IOWA STATE UNIVERSITY
Digital Repository

Retrospective Theses and Dissertations

Iowa State University Capstones, Theses and Dissertations

2006

Monitoring the structural condition of fracture-critical bridges using fiber optic technology

Justin Dale Doornink
Iowa State University

Follow this and additional works at: https://lib.dr.iastate.edu/rtd

 Part of the Civil Engineering Commons

Recommended Citation
Doornink, Justin Dale, "Monitoring the structural condition of fracture-critical bridges using fiber optic technology " (2006). *Retrospective Theses and Dissertations*. 3065.
https://lib.dr.iastate.edu/rtd/3065

This Dissertation is brought to you for free and open access by the Iowa State University Capstones, Theses and Dissertations at Iowa State University Digital Repository. It has been accepted for inclusion in Retrospective Theses and Dissertations by an authorized administrator of Iowa State University Digital Repository. For more information, please contact digirep@iastate.edu.

www.manaraa.com

Monitoring the structural condition of fracture-critical bridges using fiber optic technology

by

Justin Dale Doornink

A dissertation submitted to the graduate faculty

in partial fulfillment of the requirements for the degree of

DOCTOR OF PHILOSOPHY

Major: Civil Engineering (Structural Engineering)

Program of Study Committee:
Terry J. Wipf, Co-major Professor
Brent M. Phares, Co-major Professor
Lowell F. Greimann
Loren W. Zachary
Partha P. Sarkar

Iowa State University

Ames, Iowa

2006

Copyright © Justin Dale Doornink, 2006. All rights reserved.

www.manaraa.com

UMI Number: 3243547

UMI

UMI Microform 3243547

Copyright 2007 by ProQuest Information and Learning Company.
All rights reserved. This microform edition is protected against unauthorized copying under Title 17, United States Code.

ProQuest Information and Learning Company
300 North Zeeb Road
P.O. Box 1346
Ann Arbor, MI 48106-1346

www.manaraa.com

TABLE OF CONTENTS

www.manaraa.com

www.manaraa.com

www.manaraa.com

LIST OF TABLES

www.manaraa.com

LIST OF FIGURES

www.manaraa.com

www.manaraa.com

www.manaraa.com

www.manaraa.com

www.manaraa.com

www.manaraa.com

ABSTRACT

Structural health monitoring (SHM) enables bridge engineers to monitor the structural behavior of entire bridges or individual bridge components. At the request of the Iowa Department of Transportation, a fiber optic SHM system was developed and deployed by the Iowa State University (ISU) Bridge Engineering Center (BEC) to detect gradual or sudden damage in fracture-critical bridges (FCBs). With the equipment that was selected and the software that was developed in this research, the SHM system is deployable to any girder bridge that supports one-way traffic.

Significant laboratory and field testing was conducted as part of this research to select hardware components for the SHM system. In the laboratory testing, several fiber bragg grating (FBG) fiber optic sensors (FOSs) were bonded to steel coupons with multiple adhesives, and the coupons were subjected to cyclic and sustained tensile loads. The FOS/adhesive combinations with the best performance were selected for use in the FCB SHM system. After FOSs were installed at critical locations in the US Highway 30 (US30) demonstration bridge, conventional strain sensors were installed next to the FOSs, and measurements between the technologies for bridge responses to ambient traffic loads were compared. Results revealed good agreement between the sensing technologies.

Using the software developed in this research, the FCB SHM system was trained with measured US30 bridge performance data that were collected by the FOSs. During the training process, the SHM system filtered data and extracted event extrema from quasi-static strain records. The SHM system used the extrema to develop relationships among the FOSs, which are similar to those that are used with bivariate control charts in statistical process control (SPC). Since the relationships were developed from measured data, the SHM system was essentially trained to identify the typical bridge behavior for the structural condition that existed when the training data was collected. Relationships that were established during training are used to evaluate future strain data that are collected. Daily evaluation reports, which utilize histograms to summarize evaluations, are autonomously generated by the SHM system and delivered to the bridge engineer for interpretation and decision making. Changes in histogram distributions are predicted to be indicative of damage formation.

Significant effort was given to address the areas of SHM that are considered to hinder its general acceptance for practical applications. Specifically, data mining and storage procedures, as well as methods of presenting SHM results to bridge engineers, were addressed. Improved data mining procedures were developed and the amount of saved data from the monitoring has been significantly reduced. In addition, evaluation reports are presented to bridge owners in a familiar format that allows for rapid visual assessment. With the SHM system developed in this research, FCBs are able to be continuously monitored for damage formation, and thus, bridge owners are able to better manage their bridge inventory.

www.manaraa.com

1. INTRODUCTION

For decades structural health monitoring (SHM) has enabled bridge engineers to monitor the structural behavior of entire bridges or individual bridge components. Short-term SHM has dominated the field for most of its existence. However, technological advancements within the last decade have resulted in the evolution of long-term SHM, which has allowed for monitoring and evaluation of a bridge or bridge components continuously for years. As these systems have developed and proven their abilities, the degree to which bridge owners have invested, implemented, and utilized them has also increased. Serving as an example, the research presented in this report has been sponsored by, and conducted in cooperation with, the Iowa Department of Transportation (DOT) to develop a long-term, continuous SHM system for monitoring fracture-critical bridges (FCBs) in Iowa.

1.1 Background

A FCB is one that has at least one fracture-critical member (FCM) or member component; FCMs or member components are members whose failure would be expected to result in the collapse of the bridge [1]. There are more than 50 FCBs within the state of Iowa in the primary road system that were designed and constructed in the 1960's. A typical Iowa FCB has a two-girder cross section with stringers that are supported by floor beams as illustrated in Fig. 1.1; the welded plate girders are continuous over multiple spans, and the stringers are continuous over the floor beams. While the sizes of the structural members change to accommodate different span lengths for each bridge, the transverse spacing among the girders and stringers is constant for the FCBs in Iowa of this type.

When the FCBs were constructed, standard practice was to not weld stiffeners and

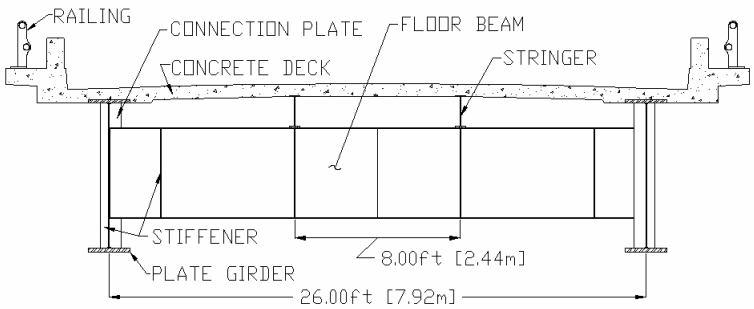

Figure 1.1. Typical Iowa FCB cross section.

www.manaraa.com

connection plates to the girder tension flanges due to concern that the strain concentrations from welds would cause fatigue cracks to form. This practice, unfortunately, merely moved the fatigue issue to other locations. Within a given cross section, the girders deflect different amounts, and the relative vertical displacement between the girders produces out-of-plane bending in the web gaps of connection plates that are not welded to the girder flanges (See Fig. 1.2). This out-of-plane bending caused fatigue cracks to develop in the web gap areas above the floor beam connection plates in the negative moment regions (NMRs) in several of Iowa FCBs. The confinement of fatigue cracks to the NMRs is explainable when considering the boundary conditions that are imposed on the tension flange throughout the bridge. In the NMRs of a bridge, the concrete deck restrains the tension flange from rotating, whereas in the positive moment regions (PMRs), the tension flange is free to rotate. Because of the difference in rotational restraint, out-of-plane bending in the NMRs is usually larger than that in the PMRs, and thus, the likelihood of fatigue crack formation increases. The magnitude of the out-of-plane bending is heavily influenced by the girder spacing and bridge skew. For example, the relative displacement between girders at a cross section will be larger for skewed bridges, which produces larger out-of-plane bending in the web gaps [2].

With concern of the fatigue cracks propagating vertically through the girders and causing structural failure, retrofit procedures were developed and implemented in the FCBs. Each retrofit involved cutting back the floor beam connection plates and any accompanying stiffeners in the

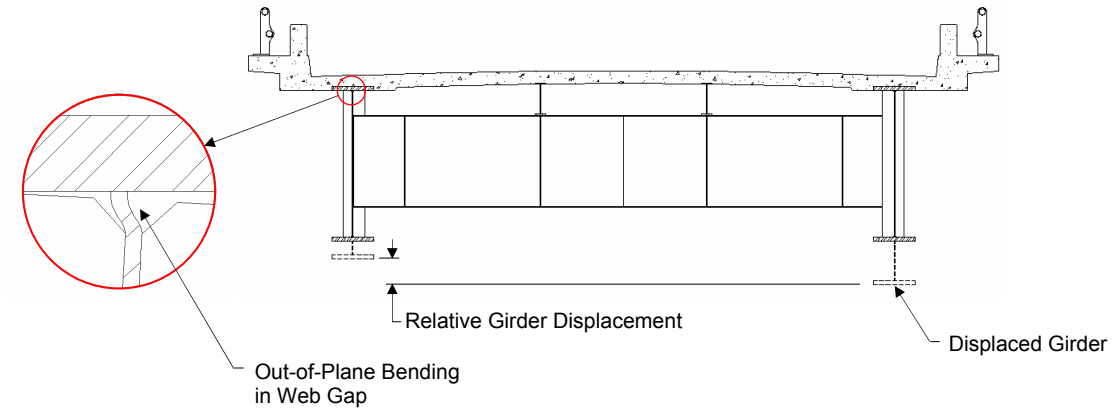

Figure 1.2. Out-of-plane bending in the web gap due to relative girder displacement.

www.manaraa.com

NMR to reduce out-of-plane bending stress levels. Figure 1.3 illustrates the retrofit procedure for the US Highway 151 (US151) bridge crossing the Wapsipinicon River.

During the retrofit of the US151 bridge, a 67.5-in. (1.7-m) - long crack spontaneously propagated vertically through the girder web. The longitudinal location of the crack is presented in Fig. 1.3c, and a detail of the crack is shown in Fig. 1.4a. Figure 1.4b presents the web splice plates that were used to repair the crack and restore the US151 bridge to operating condition. The US151 crack formation is an example that illustrates the severe dangers that fatigue cracks impose on FCBs, and as a result of this threat, FCBs are manually inspected for fatigue cracks during their biennial inspections. However, the Iowa DOT expressed interest in a SHM system with the ability to monitor the FCBs continuously between inspections. With advanced identification of crack development, necessary bridge repair can be accomplished before cracks have reached a critical state that causes bridge failure.

1.2 Scope and Objective of Research

The SHM system developed in this study has been developed for the Iowa DOT bridge engineers to remotely and continuously monitor a FCB in order to aid detection of crack formation by identifying gradual changes in bridge structural behavior. The specifications for the system were identified as follows:

- Monitoring must be continuous and capable of identifying changes in bridge structural behavior (elastic or inelastic) from a preexisting state, which may be indicative of crack development and/or propagation.
- Data collection, reduction, evaluation, and storage must be autonomous.
- Summaries of reduced data and evaluations must be presented in a clear, understandable format to bridge engineers; the presentation of the data must be in a report that is autonomously generated and electronically delivered.
- DOT work forces with proper training must be capable of installing the system.

Previous experience with long-term SHM at the ISU BEC resulted in the accumulation of massive amounts of data, but it was determined that only a small percentage of the data was useful for assessing the condition of the structure [3]. As a result, in addition to the previously defined objectives, this study also included significant efforts to (1) develop data reduction procedures that

www.manaraa.com

a. Photograph of the US151 bridge

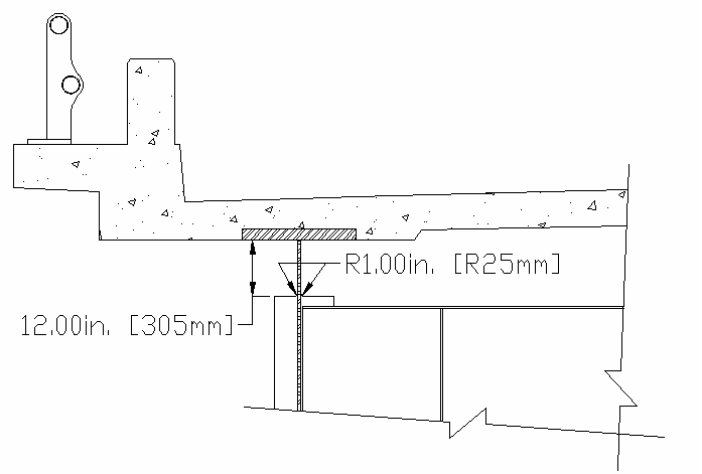

b. Detail of the cut-back retrofit

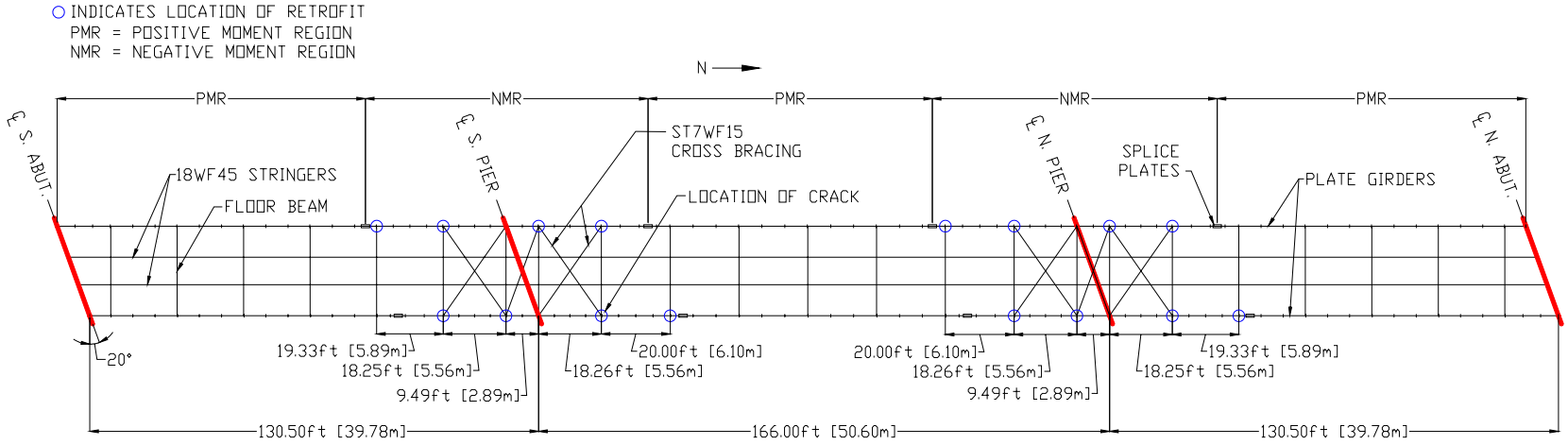

c. Plan view of US151 identifying locations of retrofit

Figure 1.3. Retrofit procedure and details of the US151 bridge crossing the Wapsipinicon River.

www.manaraa.com

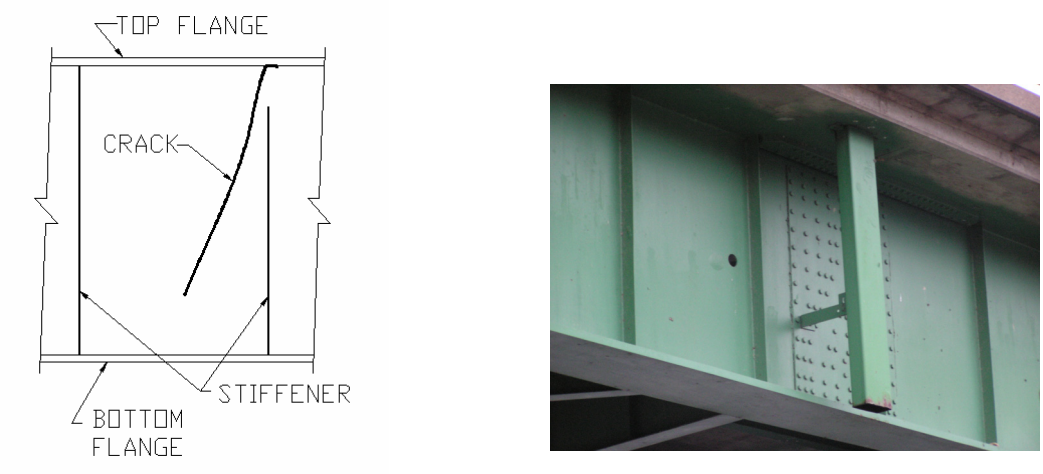

a. Crack formation during the US151 retrofit (View from exterior face of girder)

b. Photograph of web splice retrofit

Figure 1.4. Crack formation and repair during the US151 retrofit (See Fig. 1.3c for crack location).

identify and extract the information in data files that is useful for evaluating the condition of the bridge, and (2) develop evaluation methods that effectively utilize the extracted data to correctly report the structural condition of the bridge.

1.3 Proposed Research Approach and SHM Solution

The proposed SHM solution is a monitoring system that utilizes strains measured at various locations that result from ambient traffic crossing the bridge. Strain has been selected as the damage detection parameter in this study because it is a highly dependent indicator of damage, and in addition, it is usually the parameter that is best understood by bridge engineers. In this approach, sensors are installed in regions of the bridge that are expected to experience damage, such as the cutback region of the retrofit, and also in regions of the bridge that are not expected to experience damage. Fiber optic sensors (FOSs) have been chosen as the strain sensors based on their previous success with long-term strain monitoring and distinct advantages that are discussed subsequently.

The recorded strains resulting from ambient traffic for a given period of time are used to develop relationships between sensors in the damage prone regions of the bridge and those that are not in damage prone regions of the bridge; each relationship is formed and defined with upper and

www.manaraa.com

lower limits similar to the methods used with control chart analyses, which are commonly used to monitor process controls of chemical plants, manufacturing facilities, and nuclear power plants. By developing the relationships with recorded strain data, the system has been trained to recognize typical performance for the existing condition of the bridge.

After the relationships have been established, they are used to evaluate every traffic event measured by the system. The assessment from each relationship is “Pass” or “Fail”, and at the end of a specified evaluation period, the assessments are summarized in histograms. Structural changes in the bridge, such as the formation of cracks, are expected to be evident through changes in histogram distributions for successive evaluation periods. When the distribution changes are identified, bridge owners are able to take necessary actions, investigations, repairs, etc., before the damage reaches a critical state.

1.4 SHM System Demonstration Bridge

The Iowa FCB that was selected as the demonstration bridge for the showcased project is the US Highway 30 (US30) bridge crossing the Skunk River near Ames, IA (See Fig. 1.5). The demonstration bridge has a 30-ft (9.1-m) - wide roadway that supports two east-bound traffic lanes; the posted speed limit is 65 miles per hour (mph) [105 kilometers per hour (kph)]. The composition and layout of the bridge is presented in Fig. 1.6. As illustrated, the bridge is a three span structure consisting of 97.5-ft (29.7-m) - long side spans and a 125-ft (38.1m) - long middle span. Review of Figs. 6a-b reveals that the floor beam connection plates in the NMR have been cut back during the retrofit procedure (See Figs. 1.3b, 1.5d, and 1.6c), whereas those in the PMR have not been cut back. To date, no fatigue cracks have developed in the cut-back regions of the girders above the floor beam connection plates in the US30 bridge.

1.5 Report Content

The contents of this report discuss all aspects of the research project pertaining to the development of the proposed SHM system. The information in Chapter 2 provides a brief overview of the current international state of SHM in bridge structures. Presented in Chapter 3 are the procedures that were used to select the technology for this research, and in addition, the laboratory

www.manaraa.com

a. Side view

b. Girders, stringers, floor beams, and stiffeners

c. Cross bracing

d. Retrofitted floor beam connection plate

e. Negative moment region flange taper

Figure 1.5. Photographs of the US30 bridge.

www.manaraa.com

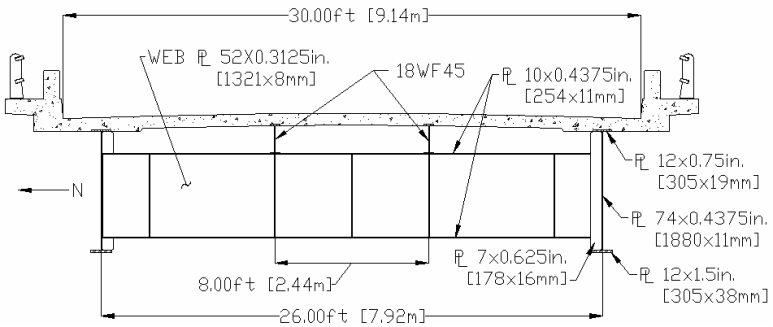

a. Cross section in positive moment regions

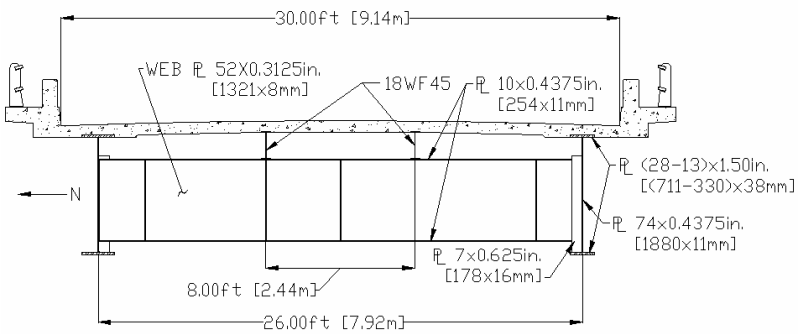

b. Cross section in negative moment regions

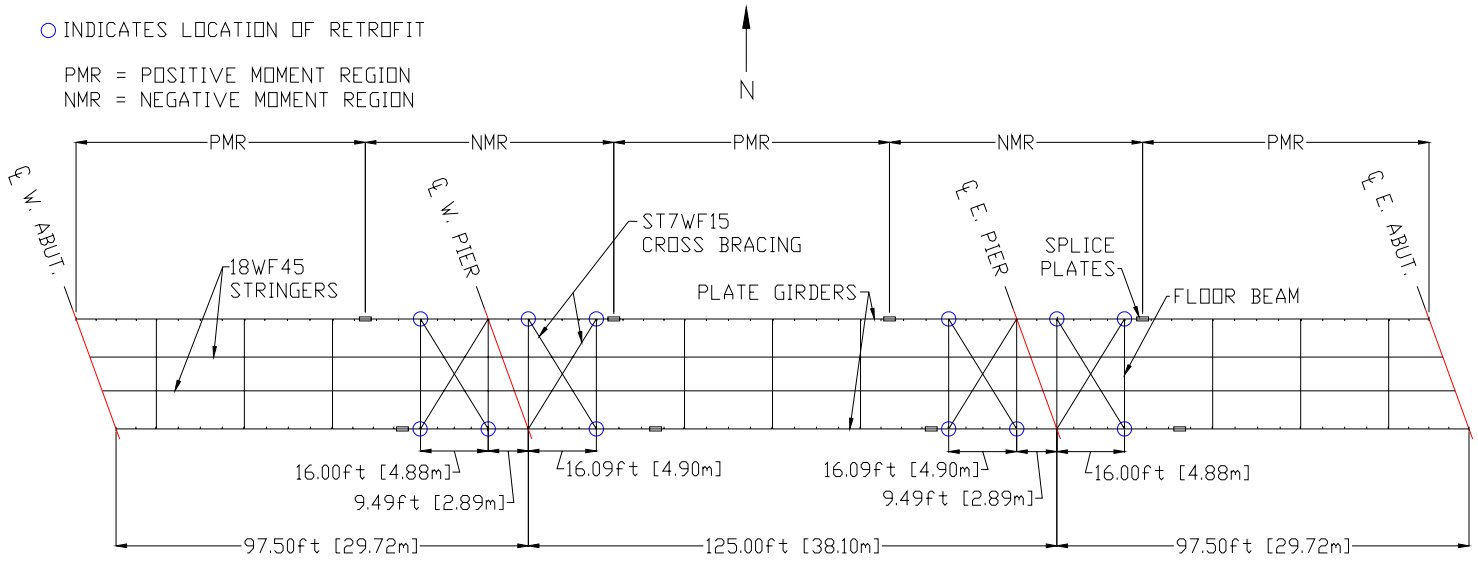

c. Layout of structural steel, identification of positive and negative moment regions, and locations of cut-back retrofits

Figure 1.6. Composition and layout of the US30 bridge.

www.manaraa.com

validation testing that was performed to ensure that the technology was suitable for use in the SHM system. Chapter 4 illustrates the hardware layout at the US30 bridge and presents the in-service validation testing that was performed. In Chapter 5, the SHM system software is discussed; the details of the operations that are performed by the system are described, and examples of collected and analyzed data are provided. Finally, Chapter 6 summarizes the conclusions that were determined from the research, and Chapter 7 provides recommended future research that is required to further expand the SHM system that was developed.

www.manaraa.com

2. LITERATURE REVIEW

The material presented in this chapter provides a general overview of the status of bridge SHM. However, for the topics pertaining to the development of the FCB SHM system discussed in Section 1.3, specific attention and detail is provided. The sections in this chapter address the following topics in respective order:

- History and progression of bridge field inspections as well as current manual methods of crack detection in structures
- Research specifically pertaining to crack detection with advanced methods and sensors that has been demonstrated on basic experiments or analytical methods
- An introduction to SHM procedures, systems installed on or analytically demonstrated for in-service structures, and discrimination methods used in the systems for damage detection
- Current challenges and criticisms of SHM
- Miscellaneous topics related to SHM system installation and data reduction
- Summary of selected literature and discussion that identifies the uniqueness of the proposed FCB SHM system

2.1 Background to Field Inspection of Bridges

The need for a structured method of recording and tracking the condition of bridges in the United States became evident in 1967 when the Silver bridge between Point Pleasant, West Virginia, and Gallipolis, Ohio, collapsed during rush hour traffic resulting in the deaths of 46 civilians. In response, the National Bridge Inspection Standards (NBIS) were implemented in the 1970's to guide the inspection and inventory of bridges on public roads. In general, bridges are inspected every two years with exceptions given to bridges with special conditions that warrant shorter or longer inspection cycles [4].

Inspection information is kept in the National Bridge Inventory (NBI) data base and serves as a basis for the prioritization, allocation, and distribution of federal funding. To date, there are more than 590,000 bridges and culverts in the USA consisting of various shapes, sizes, and materials that are included in the NBI [5]. Approximately 11% of the steel bridges have FCMs, and thus, are categorized as FCBs. From this population of FCBs, 83% are two-girder bridges and two-line trusses

www.manaraa.com

[6]. As a result, it is evident that the population of FCBs in the USA extends well beyond the state of Iowa.

The evaluations of each bridge in the NBI currently rely heavily on visual inspections. For many years visual inspection was the only alternative to evaluating a bridge, and the method has advantages in terms of cost and ease of application [5]. However, its limitations have been shown to sometimes result in inconsistent and erroneous bridge evaluations [7]. The limitations of visual inspection are the result of many factors, and two of the major ones include (1) they are subject to the opinions and variability in experience and training among the inspectors, and (2) they are limited to structural condition that can only be perceived by the human eye, and thus, if signs of damage are not visually evident, such as subsurface cracks, then they may be overlooked and not included in the evaluation.

To enhance the quality of the inspections, manual non-destructive testing (NDT) techniques are often included to verify the presence and/or the extent of cracks that are visually suspected or detected in a bridge. Such methods include the following [5, 6, 8]:

- Dye penetrant testing [9]
- Magnetic particle testing [10]
- Ultrasonic testing [11, 12, 13, 14]
- Acoustic emission [15, 16, 17]
- Coating tolerance thermography
- Radiography [18, 19]

Dye penetrant and magnetic particle testing are presently the methods most commonly used to investigate cracks during in-service field inspections of bridges [6] because they are effective, inexpensive, and relatively basic procedures. However, both methods are limited to cracks that are at or near the surface being tested. Ultrasonic testing is a method that can identify internal defects of a component and is commonly used during the fabrication inspection of steel bridges, but the interpretation of results requires a skilled operator. Acoustic emission testing and radiography have been utilized less frequently than other methods. Coating tolerance thermography requires extremely

www.manaraa.com

expensive equipment and is rarely utilized [8]. Even though some methods are more applicable and are used more frequently than other methods, implementation of some of these methods in field or manufacturing inspections has enhanced the quality and reliability of visual inspections.

Bridge owners spend a major portion of their budget inspecting and maintaining bridges within their inventory. Unfortunately, FCBs have been proven to consume a large fraction of that budget even when they represent a small fraction of the bridge inventory. In a National Cooperative Highway Research Program (NCHRP) synthesis study [6], bridge owners reported that FCBs cost two to five times the amount to inspect than redundant bridges. Reasons for increased inspection costs were reported as specialized access equipment (requiring additional traffic control) for hands-on inspection, additional employee hours to conduct the detailed inspections, more frequent use of NDT methods, and more frequent inspections required for the FCBs. Also included in the study was a questionnaire that asked agencies to identify research needs for FCBs. Field monitoring of FCBs was listed among the top three responses.

Based on the review presented, field inspection of bridges has heavily relied on visual inspection for finding damage and utilized advanced technologies to confirm and identify the extent of damage. While this approach has been suitable for many years, the influence of human limitations and variability among inspectors has sometimes resulted in erroneous and inconsistent bridge evaluations. In addition, inspections for FCBs have been proven to cost more than non-FCBs. The development of a continuous SHM system for FCBs is an alternative that uses science and technology to autonomously and consistently detect and quantify damage. The funding required to implement such a system is justified by the capitol that it will save bridge owners by reducing the frequency and additional costs of inspecting FCBs. Interest in developing such a system is evident through the funding provided in this research by the Iowa DOT and through the interest expressed by practitioners in the NCHRP synthesis study.

2.2 Crack Detection with Advanced Methods

Laboratory research solely dedicated to the investigation of crack detection in structures has been conducted for decades. The selected research focused on using equipment and sensors with

www.manaraa.com

autonomous capabilities that were applicable in SHM systems. Review of the literature illustrates that two parameters have been primarily utilized for crack detection: vibration-based measurements and strain-based measurements. However, automated ultrasonic methods have also been briefly investigated. Regardless of the technology utilized, past research involving crack detection in a structural material has included efforts to investigate the ability of the equipment to accurately and reliably measure a parameter, and in addition, to investigate the sensitivity of a parameter to crack formation and /or propagation.

In the following sections, selected projects involving crack detection are showcased for vibration-based, strain-based, and ultrasonic-based sensing and have been organized according to the type of technology utilized in the research: conventional technology or fiber optic technology. For discussion purposes, conventional technology has been defined as any technique that does not include fiber optic technology.

2.2.1 Crack Detection with Conventional Technology

As previously mentioned, past research involving crack detection has involved vibration-based sensing and strain-based sensing, which involves the use of accelerometers and strain gages, respectively. A basic understanding or estimation of the event being measured is critical to the accuracy of the measurement in either case. With accelerometers, the amplitude and frequency content of the event are required for proper accelerometer selection. With conventional strain gages, two common types of sensors are available and selected based on the type (static or dynamic) of event being measured. Electrical resistance strain gages, also known as foil gages, are capable of measuring dynamic events, but they have low zero-stability which ultimately results in signal drift. Vibrating wire strain gages have high zero-stability, but they can only be used for quasi-static strain measurement [20]. Applications of accelerometers, strain gages, and piezoelectric sensors for crack detection are discussed in the following paragraphs.

Yoo and Kim [21] suggested that damage detection is a localized phenomenon, and as a result, the sensor being utilized must also measure a localized response. The project presented analytical work to illustrate the use of strain measurements to determine strain mode shapes of in a

www.manaraa.com

plate before and after crack formation. Results concluded that a cross grid (strain gages directly above and to the sides of a crack) of five sensors was sufficient to characterize the strain modes for crack detection. In addition, this method was analytically proven to identify the existence of a crack, but not the size crack. The results of this research were not experimentally tested, however.

Patil and Maiti [22] presented another analytical study that involved detection of multiple cracks in slender Euler-Bernoulli beams. This approach is one of few that is capable of identifying more than one crack at a time. The method was based on transverse vibration (natural frequencies) in the beam at one point. The beam was divided into a number of segments, and each segment was associated with a damage parameter. Through knowledge of changes in natural frequencies of the beam, damage parameters such as crack size and location were determined. Several successful numerical examples were presented, but the method was not proven experimentally.

Wang and Barkey [23] illustrated the use of impact hammer-accelerometers to determine frequency response functions of spot welded specimens. Finite element analyses (FEAs) were conducted for the uncracked and cracked spot welded joints and proved to be in good agreement with experimental results. Through their research, it was shown that natural frequencies of the spot welded joints nonlinearly decreased with the growth of fatigue cracks, and that variation in natural frequencies and vibrating modes was indicative of fatigue crack formation for the spot welded joints.

Verreman [24] displayed the ability to measure propagation of fatigue cracks with miniature strain gages in cruciform welded joints. Strain gages in this research were installed above a crack in a cruciform joint with varying distances between the sensors and the crack. Cyclic loads were applied to the joint and the strain gages monitored the propagation of the crack; when the reading from the strain gage closest to the crack saturated, other gages farther away monitored the crack. It was shown that strains that were measured above the crack changed as the crack propagated during identical cyclic loading conditions. The results of the research provided relationships between crack length and cycle life of the joint.

Fujimoto and Yue [25] introduced a new method to estimate the depth of a surface crack based on the measurement of the crack opening deformation (COD) by using strain gages. Strain

www.manaraa.com

gages were bonded along the crack line to measure the COD, and a reference strain gage was bonded farther away from the crack to measure the nominal strain for the region. To estimate the depth of the crack, the COD distribution per unit of normalized strain was multiplied by a proportional factor obtained from analytical modeling. The method illustrated favorable results when compared with FEA and was proposed for use in place of other NDT techniques.

Younis and Mize [26] investigated the averaging effects of strain gages in nonuniform strain fields near crack tips. This study focused more on the affects of sensor limitations on the measured parameter, rather than the ability of the sensor to measure a change in the parameter. The research presented analytical modeling to illustrate that strain gage readings nearly always underestimate the true strains at a crack tip, and the magnitude of the error is related to strain gage width, length, and misalignment. Due to the averaging effects of strain gages, the paper reinforced the familiar concept that strain gages should be small when compared to the size of the crack and the strain gradient near the crack tip. Finally, it was suggested that in order to correctly interpret strain measurements to determine crack properties such as size, location, and stress intensity factors, the averaging effects of strain gages needs to be considered.

Ihn and Chang [27] demonstrated the ability to detect cracks by using ultrasonic, piezoelectric-based sensors that are built into metallic structures. The actuating sensors used ultrasonic guided Lamb waves to maximize measurements at the receiving sensors. The assumption was that any change in the received signal from the constant transmitted signal was due to a change in structural condition. Methods were developed to select an individual mode for damage detection, and a physics-based damage index was developed from extracting features in the sensor signals related to crack growth. The method was demonstrated with a fatigue test on a notched aluminum plate, and results showed good correlation with visual inspection. In a follow-up study [28], the researchers applied the method to a riveted fuselage joint, and damage predictions from the proposed system showed good correlation with visual inspection, eddy current testing, and ultrasonic scan methods.

www.manaraa.com

Based on the findings from the discussed research, conventional sensing methods have been proven to be capable of measuring changes in parameters due to the formation of cracks in fundamental laboratory experiments. For the selected investigations, the existence, locations, and sizes of cracks were known.

2.2.2 Crack Detection with Fiber Optic Technology

As technology has continued to improve, so has the market for sensors. Within the last decade, fiber optic technology has evolved and been researched to demonstrate its potential for crack detection. In the proceeding paragraphs, a background for fiber optic sensing has been presented along with selected research projects that utilize the technology for crack detection.

Fiber optic sensors measure some type of change in guided light, and two general categories of FOSs exist based on where the change in guided light is measured: intrinsic (inside the fiber) and extrinsic (outside the fiber). The four primary changes in guided light that can be measured are as follows: phase, polarization state, intensity, and wavelength. Thus, four refined categories of FOSs are as follows, respectively: (1) interferometric sensors, (2) polarimetric sensors, (3) intensity modulated sensors, and (4) spectrometric sensors. Intensity modulated sensors and spectrometric sensors are the most commonly used strain sensors [29].

Intensity modulated sensors are intrinsic and measure changes in the intensity of the input light, and optical time domain reflectometry (OTDR) is used in almost all sensors of this type. With OTDR, an optical signal is pulsed into a fiber, and the intensity of backscatter (Raleigh scattering) due to microscopic variations in the fiber core are monitored along the length of the entire fiber. When an external load is applied to the fiber, it becomes deformed and causes a change in the magnitude of the reflected signal; thus, mechanical strain can be extracted from the change in the reflected signal. Monitoring the entire length of the fiber allows each point along its length to serve as a sensor, and this type of arrangement is referred to as a fully distributed network [29, 30, 31].

Spectrometric sensors are intrinsic and measure changes in wavelength of light, and these sensors are more commonly known as fiber bragg grating (FBG) sensors. While these sensors are not as sensitive as interferometric sensors, their configuration, installation, and data processing are

www.manaraa.com

extremely easy, which as has made them very popular [29]. The sensors are engraved into the fiber for a finite length (typically one cm) with the pitch spacing of the grating controlled to reflect one wavelength of light. When external load is applied to the sensor, the grating pitch spacing changes and a different wavelength of light is reflected; changes in the reflected wavelength of light are linearly related to the strain on the sensor. In general, advantages of using FBGs over conventional resistance or vibrating wire strain gages include the following [29, 30, 31]:

- They are immune to electromagnetic and radio frequency interference.
- They measure wavelength shift and not signal amplitude, and thus, there is no signal drift.
- There is low loss with long lead lengths, enabling measurements on very long structures.
- They are not electrically conductive, and thus, can be used in moist environments.
- They are comprised of generally inert material (glass) that does not corrode, resulting in a long sensor lifetime.
- Several FBGs can be multiplexed into one fiber, a sensor arrangement referred to as a quasi-distributed network.

FBGs can be used to measure quasi-static and/or dynamic events on a structure. In addition, they can measure long-term events without recalibration, which is not possible with conventional strain sensors. However, the disadvantages of using FBGs are as follows [29, 30, 31]:

- They are sensitive to temperature variations in addition to mechanical loading.
- The fiber can be broken if it is severely bent, twisted, or pinched, which makes them less advantageous for construction monitoring.
- The cost of the sensors and equipment is currently several magnitudes higher than that of conventional equipment.

The largest disadvantage to using FBGs is that part of the change in wavelength is caused by strain in the host material (mechanical plus thermal), and part is caused by changes in optical properties of the fiber due to temperature changes [29]. Thus, for measurement of any event that is long enough for temperature variations to occur, results must be compensated for the wavelength change resulting from temperature-induce changes in the fiber.

Hale [32] presented some of the earliest attempts to use fiber optic technology for crack detection in a specimen. In the research, a prepackaged crack-detection sensor was developed.

www.manaraa.com

The sensor was designed to be bonded to a structure in the crack-prone region. If a crack formed in the substrate material below the sensor, the optical fiber was damaged or broken; thus, light being transmitted through the fiber was attenuated, and the measured attenuation change was indicative of structural cracking. Each sensor was designed with three parallel optical fibers, an attempt to monitor crack propagation through sequential damage in the fibers. Infrared light sources and detectors were displayed in the research, but it was also suggested that OTDRs could be used. Simple laboratory tests on tensile coupon proved that the sensor is capable of detecting cracks as small as 5-30μm.

Leung et al. [33, 34] illustrated a fully distributed fiber optic network with OTDR to determine crack formation and/or propagation. The method consisted of installing a single mode fiber (SMF) in a 'zigzag' pattern throughout a region where cracks were expected to develop in a concrete structure. Before the formation of cracks, the OTDR was used to establish a baseline of signal intensity versus fiber length. If a crack formed in the structure at an angle other than 90° to the fiber, a sharp bend formed in the fiber and caused a significant drop in the power signal on the OTDR record. The location of the crack was known based on the OTDR record, and the magnitude of the drop was related to the size of the crack. Olson et al. [35] demonstrated theoretically and experimentally that using this approach with multimode fiber (MMF) increased the dynamic range of the measurement, which is the total loss that can be monitored. Thus, more cracks were able to be monitored by the network with MMF.

Yang et al. [36] showcased a procedure to use integral strains (total change in length of the fiber) to detect the presence of cracks in a specimen. Fibers were bonded to a surface expected to crack, and when the crack formed, the change in length of the fibers (deformation of the specimen) were determined by measuring phase shifts of the system and were used in an algorithm to determine the crack size and location. Numerical models were presented to support the research, but experimental procedures were not performed.

Peters et al. [37] investigated the effects of a nonuniform strain field on the accuracy of FBG strain measurement. The study provided laboratory proof that the reflected spectrum of a FBG was not a single peak when the grating was bonded in a region with a nonuniform strain field. Thus,

www.manaraa.com

conversion between wavelength change and mechanical strain required more complex analysis. Thus, it was shown that FBG sensors have an error associated with measurements in regions with high strain gradients, such as at a crack tip, which resembles the averaging effects of conventional sensors. As a result, it was proven the length of FBG sensors must be sufficiently small when compared to strain gradient to avoid significant measurement errors. This criterion is consistent with that of conventional electrical resistance or vibrating wire strain gages.

Struder and Peters [38] proposed to monitor a structural volume with an embedded fiber optic sensor network that measures strain, integrated strain (displacement), and strain gradients. The approach used FBGs to monitor strain, interferometers for integrated strain, and long FBGs to measure strain gradients. Long FBGs were selected to ensure that the entire strain gradient was captured by the FBG. However, rather than calculating a strain reading from wavelength shift, the strain gradient was calculated directly by using the change in bandwidth of the reflected spectrum; the researchers referenced the work by Hill and Eggleton [39] to accomplish this calculation. Analytical examples were provided to showcase two approaches that utilized the measured parameters: strain mapping and an artificial neural network (ANN). The ANN proved to be a better method for utilizing the multi-scale sensing in the procedure. No experimental work was performed to support the conclusions from the analytical work.

Degen [40] illustrated the use of embeddable FBGs to monitor strains in an ultra-high-performance concrete (UHPC) beam that was tested in flexure and shear. The FOSs were installed in the bottom of the beam and were used to determine the presence of tension cracking. Knowing the loading condition that produced the cracking, the tensile strength of the new type of concrete was determined.

Fiber optic sensors are available as accelerometers, strain gages, tilt meters, displacement transducers, temperature sensors, load cells, etc., and thus offer all of the capabilities of conventional sensors. In addition, fiber optic sensing also allows for fully distributed sensing networks that allow for spatial resolution in addition to parameter measurement. This versatility along with several other beneficial characteristics has helped make FOSs a popular choice for long-term SHM of bridges.

www.manaraa.com

The research presented in the Sections 2.2.1-2.2.2 illustrates the ability to use various measured parameters, technologies, and methods to detect cracks with known properties in carefully controlled laboratory experiments. Building on this success, SHM systems have been developed, deployed, and tested in the field on full-scale, in-service bridges as will be presented in Section 2.3.

2.3 Structural Health Monitoring for Damage Detection in Bridges

Structural health monitoring is a broad term used to describe monitoring that produces an overall depiction of the structure's condition. Thus, SHM should not be considered as only damage detection; damage detection is just one aspect of SHM. Within the last decade, research pertaining to continuous field monitoring of bridges has increased dramatically. A few of the major factors contributing to the increase in SHM research include the following [41]:

- The current state of the aging bridge infrastructure and economics associated with rehabilitation and repair versus new construction.
- Technological advancements such as increases in computing memory and speed, as well as advancements in sensors.
- Recent failures receiving media coverage, which in turn creates public concern, political pressure, and increased funding for research.

In addition to the complexities of detecting damage in controlled laboratory experiments, SHM that includes damage detection for in-service bridges introduces more challenges:

- The system components and functionality must be capable of withstanding and compensating for environmental conditions such as extreme temperatures, moisture, wind, etc.
- The structure being monitored is larger and more complex.
- The magnitude and frequency of external loads on the structure cannot be controlled for most practical in-service monitoring approaches.
- Power for electrical equipment may not be available due to the remote location of some bridges, and solar power equipment may not be suitable to supply sufficient electricity for some SHM systems.
- Wireless communication is usually the only practical method to communicate with SHM components at the bridge site, which is slower and less reliable than wired communication that is typically available in laboratories.

In general, damage detection in bridges presents a more complex situation than that of laboratory experiments, and in addition, demands on equipment increase while the resources for the equipment

www.manaraa.com

decrease. Selected SHM systems are presented in this section to demonstrate the wide variety of equipment and methods that are used to monitor the condition of bridges. Prior to the presentation of these projects, and a brief background to SHM process is presented.

2.3.1 Background to Structural Health Monitoring Procedures

The complexity and capability of SHM systems are different, and thus, the information pertaining to structural condition and/or damage that is presented to the bridge engineer varies for each system. Research by Rytter [42] defines four levels of damage detection:

- Level 1: Determination that damage is present in the structure
- Level 2: Determination of the geometric location of the damage
- Level 3: Quantification of the severity of the damage
- Level 4: Prediction of the remaining service life of the structure

Level 1 is a forward problem that identifies a change in a parameter and relates it to the presence of damage. Levels 2 and 3 are inverse procedures that use the change in the parameter to back-calculate the extent and location of the damage that caused the parameter change. Some type of modeling is usually required to reach level 3 damage detection.

Damage can also be classified as linear or nonlinear. Linear damage assumes that elastic structural behavior prior to damage remains elastic after damage, while nonlinear damage assumes that elastic structural behavior prior to damage becomes inelastic after damage (i.e. crack opening and closing during an event). Most research reported in literature addresses linear damage detection for levels 1 to 3 [41].

Literature for SHM systems describes several aspects of each approach, but in general, many researchers and practitioners agree that long-term SHM is fundamentally a process of pattern recognition that is composed of four processes [43]:

1. Operational evaluation
2. Data acquisition, fusion, and cleansing
3. Feature extraction and information condensation
4. Statistical model development for feature discrimination

www.manaraa.com

Operational evaluation begins to define why the monitoring is being performed, how long to perform the monitoring, and how to tailor the monitoring for the measurable changes related to the damage condition. Data acquisition is application specific, and the interval and sampling rate are dependent on the measured parameter as well as the damage type being detected. The purpose of data fusion is to integrate the data from a multitude of sensors in order make a decision that is more robust and confident than that which could be made with just one sensor. Data cleansing is the process of selecting the data to be kept from the original set and to be passed on for further evaluation; filtering and decimation are both examples of data cleansing [43].

Feature extraction is the process of identifying the useful information within a data set that is useful in analysis, which is usually application specific. Almost all feature extraction is some form of information condensation, meaning that the size of the information remaining to be processed has been significantly reduced. For example, vibration-based monitoring often extracts mode shape and frequencies as the damage-sensitive feature from a continuous set of acceleration measurements on a structure [43].

Feature discrimination is the process of identifying the changes in a feature or parameter that are indicative of the extent of damage in a structure. As previously mentioned, many SHM systems use statistical pattern recognition to achieve this task. If an algorithm is a statistical-based model that uses information from both the damaged and undamaged structure to identify damage, then the algorithm has used what is referred to as *supervised learning*. However, if the algorithm only uses information relating to the undamaged structure, then the algorithm uses *unsupervised learning*. To identify the existence and location of damage (Level 1 and Level 2), unsupervised learning is usually adequate. To quantify the extent of damage from the data (Level 3), however, supervised learning is usually required [43].

2.3.2 Structural Health Monitoring of Bridges with Conventional Technology

Most SHM bridge projects have utilized conventional technology to accomplish their sensing needs. These projects include SHM on FCBs similar to the US30 bridge (Fig. 1.6) as well as many

www.manaraa.com

redundant styles of bridges. Selected research projects pertaining to each category are presented in the subsequent sections.

2.3.2.1 Monitoring of Fracture-Critical Bridges

In 1993 the I-40 bridges over the Rio Grande in Albuquerque, NM, were scheduled to be demolished, and thus, created an opportunity to investigate the post-damage performance of a full scale bridge. The I-40 bridges were classified as fracture-critical since they were two-girder designs very similar to the US151 (Fig. 3) and US30 (Fig. 6) bridges. There were two primary differences between the designs of the I-40 bridges and the designs of the US151 and US30 bridges: (1) the I-40 bridges had three stringers positioned between the two exterior plate girders, while the US151 and US30 bridges have two stringers, and (2) the I-40 bridges had cross bracing between each set of floor beams, but the US151 and US30 bridges only have diagonal bracing between floor beams near the piers.

The research approach consisted of first testing the bridge in the pristine condition, and then the bridge was retested after damage was inflicted to the middle span of the three-span segment of the bridge. The damage consisted of four sequential cuts to the web and bottom flange of an exterior girder at midspan of the middle span; the final damage case resulted in a cut that completely severed the bottom flange and extended upward through approximately 60% of the web. Two different parameters, vibrations [44, 45, 46] and strains [47], were utilized to scrutinize three different SHM approaches.

Farrar and Jauregu [44] used two sets of accelerometers to measure the I-40 bridge accelerations; one coarse set of accelerometers measured the global response of the bridge over the three spans, and a refined set that was confined to the damaged area of the bridge. A hydraulic shaker was used to subject the structure to a random vibration signal over the range of 2 to 12 Hz. Many analyses were performed to investigate the changes in bridge properties due to damage and included: changes in resonant frequencies, mode shapes, mode shape curvature, load surface curvature, flexibility, and stiffness. Results from the study indicated that resonant frequencies and mode shapes were poor indicators of damage and that all other methods did not clearly identify

www.manaraa.com

damage until the most severe damage case when the entire bottom flange and 60% of the web were cut. The researchers also conducted a follow-up study [45] that investigated the accuracy the damage identification methods when applied to numerical models. Conclusions from the numerical study were approximately the same as those of the experimental study.

Woodward et al. [46] describe the analysis that was conducted on the I-40 bridge that utilized the resonant ultrasound spectroscopy (RUS) method, which relies on changes in the resonant frequencies of the structure as indicators of damage. While the structure was vibrated with the driving force from low to high frequency, a narrow band measurement was swept over the same frequency range. Since noise is significantly reduced with this method, slight changes in frequencies and mode shapes were detectable. Results of the study indicated that only the most severe case of damage was identifiable.

Idriss et al. [47] instrumented the I-40 bridge with strain gages to monitor the positive and negative moments in the girders, forces in the cross bracing, moments in the floor beams in the vicinity of the crack, and forces in the stringers. Dead load strains and static live load strains were measured before and after each damage case. Results illustrated that redistribution of forces did not occur until the last state of damage; most of the redistribution was longitudinal in the damaged girder, but there was also transverse redistribution to the undamaged girder. In addition, results showed that the cross bracing had very large increases in strain during the most severe damage case, which indicated that the cross bracing significantly contributed to the stability of the bridge after damage was inflicted. Conclusions of the research indicated that the damage was directly detectable through strain measurements during the most severe damage case, and that follow-up research should be conducted to develop a monitoring system for the family of FCBs.

2.3.2.1 Monitoring of Redundant Structures

Most projects involving SHM are demonstrated on redundant structures. A review of literature for these projects reveals a wide variety of sensors that have been utilized among the most successful projects: accelerometers, strain gages, load cells, displacement transducers, level sensors, anemometers, temperature sensors, weigh-in-motion sensors, etc. Although the selected

www.manaraa.com

projects presented in this section attempt to illustrate the broad use of these sensors, vibration-based monitoring has been investigated far more than any other method.

Iwasaki et al. [48] showcased the use of load cells to monitor the turnbuckle supports of a jet-fan installed in an expressway tunnel as a ventilator. Load cells were installed on each of the four main turnbuckle supports, and data from the undamaged, operating condition were used to generate a response surface (i.e. unsupervised training), and damage was automatically determined by testing changes in the identified system by means of a probability distribution. The method was tested on a full scale system and determined to be successful.

Kesavan et al. [49] analytically illustrated the use of static strain distributions with an ANN to detection delaminations in a glass fiber reinforced polymer (GFRP) retrofit. Strain distributions obtained from FEA for various damage scenarios were used to train an ANN. Results of the study concluded that as distances between strain gages on the FEA decreased (more sensors in the area of damage), the percentage of error for the ANN decreased.

Wong et al. [50] presented the Wind And Structural Health Monitoring System (WASHMS) installed on the Tsing Ma Bridge, Kap Shui Mun Bridge, and Ting Kau Bridge. The systems installed on these bridges are some of the largest and most diverse to date. Approximately 774 sensors have been installed on these suspension and cable-stayed bridges and include the following: accelerometers, strain gages, displacement transducers, level sensors, anemometers, temperature sensors, and weigh-in-motion sensors. Data are interpreted in the amplitude, time, and frequency domains for analysis and interpretation. Several examples of data collected were presented. Li et al. [51] demonstrated the use of strain gage measurements in a fatigue damage model to estimate the remaining fatigue life of the Tsing Ma Bridge. In addition, Ni et al. [52] illustrated the use of probabilistic neural networks (PNNs) for damage identification and location in the Ting Kau Bridge.

Caicedo and Dyke [53] presented the use of accelerometers to measure changes in dynamic characteristics of a cable-stayed bridge to detect damage. The method was developed utilizing information from FEA, and then it was compared to results from experimental testing on a scaled laboratory model in both the undamaged and damaged state. Results of the testing indicated that

www.manaraa.com

damage was detectable in the structure by comparing natural frequencies for the undamaged and damaged bridge.

Maeck et al. [54] investigated the ability to detect damage in a prestressed concrete bridge through vibration monitoring. The presented techniques are based on changes in eigenfrequencies and mode shapes of the structure. The calculation of bending moments and curvatures were used to derive the bending stiffness at each critical location of the bridge. The underlying assumption was that decreases in structural stiffness are indicative of damage. The approach was tested on the Z24 bridge in Switzerland - a three-span prestressed concrete bridge. A series of damage scenarios were inflicted into the bridge, and the dynamic properties of the bridge were monitored. Results from the research reported that high modes of vibration gave bad damage indication results due to numerical inaccuracies with the modes. It was anticipated that curvatures would have given better damage indication results.

Another vibration-based study was illustrated by Zhao and DeWolf [55] in an attempt to use SHM to identify restrained bearings in cold weather for a two-span, welded steel plate girder bridge. The system measured ambient traffic vibrations with accelerometers and used the results to compare the potential of three approaches to identify damage: (1) natural frequencies, (2) mode shapes, and (3) modified modal flexibility. When the bearings were restrained, testing results revealed identifiable changes in natural frequencies. Changes in modal displacements, however, were not good indicators of damage. The modal flexibility method presented in the research was reported to most clearly identify structural damage.

Khalil et al. [56, 57] investigated the use of modal testing that utilized ambient excitation to detect, locate, and determine the measurable size of defects in steel plate girder bridges. Three-dimensional FEA was used in the preliminary analysis to study the modal behavior of a three-span steel girder bridge; in-service vibration testing was then performed on the undamaged and pseudo-damaged bridge. Results of the study concluded that mode shape changes are more sensitive to localized damage and frequency shifts, but both mode shapes and frequencies of vibrations are

www.manaraa.com

capable of detecting major (global) damage to the bridge. In addition, it was found that frequencies of vibration were influenced by temperature; frequencies decreased with temperature increase.

Several additional projects and SHM approaches are discussed in literature reviews by Hoon et al. [43], Doebling et al. [41], and Farrar et al. [58].

2.3.3 Structural Health Monitoring of Bridges with Fiber Optic Technology

As previously mentioned, FOSs are available as accelerometers, strain gages, tilt meters, displacement transducers, temperature sensors, load cells, etc., and as a result, have been incorporated into many SHM systems. Examples of bridges and bridge components requiring performance monitoring that include FOS are as follows:

- Performance/condition evaluation of an important structure
- Arson prevention in historic structures
- Prestressing losses in tendons
- Stay-cable forces in bridges
- Immediate and long-term performance of a retrofit
- Performance of a new material in a structure
- Pavement management

Further description of each monitoring approach is described in the following paragraphs.

Some of the earliest uses of fiber optic sensors are illustrated by Tennyson et al. [59] and Maalej et al. [60]. Six bridges in Canada were instrumented with FBGs for a variety of monitoring applications. The Beddington Trail, Taylor, and Joffre Bridges were primarily instrumented with FOSs to evaluate the immediate and long-term performance of GFRP and carbon fiber reinforced polymer (CFRP) as prestressing tendons, as well as flexural and shear reinforcement. The Crowchild Trail Bridge and Salmon River Bridge were the first bridges to be constructed with steel-free decks. Transverse steel straps across the tops of the girders provide transverse confinement to the deck. Strain gages consisting of foil resistance gages, FBGs, and Fabry-Perot sensors were installed on the girders, transverse steel straps, and in the deck to monitor the performance of the new designs. Finally, the Confederation Bridge, which is the longest bridge over iced-ocean water, was

www.manaraa.com

instrumented with FBGs to monitor its loadings and structural performance to ensure that it is maintaining adequate strength in the harsh environment. For nearly every bridge, temperature sensors were installed to help temperature-compensate the FOS.

Doornink et al. [61], Graver et al. [62], as well as Phares and LaViolette [63] describe the use of FBG sensors to monitor the performance of new materials. A high-performance steel (HPS) bridge was continuously monitored with 40 FBG sensors to determine its structural response to ambient traffic traversing the bridge. In addition, the performance of a prestressed, UHPC beam was laboratory tested to verify its shear and flexural properties to aid the design of the first UHPC bridge in the USA.

Seim et al. [64] used fiber bragg grating sensors to monitor the retrofit of the historic Horsetail Falls Bridge. The bridge was retrofitted with fiber reinforced plastic composite (FRPC) to increase its load-carrying capacity. The structure was instrumented with FBGs to monitor the performance of the retrofit additions as well as the existing concrete structure.

Doornink et al. [65] as well as Phares and LaViolette [62] demonstrate the use of FBGs to help guard a historic covered bridge in Madison County, IA from arson. The FBGs installed on the bridge measure the temperature of the wood to detect fire. Flame detectors and infrared cameras were also installed in conjunction with the FBGs. When the components of the SHM system agree to the presence of fire, authorities are autonomously alerted.

Huang et al. [66] discuss the use of multimode FOSs to aid in the selection of the pavement structure for the Humen Bridge in China. A test structure was constructed in the form of a ring and consisted of each type of pavement being considered for use in the bridge. Multimode fibers were installed in each of the pavement samples, and the interference and coupling of the different modes propagating down the fiber were monitored. The samples were subjected to wheel loads for three months, and when the fiber was vibrated, the intensity and phase of each mode was modulated and used to measure changes in pavement frequencies. The changes in natural frequencies of the pavements were compared over time to determine the pavement type with the longest lifetime.

www.manaraa.com

Wang and Tang [67] described a new sensor that simultaneously measures strain and temperature with FBG technology within the pavements. The reliability and long-term stability of the sensor was tested in both concrete and asphalt specimens. Results indicated that the performance of the sensor was comparable to that of the conventional thermocouple, and that its long-term stability was four times better than a long period grating (LPG).

Idriss et al. [68] illustrated the use of FBGs to measure strain on a full scale laboratory bridge. The single-span steel girder bridge had a concrete deck and was instrumented with 48 FBGs and 48 electrical resistance sensors installed on the steel girders and embedded in the concrete deck. Damaged was introduced at midspan of an exterior girder with a series of torch cuts, and the redistribution of the structure dead load was measured by the FBGs and identified damage to the structure. Davis et al. [69] conducted vibration-based testing on the same bridge and instrumentation. Dynamic measurements were taken with the same FBG array for the damaged and undamaged bridge. A noticeable difference in the modal behavior of the damaged and undamaged bridge was identified.

Yong et al. [70] presented a fiber optic SHM system for the monitoring of the Dafosi Bridge, the largest cable-stayed bridge across the Yangtze River in western China. The system monitors fiber optic strains sensors, displacement sensors, temperature sensors, and dynamic measurements to evaluate the structural condition of the bridge. Evaluation of data includes on-site preprocessing before it is sent to a host computer at a management center for further evaluation.

The selected projects presented in this section are a small sample of the SHM systems that use or have used fiber optic technology. As can be seen, the functions of the technology among the systems are quite different. Note that for nearly all of the systems that utilized FBG strain sensors in the field environment, temperature sensors were included in the system to compensate the measurements of the FBGs. This was often performed because long-term events were being recorded and temperature fluctuations occurred during the event, such as measuring the long-term prestressing loss in a tendon. Moreover, temperature compensation was required when the total state of mechanical and thermal stress in the bridge was desired. Once again, this long-term event

www.manaraa.com

inflicted temperature-induced strains into the structure, and thus, FBG measurement error due to temperature fluctuations was also present. Thus, the strain results were temperature compensated to remove the apparent thermal strain from the results. Finally, temperature compensation was necessary for systems that required a zero baseline prior to measurement in order to determine dead load redistribution or FRP delaminations in a structure. In this case, the systems removed all thermal effects (from FBG and the host material) from the data in order to determine if the system returned to a zero baseline after each event. Regardless of how the data were used, the projects presented in this section clearly illustrate the versatility and widespread use of FOSs.

2.3.4 Feature Discrimination in Structural Health Monitoring for Damage Detection

Feature (or parameter) discrimination has received the least amount of attention in literature. Feature discrimination often incorporates some kind of statistical methods to operate on the extracted features or parameters to determine the extent of the damage. As previously mentioned, statistical-based feature discrimination algorithms utilize either supervised or unsupervised learning. Examples of supervised learning in literature include response surface analysis, Fisher's Discriminant, neural networks, genetic algorithms, and support vector machines; examples of unsupervised learning include control chart analysis, outlier detection, neural networks, and hypothesis testing. Neural networks are perhaps the most popular of all algorithms, while control chart analyses are less commonly used [43].

Artificial neural networks are essentially crude mathematical models based on the structure of the human brain. They have simple processing units that store knowledge and make it available for future use, and the knowledge is acquired through a learning process that utilizes sets of known features and parameters for a particular condition. In addition, an ANN may utilize supervised training or unsupervised training, depending on if data from the damaged structure (usually obtained through use of a model) is available. Thus, the accuracy and abilities of the ANN depend on the quality of data available for learning. Many types of ANNs exist: perceptron networks, linear networks, multilayer feed-forward networks, radial-based networks, probabilistic networks, competitive networks, and self-organized maps. Out of all types, the multilayer feed-forward network

www.manaraa.com

is listed in the literature as the most common for data compression, data segmentation, and pattern recognition. In addition, their capacity for recognizing linear or nonlinear problems coupled with robustness to environmental noise make ANNs an ideal choice for crack detection [49].

As previously mentioned, Kesavan et al. [43] utilized a multilayer feed-forward, error back propagation network to determine delaminations in a composite beam using static strain results. Also previously presented was the research by Studer and Peters [38] that introduced the use of integral strain, strain, and strain gradient collected by FOSs in a back-propagation network to determine cracks in structural volumes. Both projects illustrate the ability to determine the severity or size of damage, and thus, require some type of supervised training.

Furthermore, Liu and Sun [71] investigate the use of bridge elongation curves in neural networks to detect localized damage in a three-span bridge. The authors assume that these curves could be calculated from strain gage measurements. Five separate ANNs work in parallel to reduce the training of the system while still providing accurate damage assessment. The ANNs presented in this research also utilize supervised training with data for damage cases generated from FEA.

Control chart analyses have been heavily utilized for process controls of chemical plants, manufacturing facilities, and nuclear power plants [43], but have been utilized far less in SHM of bridges. Control charts are one of the primary techniques of statistical process control (SPC). The concept recognizes that every process has variation. Some of the variation in the process is unavoidable, always present, and inherent to the process. This type of variation is referred to as unassignable cause, common cause, or chance cause. Other types of variation not always present, can be avoided with proper investigation, and are not normal to the process; this type of variation is termed assignable cause or special cause [72, 73].

To develop a control chart, information pertaining to a process characteristic, or parameter, is monitored and plotted versus time or sample number. A centerline (average expected values), upper control limit (UCL), and lower control limit (LCL) is developed to identify typical process behavior, which includes common cause variations. Each limit is typically established three standard deviations from the centerline, and thus, will statistically include 99.7% of all data points for the parameter if it is

www.manaraa.com

a normalized set. The area bounded by the limits is defined as the control region, which is applied to future parameter values for identifying new data (outliers) that are inconsistent with past data [72, 73].

Common types of control charts include univariate, regression, and multivariate. To monitor a process with one independent parameter, a univariate control chart is developed (Fig. 2.1). Several types of univariate control charts are available that utilize different approaches to establishing the UCL and LCL: Shewhart (X-bar and R-charts), Cumulative Sum (CUSUM), and Exponentially Weighted Moving Average (EWMA). In addition, each one has different sensitivity to process changes [72, 73].

If the process requires monitoring of one dependent parameter, a regression control chart is used, which plots the dependent versus independent parameters on a chart (Fig. 2.2). There is an assumed linear relationship between the dependent and independent parameters, and thus, the UCL and LCL are also assumed to be linear [74].

To monitor a process with two or more independent parameters, a multivariate control chart is used. Such a chart is easily explained by considering two parameters that are being monitored in a process (bivariate data). To monitor both variables simultaneously, the univariate control chart for each parameter is developed, and results from both control charts are superimposed onto one scatter plot. Corresponding times or samples between the two parameters are matched to form one data point (See Fig. 2.3). Note that in Fig. 2.3, a more accurate control region for the bivariate control chart is achieved by using an elliptical control region, rather than the rectangle defined by the UCL and LCL from the univariate analyses. The ellipses and regions identified in Fig. 2.3 represent

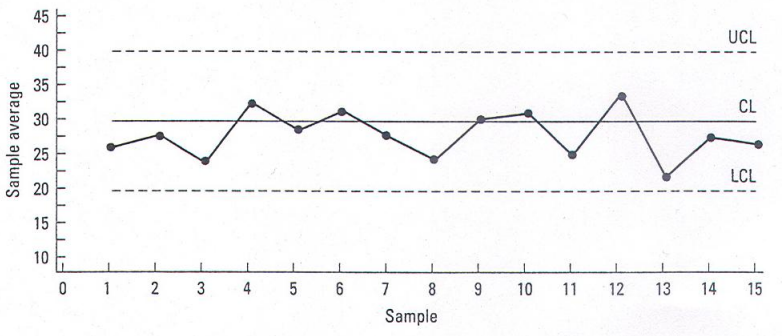

Figure 2.1. Example of a univariate control chart [73].

www.manaraa.com

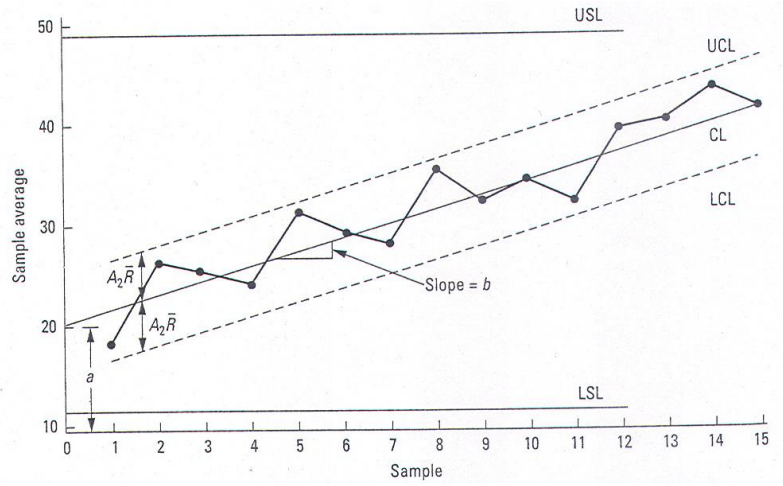

Figure 2.2. Example of a regression control chart [73].

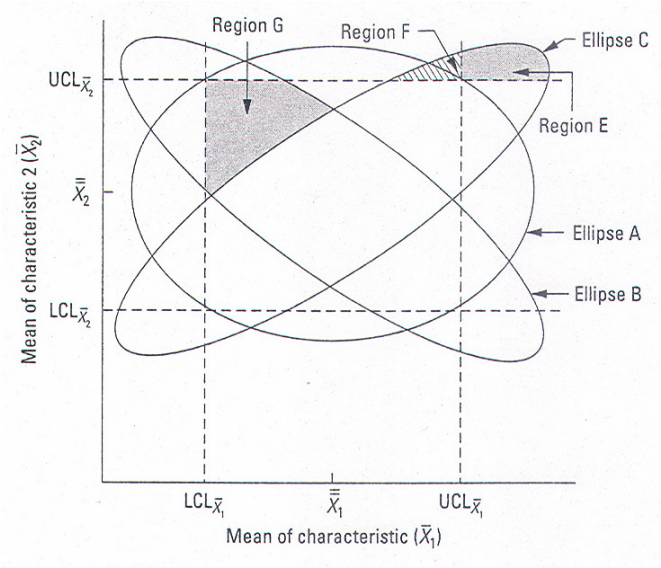

Figure 2.3. Superimposed univariate control charts with elliptical control regions [73].

the following [73]:

- Ellipse A: Control region for parameters that are not correlated.
- Ellipse B: Control region for parameters that are negatively correlated.
- Ellipse C: Control region for parameters that are positively correlated.
- Region E and Region F: Additional areas to the control region that results from using an elliptical control region rather than rectangular region.

www.manaraa.com

- Region G: Area removed from the control region due to an elliptical control region rather than a rectangular control region.

Most processes are multivariate, and thus, require multivariate SPC. The actual dimension of the multivariate control chart is equal to the number of independent process characteristics, or parameters, included in the chart. Thus, for any chart including more than two parameters, the analysis becomes complex and difficult or impossible to display in its true dimension. For this situation, methods are used to calculate a new term, which is a function of all parameters, and associated limits that can be displayed in a format similar to a univariate control chart. Such multivariate control charts include the following: Hotelling T^2, Chi-square, Multivariate Cumulative Sum (MCUSUM), and Multivariate Exponentially Weighted Moving Average (MEWMA).

Very few damage detection algorithms have utilized control chart analyses for SHM of bridge structures. Hoon et al. [75] applied X-bar control charts to accelerometer measurements on a damaged, reinforced concrete bridge column. A series of quasi-static cyclic tests were performed on the column to create progressive damage, and at intermittent stages during the testing, vibration tests were performed. For each accelerometer, a univariate control chart was developed at each level of damage, and as the damage progressed in the column, the number of outliers in the control chart also increased. Thus, the ability of the univariate control chart analysis to detect damage was proven.

In a follow-up study on the previously mentioned Z24 Bridge SHM project [54] that investigated vibration monitoring to detect structural damage, Kullaa [76] investigated the use of the Z24 Bridge natural frequencies, mode shapes, and damping ratios in univariate and multivariate control chart analyses. Conclusions of the research indicated that natural frequencies and mode shapes were good indicators of damage with the control chart analyses, but damping ratios were too inaccurate and insensitive for damage detection. In addition, it was noted that the multivariate control charts were more reliable than the univariate control charts in the undamaged case, but univariate control charts were able to observe smaller levels of damage than multivariate control charts. However, both univariate and multivariate control charts recognized high levels of damage in the bridge.

www.manaraa.com

Control chart analyses of SPC have illustrated their abilities to monitor processes in chemical plants and manufacturing industries for decades, and in a few projects, have been introduced as successful damage detection algorithms for bridge SHM. By using control regions and outlier analyses, the process is relatively simple to implement in to SHM systems. For detailed descriptions of other statistical-based feature discrimination methods, refer to the literature review of Sohn et al. [43].

2.4 Current Challenges and Criticisms of Structural Health Monitoring

Structural health monitoring has been a subject of major international research for over a decade, and significant progress has been achieved to develop new sensors and systems that are capable of monitoring the performance of a structure and to detect damage. However, numerous items are still identified in the literature as major obstacles that hinder the further advancement of SHM and require improvement [20]:

- Standardized approaches and consistent diagnostic methods
- Reliable and efficient data mining and knowledge discovery
- Data management and storage
- Presentation of useful and reliable information to bridge owners/managers for decision making on maintenance and management

One very big criticism is that academic goals are often very different than the needs of the infrastructure owners, and thus, there is a big disconnect between the SHM systems that are developed and the number that are actually implemented by agencies. As a result, this disconnect has impeded bridge owners/managers from benefiting from SHM systems. In addition, other literature notes that there has been a large bias toward the use of dynamic response data for bridge SHM, and thus, many bridge research projects have a very narrow focus. The literature states that strain measurement is essential for bridge health assessment, and thus, should be included more often [77]. Most literature, however, acknowledges that even though SHM techniques have not been perfected, the bridge community has benefited from the knowledge of bridge performance obtained from the SHM systems.

www.manaraa.com

2.5 Other Miscellaneous Topics Requiring Review

The discussion prior to this section has focused on the status of SHM and damage detection for both laboratory and field applications. However, successful monitoring is dependent on the ability to accurately collect and prepare data prior to its discrimination. Thus, two additional topics have been addressed in this section: adhesives for long-term SHM and data filtering methods.

2.5.1 Sensor Adhesives for Long-Term Structural Health Monitoring

The demands on adhesives for long-term SHM are far greater that those for typical applications. For an adhesive to be adequate for field installation and use in SHM, it must meet several requirements:

- It must have a short fixture (working) time.
- It must have superior bond to the sensor packaging and host material.
- It must be capable of maintaining its strength in the midst of long-term environmental exposure.

The group of adhesives that satisfies these specifications is referred to as structural adhesives. Structural adhesives maintain high tensile strength as well as toughness and flexibility to resist peel and impact in extreme service environments. The most common classifications of structural adhesives include polyurethanes, acrylics, toughened acrylics, epoxide adhesives, and toughened epoxide adhesives. Among these classifications, acrylics are characterized as having very rapid cure and are divided in two main categories: (1) cyanoacrylates and (2) acrylates and methacrylates. Table 2.1 presents the comparative benefits of industrial structural adhesives. As can be seen, structural acrylics achieve the best combination of fixture time, bond strength, and environmental resistance [78, 79, 80]. One large concern with adhesives is shear lag, the result of shear deformation on an adhesive layer [78]. With strain gages, this usually results in lower strain measurements than those that actually exist in the substrate. Shear lag can be minimized by reducing the thickness of the bond layer between the strain gage and the host material.

An even bigger concern with strain sensing is adhesive viscoelastic behavior, or viscoelasticity. Viscoelasticity is a phenomenon that causes stress relaxation in adhesives and is composed of two components: elastic behavior and viscous behavior. The elastic component is

www.manaraa.com

Table 2.1. Relative comparison of structural adhesives [78].

	Structural acrylic	Structural polyurethanes (with primers)	Structural epoxides	
			Two-part mixed	One-part heat cure
Bond Strength				
Metals/ferrites	++	+	+	++
Metals/plastics	++	+	0	-
Toughness	++	+	+	+
Impact resistance	+	++	+	0
Temperature/humidity	+	-	+	++
Speed of bonding	++	-	0	-
Ease of cure				
Automatic application	++	-	-	++

Note: ++ great benefit, + significant benefit, 0 no benefit, - significant disadvantage.

instantaneous, rate-independent deformation that occurs immediately upon application or release of stress, and the deformation is completely recoverable. The viscous component of viscoelasticity is not instant; the viscous deformation is dependent on time and is not completely recoverable. Two common static methods for measuring viscoelastic characteristics of an adhesive include measurement of the following:

- Creep: the time-dependent deformation of a polymer sample under constant load [78].
- Stress relaxation: the time-dependent load required to maintain a polymer sample at a constant extent of deformation [78].

The results from each test are expressed as either a creep modulus or a relaxation modulus [81]. Some of the most common factors affecting viscoelasticity, and thus, the performance of an adhesive include the initial magnitude of loading, loading and unloading rate, time duration of the sustained load, time duration of the released load, and adhesive temperature [78, 79, 80, 81].

The effects of viscoelasticity in adhesives have been addressed in literature. Takiguchi et al. [82] investigated the rate-dependent deformation behavior and stress relaxation of an acrylic adhesive. Tensile lap shear tests were performed at various ramping speeds at room temperature, and it was determined that increasing the shearing speed resulted in higher shear stresses. In addition, stress relaxation results were performed to verify viscoelastic behavior in the acrylic

www.manaraa.com

adhesive. Results from the test illustrated typical viscoelastic behavior with rapid stress decrease at the beginning of the test, which eventually slowed to become a constant stress value.

Gunawan et al. [83] investigated the stress relaxation of adhesives over time, rather than just for one loading. Static and cyclic relaxation tests were performed on adhesives, and results illustrated that the rate of relaxation is slower under cyclic loading than that in static loading for the same displacement amplitude. In addition, it was proven that the rate of relaxation of adhesives increases with increasing hold time and with decreasing ramp time and no-load time.

Finally, Chernenkoff [84] investigated the effects of temperature/humidity exposure on the cyclic-creep behavior of adhesives. Three adhesives, a toughened epoxy, a vinyl/epoxy, and an epoxy/acrylic were studied in an ambient condition and after being exposed to a new temperature/humidity environment. Results showed that environmental exposure can increase the creep rate by as much as 80% in an adhesive.

2.5.2 Data Collection and Filtering for Long-Term Structural Health Monitoring

One must ensure that an appropriate sampling frequency, or data acquisition rate (DAR), is selected such that the recorded signal accurately portrays the original event, and in addition, to ensure that filtering processes do not incorrectly alter the recorded event. Two general rules usually govern the sampling frequency for bridge monitoring [85, 86]:

1. The sampling frequency must be at least two times the maximum frequency within the measured record. This avoids aliasing effects and is known as the Nyquist criterion.
2. For peak value determination, the sampling frequency should be at least 10-20 times the maximum frequency within the measured record. This ensures that all peak values within the record can be obtained.

By applying a digital filter to a data set, the frequency content of the record is altered. Four common types of filters are available depending on the desired frequency alteration in the data:

- Lowpass: Passes low frequencies and blocks high frequencies
- Highpass: Passes high frequencies and blocks low frequencies
- Bandpass: Passes a certain band of frequencies
- Bandstop: Blocks a certain band of frequencies

www.manaraa.com

In addition, filter operations are also governed by their impulse response. The output from Finite Impulse Response (FIR) filters, also known as moving average (MA) filters, depends on current and past input values to filter data. Common FIR filters utilize windowing techniques or the Parks-McClellan algorithm. Windowing is the fastest technique, but the disadvantage is that it truncates data. The Park-McClellan algorithm has optimal performance, but it requires significant computational resources [86, 87].

The output from Infinite Impulse Response (IIR) filters, also known as autoregressive moving average (ARMA) filters, depends on current and past input values, as well as current and past output values. Common types of IIR filters include: Butterworth, Chebyshev, Chebyshev (Type II), Elliptical, and Bessel. In relative comparison, results from Butterworth and Bessel filters have lower error in frequency, but higher error with peak detection than Chebyshev and Elliptical filters. In contrast, Chebyshev and Elliptical filters have higher error frequency, but lower error with peak detection [86, 87].

In general, it is recommended that IIR filters be used for applications that do not require phase information, such as signal monitoring applications, and FIR filter be used when phase information is required [86].

2.6 Conclusions from Literature Review

The dominant SHM approach for damage detection in bridges has been vibration-based monitoring, which utilizes changes in frequencies, mode shapes, and mode shape derivatives to identify damage in a structure. For those that have utilized strain measurements to detect damage in bridges, they have not utilized the approach described in Section 1.3 that utilizes unsupervised learning methods to establish relationships between sensors to account for the unknown characteristics of the ambient traffic. In addition, no systems were identified that used methods similar to control chart analyses, or more specifically bivariate control charts, for parameter discrimination with strain-based SHM systems for bridges. Moreover, most projects that incorporate FBG sensors, such as those in this research, temperature-compensate the data before it is used.

www.manaraa.com

3. SHM TECHNOLOGY EXAMINATION AND SELECTION

During the design of a SHM system, the measured parameters for assessing the condition of the structure must first be determined, and then the hardware components can be selected to perform the measurement and to function with other system components. The proceeding sections of this chapter discuss this process for the US30 bridge by addressing the following topics:

- Selection of strain as the measured parameter
- Conceptual identification of equipment specifications and data reduction methods
- Laboratory examination and validation of data reduction methods and equipment performances
- Selection of equipment for use in the FCB SHM system

3.1 Parameter Selection for Discrimination and Damage Detection

As previously mentioned, strain was selected as the parameter for discrimination and damage detection. Selection of this parameter was based on (1) ease of its measurement and collection while ambient traffic crosses the bridge and (2) flexibility in the formats that can be used to present the results to bridge owners. With these considerations, the SHM system was designed to measure and analyze a reliable parameter while maintaining usefulness and attractiveness to bridge engineers.

As mentioned in Chapter 2, two primary parameters have been researched and investigated for use in SHM systems for damage detection: vibrations and strains. Vibrations have been utilized more frequently than strains in previous research. One attractive feature of vibration-based monitoring that has contributed to its popularity is that the dynamic properties of a bridge are generally not affected by the magnitude of the events (weight of traffic). This eliminates an unknown involved in any monitoring that utilizes ambient traffic loads. However, most literature discussing results from these SHM systems agrees that there are notable limitations of using vibration-based measurements and dynamic properties for bridge damage detection [41, 43, 58]:

- Modal properties are estimated from a measured response, and thus, error within the estimation and data lost during this compression process potentially lead to inaccurate or misleading results.

www.manaraa.com

- Damage is a local phenomenon that is most likely only captured with higher frequencies of vibration. However, it is difficult to extract accurate information from higher frequencies due to greater modal density and coupling between modes. In addition, ambient traffic rarely produces the required excitation for higher frequencies.

- Variation in excitation or environmental conditions can cause changes in the dynamic properties that are large enough to mask changes due to damage formation.

Because of these reasons, vibration-based monitoring was rejected from use in the FCB SHM system.

The FCB SHM system utilizes FBG sensors to achieve strain-based monitoring. The attractive characteristics for this type of system are as follows:

- Strain measurements from ambient traffic loads are dependent on the magnitude of the event, which results in a large and diverse population of measurements.

- Assuming elastic bridge behavior, strain measurements are repeatable for similar events, a condition that supports pattern recognition as a possible analysis technique.

- Appropriate analysis of strain measurements can reveal both static and dynamic properties.

- A bridge's static response to ambient traffic loads is affected very little, if at all, by environmental factors.

- Measurements can be used directly in calculations without being converted into another parameter.

- Bridge engineers are typically more familiar with strain measurements than any other measurement metric.

In addition, the use of FBGs incorporates all of the favorable characteristics discussed in Section 2.2.2 such as sensor stability and longevity.

An unfavorable characteristic of FBG sensors, as previously mentioned, is that they are sensitive to temperature variations. Thus, for any event occurring simultaneously with temperature fluctuations, FBG sensors measure the thermal and mechanical strain of the host material as well as an apparent strain resulting from temperature effects on the sensor itself. Compensation for this issue was avoided in the FCB SHM system by utilizing only mechanical strain measurements resulting from vehicles traversing the bridge. These events occur too quickly for temperature variation to simultaneously occur.

The dependency of strain on magnitude of loading was previously considered to be favorable because it creates a large population of events for evaluation, but it also creates difficulties since the

www.manaraa.com

weights of the ambient traffic events are not known. This challenge, however, was overcome in the FCB SHM system by using relative relationships among the sensors on the bridge, rather than an analysis that utilizes independent measurements from each sensor. The SHM data reduction techniques will be discussed in further detail in Chapter 5.

3.2 Conceptual Equipment Specifications

Equipment specifications must be considered for both the data acquisition equipment and strain sensors together to ensure proper system operation. For fiber optic sensing, the interrogator performs the data acquisition and must be capable of sampling at adequate rates for the event being recorded. As discussed in Section 2.5.2, a DAR of 10-20 times the maximum frequency in the strain record is sufficient to avoid filter aliasing effects and to accurately determine peak strain values within the record. Strain records for measured bridge responses typically include both quasi-static and dynamic frequencies from traffic events; fundamental frequencies for highway bridges are usually within 2-5 Hz [88], and quasi-static frequencies are often slower than the dynamic frequencies. Thus, to capture quasi-static events and the fundamental dynamic responses of most typical highway bridges, a DAR of 50-100 Hz is adequate. The Micron Optics si425-500 interrogator has sampling capabilities as high as 250 Hz, and thus, was determined to be adequate for use in the FCB SHM system. To fully capture each traffic event, a DAR equal to 125 Hz was chosen for the FCB SHM system.

Sensor specifications were investigated to ensure accurate measurements. As presented in Section 2.2.2, the conversion of FBG reflected spectrums to strains requires an understanding of the strain field being imposed on the FBG. Standard FBGs with 10mm lengths are sufficient in relatively uniform strain fields, but shorter FBGs are required in nonuniform strain fields. As a result, locations for strain measurements in the FCBs were identified, and the corresponding structural responses were considered to determine sensors specifications. Keeping in mind that large and repeatable strain measurements are most the most dependable strains within a record, and thus desirable for use in SHM, five different sensor orientations and locations were identified:

- Vertical orientation: cut-back regions of the retrofits and stringer webs above floor beams

www.manaraa.com

- Horizontal orientation: bottom flanges of girders, stringers, and floor beams

Horizontal strains on bottom flanges of structural members develop from global bridge responses, and thus, those regions were assumed to have uniform strain fields that were measurable with FBGs having 10mm lengths. However, vertical strains in the retrofit cut-back regions and stringer webs above floor beams measure local bridge responses. A uniform strain field was assumed for the local vertical response of the stringer webs, and thus, 10mm FBGs were again considered to be suitable. However, the reverse curvature condition in the retrofit cut-back regions was considered to create a nonuniform strain field that required shorter FBG lengths. Thus, 5mm FBGs were selected to measure strains in the retrofit cut-back regions.

Previous bridge research involving FBG sensors at ISU [3] utilized surface-mountable sensors (SMSs) that were manufactured by Avensys, Inc. A photograph of a 210x20mm SMS is given in Fig. 3.1. Each SMS consists of a 10mm FBG with polyimide recoating that was embedded within a 210x20x1mm (length x width x thickness) CFRP packaging. The CFRP packaging protected the sensor and made it more robust for installation purposes, and at the same time, increased its bonding surface area. The fiber pigtails exiting from each side of the packaging (entry fiber and exit fiber) consist of SMF simplex cable (3mm jacketing) and FC/APC mechanical connectors. To bond the 210x20mm SMS to the bridge, Loctite 392 adhesive with Loctite 7387 activator were used. The field installation and performance of this sensor was proven in the previous research, and as a result,

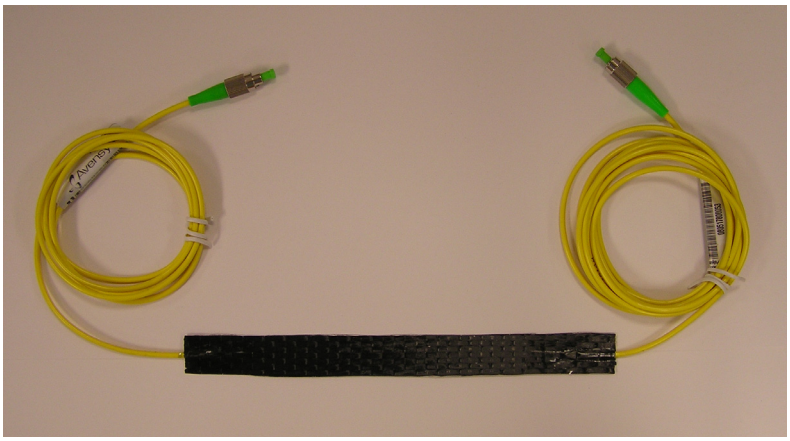

Figure 3.1. The 210x20mm SMS used for sensing in uniform strain fields.

www.manaraa.com

was selected as the sensor for use in all strain fields identified as suitable for measurement with a 10mm FBG.

For sensing in the retrofit cut-back regions, the size of the FBG and packaging of the 210x20mm SMS was determined to be unsuitable. It was desired to use 5mm FBGs to measure strains every 2 in. (55 mm) along the height of two cut-back regions, as well as at the top and bottom of other cut-back regions. To achieve this sensing, two different types of SMSs were envisioned and designed: (1) a single 5mm FBG encased in a small form factor (SFF) CFRP packaging, and (2) an array of 5mm FBGs entirely encased in a single CFRP packaging. Once again, each FBG utilized polyimide recoating, but the SMF pigtails exiting from each side of the packaging had 900μm furcation tube for protection and did not have mechanical connectors.

As will be presented in Section 3.3, laboratory testing was performed to determine and/or validate the following:

- The data reduction methods developed to extract vehicular mechanical strains from the aggregate strain record of each sensor.
- The performance of the 210x20mm SMS sensor bonded to steel with Loctite 392 adhesive (Loctite 7387 activator).
- An appropriate size for the CFRP packaging and a suitable adhesive for use with the SFF SMS sensor.

The laboratory validation testing was performed to ensure that the interrogator, sensors, adhesives, and accessory equipment were capable of achieving the desired measurements and to reduce the likelihood of hardware deficiencies and malfunctions after field installation.

3.3 Laboratory Validation Testing

The laboratory validation testing included the following sensors, equipment, and materials:

- Traditional electrical resistance (foil) sensors, equipment, and materials
  - Data acquisition system: Megadac (Model 5108)
  - Sensors: TML FLA-6-11 sensors from Tokyo Sokki Kenkyujo Co., Ltd.
  - Adhesives: TML CN from Tokyo Sokki Kenkyujo Co., Ltd.
- FOSs, equipment, and materials
  - Interrogator: Micron Optics si425-500
  - Sensors: Avensys Strain Sense™ Surface Mountable FBG Sensor and unpackaged FBGs
  - Adhesives: 3M (4926, 4936, 4941, and 9500PC), Loctite (330, 392, 410, H3000, H3300, H4500), Plexus MA820, Pliogrip 7771

www.manaraa.com

- Test frame and equipment
  - MTS Fatigue Frame (Model 810)
  - Flextest GT Controller and MPT Software
- A-36 structural steel tensile coupons
  - Coupon A (Tests 1 and 2)
  - Coupon B (Tests 3, 4, 5, and 6)
  - Coupon C (Tests 7 and 8)

The adhesives selected for the research were based on manufacturers' recommendations for structural adhesives (See Section 2.5.1) with the following criteria:

1. Short fixture (working) time
2. Superior bond to both FRP and structural steel
3. Long-term durability in variable environments

While adhesives are listed for 3M, Loctite, Plexus, and Pliogrip, initial testing identified that the 3M products were inadequate for bonding the FOSs and steel. As a result, only the results for tests conducted with Loctite, Plexus, and Pliogrip adhesives are included in this report.

Eight laboratory tests were conducted with tensile coupons instrumented with both FOSs and foil sensors. For all tests, the foil sensor results were compared with theoretical calculations and proven to accurately represent the actual strain condition in the coupon, and thus, they are used as baselines for comparison with the FOS results. For each test described in the following sections, the following have been identified:

- Objectives of testing
- Testing procedure
- Sensors and adhesives being investigated
- Testing equipment and acquisition system settings
- Testing results
- Conclusions from testing

For FBG specifications for each type of tested FOS, refer to Appendix A; for adhesive specifications used in this research, refer to Appendix B.

www.manaraa.com

3.3.1 Coupon Test 1 (CT1)

3.3.1.1 CT1 Objectives and Testing Procedure

The objective of Coupon Test 1 (CT1) was to investigate the impact of the CFRP packaging on FOS performance. Tensile Coupon A with associated sensors and respective adhesives used in CT1 are presented in Fig. 3.2. As illustrated, CT1 FOSs included the following:

- One commercially-available 210x20mm SMS with CFRP packaging that was bonded to the coupon using Loctite 392 adhesive with Loctite 7387 activator.
- One custom-made 15x10mm SMS with CFRP packaging that was bonded to the coupon using Loctite 392 adhesive with Loctite 7387 activator.
- One unpackaged FBG with acrylate recoating that was bonded to the coupon using Loctite 410 adhesive with Loctite 7452 accelerator.

The 210x20mm SMS/Loctite 392 and unpackaged FBG/Loctite 410 combinations were selected because they have been previously field proven to perform accurately for controlled tests [3]. As a result of the FOSs utilized, CT1 allowed for direct comparison of results between packaged and unpackaged FOS to identify the effect of packaging on performance, and also for a comparison between different packaged FOS to reveal the effect of packaging size on performance.

To achieve the objectives of CT1, Coupon A was subjected to tensile cyclic loading producing amplitudes of approximately 450με and 900με for 950,000 cycles and 325,000 cycles (1,275,000 total cycles), respectively, at 4.0 Hz. During the testing, an si425-500 interrogator recorded FOS strains continuously at 250 Hz, and the Megadac recorded foil sensor strains at 250 Hz for five continuous seconds at the beginning of each hour of testing. Figure 3.3 presents a photograph of Coupon A in the MTS fatigue frame during CT1.

3.3.1.2 CT1 Results

Since only mechanical strains were being used for analysis in the laboratory testing and in the FCB SHM system, FOS wavelength shifts were converted to strains by using the traditional conversion factor for mechanical strains: 1.2 picometer (pm) change in wavelength = 1.0 με. Since temperature influences have been neglected in the conversion, the only accurate and useful portions of the strain files are the relative changes in strain due to mechanical loads that occur during constant temperature. Figure 3.4 presents a randomly selected portion of CT1 results to illustrate the data

www.manaraa.com

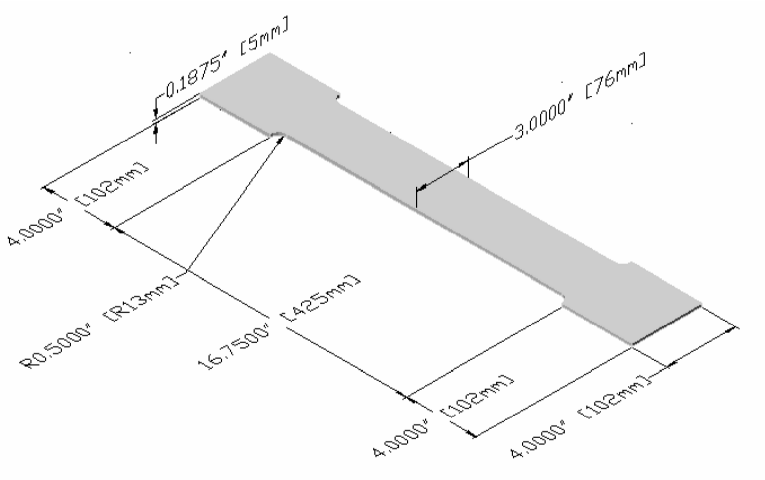

a. Coupon A

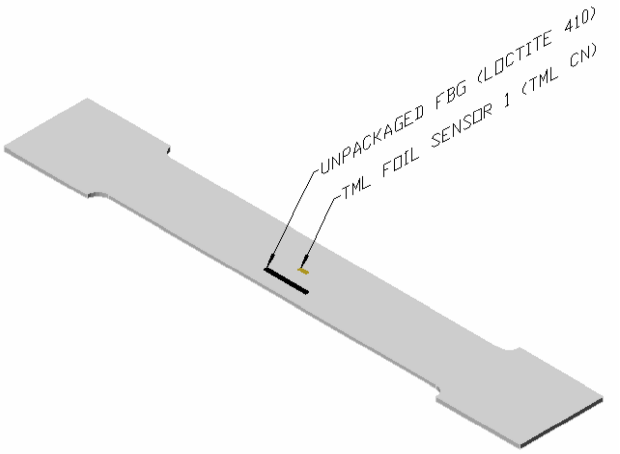

b. Coupon A: side 1 sensors and adhesives

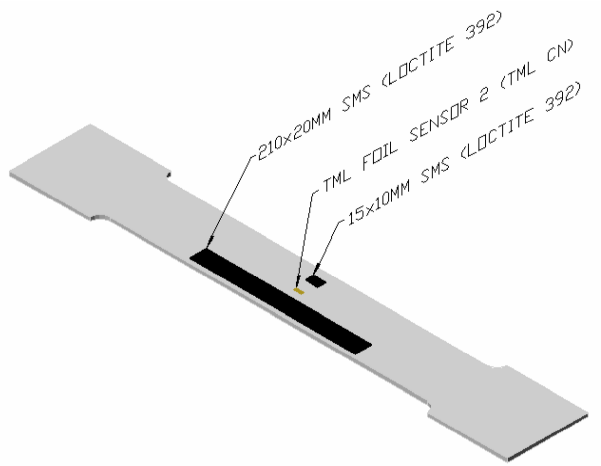

c. Coupon A: side 2 sensors and adhesives

Figure 3.2. Coupon A, sensors, and adhesives used in CT1.

www.manaraa.com

Figure 3.3. Photograph of Coupon A and testing frame used in CT1.

reduction process that extracts the cyclic mechanical strain from the aggregate strain results. For each sensor, the data reduction algorithm loaded the raw strain data file and identified the extrema for each cycle (Fig. 3.4a), plotted cycle extrema vs. cycle number (Fig. 3.4b), and finally calculated the cycle amplitudes (change in strain between cycle extrema) and plotted them vs. cycle number (Fig. 3.4c). Reduced CT1 results are presented in Figs. 3.5 - 3.8. In each figure, the FOS results are presented with the corresponding foil sensor results.

Examination of Figs. 3.5 and 3.6 reveals that the cycle extrema for the foil sensors remain nearly constant when compared with other cycles with the same magnitude of loading. This is not true for the FOS results; large deviations are present among the FOS cycle extrema when compared

www.manaraa.com

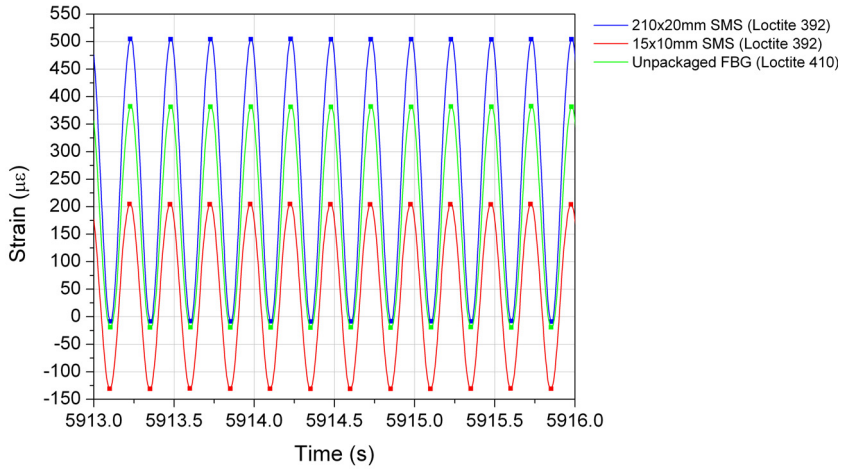

a. Raw data and identified cycle extrema

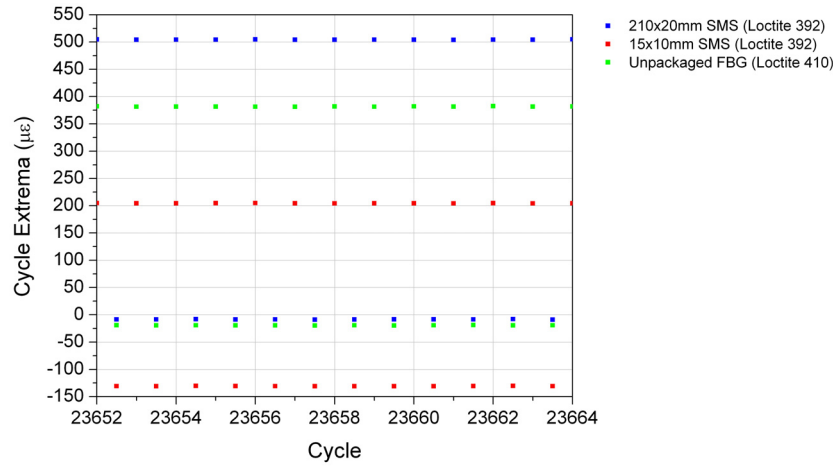

b. Plot of cycle extrema

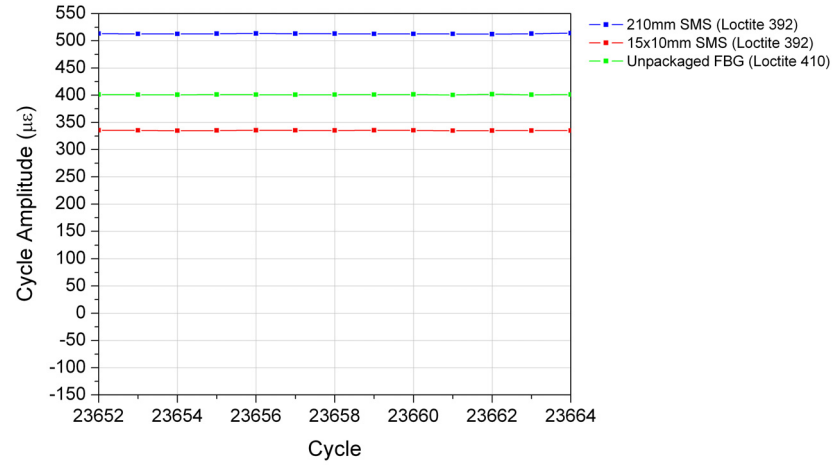

c. Calculation of cycle amplitudes

Figure 3.4. Example of data reduction process for all cyclic loading tests.

www.manaraa.com

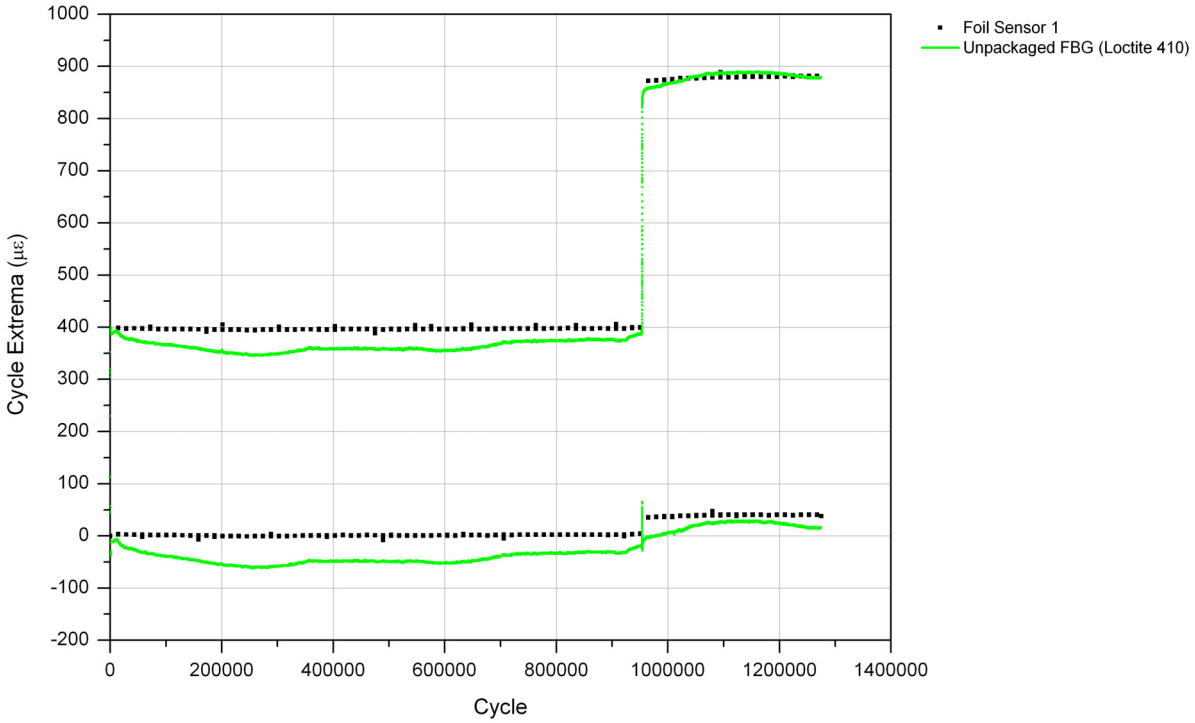

Figure 3.5. CT1: cycle extrema vs. cycle number for Coupon A, side 1 sensors.

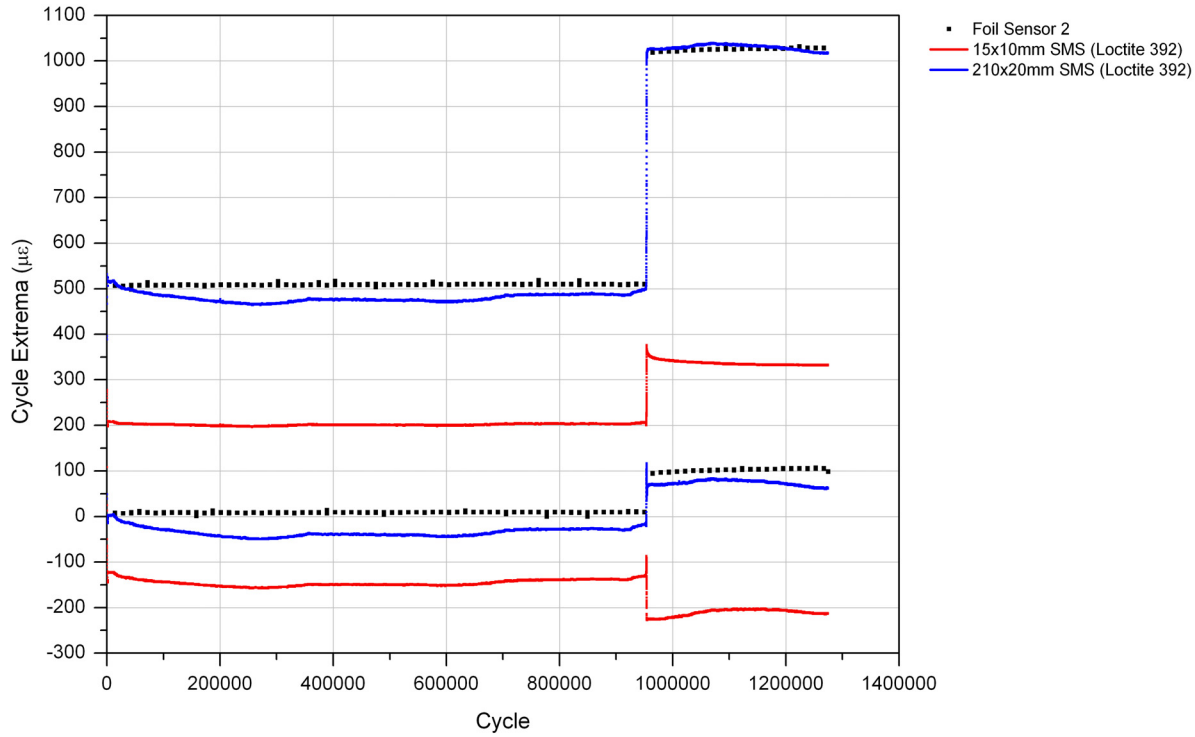

Figure 3.6. CT1: cycle extrema vs. cycle number for Coupon A, side 2 sensors.

www.manaraa.com

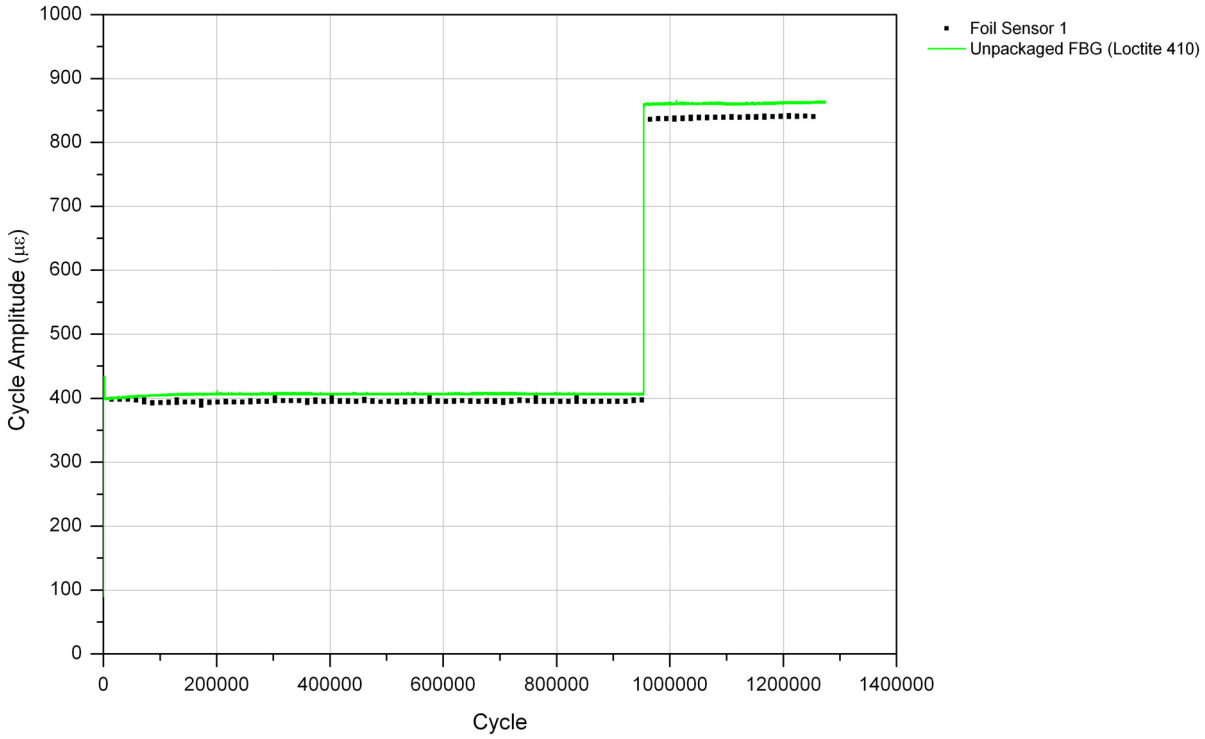

Figure 3.7. CT1: cycle amplitude vs. cycle number for Coupon A, side 1 sensors.

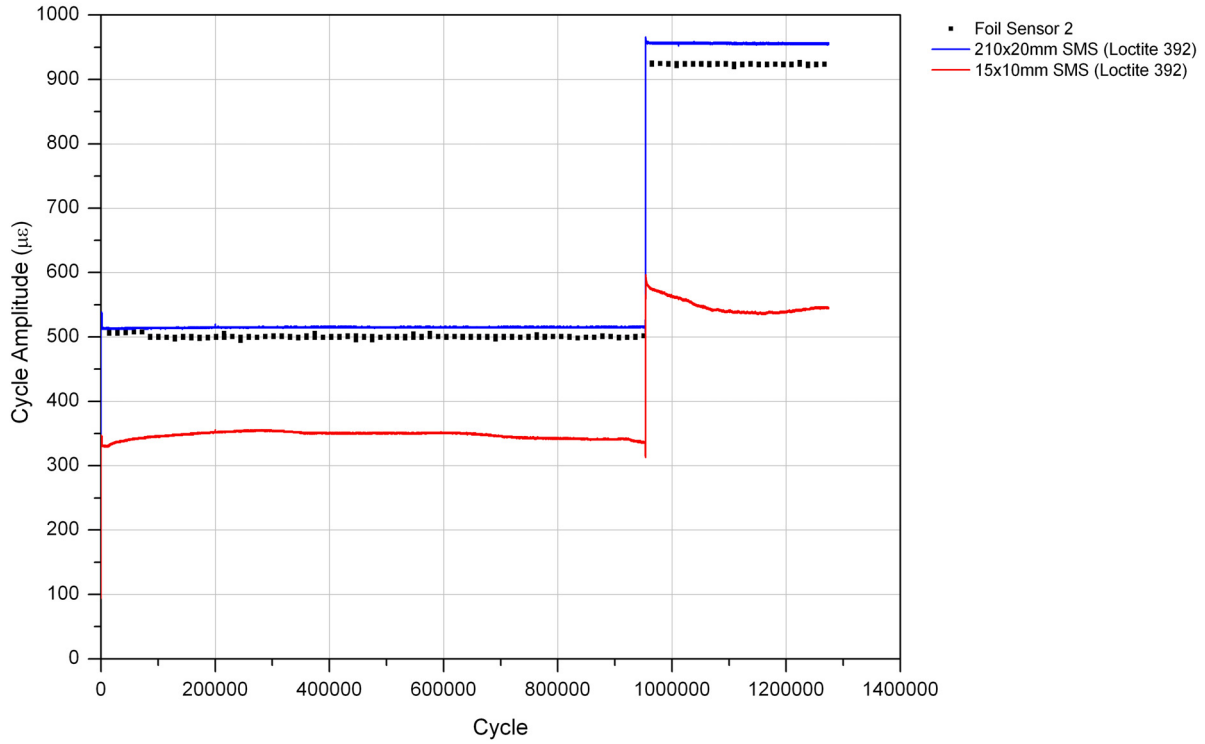

Figure 3.8. CT1: cycle amplitude vs. cycle number Coupon A, side 2 sensors.

www.manaraa.com

with other cycles with the same magnitude of loading. In addition, an unexpected residual strain was maintained in the Loctite 392 adhesive of the 15x10mm SMS for all cycles. Similarly, a temporary residual strain was evident at the onset of the 900με cyclic loading in the Loctite 410 adhesive of the unpackaged FBG and in the Loctite 392 adhesive of the 210x20mm SMS.

Figures 3.7 and 3.8 present the cycle amplitudes measured by each sensor. Investigation of these figures reveals that the 210x20mm SMS and the unpackaged FBG measured constant amplitude cycles that were in good agreement with the corresponding foil sensors. The 15x10mm SMS, however, did not measure constant amplitude cycles, and thus, was not in good agreement with the foil sensor. Thus, this sensor and adhesive combination was proven to perform unsatisfactorily. For all cycles of CT1 where FOS and foil sensor results were available, comparisons between the technologies were conducted. The foil sensor results were assumed to be the correct strain measurement for the testing, and thus, were used as the baseline for comparison. Error analysis results for CT1 are presented in Table 3.1.

The CT1 results presented in Figs. 3.5 - 3.8 are explainable when considering the differences between FOS and foil sensors. One major difference (other than the type of technology) is that the foil sensors were self-temperature-compensated (STC) for the temperature range 50°F - 176°F (10°C – 80°C), while the FOS had no STC. As a result, the foil sensors responded only to coupon mechanical strains while operating in the STC range, and the FOS responded to mechanical and temperature-induced strains at all temperatures. Examining Figs. 3.5 and 3.6, the deviations in cycle extrema for the 210x20mm SMS and the unpackaged FBG therefore likely represent temperature-

Table 3.1. Error analysis results for FOSs in CT1.

CT1 Loading	Sensor (Adhesive)	Error Statistics							
		Minimum		Maximum		Average		Standard Deviation	
		Strain (με)	%	Strain (με)	%	Strain (με)	%	Strain (με)	%
950,000 cycles @ 450με	Unpackaged FBG (Loctite 410)	1	0.3	18	4.6	11	2.8	2.3	0.57
	210x20mm SMS (Loctite 392)	5	1.0	21	4.3	15	2.9	2.3	0.46
	15x10mm SMS (Loctite 392)	140	28.3	176	34.8	153	30.6	6.1	1.15
325,000 cycles @ 900με	Unpackaged FBG (Loctite 410)	19	2.3	25	3.0	22	2.6	1.1	0.14
	210x20mm SMS (Loctite 392)	28	3.0	36	3.9	33	3.5	0.9	0.10
	15x10mm SMS (Loctite 392)	348	37.7	388	42.0	377	40.8	11.0	1.20

www.manaraa.com

induced strain in the steel, FBG, and adhesive that was only recorded by the FOSs; the sinusoidal data connecting the cycle extrema represents the mechanical strain subjected to the coupon, which was recorded by both the FOSs and foil sensors. Since the cycle amplitudes plotted in Figs. 3.7 and 3.8 represent the measured mechanical strain that was extracted from the aggregate strain file, the 210x20mm SMS and the unpackaged FBG data likely illustrate proper performance as they measured constant amplitude loading to the coupon during both segments of CT1. The poor performance of the 15x10 SMS is assumed to be the result of inadequate adhesive strength to fully develop the SFF CFRP packaging.

3.3.1.3 CT1 Conclusions

Considering the CT1 results, the following conclusions were determined:

- The third step in the data reduction process (Fig. 3.4c) adequately extracted mechanical strains from the aggregate record.
- With the small average errors presented in Table 3.1 for the unpackaged FBG with Locite 410 and the 210x20mm SMS with Loctite 392, both FOSs have been shown to be accurate for cyclic loading with up to 900με amplitudes.
- The large average error presented in Table 3.1 for the 15x10mm SMS illustrates very poor performance, and thus, this FOS is not considered to be an acceptable sensor for use with the Loctite 392 adhesive.
- The addition of the 210x20mm CFRP packaging had essentially no influence on FOS performance, but reducing the CFRP packaging to 15x10mm had a large impact on FOS performance.
- Further examination was required to determine the following:
  - The reason for the overall poor performance of the 15x10mm SMS.
  - The cause of the residual strain maintained in the Loctite 392 adhesive of the 15x10mm SMS for all cycles, and in addition, the temporary residual strain at the onset of the 900με cyclic loading in the Loctite 410 adhesive of the unpackaged FBG and in the Loctite 392 adhesive of the 210x20mm SMS.

3.3.2 Coupon Test 2 (CT2)

3.3.2.1 CT2 Objectives and Testing Procedure

The objectives of Coupon Test 2 (CT2) were to investigate (1) the impact of loading rate and magnitude on FOS performance, and (2) the performance of the 15x10mm SMS with a different adhesive. Tensile Coupon A and the sensors/adhesives used in CT1 (See Fig. 3.2) were used again

www.manaraa.com

in CT2. However, a 15x10mm SMS with Pliogrip 7771 adhesive was added to side 1 of Coupon A as illustrated in Fig. 3.9.

To achieve the objectives of CT2, Coupon A was subjected to tensile cyclic loading producing amplitudes of approximately 200με for 104,500 cycles at 1.0 Hz. Note, however, that the loading during CT2 gradually increased throughout the first 88,000 cycles, resulting in coupon strains increased by as much as 15με, but the load was corrected to produce approximately 200με in the coupon for the remaining 16,500 cycles. During the testing, a si425-500 interrogator recorded FOS strains continuously at 250 Hz, and the Megadac recorded foil sensor strains at 250 Hz for five continuous seconds at the beginning of each hour of testing.

3.3.2.2 CT2 Results

CT2 results were reduced with the same methods as those of CT1, and summaries of the testing are presented in Figs. 3.10 - 3.13. Table 3.2 presents FOS error analysis results for CT2. Examination of Figs. 3.10 and 3.11 once again revealed that FOS results included both temperature-induced and mechanical strains, while the foil sensor results only included mechanical strains. Figures 3.12 and 3.13 present the amplitudes of tensile cyclic loading for the 104,500 cycles with good agreement between the FOS and foil sensor results for the 210x20mm SMS with Loctite 392 adhesive and the unpackaged FBG with Loctite 410 adhesive. However, poor agreement between the FOS and foil sensor results is evident for both 15x10mm SMS with Loctite 392 and Pliogrip 771

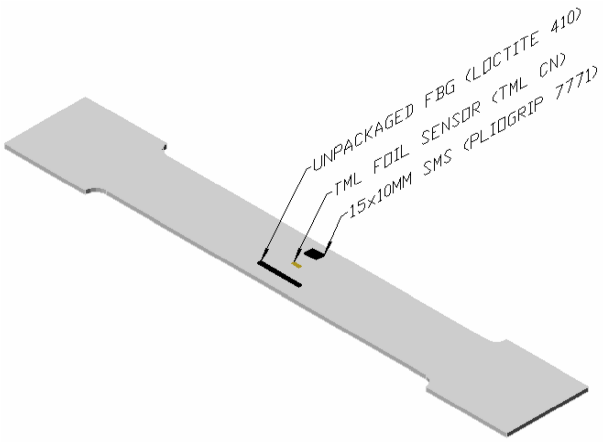

Figure 3.9. Coupon A: side one sensors and adhesives for CT2 (side two same as those in CT1).

www.manaraa.com

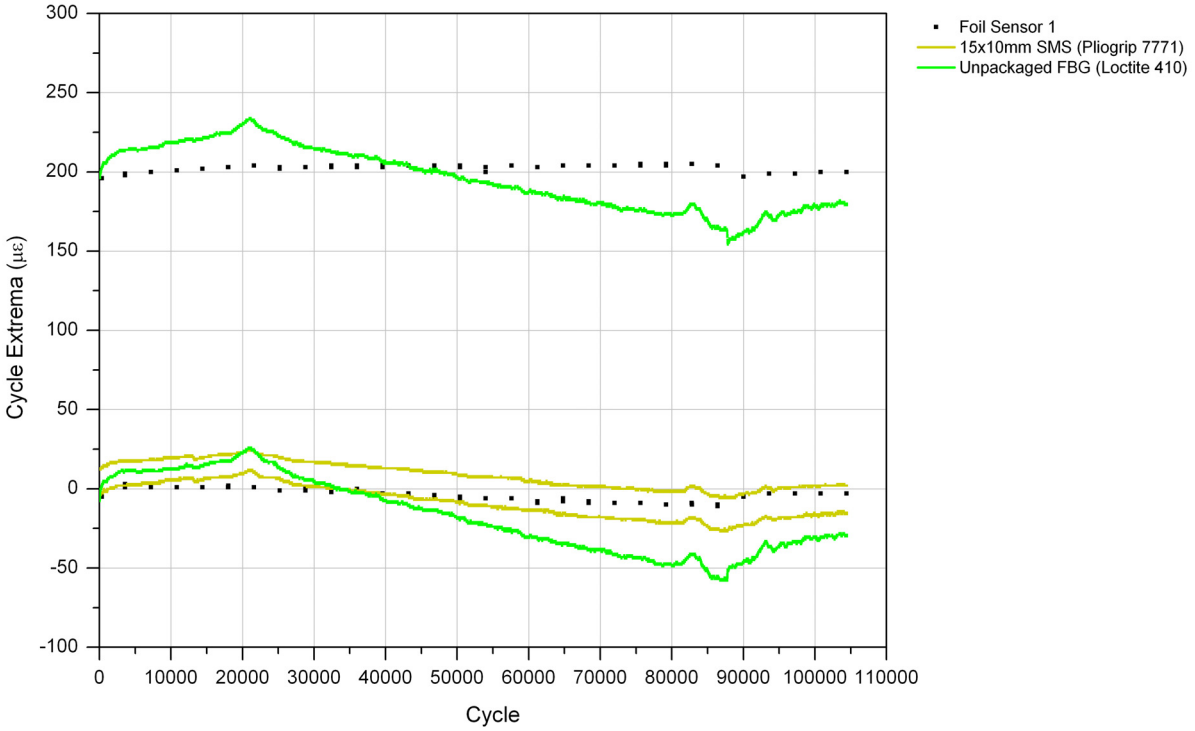

Figure 3.10. CT2: cycle extrema vs. cycle number for Coupon A, side 1 sensors.

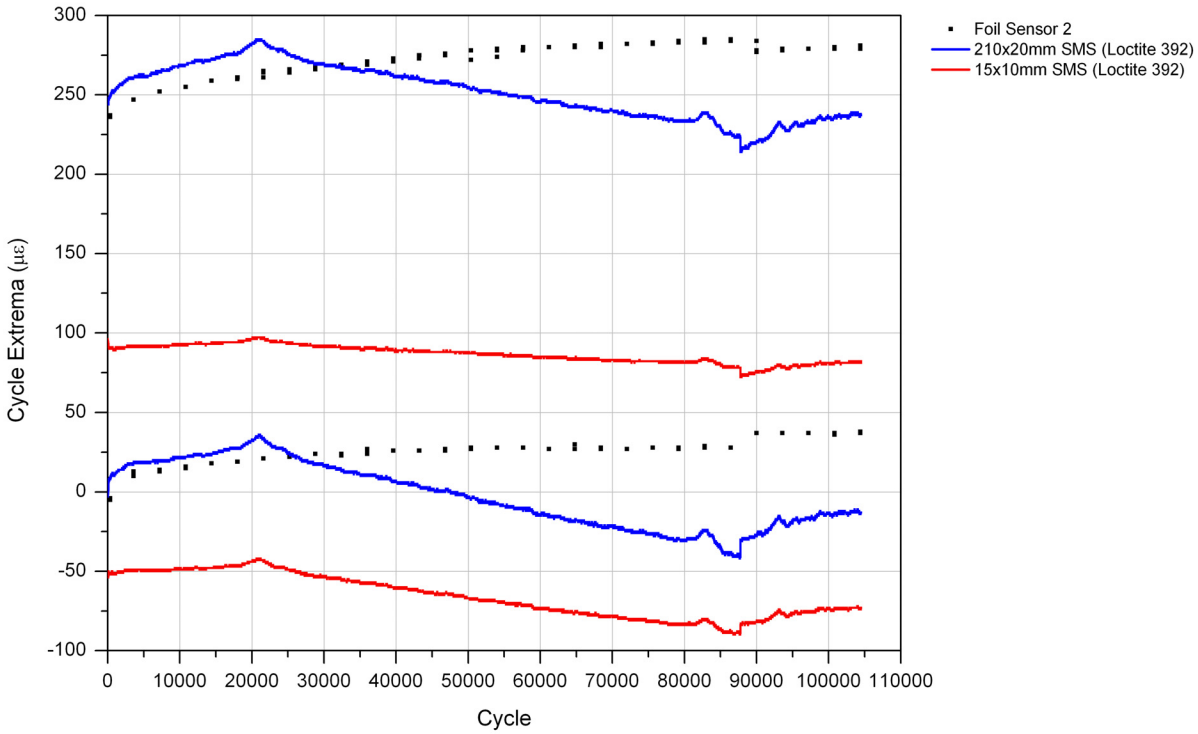

Figure 3.11. CT2: cycle extrema vs. cycle number for Coupon A, side 2 sensors.

www.manaraa.com

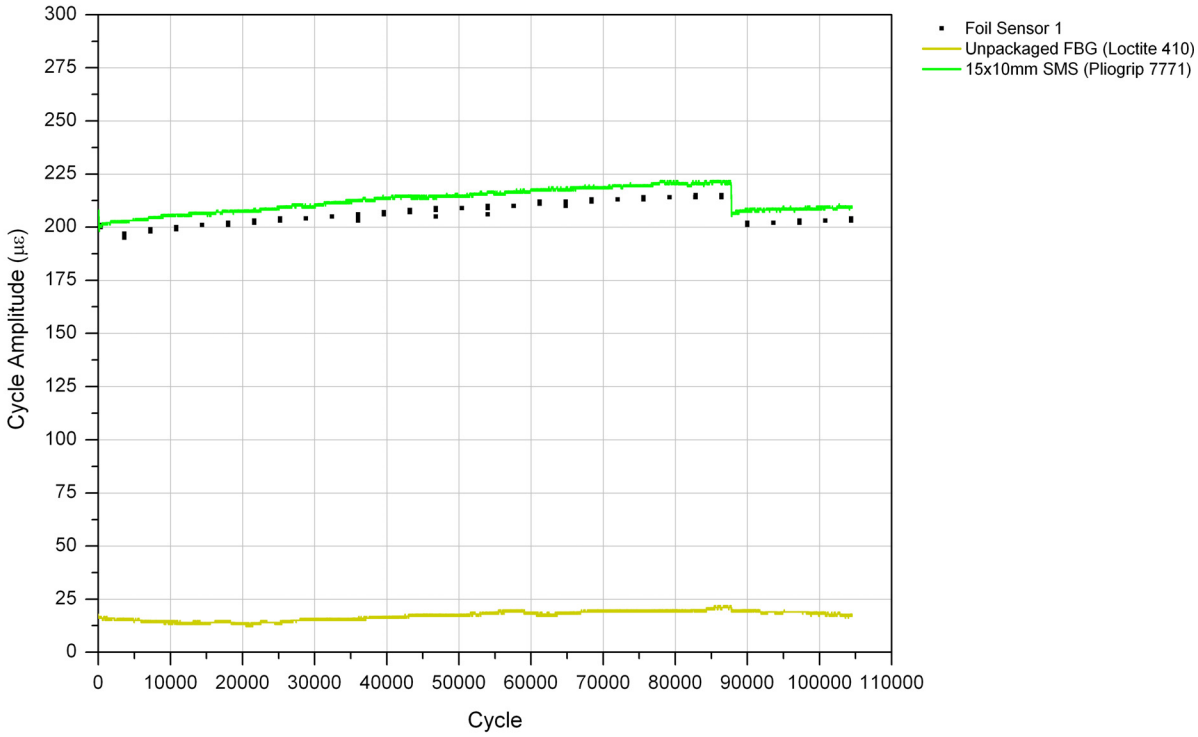

Figure 3.12. CT2: cycle amplitude vs. cycle number for Coupon A, side 1 sensors.

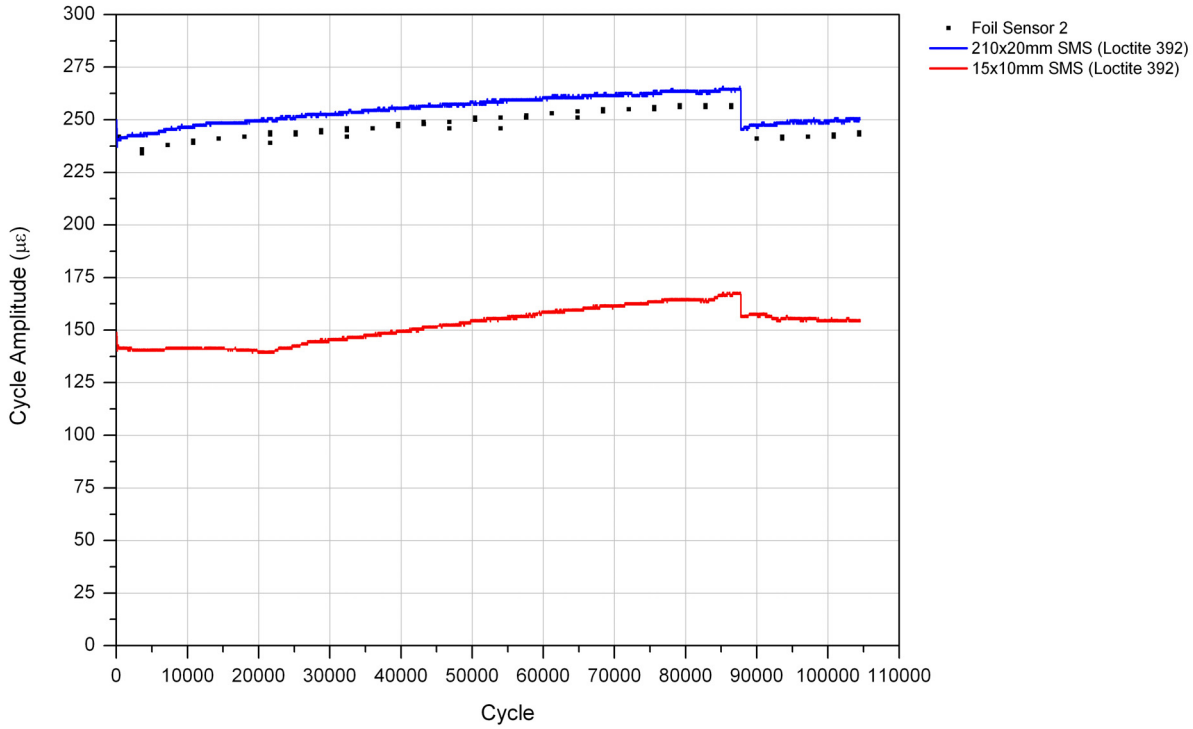

Figure 3.13. CT2: cycle amplitude vs. cycle number for Coupon A, side 2 sensors.

www.manaraa.com

Table 3.2. Error analysis results for FOSs in CT2.

CT2 Loading	Sensor (Adhesive)	Error Statistics							
		Minimum		Maximum		Average		Standard Deviation	
		Strain (με)	%	Strain (με)	%	Strain (με)	%	Strain (με)	%
104,500 cycles @ 200με	Unpackaged FBG (Loctite 410)	1	0.5	10	4.9	6	3.0	1.4	0.68
	210x20mm SMS (Loctite 392)	1	0.4	13	5.3	7	3.0	1.7	0.68
	15x10mm SMS (Loctite 392)	83	34.4	105	43.0	95	38.5	4.8	2.33
	15x10mm SMS (Pliogrip 7771)	180	90.0	195	93.6	189	91.7	4.0	0.95

adhesives. The poor performance of the 15x10mm SMS is again assumed to be the result of inadequate adhesive strength and/or inadequate cure time for the Pliogrip 7771 to fully develop the SFF CFRP packaging. Finally, note that the gradual increase in loading amplitude during CT2 is evident in Figs. 3.12 and 3.13 until a correction after 88,000 cycles.

3.3.2.3 CT2 Conclusions

The following additional conclusions were determined considering all testing through CT2:

- Changing the loading rate and magnitude resulted in essentially no change in error for any FOSs. The 210x20mm SMS and unpackaged FBG performed well and had essentially the same percent error in CT2 as in CT1. The 15x10mm SMS with Loctite 392 adhesive exhibited error in CT2 that was within the range of error that was displayed in CT1. The error of the 15x10mm SMS with Pliogrip 771 adhesive was several magnitudes worse than that bonded with Loctite 392, and thus, the adhesive type has been identified as at least one factor contributing to the inadequacy of the 15x10mm SMS.

- Reducing the loading magnitude and rate reduced the magnitude of residual strain maintained in the Loctite 392 adhesive of the 15x10mm SMS for all cycles. In addition, the Loctite 410 adhesive and Loctite 392 adhesive of the 210x20mm SMS did not maintain any residual strain during CT2. Therefore, testing thus far indicates that residual strain maintained during FOS loading is dependent upon adhesive type, loading magnitude, and/or loading rate.

- Further examination was required to determine the following:
  - Adhesives, if any, that sufficiently improve the SFF FOS performance to produce accurate strain measurements.
  - The underlying cause and factors affecting the magnitude of the residual strains maintained in adhesives during their long-term measurement history.

3.3.3 Coupon Test 3 (CT3)

3.3.3.1 CT3 Objectives and Testing Procedure

The objectives of Coupon Test 3 (CT3) were to (1) investigate several adhesives for use with SFF fiber optic SMSs, and (2) attempt to identify any factors affecting the adhesive performance, and thus, accuracy of the SFF SMSs. Since the increased adhesive shear stress, resulting from a smaller

www.manaraa.com

bond area with the 15x10mm SMS, was believed to be a factor causing deficient adhesive performance for the SFF SMSs in CT1 and CT2, the width of the CFRP packaging was doubled in CT3 to increase the bonding area, and thus reduce the adhesive shear stress. Therefore, all SFF SMSs used in CT3 were 15x20mm in size.

Tensile Coupon B with associated sensors and respective adhesives used in CT3 are presented in Fig. 3.14. As illustrated, eight structural adhesives consisting of acrylics, cyanoacrylates, methacrylates, and polyurethanes were tested with the 15x20mm SMSs: Loctite (330, 392, 410, H3000, H3300, H4500), Pliogrip 7771, and Plexus MA820 (See Appendix B for specifications). As previously mentioned, these adhesives were selected based on fixture time, bond strength, and long-term durability. The eight 15x20mm SMSs were each bonded to the coupon using a different adhesive and were organized into four groups (2 groups per side); each group had one foil sensor to serve as the baseline for comparison between the technologies.

To achieve the objectives of CT3, Coupon B was subjected to tensile cyclic loading producing amplitudes of approximately 500με for 2,100,000 cycles at 4.0 Hz. During the testing, a si425-500 interrogator recorded FOS strains and the laboratory temperature (with a fiber optic temperature sensor) continuously at 250 Hz. In addition, the Megadac as well as the Flextest GT Controller and MPT Software recorded foil strains and coupon loading, respectively, at 250 Hz for five continuous seconds at the beginning of each hour of testing. Laboratory temperature and loading magnitude were recorded to help isolate and identify parameters affecting CT3 results.

3.3.3.2 CT3 Results

Data from CT3 were reduced with the same methods as those of CT1 and CT2, and Figs. 3.15 - 3.22 present summaries of the results. Due to the consistency and repeatability of the MTS Data, linear interpolation was assumed and displayed between data points in the loading graphs. All other data has been displayed as it was collected, continuous or intermittent. Table 3.3 presents FOS error analysis results for CT3. As illustrated, the range of error and average error varies significantly among the eight adhesives tested with the 15x20mm SMSs.

Examination of Figs. 3.15 - 3.18 reveals that the maximum load for each cycle in CT3 was

www.manaraa.com

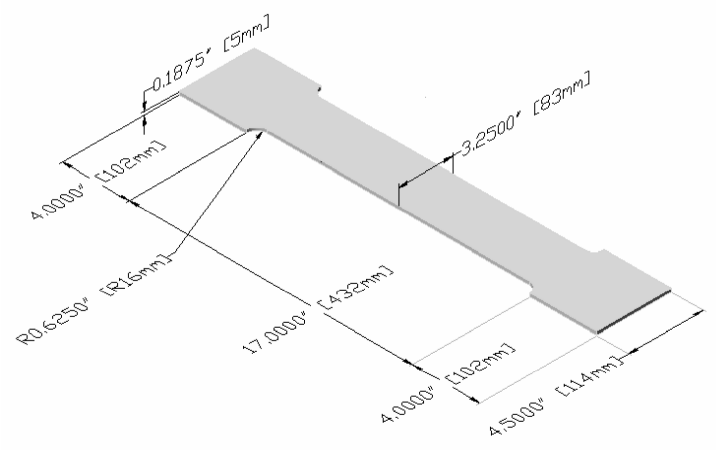

a. Coupon B

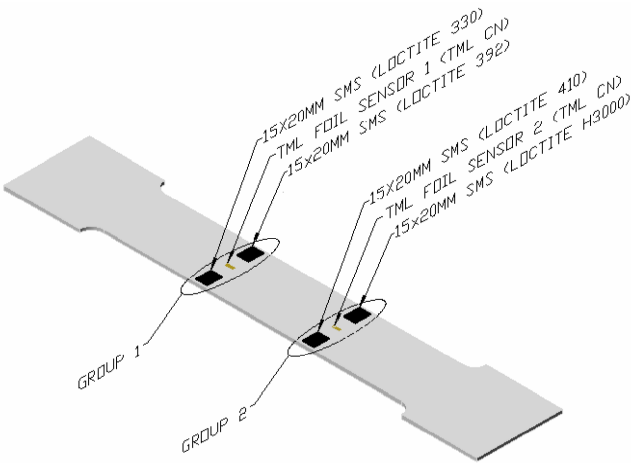

b. Coupon B: side 1 sensors and adhesives

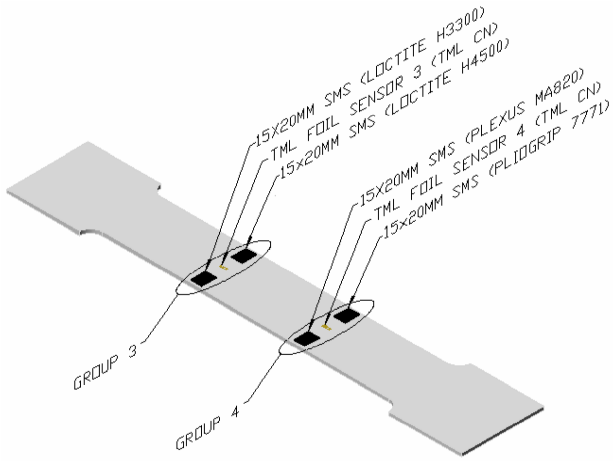

c. Coupon B: side 2 sensors and adhesives

Figure 3.14. Coupon B, sensors, and adhesives used in CT3.

www.manaraa.com

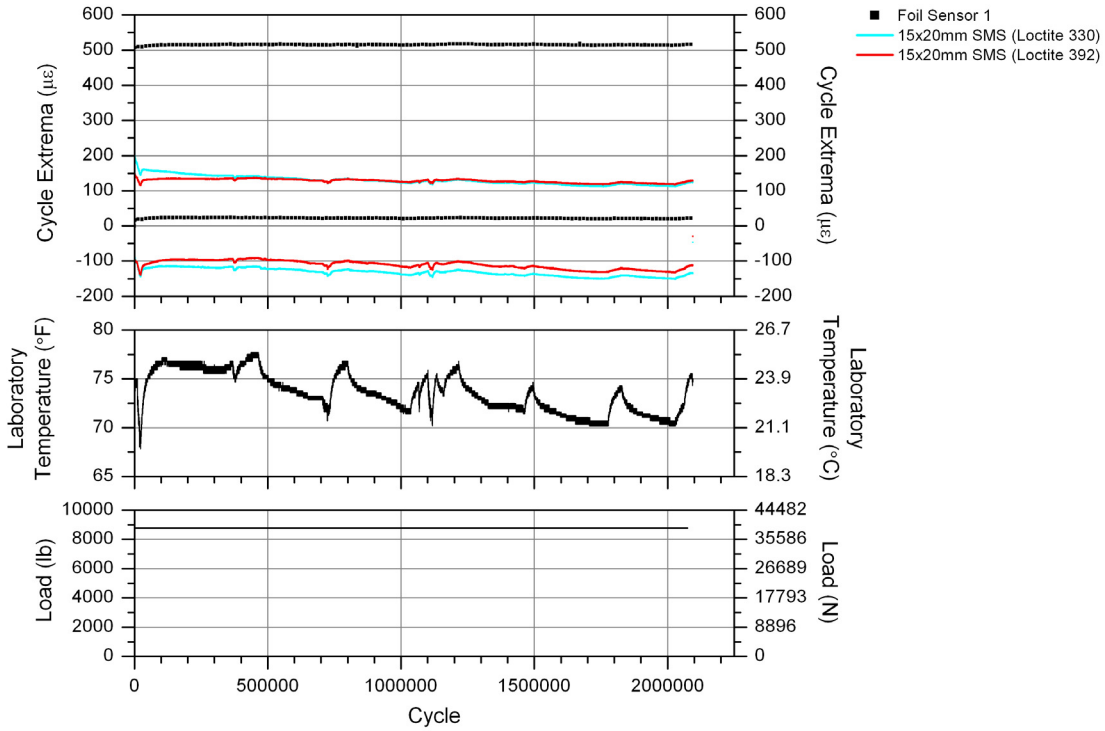

Figure 3.15. CT3: cycle extrema vs. cycle number for Coupon B, group 1 sensors.

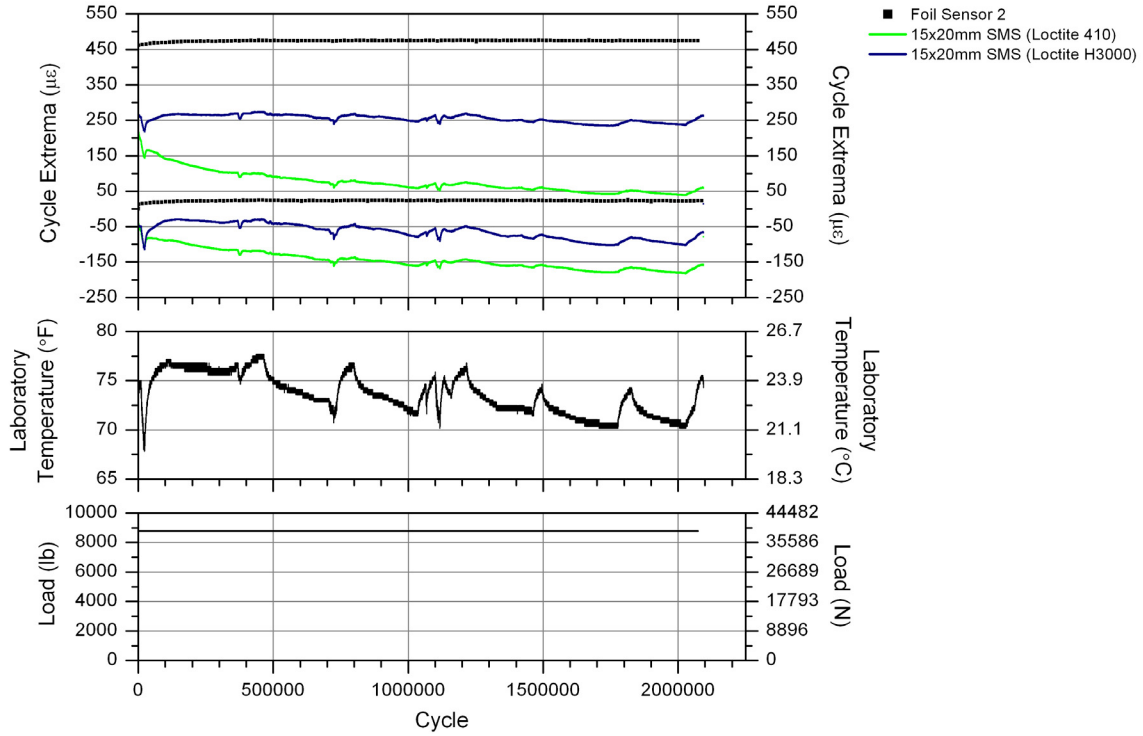

Figure 3.16. CT3: cycle extrema vs. cycle number for Coupon B, group 2 sensors.

www.manaraa.com

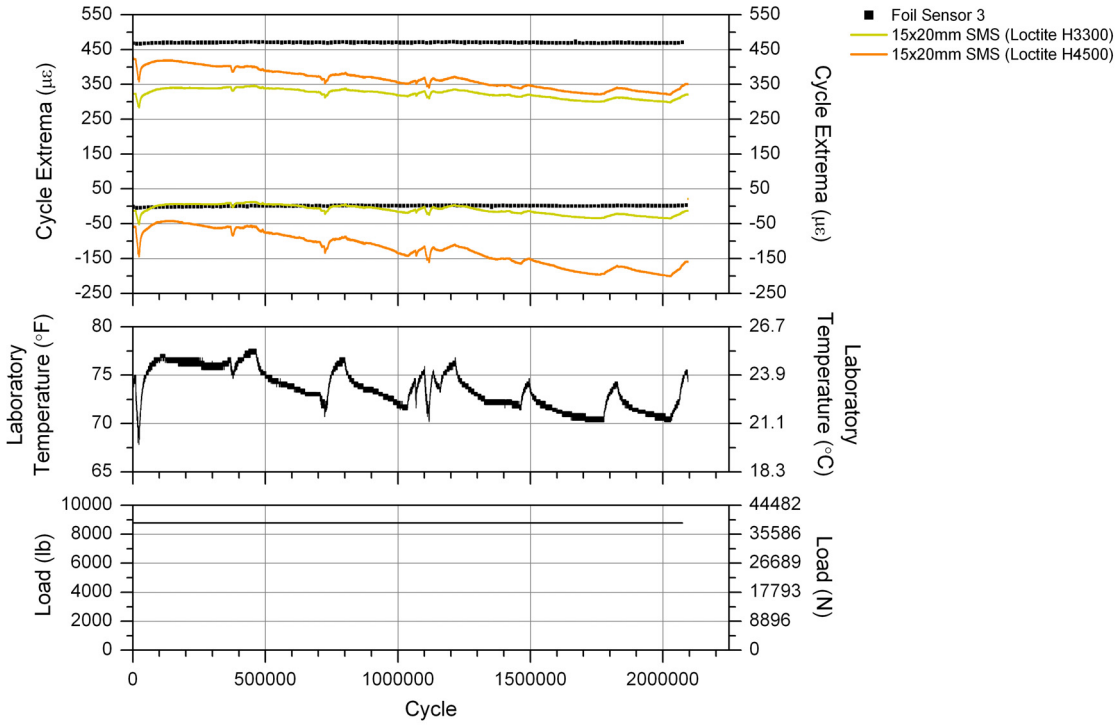

Figure 3.17. CT3: cycle extrema vs. cycle number for Coupon B, group 3 sensors.

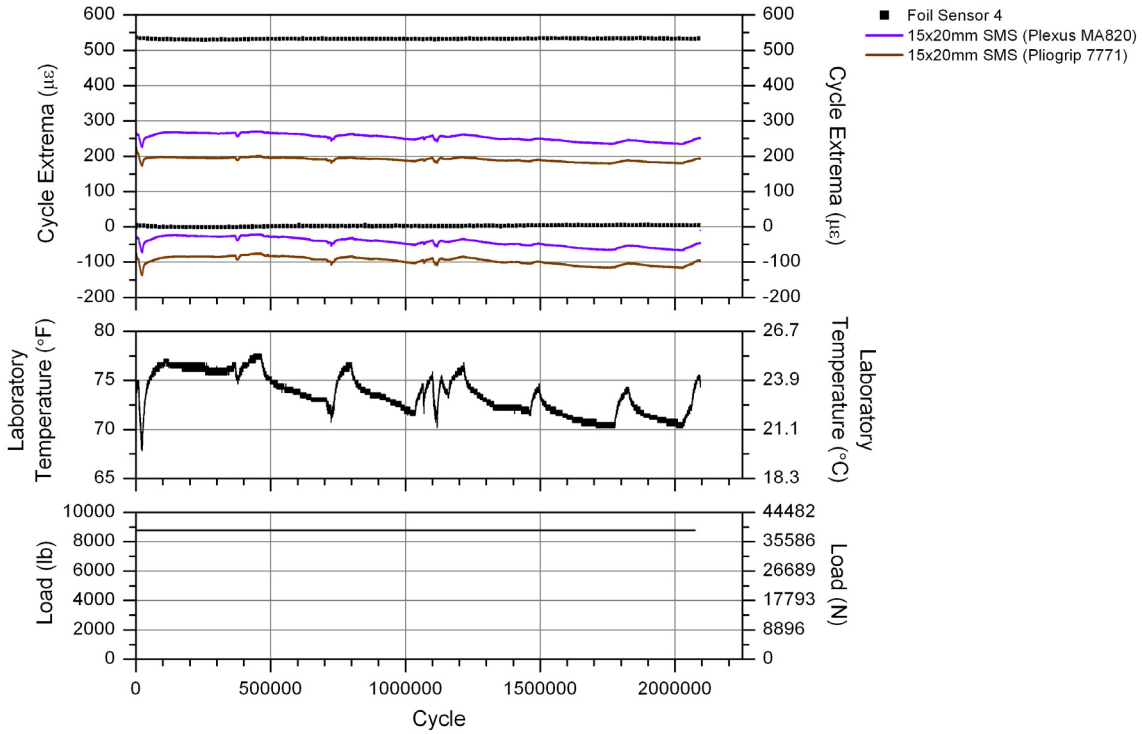

Figure 3.18. CT3: cycle extrema vs. cycle number for Coupon B, group 4 sensors.

www.manaraa.com

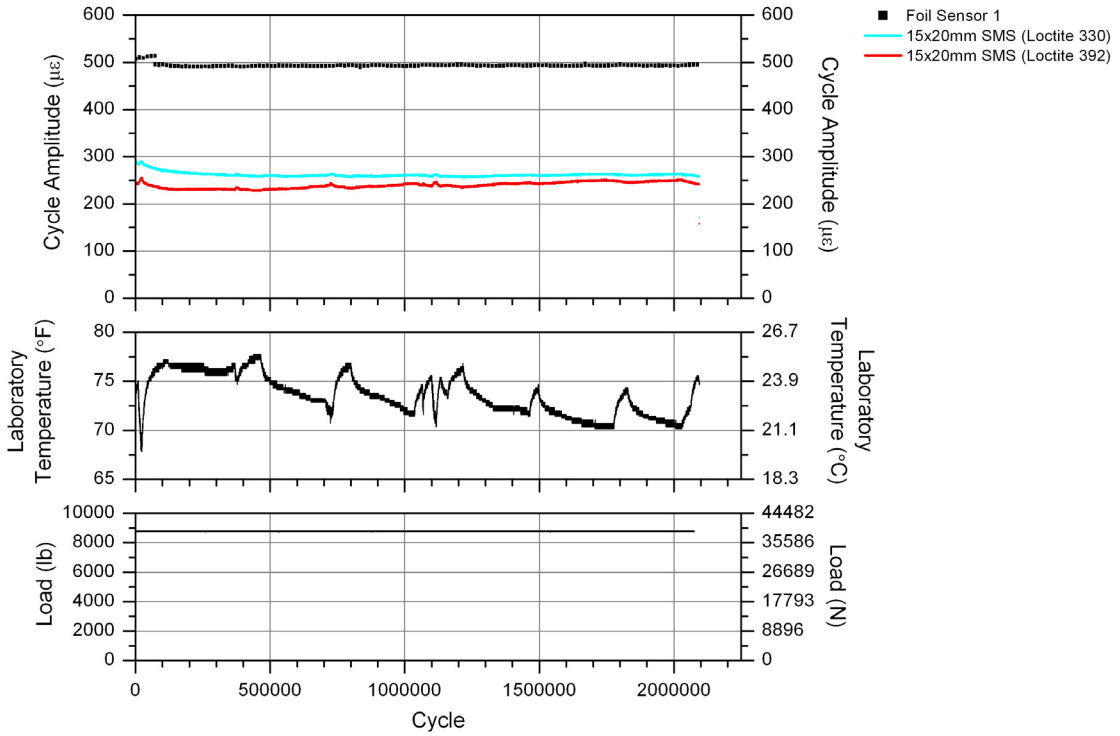

Figure 3.19. CT3: cycle amplitude vs. cycle number for Coupon B, group 1 sensors.

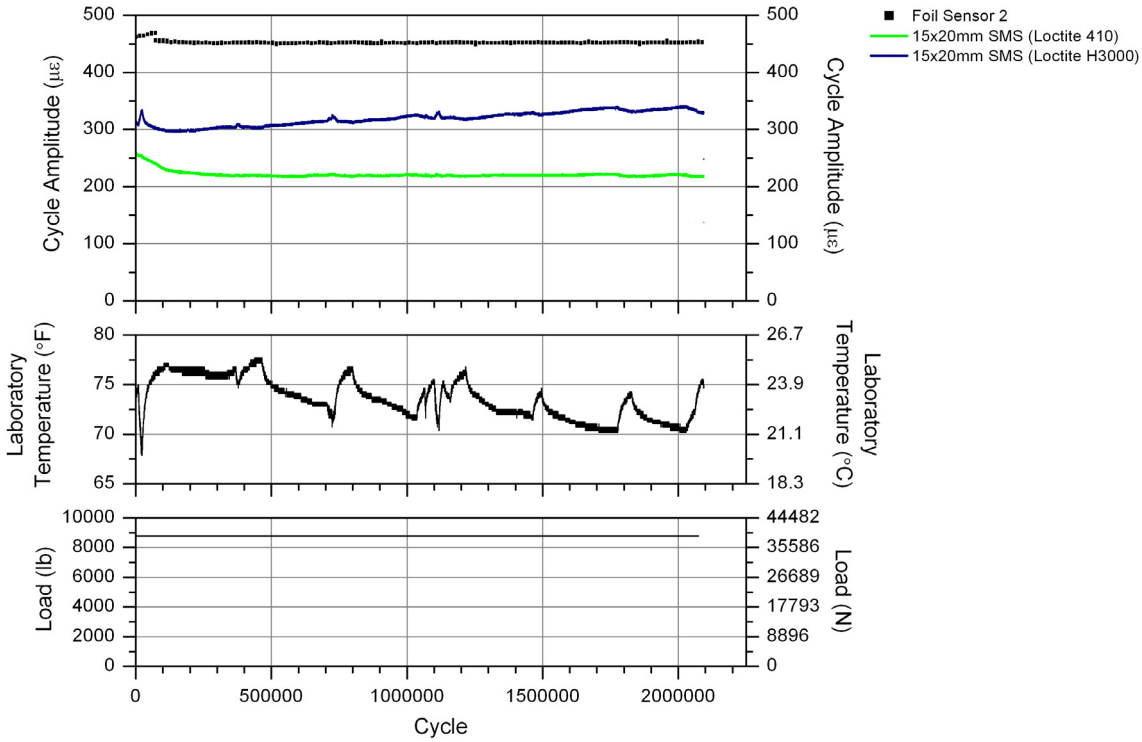

Figure 3.20. CT3: cycle amplitude vs. cycle number for Coupon B, group 2 sensors.

www.manaraa.com

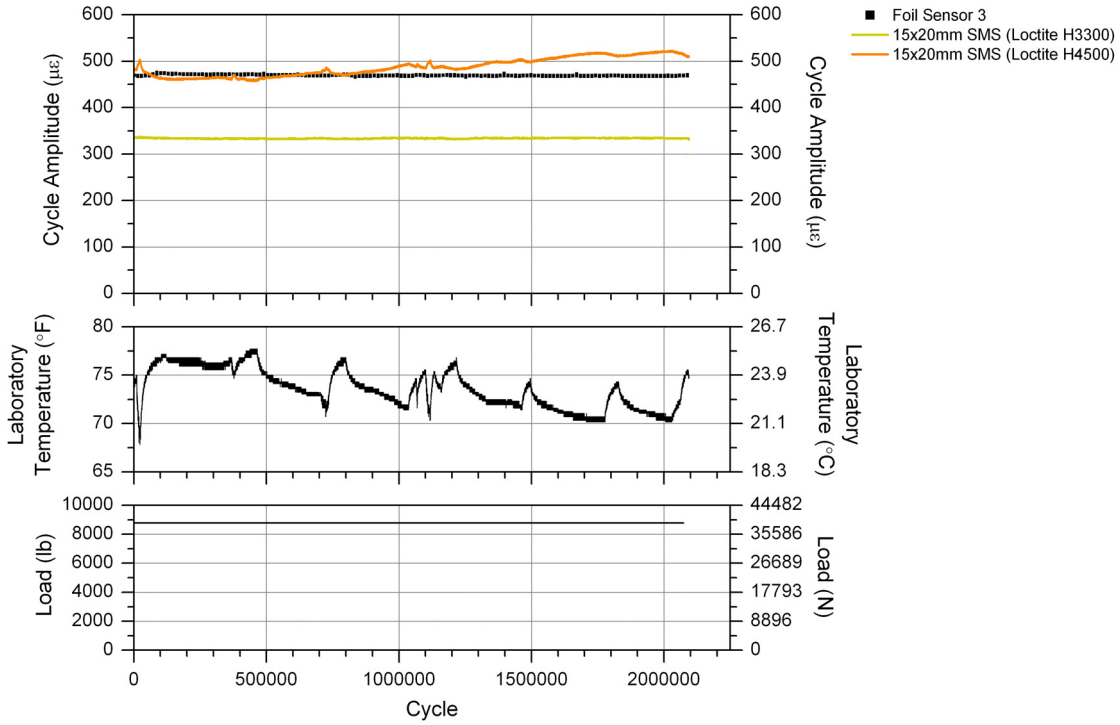

Figure 3.21. CT3: cycle amplitude vs. cycle number for Coupon B, group 3 sensors.

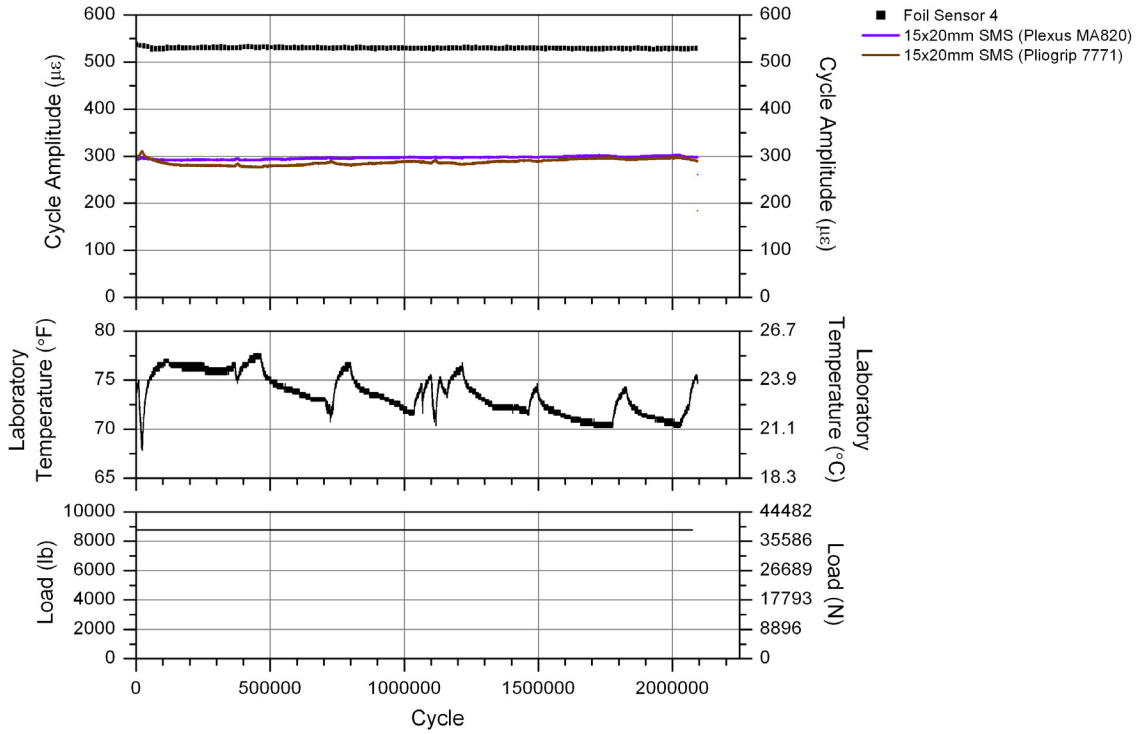

Figure 3.22. CT3: cycle amplitude vs. cycle number for Coupon B, group 4 sensors.

www.manaraa.com

Table 3.3. Error analysis results for FOSs in CT3.

CT3 Loading	Adhesive *	Error Statistics							
		Minimum		Maximum		Average		Standard Deviation	
		Strain (με)	%	Strain (με)	%	Strain (με)	%	Strain (με)	%
2,100,000 cycles @ 500με	Loctite 330	216	42.6	239	48.3	232	47.0	3.5	0.63
	Loctite 392	241	49.0	278	54.1	254	51.5	6.6	1.61
	Loctite 410	203	44.0	238	52.3	232	51.2	4.2	1.29
	Loctite H3000	111	24.6	168	35.8	133	29.5	12.9	7.70
	Loctite H3300	131	28.0	142	30.0	136	29.0	2.1	0.12
	Loctite H4500	1	0.2	55	11.8	22	4.7	16.4	12.30
	Plexus MA820	225	42.7	247	45.8	234	44.1	4.0	0.43
	Pliogrip 7771	229	43.0	258	48.3	243	45.8	6.7	1.45

* Note: All FOSs = 15x20mm SMSs

nearly constant, and thus, variation in load was eliminated as a possible source of error in CT3 FOS results. Similar to CT1 and CT2, both temperature-induced and mechanical strains were measured by the FOS in CT3, but only mechanical strains were measured by the foil sensors. Even more evident in CT3 than in the other tests was the influence of laboratory temperature on the cycle extrema.

Examination of Figs. 3.19 - 3.22 clearly illustrates that the foil sensors accurately measured constant amplitude cyclic loading in CT3, whereas the FOS did not accurately capture this behavior. Only the 15x20mm SMS with Loctite H4500 measured mechanical strains within 5% average error of the actual strain. In addition, all 15x20mm SMSs measured variable cycle amplitudes for the constant-amplitude cyclic testing, and the variation is clearly related to the laboratory temperature. As the laboratory temperature decreased and increased, the measured cycle amplitudes for all FOSs increased and decreased, respectively. While Loctite H4500 was the CT3 adhesive with the smallest mechanical strain measurement error, it had the highest standard deviation in the error analysis, which identified it as the adhesive most heavily influenced by temperature.

3.3.3.3 CT3 Conclusions

The following additional conclusions were determined considering all testing through CT3:

- One factor contributing to the inaccurate performance of the 15x20mm SMS was proven to be the adhesive used to bond the SMSs to the coupon.

www.manaraa.com

- The 15x20mm packaging surface area of the SMSs was not sufficient for adhesives other than Loctite H4500 for the loading conditions in CT3.
- Adhesive performance was inversely related to the laboratory temperature for the testing conducted in CT3.
- Further examination was required to determine the following:
  - FOS/adhesive performance and degree of accuracy during two isolated conditions:
    a. Fluctuating, temperature-induced coupon strains in the absence of mechanical strain.
    b. Sustained mechanical strains in the coupon in the presence of constant laboratory temperature.
  - The primary cause for the inverse relationship between FOS mechanical strain measurement error and changes in laboratory temperature.

3.3.4 Coupon Test 4 (CT4)

3.3.4.1 CT4 Objectives and Testing Procedure

The objective of Coupon Test 4 (CT4) was to investigate the sensitivity of each adhesive to temperature change while Coupon B was subjected to only temperature changes. Coupon B and associated sensors with respective adhesives presented in Fig. 3.14 were again utilized in CT4. To achieve the objective of CT4, Coupon B was removed from all restraints to allow for free expansion and contraction, and then subjected to fluctuating temperatures in the range of approximately 9°F to 43°F (-13°C to 6°C). During the testing, a si425-500 interrogator recorded the air temperature and FOS strains continuously at 1.0 Hz, and the Megadac recorded foil sensor strains at 1.0 Hz. Both FOSs and foil sensors were zeroed when the coupon steel temperature was 18°F (-7.7°C).

3.3.4.2 CT4 Results

Since CT4 temperatures were not within the STC range of the foil sensors, the foil results were compensated for thermal influence by using the STC information provided from TML for FLA-6-11 sensors (See Appendix C). Figure 3.23 presents foil sensor results before and after temperature compensation. As illustrated, nearly all thermal influence has been removed from CT4 foil sensor results, and thus, the temperature compensation process for the foil sensors has been verified to be accurate.

Figure 3.24 presents continuous strain data for all FOSs in CT4, and as demonstrated,

www.manaraa.com

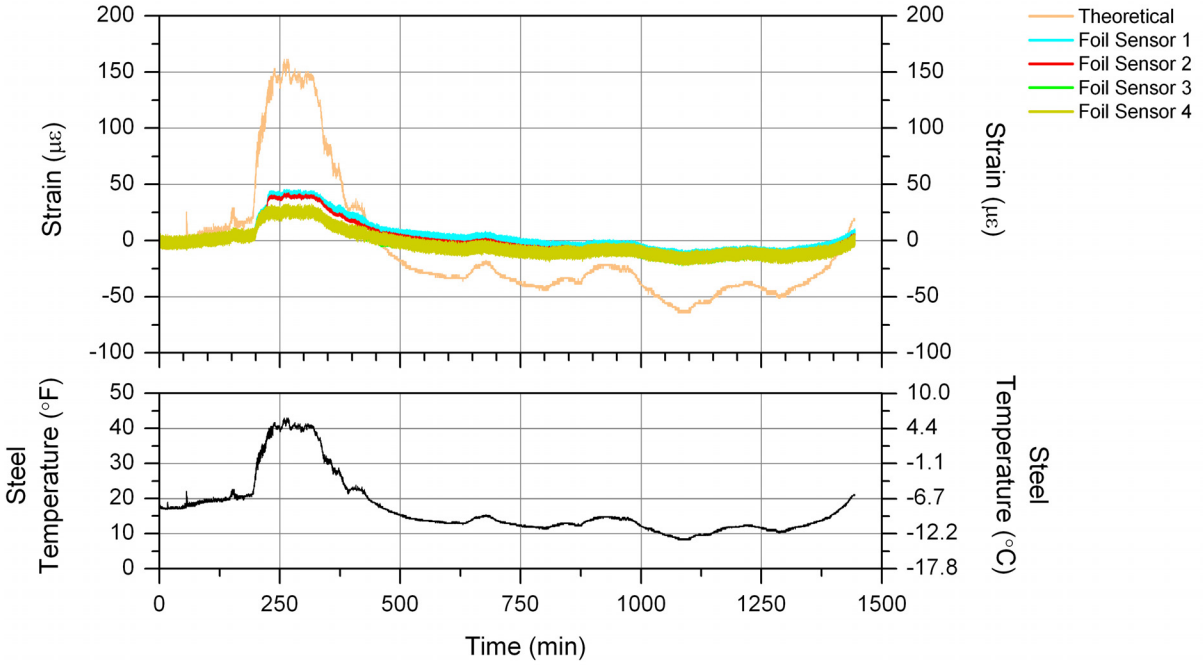

a. Foil sensor results before temperature compensation

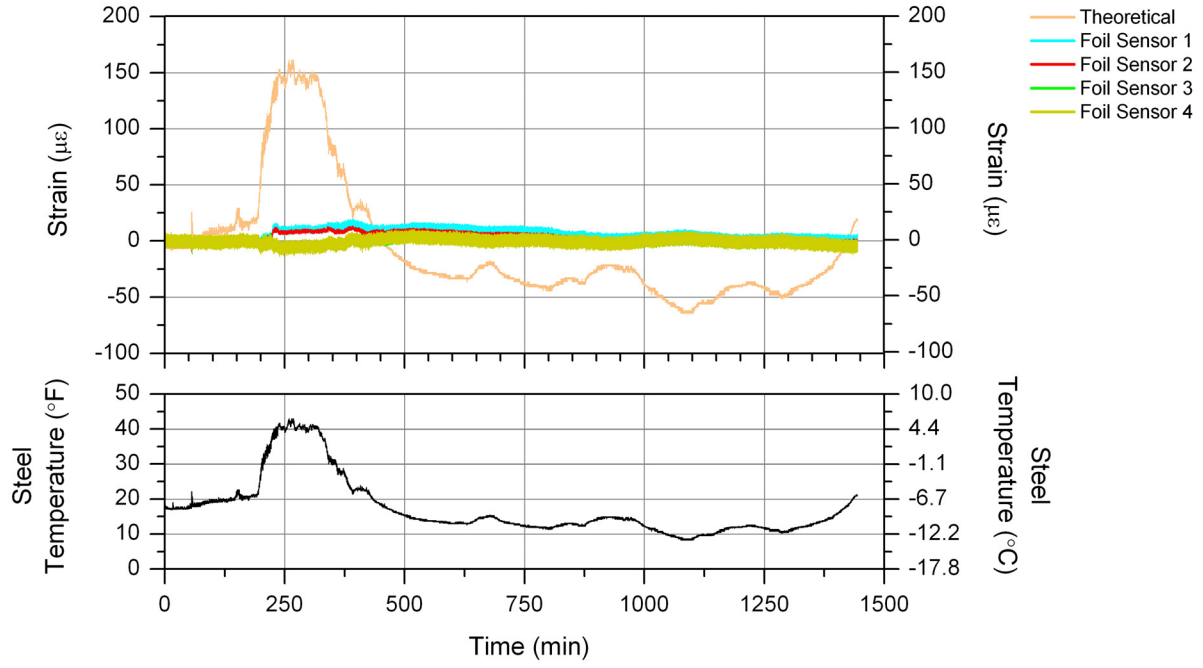

b. Foil sensor results after temperature compensation

Figure 3.23. CT4: foil sensor results compared with theoretical analysis for Coupon B.

www.manaraa.com

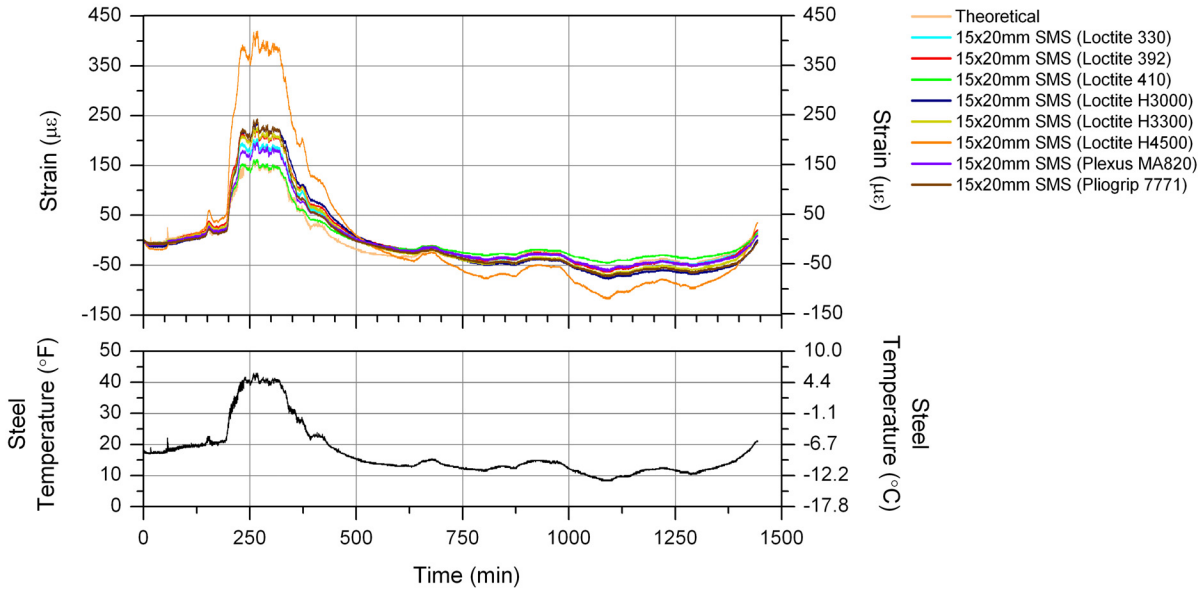

Figure 3.24. CT4: FOS results compared with theoretical analysis for Coupon B.

results among the sensors vary significantly. Since Coupon B was subjected to uniform temperature change and all FOSs were identical, the discrepancies among the FOS results were due to differing thermal properties of the adhesives. It should also be noted that FOS results presented in Fig. 3.24 include temperature-induced effects on the FBGs, while the theoretical calculation accounts only for temperature-induced strains in the steel. Thus, differences between the theoretical and experimental results in Fig. 3.24 were expected. However, the theoretical results were still used as a baseline and compared to each FOS. The results of the comparisons are presented in Table 3.4 and are useful for relative comparison among the FOSs, but not as a measure of accuracy.

3.3.4.3 CT4 Conclusions

The following additional conclusions were determined considering all testing through CT4:

- STC compensation for the foil sensors was verified to be accurate and repeatable.
- The adhesives were proven to have differing thermal expansion/contraction properties.
- The influence of temperature on adhesives explains deviations among FOS extrema during constant amplitude cyclic loading, but it does not explain the inverse relationship between cycle amplitude measurement error and temperature fluctuation in CT1, CT2, and CT3.

www.manaraa.com

Table 3.4. Error analysis results for FOSs in CT4.

CT4 Loading	Adhesive *	Statistics for Relative Comparison							
		Minimum		Maximum		Average		Standard Deviation	
		Strain (με)	%	Strain (με)	%	Strain (με)	%	Strain (με)	%
Fluctuating Temperature: 9 to 43°F (-13 to 6°C)	Loctite 330	0.1	0.2	68	325.5	12	28.6	13.1	32.52
	Loctite 392	0.1	0.2	91	405.3	16	35.8	19.2	41.65
	Loctite 410	0.1	0.1	27	184.0	9	26.9	5.4	20.36
	Loctite H3000	0.1	0.1	93	511.7	23	53.3	21.0	47.19
	Loctite H3300	0.1	0.2	83	370.2	17	38.2	17.4	32.89
	Loctite H4500	0.2	0.6	262	840.4	58	112.5	64.9	77.97
	Plexus MA820	0.1	0.1	52	308.5	10	26.2	9.9	28.98
	Pliogrip 7771	0.1	0.3	95	312.8	19	41.5	19.3	31.88

* Note: All FOSs = 15x20mm SMSs

- Further examination was required to determine the following:
  - The performance and degree of accuracy of the 15x20mm SMSs during sustained mechanical load and approximately constant steel temperature.
  - The primary cause for the relationship between mechanical strain measurement error and temperature fluctuations.

3.3.5 Coupon Test 5 (CT5)

3.3.5.1 CT5 Objectives and Testing Procedure

The objective of Coupon Test 5 (CT5) was to investigate the performance and accuracy of the 15x20mm SMSs and corresponding adhesives during sustained mechanical loading on Coupon B while maintaining approximately constant laboratory temperature. Coupon B with associated sensors and respective adhesives presented in Fig. 3.14 was again utilized in CT5. To achieve the objective of CT5, Coupon B was subjected to five tensile loads, each of which was statically sustained for 30 minutes and then released for 30 minutes before the next load was applied. The five sustained tensile loads were applied to produce approximately 100με, 200με, 300με, 400με, and 500με in the coupon, and the time required to ramp and release each load was approximately 0.1 seconds. During the testing, a si425-500 interrogator recorded FOS strains and the laboratory temperature continuously at 250 Hz, and the Megadac recorded foil sensor strains continuously at 1.0 Hz. In addition, the coupon loading was recorded by the Flextest GT Controller and MPT Software continuously at 1.0 Hz throughout CT5.

www.manaraa.com

3.3.5.2 CT5 Results

Figures 3.25 - 3.28 present continuous strain results for the four groups of sensors on Coupon B in CT5. As illustrated, the strain history pattern of each foil sensor mimics the load history pattern; a maximum strain measurement was reached immediately upon application of the load, and that strain measurement was maintained throughout the 30 minutes of the sustained load. When the load was released, foil sensors 1-3 returned to essentially zero strain while foil sensor 4 maintained some residual strain after each event. In general, the foil sensors behaved as expected.

The strain history patterns of the 15x20mm SMSs display different behavior, however. As illustrated in Fig. 3.29, starting at a value of E_{RL} (extreme strain in released coupon immediately prior to loading), load was applied and an instantaneous strain measurement, E_L (extreme strain immediately after loading) was reached, but it was lower than the actual strain condition for all FOSs in Events 1-5. In addition, E_L was immediately followed by a severe reduction in strain. The rate of strain reduction was time-dependent, and for the 15x20mm SMSs bonded to the coupon with Loctite (330, 392, 410, H4500), and Pliogrip 7771, the rate eventually stabilized and became steady-state reduction throughout the rest of the 30 minutes of sustained load. However, for the 15x20mm SMSs bonded to the coupon with Loctite H3000, Loctite H3300, and Plexus MA820, the strain reduction rate eventually diminished to essentially zero for the remaining time of sustained load. Figure 3.30 presents a close up view of the strain reduction behavior for all 15x20mm SMSs in Event Four. Note that this strain reduction occurred during a time interval that had an approximately constant laboratory temperature and coupon load. With E_L reduced to the value E_{LR} (extreme strain in the loaded coupon immediately prior to load release), the load was released and a residual strain was initially maintained to produce E_R (extreme strain in the released coupon immediate after load release), which experienced reduction in the same manner as E_L. Interestingly, E_R never completely recovered for any of the 15x20mm SMSs for any CT5 events.

Note that the 15x20mm SMS bonded with Loctite 410 recorded essentially zero mechanical strain in CT5. Since this FOS was multiplexed with all other FOSs in the same fiber, and since measurements were obtained from other FOSs during CT5, it is thought that the zero strain

www.manaraa.com

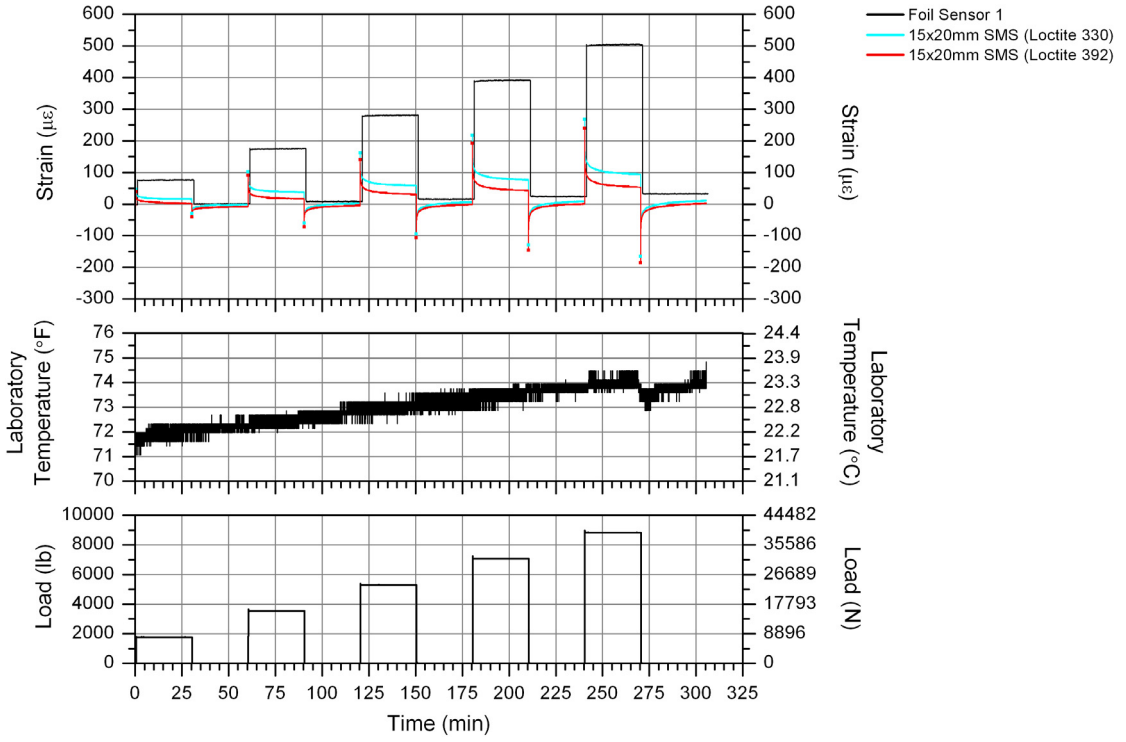

Figure 3.25. CT5: continuous strain results for Coupon B, group 1 sensors.

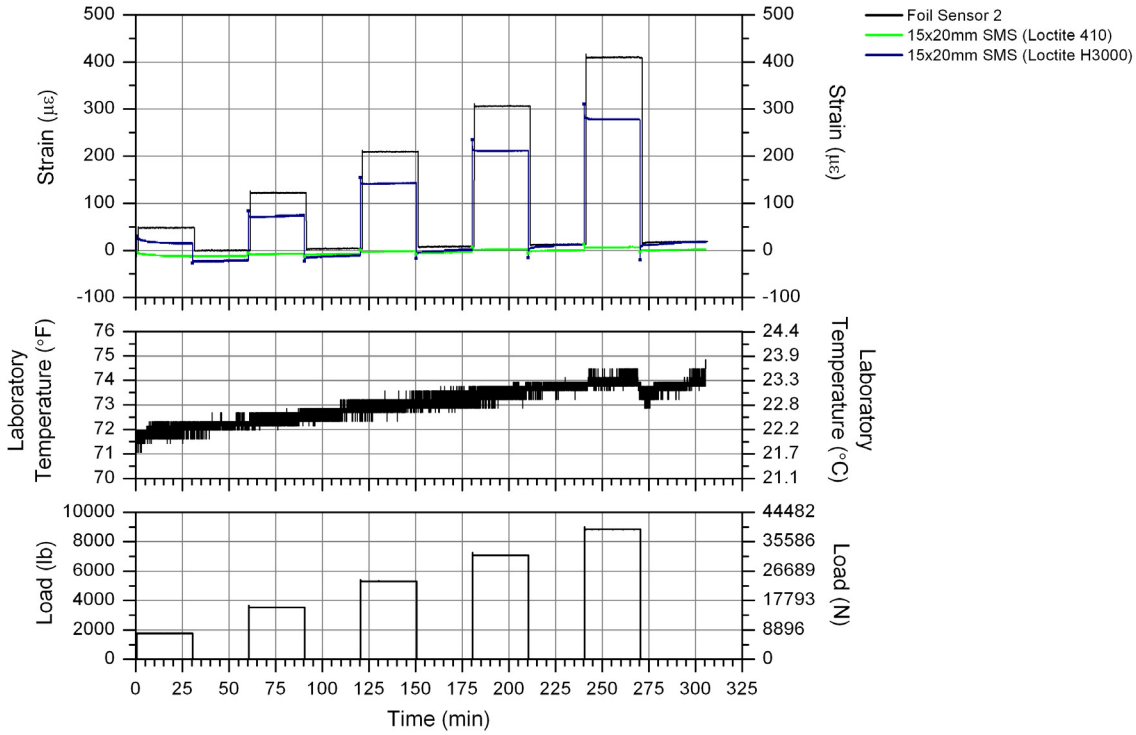

Figure 3.26. CT5: continuous strain results for Coupon B, group 2 sensors.

www.manaraa.com

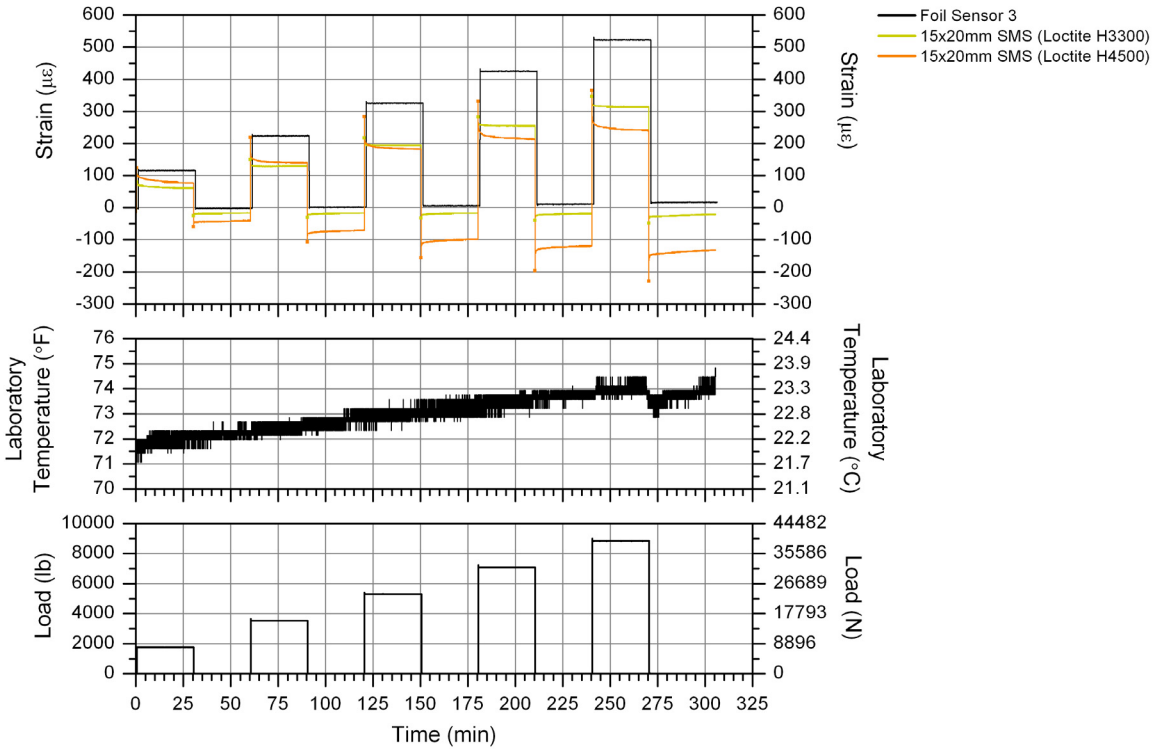

Figure 3.27. CT5: continuous strain results for Coupon B, group 3 sensors.

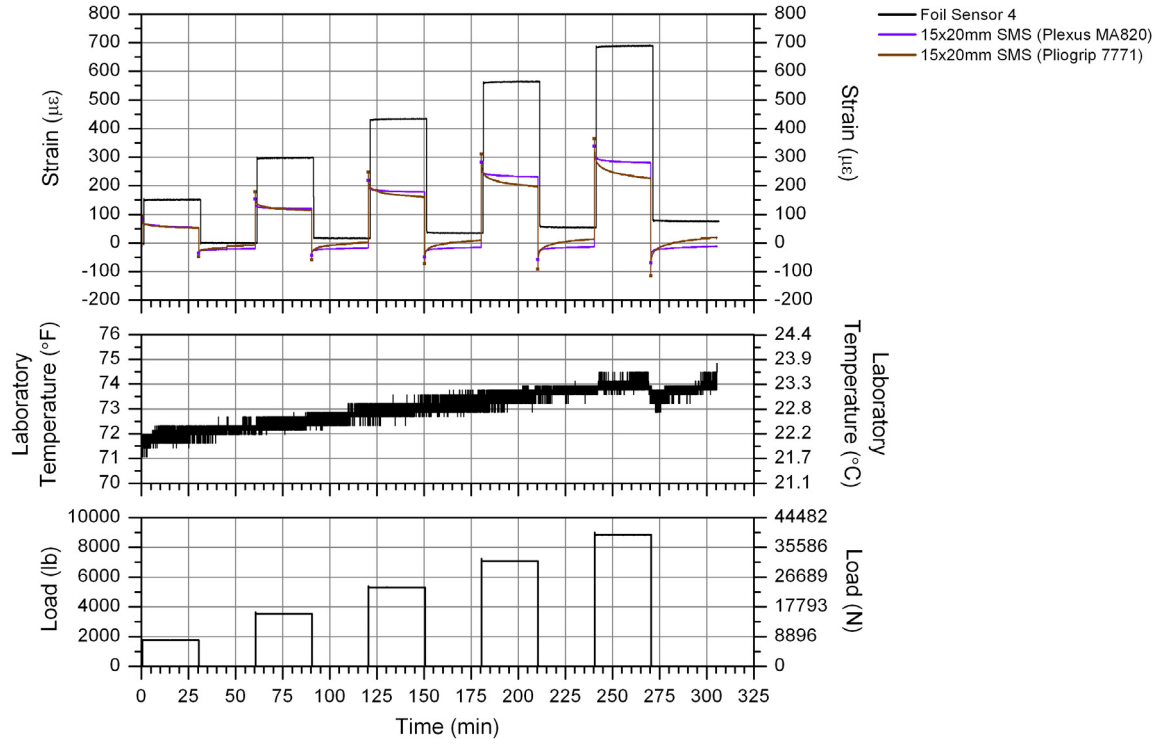

Figure 3.28. CT5: continuous strain results for Coupon B, group 4 sensors.

www.manaraa.com

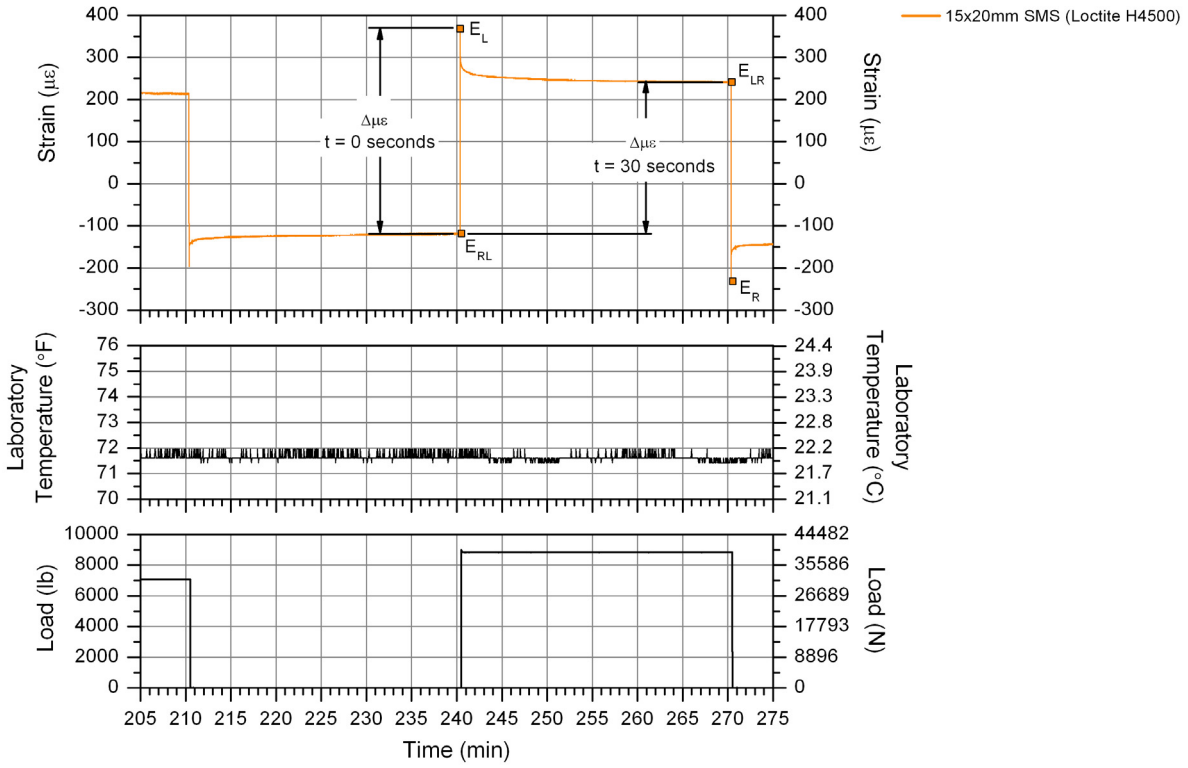

Figure 3.29. CT5: typical behavior and determination of measured mechanical strain, Δμε.

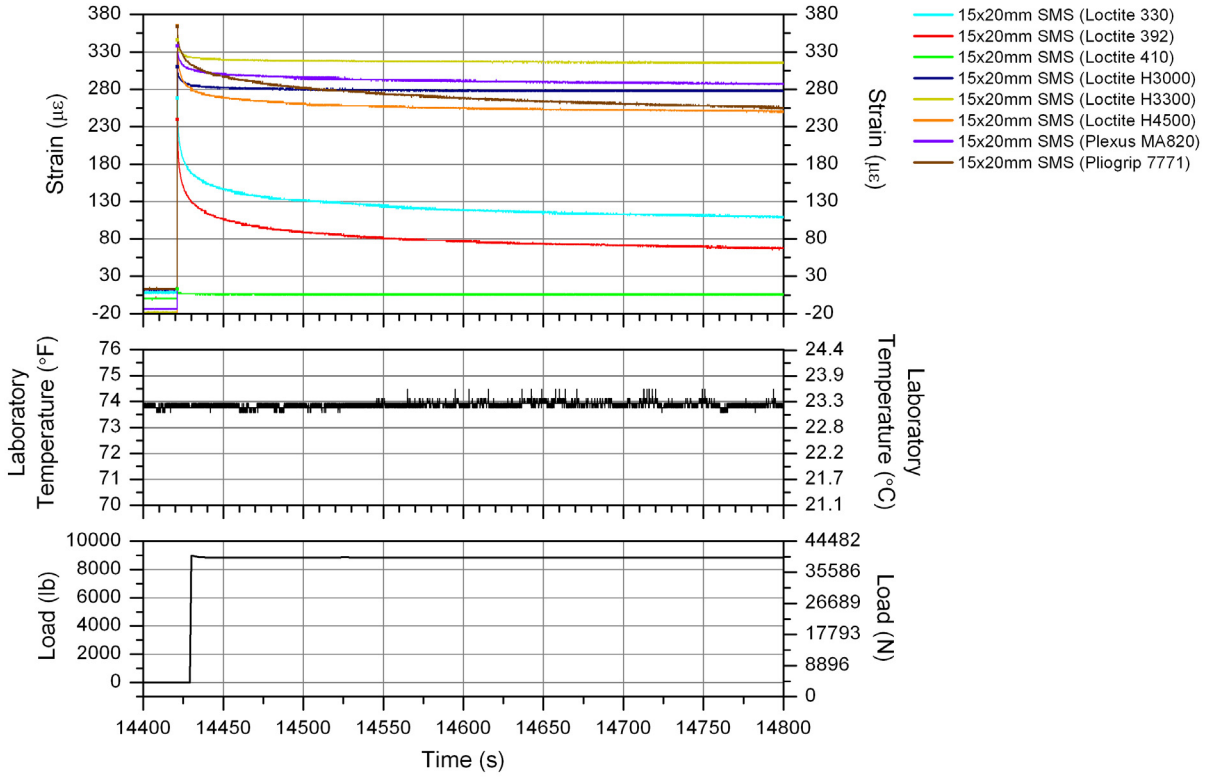

Figure 3.30. CT5: close up view of Event 5 for all 15x20mm SMS.

www.manaraa.com

measurement was the result of adhesive failure and not sensor failure. This failure could have been unobservable failure in the Loctite 410 or in the adhesive used to bond the FBG and CFRP.

As demonstrated in Fig. 3.29, the magnitude of mechanical strain measured by each sensor continuously throughout each event was calculated as the change in strain, $\Delta\mu\varepsilon$, between E_{RL} and the recorded strains values of the event. Using the foil sensor results as baselines for comparison, an error analysis was conducted and is summarized in Table 3.5; both immediate (t = 0 minutes) and long-term (t = 30 minutes) error is presented for all FOS/adhesive combinations. Review of Table 3.5 reveals that the measurement error in each 15x20mm SMSs increased with time throughout each event, and the magnitude of the immediate and long-term error varied significantly among the eight FOSs. When comparing the five events within one 15x20mm SMS, however, the immediate and long-term errors remained relatively constant for all five events, regardless of the change in the coupon loading magnitude. Compiling all FOS results in CT1-CT5, the factor contributing to all abnormal performance in the FOS results was identified as viscoelastic behavior in the adhesives.

3.3.5.3 Explanation of Viscoelastic Behavior

As discussed in Section 2.5.1, viscoelastic behavior, or viscoelasticity, is a phenomenon that causes stress relaxation in adhesives and is composed of two components: elastic behavior (instant, rate-independent, and recoverable) and viscous behavior (delayed, time-dependent, and unrecoverable). The elastic behavior is identified in CT5 results as the changes in strains that are immediately measured by each FOS upon application and release of the tensile loads, and the viscous behavior is identified in CT5 results as (1) the time-dependent reduction in the measured strain during an event with sustained load, and (2) the residual strain that is not recovered after each loading event. Stress relaxation and creep tests are both methods for determining the degree of viscoelasticity occurring in an adhesive. In a stress relaxation test, the calculated relaxation modulus decreases with time, and in a creep test, the creep modulus increases with time. While neither of these procedures was directly followed in this research, the FOS results obtained in CT5 resemble those of stress relaxation tests.

Having identified viscoelastic behavior in the adhesives, effort was given to determine its

www.manaraa.com

Table 3.5. Error analysis results for FOSs in CT5.

CT5 Loading	Adhesive *	Error Label	Error Statistics									
			Event 1		Event 2		Event 3		Event 4		Event 5	
			t = 0 min	t = 30 min	t = 0 min	t = 30 min	t = 0 min	t = 30 min	t = 0 min	t = 30 min	t = 0 min	t = 30 min
Incremental Sustained Loads	Loctite 330	Strain (με)	31	58	70	132	109	213	162	301	219	388
		%	39.4	74.5	39.7	75.9	40.2	78.1	43.3	80.3	45.5	81.0
	Loctite 392	Strain (με)	33	67	76	147	124	235	181	329	239	423
		%	41.9	86.0	43.1	84.5	45.8	86.1	48.3	87.7	49.7	88.3
	Loctite 410	Strain (με)	47	51	119	112	201	199	292	289	389	384
		%	90.3	104.1	94.4	92.6	95.7	96.1	96.4	97.0	96.3	97.2
	Loctite H3000	Strain (με)	8	18	19	21	43	51	68	86	105	127
		%	14.9	36.4	15.0	17.3	20.4	24.6	22.5	28.8	25.9	32.1
	Loctite H3300	Strain (με)	35	47	64	77	94	113	127	144	154	177
		%	28.3	39.3	27.7	34.4	28.7	34.6	29.7	34.3	29.7	34.6
	Loctite H4500	Strain (με)	17	24	29	41	27	70	5	103	33	148
		%	13.6	19.9	12.5	18.4	8.1	21.4	1.2	24.6	6.4	28.9
	Plexus MA820	Strain (με)	63	87	124	154	176	219	231	280	279	338
		%	40.0	56.0	41.7	51.9	42.5	52.3	43.5	52.8	44.1	53.1
	Pliogrip 7771	Strain (με)	57	93	111	172	168	255	226	337	281	420
		%	36.2	59.9	37.4	57.9	40.5	60.8	42.6	63.6	44.4	66.0

* Note: All FOSs = 15x20mm SMSs

www.manaraa.com

influence, if any, on the mechanical strain measurement error observed in CT3. Considering all identified factors contributing to viscoelasticity (See Section 2.5.1), the only factor that varied during CT3 was the laboratory temperature, which was previously recognized from CT3 results as the factor having an inverse relationship with mechanical strain measurement error. Through literature review, it was found that increasing the temperature of an adhesive is equivalent to sustaining a load for a longer period of time, and thus, allowing for more viscoelastic effects to take place [78]. By knowing the change in adhesive temperature, a time shift factor, a_T, can be calculated and used with appropriate results from stress relaxation and creep tests to determine the properties of the adhesive at the new temperature.

While a_T cannot be quantified from the limited testing that was conducted in this research, it is conceptually presented to illustrate the effect of temperature on FOS mechanical strain measurement in CT3. In Fig. 3.31 the CT5 viscoelastic behavior of Loctite 392 at temperature, T_0 = 71.5°F (21.9°C), has been presented and has been considered for new test temperatures T_1 and T_2, where $T_2>T_1>T_0$. To determine a strain at time = t for a new test temperature = T_i, the FOS results for T_0 are evaluated at time = $t+a_T$. With this approach, a_{T1} and a_{T2} were the shift factors used for T_1 and T_2, respectively, to determine $E_{L,T1}$, $E_{R,T1}$, $E_{L,T2}$, and $E_{R,T2}$, which are the extrema for each temperature. Finally, using the new extrema and the data reduction process used for cyclic loading in CT1-CT3, measured mechanical strains $\Delta\mu\varepsilon_0$, $\Delta\mu\varepsilon_1$, and $\Delta\mu\varepsilon_2$ for T_0, T_1, and T_2, respectively, have been conceptually displayed. As illustrated, there is an inverse relationship between the temperature and measured mechanical strains; the measured mechanical strains decrease and increase as the adhesive temperature increases and decreases, respectively. This is the exact behavior observed in Figs. 3.19 - 3.22.

3.3.5.4 CT5 Conclusions

The following additional conclusions were determined considering all testing through CT5:

- The adhesive used to bond the foil sensors to Coupon B did not experience viscoelastic behavior, and thus, time-dependent error did not exist for the foil sensors when subjected to sustained loads.

www.manaraa.com

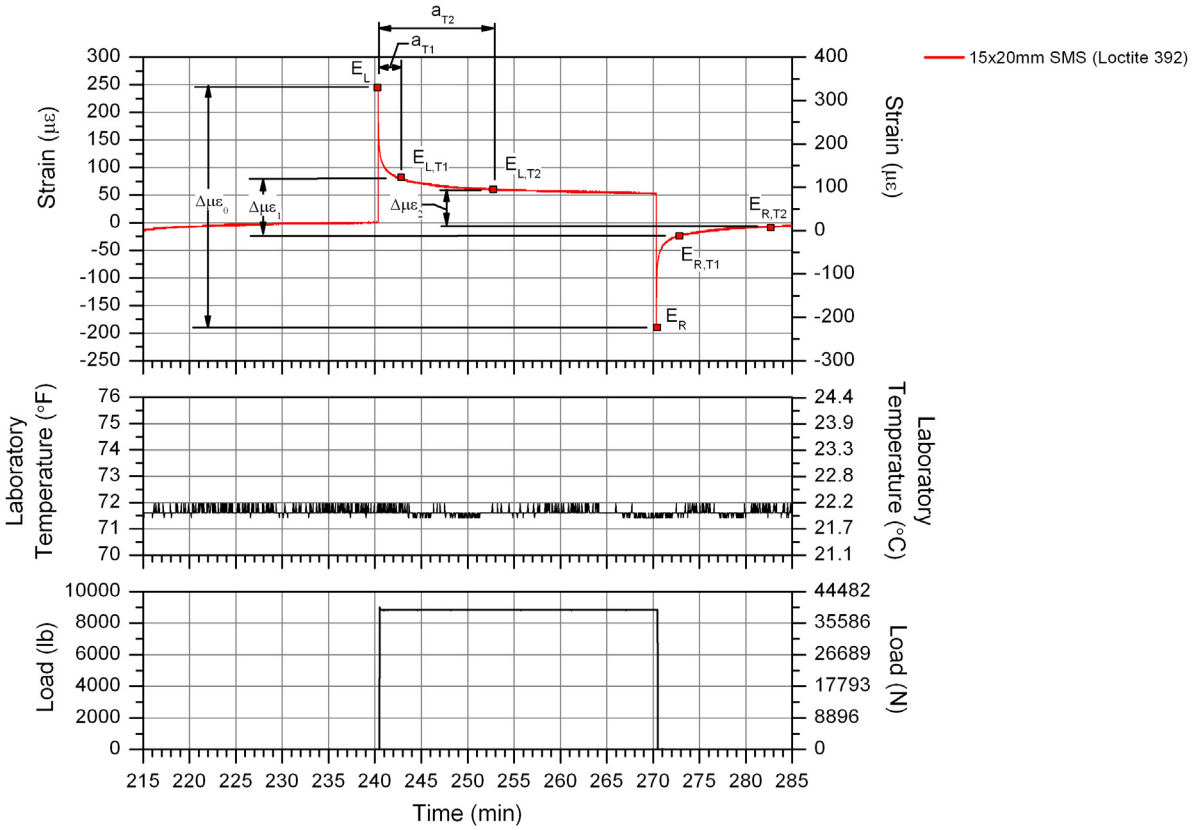

Figure 3.31. Impact of temperature change on viscoelastic adhesive behavior and FOS results.

- All adhesives used to bond the eight 15x20mm SMSs to Coupon B experienced viscoelastic behavior during sustained loading, and thus, the error of each sensor increased as a function of time.

- Examining the measurement error for each FOS immediately after load application, most of the 15x20mm SMSs had considerable error even before viscoelasticity occurred in the adhesive, and the magnitude of the immediate error was variable among the eight adhesives utilized in CT5. Thus, it is still thought that the immediate error was the result of inadequate strength of the adhesive to fully develop the CFRP packaging.

- Further examination is required to determine the following:
  - The influence of loading rate and amplitude on the performance of the 15x20mm SMS/adhesive combinations.
  - The impact of FOS packaging on viscoelasticity in the adhesives.

3.3.6 Coupon Test 6 (CT6)

3.3.6.1 CT6 Objectives and Testing Procedure

The objective of Coupon Test 6 (CT6) was to investigate the influence of loading rate and amplitude on the performance of the 15x20mm SMS/adhesive combinations during temperature

www.manaraa.com

fluctuations. Specifically, it was desired to determine if the inverse relationship between mechanical strain measurement error and temperature fluctuations (due to viscoelasticity) existed in the 15x20mm SMSs and adhesives when they were subjected to the loading conditions that were expected in the cut-back regions of the US30 bridge. Coupon B and associated sensors with respective adhesives presented in Fig. 3.14 were again utilized in CT6.

To achieve the objectives of CT6, Coupon B was subjected to tensile cyclic loading producing amplitudes of approximately 200με for 30,300 cycles at 0.35 Hz; the frequency and amplitude of the loading was determined from a preliminary field test on the US30 bridge. During CT6, a si425-500 interrogator recorded FOS strains continuously at 125 Hz, which was previously identified as the DAR for the FCB SHM system. The Megadac as well as the Flextest GT Controller and MPT Software recorded foil sensor strains and cyclic loads, respectively, at 125 Hz for 15 continuous seconds at the beginning of each hour of testing.

3.3.6.2 CT6 Results

Results from CT6 were reduced with the same methods as those in CT1, CT2, and CT3. Figures 3.32 - 3.39 present summaries of CT6 results, and Table 3.6 presents FOS error analysis results. Examination of Figs. 3.32 - 3.35 once again reveals that FOS results include both temperature-induced and mechanical strains, while the foil sensor results only include mechanical strains; Figures 3.36 - 3.39 present the amplitudes of the FOSs for the 30,300 cycles and illustrates that only the 15x20mm SMS bonded with Loctite H4500 was able to achieve the strain levels subjected to the coupon. Comparison of Tables 3.3 and 3.6 reveals that the average error for each FOS/adhesive combination remained approximately the same between the tests regardless of the change in loading conditions. However, the CT6 temperature changed by five degrees Fahrenheit, but the inverse relationship between the FOS mechanical strain measurement error and temperature change was not evident in CT6 results. For the same temperature change in CT3, the inverse relationship was present in the FOS results.

www.manaraa.com

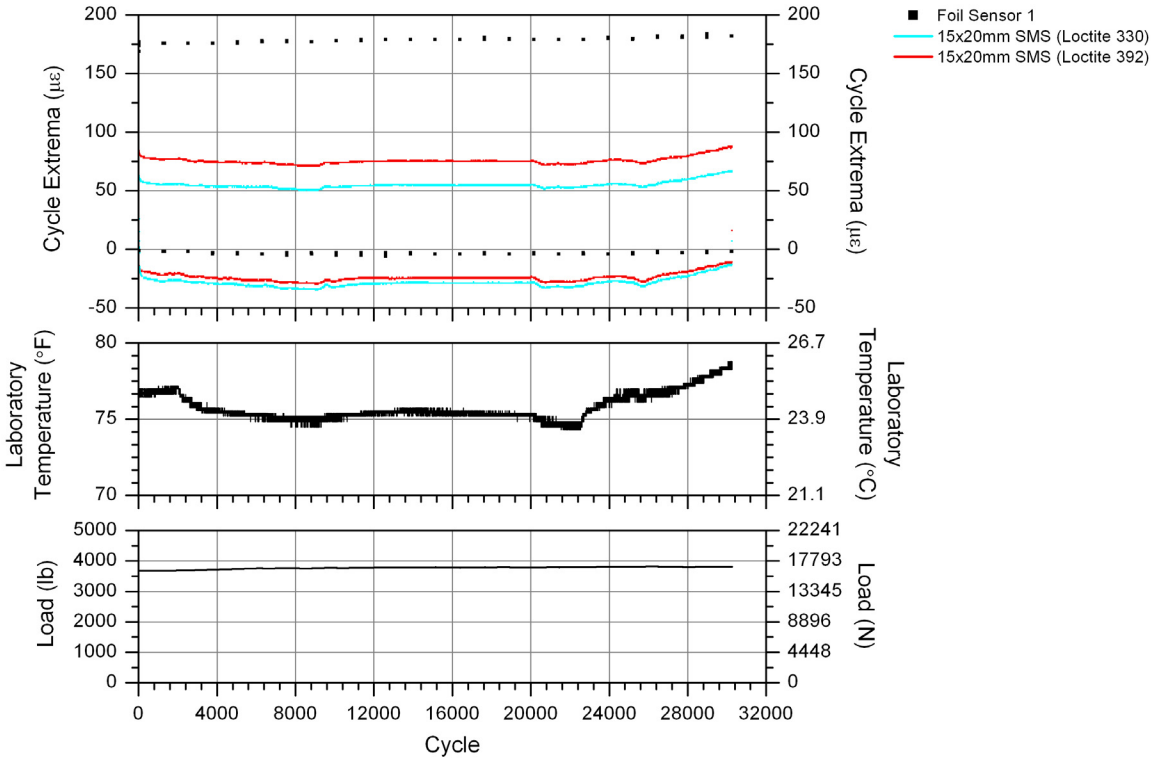

Figure 3.32. CT6: cycle extrema vs. cycle number for Coupon B, group 1 sensors.

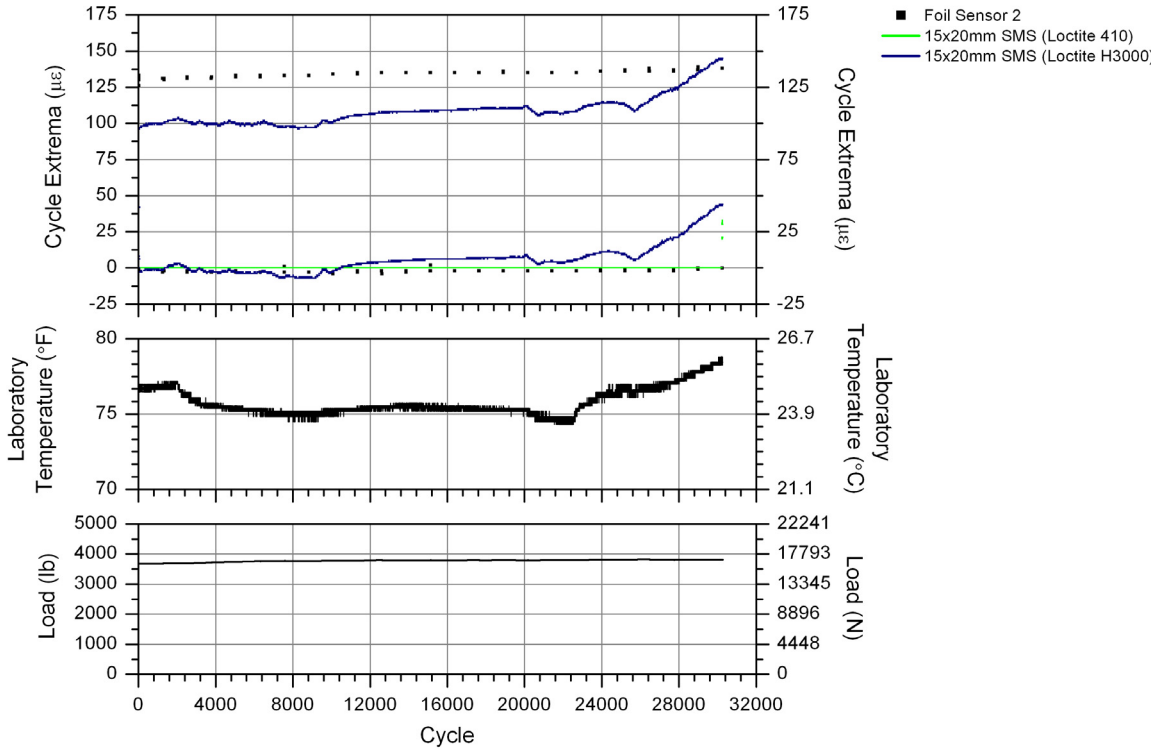

Figure 3.33. CT6: cycle extrema vs. cycle number for Coupon B, group 2 sensors.

www.manaraa.com

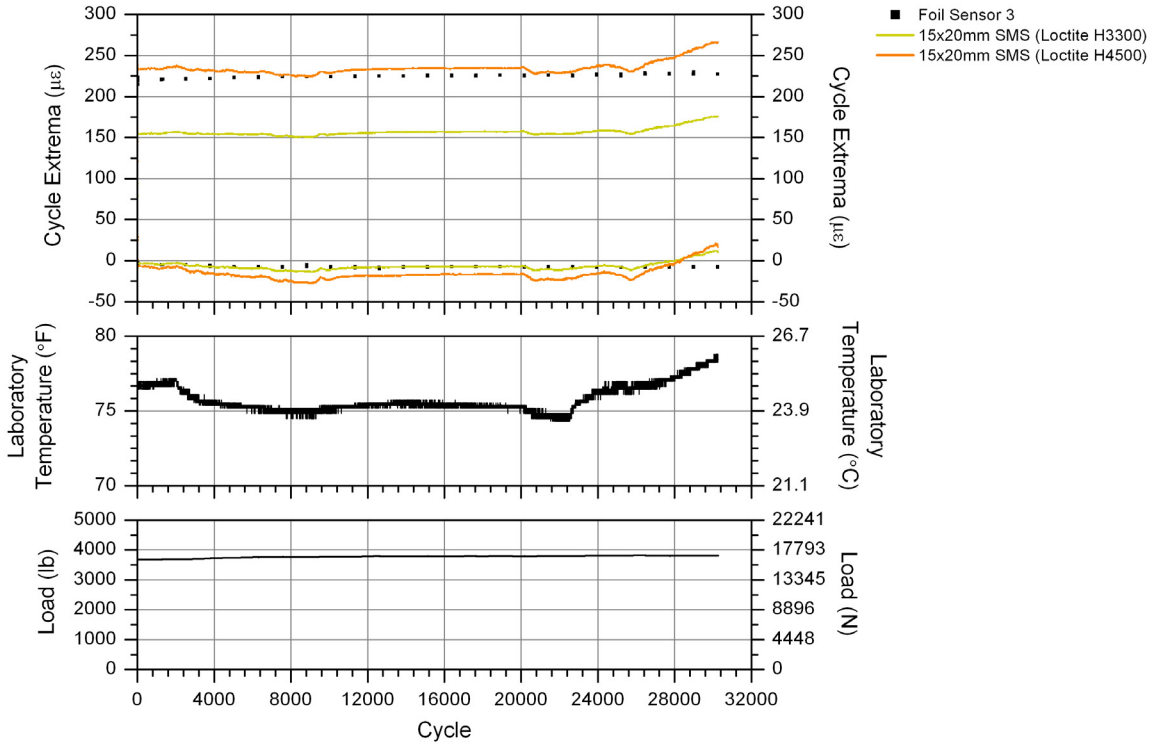

Figure 3.34. CT6: cycle extrema vs. cycle number for Coupon B, group 3 sensors.

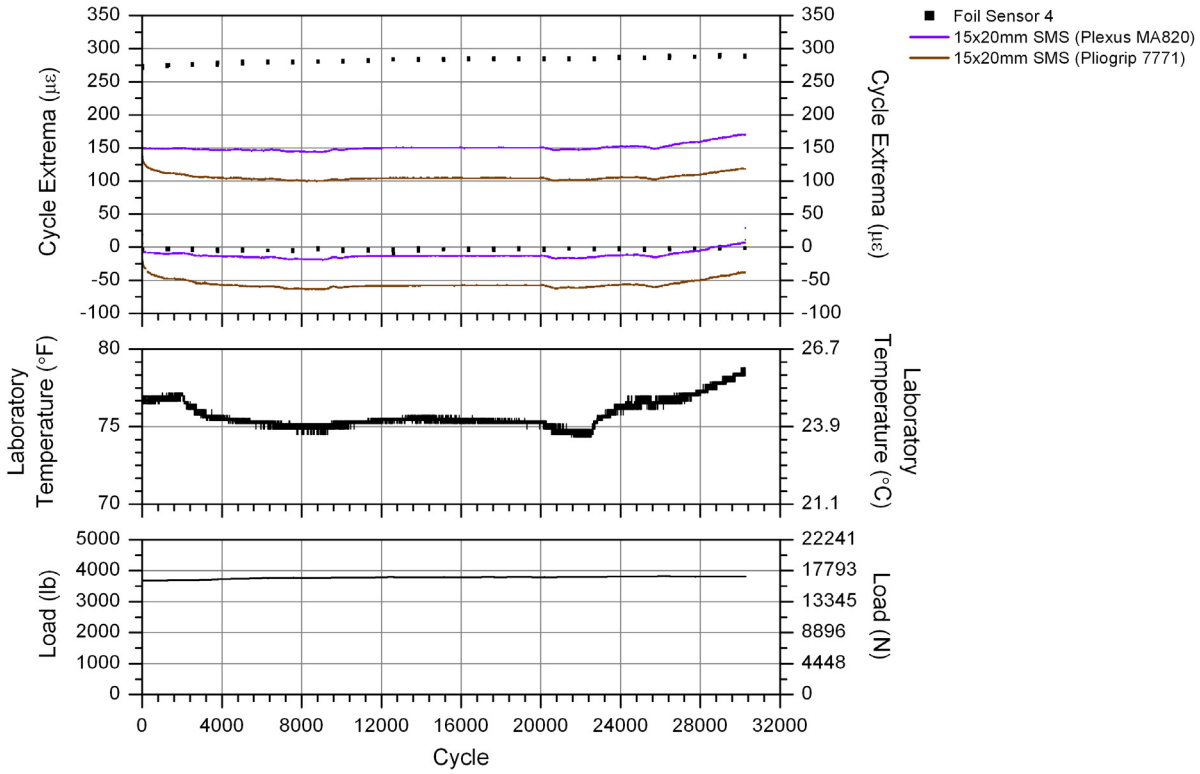

Figure 3.35. CT6: cycle extrema vs. cycle number for Coupon B, group 4 sensors.

www.manaraa.com

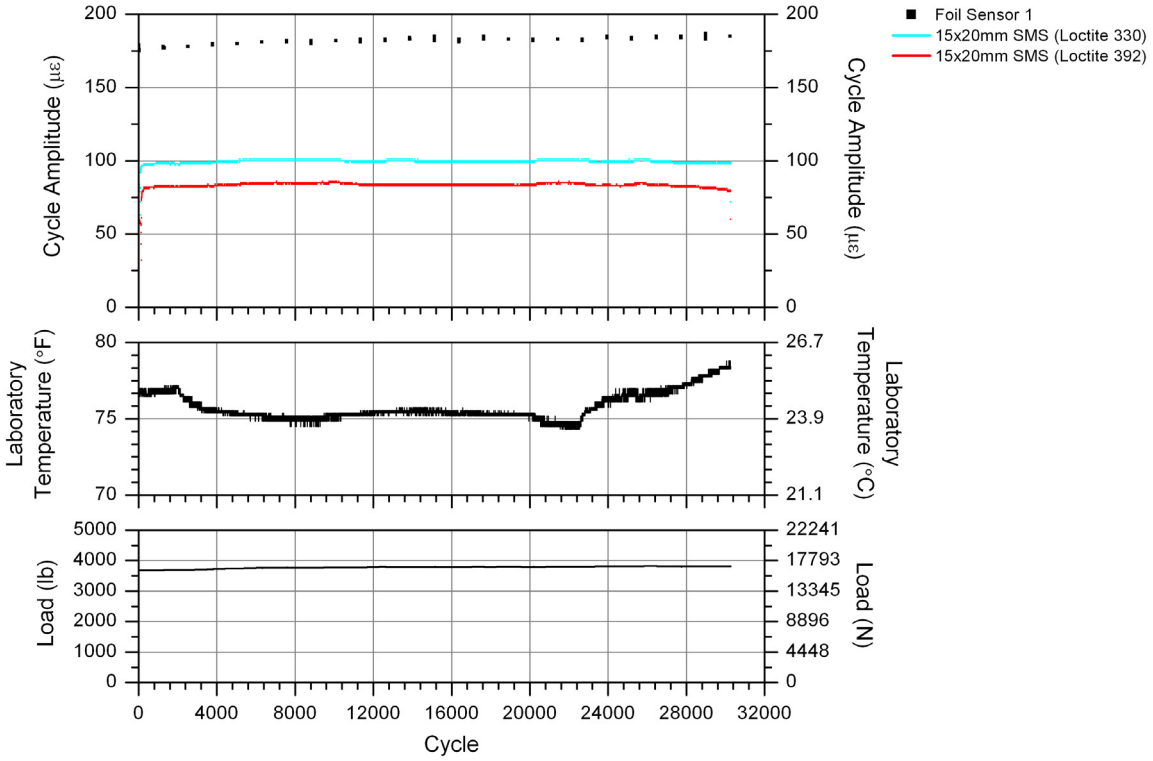

Figure 3.36. CT6: cycle amplitude vs. cycle number for Coupon B, group 1 sensors.

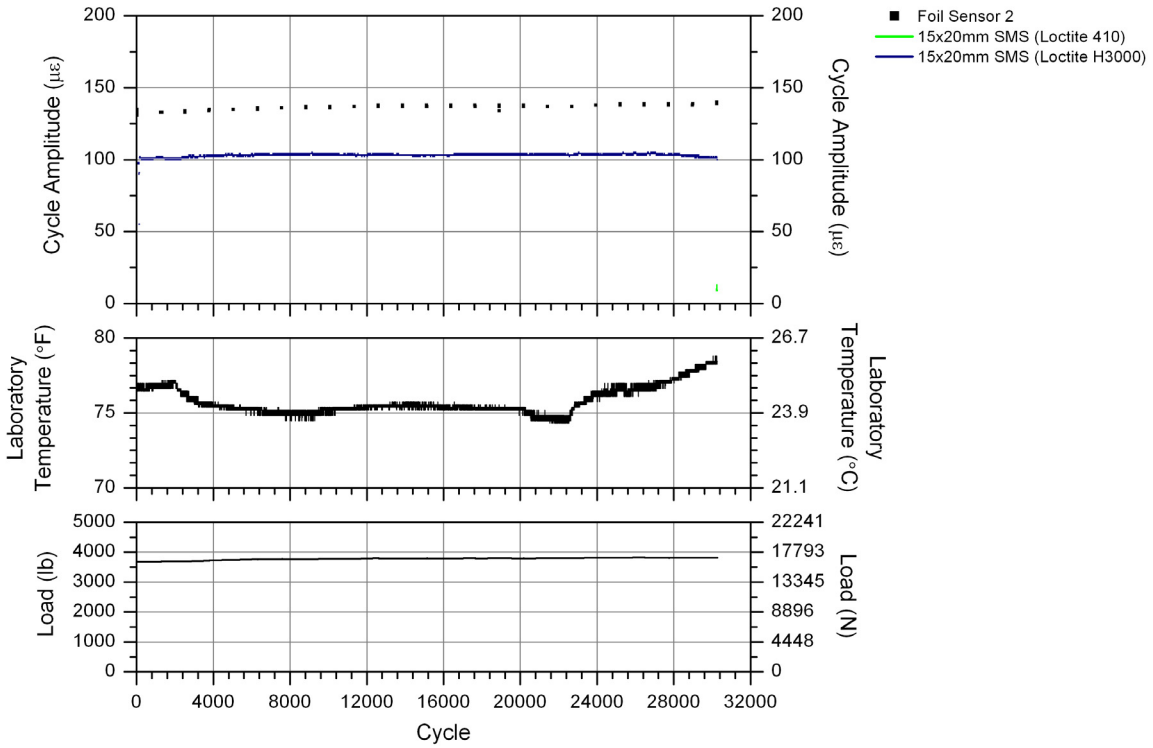

Figure 3.37. CT6: cycle amplitude vs. cycle number for Coupon B, group 2 sensors.

www.manaraa.com

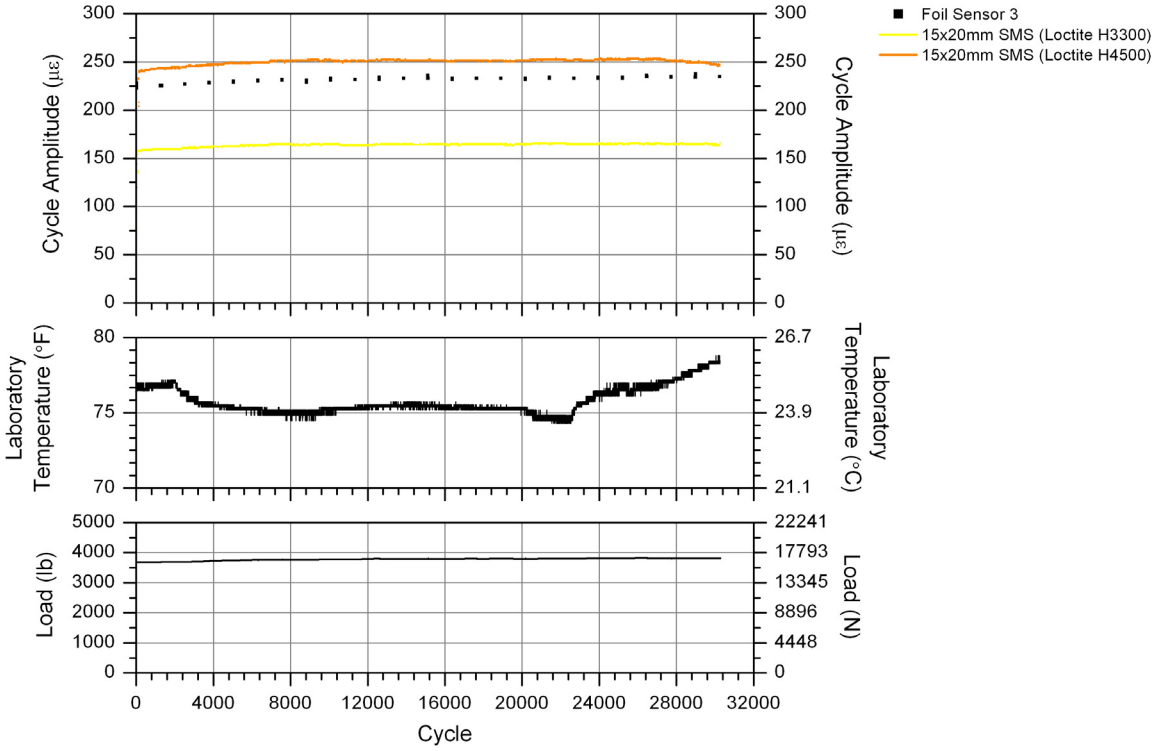

Figure 3.38. CT6: cycle amplitude vs. cycle number for Coupon B, group 3 sensors.

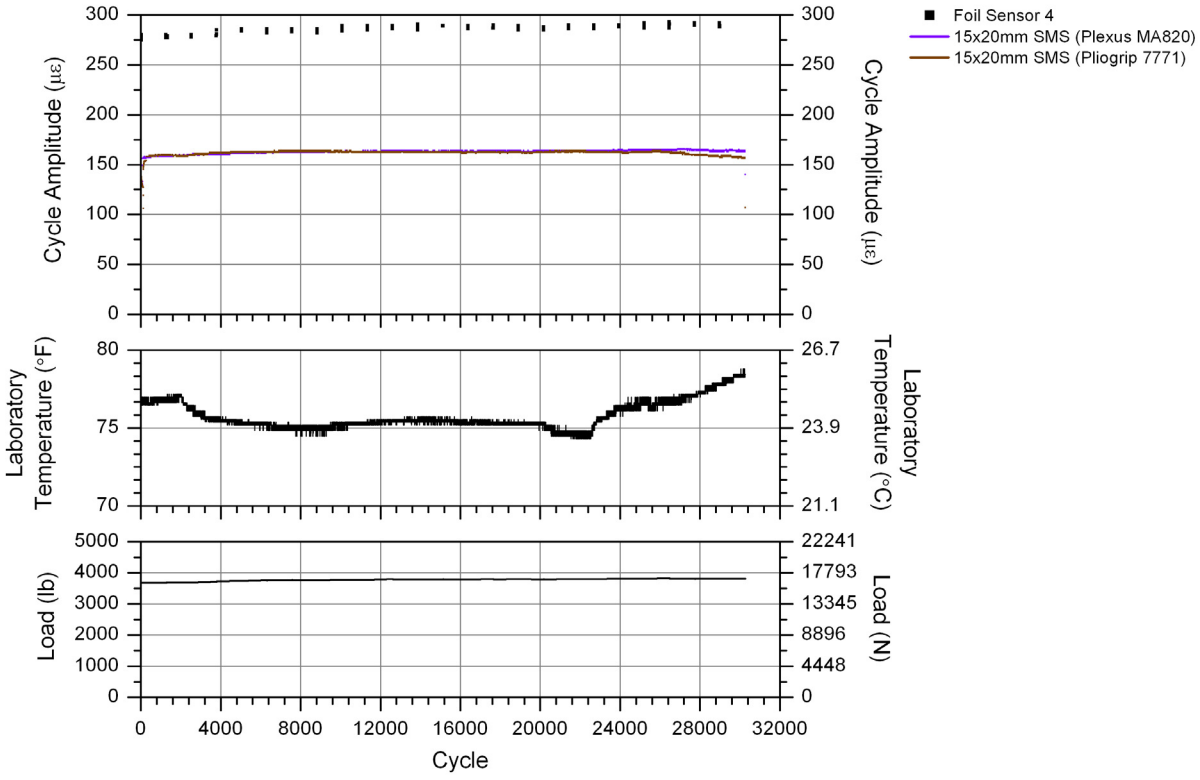

Figure 3.39. CT6: cycle amplitude vs. cycle number for Coupon B, group 4 sensors.

www.manaraa.com

Table 3.6. Error analysis results for FOSs in CT6.

CT6 Loading	Adhesive *	Error Statistics							
		Minimum		Maximum		Average		Standard Deviation	
		Strain (με)	%	Strain (με)	%	Strain (με)	%	Strain (με)	%
30,300 cycles @ 200με	Loctite 330	78	44.1	95	53.1	84	45.9	3.4	2.03
	Loctite 392	94	53.0	118	65.9	100	55.1	5.2	3.15
	Loctite 410	122	93.1	140	100.0	136	99.5	4.0	1.84
	Loctite H3000	30	22.4	39	28.1	34	25.0	1.6	1.05
	Loctite H3300	65	28.4	74	31.6	68	29.5	1.5	0.47
	Loctite H4500	5	2.2	22	9.6	18	7.6	3.0	1.30
	Plexus MA820	118	42.3	131	46.8	124	43.4	2.7	0.88
	Pliogrip 7771	117	41.9	144	51.4	126	44.0	5.6	2.06

* Note: All FOSs = 15x20mm SMSs

3.3.6.3 CT6 Conclusions

The following additional conclusions were determined considering all testing through CT6:

- Changing the loading rate and magnitude resulted in essentially no change in the average error for any FOS. However, the inverse relationship between FOS mechanical strain measurement error and temperature fluctuation was not present. Thus, the changes in loading rate and magnitude reduced the influence of viscoelasticity in the adhesive.
- The 15x20mm SMS bonded with Loctite H4500 was determined to be a suitable combination for measuring mechanical strains in the cut-back regions of the FCBs. This conclusion was based on the accuracy demonstrated in CT3 and CT6, and as well as the insensitivity to temperature fluctuations demonstrated in CT6 while being subjected to typical FCB mechanical strains.
- Further examination is required to determine the impact of FOS packaging on viscoelasticity in the adhesives.

3.3.7 Coupon Test 7 (CT7)

3.3.7.1 CT7 Objectives and Testing Procedure

The objective of Coupon Test 7 (CT7) was to investigate the change in FOS accuracy and adhesive viscoelasticity while measuring cyclic loads with the CFRP packaging removed from the FBGs. Coupon C and associated sensors with respective adhesives used in CT7 are presented in Fig. 3.40; the coupon loading conditions, FOS adhesives, and foil sensors were exactly the same as those used in CT3. However, the FOSs used were unpackaged FBGs identical to those embedded in the CFRP packaging of the 15x20mm SMSs. As previously mentioned, these FBGs were 5mm long and utilized polyimide recoating. To aid installation of these eight unpackaged FBGs, they were first

www.manaraa.com

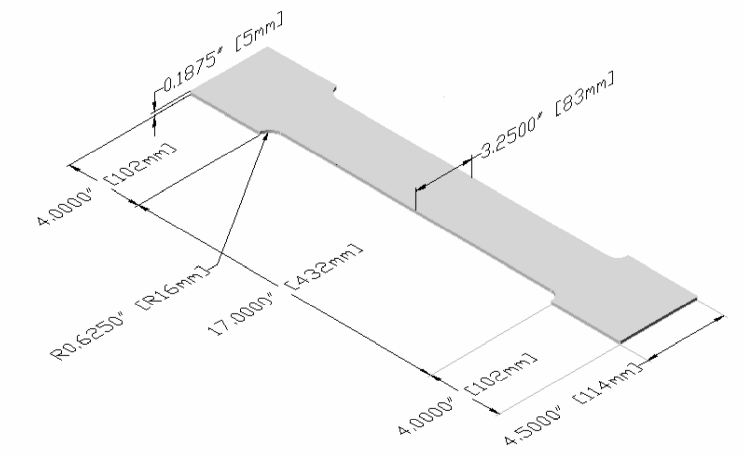

a. Coupon C

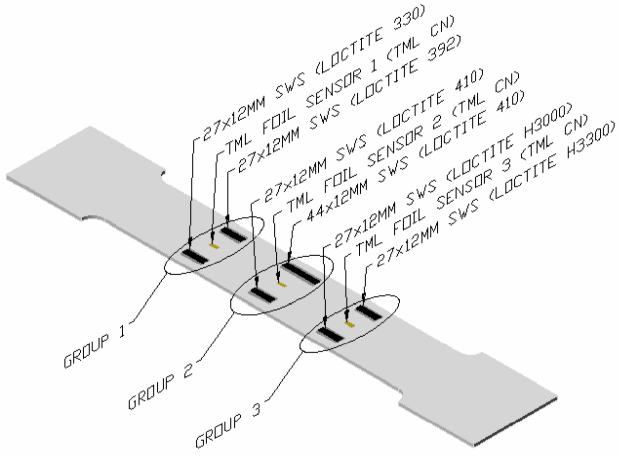

b. Coupon C: side 1 sensors and adhesives

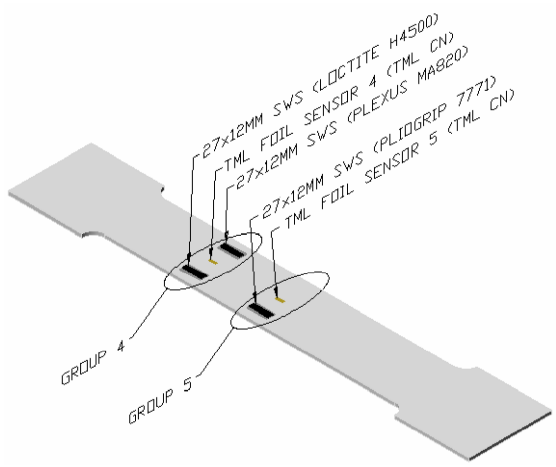

c. Coupon C: side 2 sensors and adhesives

Figure 3.40. Coupon C, sensors, and adhesives used in CT7.

www.manaraa.com

bonded to a 27x12mm stainless steel shim with the desired adhesive, and then they were spot welded to Coupon C with a Vishay Micro-Measurements Model 700 Portable Strain Gage Welding Unit. These FOSs are referred to as 27x12mm surface weldable sensors (SWSs). In addition, one 10mm FBG with acrylate recoating was bonded a 44x12mm stainless steel shim and spot welded to Coupon C; this FOS is referred to as the 44x12mm SWS. The nine FOSs and five foil sensors were organized into five groups as illustrated in Fig. 3.40. This setup allowed comparison of CT3 and CT7 results to reveal the change in FOS accuracy and adhesive viscoelasticity due to the removal of the CFRP packaging. In addition, comparison of the 44x12mm SWS and 27x12mm SWS with Loctite 410 adhesive within CT7 results revealed the impact of the FBG recoating type on FOS performance under cyclic loads.

To achieve the objectives of CT7, Coupon C was subjected to tensile cyclic loading producing amplitudes of approximately 500με for 360,000 cycles at 4.0 Hz. During CT6, a si425-500 interrogator recorded FOS strains continuously at 250 Hz. The Megadac as well as the Flextest GT Controller and MPT Software were programmed to record foil sensor strains and cyclic loads, respectively, at 250 Hz for five continuous seconds at the beginning of each hour of testing. However, the Megadac system malfunctioned during the test and recorded the first 5,200 cycles continuously at 250 Hz. Since the foil sensors proved to be stable with repeatable behavior in previous coupon tests, the 5,200 cycles of acquired information were used to establish calibrated relationships with the loading information. With these relationships, projected foil sensor results were generated for the remaining portion of CT7 and are thought to be in good agreement with those that would have been measured.

3.3.7.2 CT7 Results

Results from CT7 were reduced with the same methods as those in CT1, CT2, CT3, and CT6. Figures 3.41 - 3.50 present summaries of CT7 results, and Table 3.7 presents FOS error analysis results. Examination of Figs. 3.41 - 3.45 once again revealed that FOS results include both temperature- induced and mechanical strains. However, the residual strains in cyclic loading that were identifiable in previous tests through significant offsets of the minima extreme values were not

www.manaraa.com

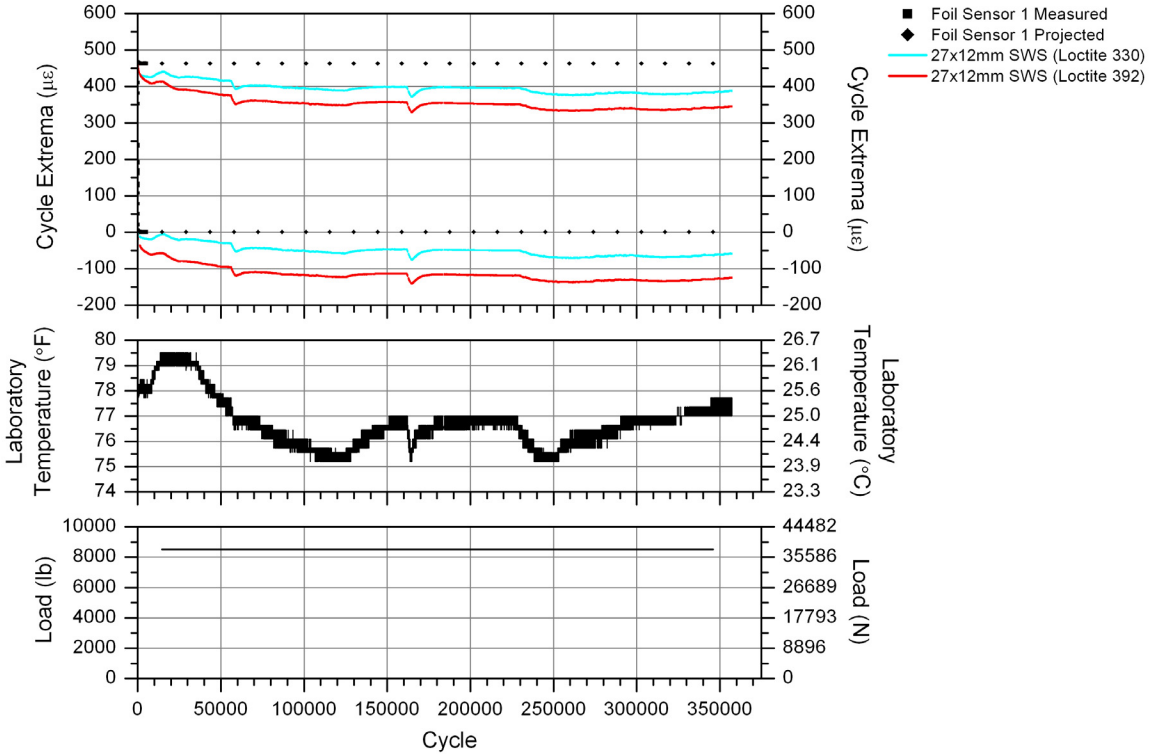

Figure 3.41. CT7: cycle extrema vs. cycle number for Coupon C, group 1 sensors.

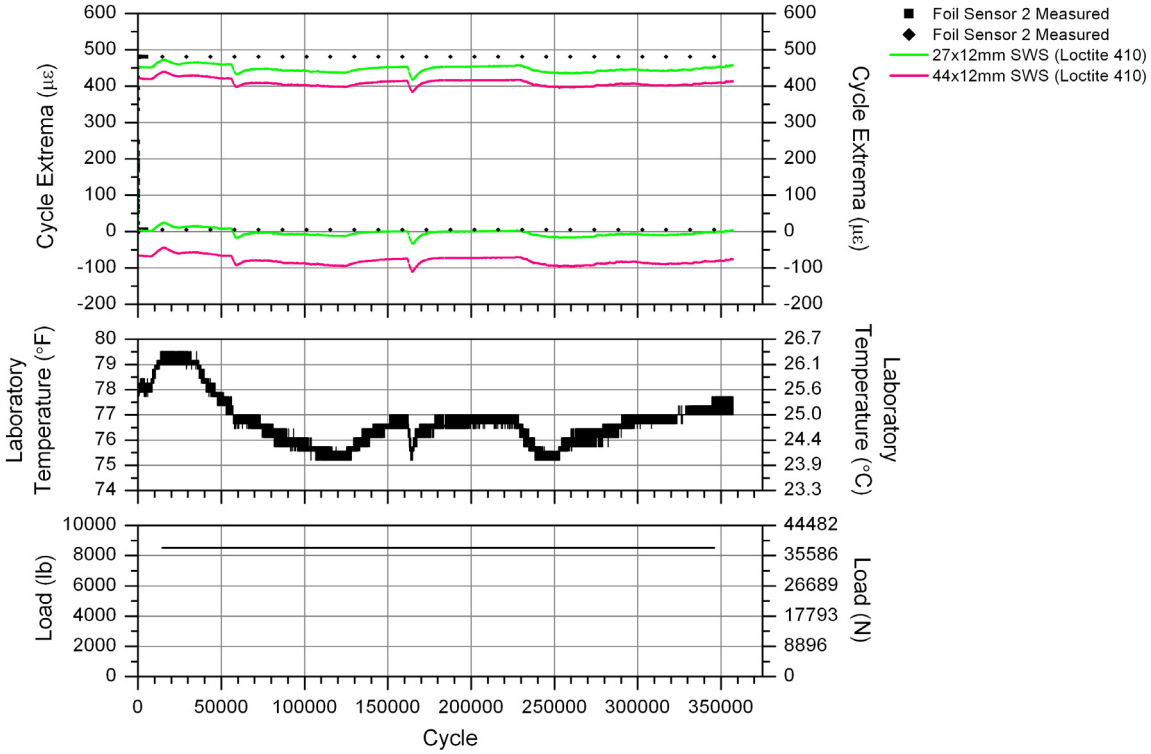

Figure 3.42. CT7: cycle extrema vs. cycle number for Coupon C, group 2 sensors.

www.manaraa.com

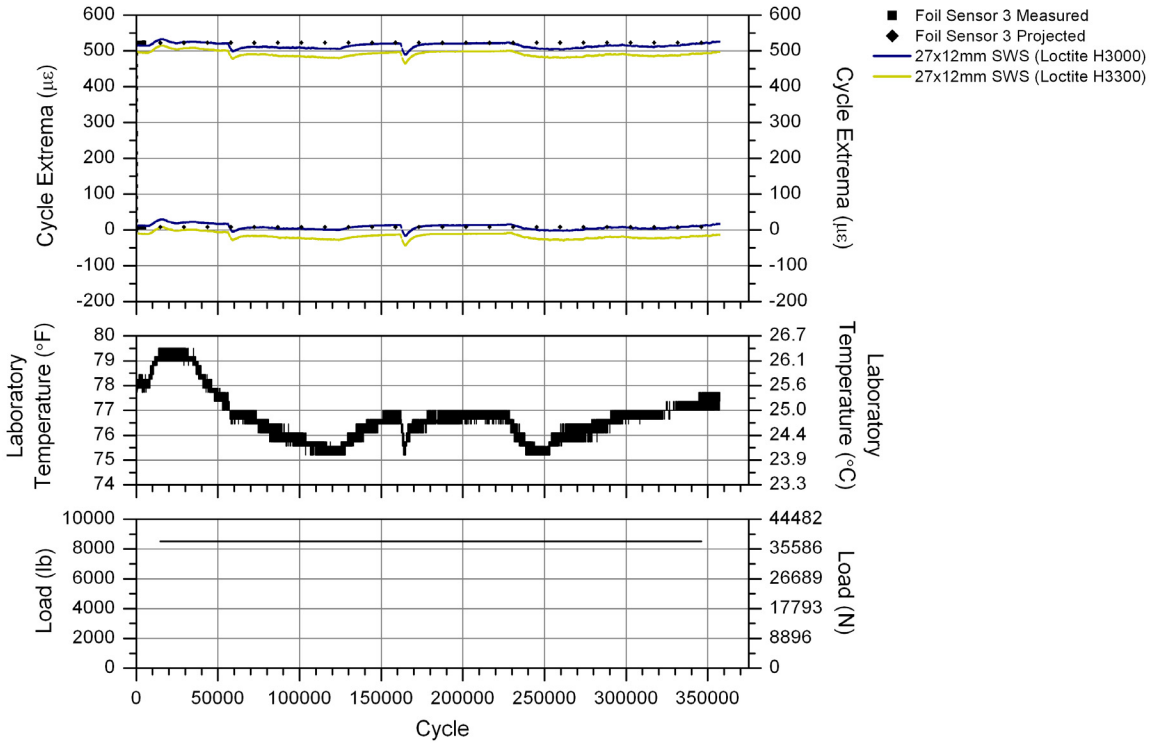

Figure 3.43. CT7: cycle extrema vs. cycle number for Coupon C, group 3 sensors.

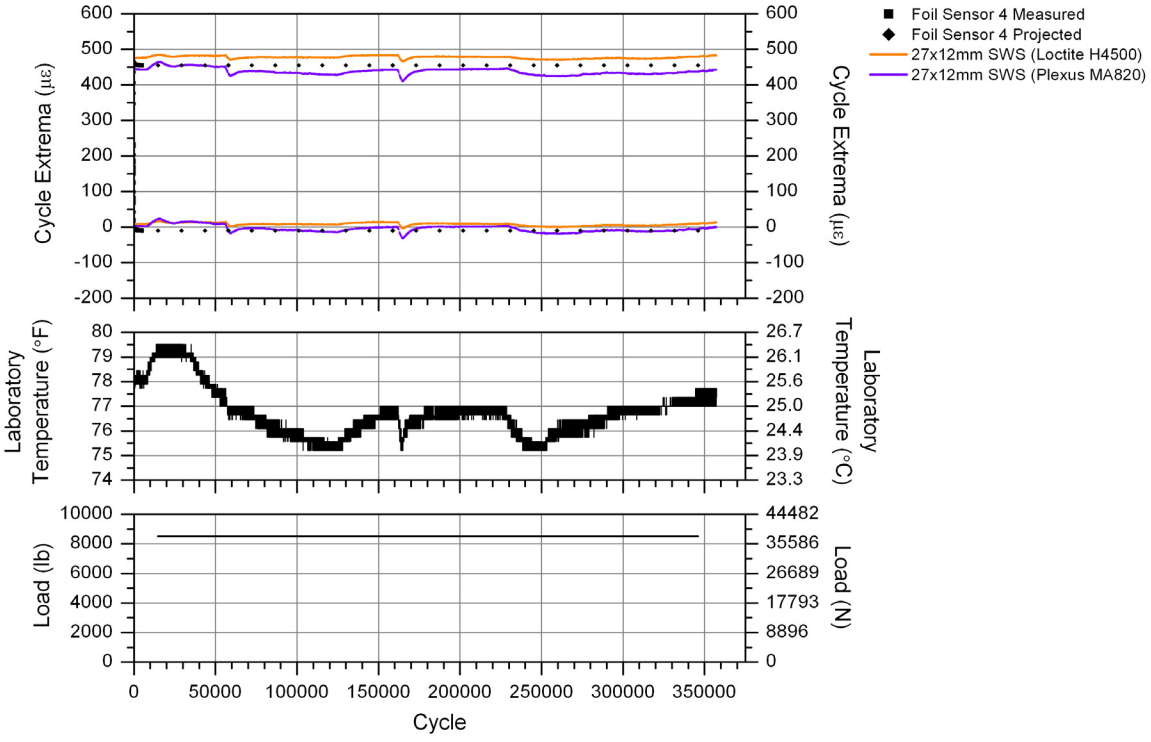

Figure 3.44. CT7: cycle extrema vs. cycle number for Coupon C, group 4 sensors.

www.manaraa.com

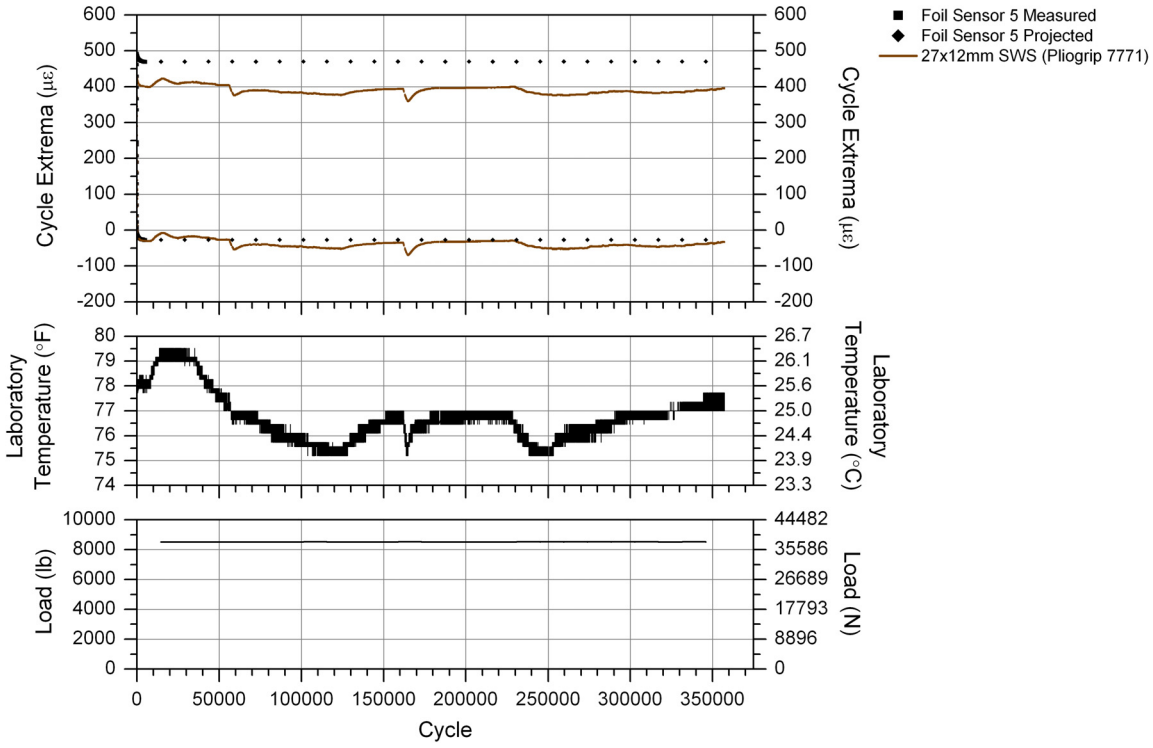

Figure 3.45. CT7: cycle extrema vs. cycle number for Coupon C, group 5 sensors.

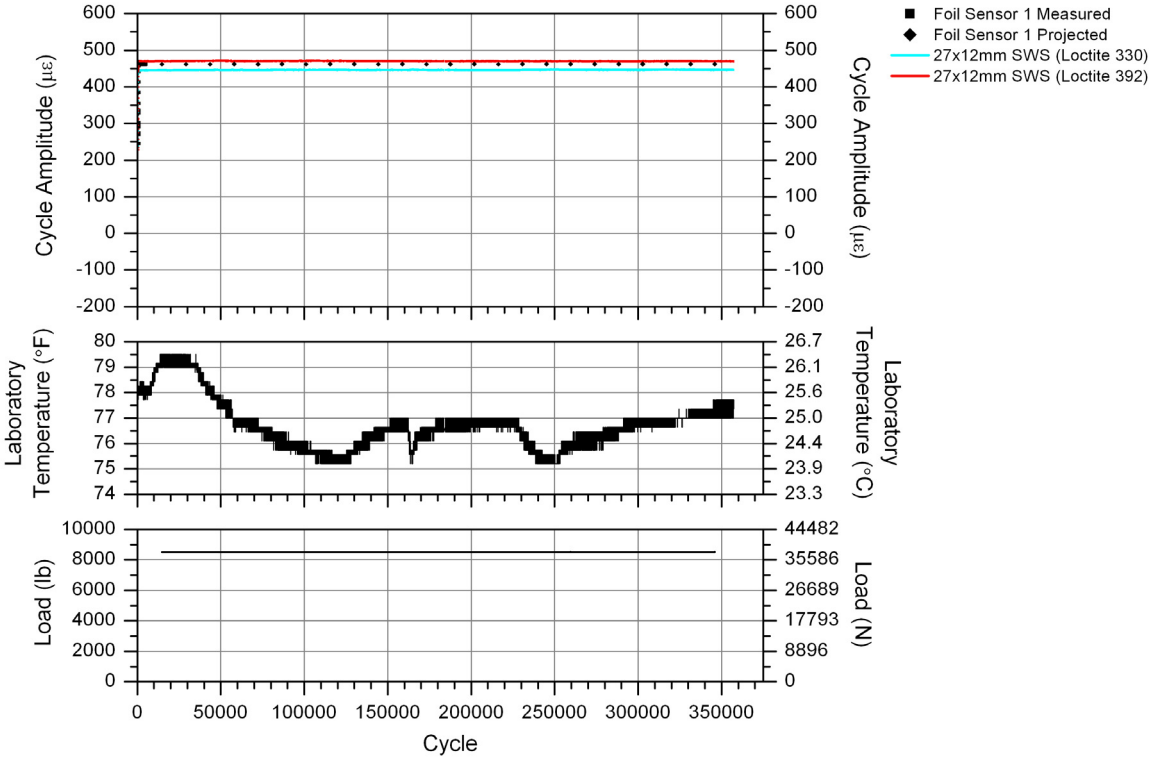

Figure 3.46. CT7: cycle amplitude vs. cycle number for Coupon C, group 1 sensors.

www.manaraa.com

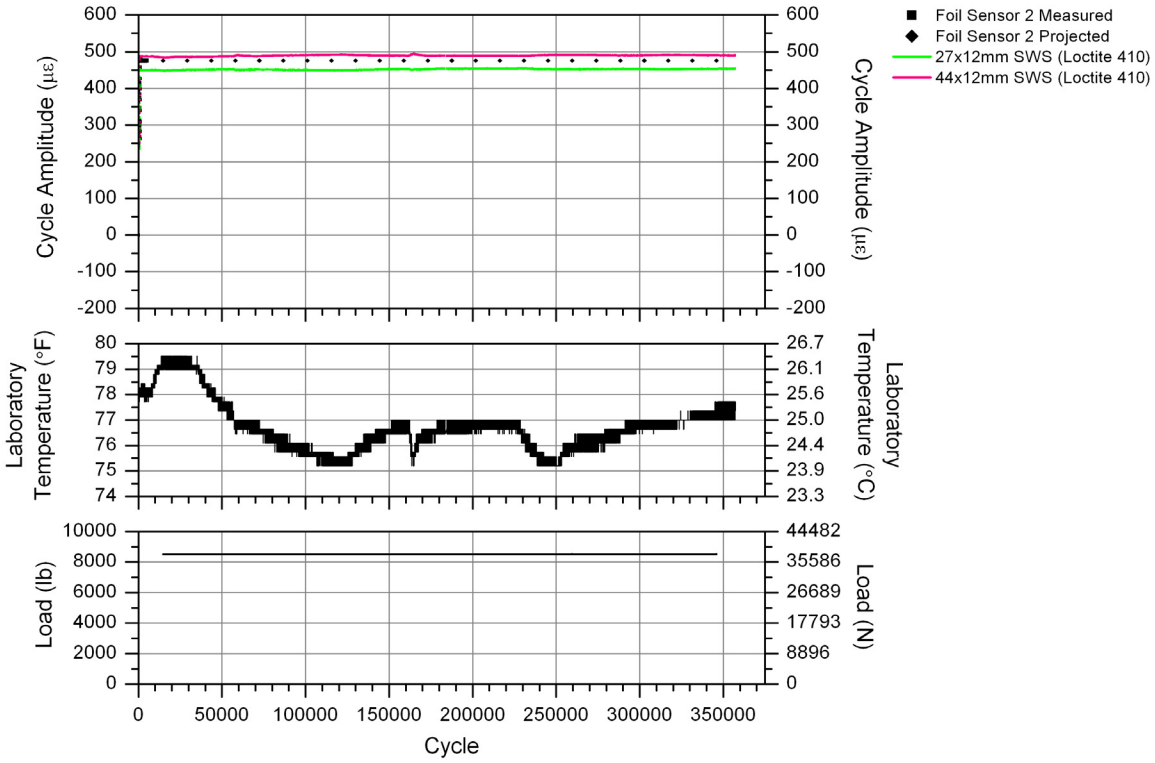

Figure 3.47. CT7: cycle amplitude vs. cycle number for Coupon C, group 2 sensors.

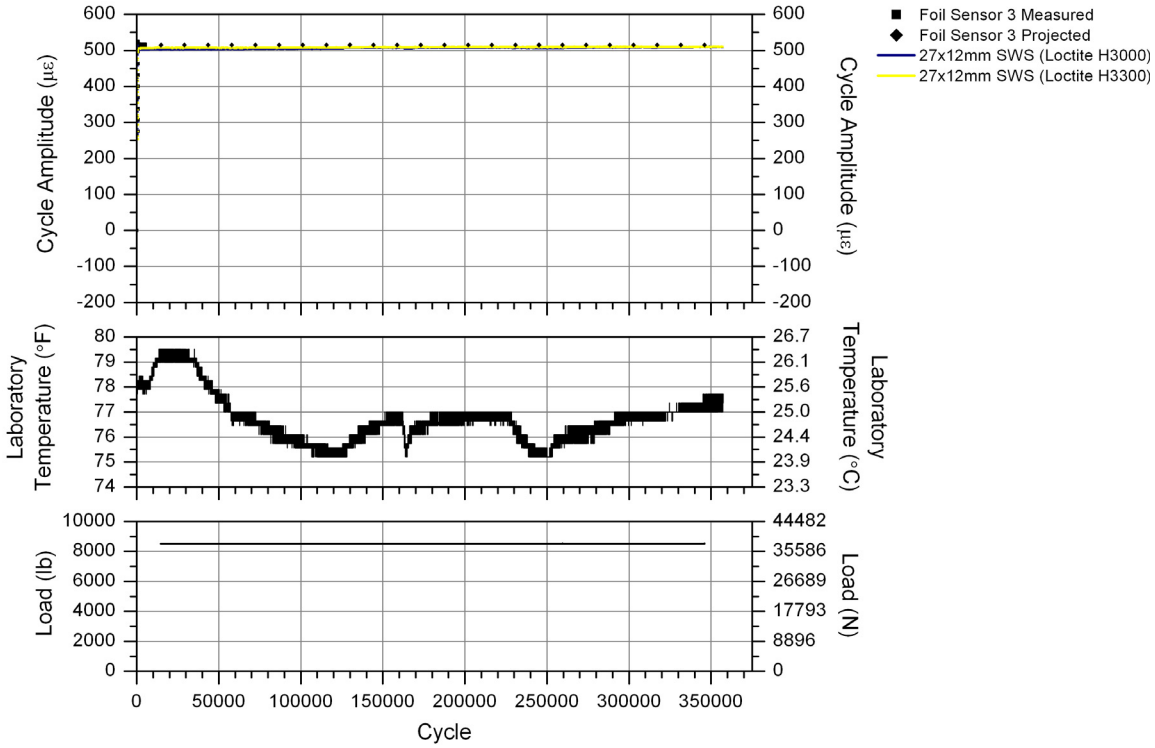

Figure 3.48. CT7: cycle amplitude vs. cycle number for Coupon C, group 3 sensors.

www.manaraa.com

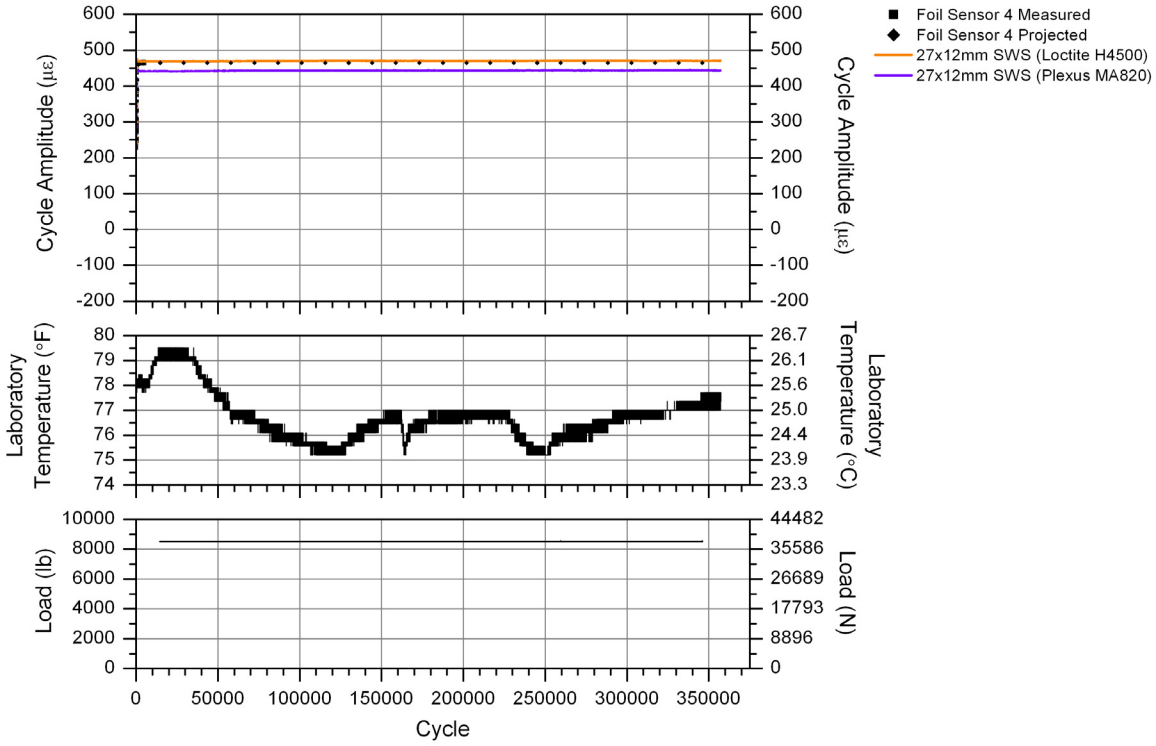

Figure 3.49. CT7: cycle amplitude vs. cycle number for Coupon C, group 4 sensors.

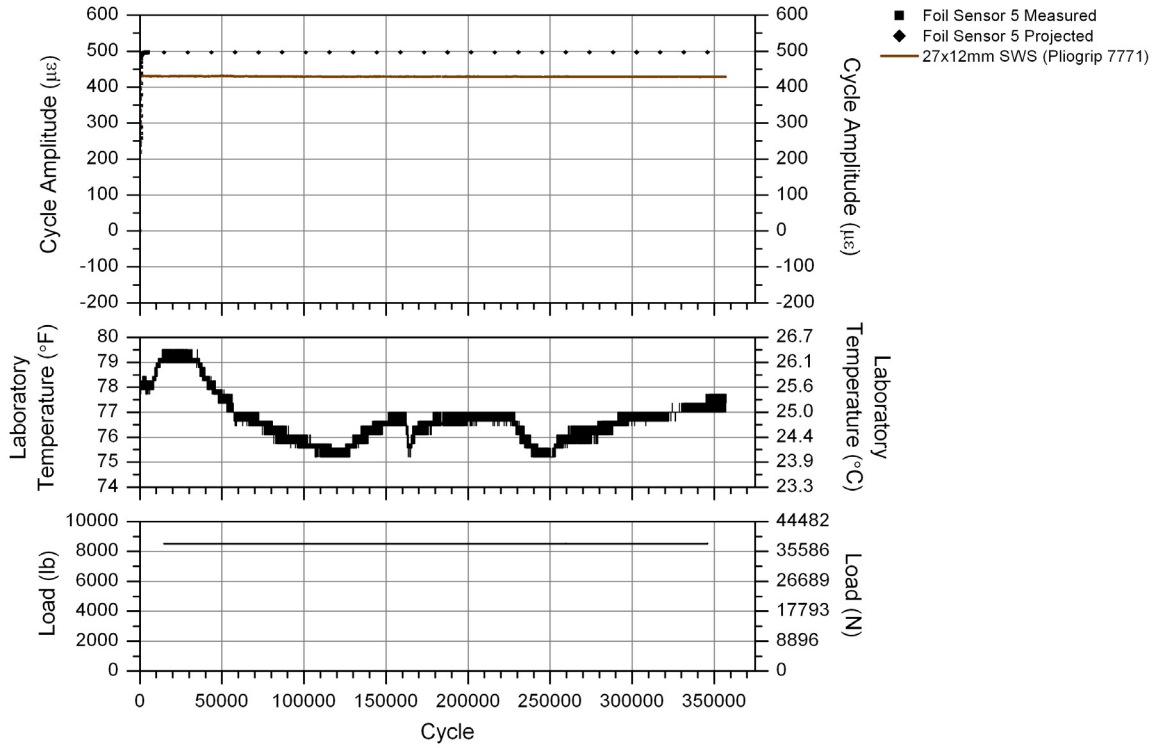

Figure 3.50. CT7: cycle amplitude vs. cycle number for Coupon C, group 5 sensors.

www.manaraa.com

Table 3.7. Error analysis results for FOSs in CT7.

CT7 Loading	Adhesive	Error Statistics							
		Minimum		Maximum		Average		Standard Deviation	
		Strain (με)	%	Strain (με)	%	Strain (με)	%	Strain (με)	%
360,000 cycles @ 500με	Loctite 410 *	9	1.8	18	3.7	14	2.9	1.9	0.39
	Loctite 330 **	14	3.0	18	3.9	16	3.5	0.7	0.15
	Loctite 392 **	6	1.3	10	2.2	8	1.8	0.7	0.15
	Loctite 410 **	20	4.3	27	5.8	24	5.0	1.5	0.32
	Loctite H3000 **	5	1.0	13	2.5	8	1.6	1.8	0.34
	Loctite H3300 **	4	0.8	9	1.8	7	1.3	1.2	0.23
	Loctite H4500 **	3	0.7	7	1.4	5	1.1	0.8	0.16
	Plexus MA820 **	20	4.4	24	5.3	22	4.7	0.8	0.17
	Pliogrip 7771 **	66	13.2	70	14.1	68	13.7	0.8	0.16

Note: * 44x12mm SWS

** 27x12mm SWS

present for most FOS results in CT7. Figures 3.46 - 3.50 present the amplitudes of the FOSs and illustrate that all FOS/adhesive combinations, except for the 27x12mm SWS with Pliogrip 7771, were able to accurately measure the mechanical strains subjected to Coupon C. Comparison of Tables 3.3 and 3.7 revealed significantly reduced average errors for the FOSs due to the removal of the 15x20mm CFRP packaging.

3.3.7.3 CT7 Conclusions

The following additional conclusions were determined considering all testing through CT7:

- Removal of the 15x20mm CFRP packaging from the FBGs reduced the stiffness of each FOS, which also reduced the strength demands on the adhesives. As a result, each FOS had significantly less measurement error. In addition, viscoelasticity causing the adhesives to be sensitive to temperature changes diminished.
- Except for Pliogrip 7771, the tested adhesives proved to be adequate for use with unpackaged FBGs for the cyclic loading conditions in CT7.
- The acrylate recoating of the 10mm FBG in the 44x12mm SWS appeared to have no affect on measurement accuracy during the cyclic loading of CT7. This is consistent with the results of CT1 and CT2.
- Further examination is required to determine the impact of FOS packaging on FOS and adhesive performances during sustained loads.

www.manaraa.com

3.3.8 Coupon Test 8 (CT8)

3.3.8.1 CT8 Objectives and Testing Procedure

The objective of Coupon Test 8 (CT8) was to investigate the change in FOS accuracy and adhesive viscoelasticity while measuring sustained loads with the CFRP packaging removed from the FBGs. Coupon C and associated sensors with respective adhesives presented in Fig. 3.40 were used again in CT8; the coupon loading conditions, FOS adhesives, and foil sensors were exactly the same as those used in CT5. Just as CT7 was comparable to CT3 to reveal the influence of the CFRP packaging on cyclic loading measurements, comparison of CT8 and CT5 revealed the influence of the CFRP packaging on FOS accuracy and adhesive viscoelasticity under sustained loads. In addition, comparison of the 44x12mm SWS and 27x12mm SWS with Loctite 410 adhesive within CT5 results showed the impact of the FBG recoating type on FOS performance under sustained loads.

To achieve the objectives of CT8, Coupon C was subjected to five tensile loads, each of which was statically sustained for 30 minutes and then released for 30 minutes before the next load was applied. The five sustained tensile loads were applied to produce approximately 100με, 200με, 300με, 400με, and 500με in the coupon, and the time required to ramp and release each load was approximately 0.1 seconds. During the testing, a si425-500 interrogator recorded FOS strains and the laboratory temperature continuously at 250 Hz, and the Megadac recorded foil sensor strains continuously at 1.0 Hz. In addition, the coupon loading was recorded by the Flextest GT Controller and MPT Software continuously at 20 Hz throughout CT8.

3.3.8.2 CT8 Results

Figures 3.51 - 3.55 present CT8 results, and Table 3.8 summarizes the FOS error analysis. While it was desired to maintain constant temperature during the test, results illustrate that thermal responses were evident during the time period of 140-175 minutes. Examination of Figs. 3.51 - 3.55 and Table 3.8 revealed that Loctite (330, 392, 410, H3300, H4500) and Plexus MA820 adhesives were capable of measuring the coupon mechanical strain immediately upon loading for all events, which reinforced the results from CT7. However, error among measurements immediately upon

www.manaraa.com

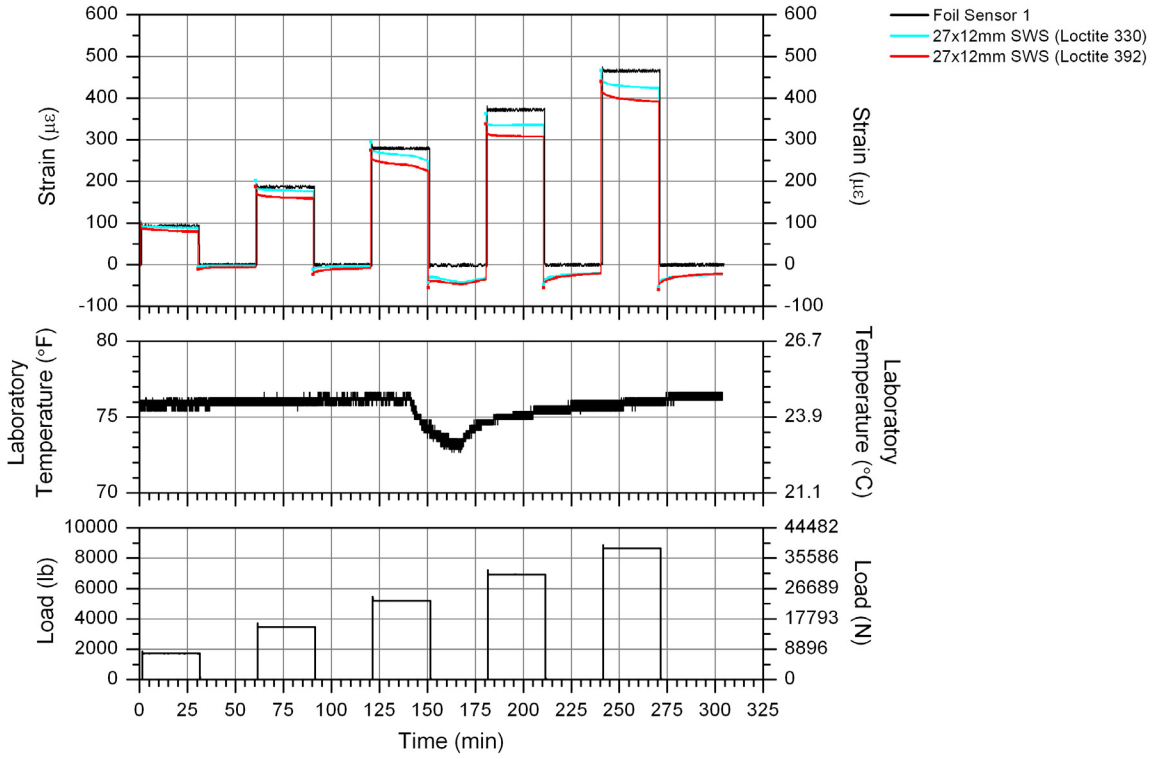

Figure 3.51. CT8: continuous strain results for Coupon C, group 1 sensors.

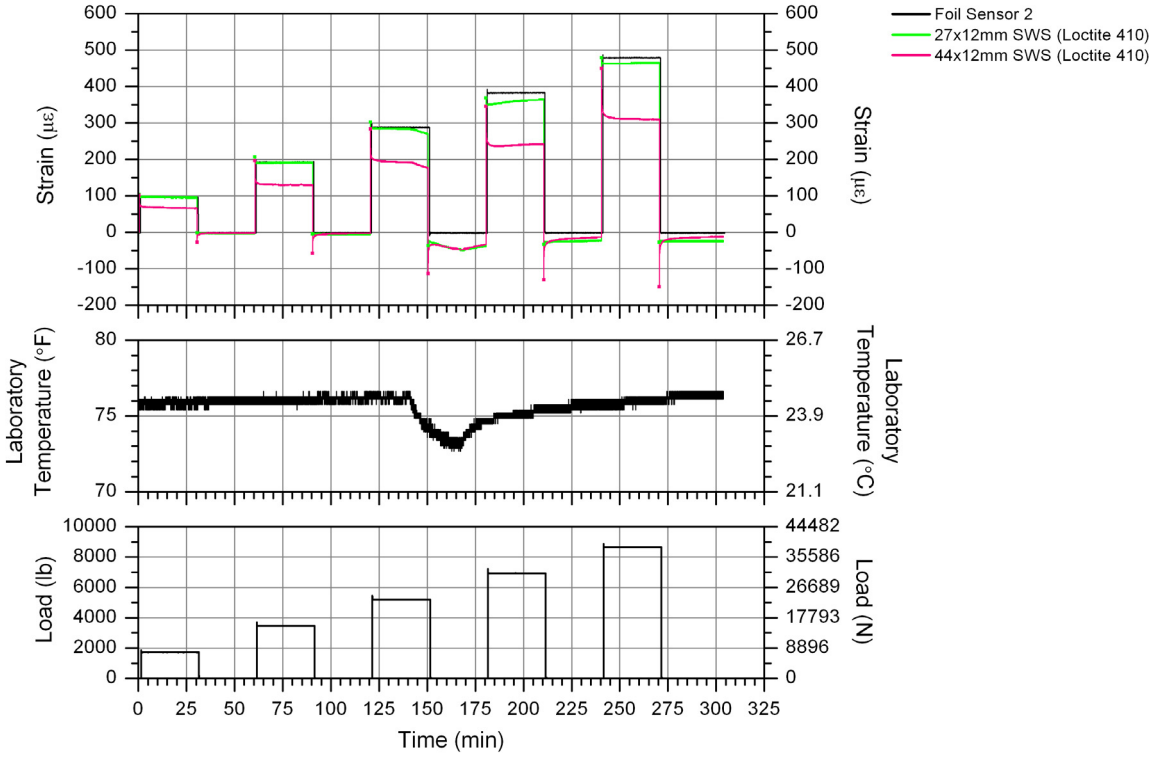

Figure 3.52. CT8: continuous strain results for Coupon C, group 2 sensors.

www.manaraa.com

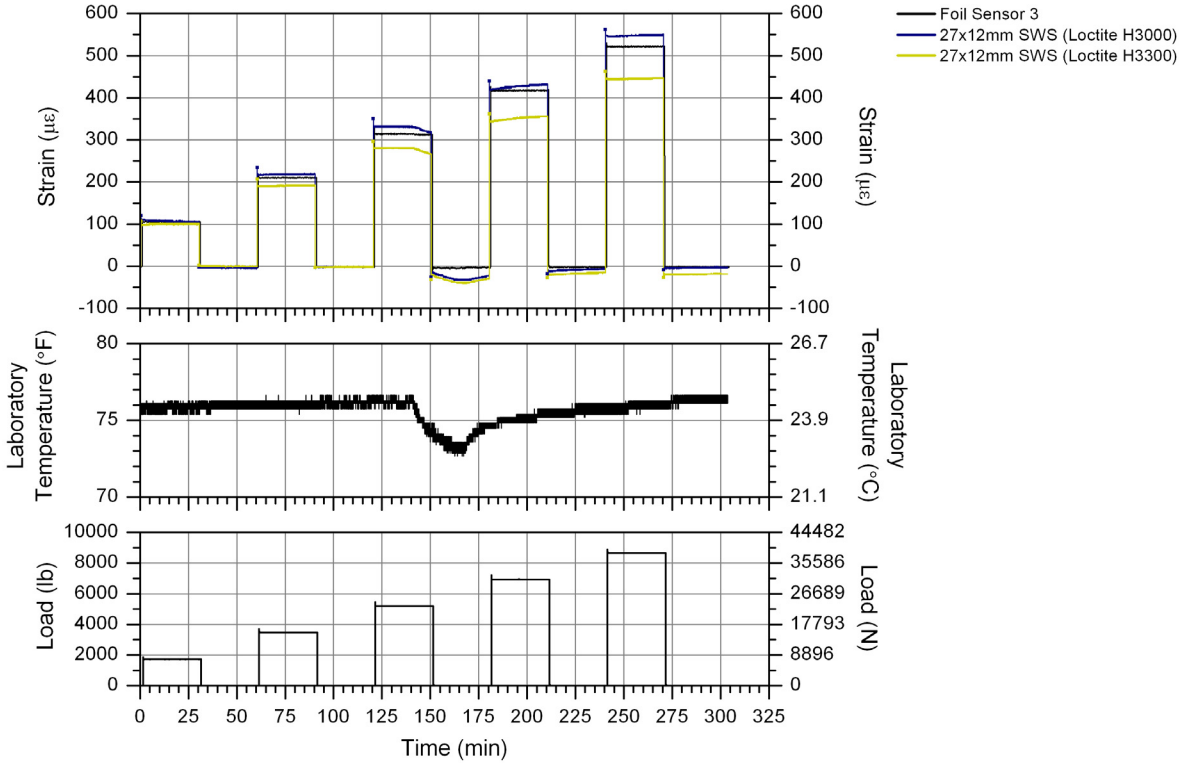

Figure 3.53. CT8: continuous strain results for Coupon C, group 3 sensors.

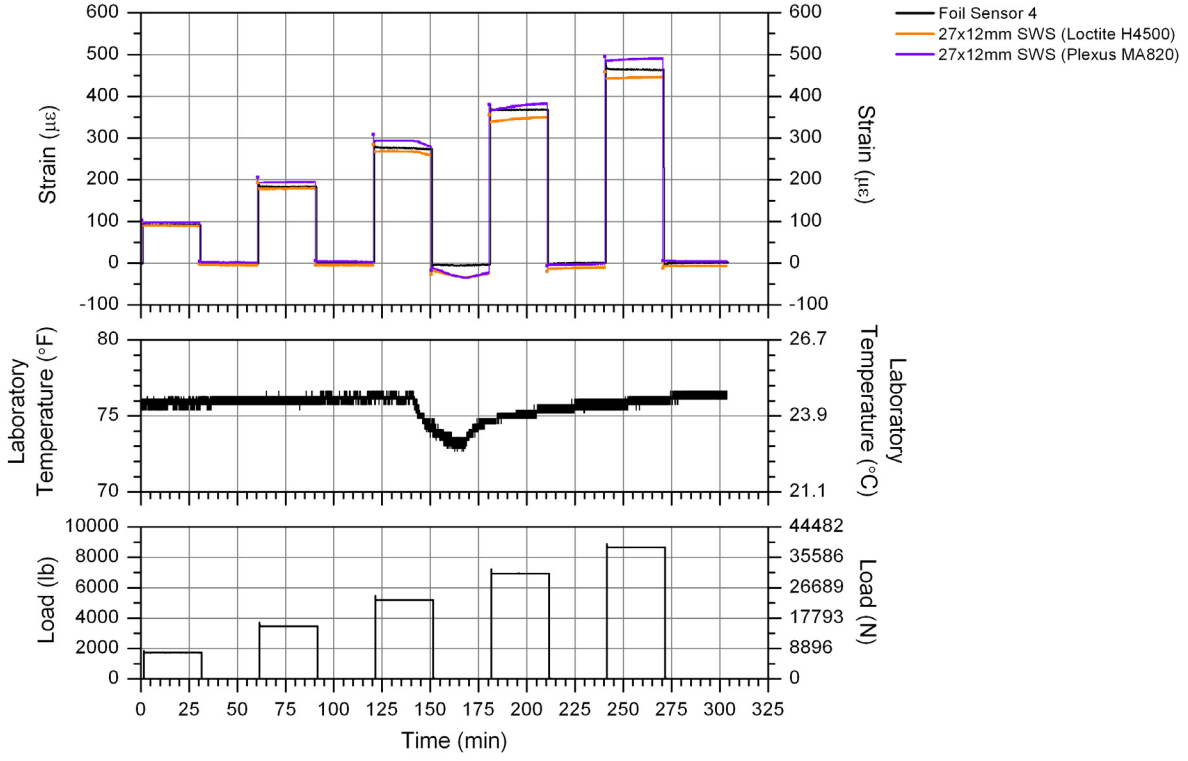

Figure 3.54. CT8: continuous strain results for Coupon C, group 4 sensors.

www.manaraa.com

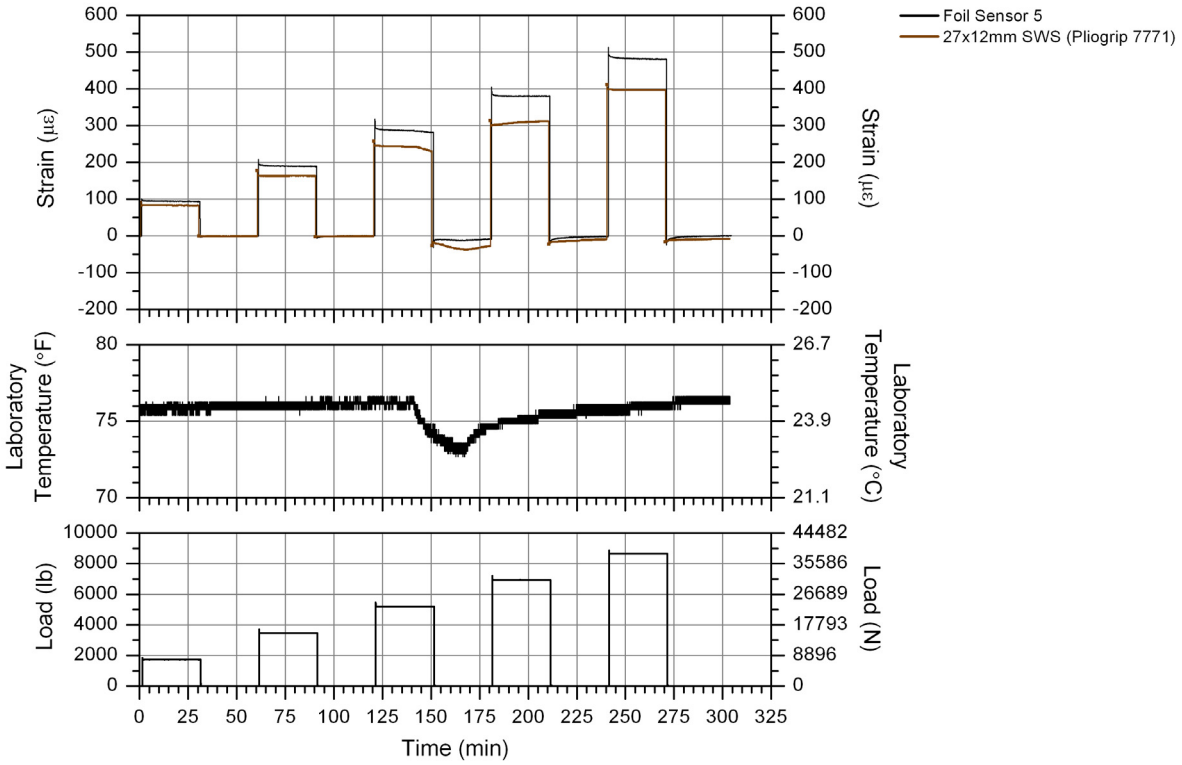

Figure 3.55. CT8: continuous strain results for Coupon C, group 5 sensors.

loading for FBGs bonded with Loctite H3000 and Pliogrip 7771 appeared to be a related to the magnitude of the loading. It should be noted that this observed behavior could have also been the result of transverse bending on the coupon.

As load was sustained on the coupon, adhesive viscoelasticity was evident in Loctite 330 and 392, but it was significantly less than that which was present in CT5. For Loctite (410, H3000, H3300, H4500), Plexus MA820, and Pliogrip 7771, the small reduction in strains at the beginning of the sustained loading suggested that viscoelasticity also existed in those adhesives. However, examination of the loading reveals that there was a small amount of overshoot and correction by the Flextest GT Controller and MPT Software during the rapid load application. This small amount of overloading caused the small spike at the beginning of the FOSs, and it was also recorded by the foil sensors. Thus, long-term viscoelasticity that was evident in CT5 results was eliminated through removal of the CFRP packaging for all adhesives other than Loctite 330 and 392. This conclusion is

www.manaraa.com

Table 3.8. Error analysis results for FOSs in CT8.

CT8 Loading	Adhesive *	Error Label	Error Statistics									
			Event 1		Event 2		Event 3		Event 4		Event 5	
			t = 0 min	t = 30 min	t = 0 min	t = 30 min	t = 0 min	t = 30 min	t = 0 min	t = 30 min	t = 0 min	t = 30 min
Incremental Sustained Loads	Loctite 410 - ACR *	Strain (με)	5	28	1	60	16	109	14	108	24	155
		%	4.9	29.6	0.3	30.9	5.4	37.6	3.6	28.1	4.9	32.3
	Loctite 330 **	Strain (με)	10	3	10	7	6	28	14	5	12	23
		%	10.6	3.2	5.1	3.8	2.0	9.9	3.7	1.3	2.5	5.0
	Loctite 392 **	Strain (με)	8	3	0	21	10	49	8	31	13	54
		%	8.4	3.6	0.1	11.2	3.4	17.3	2.1	8.2	2.8	11.6
	Loctite 410 **	Strain (με)	8	4	11	4	7	12	15	21	15	10
		%	8.0	4.0	5.7	2.1	2.2	4.1	3.8	5.4	3.1	2.1
	Loctite H3000 **	Strain (με)	13	4	19	12	22	8	35	36	36	32
		%	12.3	3.5	8.5	5.5	6.7	2.4	8.2	8.4	6.8	6.0
	Loctite H3300 **	Strain (με)	1	0	11	18	32	45	36	33	55	61
		%	1.0	0.4	5.2	8.6	9.6	14.4	8.4	7.9	10.3	11.7
	Loctite H4500 **	Strain (με)	9	5	6	6	3	8	1	8	11	3
		%	9.1	5.1	3.0	3.0	1.2	3.1	0.3	2.3	2.3	0.7
	Plexus MA820 **	Strain (με)	10.5	11.5	11.8	12.6	12.6	5.7	19.9	37.4	15.9	32.0
		%	11.3	13.0	6.1	6.9	4.3	2.1	5.2	10.1	3.3	6.9
	Pliogrip 7771 **	Strain (με)	5	5	28	22	58	49	71	47	94	75
		%	5.2	5.3	13.6	11.6	18.3	17.4	17.2	12.2	18.2	15.6

Note: * 44x12mm SWS

** 27x12mm SWS

www.manaraa.com

supported by comparing the immediate and long-term FOS errors presented in Tables 3.5 and 3.8.

Figure 3.52 presents behavior in the 44x12mm SWS that resembled long-term viscoelastic effects in adhesives. However, as proven in the same figure, viscoelasticity did not exist in the Loctite 410 adhesive for the 27x12mm SWS. Thus, the long-term reduction in measured strain in the 44x12mm SWS was the direct result of the unfavorably soft acrylate recoating on the 10mm FBG.

3.3.8.3 CT8 Conclusions

The following additional conclusions were determined considering all testing through CT8:

- Removal of the 15x20mm CFRP packaging from the FBGs eliminated viscoelasticity in all FOS adhesives except Loctite 330 and 392.
- Except for Pliogrip 7771, Loctite 330, and Loctite 392, the adhesives tested have been proven to be adequate for use with unpackaged FBGs with polyimide recoatings for the sustained loading conditions in CT8.
- The soft acrylate coating of the 10mm FBG in the 44x12mm SWS resulted in long-term measured strain reduction in the 44x12mm SWS, and thus, is not suitable for measuring sustained loadings.

3.3.9 Conclusions from Laboratory Validation Testing

The laboratory validation testing presented herein was performed to determine and/or validate the best FOS design and adhesive for use in the FCB SHM system. Different combinations of FOS designs and adhesives were bonded to coupons and subjected to mechanical loadings with varying magnitudes, frequencies, temperatures, and durations of sustained loading. In general, the following conclusions were determined:

- The CFRP packaging on the SFF SMSs proved to create viscoelastic effects in the eight adhesives tested in this study.
- The 210x20mm SMS bonded to steel with Loctite 392 proved to accurately and consistently measure cyclic mechanical strains, such as those defined in CT1, without being influenced by temperature variations.
- The 15x20mm SMS bonded with Loctite H4500 proved to be the only SFF SMS/adhesive combination that was capable of accurately measuring mechanical strains in the presence of temperature variations. However, this accuracy and temperature independence was proven for the loading conditions demonstrated in CT6. With larger mechanical strains, higher frequencies of loading, and during sustained load, viscoelasticity in the adhesive affected the accuracy of the SFF SMS.
- Loctite (330, 392, 410, H3000, H3000, H4500) and Plexus MA820 adhesives were proven to be adequate for use with unpackaged FBGs utilizing polyimide recoating to measure the cyclic loading presented in CT7.

www.manaraa.com

- Loctite (410, H3000, H4500) and Plexus MA820 were proven to be adequate for use with unpackaged FBGs utilizing polyimide recoating to measure the sustained static loads presented in CT8.

- FBGs with acrylate recoatings proved to accurately measure cyclic loadings in CT1, CT2, and CT7, but the soft recoating relaxed and caused significant error when subjected to sustained loadings such as those presented in CT5 and CT8.

The preceding conclusions were based on limited laboratory testing with the specific purpose of testing FOS designs and adhesive for use with the FCB SHM system. For a more thorough understanding of the FOS and adhesive behaviors revealed through this investigation, additional research is required.

3.4 FCB SHM System Equipment Selection

Based on the laboratory validation testing presented in Section 3.3, the following components were selected for use in the FCB SHM system:

- The 210x20mm SMS bonded with Loctite 392 was chosen for strain measurements in uniform strain fields.

- The 15x20mm SMS bonded with Loctite H4500 was chosen for strain measurements at single locations within the cut-back regions of the retrofits.

- A 220x20mm surface-mountable array (SMA), utilizing a five-FBG array and bonded with Loctite H4500, was designed and chosen for strain measurements at multiple locations within the cut-back regions of the retrofits. The design of this SMA was based on results from the 15x20mm SMS in the laboratory validation testing.

- A si425-500 interrogator was chosen for use with the FBG-based FOSs based on its proven ability to interrogate four channels of sensors at rates up to 250 Hz.

- A 1.70 GHz Dell desktop computer (40 GB hard drive) was chosen based on its ability to save and manage the data output from the si425-500 without becoming backlogged.

- Various wireless networking components were chosen based on proven abilities with previous research projects.

Additional details for each of the components within the FCB SHM system will be provided in Chapters 4 and 5.

www.manaraa.com

4. FCB SHM SYSTEM HARDWARE

The hardware components that were implemented in the FCB SHM system include a FOS network, data collection and management equipment, and wireless communication equipment. The proceeding sections present an overview of the system bridge components as well as field validation testing procedures that were performed.

4.1 SHM System Components

Section 3.4 briefly mentioned the hardware components that were selected for use in the FCB SHM system based on their performance during the laboratory validation testing. The following sections provide information regarding the configurations and abilities of the components to function together to achieve the strain-based monitoring process.

4.1.1 Fiber Optic Sensor Network

Conceptual sensor locations and orientations were identified in Section 3.2, and the design and validation of FOSs and adhesives for strain measurement was discussed Section 3.3. As a result, 40 FBG-based FOSs (SMSs and SMAs) were strategically distributed in six cross sections of the US30 bridge. Figure 4.1a identifies the six cross sections, and Figs. 4.1b-g illustrate the locations and orientations of the sensors within each section. Each FOS has been assigned a label with the following format:

Section – Member – Part – Orientation

where,

BF = Bottom flange	NS = North stringer
CB = Cut-back region	SG = South girder
FB = Floor beam	SS = South stringer
H = Horizontal	V = Vertical
NG = North girder	WB = Web

The instrumentation layout was specifically designed to monitor the cut-back regions above the north and south floor beam connection plates of Section C for damage formation. Since the cut-back regions are the primary areas of concern with these FCBs, the FOSs could be placed near the critical damage areas.

As was discussed in Chapter 3, sensors installed horizontally on bottom flanges of members

www.manaraa.com

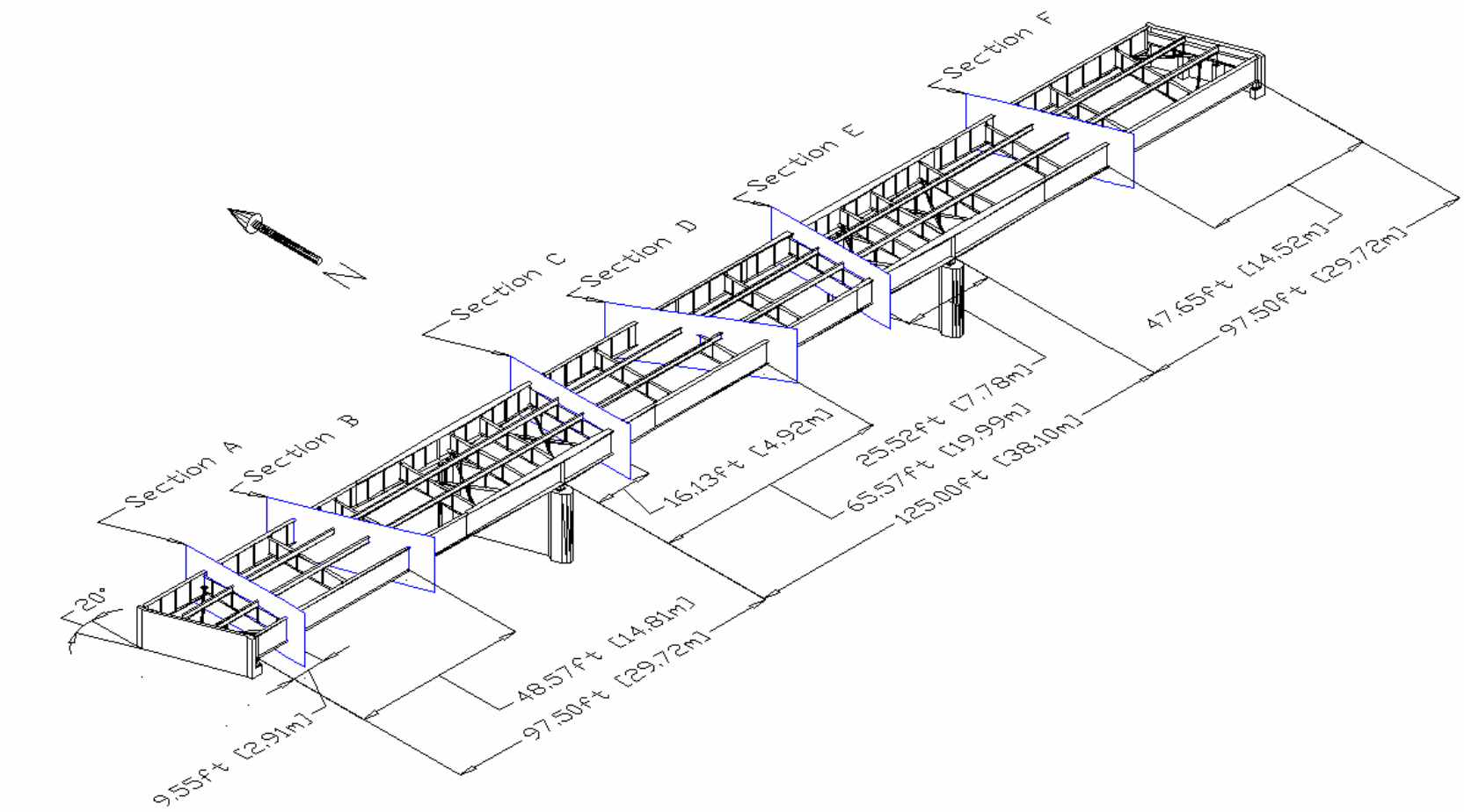

a. Longitudinal locations of the six instrumented cross sections

Figure 4.1. FOS layout of the FCB SHM system in the US30 bridge.

www.manaraa.com

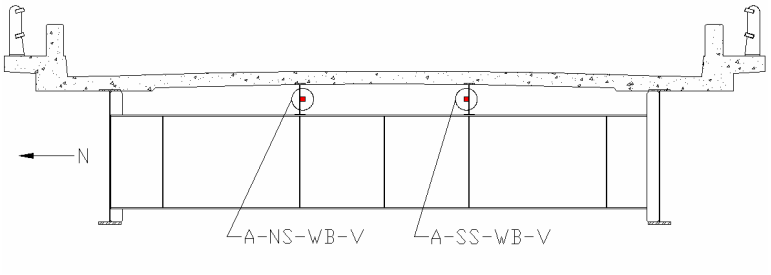

b. FOS Cross Section A

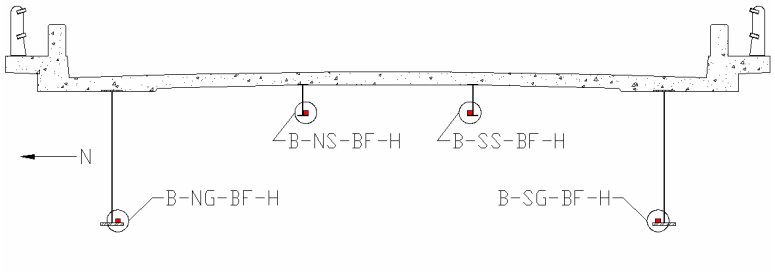

c. FOS Cross Section B

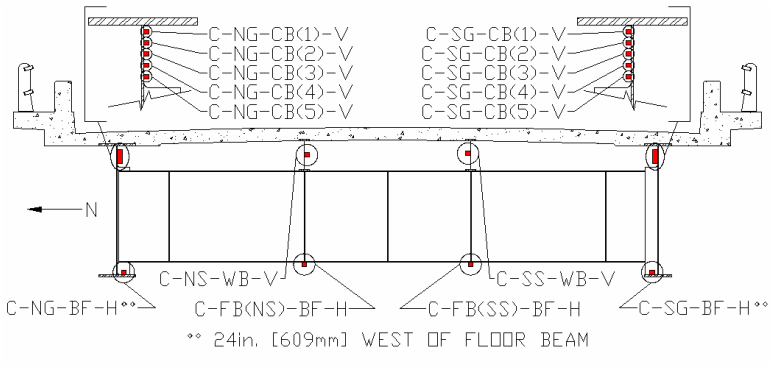

d. FOS Cross Section C

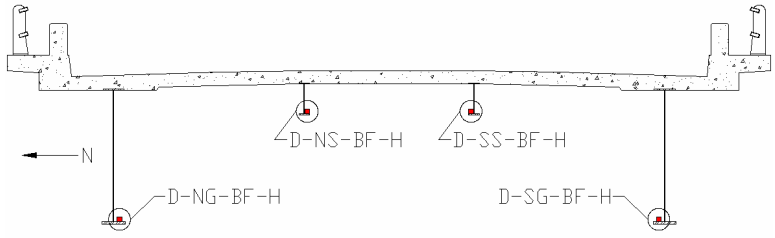

e. FOS Cross Section D

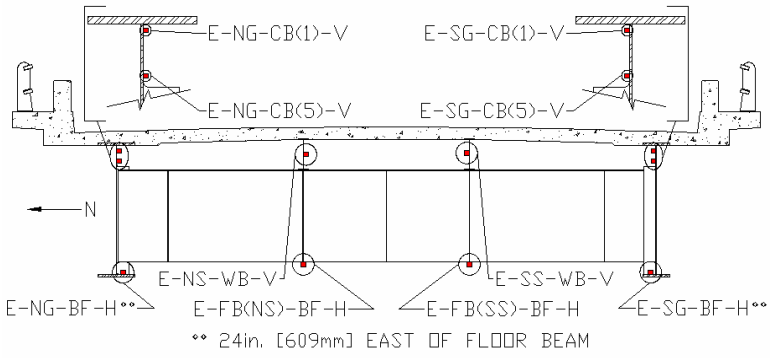

f. FOS Cross Section E

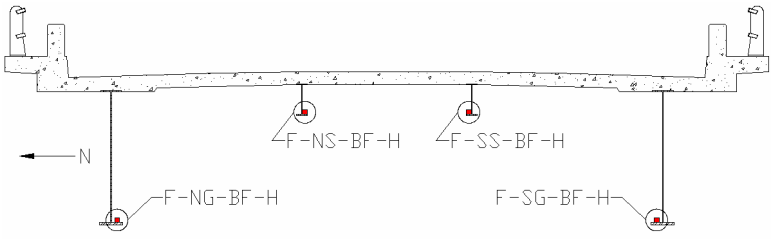

g. FOS Cross Section F

Figure 4.1. Continued.

www.manaraa.com

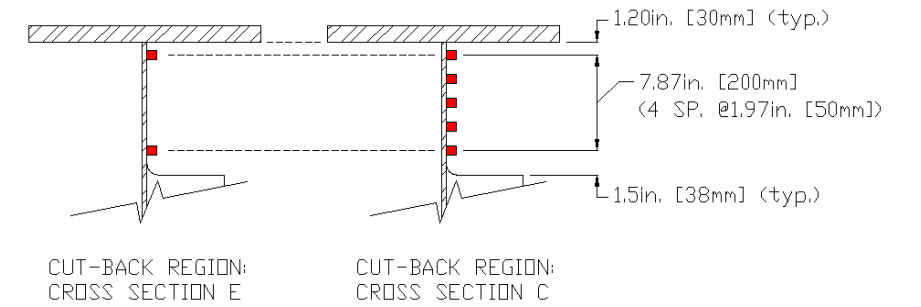

Figure 4.2. Alignment of the FOSs in the cut-back regions of Cross Sections C and E.

(girders, stringers, and floor beams) or vertically in the webs of the stringers utilized the 210x20mm SMS design with Loctite 392 adhesive. Within Section E of the FOS layout, sensors in the cut-back regions utilized the 15x20mm SMS design with Loctite H4500 adhesive to measure strains at the top and bottom of the cut-back region. Within Section C, FOSs in the cut-back regions utilized the 220x20mm SMA design with Loctite H4500 adhesive to measure strains at five evenly-spaced locations throughout the height of the cut-back region. As shown in Fig. 4.2, the 15x20mm SMSs were installed vertically in each cut-back region to match the corresponding FOSs in Section C. Photographs of installed FOSs are presented in Fig. 4.3. In Appendix A, Table A2 includes specifications for all FOSs installed at the US30 bridge, and Fig. A1 presents design details and specifications for the 220x20mm SMAs.

The 40 FOSs are distributed among three individual fiber optic leads, and each fiber was connected to one channel of the si425-500 interrogator. The FOSs within any one fiber were designed with approximately 5 nanometers (nm) of separation between adjacent center (reflected) wavelengths. Two methods were used to multiplex the FOSs: mechanical connectors and fusion splices. When FC/APC mechanical connectors were available on both fiber ends to be joined, the FOSs were mechanically multiplexed with mating sleeves. When mechanical connectors were not available on one or both fibers, the FOSs were multiplexed with fusion splices. Although fusion splices typically create lower optical loss in the fiber, the process requires more time and is nearly impractical for field use. Figure 4.4 presents photographs of a typical mechanical connection, a

www.manaraa.com

a. SMS: B-NG-BF-H

b. SMS: B-SS-BF-H

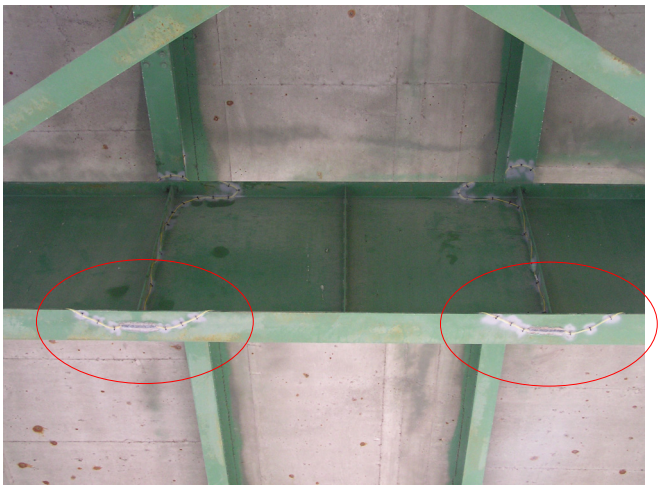

c. SMSs: C-FB(NS)-BF-H and C-FB(SS)-BF-H

d. SMS: C-SS-WB-V

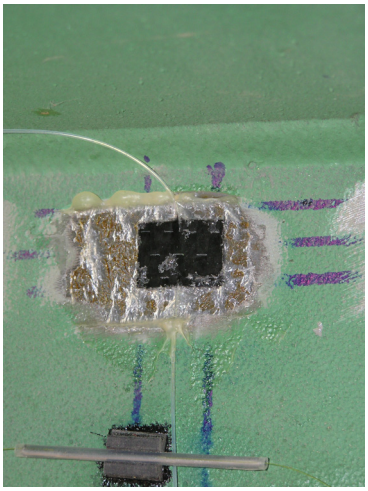

e. SMS: E-SG-CB(1)-V

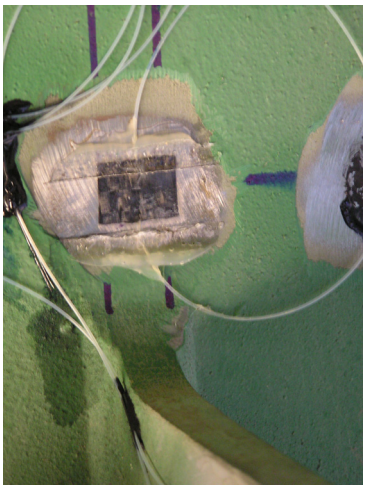

f. SMS: E-SG-CB(5)-V

g. SMA: C-SG-CB(1,2,3,4,5)-V

Figure 4.3. Photographs of FOSs (SMSs and SMA) in the FCB SHM system of the US30 bridge.

www.manaraa.com

a. FC\APC mechanical connection

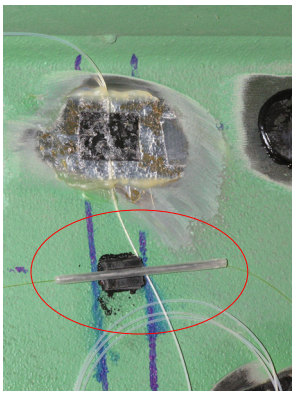

b. Fusion splice

c. Fiber optic equipment used for fusion splicing

d. Fusion splicer during the arcing process

Figure 4.4. Methods and equipment used for multiplexing the FOSs.

typical fusion splice, and equipment required for fusion splicing.

Several procedures were performed to aid longevity of the system. The optical fibers were intermittently secured with cable ties to mounting bases that were bonded to the bridge. In addition, all FOSs, fusion splices, and mechanical connectors were covered with a layer of silicone sealant to protect them from moisture. Finally, after the fiber optic network was installed, an OTDR was used to scan the network and check for regions with large optical attenuation. Examples of such optical loss include sharp bends or pinches in the fiber that could lead to extremely low optical levels or even fiber breakage. This would result in the inability to interrogate the FOSs. Fortunately, no severe attenuation issues were identified in the three-fiber network. In addition to attenuation purposes, the OTDR scans were used to identify the locations of the FOSs, or their distances from the beginning of the fiber, which aided in the setup of the si425-500 interrogator. Each fiber was scanned four times,

www.manaraa.com

and the locations of the FOSs used in the interrogator setup were taken to be the averages of the four scans. Refer to Table A2 in Appendix A for the locations of each FOS in the fiber optic network of the US30 FCB SHM system.

4.1.2 Data Collection and Management Equipment

The data collection and management equipment consist of a si425-500 interrogator, a 1.7 GHz Dell desktop computer, and a Linksys wireless router. As illustrated in Fig. 4.5, this equipment is stored in a temperature-controlled cabinet that is mounted on the north corner of the west abutment at the US30 bridge; power to the cabinet and equipment is provided through direct feed from an underground line that conveniently preexisted in the area. The si425-500 interrogator and Dell computer operate within a private network at the bridge site that is managed by the Linksys router through hardwired connections. As mentioned in Section 4.1.3, the private network at the bridge is connected to ISU's network via wireless communication (due to the proximity of the bridge to Ames, IA). With this setup, DOT personnel and ISU researchers are able to access the private network via encrypted wireless transmission at the bridge site or remotely from an off-site internet connection.

Figure 4.5. Temperature-controlled cabinet containing the data management and collection equipment at the US30 bridge.

www.manaraa.com

As previously discussed, the interrogator collects strain information at 125 Hz from the 40 FOSs. These data are relayed through the router to the Dell computer where it is stored and immediately processed. After the data have been processed, summarized information is sent to the DOT personnel and ISU researchers via the internet. For more information regarding the specifications and capabilities of the si425-500 interrogator, see Appendix D.

4.1.3 Wireless Communication Equipment

Wireless communication equipment was installed at the ISU BEC and at the US30 bridge site to provide network access to the SHM system. Figure 4.6 presents photographs of the wireless equipment at the bridge site. As illustrated, the antenna is mounted on an overhead sign frame located at the west end of the bridge. Electrical power wires and a Category 5e communication cable between the antenna and the equipment cabinet were installed through the inside of the sign frame and through underground conduit. The power wires terminated at the breaker box within the cabinet while the Category 5e cable was wired into the Linksys router. Figure 4.7 presents a photograph of the antenna at the ISU BEC. While the wireless transmission is only approximately two miles (3.2 km), other types of wireless communication could be used with the FCB SHM system for bridges in remote and/or secluded areas. Figure 4.8 presents a basic schematic of the SHM system discussed in this chapter.

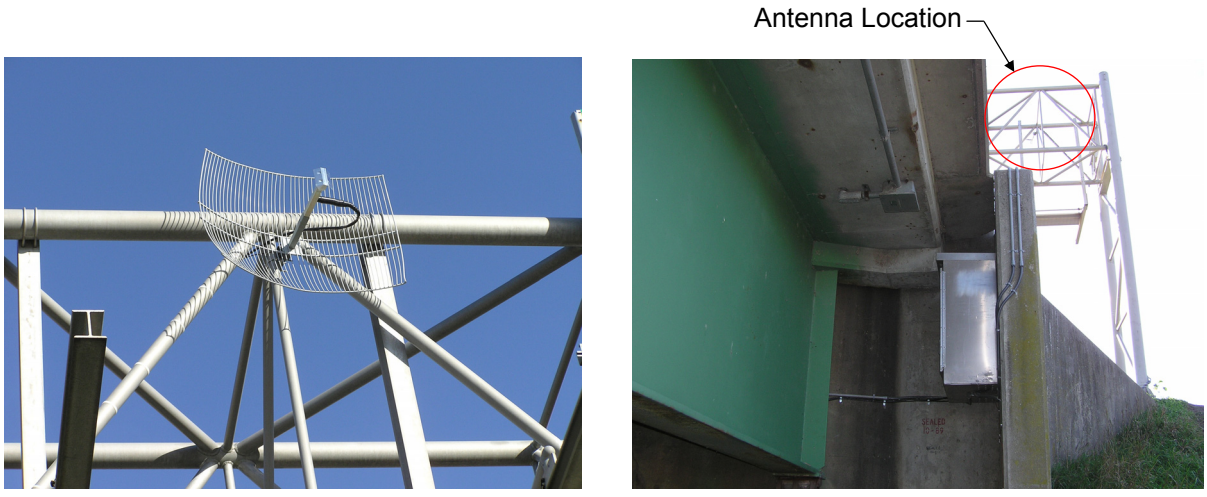

a. Antenna mounted on overhead sign frame b. Antenna location relative to the field cabinet

Figure 4.6. Wireless communication equipment installed at the US30 bridge site.

www.manaraa.com

Figure 4.7. Antenna mounted on the rooftop of the ISU BEC.

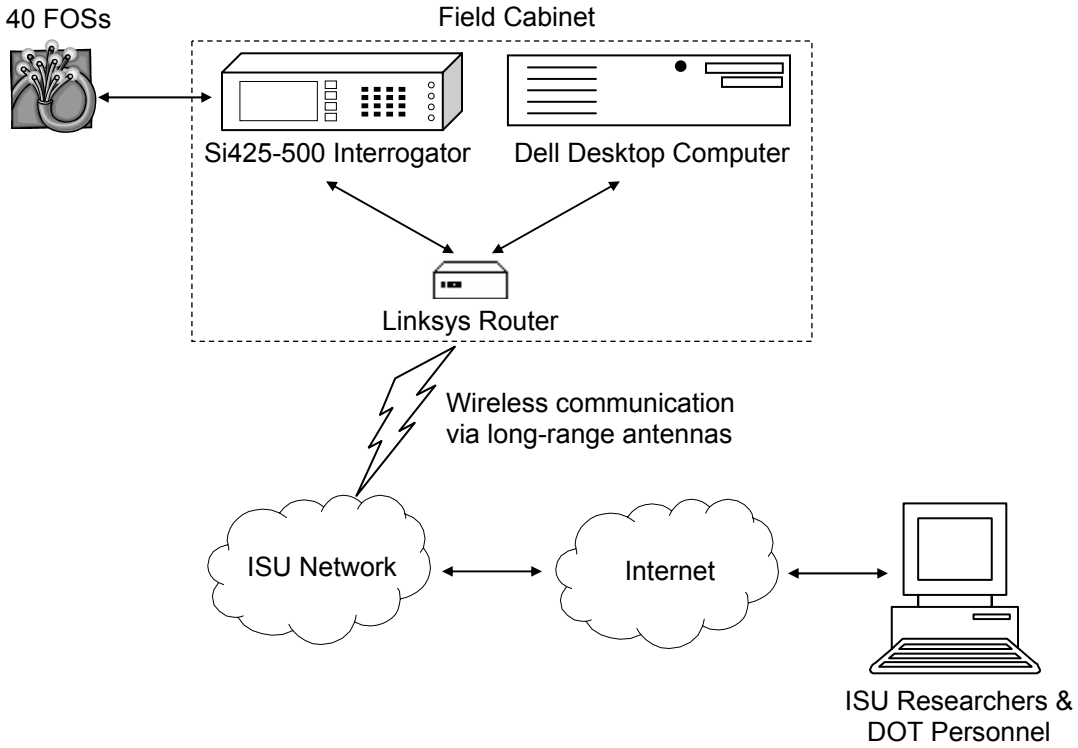

Figure 4.8. Overview of the US30 FCB SHM system components.

www.manaraa.com

4.2 In-Service Validation Testing of SHM System Components

Although each type of FOS/adhesive combination and the si425-500 interrogator that were used in the US30 FCB SHM system were laboratory tested and verified to collect accurate strain measurements, field testing of the sensors was also conducted to validate their in-service performance. High river water made the east and middle spans of the bridge inaccessible, and thus, only FOSs in the west span of the bridge (Sections A and B) were included in the validation testing. In the testing procedure, Bridge Diagnostics, Inc. (BDI) strain transducers were installed next to the FOSs, and measured strains were compared between the technologies. Figure 4.9 illustrates typical positioning of a BDI sensor relative to a FOS. At least one FOS for each typical application was included in the validation testing.

Fiber optic sensors measuring strains in the bottom flanges of floor beams and in the cut-back regions of retrofits were inaccessible because they are entirely located in Sections C and E. Thus, direct validation of the FOSs in those regions was not possible. However, BDI sensors were installed on the bottom flange of the floor beam in Section A and were in alignment with the corresponding FOSs in Section C and E. Assuming that vehicles maintained approximately the same transverse positions as they traversed the bridge and that similar loads were subjected to each floor beam, comparisons were conducted between the bottom flange BDI sensors on the floor beam in Section A and the corresponding FOSs in Section C. Due to the localized nature of the strains in the

Figure 4.9. Typical placement of a BDI sensor relative to a FOS during in-service validation testing.

www.manaraa.com

cut-back region and the large gage length (three inches) of the BDI sensors, this projection technique was not attempted for the FOSs in the retrofit cut-back regions.

The testing procedure consisted of simultaneously recording FOS and BDI strains for randomly selected segments of ambient traffic for approximately two and one-half hours. During this time period, 45 traffic segments were recorded, and the length of time contained in the data files varied from 17-122 seconds. Sampling rates differed between the FOS (250 Hz) and BDI sensors (100 Hz), but both sets of data were reduced with methods identical to those that are used in the FCB SHM system (See Chapter 5). Examples of reduced data with extrema identified in each event are presented in Fig. 4.10, and it is visually evident that there was good agreement in frequency and magnitude between the FOSs and BDI sensors. Extrema comparisons for all 45 traffic segments were conducted for the eight FOS/BDI pairs that were included in the validation testing and are summarized in Table 4.1. With the exception of A-SS-WB-V, measurement differences between FOSs and BDI sensors were less than five microstrain for the largest extrema measured; for the entire sample of approximately 2,100 extrema, the average measurement difference was less than one microstrain. Percentage differences are also included in Table 4.1, but it should be noted that most extrema that were used to calculate the percentages were small values. As a result, percentage differences appear higher than expected and are considered to be misleading.

Effort was given to investigate the large measurement difference between A-SS-WB-V and the corresponding BDI sensor. Review of several data files revealed that A-SS-WB-V was recording strain values consistent with C-SS-WB-V and E-SS-WB-V, and thus, was determined to be functioning properly. It was also noted that for every extrema comparison, the BDI sensor measurement was always lower than A-SS-WB-V. As a result, it is thought that the BDI sensor was not capturing the same localized strain condition as A-SS-WB-V, and thus, significant measurement differences were evident between the sensors. While this may also have been the case for A-NS-WB-V, the situation was apparently not as severe since measurement differences between the technologies were acceptable. As a result of the validation testing, it was determined that the US30

www.manaraa.com

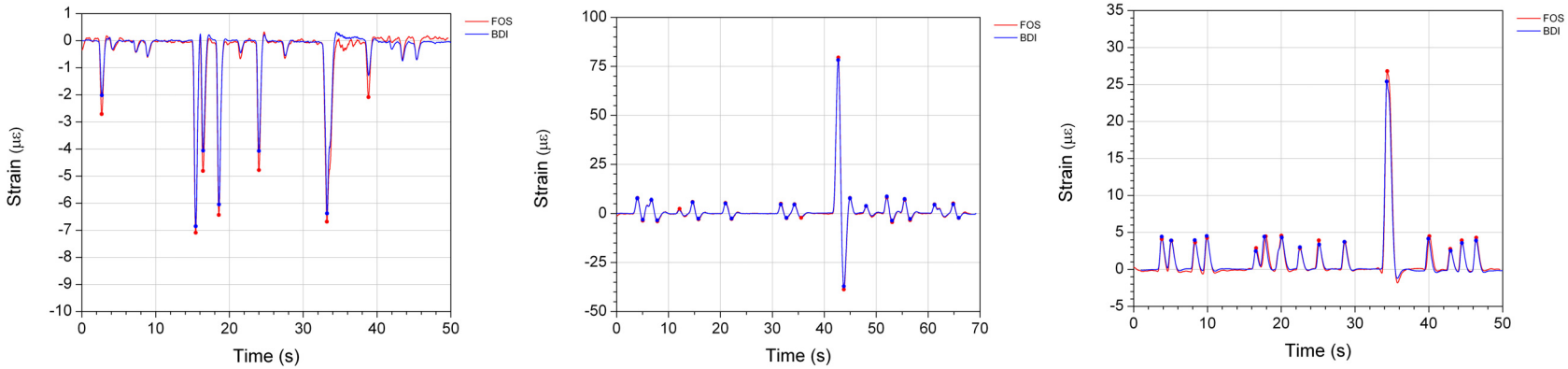

a. A-NS-WB-V b. B-SG-BF-H c. C-FB(SS)-BF-H

Figure 4.10. In-service validation testing: examples of comparisons between sensing technologies at various US30 bridge locations.

Table 4.1. Comparative results between FOSs and BDI sensors during in-service validation testing.

FOS	Number of Extrema	Smallest Traffic Extrema			Largest Traffic Extrema			Average of Traffic Extrema		
		FOS Measurement (με)	FOS and BDI Difference		FOS Measurement (με)	FOS and BDI Difference		FOS Measurement (με)	FOS and BDI Difference	
			Strain (με)	%		Strain (με)	%		Strain (με)	%
A-SS-WB-V	10	-4.5	2.5	126.1	-25.4	17.5	221.5	-15.3	10.9	240.7
A-NS-WB-V	149	-2.1	0.3	12.1	-34.6	4.4	11.3	-4.4	0.6	14.9
B-NG-BF-H	325	2.0	0.2	9.5	68.2	1.1	1.7	3.0	0.3	7.5
B-SG-BF-H	667	2.0	0.2	7.6	79.5	1.3	1.6	2.9	0.6	13.9
B-NS-BF-H	75	2.0	0.4	15.5	24.1	0.4	1.5	3.1	0.2	6.3
B-SS-BF-H	195	2.0	0.1	4.5	25.4	1.0	4.0	2.9	0.3	9.1
C-FB(NS)-BF-H *	209	2.1	0.01	0.5	45.8	4.0	9.5	4.6	0.6	15.5
C-FB(SS)-BF-H *	471	2.1	0.1	2.7	55.2	4.9	9.8	4.5	0.6	14.4

* BDI installed on Section A floor beam

www.manaraa.com

SHM system hardware was properly functioning and accurately measuring bridge strains resulting from ambient traffic loads.

www.manaraa.com

5. SHM SYSTEM SOFTWARE AND EVALUATION PROCEDURES

The FCB SHM system software includes two groups of components: (1) graphical user interfaces (GUIs) that are required to configure and train the system for the bridge being monitored, and (2) the autonomous applications that perform the data collection, reduction, and evaluation procedures, as well as the report generation process. During the development of the system software, significant efforts were undertaken to address the obstacles that were identified in Section 2.4 that hinder the advancement of SHM. Specifically, attention was given to improve data management, mining, and storage procedures, and in addition, presentation of information to bridge owners for decision making.

In general, Section 5.1 presents explanations of the various elements included in the strain records of the FOSs, overviews of the basic procedures for preparing and analyzing the strain data, and brief introductions to the numerous procedures that are contained within the training and monitoring modes of the SHM system. Moreover, a brief review of the measured behavior occurring in the cut-back regions is presented. In Section 5.2, the procedures involved with the training process of the SHM system are presented along with detailed discussions of the GUIs and algorithms that were developed for this mode of operation. Section 5.3 includes discussion of the autonomous applications that are used by the SHM system while it operates in monitoring mode. During discussion of the software in Sections 5.2 and 5.3, US30 bridge data are used to help illustrate each process. In addition, examples of US30 evaluation results are presented. Finally in Section 5.4, the overall performance of the US30 SHM system is summarized, and recommendations are given for the distribution of the SHM system software.

5.1 Overview of Bridge Behavior and Data Preparation, Reduction, and Interpretation

As previously discussed, the data collection equipment at the US30 bridge record strains from the FOSs at 125 Hz, and thus, large amounts of data are available for analysis. However, analyzing every byte of the continuous data would not only required significant processing time and resources, but it would also be impractical since not every byte of data is useful. Thus, the FCB SHM

www.manaraa.com

system functions to identify, extract, and utilize only the useful strain information contained within each strain record for the evaluation process used in this approach.

As demonstrated in Sections 5.2 and 5.3, the useful information for the evaluation procedures in the FCB SHM system is the quasi-static response of the bridge to ambient traffic loads. Since the evaluation process is only as reliable as the data being evaluated, the data preparation, reduction, and extraction procedures are extremely important. As will be illustrated, raw strain data contains many components pertaining to the different elements of a bridge response. The basic approach in the data preparation and reduction process is to remove the unwanted elements from the strain data to produce consistent and accurate information that clearly represents the quasi-static response of the bridge to ambient traffic. The subsequent sections present introductions to the following topics related to data analysis and bridge behavior:

- Segmental analysis of continuous strain records
- Data zeroing and filtering
- Identification of vehicular events in strain records
- Extraction of event extrema for evaluation
- Review of bridge behavior from strain records

The details of each process as well as the software procedures to accomplish each task are discussed in further detail in Sections 5.2 and 5.3.

5.1.1 Segmental Analysis of Continuous Strain Records

Continuous strain measurements are affected by many components, but in general, the two primary components are as follows: (1) mechanical strains in the substrate material, and (2) environmental factors causing thermal expansion and contraction in the substrate material, bonding adhesive, sensor packaging, and/or sensor. For highway bridges, mechanical strains resulting from traffic loadings occur at much higher frequencies than those that those of temperature-induced strains. Figure 5.1 presents 24-hr continuous strain records for six selected FOSs that provide evidence of this behavior. In each 24-hr record, the long rolling movement of the sensor baseline is the result of environmental temperature fluctuations, while the short vertical spikes extending from

www.manaraa.com

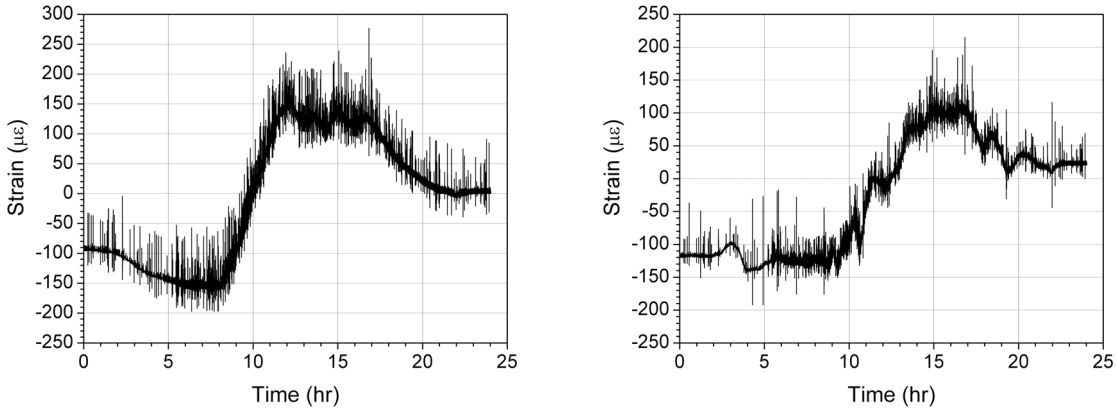

a. B-SG-BF-H

b. F-SG-BF-H

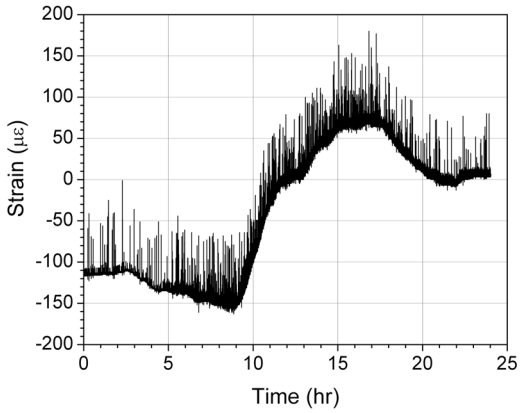

c. C-FB(SS)-BF-H

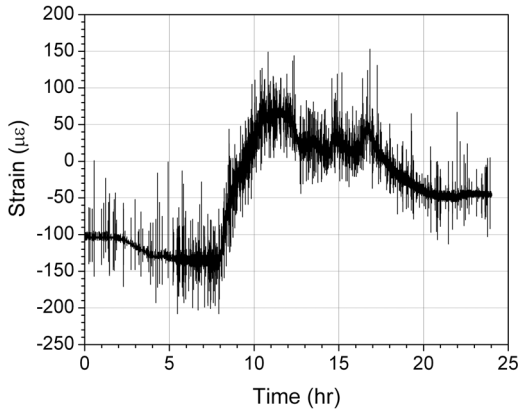

d. F-SG-CB(5)-V

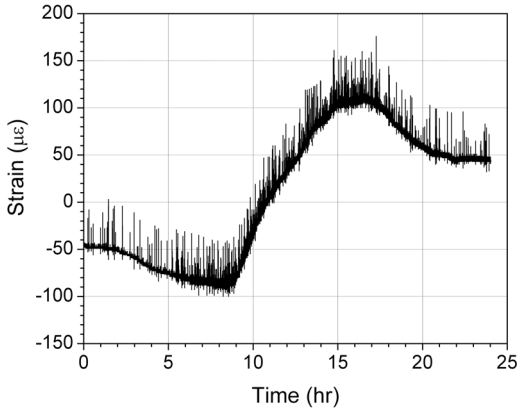

e. D-SS-BF-H

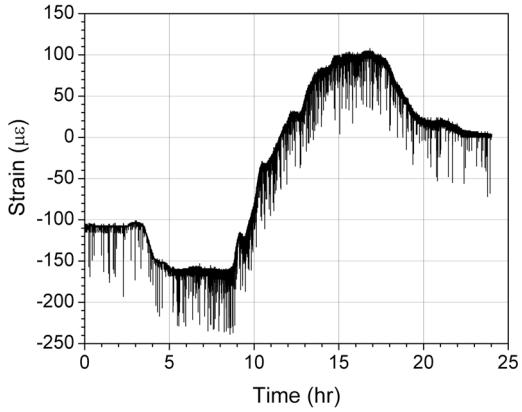

f. E-SS-WB-V

Figure 5.1. Continuous 24-hr time history strain plots for selected FOSs.

www.manaraa.com

each baseline are mechanical strains resulting from the ambient traffic. Note that in Figs. 5.1a-f, the baseline changes are different in shape and magnitude for each FOS, which indicates that each FOS experienced different temperature fluctuations during the same time period.

As was discussed in Section 3.3, changes in reflected wavelengths for each sensor are converted to strains in the SHM system by using the traditional conversion factor for mechanical strains: 1.2 pm = 1.0 με. Since temperature influences have been neglected in the conversion, only relative mechanical strain measurements occurring during a time period with essentially constant temperature, and thus constant baseline strain, are accurate and useful. To address this condition and to properly use the developed data reduction algorithms, the strain data at the US30 bridge are saved in data segments that maintain an essentially constant baseline strain. The data segmentation process is illustrated in Fig. 5.2. Figure 5.2a presents a continuous 24-hr strain record for B-SG-BF-H; Figs. 5.2b-c present data segments that are approximately ten megabytes (MB) of data (270 seconds) in size; and Figs. 5.2d-e display data segments that are approximately one MB of data (27 seconds) in size. From Fig. 5.2a, it is evident that the baseline rate of change is much greater for the segment presented in Fig. 5.2b than the segment in Fig. 5.2c. As a result, dividing the 24-hr continuous data into 270-second segments was sufficient to maintain a constant baseline in Fig. 5.2c, but baseline variation was still evident in Fig. 5.2b. However, it is has been shown that dividing the data into 27-second segments was sufficient to maintain constant baselines in both Figs. 5.2d-e. As a result, the strain data at the US30 bridge is saved in files approximately one MB in size, where each file contains the raw strain data for every FOS for the same 27-second time period.

5.1.2 Data Zeroing and Filtering

The baseline strain for each sensor does not contain information related to the quasi-static response of the bridge to traffic loads, and thus, it is removed from each sensor strain record through a process referred to as *zeroing the data*. For a given strain record in this process, the baseline strain is determined and subtracted from all measurements, and the resulting segmented strain data represents a relative measurement. This process is repeated for every strain record in the data file. In the resulting data, all significant deviations from zero are assumed to be mechanical responses of

www.manaraa.com

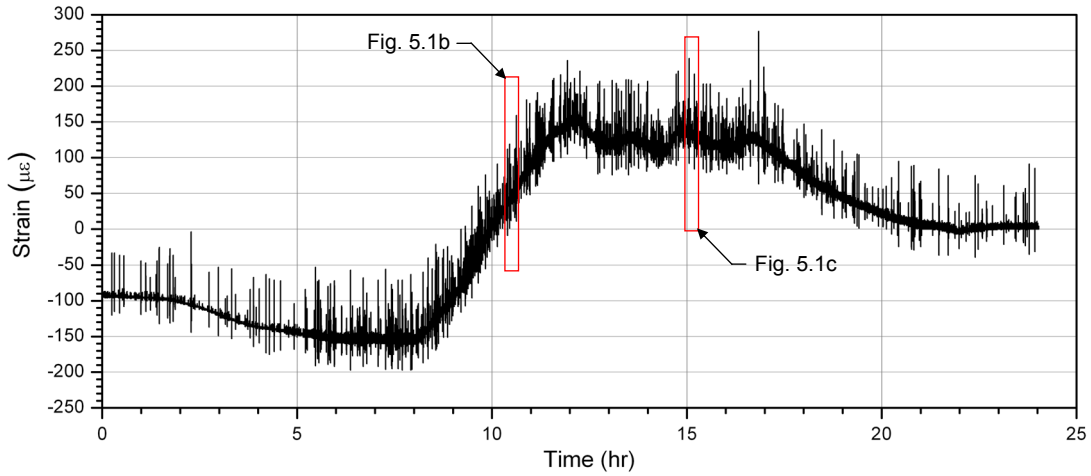

a. Continuous 24-hr time history

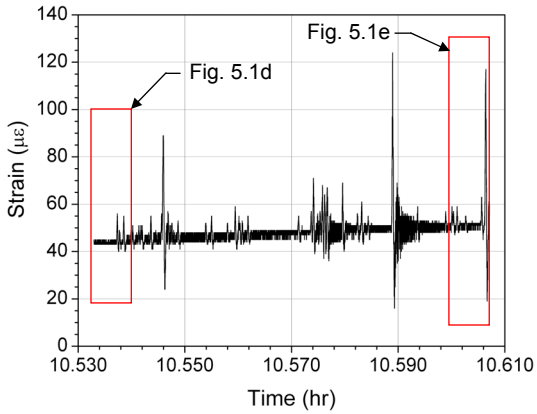

b. Ten MB segment with a varying baseline (See Fig. 5.1a)

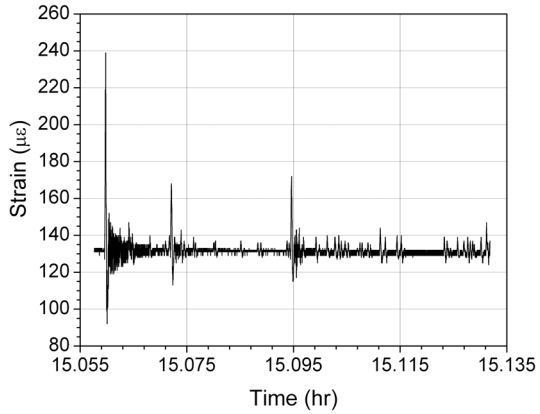

c. Ten MB segment with a constant baseline (See Fig. 5.1a)

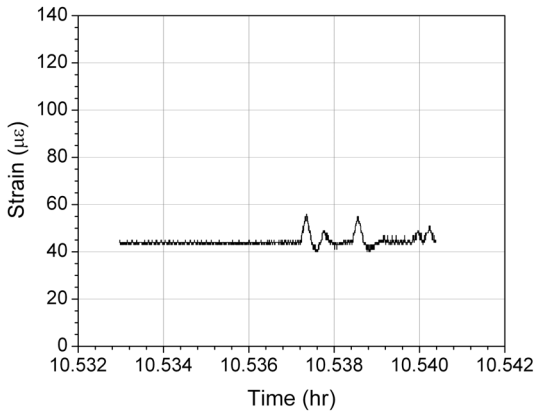

d. One MB segment with a constant baseline (See Fig. 5.1b)

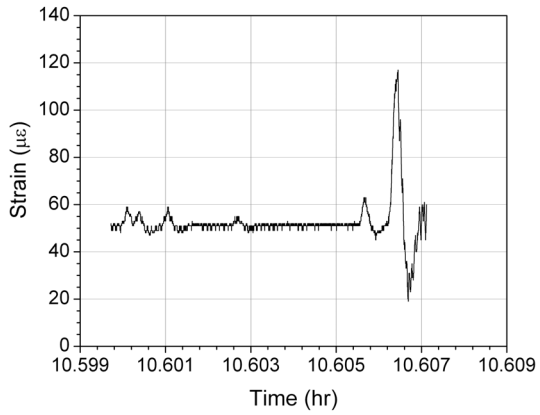

e. One MB segment with a constant baseline (See Fig. 5.1b)

Figure 5.2. Identification of B-SG-BF-H raw data file segments with constant baselines.

www.manaraa.com

the bridge to traffic, which were previously identified to be the most useful information in a record.

Presented in Fig. 5.3 are zeroed data for the raw data segments previously introduced in Figs. 5.2b-e. Even more obvious are the constant baselines for the data segments in Figs. 5.3b-e and the variation in the baseline in Fig. 5.3a. Note that by zeroing the data, the magnitudes of the mechanical strain response are more easily obtained.

The measured mechanical response remaining in the data file after the zeroing process is composed of three main elements: (1) noise in the data file, (2) a quasi-static bridge response resulting from the traffic loads, and (3) dynamic responses that include dynamic influence from the vehicles as well as structural dynamics of the bridge. The quasi-static response of the bridge has been identified as the strains that would have developed if the vehicles were moving very slowly (crawl speed) rather that at the speed limit. Assuming that the frequencies of the quasi-static responses are significantly different than those of the dynamic responses and the data noise, a frequency filter can be used to remove the dynamic response and noise from the data file. After such removal, the remaining information in the data file is the quasi-static bridge response to ambient traffic loads. Presented in Fig. 5.4 are the zeroed and filtered data for the largest mechanical response recorded in Fig. 5.3b. As illustrated, the quasi-static response of the bridge occurred at a frequency that was much lower than that of the dynamic response and noise that were filtered out of the data. More details for the data zeroing and filtering processes are presented in Section 5.2.3.

5.1.3 Vehicular Events in Strain Records

The pattern and magnitudes of the mechanical bridge strains that are generated when a vehicle traverses the bridge are dependent on several factors, and the major contributing factors are as follows:

- Static vehicular weight
- Bridge geometry
- Vehicle geometry
- Sensor location and orientation
- Vehicle(s) transverse location in the bridge

www.manaraa.com

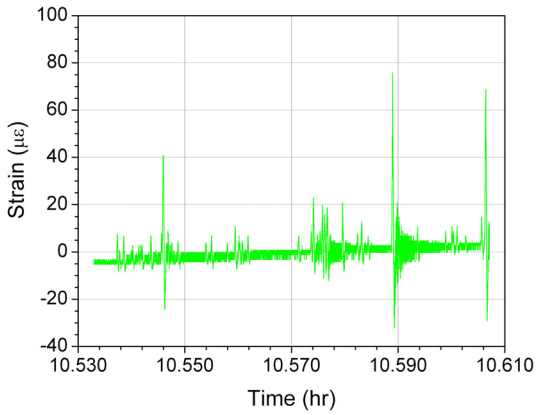

a. Ten MB segment with a varying baseline (See Fig. 5.2b)

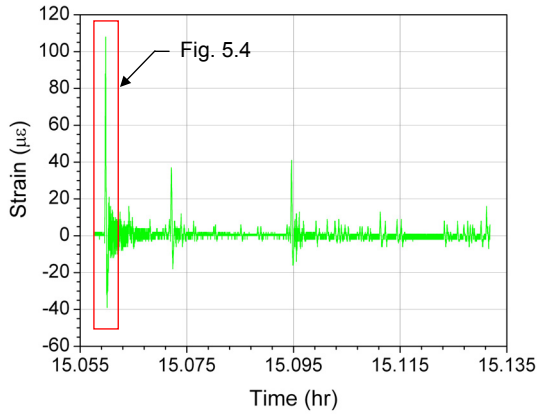

b. Ten MB segment with a constant baseline (See Fig. 5.2c)

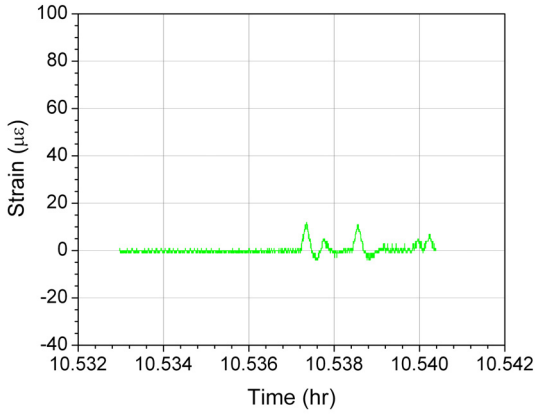

c. One MB segment with a constant baseline (See Fig. 5.2d)

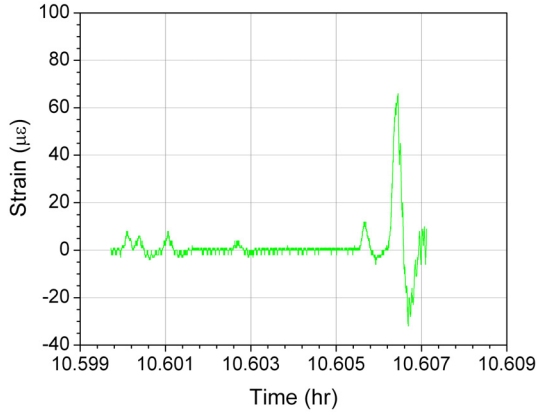

d. One MB segment with a constant baseline (See Fig. 5.2e)

Figure 5.3. Zeroed B-SG-BF-H data file segments.

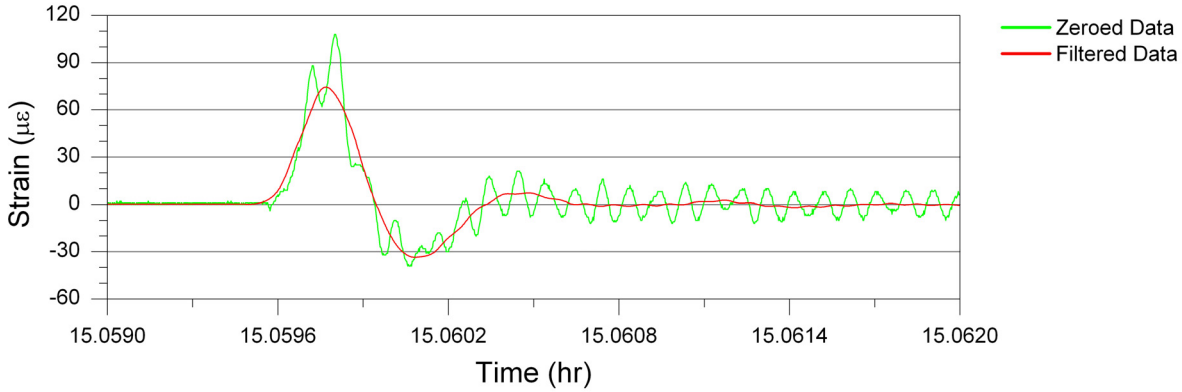

Figure 5.4. Zeroed and filtered strain data for B-SG-BF-H (See Fig. 5.3b).

www.manaraa.com

- Dynamic properties of the vehicular suspension systems

For a SHM system that has been installed in a bridge, the bridge geometry as well as the locations and orientations of the sensors cannot be changed. The remaining listed factors are characteristics of the vehicles traveling on the bridge. As a result, each type of vehicle traversing the bridge should theoretically produce a unique pattern of mechanical strains in the strain record of the sensor. These patterns of mechanical strains have been referred to in literature as vehicular events, footprints, fingerprints, and signatures; in this report, they will be referred to as vehicular events.

Comparing vehicular events within a sensor strain record, pattern variations are primarily affected by vehicle geometry while magnitude variations are dominated by the weight of the vehicle. In addition, dynamic effects in the strain record influence both the pattern and magnitude of the events. However, assuming an essentially elastic bridge response, the quasi-static events produced from each type of vehicle (i.e. car, straight truck, semi truck, utility vehicle, etc.) are repeatable.

Since the proposed SHM system utilizes the quasi-static events within strain records for evaluation and analysis of the bridge, the variation in the events must be minimized in order to produce a reliable and consistent system. The largest sources of variation presented thus far for vehicular events are dynamic responses in the data file that were previously shown to be removable through use of an appropriate filter. Since dynamic effects in a response are removable sources of variation in vehicular events, they are examples of assignable causes of variation in the monitoring process (See Section 2.3.4). All other factors causing variation are inherent characteristics of ambient traffic and are not capable of being removed from the data, and thus, are unassignable causes of variation in the monitoring process. As a result, the SHM system must account for these variable factors in the evaluation process.

Prior to software development, it was necessary to obtain a general understanding of the changes in event patterns that result from variations in the geometries of the vehicles. For this investigation, analytical models of the US30 bridge were developed and subjected to various moving loads. Independent models were constructed for the girders and stringers in STAAD.Pro 2005; in each model, the girder or stringer was represented with two-dimensional (2-D) prismatic beam

www.manaraa.com

elements, the west pier was considered to be a pinned support, and both abutments as well as the east pier were represented by roller supports. For the stringer models, the floor beam supports were modeled as elastic vertical springs. Composite girder or stringer section properties were calculated and assigned to prismatic beam elements; nonprismatic regions of the girders were modeled as a series of 6-in. (152-mm)-long prismatic beam elements with section properties that were determined by averaging those at the beginning and end of the tapering segment. In addition to the nodes required to model the geometry of each member, additional nodes were inserted into the models at FOS locations.

In each model, the girder or stringer was subjected to moving loads that traveled across the entire length of the bridge. The moving loads utilized in the analyses consisted of a unit concentrated force, as well as load patterns representing the geometries of Iowa Group One truck loads that are presented in Fig. 5.5. In Figs. 5.5a, 5.5c, and 5.5e, the geometries and legal axle loads are presented for the straight truck (Type 3), semi (Type 3S2A), and semi (Type 3S2B), respectively. However, the actual moving truck loads that were applied to the models are displayed in Figs. 5.5b, 5.5d, and 5.5f, where the total weight of each truck was reduced to unity while retaining the original axle weight ratios. These vehicles will be individually referred to as the unit straight truck (Type 3), unit semi (Type 3S2A), and unit semi (Type 3S2B); in general, they will be referred to as the unit trucks. Because the total weight for all moving loads was unity, differences in results for analyses that utilize different moving loads could be directly attributed to changes in vehicle geometry.

Figures 5.6 and 5.7 present schematics of the south girder and stringer models, respectively. In addition, the beginning and ending positions of the moving loads in each analysis are displayed. With each of the four analyses starting when the load was positioned immediately prior to entering the bridge, they were moved across the structure in 6-in. (152-mm) increments until the they were entirely off of the structure. For each load position, a static analysis was performed. As shown, the position of the unit concentrated load, x, during the analysis was measured from the west abutment; for the analyses involving unit trucks, the position of the truck, x, was recorded as the distance between the west abutment and the front axle load of the vehicle. Since the moving load geometries had different

www.manaraa.com

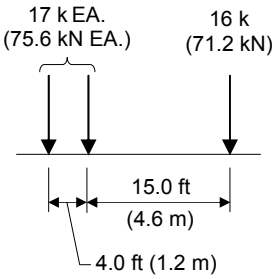

a. Straight Truck (Type 3)

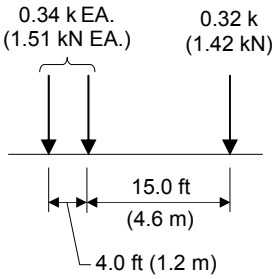

b. Unit Straight Truck (Type 3)

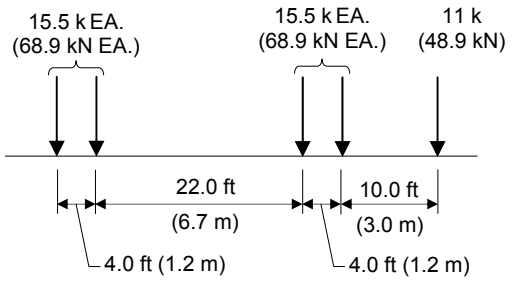

c. Semi (Type 3S2A)

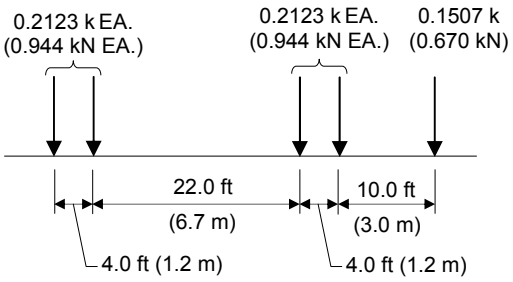

d. Unit Semi (Type 3S2A)

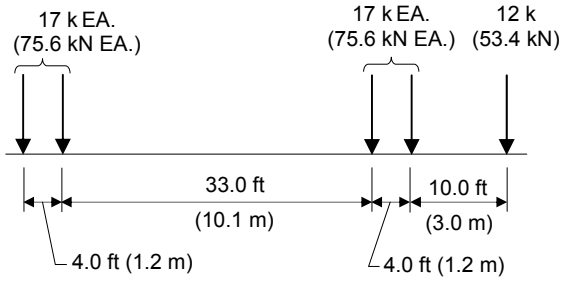

e. Semi (Type 3S2B)

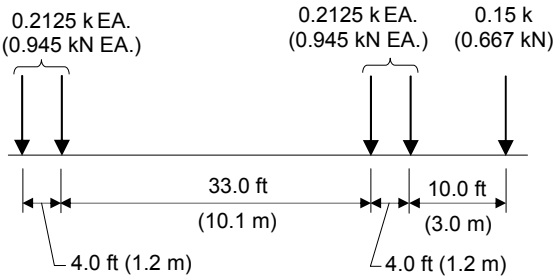

f. Unit Semi (Type 3S2B)

Figure 5.5. Iowa legal truck loads (Group 1) and unit equivalencies for the moving load analyses.

www.manaraa.com

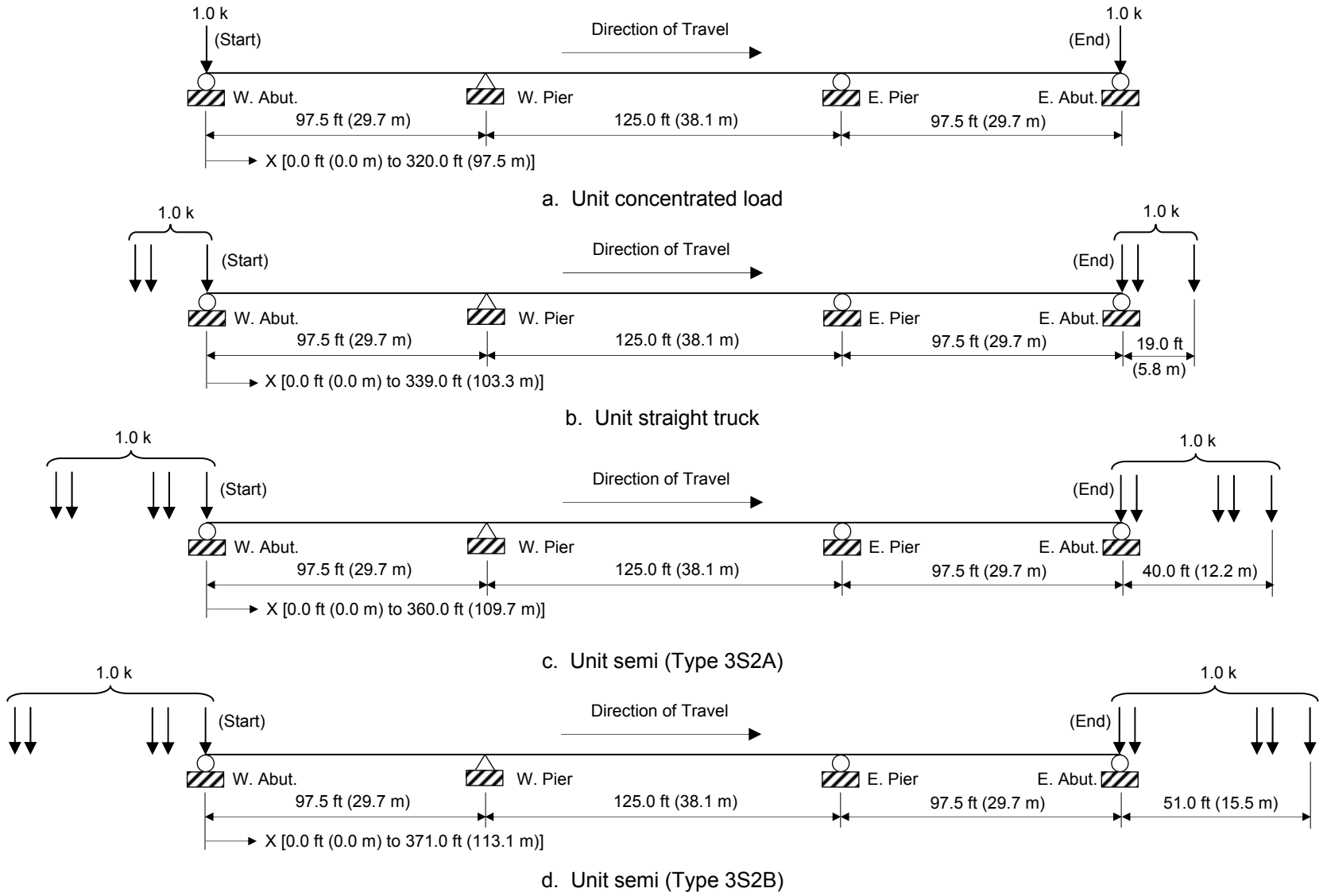

Figure 5.6. Positioning and length of travel for the unit concentrated load and unit trucks in the south girder static analyses.

www.manaraa.com

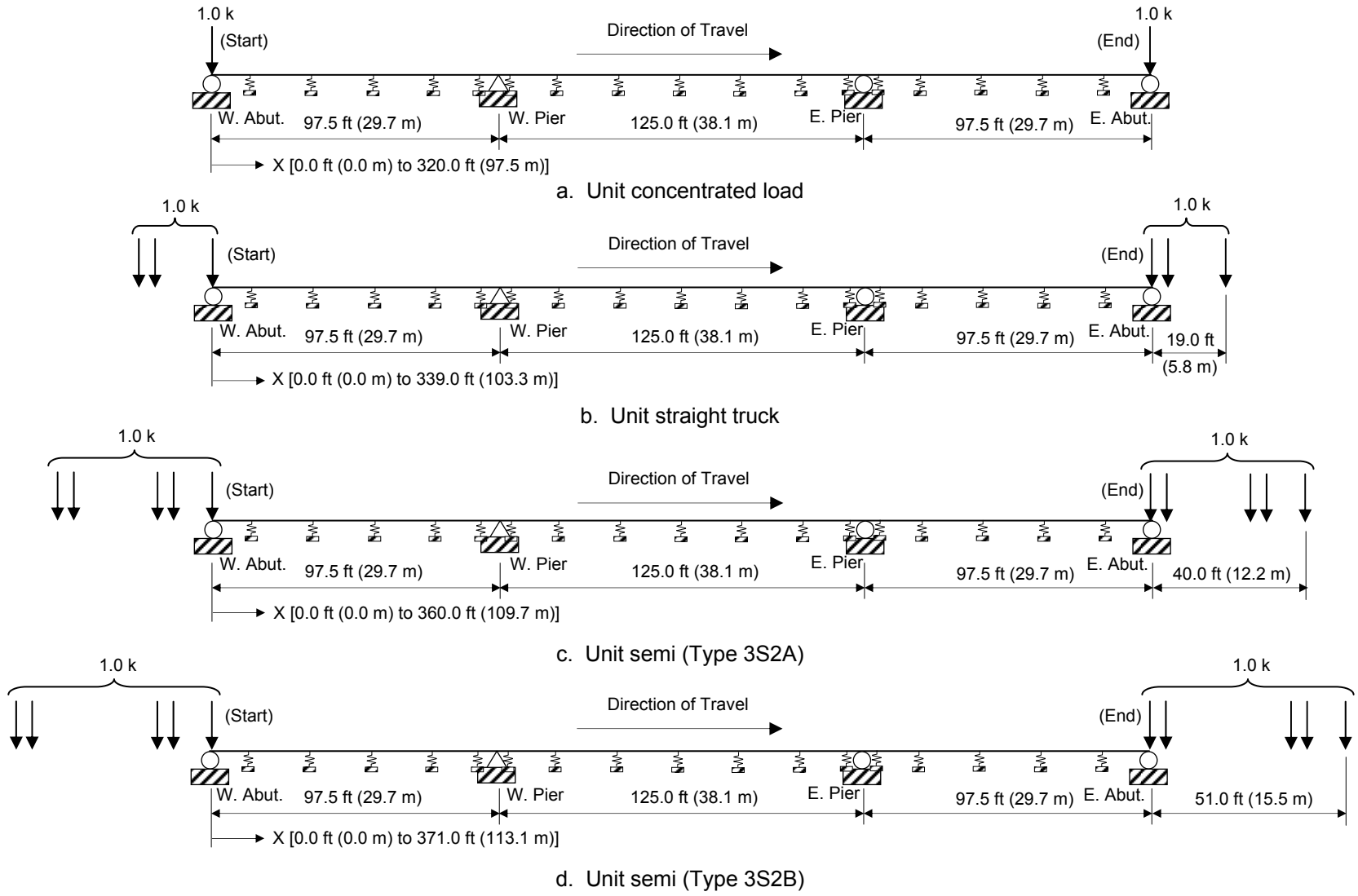

Figure 5.7. Positioning and length of travel for the unit concentrated load and unit trucks in the south stringer static analyses. [spring flexibility, f_s = 869.6 k/in (152.29 kN/mm for all springs)].

www.manaraa.com

lengths, the total distance traveled by each was different; the unit concentrated load traveled the shortest distance while the unit semi (Type 3S2B) traveled the longest distance.

The desired results from each analysis were the beam end forces and nodal reactions that corresponded to the measured strains at each FOS location. With these results, plots were generated for each sensor in the form of force versus moving load position. For the analyses utilizing a unit concentrated moving load, the resulting plot was an influence line. For each unit truck analysis, the resulting plot was essentially a force history for the girder or stringer section as the truck traversed the bridge. It was predicted that the force history patterns and relative magnitudes would resemble those of actual events obtained from FOS strain records at the US30 bridge. The resulting influence lines and force histories obtained from the analyses are presented in Figs. 5.8 - 5.18 for eleven girder and stringer sections that contain FOSs. Review of these figures reveals the following observations and conclusions about the forces generated at each member section and the predicted corresponding strains that develop in the FOSs:

- The total weight of each moving load was unity in each analysis, but the geometry of the moving load was variable. As a result, pattern changes among the influence line and force histories for a given girder or stringer section are the result of changes in the moving load geometry. Therefore, these pattern changes also reflect how the vehicular events in sensor strain records will change as the geometries of the vehicles traversing the bridge change.
- Forces in girder sections continually change as the position of the moving load changes throughout the entire length of the bridge. Therefore, measured strains at these girder sections will also continually change as the ambient traffic traverses the bridge.
- Forces in stringer sections change only when the moving load is in close proximity of the stringer section under investigation. Thus, measured strains at these locations will only change when ambient traffic is near the location of the sensor. As a result, the patterns of corresponding vehicular events in strain records will be shorter in FOSs that are installed on stringers than those that are installed on girders.
- The pattern differences among the influence line and three force history for a given stringer section are much greater than those of a girder section. Therefore, there will be more variability in vehicular event patterns within a FOS strain record that is installed on a stringer than for a sensor that is installed on a girder.
- For both girders and stringers, the maximum absolute response in each section force history decreases as the distances between the axles within the moving loads increase. Thus, for two vehicles that have essentially identical weights but different geometric lengths, the strains produced by the longer vehicle could be smaller than those produced by the shorter vehicle.

www.manaraa.com

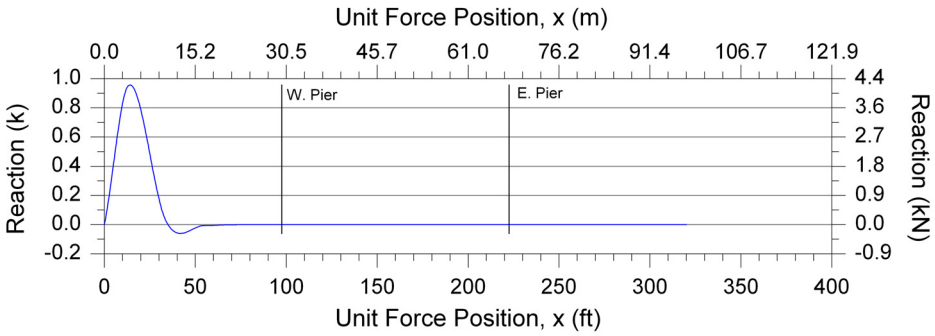

a. Influence Line (unit concentrated force)

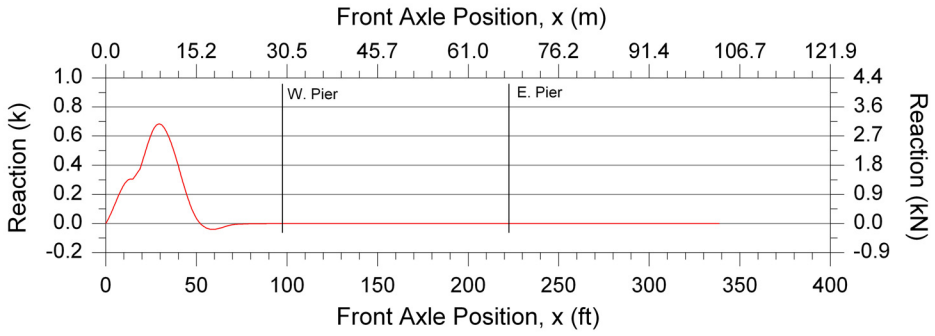

b. Unit straight truck (Type 3)

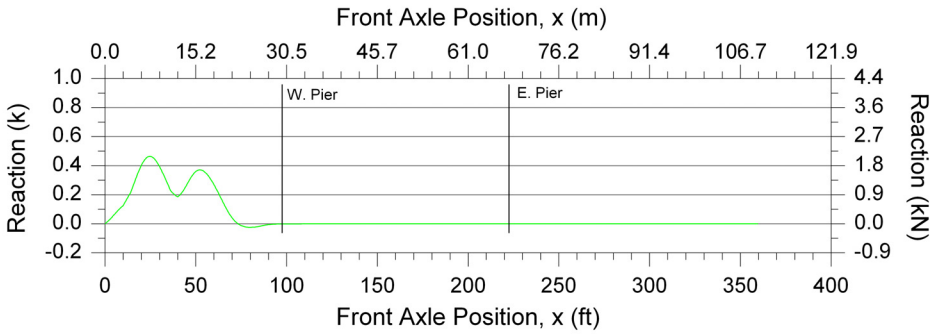

c. Unit semi (Type 3S2A)

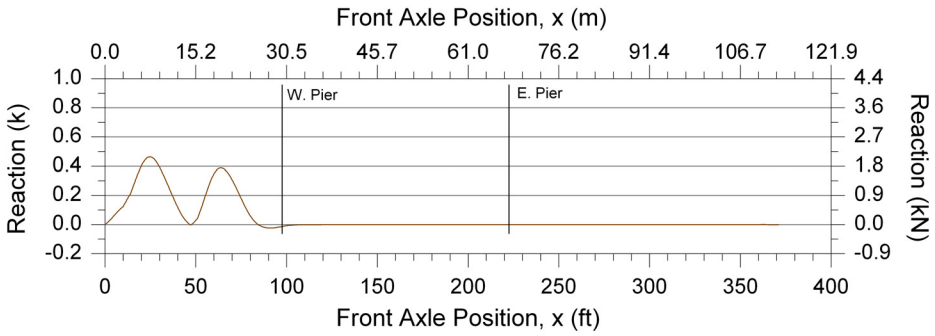

d. Unit semi (Type 3S2B)

Figure 5.8. A-SS-WB-V: Influence line and analytical vertical reaction histories from moving loads.

www.manaraa.com

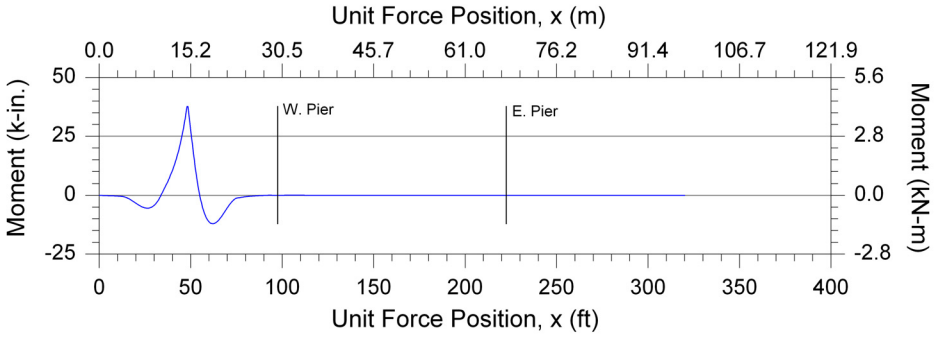

a. Influence Line (unit concentrated force)

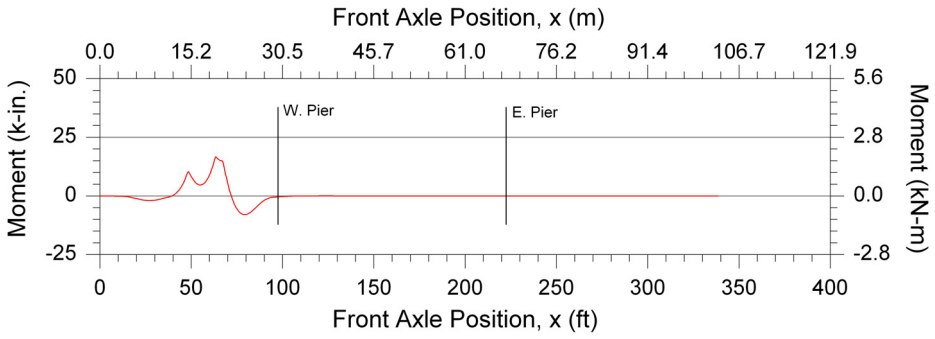

b. Unit straight truck (Type 3)

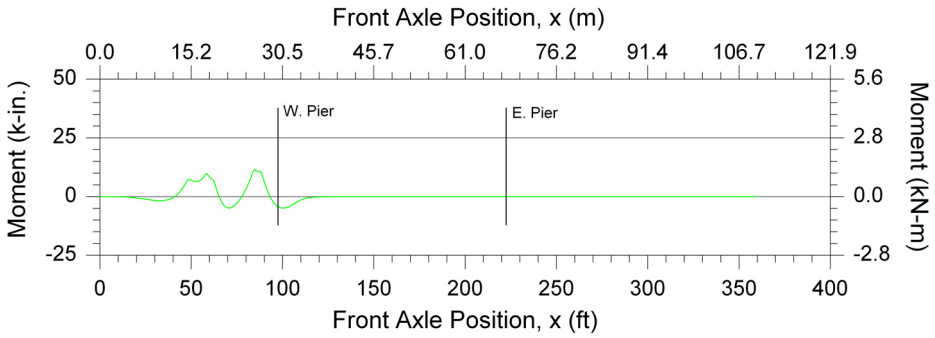

c. Unit semi (Type 3S2A)

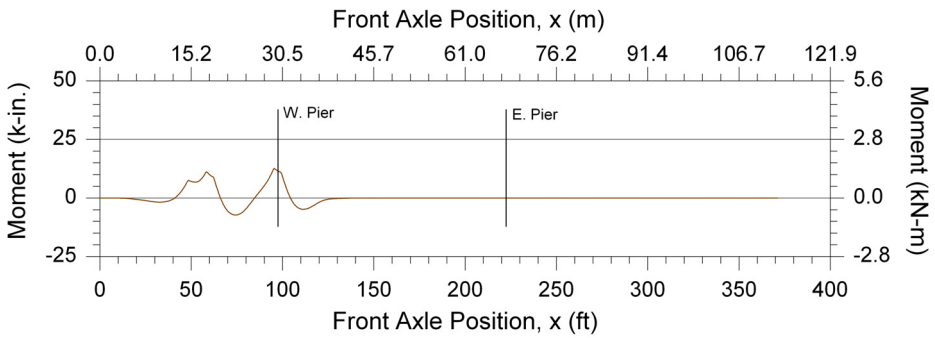

d. Unit semi (Type 3S2B)

Figure 5.9. B-SS-BF-H: Influence line and analytical nodal moment histories from moving loads.

www.manaraa.com

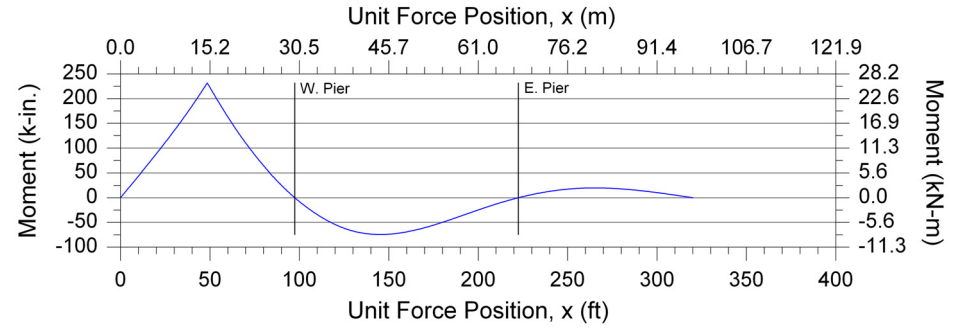

a. Influence Line (unit concentrated force)

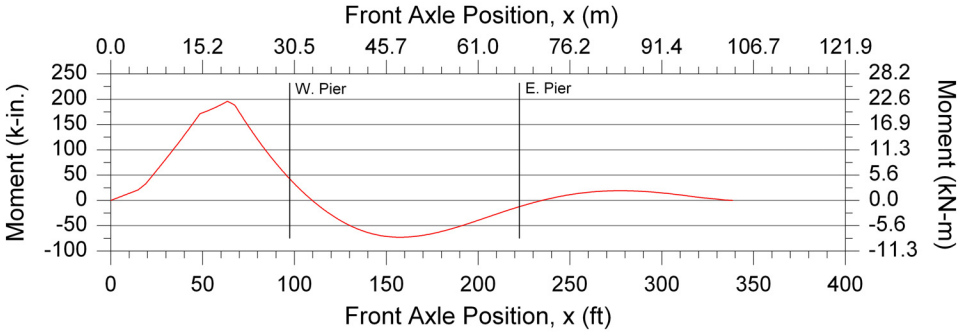

b. Unit straight truck (Type 3)

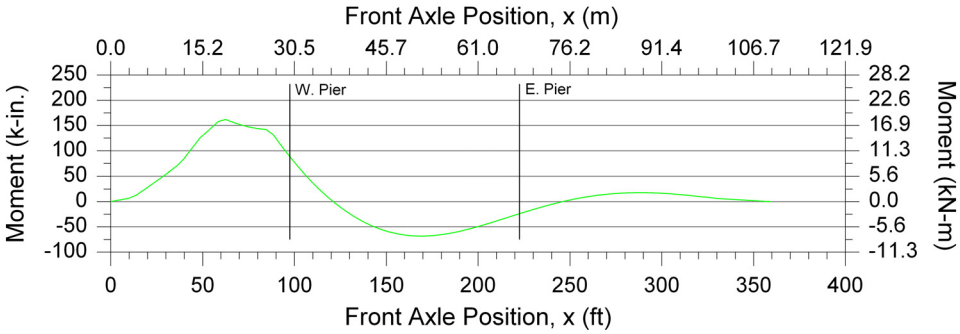

c. Unit semi (Type 3S2A)

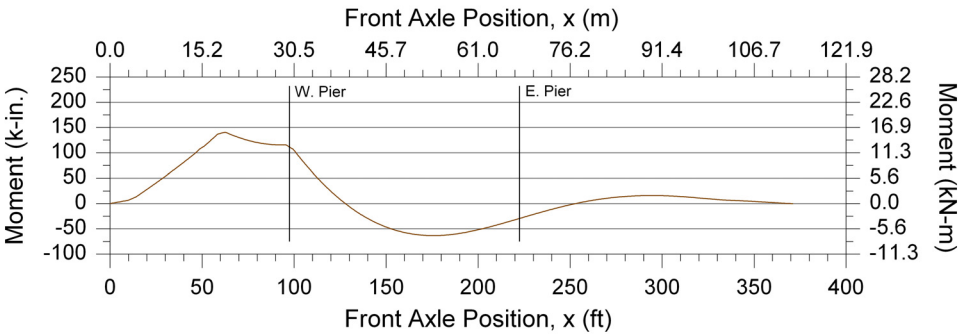

d. Unit semi (Type 3S2B)

Figure 5.10. B-SG-BF-H: Influence line and analytical nodal moment histories from moving loads.

www.manaraa.com

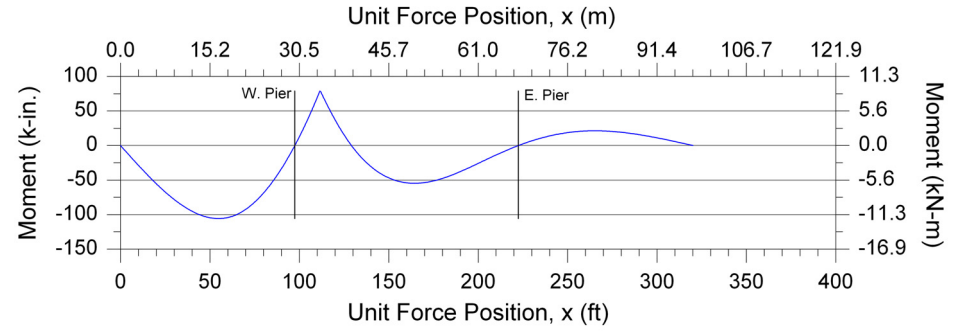

a. Influence Line (unit concentrated force)

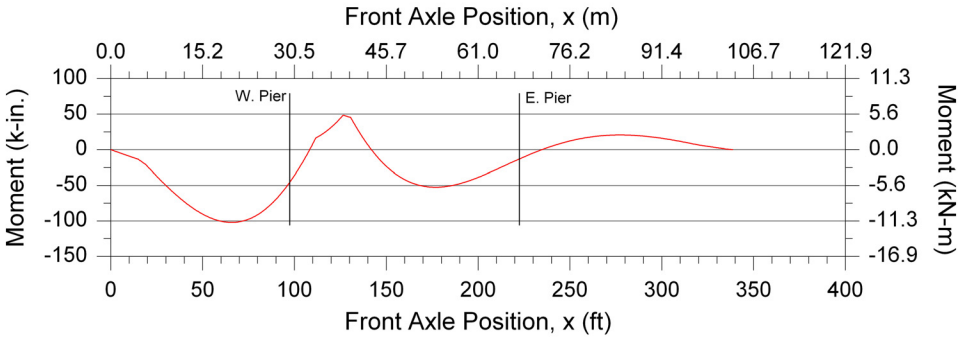

b. Unit straight truck (Type 3)

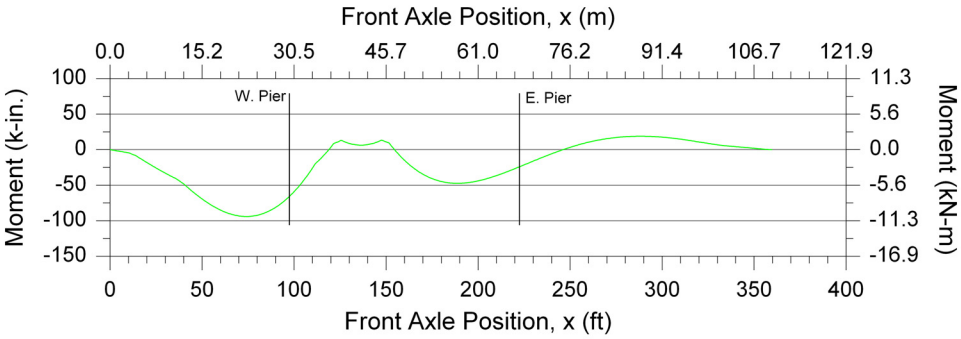

c. Unit semi (Type 3S2A)

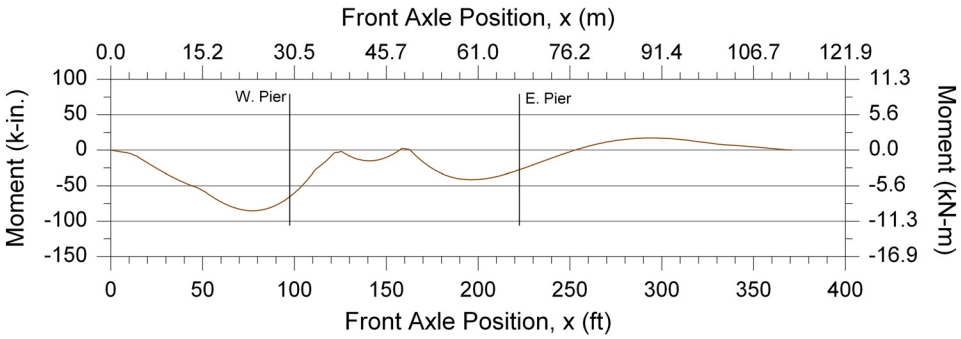

d. Unit semi (Type 3S2B)

Figure 5.11. C-SG-BF-H: Influence line and analytical nodal moment histories from moving loads.

www.manaraa.com

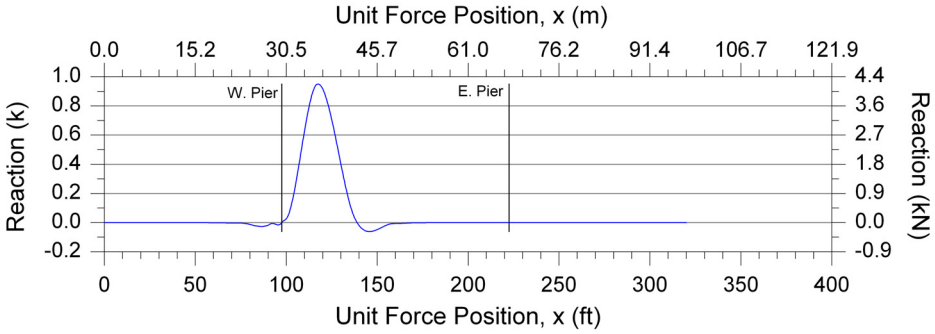

a. Influence Line (unit concentrated force)

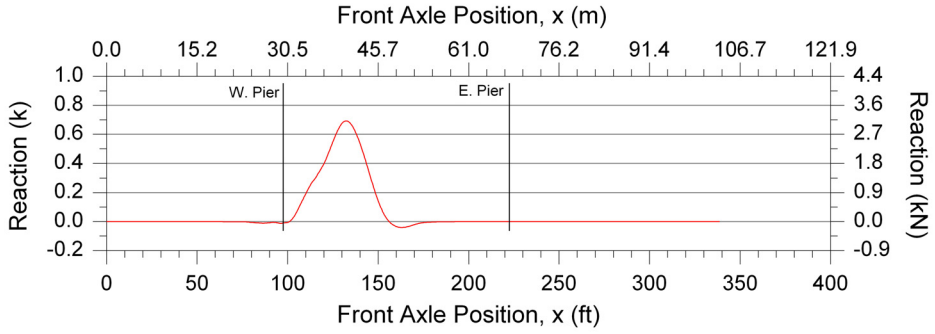

b. Unit straight truck (Type 3)

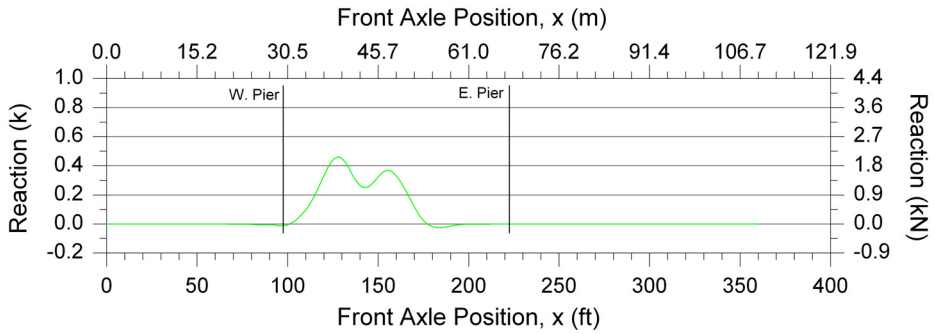

c. Unit semi (Type 3S2A)

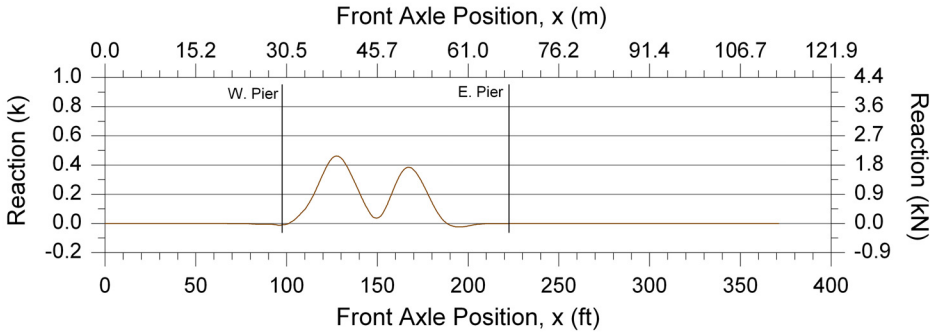

d. Unit semi (Type 3S2B)

Figure 5.12. C-SS-WB-V: Influence line and analytical vertical reaction histories from moving loads.

www.manaraa.com

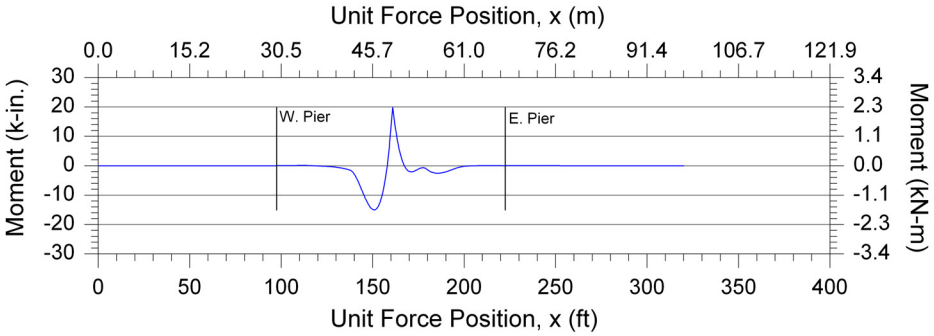

a. Influence Line (unit concentrated force)

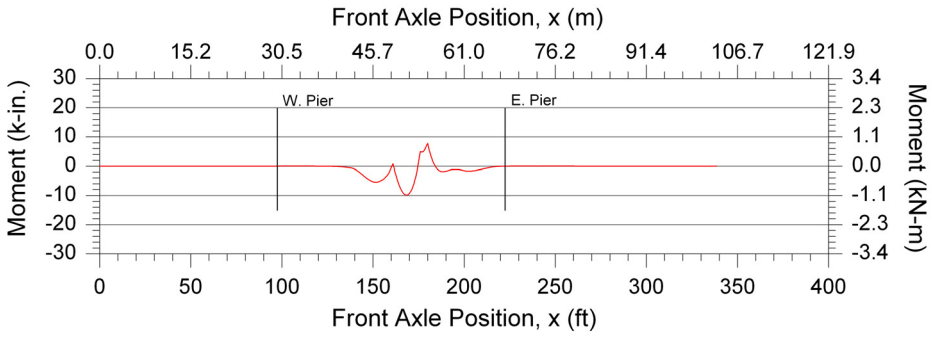

b. Unit straight truck (Type 3)

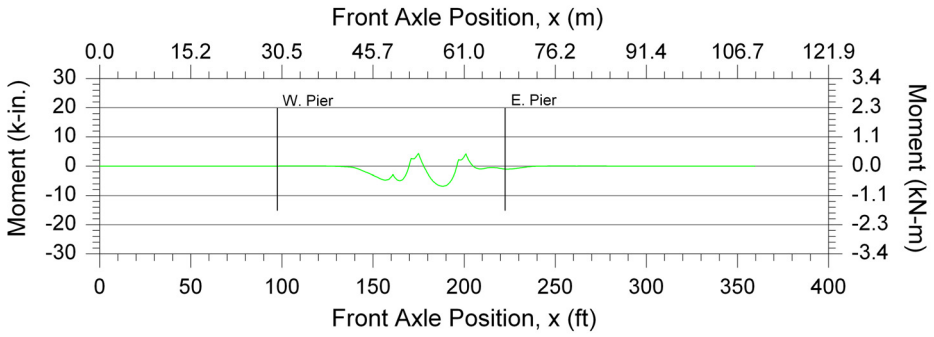

c. Unit semi (Type 3S2A)

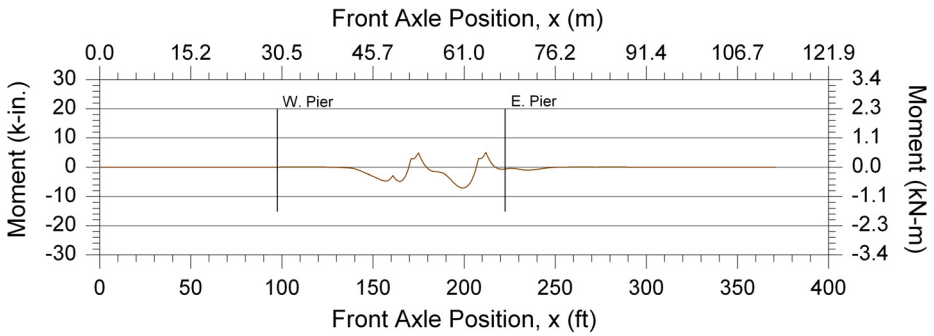

d. Unit semi (Type 3S2B)

Figure 5.13. D-SS-BF-H: Influence line and analytical nodal moment histories from moving loads.

www.manaraa.com

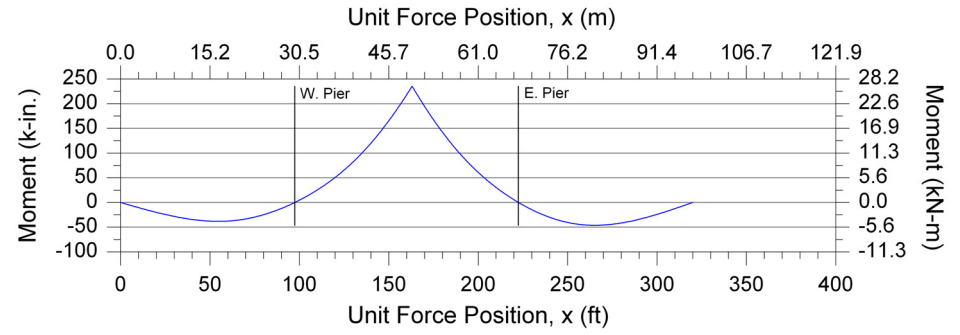

a. Influence Line (unit concentrated force)

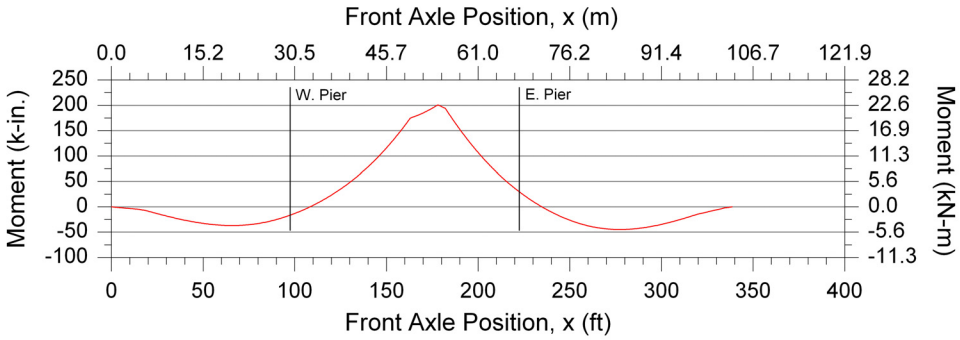

b. Unit straight truck (Type 3)

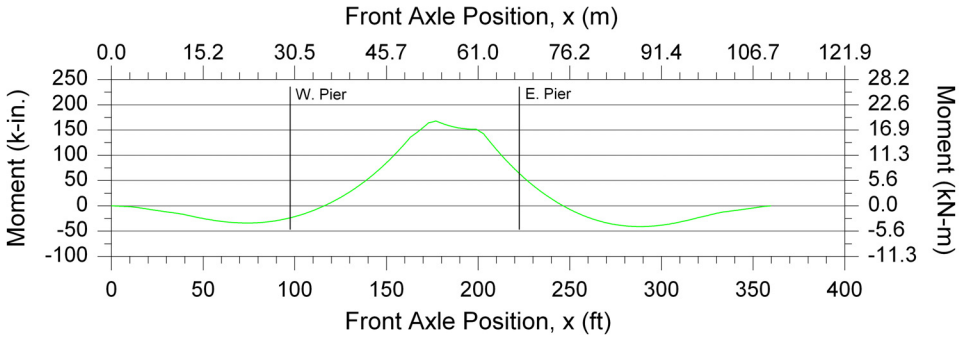

c. Unit semi (Type 3S2A)

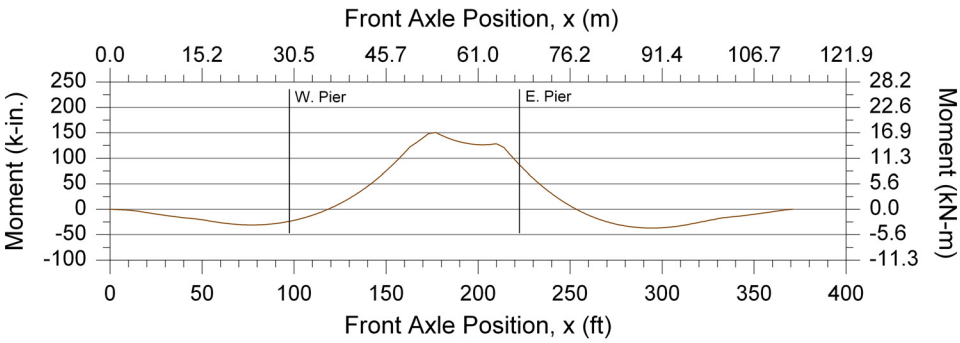

d. Unit semi (Type 3S2B)

Figure 5.14. D-SG-BF-H: Influence line and analytical nodal moment histories from moving loads.

www.manaraa.com

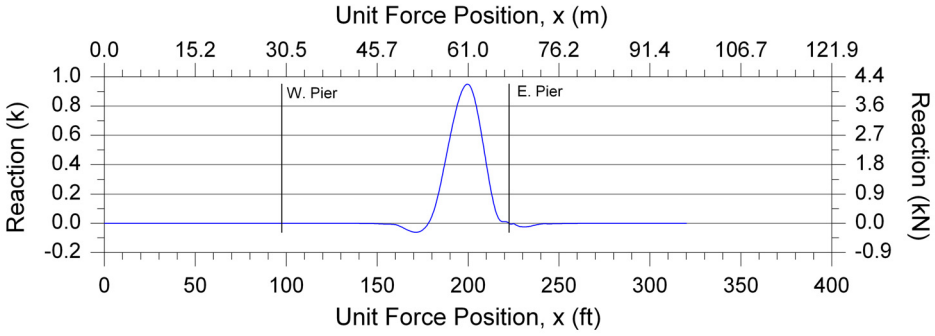

a. Influence Line (unit concentrated force)

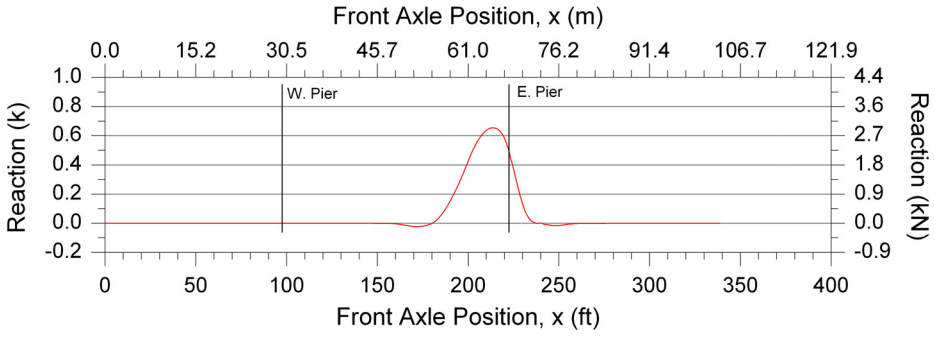

b. Unit straight truck (Type 3)

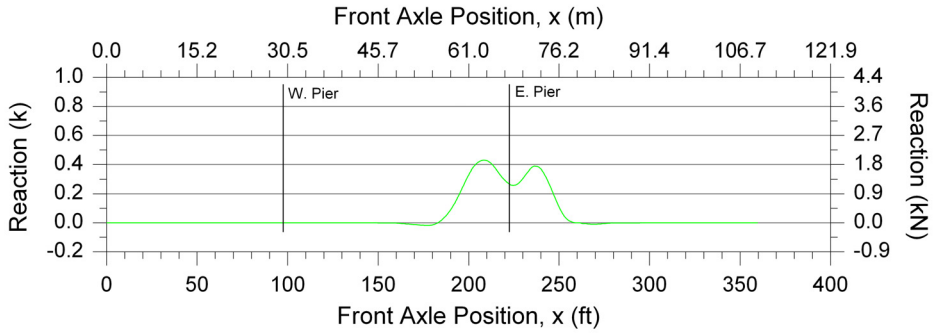

c. Unit semi (Type 3S2A)

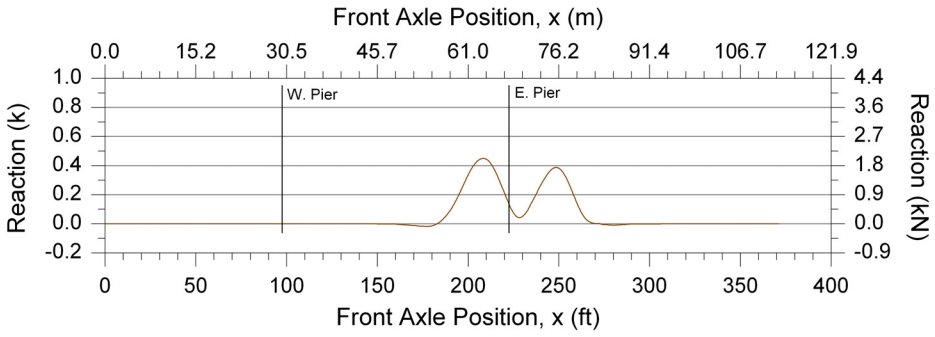

d. Unit semi (Type 3S2B)

Figure 5.15. E-SS-WB-V: Influence line and analytical vertical reaction histories from moving loads.

www.manaraa.com

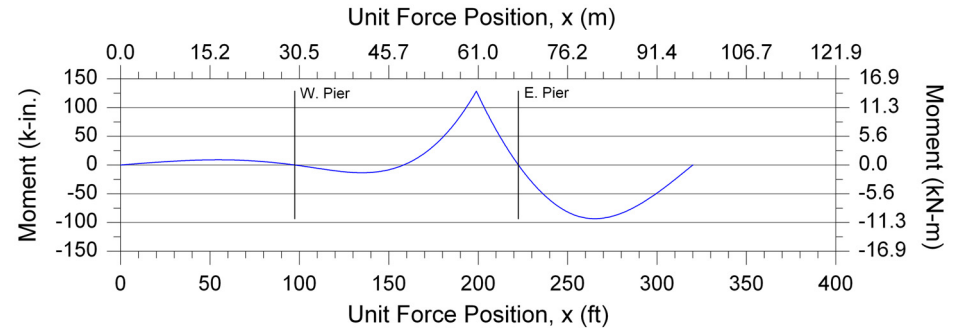

a. Influence Line (unit concentrated force)

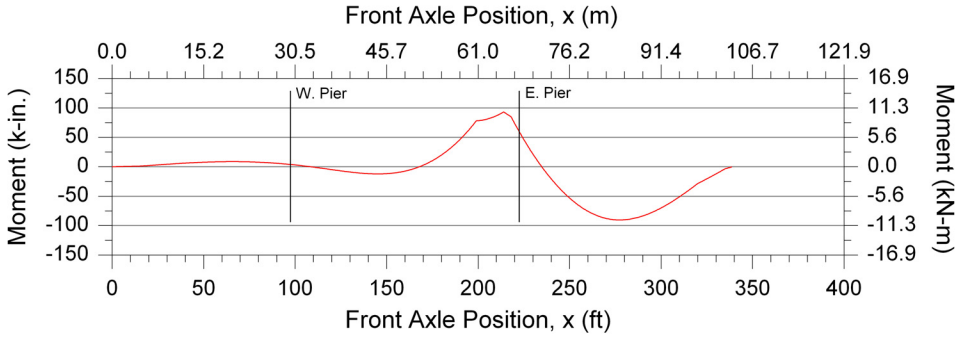

b. Unit straight truck (Type 3)

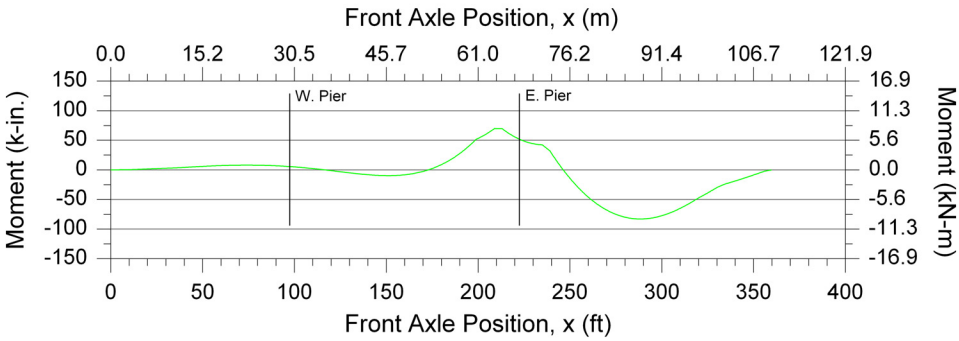

c. Unit semi (Type 3S2A)

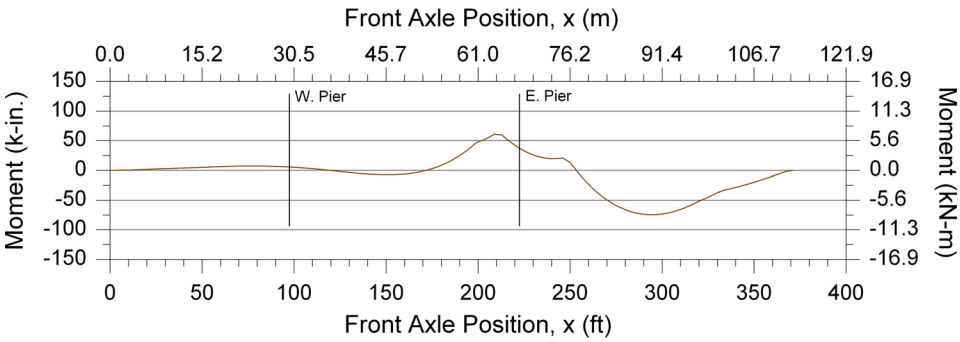

d. Unit semi (Type 3S2B)

Figure 5.16. E-SG-BF-H: Influence line and analytical nodal moment histories from moving loads.

www.manaraa.com

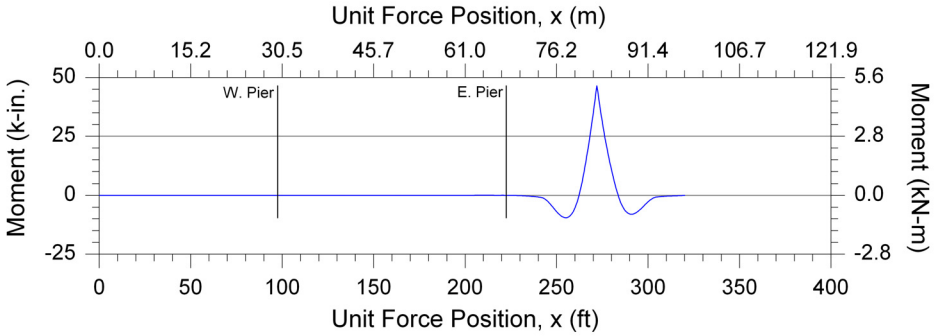

a. Influence Line (unit concentrated force)

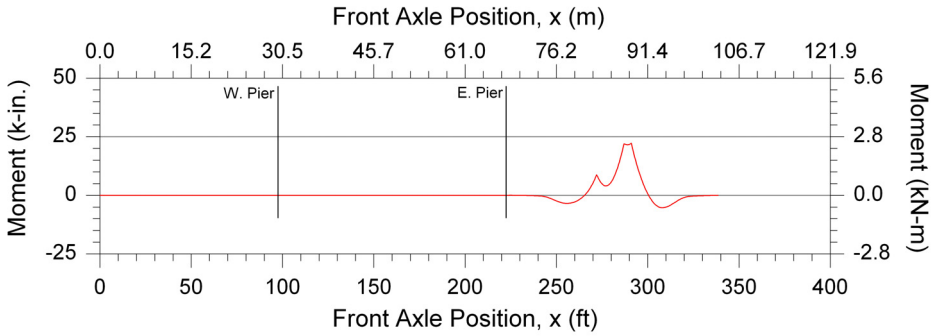

b. Unit straight truck (Type 3)

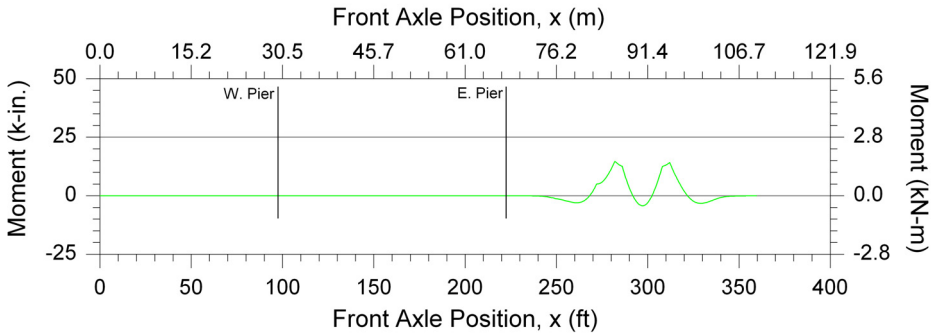

c. Unit semi (Type 3S2A)

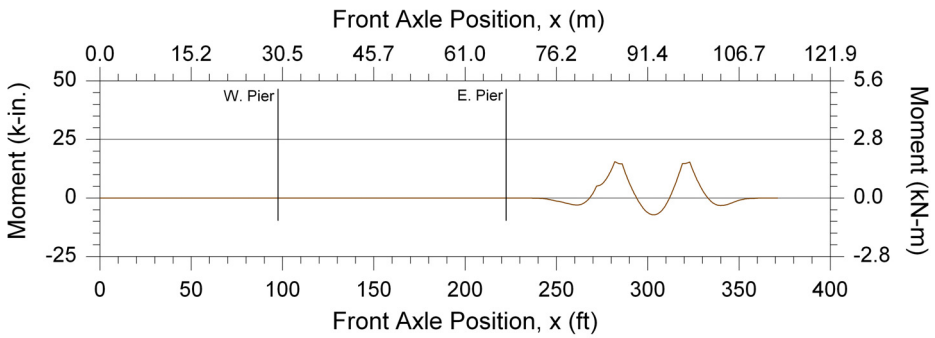

d. Unit semi (Type 3S2B)

Figure 5.17. F-SS-BF-H: Influence line and analytical nodal moment histories from moving loads.

www.manaraa.com

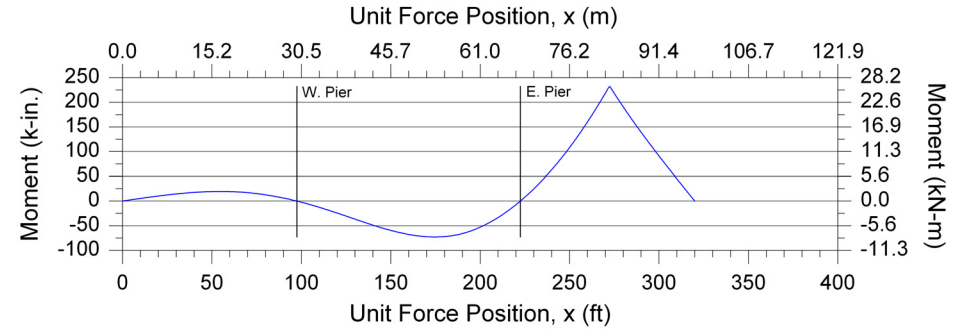

a. Influence Line (unit concentrated force)

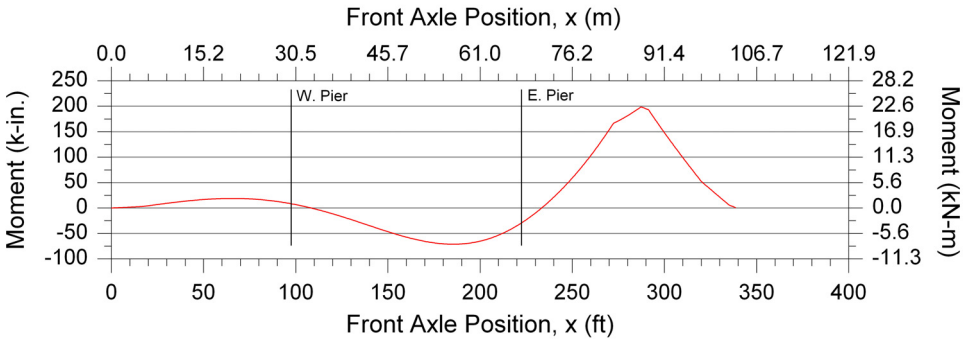

b. Unit straight truck (Type 3)

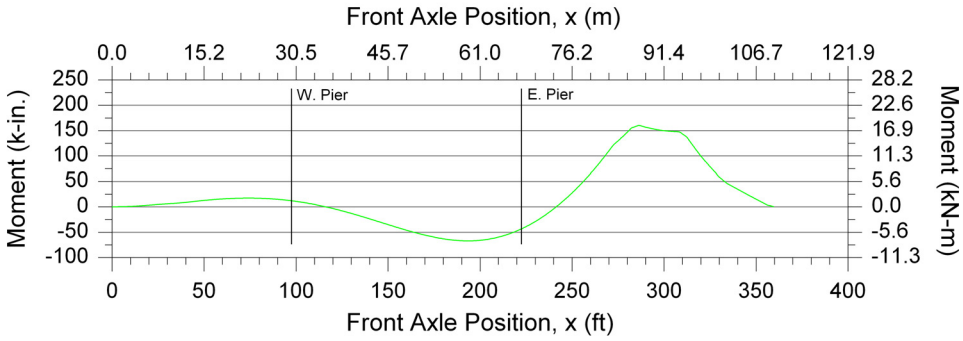

c. Unit semi (Type 3S2A)

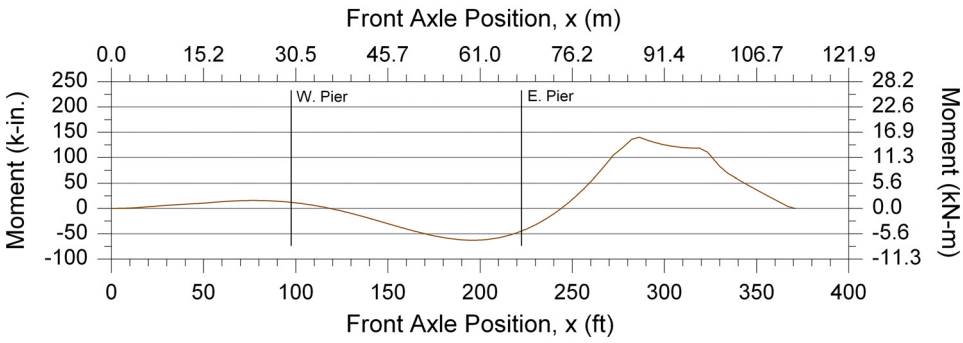

d. Unit semi (Type 3S2B)

Figure 5.18. F-SG-BF-H: Influence line and analytical nodal moment histories from moving loads.

www.manaraa.com

- For both girders and stringers, the influence lines predict that the maximum absolute response in each section force history is obtained when the unit concentrated force is positioned at the same longitudinal location as the section under investigation. While actual vehicles are not single concentrated forces, this conclusion suggests that the maximum strains for a section are produced when the ambient traffic passes over that region of the bridge. Since the FOSs are positioned at several longitudinal locations in the bridge, the maximum absolute response for an event will occur at different times in the strain records of the sensors.

- Expanding on the previous conclusion, for analyses involving unit truck moving loads, the peaks and valleys producing extreme values in the force histories generally shift to the right.
    - As the unit truck geometry length increases, the shift distance increases.
    - For a given unit truck geometry, the shift distance is relatively constant among all section force histories.

The force history plots displayed in Figs. 5.8 - 5.18 were presented as functions of the moving load position. These plots were useful for gaining a conceptual understanding of the patterns and relative magnitudes of the vehicular events in a sensor strain record, but in order to validate the patterns of the analytical results, it was necessary to compare them to actual events recorded by the US30 SHM system. Measured strains at the US30 bridge site are saved as functions of time (or index position). Thus, the moving loads utilized in the analytical models were assumed to be traveling 60 mph (97 kph), and the force histories were converted to be functions of time. For a comparison with the analytical results, the vehicular event presented in Fig. 5.4 was identified in the strain record of every sensor. For each of the eleven FOSs considered in Figs. 5.8 - 5.18, all analytical force history patterns from the unit trucks were compared with that of the experimental vehicular event, and it was determined that the unit semi (Type 3S2A) analytical patterns agreed most closely with the experimental patterns in most cases. To illustrate the similarities, unit semi (Type 3S2A) analytical force history patterns are displayed along with the corresponding experimental vehicular event patterns in Figs. 5.19 - 5.29. For these figures, note that for A-SS-WB-V, C-SS-WB-V, and E-SS-WB-V, the sign convention that was used in the analyses was opposite of that in the experimental results; for all other comparisons, the sign conventions were the same.

Review of Figs. 5.19 - 5.29 reveals that in many cases, the vehicular event in the zeroed strain record was significantly different than the event in the filtered data, and the patterns of the analytical events agreed much more closely with the filtered experimental data than with the zeroed

www.manaraa.com

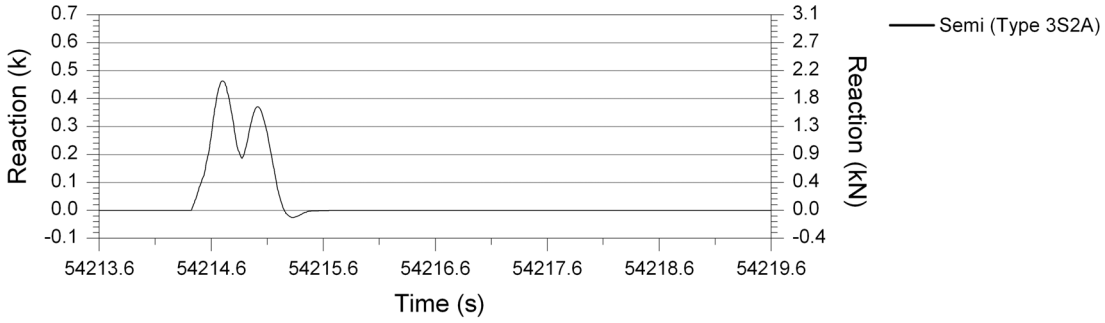

a. Analytical vertical reaction history

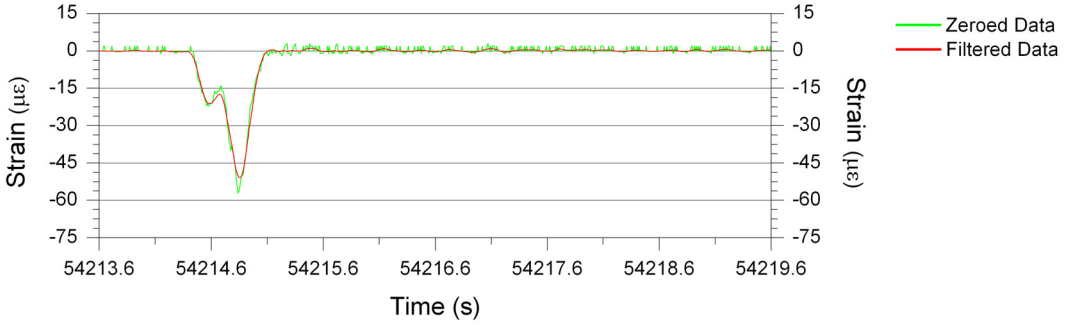

b. Experimental vehicular event

Figure 5.19. A-SS-WB-V: experimental vehicular event and corresponding analytical reaction history.

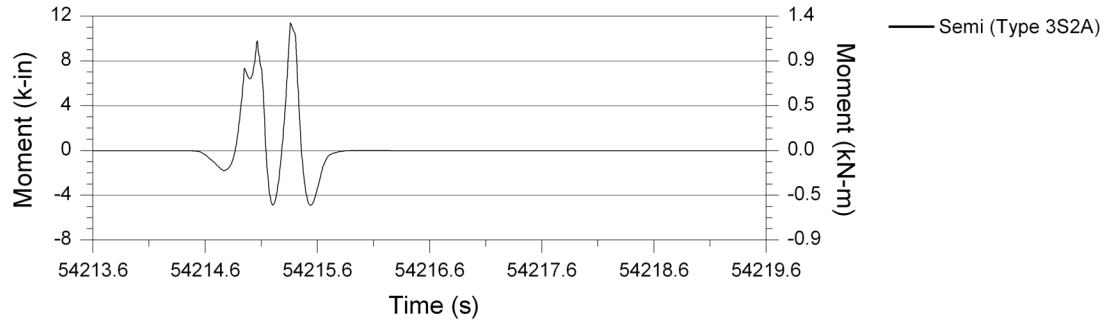

a. Analytical nodal moment history

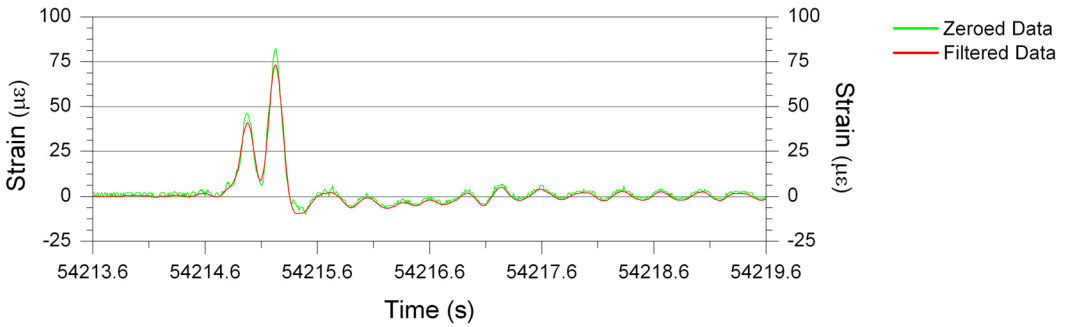

b. Experimental vehicular event

Figure 5.20. B-SS-BF-H: experimental vehicular event and corresponding analytical moment history.

www.manaraa.com

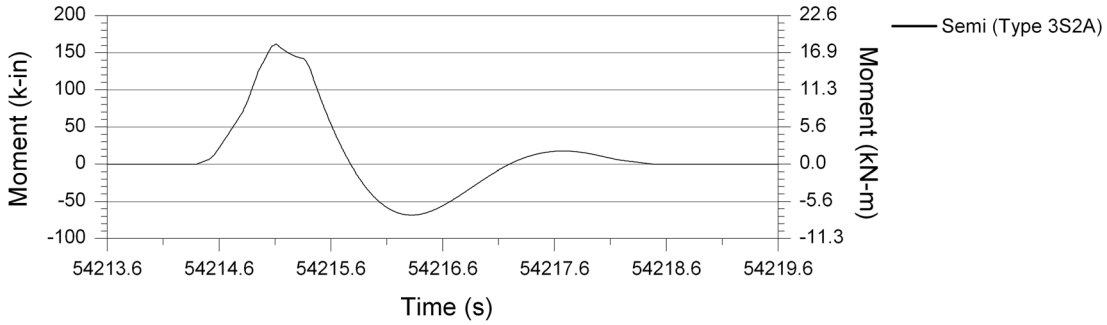

a. Analytical nodal moment history

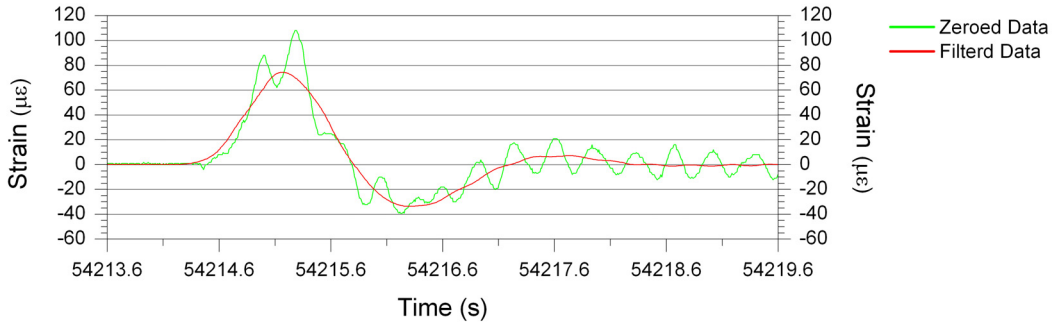

b. Experimental vehicular event

Figure 5.21. B-SG-BF-H: experimental vehicular event and corresponding analytical moment history.

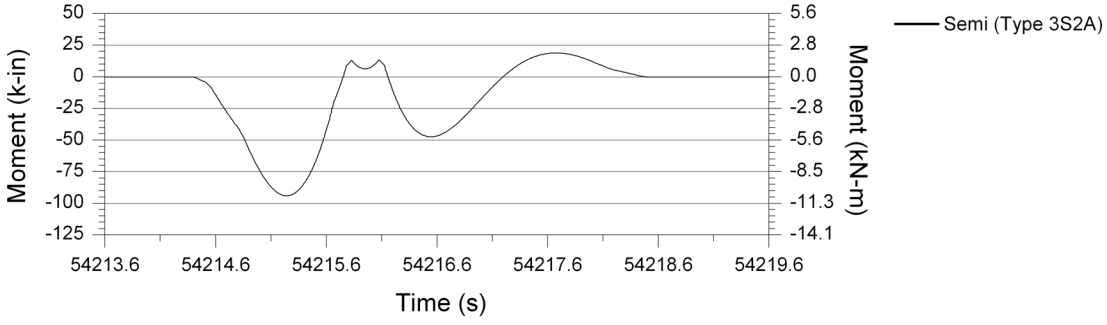

a. Analytical nodal moment history

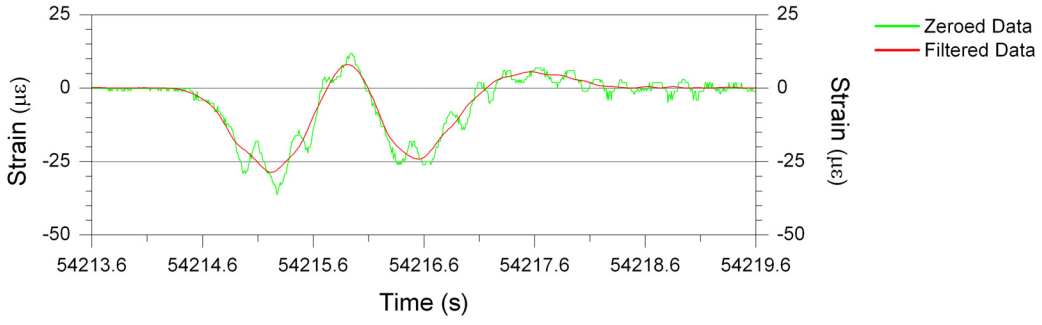

b. Experimental vehicular event

Figure 5.22. C-SG-BF-H: experimental vehicular event and corresponding analytical moment history.

www.manaraa.com

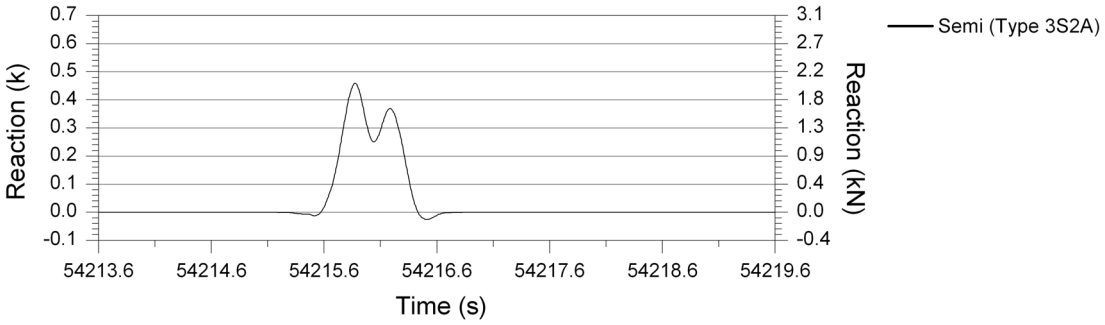

a. Analytical vertical reaction history

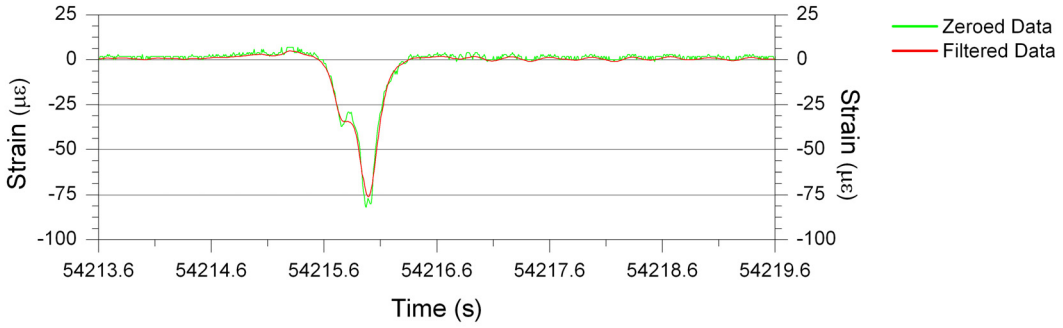

b. Experimental vehicular event

Figure 5.23. C-SS-WB-V: experimental vehicular event and corresponding analytical reaction history.

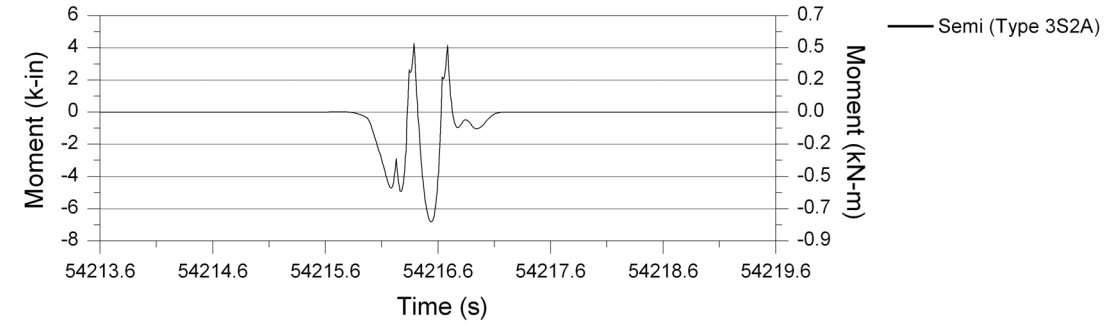

a. Analytical nodal moment history

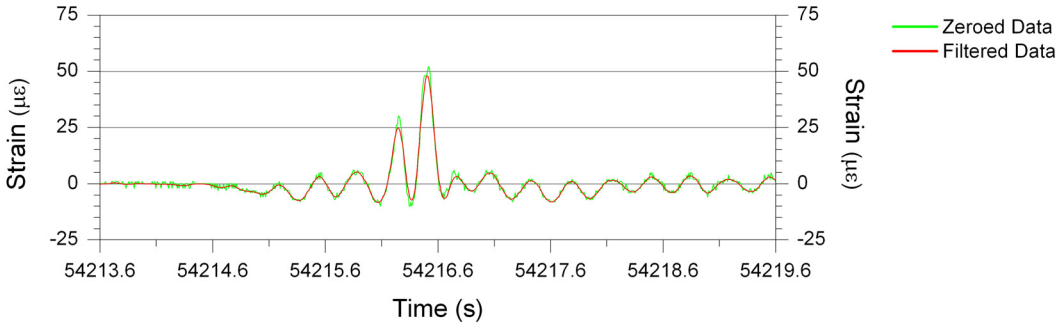

b. Experimental vehicular event

Figure 5.24. D-SS-BF-H: experimental vehicular event and corresponding analytical moment history.

www.manaraa.com

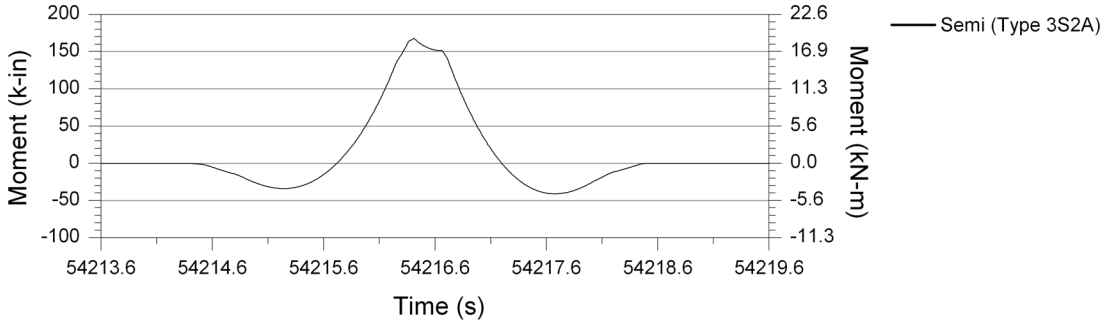

a. Analytical nodal moment history

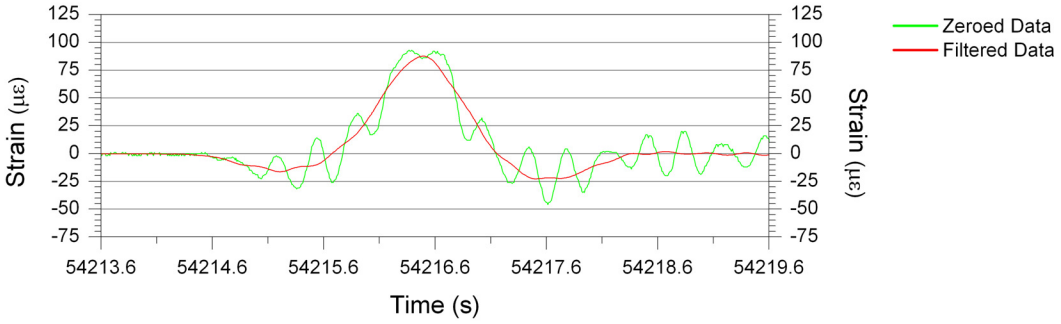

b. Experimental vehicular event

Figure 5.25. D-SG-BF-H: experimental vehicular event and corresponding analytical moment history.

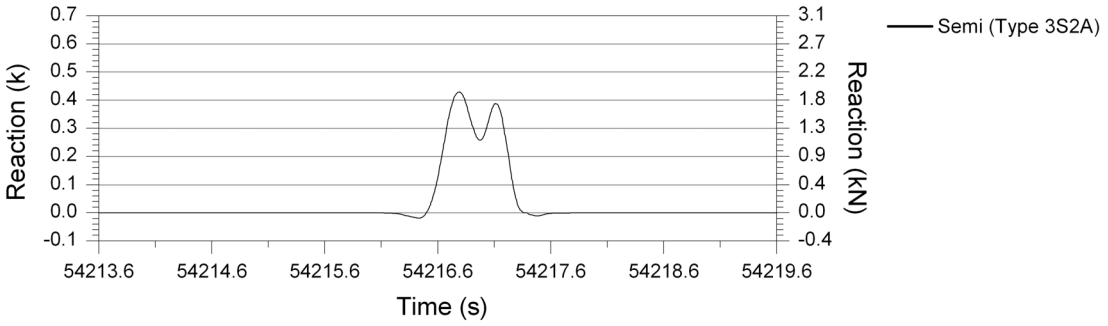

a. Analytical vertical reaction history

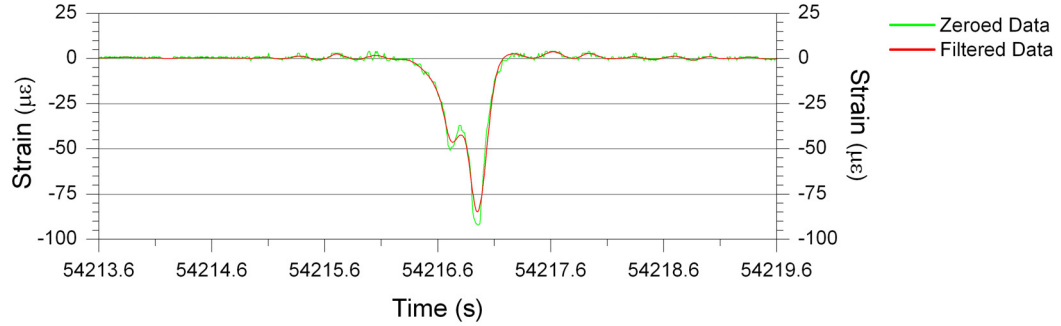

b. Experimental vehicular event

Figure 5.26. E-SS-WB-V: experimental vehicular event and corresponding analytical reaction history.

www.manaraa.com

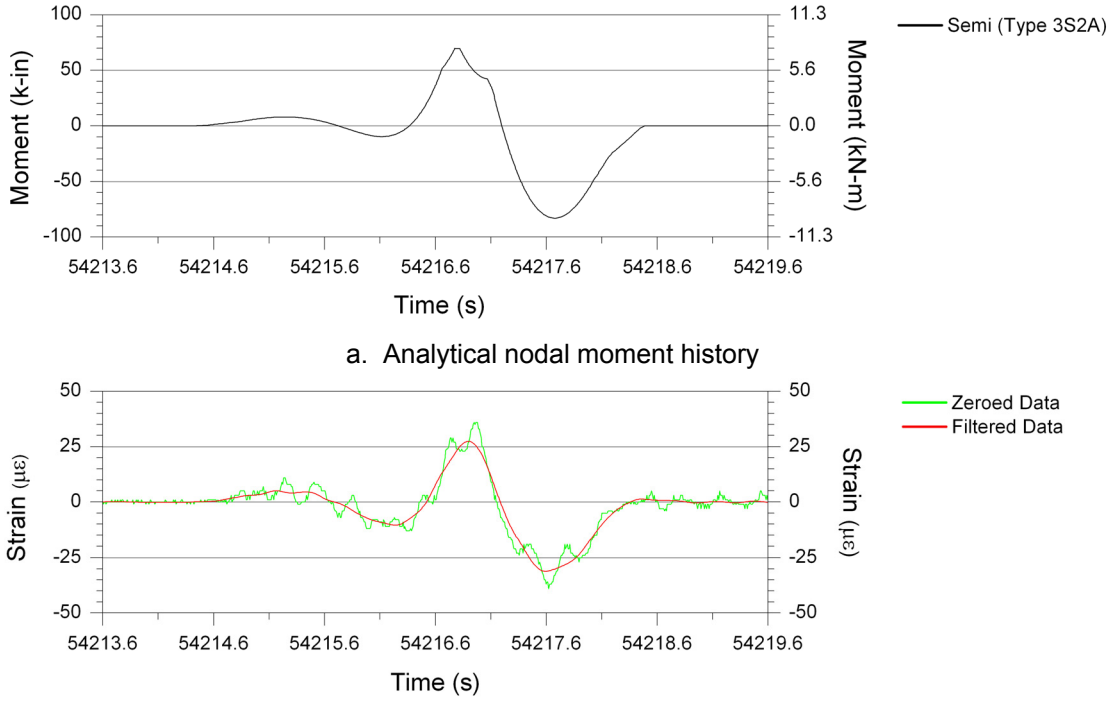

a. Analytical nodal moment history

b. Experimental vehicular event

Figure 5.27. E-SG-BF-H: experimental vehicular event and corresponding analytical moment history.

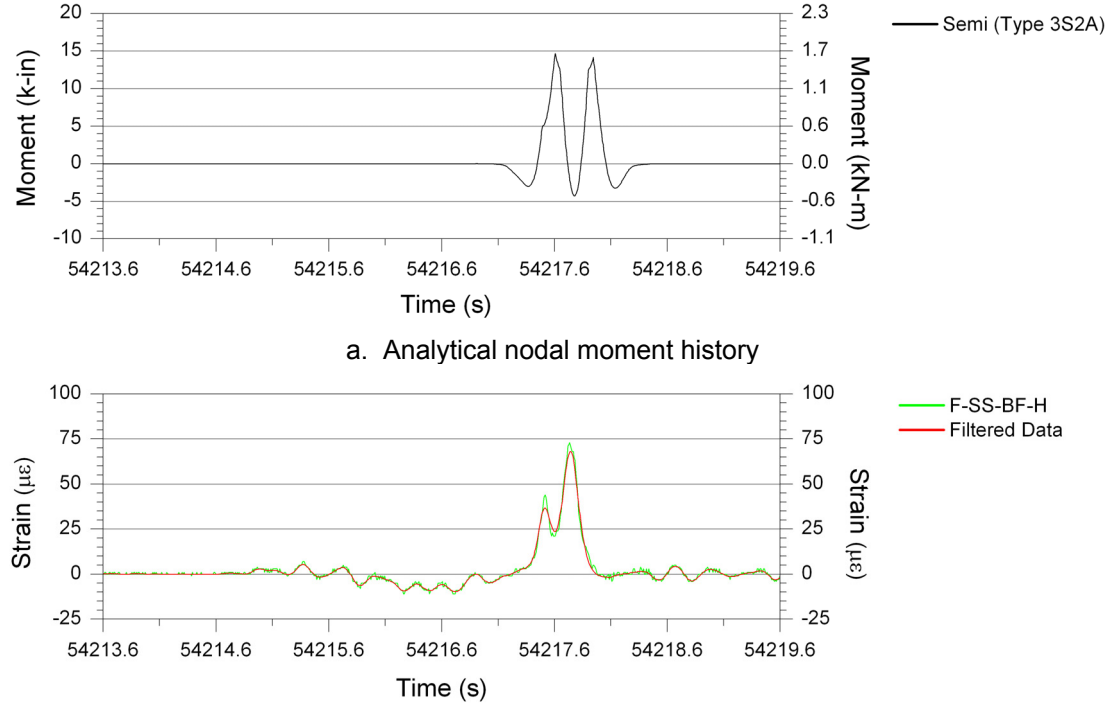

a. Analytical nodal moment history

b. Experimental vehicular event

Figure 5.28. F-SS-BF-H: experimental vehicular event and corresponding analytical moment history.

www.manaraa.com

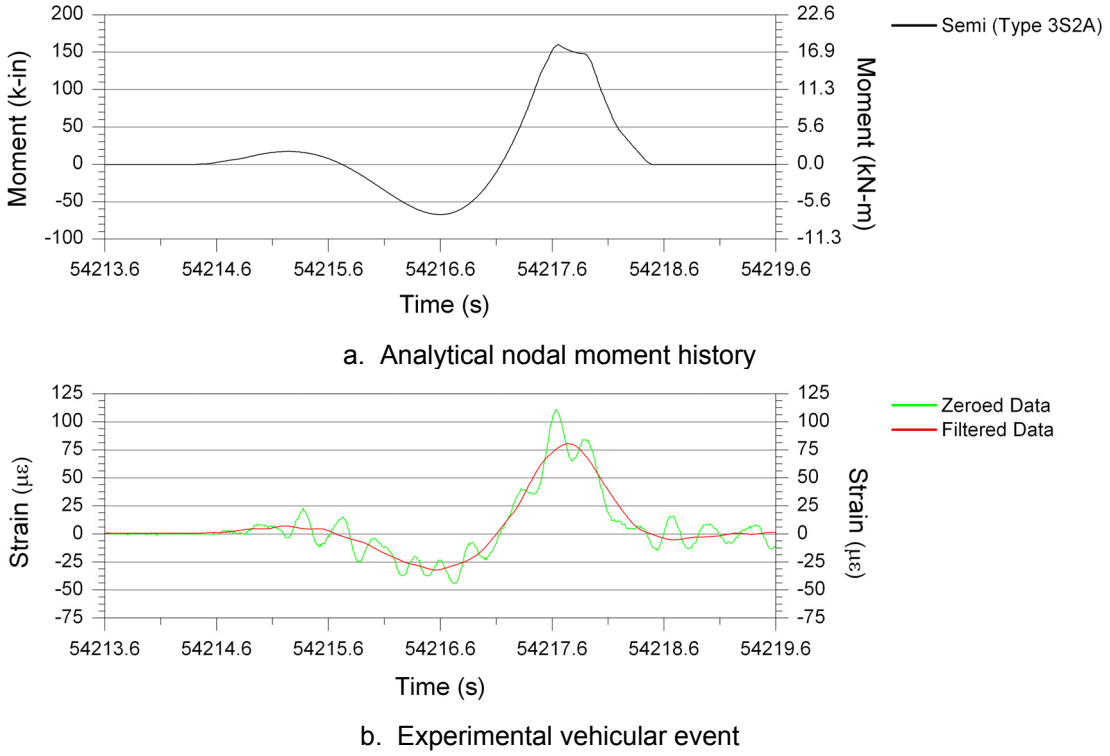

Figure 5.29. F-SG-BF-H: experimental vehicular event and corresponding analytical moment history.

data. This was expected since static analyses were performed, and the resulting data after filtering are the quasi-static response of the bridge to the ambient traffic. As a result, the need to filter the dynamic response and noise from the data file to reveal the quasi-static vehicular event was further reinforced.

Comparison of the static analytical and quasi-static experimental event patterns of Figs. 5.19 - 5.29 revealed two main observations: (1) the discontinuities in the analytical event patterns were not present in the experimental event patterns, and (2) the relative magnitudes of the experimental event patterns are not always in agreement with those of the analytical results. These observations are explainable when considering the differences between the modeled structure and the actual structure. One large difference is that the model did not include the load distributing capabilities of the bridge deck or influence of the bridge overhands and guardrails on the member section properties. In addition, because 2-D analyses were performed, the transverse stiffness of the bridge was neglected. As a result of the simplified analysis, exact agreement in the event patterns between the analysis and

www.manaraa.com

the experimental results did not exist and was not expected. However, the analyses were performed to obtain a general understanding of the factors that affect vehicular events in strain records, and the objective was achieved. Since analytical and experimental results are similar in most cases, the conclusions determined from the analytical results have been proven to be applicable for the strain data recorded at the US30 bridge.

An understanding of vehicular events in strain records is essential for understanding the operations performed by the data reduction, extraction, and evaluation algorithms presented in Sections 5.2 and 5.3. Summarizing the results and discussion in this section, the four most important conclusions pertaining to the discussion and application of vehicular events in the proceeding sections are as follows:

- For a given sensor, variations among events in the strain records of sensors are produced by different types of vehicles (i.e. car, straight truck, semi truck, utility vehicle, etc.) traversing the bridge.
- For a given type of vehicle, its event pattern and magnitude are different in strain records depending on the sensor location, orientation, and member to which it is attached.
- An event may be composed of many peaks and valleys, but the maximum absolute response of an event theoretically occurs when the vehicle is in close vicinity of the sensor (as predicted by influence lines).
- As a vehicle traverses the bridge, its event occurs at different times in the strain records of the sensors in the bridge.

For simplicity, vehicular events were introduced and discussed for the situation where one vehicle traversed the bridge. It is important to note, however, that it is more common that multiple vehicles traverse the bridge in a group. The density of the vehicles and their patterns as they cross the bridge are additional factors with potential to affect the patterns and magnitudes of events in strain records. Compensation for these factors is illustrated in Section 5.2.

5.1.4 Feature Extraction, Relationship Development, and Evaluation Procedures

After zeroed strain data have been filtered and all events have been identified in the resulting data, the maximum and minimum strain values for each peak and valley, respectively, are identified in the strain records. These values are referred to as the event extrema, and they are the extracted from the data sets. Figure 5.30 illustrates the identification of event extrema from the filtered data

www.manaraa.com

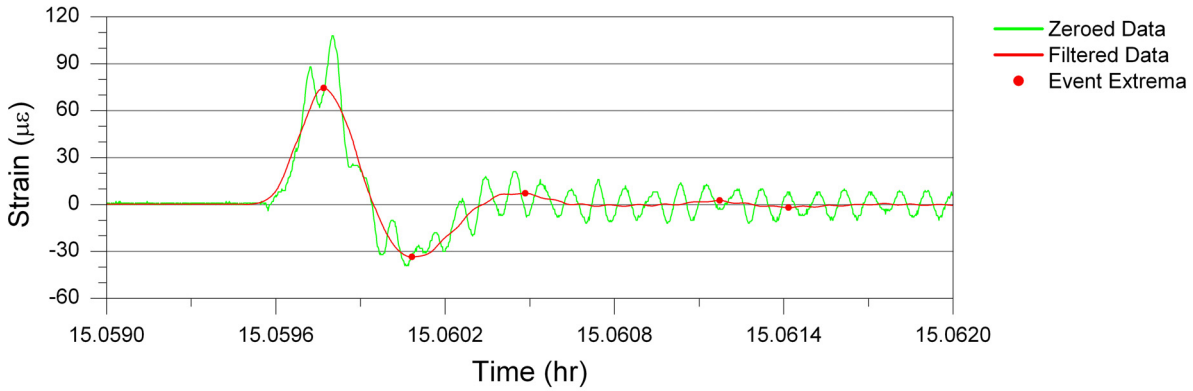

Figure 5.30. Identified extrema for a vehicular event in the B-SG-BF-H strain record (See Fig. 5.4).

previously introduced in Fig. 5.4. Note that five extrema have been identified for the presented data. The first three extrema apply to the actual event and are the most important. However, the last two have been identified as part of the free vibration response of the structure, and since they are not part of the actual event, they are not useful. While these two unwanted extrema have been identified from the free vibration response, many more could have been identified if the zeroed data had been used instead of the filtered data. As will be shown, procedures have been developed to help find and eliminate the unwanted extrema before the evaluation process. The details of the algorithm that identifies and extracts event extrema from strain records is discussed in Section 5.2.3.

The event extrema are extremely important in the evaluation process utilized by the SHM system. The event extrema alone, however, cannot be used to analyze the condition of a bridge or bridge component because the characteristics of the ambient traffic causing the bridge response are not known. Examples of such characteristics include geometries and weights of the vehicles, longitudinal and transverse combinations of traffic on the bridge, paths of the vehicles as they traverse the bridge, etc. Without knowledge of such characteristics, it would be difficult to perform a classical structural evaluation of the bridge. For example, if abnormal behavior was detected in the strain record of a sensor and only that sensor was used to diagnose the situation, it would not be known if the change in behavior was the result of damage formation or if it was the result of a change in a characteristic of the ambient traffic.

www.manaraa.com

The uncertainties of the previous discussion can be overcome, however, if multiple sensors were used to diagnose the situation. Except for extreme instances, damage is a localized phenomenon. Therefore, sensors in the area of damage, which are referred to as target sensors (TSs), may detect strain changes caused to the formation of damage; sensors farther away from the damage, referred to as non-target sensors (NTSs), would not likely detect the bridge behavior change. Therefore, if changes in event extrema were detected in TSs and NTSs, then the cause of such a change would likely be a change in the ambient traffic. However, if changes in event extrema were detected in TSs but not in NTSs, then the cause of such a change could be the result of damage formation in the location of the TS. If such relationships between sensors are known, then pattern recognition techniques can be used to detect the outliers that are indicative of damage.

As mentioned in Section 2.3.4, control chart analyses are a common SPC technique used to identify atypical behavior in a process, and they can be univariate or multivariate. Since processes are rarely univariate, simultaneous monitoring of two or more parameters is often required, which is commonly referred to as multivariate SPC or multivariate quality control (MQC). In one method for monitoring bivariate data, univariate control charts are independently established for each parameter in the data and superimposed on a single scatter plot; corresponding data points for each time value or sample number form (x,y) pairs in the scatter plot. With this bivariate analysis, however, an elliptical joint control region is established that is different from the control regions determined in each independent control chart analysis. A bivariate plot of this type was previously presented in Fig. 2.3, where the orientation of the elliptical control region was described to be dependent on the correlation between the two samples. For multivariate procedures involving several parameters or variables, the process becomes more complicated and multivariate control charts such as Hotelling T^2, Chi-square, Multivariate Cumulative Sum (MCUSUM), and Multivariate Exponentially Weighted Moving Average (MEWMA) are commonly used.

The FCB SHM system utilizes methods of pattern recognition and analysis similar to the control chart procedures that were previously discussed for bivariate data, but deviations from these methods have been incorporated to address specific needs of the proposed system. In the system,

www.manaraa.com

each sensor is classified as a TS or a NTS. The cut-back regions in the US30 bridge are the known problematic areas that are susceptible to crack formation. Thus, the cut-back regions in Section C (See Fig. 4.1d) were selected as demonstration target regions. As a result, the ten FOSs within these regions have been classified as TSs and are listed as follows:

- C-NG-CB(1)-V
- C-NG-CB(2)-V
- C-NG-CB(3)-V
- C-NG-CB(4)-V
- C-NG-CB(5)-V
- C-SG-CB(1)-V
- C-SG-CB(2)-V
- C-SG-CB(3)-V
- C-SG-CB(4)-V
- C-SG-CB(5)-V

The remaining 30 FOSs have been classified as NTSs. Considering two FOSs (one TS and one NTS) at a time, the extrema from corresponding quasi-static vehicular events are matched to form an (x,y) pair on a scatter plot. As data are continuously collected through the training process, the matched event extrema form relationships on the x-y plot.

After completion of extrema matching, limit sets that are comparable to elliptical control regions are manually established via a graphical user interface (GUI) to define the “typical” region for each relationship. The initial process of matching event extrema to identify and define relationships with limits sets is referred to as the training process. When the training process has been completed for all applicable and desired sensor pairs, the defined relationships are used with newly collected strain data to evaluate the TS extrema and determine if their values are typical (within the limit sets) or atypical (outside of the limit sets) to that of the trained behavior. After evaluation is complete, a report is autonomously generated that summarizes the results.

In summary, by establishing relationships among the event extrema captured by all of the sensors, knowledge of variable parameters associated with ambient traffic such as such as the weights and geometries of vehicles, longitudinal and transverse combinations of traffic, paths of the vehicles as they traverse the bridge, etc., is not required to evaluate the structural condition of the bridge. More details and results of the extrema matching process, evaluation process, and report generation process are described in Section 5.2 and 5.3.

www.manaraa.com

The two modes of operation for the SHM system process include: (1) training mode, which is described in Section 5.2, and (2) monitoring mode, which is presented in Section 5.3. Figure 5.31 presents a general flowchart for the order of procedures that are undertaken in each mode. The training mode includes procedures that are required for configuring the SHM system software for the bridge and sensor network. The monitoring mode uses the relationships that were established in the training mode to evaluate performance data as soon as they have been saved, and in addition, to ultimately generate a report that summarizes the performance of the bridge for a given period of time.

5.1.5 Review of Measured Behavior in Cut-back Regions

An understanding of the behavior causing TS strains in the cut-back regions is important prior to the detailed discussions of the evaluation methods that have been developed. For the vehicle that traveled across the bridge and generated the NTS events displayed in Figs. 5.19 - 5.29, the same event was identified in the strain records of the TSs. Figure 5.32 presents zeroed and filtered data for the event in the TSs that are located in the north cut-back region of Section C (See Fig. 4.1d). Similarly, Fig. 5.33 presents zeroed and filtered data for the same event within the TS strain records of the south cut-back region. Note once again that removal of dynamic responses from the data significantly changed the shape of the event in all sensors. Moreover, all FOSs have three identified extrema from the event, which corresponds to one extrema per span that was traversed by the vehicle.

Review of Figs. 5.32 and 5.33 reveals that out-of-plane bending occurred in both cut-back regions. In addition, results between sensors corresponding to the same vertical position in the cut-back regions have opposite signs. For example, event extrema for C-SG-CB(1)-V in Fig. 5.32b were approximately 54.3 με, -108 με, and 19 με. However, the corresponding event extrema in C-SG-CB(1)-V were approximately -55με, 67 με, and -17 με. Since the sensors in both regions were installed on the inner faces of the webs, it can be concluded that both regions experienced the same reverse curvature behavior, but at different magnitudes. This out-of-plane behavior is depicted in Fig. 5.34, and for illustration purposes, the out-of-plane bending has been extremely exaggerated. Due to the relative girder displacement, δ, the floor beam experienced a rotation, θ; as a result of the

www.manaraa.com

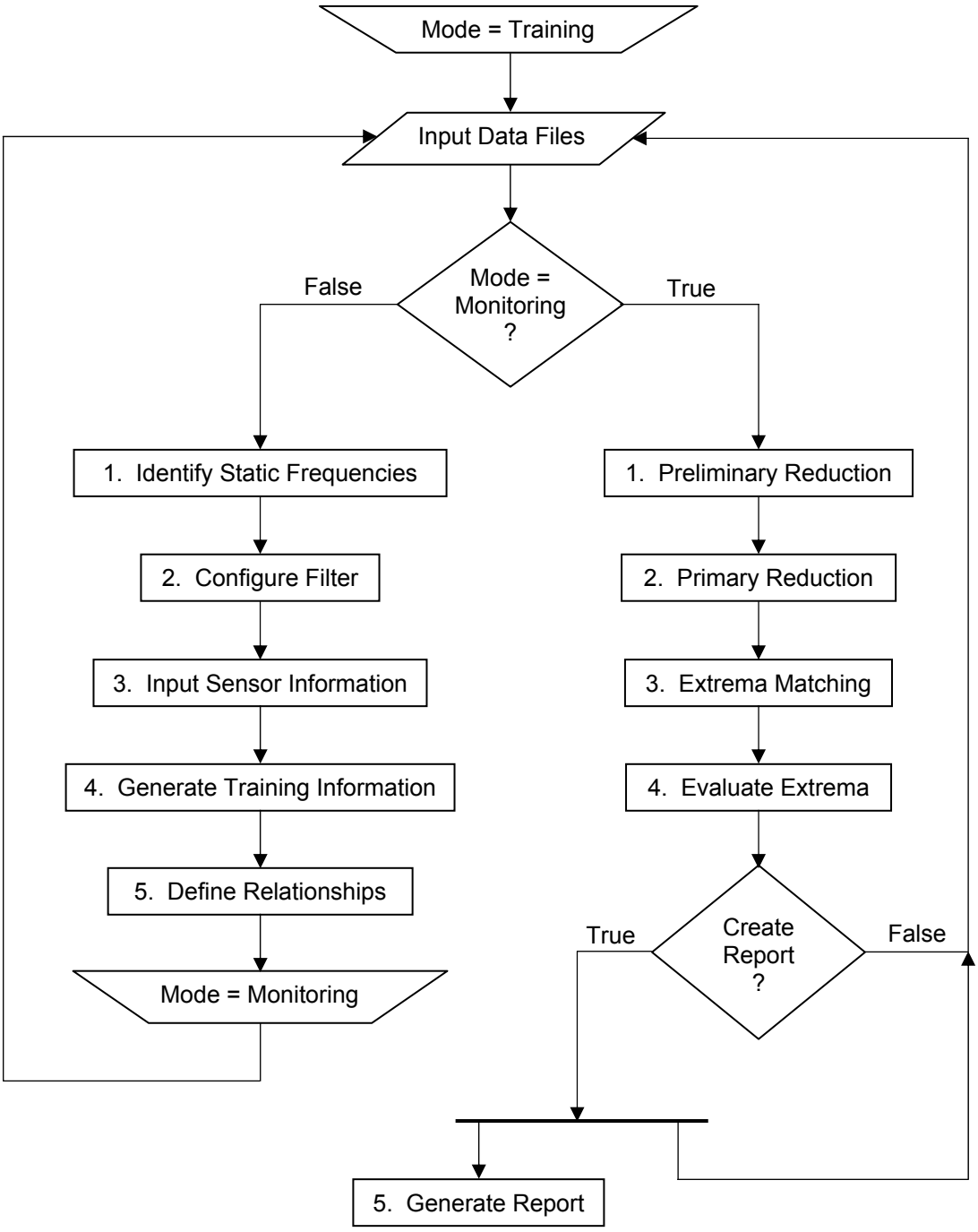

Figure 5.31. General flowchart for setup and monitoring modes of the FCB SHM system.

www.manaraa.com

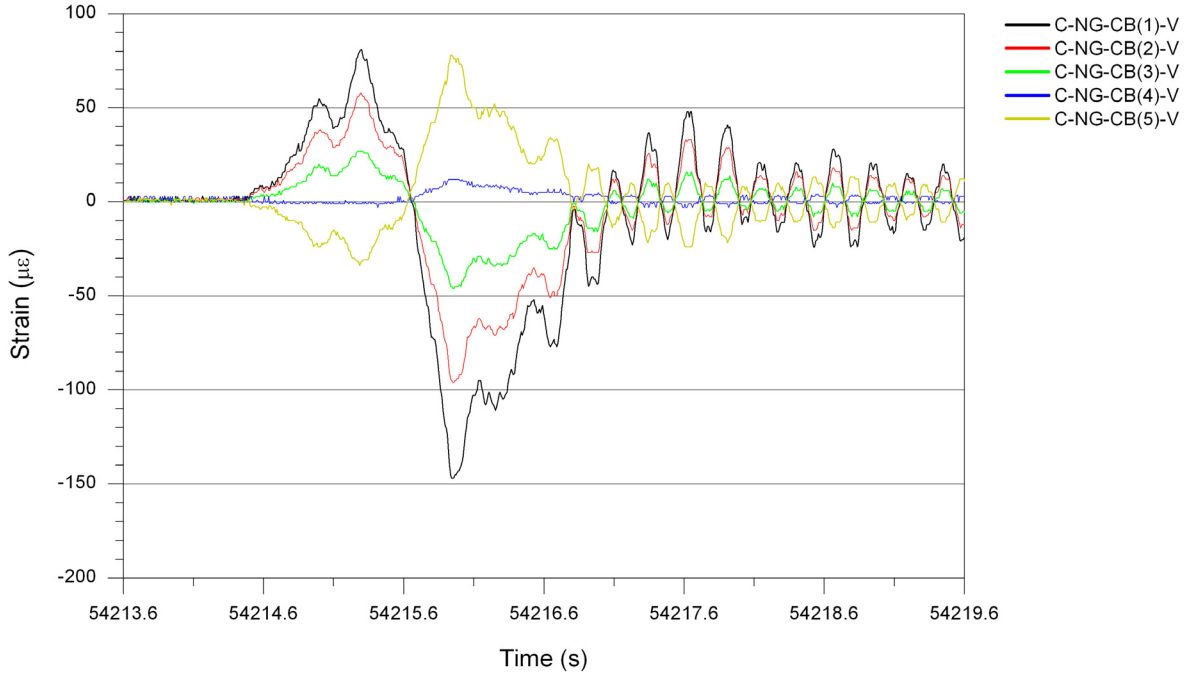

a. Zeroed data

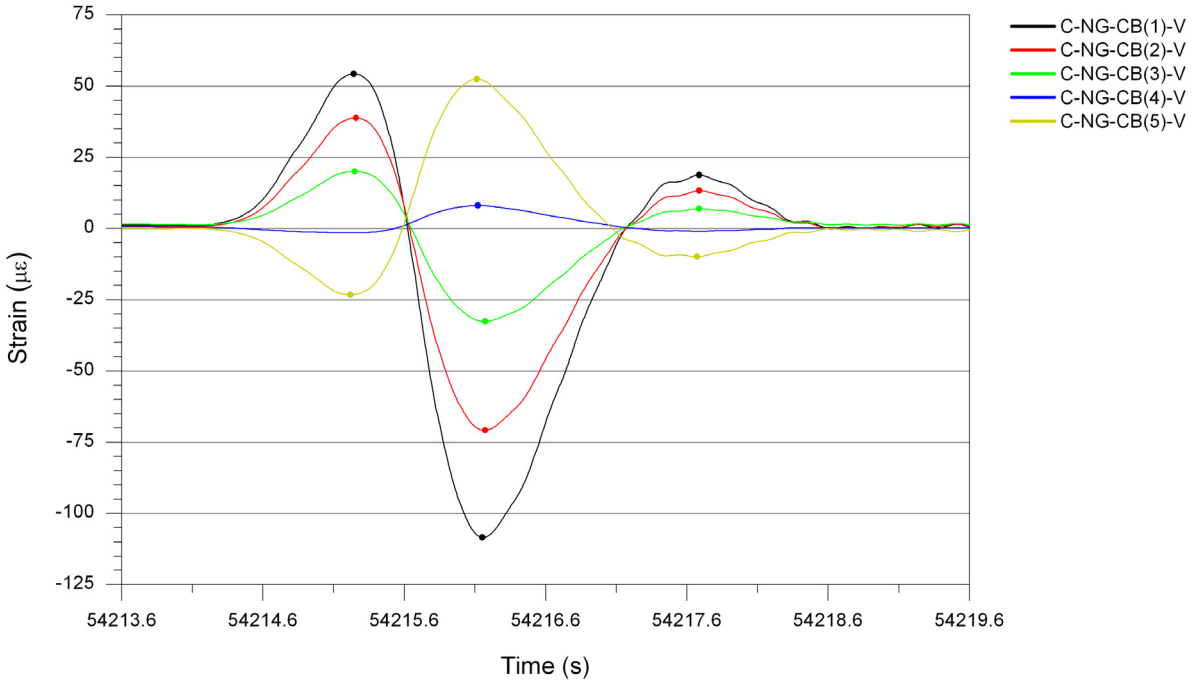

b. Filtered data with identified event extrema

Figure 5.32. Out-of-plane bending measured by FOSs in the north cut-back region in the US30 bridge.

www.manaraa.com

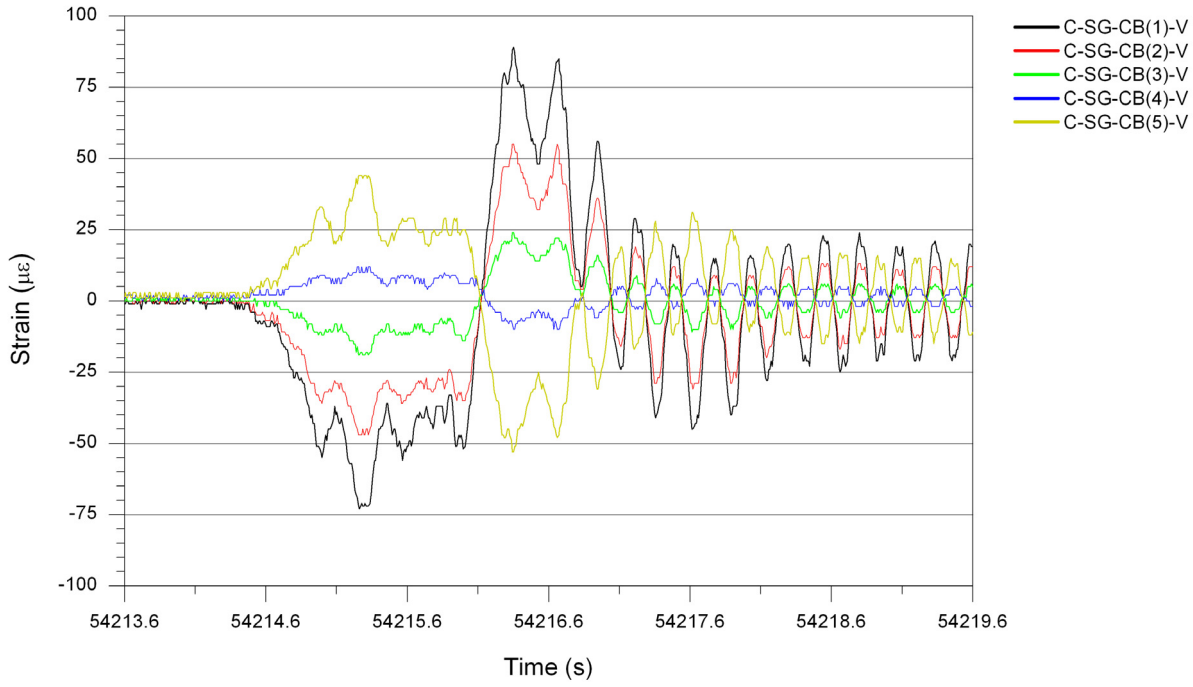

a. Zeroed data

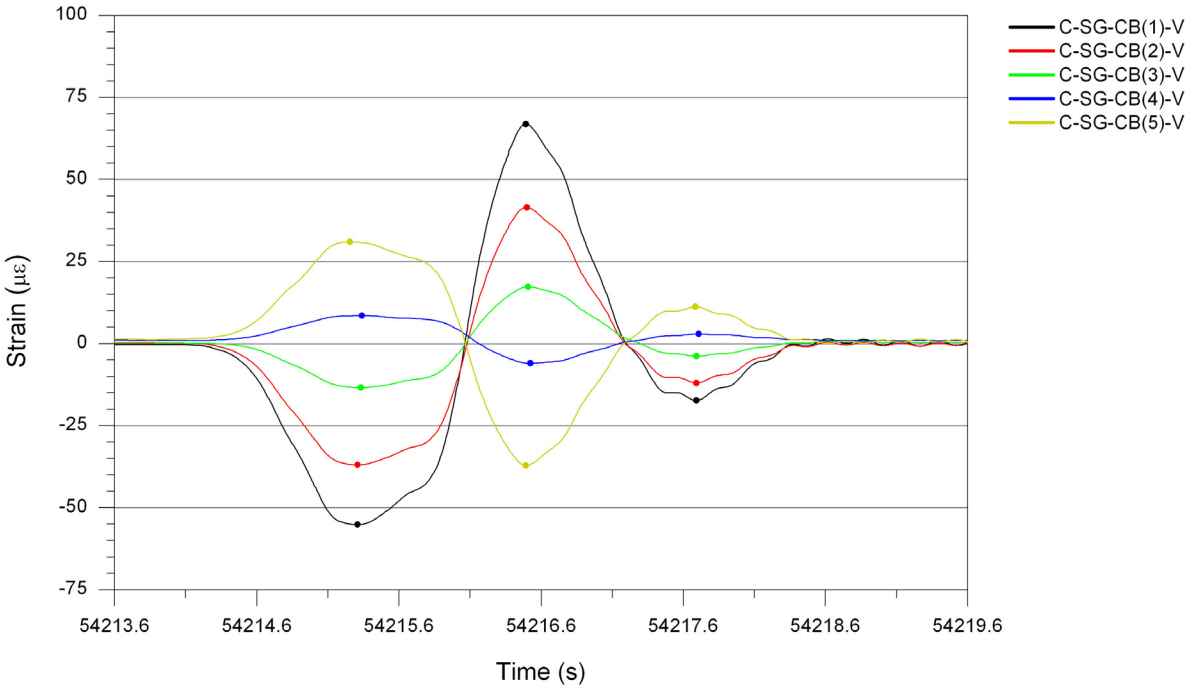

b. Filtered data with identified event extrema

Figure 5.33. Out-of-plane bending measured by FOSs in the south cut-back region in the US30 bridge.

www.manaraa.com

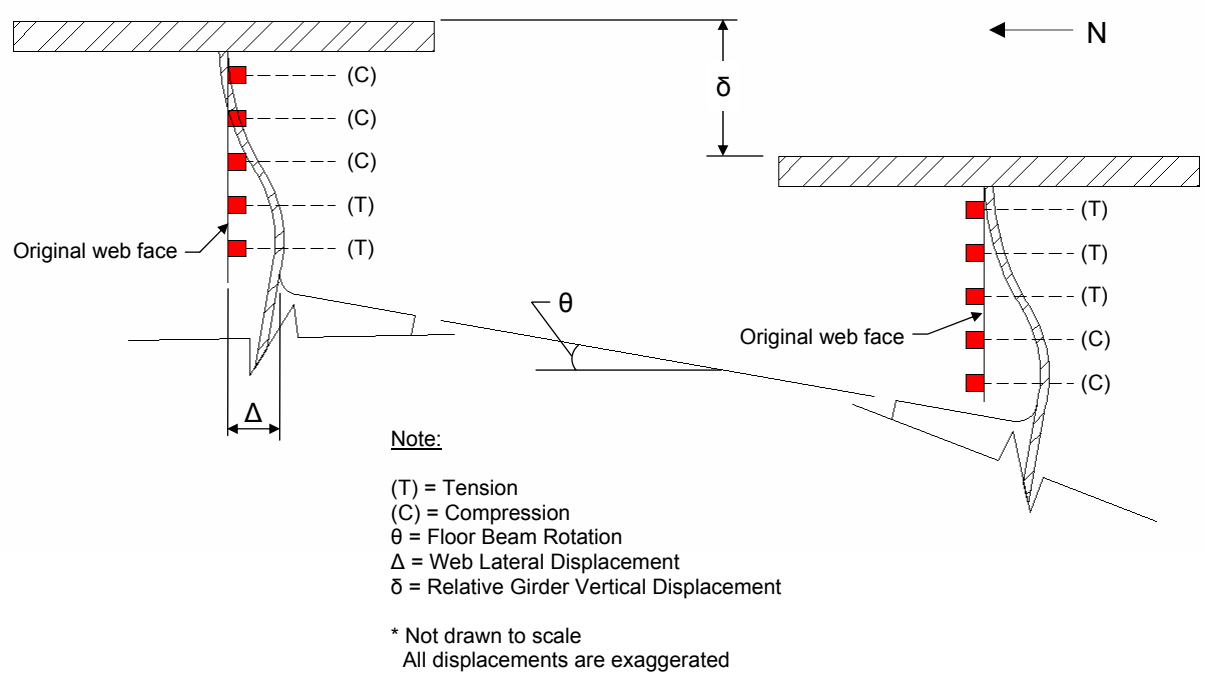

Figure 5.34. Explanation of out-of-plane bending in cut-back regions due to relative girder displacement.

floor beam rotation, the connection plates also rotated and were subjected to a lateral displacement, Δ. The combined effect of the rotation and lateral displacement produced the out-of-plane bending in the cut-back regions [2]. From the results presented in Figs. 5.32 - 5.33, it is evident that the inflection point for the reverse curvature consistently occurred between FOSs #3 and #4 in each region.

The relative girder displacement presented in Fig. 5.34 was determined by comparing strain values in the records of C-NG-WB-V and C-SS-WB-V. As illustrated in Fig. 5.35, the event strains in C-SS-WB-V were much higher than those in C-NS-WB-V. Thus, it was concluded that the vehicle was in the south lane as it traversed the bridge, which would have produced a larger deflection in the south girder than in the north girder.

Since out-of-plane bending is related to relative girder displacements, the strain records of the TSs in the cut-back regions were compared to those of the C-NG-BF-H and C-SG-BF-H on the girders. Girder flexural strains are produced by moments, and given that girder displacements are

www.manaraa.com

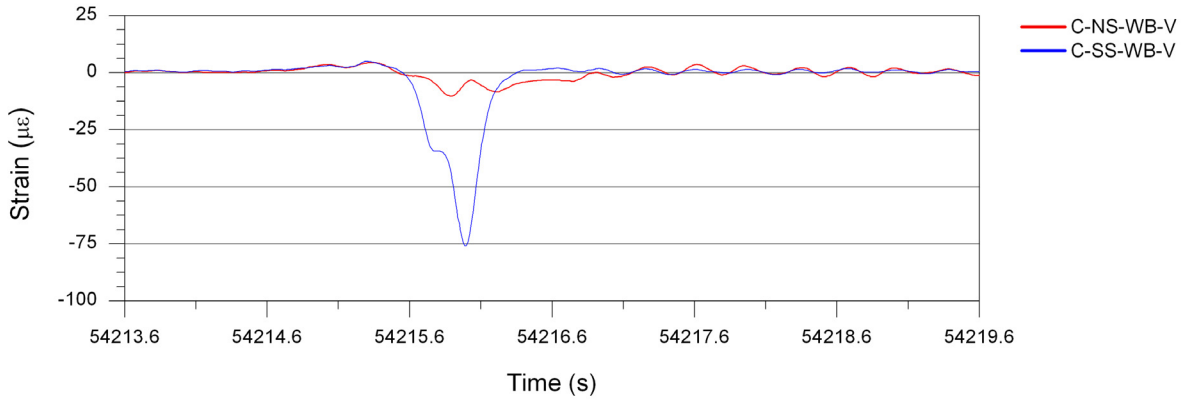

Figure 5.35. Comparison of filtered data for C-NS-WB-V and C-SS-WB-V to determine the transverse position of the vehicle.

related to the moments through curvature, it was expected that an event extrema would be produced in the strain records of the FOSs in the cut-back regions when the absolute difference between the strains in C-NG-BF-H and C-SG-BF-H were maximized (i.e. the relative girder displacement at Section C was maximized). In Fig. 5.36, strains for the same event in C-NG-CB(1)-V, C-SG-CB(1)-V, C-NG-BF-H, and C-SG-BF-H have been displayed. As can be seen, event extrema in C-NG-CB(1)-V and C-SG-CB(1)-V coincide approximately at the time of the maximum strain difference between C-NG-BF-H and C-SG-BF-H when the vehicle was traveling on the west or east span (the first and third extrema in each TS strain record). When the vehicle was traveling on the middle span (second extrema in each TS strain record), however, deviation from this behavior was observed. As illustrated, the extrema for C-NG-CB(1)-V and C-SG-CB(1)-V did not occur at the same time; the C-SG-CB(1)-V extrema coincided with the time of maximum difference between strains in C-NG-BF-H and C-SG-BF-H, but the corresponding C-NG-CB(1)-V extrema occurred at a slightly earlier time. This behavior was verified in several other events within the strain records of the sensors in the cut-back regions. As a result, it has been concluded that the conditions contributing to out-of-plane bending become more complex when the vehicle traversing the bridge is in the area of the cut-back region under investigation.

Changes in the load path through the structure as vehicles traverse the bridge were considered to be one cause of the observed variation in cut-back region behavior. As demonstrated

www.manaraa.com

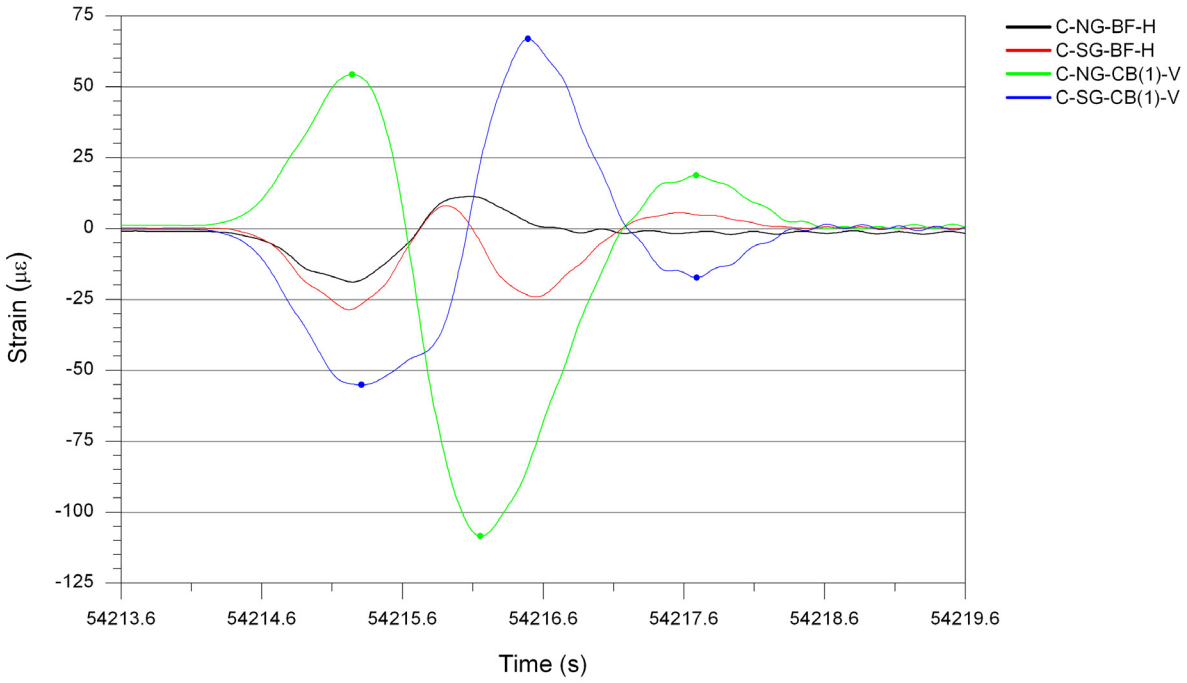

Figure 5.36. Comparison of event patterns among the girders and cut-back regions in Section C.

in Fig. 5.35, the vertical forces acting of the floor beam, which are evident through strains in C-NS-WB-V and C-SS-WB-V, increased as the vehicle passed over Section C. Therefore, the action of the floor beam on the girders webs theoretically should have changed. Validation of this situation was not possible, however, by reviewing the strain records in Figs. 5.32 and 5.33. If fluctuating floor beam forces caused intermittent changes in the out-of-plane bending, it was not uniquely distinguishable from the dynamic responses in Figs. 5.32a and 5.33a. Moreover, if the frequency of the fluctuating floor beam forces was similar to that of the dynamic response in the zeroed data, it unfortunately would have been removed from the strain records (along with the dynamic response) during the filtering process. While an absolute understanding of the factors causing out-of-plane bending in cut-back regions is not required for the SHM system developed in this study, investigation and identification of event patterns in the TSs was essential for the discussion that follows in Sections 5.2 and 5.3.

www.manaraa.com

5.2 SHM System Training Mode Procedures

As mentioned in Section 5.1, measured performance data are used to help the SHM system learn how to identify typical bridge performance. As briefly illustrated in Fig. 5.31, this process is accomplished while the system is in training mode. After the training process is complete, the SHM system is switched to monitoring mode where the information learned during training is applied to measured data in the future. The information presented in this section provides detailed information pertaining to system training.

Figure 5.37 displays a detailed schematic of the procedures involved with SHM system training. As illustrated in Figs. 5.31 and 5.37, six processes are performed:

1. Collection of raw strain data from which training information is developed
2. Identification of frequencies for quasi-static vehicular events
3. Configuration of a lowpass frequency filter to remove noise and dynamic responses from strain records
4. Defining sensor classification and longitudinal location within the bridge
5. Generation of training information from matched event extrema
6. Defining limit sets for relationships between TSs and NTSs

For ease of operation for the user, GUIs were developed to control the execution sequence of the algorithms that perform the processes listed above with minimized user interaction. Each GUI and algorithm that was developed in this research and is used in the training process is discussed in detail in the proceeding sections.

All software applications that were created in this work were developed in LabVIEW, which is a graphical programming language that uses icons instead of text to create applications. Programs that are developed in LabVIEW are called virtual instruments (VIs). A VI that is called by another VI is referred to as a subVI, which is comparable to a subroutine in a text-based programming language. To avoid the need for third party software for file compression and unzipping, dynamic link libraries (DLLs) were developed and compiled with Microsoft Visual Basic (VB) programming language to access the appropriate Windows XP compression and unzipping utilities. The VB DLLs are called by the LabVIEW VIs to perform these operations since LabVIEW uses Win32 application program

www.manaraa.com

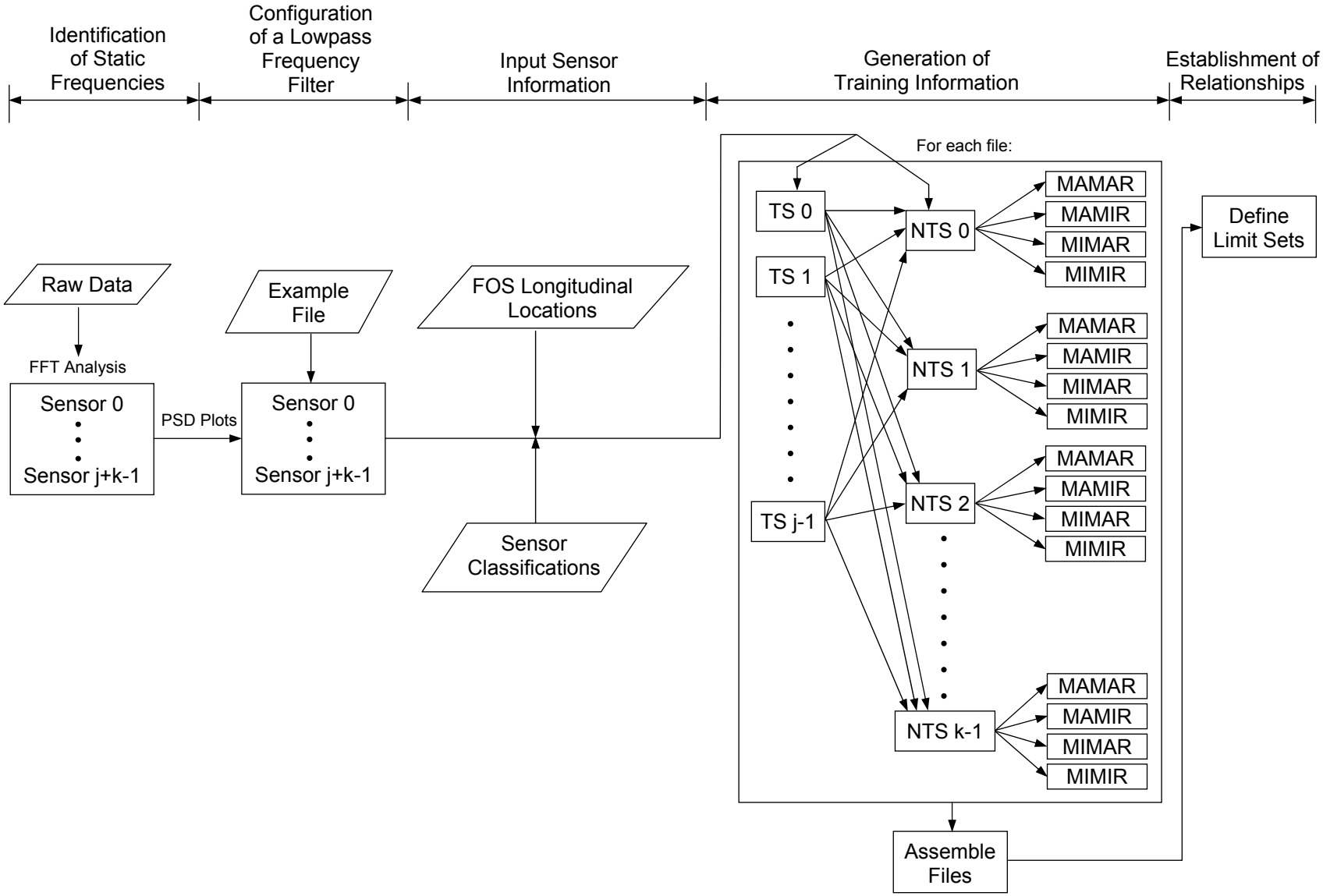

Figure 5.37. Overview of the steps included in the FCB SHM training process.

www.manaraa.com

interfaces (APIs) that do not have access to such Windows XP utilities. All SHM software applications that have been developed in this study are available as open source code in Appendix E and are referenced during the discussion in the proceeding sections.

5.2.1 Training Mode Data Collection and Storage

All completely autonomous operations that are performed by the FCB SHM software are performed within the VI, *Master FCB SHM System.vi* (See Appendix E), and the font panel for this VI is presented in Fig. 5.38. Note that this front panel contains two displays of controls and indicators: one display controlling the data collection and storage operations (Fig. 5.38a), and one display controlling the data reduction, extraction, evaluation, and report generation (Fig. 5.38b). While only Fig. 5.38a applies to the discussion in Section 5.2, Fig. 5.38b has also been presented to show the front panel in entirety and also for future reference in Section 5.3. As illustrated, selected controls and indicators have been labeled in Fig. 5.38, and a brief description of each labeled item is as follows:

1. **si425 IP Address Control:** Internet protocol (IP) address for the si425-500, which is required for networking purposes.
2. **Data Acquisition Rate Indicator:** Number of samples per second that strain data are saved for a sensor.
3. **Buffer Indicator (%):** Percentage of overflow storage that is available.
4. **Timestamp and Sensor Indicator:** Table that presents the current timestamp along with the selected parameter (strains or wavelengths) for each sensor.
5. **Parameter Control:** The parameter to be displayed and saved, either strains or wavelengths (either absolute or relative).
6. **Set References Control:** If depressed, the current wavelength values for each sensor are stored as reference wavelengths.
7. **References Control:** If depressed (as shown), the si425-500 uses stored reference wavelengths to calculate and return relative wavelength changes (nm) for each sensor. Otherwise, absolute sensor wavelengths are reported.
8. **Save Strain Data Control:** If depressed (as shown), data is continuously written to the temporary directory. Otherwise, data is not saved at all.
9. **Mode Control:** If depressed, the system operates in monitoring mode. Otherwise (as shown), the system operates in training mode.
10. **File Size Limit Control:** The desired data file size (bytes).

www.manaraa.com

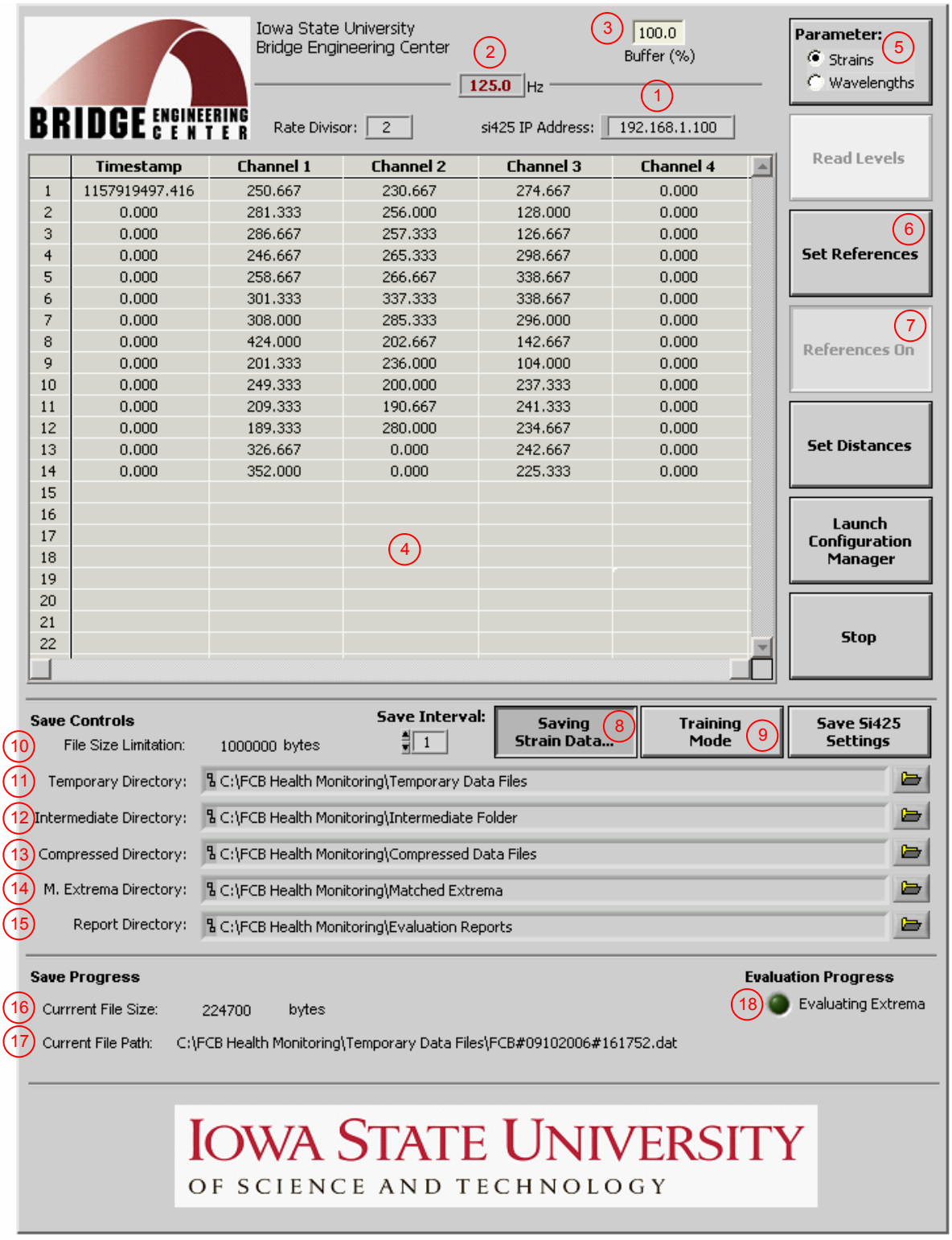

a. Display for data collection and storage

Figure 5.38. Front controls and indicators of FCB SHM system while operating in training mode (*Master FCB SHM System.vi*).

www.manaraa.com

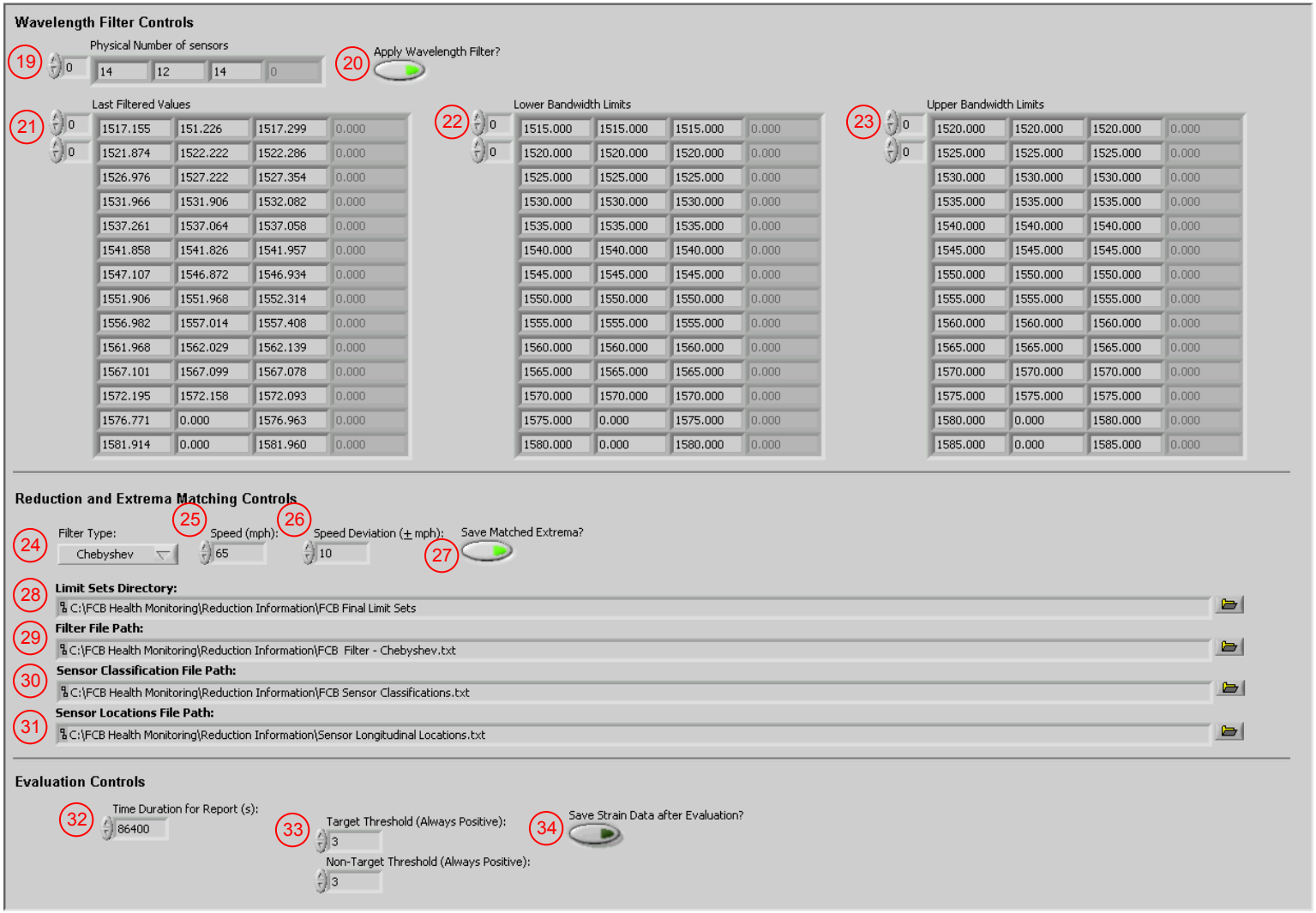

b. Display for data reduction, extraction, evaluation, and report generation

Figure 5.38. (Continued).

www.manaraa.com

11. **Temporary Base Path Control:** Directory for the data to which sensor information is currently being written.

12. **Intermediate Base Path Control:** Directory to which temporary files are moved when they have exceeded the file size limit and are awaiting evaluation.

13. **Compressed File Path Control:** Directory in which data files are stored after they have been evaluated (if system is in monitoring mode) and compressed.

14. **M. Extrema Path Control:** Directory in which the matched event extrema are stored after the data file contents have been evaluated.

15. **Report Path Control:** Directory in which all evaluation reports are stored after they have been generated.

16. **Current File Size Indicator:** Reports the size (bytes) of the file to which data is currently being written.

17. **Current File Path Indicator:** Reports the path of the file to which data is currently being written.

18. **Evaluating Extrema Indicator:** Turns green when the evaluation process is being conducted for a data file.

19. **Physical Number of Sensors Control:** The actual number of sensors in the fiber of each channel.

20. **Apply Wavelength Filter? Control:** If set to true (depressed as shown), the wavelength filter is applied to the data in the file. Otherwise, the filter is not applied.

21. **Last Filtered Values Control:** Last known wavelength values for each sensor, which are used in the first iteration of the wavelength filter.

22. **Lower Bandwidth Limits Control:** Lowest wavelength values considered to be achievable by the sensors.

23. **Upper Bandwidth Limits Control:** Highest wavelength values considered to be achievable by the sensors.

24. **Filter Type Control:** The type of lowpass frequency filter, Chebyshev or Butterworth, to be applied to the data file.

25. **Speed (mph) Control:** Expected average speed for a representative sample of traffic.

26. **Speed Deviation (± mph) Control:** Deviation (mph) to be used with the expected average speed to define the expected speed range for a representative sample of traffic.

27. **Save Matched Extrema? Control:** If set to true (depressed as shown), the matched extrema are saved after the data file is analyzed. Otherwise, the matched event extrema are deleted after the data file is evaluated.

28. **Limit Sets Directory Control:** Directory to the folders that contain the limit sets for the defined TS-NTS relationships.

www.manaraa.com

29. **Filter File Path Control:** Path to the file that contains the settings for selected lowpass frequency filter.

30. **Sensor Classification File Path Control:** Path to the file that defines each sensor as a TS or NTS.

31. **Sensor Locations File Path Control:** Path to the file that contains the longitudinal location of each sensor within the bridge.

32. **Time Duration for Report (s) Control:** Time limit in seconds for each evaluation report that is generated.

33. **Target and Non-Target Threshold Control:** Minimum absolute value of an event extrema in order to be included in the evaluation process.

34. **Save Strain Data after Evaluation? Control:** If set to true, data is compressed and saved after it is evaluated. If set to false (as shown), the original data file is deleted after evaluation.

To develop the SHM program, the basic LabVIEW data collection utility that was provided for use with the si425-500 and developed by Micron Optics, Inc., was significantly rebuilt and restructured. From the previously listed items, only controls and indicators #1 - 4, and #6 - 8 were part of the original data collection utility.

Figure 5.38a illustrates the data collection and storage settings while the SHM system was operating in training mode and collecting strain data. The si425-500 was configured for the static IP address 129.186.1.100 on the private network behind the Linksys router, and thus, this address was set as default in control #1. In addition, indicator #2 verifies data acquisition is being performed at 125 Hz. As displayed in indicator #3, the buffer was running at 100%, which means that all overflow storage was available because the SHM software is receiving data at the same rate as they are being collected by the si425-500. If the SHM software is unable to maintain an adequate receiving rate, data overflows to the buffer and the indicator level drops; if the buffer level reaches zero, all overflow storage is cleared, and data are lost.

The timestamp and sensors strain values (as specified in control #5) are displayed in indicator #4. To convert between sensor wavelengths and strains, the sensor references (control #7) must be activated as shown, which prompts the si425-500 to use previously stored sensor references to directly output relative wavelength changes rather than absolute wavelengths for each sensor. The subVI, *Convert to Strain.vi* (Appendix E), is called to convert the given wavelength changes to strain

www.manaraa.com

values for each sensor with the conversion factor provided in Sections 3.3.1.2 and 5.1.1. Reviewing the contents of indicator #4, the number of FOSs that are installed in channel one, channel two, and channel three are 14, 12, and 14, respectively.

To set the SHM system to training mode (as shown), control #9 was released. In addition, to begin storing data, control #8 was depressed. Upon execution, the subVI *Create File Name.vi* (See Appendix E) is called and used to autonomously generate a file name from the date and time of the local computer system in the following format:

FCB#MMDDYYY#hhmmss.dat

where,

FCB = fracture-critical bridge (constant)
MM = two digit month (00-12)
DD = two digit day (1-31)
YYYY = four digit year
hh = hour of the day (00-23)
mm = minutes of the hour (00-59)
ss = seconds of the minute (00-59)
.dat = file extension

A data file with this file name is created in the temporary directory, which is specified in control #11. As data are written to the file, its running size and path are displayed in indicators #16 and #17, respectively. When the data file size limitation (control #10) is exceeded, the data file is closed and moved to the intermediate directory specified in control #12. After the move is complete, the subVI, *Compress, Move, Delete Data File.vi* (Appendix E), is called to compress the completed data file through use of *CompressDataXP.dll* (Appendix E), to move the compressed file (now named FCB#MMDDYYYY#hhmmss.zip) to the directory specified in control #13, and to delete the original uncompressed data file that remained in the intermediate directory. Meanwhile, a new data file was created in the temporary directory, and the collection and storage procedure was repeated.

As illustrated in Fig. 5.38a, the data file size limitation was set to 1.0 MB, which is approximately 27 seconds of data for every FOS. This file size was selected because it was previously proven to have an approximately constant baseline in Fig. 5.2, which is a requirement for segmental analysis of continuous data in this study. Since knowledge of a suitable file size may not be known prior to data collection and storage, determination of such a size may be a repetitive

www.manaraa.com

process involving data collection, storage, and review. Past experience may be sufficient to determine an appropriate data file size or perhaps useful for reducing the number of iterations in the repetitive process.

With the wavelength detection algorithms incorporated into the si425-500, sensor side lobes were sometimes intermittently misinterpreted as sensor center wavelengths. When this error occurred, more FOSs were detected by the interrogator than the number that physically existed in the system, and as a result, several columns of data shifted and caused severe problems within the saved data file. To correct such complications, the wavelength filter subVI, *Wavelength Filter - ISU BEC.vi* (Appendix E), was created and incorporated into the data collection and storage procedure. For use with this filter, a wavelength bandwidth was defined for each sensor via controls #22 (lower limits) and #23 (upper limits); only one wavelength should exist within each bandwidth in each channel. Prior to writing data to a file, the system calls this subVI and checks the number of detected sensors in each channel with those specified in control #19. If the sensor numbers match, the data are written to the file. If the sensor numbers do not match, the channel or channels having extra sensors are identified, and wavelengths from the previous software iteration are recalled for each sensor. If a defined bandwidth contains more than one wavelength, the correct wavelength is determined to be the one that is closest to the wavelength from the previous software iteration. After all correct wavelengths have been identified, the data are written to the file and also saved for comparison with the next iteration, if needed.

If the parameter (control #5) is set for strain values, the wavelength filtering procedure operates differently. In this setup, the si425-500 provides relative wavelength changes for each FOS instead of absolute wavelengths. As a result, *Wavelength Filter - ISU BEC.vi*, cannot use the defined bandwidths to eliminate side lobe values from the data. Rather, if the incorrect number of sensors is detected in a channel, the wavelength filter writes zero strain values for all sensors in the channel. Since this phenomenon is intermittent (usually lasts less than 0.04 seconds), the sections of zeroes written to the data file appears as “flickers” in each sensor strain record. The flickers are easily

www.manaraa.com

identified and corrected after the data file has been saved, and this procedure is discussed in Section 5.2.2.

The formatting and organization of information within all data files are exactly the same. Each file consists of 42 columns of tab delimited data. The timestamp and buffer are located in columns zero and one, respectively, and each column thereafter (columns 2 - 41) contains the strain record for one sensor. Channel one sensor readings are first written to the file, followed by channel two and channel three, respectively, with the sensors in each channel arranged according to increasing center wavelengths.

When the US30 SHM system was functioning in training mode, data were saved data for approximately one week, which was found to be more than sufficient time for capturing a representative sample of bridge responses from ambient traffic. Illustrated in Fig. 5.39 are the compressed data files that were manually moved to a new directory after collection was complete at the US30 bridge.

It should be noted that the file naming scheme and compression of data files in the collection and storage procedure are a first step in addressing data management and storage issues in SHM. With the file naming scheme that is used, the absolute time of the data file is known without opening

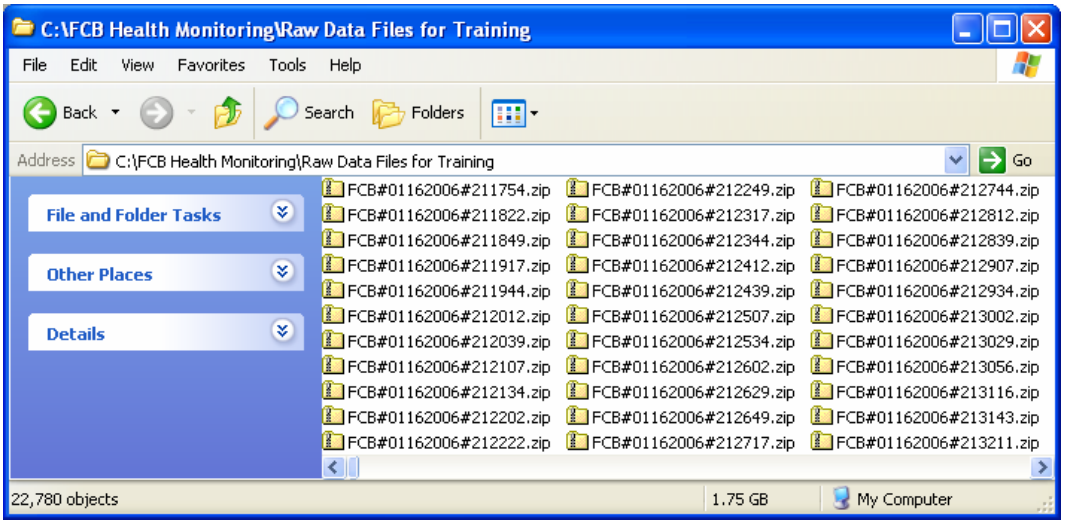

Figure 5.39. Illustration of data files that were generated by the FCB SHM system.

www.manaraa.com

and reviewing the file (See Fig. 5.39), and the 90% average compression achieved for each data file makes better use of hard drive space.

With measured performance data collected, the remaining five procedures of the training process are able to be completed through use of the following programs that have been developed (See Appendix E):

- *1 - Perform FCB FFT PSD Analysis.vi*
- *2 - Configure FCB Filter.vi*
- *3 - Input Sensor Locations.vi*
- *4 - Select Target Sensors.vi*
- *5 - Develop SHM Training Files.vi*
- *6 - Assemble SHM Training Files.vi*
- *7 - View Results - Assembled SHM Training Files.vi*
- *8 - Define Limits.vi*
- *9 - View Results - Defined Limits.vi*

Each program must be manually executed. For convenience, the order in which they must be executed is included in the name of the VI. Note that execution of programs 1, 2, 3, 4, 5, 6, and 8 are required to develop all necessary training information, while programs 7 and 9 are optional and only useful for viewing the results of the previously executed program. The operations performed by each program are discussed in Sections 5.2.2 - 5.2.6 along with operating procedure for each GUI.

5.2.2 Identification of Frequencies for Quasi-Static Vehicular Events

Identification of the quasi-static vehicular event in a strain record through use a frequency filter was illustrated in Section 5.1.2 and Fig. 5.4. As mentioned, the frequencies of the quasi-static vehicular events in FOS strain records are much lower than those of the dynamic bridge responses and noise in the data file. As a result, a lowpass frequency filter was selected for use in the SHM system. As described in Section 2.5.2, a digital filter of this type alters the frequency content of the record by blocking high frequencies and passing low frequencies, where high and low frequencies are defined according to a specified cut-off frequency. For application in this research, the frequencies

www.manaraa.com

for quasi-static vehicular events are used for the cut-off frequencies for the lowpass filter applied to each sensor.

To determine the frequencies of the quasi-static events for each sensor, a sample of data for each sensor must be investigated. With this sample data, a Fast Fourier Transform (FFT) is computed and used to develop a power spectral density (PSD) plot for each strain record. From the PSD plots, the dominant frequencies within a record are identifiable along with their relative contribution to the responses within the results. Considering frequencies with significant contributions in strain record for a typical highway bridge, the vehicular events will have lower frequencies but larger contribution than the natural frequencies of the bridge.

The VI, *1 - Perform FCB FFT PSD Analysis.vi* (Appendix E), was developed to perform the FFT analyses and generate PSD plots for all sensors in the FCB SHM system. The front panel for this VI is presented in Fig. 5.40. All controls and indicators in Fig. 5.40 have been labeled, and a brief description of each is as follows:

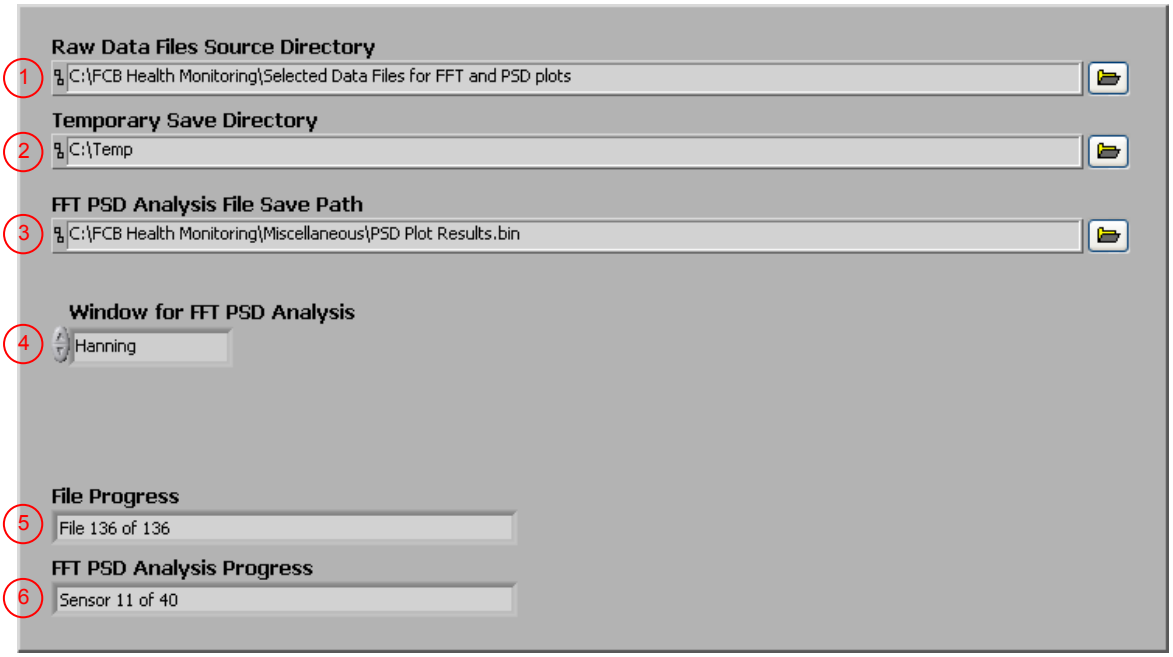

Figure 5.40. Front panel controls and indicators for program generating PSD plots (*1 - Perform FCB FFT PSD Analysis.vi*).

www.manaraa.com

1. **Raw Data Files Source Directory Control:** Directory containing the compressed raw data files that are to be used in the FFT analysis.
2. **Temporary Save Directory Control:** Directory to be used for temporary storage of the data files after they have been extracted from the compressed files in control #1.
3. **FFT PSD Analysis File Save Path Control:** Desired file path to which PSD information is written.
4. **Window for FFT PSD Analysis Control:** The time-domain window to be used in the analysis.
5. **File Progress Indicator:** Progress of the file combination process.
6. **FFT PSD Analysis Progress:** Progress of the FFT analyses and PSD plot development.

Before the program is started, a sample of data files must be selected from those that were saved (See Fig. 5.39) and copied to the directory that is specified in control #1. For the FFT analyses and generation of the PSD plots, it was determined that the entire week of raw data was not required. Rather, the amount of data that was selected was that which was collected while a representative sample of vehicles and traffic combinations traversed the bridge. For the US30 SHM system, one hour of data that was collected during dense traffic was used to generate PSD plots.

After the program is activated, the individual data files contained in the data file directory are combined into one data file. As this process is conducted one file at a time, several operations are performed on each individual data file prior to adding it to the combined file:

- Data are extracted from the compressed file.
- The DAR is determined from the timestamp.
- File continuity is checked through use of the buffer data.
- Data are checked for flickers that were created during the wavelength filtering process of data collection.
- Baselines are determined and the raw data are zeroed for each sensor.

The program calls the subVI, *WindowsXP Unzip Data.vi* (Appendix E), to unzip the data file through use of *UnzipDataXP.dll*, and the extracted data file is moved to the temporary directory specified in control #2 of Fig. 5.40. The timestamp and buffer values are removed from the 2-D array in order to calculate the DAR and check file continuity. As a result, only sensor data remains in the 2-D array (40 columns with one sensor per column); this array of sensor data will be referred to as the sensor

www.manaraa.com

array. All subVIs that perform operations on sensor strain records expect the 2-D sensor array, not the aggregate array that includes the timestamp and buffer.

File continuity is accomplished by the subVI, *Check File Continuity.vi* (Appendix E). In this subVI, the 1-D array of buffer values is scanned and checked for any sequences that cross zero. If the buffer crosses zero one or more times, the data are assumed to be discontinuous. In this case, the data are discarded and the program moves on to the next data file in the directory. If the file is determined to be continuous, the program continues with the current data set.

The timestamp values are used to compute the DAR that was used to collect the data, which is required to perform the FFT analysis. In this process, two consecutive timestamp values are subtracted, and the reciprocal of the difference results in the DAR. This procedure is repeated for all successive timestamp values, and results are averaged at the end to give an average DAR.

As mentioned in Section 5.2.1, when the measurement parameter is set to strain and the wavelength filtering process detects an incorrect number of sensors in a channel during data collection, zero values are stored for all sensors in the channel. The resulting flickers in the data, if any, must be identified and removed, and the subVI, *Remove Zero Flicker.vi* (Appendix E), is called to perform this operation. When the 2-D sensor array is read by the subVI, it is separated into subsets, and each subset contains all of the strain records for one channel. Each subset is scanned row by row to identify those that have all zero strain values (flickers). When a flicker occurs, the row of strain values immediately prior to the start of the flicker is averaged with the with row of strain values immediately after the flicker, and the resulting average values are written to all rows of the flicker that are enclosed within the averaged rows. This process is repeated for the entire array. If a flicker occurs at the beginning of an array, the row of strain values immediately after the flicker is written to all prior rows. Similarly, if the flicker occurs at the end of an array, the row of strain values immediately prior to the flicker are written to the all remaining rows. The assumption for this approach is that the time duration of each flicker is short such that minimal strain change occurred in the record during the flicker. Instances disproving this assumption have not occurred.

www.manaraa.com

With all flickers removed from the sensor array, baselines are established for all sensors with the subVI, *Determine Baselines.vi* (Appendix E). The underlying assumption for this subVI is that the baseline value within a strain record is the mode, or most frequent value. With this subVI, the mode is taken to be the center value of the bin in a histogram that contains the most values, and therefore, this approach is most accurate when the bin with the most values contains only baseline values. Such a histogram requires extremely small bin sizes, but it is not likely that a predetermined bin size would be successful for every strain record. As a result, the subVI uses an iterative process to determine when a satisfactory mode value has been calculated. For a given strain record, a histogram is generated several times, and in each iteration, the number of bins used is increased by five (increasing the number of bins results in smaller bin sizes). The determined mode value is compared among the iterations until its value change for five consecutive iterations is less than 0.05 με. At this point, it is assumed that the mode has converged and the last value obtained is the baseline for the strain record. If 10,000 iterations are performed and convergence criteria have not been satisfied, the baseline is reported as “not a number” (NaN), which signals to future calculations that a baseline was not established and that the corresponding strain record is not useable. After this process is completed for all strain records, the baselines are returned from the subVI in a 1-D array. For convenience, the bin increment, the convergence value, and maximum number of iterations performed before termination are required input values for the subVI, and thus, can be changed by the user.

After all baselines have been established, the raw strain record for each sensor is zeroed by subtracting the determined baseline value from each strain value in the raw record. Following this procedure, the zeroed array of strain records is added to the end of the combined data file. All of the procedures previously discussed are performed for each data file that is in the source directory. As displayed in Fig. 5.40, the progress of creating the combined data file is displayed in indicator #5.

After generation of the combined data file is complete, the LabVIEW subVI, *FFT Power Spectral Density.vi*, is called to perform the FFT and generate a PSD plot for each combined strain record. Vector averaging, exponential weighting, and the time-domain window specified in control #4

www.manaraa.com

define the procedures to be performed in the FFT analyses and PSD plot development. The progress of the PSD plot development is displayed in indicator #6 (See Fig. 5.40). After all plots have been developed, the results are compiled into a 3-D array, are saved in binary format to the file path specified in control #3, and are recalled and used to configure a digital filter in the next step of the training process (Section 5.2.3). Presented in Fig. 5.41 is the PSD plot that was generated for B-SG-BF-H. Note that the frequency for the quasi-static response has been identified as well as the fundamental frequency of the west span. As illustrated, the frequency for the quasi-static response is lower than the fundamental frequency, and in addition, has a larger contribution to the measured responses in the strain records. In Figs. 5.42a-nn, all resulting PSD plots that were generated from the US30 bridge data are presented. The selected frequencies for quasi-static events for all sensors are presented in Section 5.2.3.

5.2.3 Configuration of a Lowpass Frequency Filter

As illustrated in 5.37, PSD plots are used to configure a lowpass frequency filter that removes dynamic responses and noise from each strain record. Review of Figs. 5.42a-nn reveals variety in the PSD plots among the FOSs, and as a result, the configuration of the filter for each FOS strain record was different. In order to effectively use the results of the PSD plots in the filter configuration,

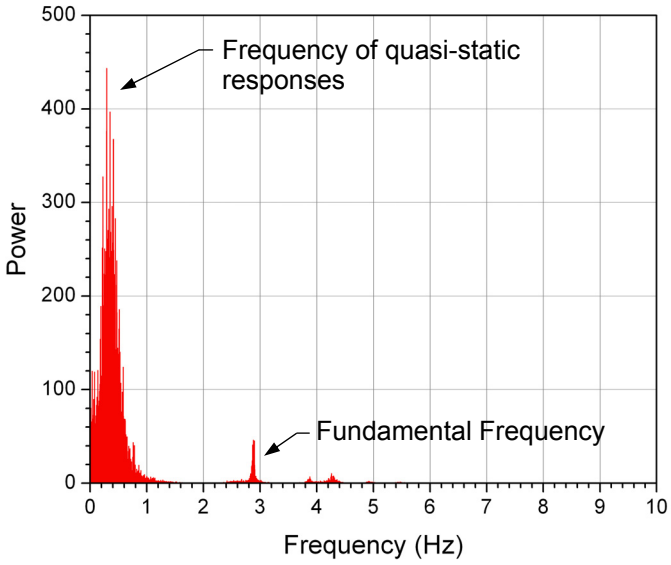

Figure 5.41. B-SG-BF-H: power spectral density (PSD) plot with identified frequencies.

www.manaraa.com

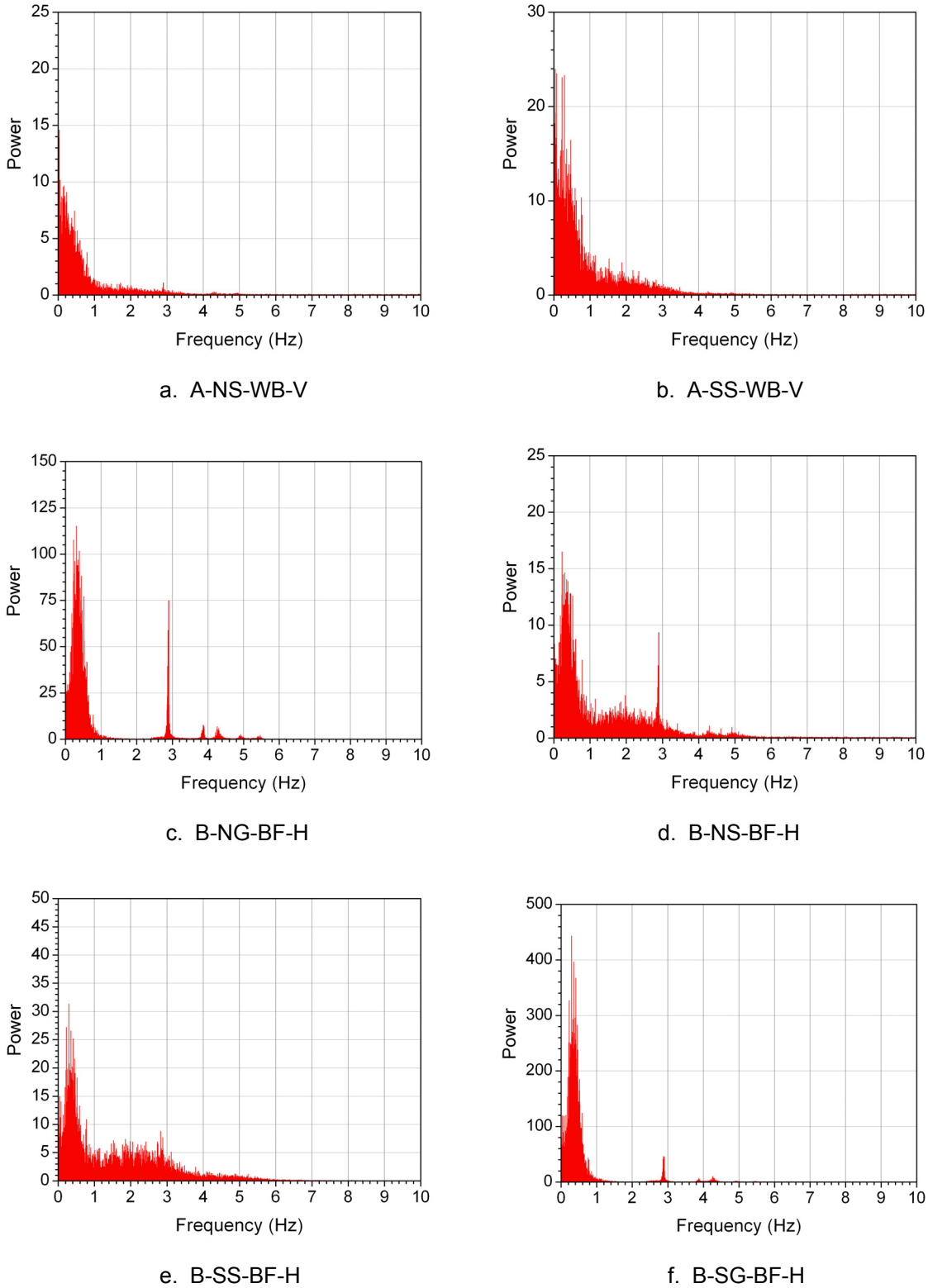

Figure 5.42. Power spectral density (PSD) plots developed during FCB SHM system training.

www.manaraa.com

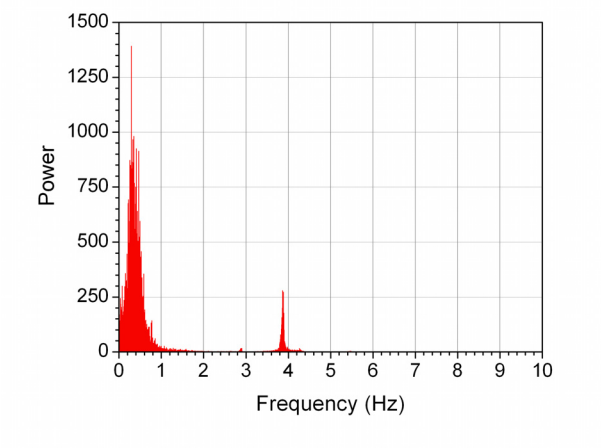

g. C-NG-CB(1)-V

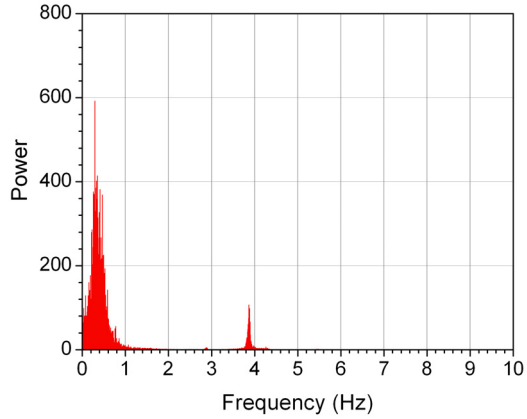

h. C-NG-CB(2)-V

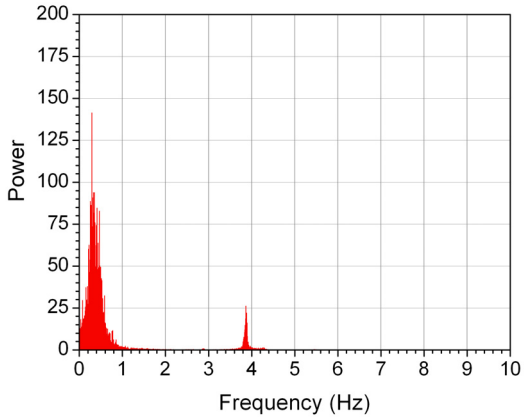

i. C-NG-CB(3)-V

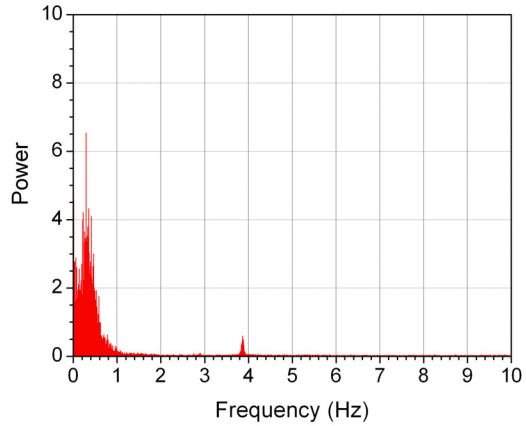

j. C-NG-CB(4)-V

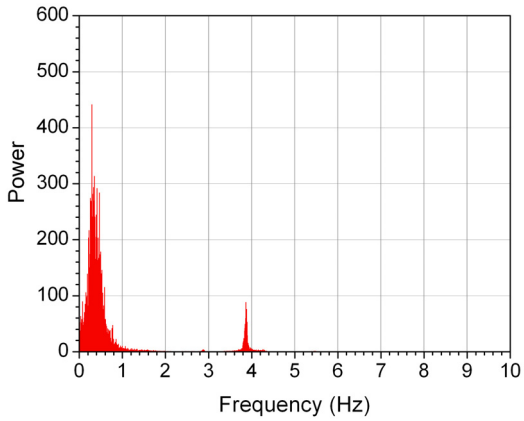

k. C-NG-CB(5)-V

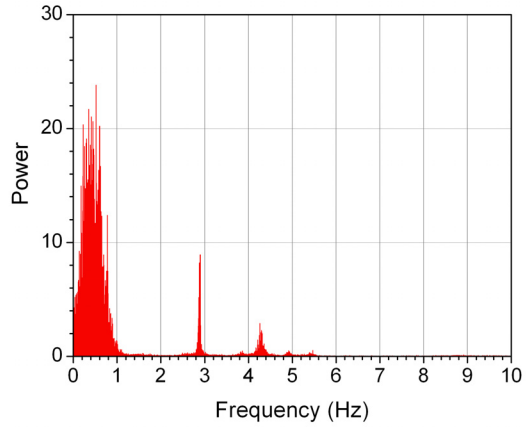

l. C-NG-BF-H

Figure 5.42 (Continued).

www.manaraa.com

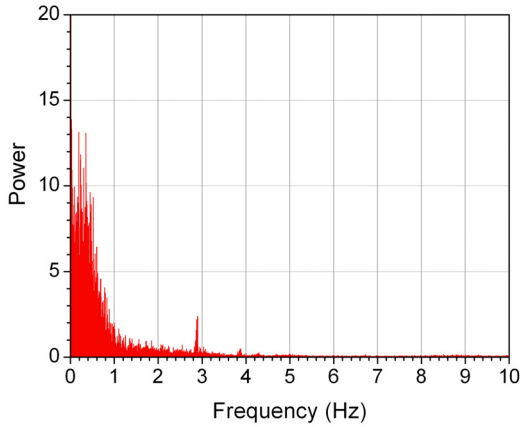

m. C-NS-WB-V

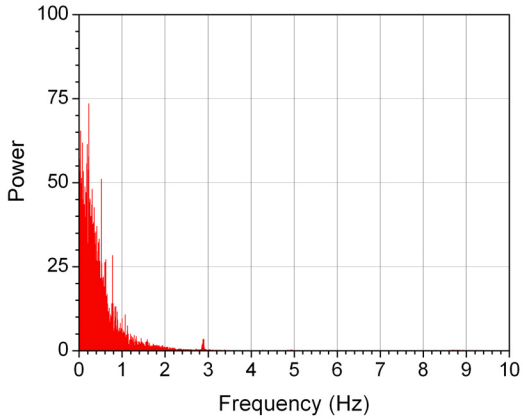

n. C-FB(NS)-BF-H

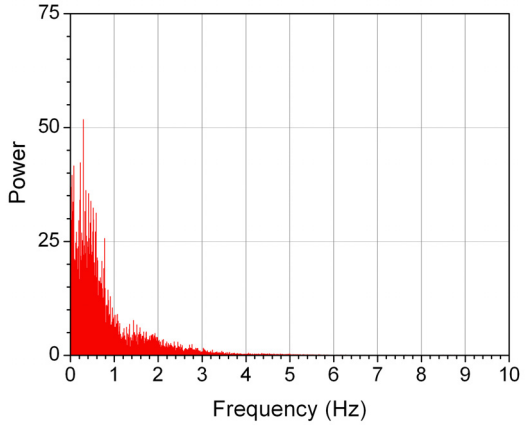

o. C-SS-WB-V

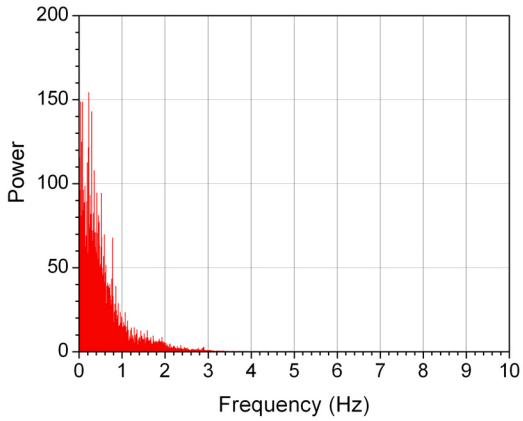

p. C-FB(SS)-BF-H

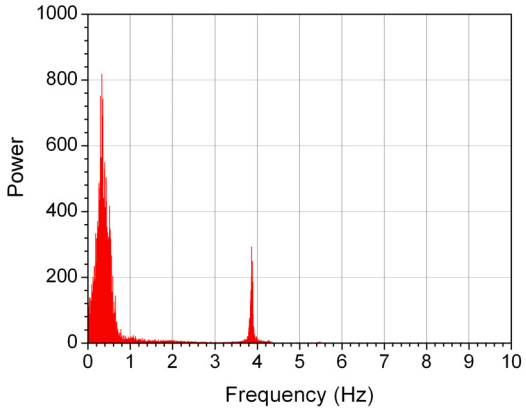

q. C-SG-CB(1)-V

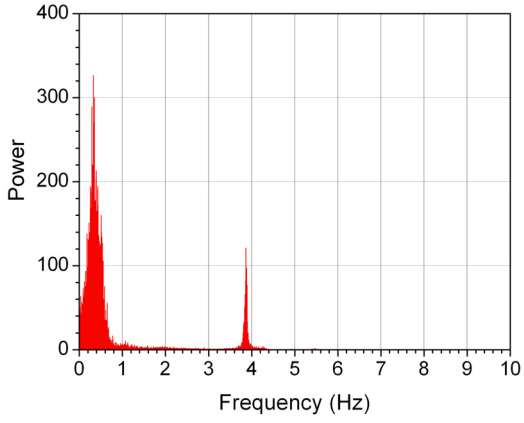

r. C-SG-CB(2)-V

Figure 5.42. (Continued).

www.manaraa.com

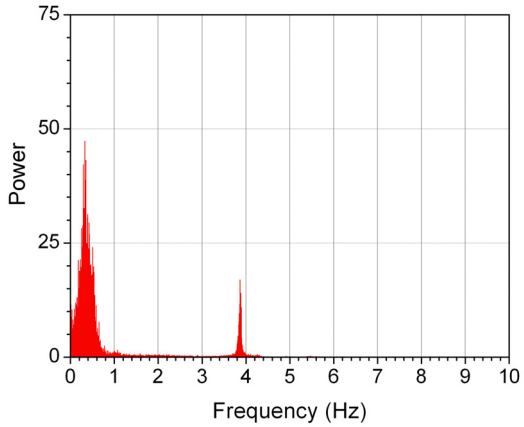

s. C-SG-CB(3)-V

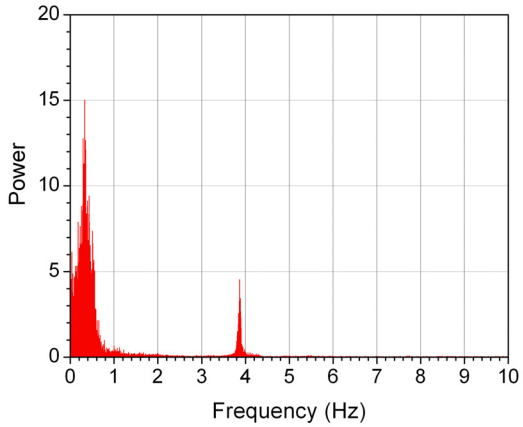

t. C-SG-CB(4)-V

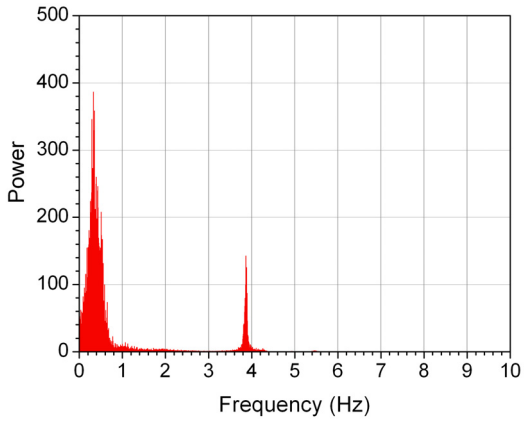

u. C-SG-CB(5)-V

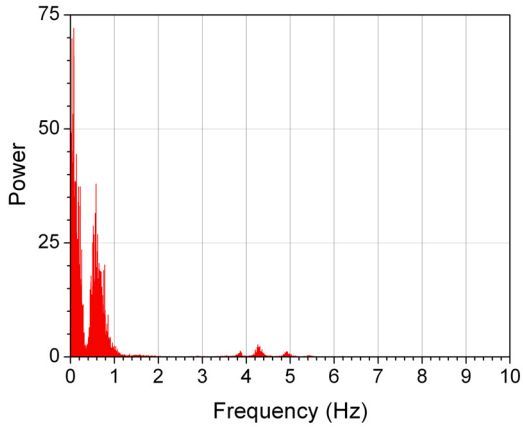

v. C-SG-BF-H

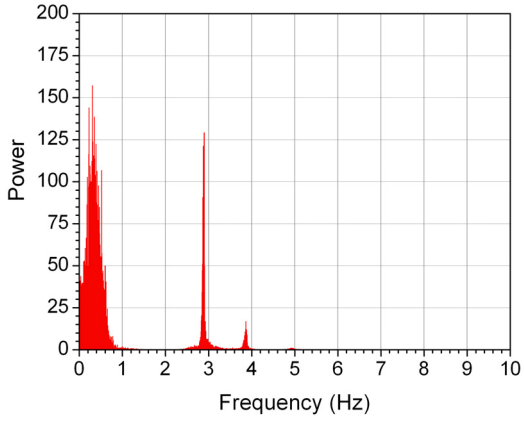

w. D-NG-BF-H

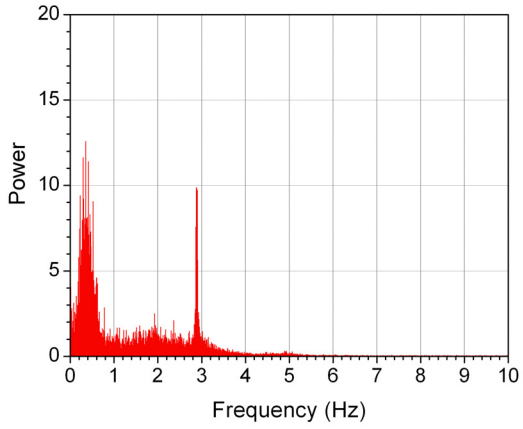

x. D-NS-BF-H

Figure 5.42. (Continued).

www.manaraa.com

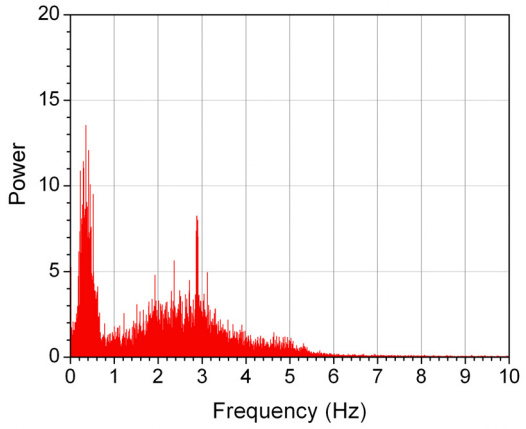

y. D-SS-BF-H

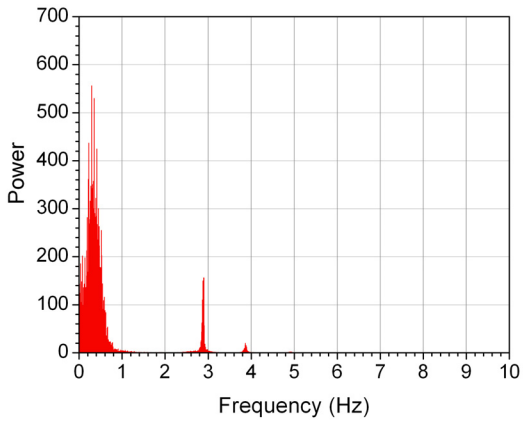

z. D-SG-BF-H

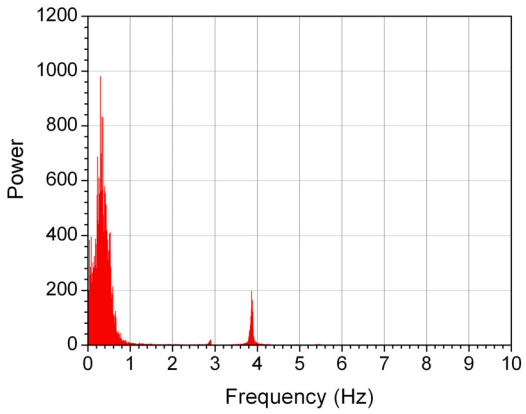

aa. E-NG-CB(1)-V

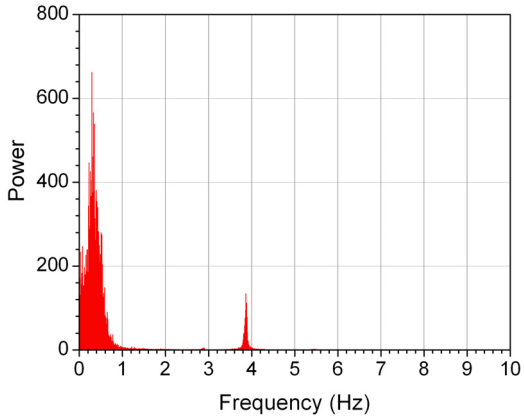

bb. E-NG-CB(5)-V

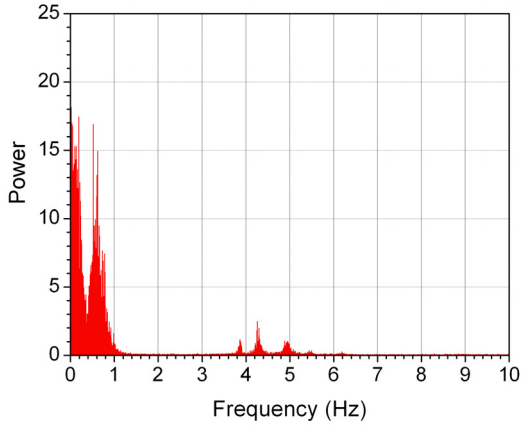

cc. E-NG-BF-H

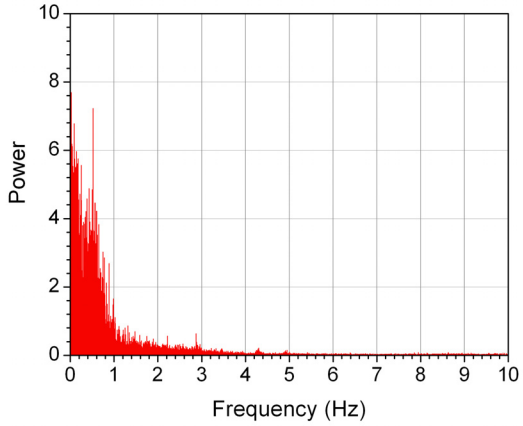

dd. E-NS-WB-V

Figure 5.42. (Continued).

www.manaraa.com

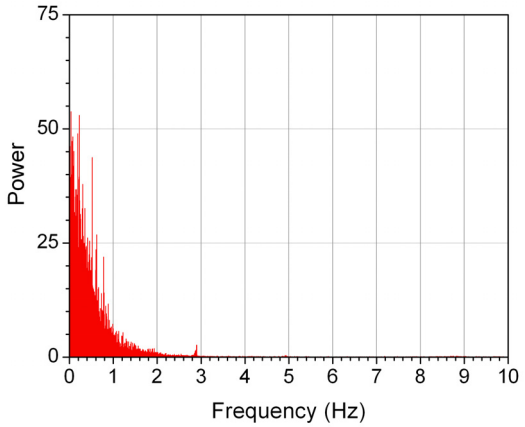

ee. E-FB(NS)-BF-H

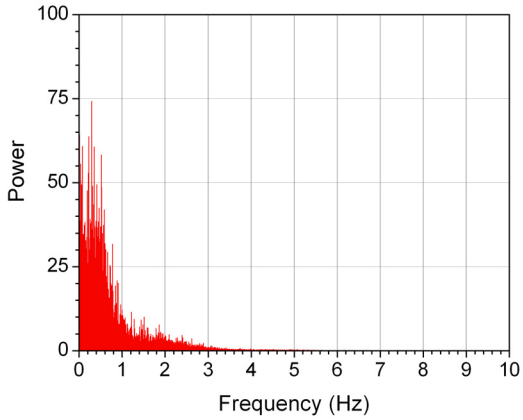

ff. E-SS-WB-V

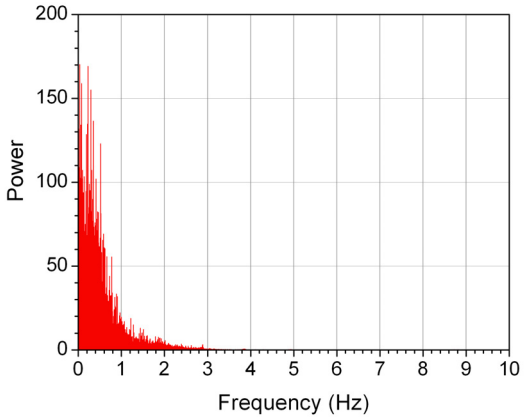

gg. E-FB(SS)-BF-H

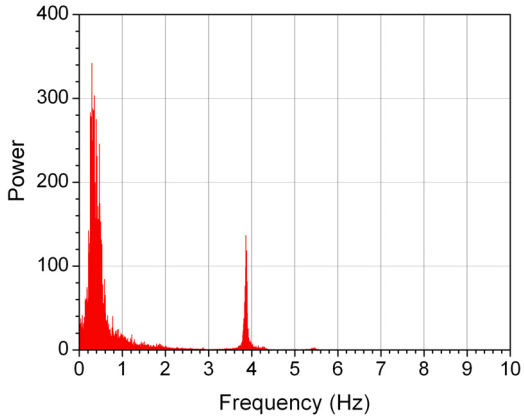

hh. E-SG-CB(1)-V

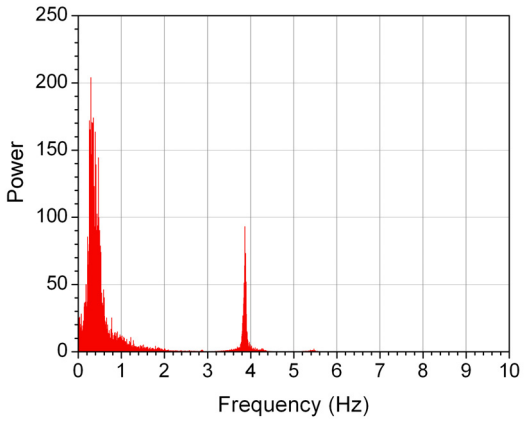

ii. E-SG-CB(5)-V

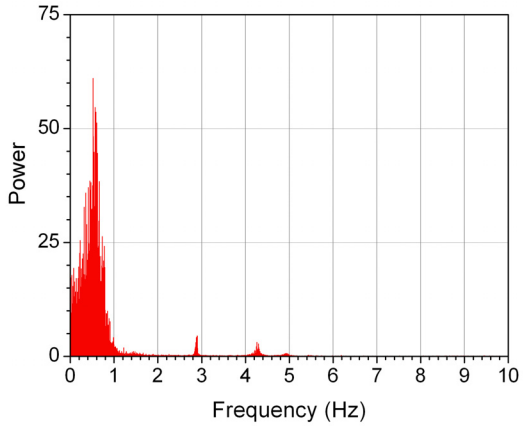

jj. E-SG-BF-H

Figure 5.42. (Continued).

www.manaraa.com

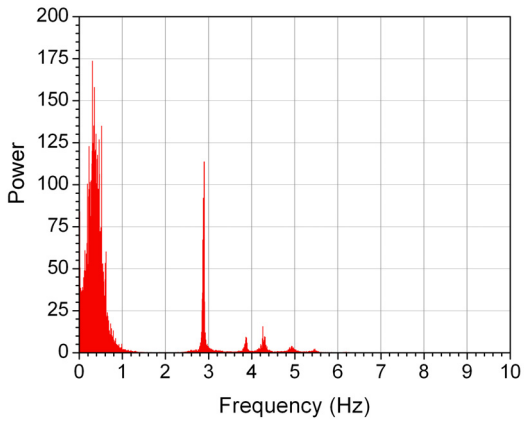

kk. F-NG-BF-H

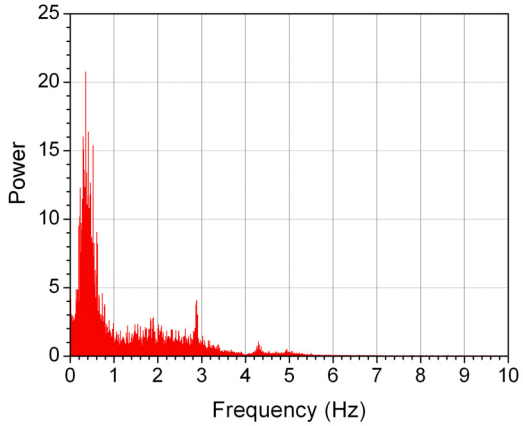

ll. F-NS-BF-H

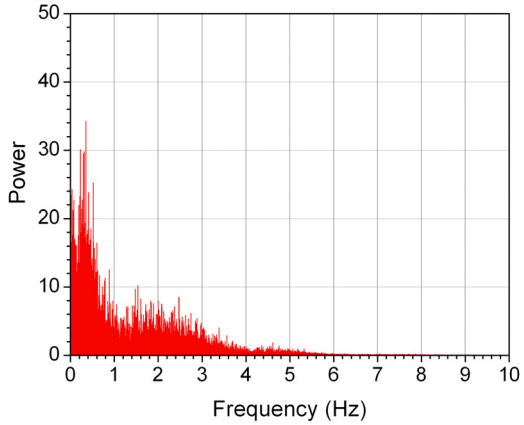

mm. F-SS-BF-H

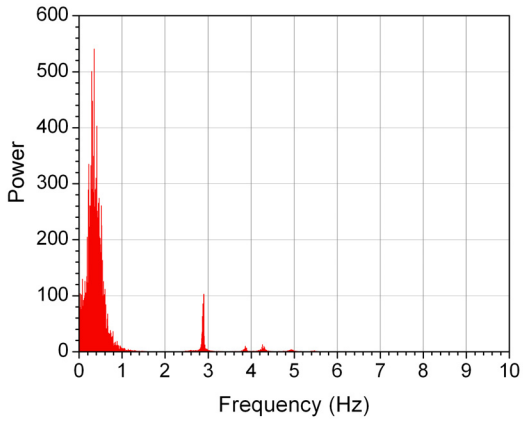

nn. F-SG-BF-H

Figure 5.42. (Continued).

the program, *2 - Configure FCB Filter.vi*, was developed. This front panel of this VI is presented in Fig. 5.43, and a brief description of the labeled controls and indicators are as follows:

1. **Demonstration Data File Source Path Control:** Path to the data file that is to be used for demonstration.

2. **FFT PSD File Source Path Control:** File path to the saved PSD plot results (control #3 in Fig. 5.40).

3. **Temporary Save Directory Control:** Directory to be used for temporary storage of the demonstration data file after it is extracted from the compressed file in control #1.

www.manaraa.com

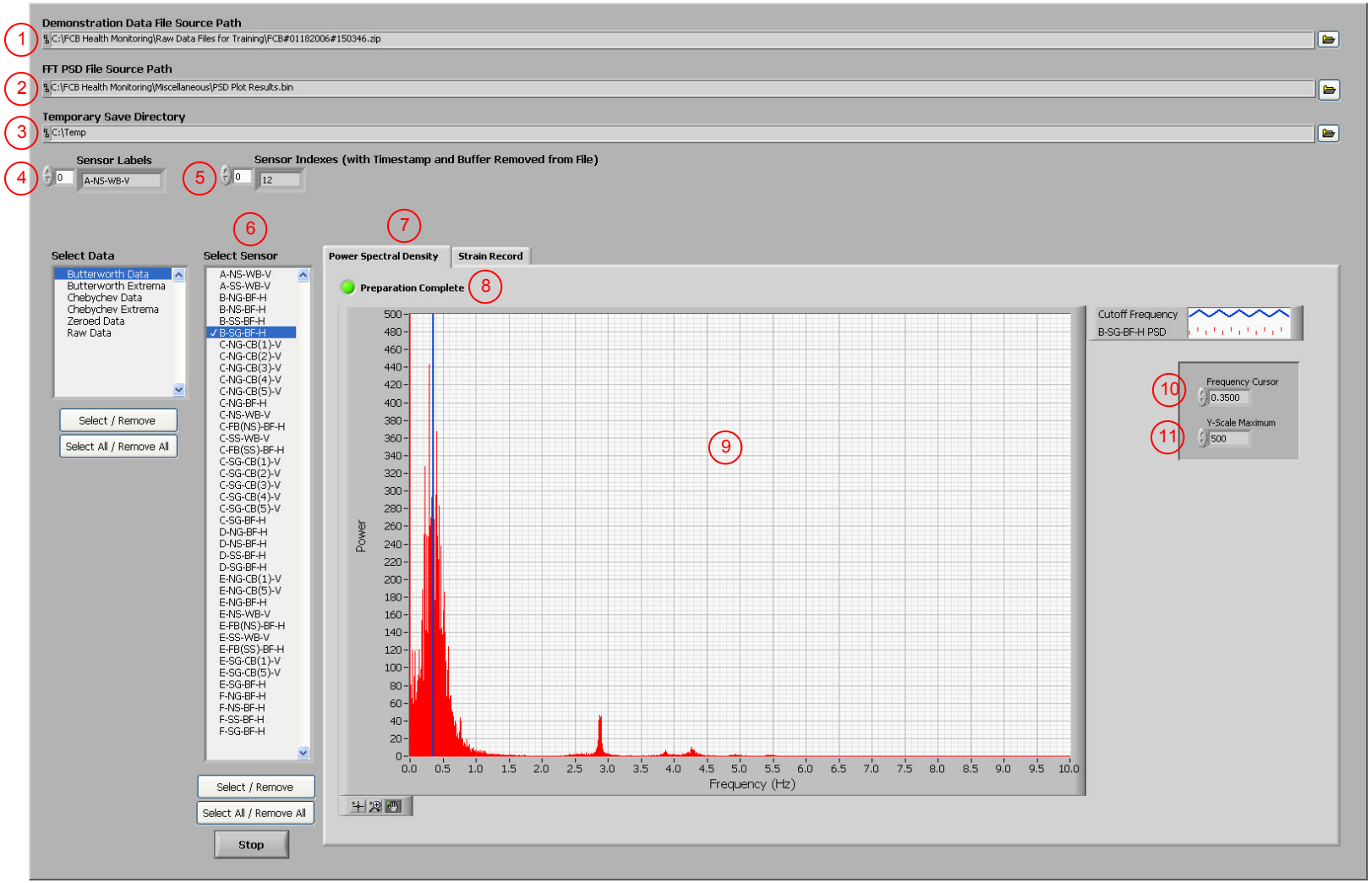

a. PSD plot display for the selected FOS

Figure 5.43. Front panel controls and indicators for configuring the lowpass frequency filter (*2 - Configure FCB Filter.vi*).

www.manaraa.com

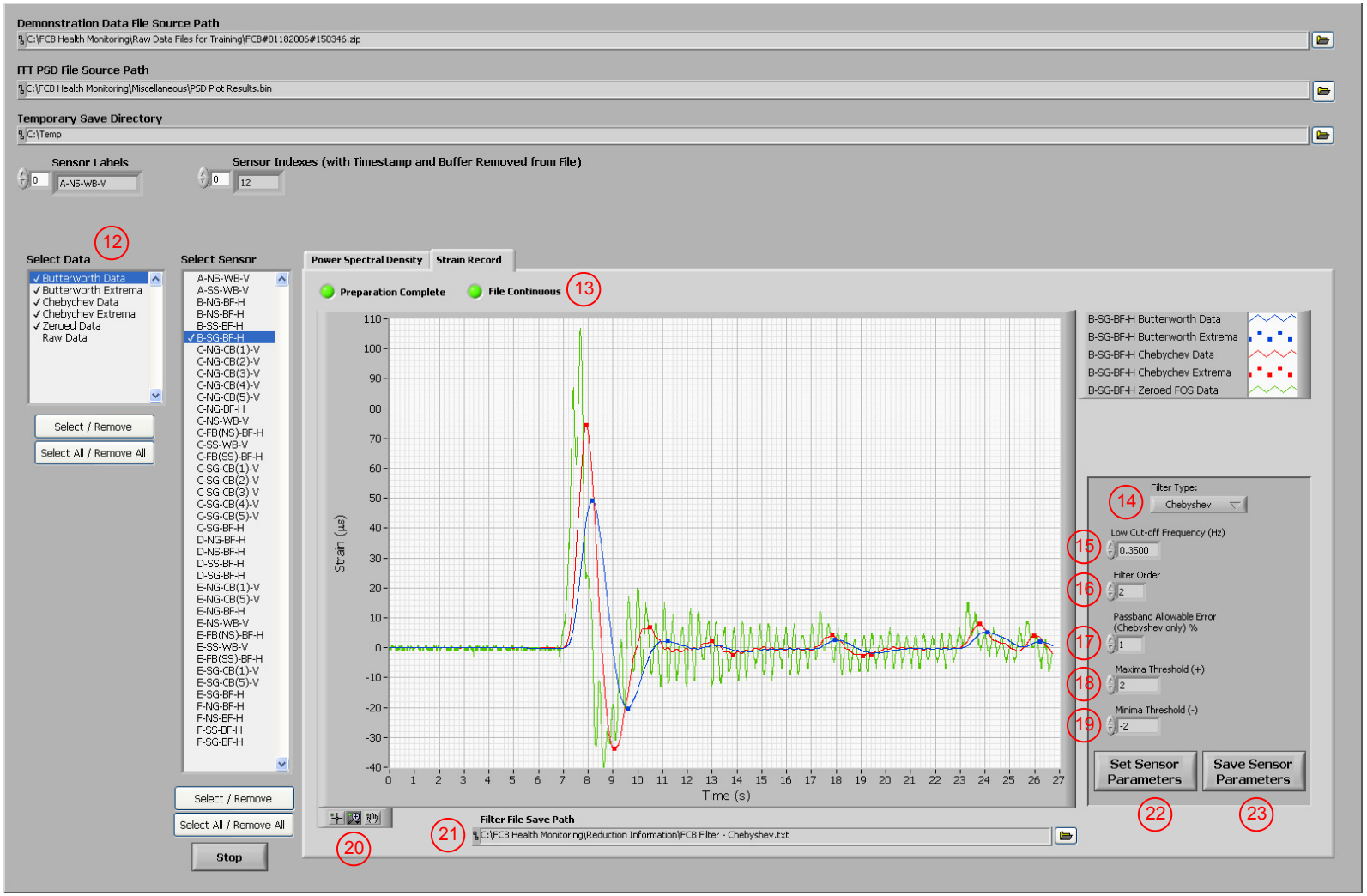

b. Strain record display for the selected FOS

Figure 5.43. (Continued).

www.manaraa.com

4. **Sensor Labels Control:** The labels to be used for each sensor, which are listed in the order of appearance in control #6.

5. **Sensor Indexes Control:** Sensor array indexes for the corresponding sensors listed in control #4.

6. **Select Sensor Control:** Activated sensor for which information is displayed and configuration settings are applied/written.

7. **Display Tab Control:** Tab control for the information display (PSD plot or strain record).

8. **Preparation Complete Indicator:** Dispays true (green) when all data is ready for display.

9. **PSD Plot Indicator:** PSD plot display for the activated sensor.

10. **Frequency Cursor Control:** Frequency cursor value and cut-off value for displayed filtered data.

11. **Y-Scale Maximum Control:** Maximum y-scale value for PSD plot display.

12. **Select Data Control:** Data to be included in the strain record display.

13. **File Continuous Indicator:** Indicates true (green) if the demonstration file was determined to be continuous.

14. **Filter Type Control:** Filter type for the parameters that are written to the filter file.

15. **Low Cut-off Frequency Control:** Cut-off frequency that is applied to the displayed data and written to the filter file.

16. **Filter Order Control:** Filter order that is applied to displayed data and written to the filter file.

17. **Passband Allowable Error Control:** Acceptable passband error in the displayed data and written to the filter file.

18. **Maxima Threshold Control:** Maxima threshold that is applied to the displayed data and written to the filter file.

19. **Minima Threshold Control:** Minima threshold that is applied to the displayed data and written to the filter file.

20. **Zoom Control:** Allows for different types of zooming to change the display view.

21. **Filter File Save Path Control:** Desired file path to which filter parameters are written.

22. **Set Sensor Parameters Control:** If button is depressed, current filter settings are temporarily stored in the program memory but not written to the file specified in control #21.

23. **Save Sensor Parameters Control:** If button is depressed, filter settings that are stored in the program memory are written to the file specified in control #21.

In general, this VI allows the user to view the PSD plot for a selected sensor, use controls to set temporary filter settings, view the effects of the filtering on the selected strain record, make alterations

www.manaraa.com

to the filter settings if desired, and save the filter setting for future application. Four main parameters must be defined to configure a filter for a sensor:

- Filter type
- Cut-off frequency
- Filter order
- Passband allowable error (%)

After all parameters have been defined for each sensor, they are saved to a filter file and used by the SHM system during the monitoring process. The information presented in this section pertains to the use of this VI to configure the filtering process for each sensor. Explanations and suggested values for each filter parameter are discussed in *LabVIEW Analysis Concepts* [86], *The Scientist and Engineer's Guide to Digital Signal Processing* [87], and many other resources discussing digital filters.

When the VI is activated, the previously discussed operations are immediately performed to prepare the data for the configuration process:

- Data is extracted from the compressed file (*WindowsXP Unzip Data.vi* and *UnzipDataXP.dll*) specified in control #1 and read into LabVIEW memory as a 2-D array.
- The timestamp and buffer columns are removed from the array. The DAR is determined from the timestamp, and file continuity is verified through use of the buffer values (*Check File Continuity.vi*).
- Data are checked for flickers (*Remove Zero Flicker.vi*).
- Baselines are determined (*Determine Baselines.vi*) and the raw strain record is zeroed for each sensor.

Moreover, the PSD results file specified in control #2, which were generated in Section 5.2.2, are read into LabVIEW memory. After these primary procedures are completed, indicator #8 displays green to notify that the data are ready to be viewed. At this point, the user has the ability to select a sensor (control #6) and use the display tab control (#7) to view the corresponding PSD plot and strain record. By default, the PSD plot (Fig. 4.42a) for the active sensor is displayed first since its use is required to determine the cut-off frequency for the lowpass filter. In this display, the user is able to use control #10 to move the frequency cursor on the PSD plot to select desired cut-off frequency for

www.manaraa.com

the filter. As illustrated in Fig. 5.43a, B-SG-BF-H was selected as the active sensor, and the cursor was moved to 0.35 Hz for the cut-off frequency, which was demonstrated in Fig. 5.41 to be the frequency for the quasi-static vehicular events for that sensor.

After a frequency for the quasi-static response has been selected with the PSD plot display, the strain record display (Fig. 5.42b) is used to further configure the filter, to set parameters for event extrema identification, to view the impact of the settings on the demonstration file, and to write the desired settings to a file that is used when the SHM system is in monitoring mode. Two types of infinite impulse response (IIR) lowpass frequency filters are available and accomplished with LabVIEW subVIs: Butterworth (*Butterworth Filter.vi*) and Chebyshev (*Chebyshev Filter.vi*) Type 1; brief advantages and disadvantages of each filter type are described in Section 2.5.2. The filter control (#14) specifies the type of filter being configured, and in the US30 SHM system, the Chebyshev filter was selected based on its ability to minimize peak detection error while also using less processing time than the Butterworth filter (and other filters capable of accomplishing the same procedures). The cut-off frequency control (#15) is automatically set to the frequency cursor value in the PSD plot display, but the control can still be changed; if the cut-off frequency is changed in the strain record display, the frequency cursor is also updated on the PSD plot display. Filter order and passband ripple are set by controls #16 and #17, respectively. The passband ripple is only required if a Chebyshev filter is selected, and as required by the subVI, *Chebyshev Filter.vi*, the ripple must be greater than zero and expressed in decibels (dB). Thus, the passband allowable error (PAE) specified in control #17 is converted as follows [86]:

$$\text{ripple (dB)} = \left| 20 \log\left(\frac{100 - \text{PAE}}{100}\right)\right| \tag{5.1}$$

After controls #14-17 have been configured, the VI filters the demonstration strain record for the active sensor according to the selected filter type. Due to the pattern of noise in the strain record, the filtered data often has a slight offset from zero. Thus, the resulting 1-D array of filtered data is zeroed with the subVI, *Determine Baselines - One Sensor.vi* (Appendix E); this subVI performs the exact same data operations as those in *Determine Baselines.vi*, except it has been configured for

www.manaraa.com

only one strain record. After the filtered data has been zeroed, the resulting 1-D array is passed to the subVI, *Determine Extrema - One Sensor.vi* (Appendix E), to identify the events and corresponding extrema within the filtered strain record based on the maxima and minima thresholds specified in controls #18 and #19, respectively. Due to the autonomous data storage, three situations are considered by the subVI to identify vehicular events in a strain record as illustrated in Fig. 5.44:

1. All events are entirely captured within the data file (Fig. 5.44a).
2. The file starts within an event peak or valley (Figs. 5.44b-c).
3. The file ends within an event peak or valley (Figs. 5.44d-e).

Based on the point-by-point bases that are illustrated for each situation in Fig. 5.44, the subVI locates the start and end of each peak or valley, as well as the resulting extrema, based on their array index within the strain record. More specifically, the subVI determines the extreme value start index (ESI), extreme value end index (EEI), and extreme value index (EI) for each event peak and valley and corresponding maxima and minima, respectively, within a strain record. If the entire event is captured within the data file Fig. 5.44a, the subVI examines four consecutive strain values to determine ESI and EEI as follows:

- **Peak start:** For the four data points being considered, the one with array index, i, must be less than or equal to the maxima threshold, and the three with indexes i+1, i+2, and i+3 must be greater than the maxima threshold. The ESI is determined to be index = i (See Detail A in Fig. 5.44a).
- **Peak end:** For the four data points being considered, the one with array index, i, must be greater than or equal to the maxima threshold, and the three with indexes i+1, i+2, and i+3 must be less than the maxima threshold. The EEI is determined to be index = i (See Detail B in Fig. 5.44a).
- **Valley start:** For the four data points being considered, the one with array index, i, must be greater than or equal to the minima threshold, and the three with indexes i+1, i+2, and i+3 must be less than the minima threshold. The ESI is determined to be index = i (See Detail C in Fig. 5.44a).
- **Valley end:** For the four data points being considered, the one with array index, i, must be less than or equal to the minima threshold, and the three with indexes i+1, i+2, and i+3 must be greater than the minima threshold. The EEI is determined to be index = i (See Detail D in Fig. 5.44a).

www.manaraa.com

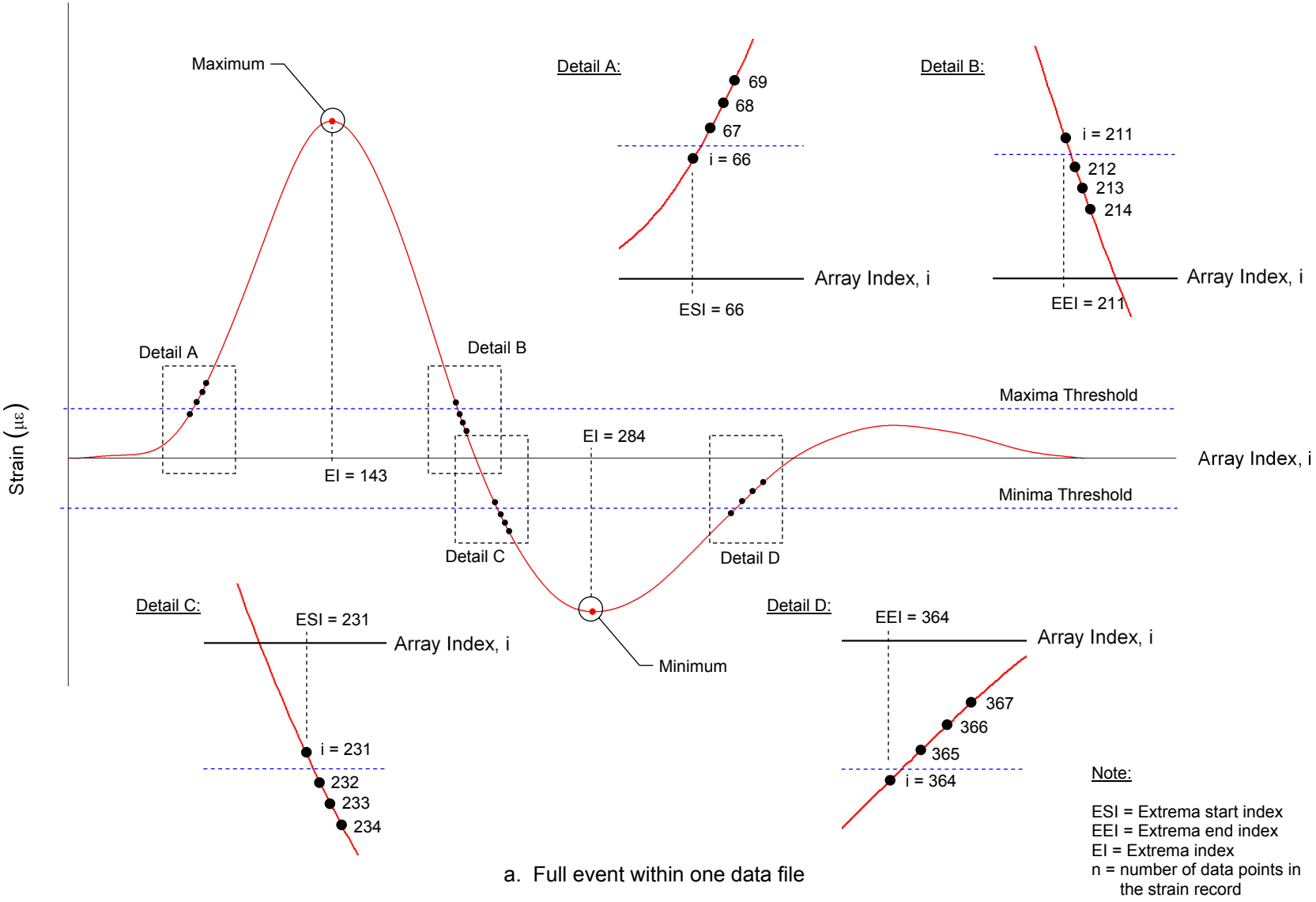

a. Full event within one data file

Figure 5.44. Details of determining event extrema in a strain record with the subVI, *Determine Extrema – One Sensor.vi*.

www.manaraa.com

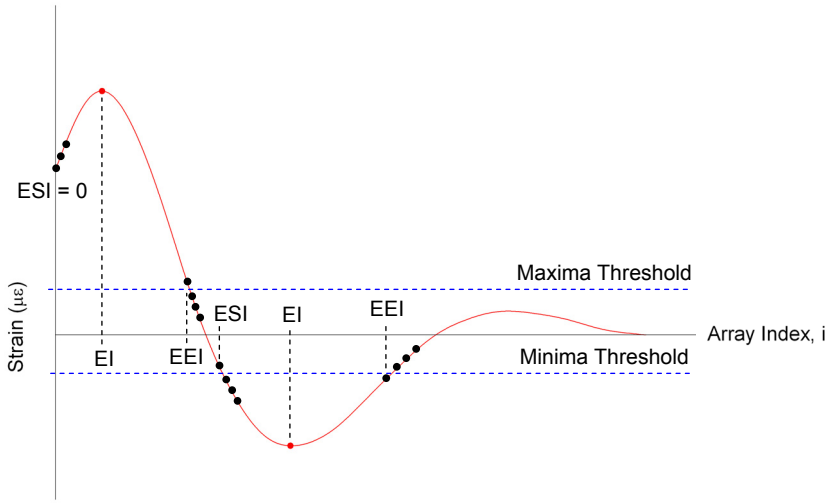

b. File starts within a peak

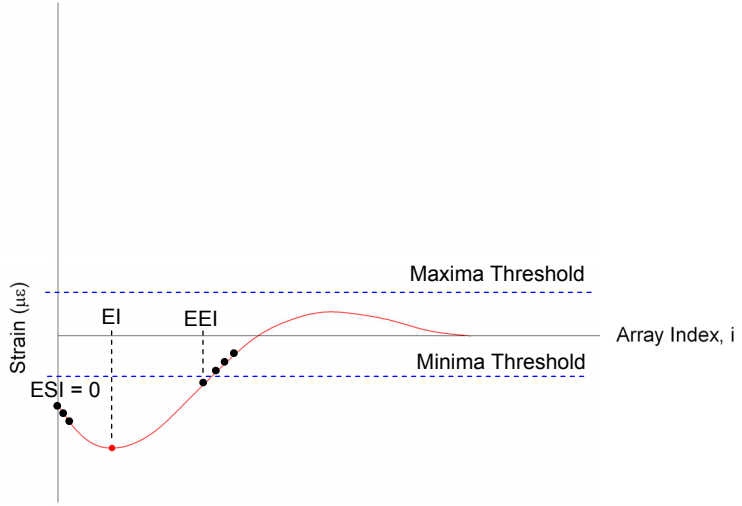

c. File starts within a valley

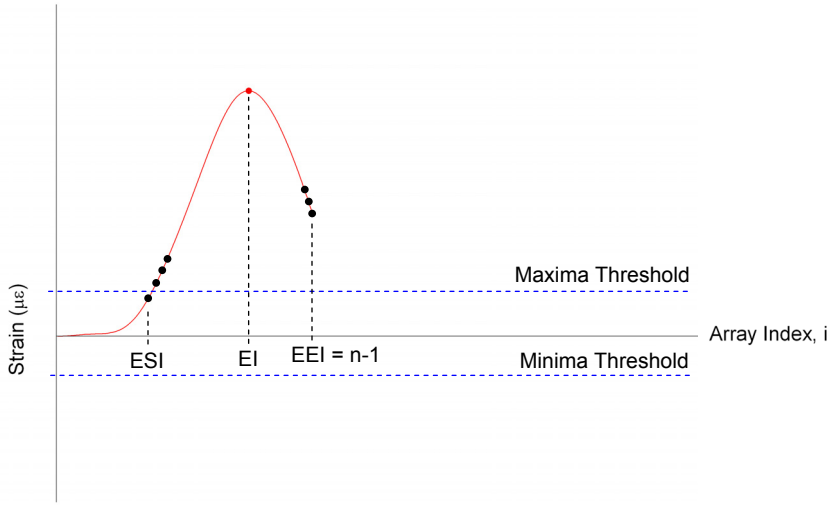

d. File ends within a peak

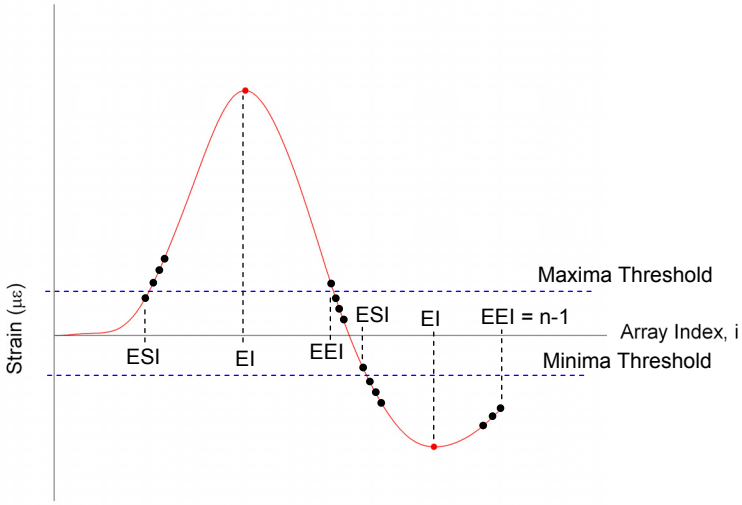

e. File ends within a valley

Figure 5.44. (Continued).

www.manaraa.com

Figures 5.44b-c illustrate the determination of ESI when the file starts within a peak or valley, respectively. If the first three data points of the strain record are all greater than the maxima threshold and consecutively increasing in value (Fig. 5.44b), or if the first three data points of the strain record are all less than the minima threshold and consecutively decreasing in value (Fig. 5.44c), then ESI is recorded as index, i = 0. Similarly, Figs. 5.44d-e illustrate the determination of EEI when the file ends within a peak or valley, respectively. If the last three data points of the strain record are all greater than the maxima threshold and consecutively decreasing in value (Fig. 5.44d), or if the first three data points of the strain record are all less than the minima threshold and consecutively increasing in value (Fig. 5.44e), then ESI is recorded as index, i = n-1, where *n* is equal to the number of data points in the strain record. After the entire sensor strain history has been considered and all ESI and EEI identified, the event extrema values are recorded as the maximum and minimum values between each set of ESI and EEI, where peaks produce maximum values and valleys produce minimum values. For every extrema value, the EI is also recorded. Input to the subVI, *Determine Extrema - One Sensor.vi*, are as follows:

- **Array of Sensor Data**: The strain record for one sensor (1-D array).
- **Maxima Threshold (+)**: The minimum value to be achieved for an event extrema to be considered an event maximum (scalar).
- **Minima Threshold (-):** The maximum value to be achieved for an event extrema to be considered an event minimum (scalar).

Output from the subVI, *Determine Extrema - One Sensor.vi*, are as follows:

- **Maxima-Extrema Indexes**: Indexes for the maxima values that were identified (1-D array).
- **Maxima Values**: The maxima values that were identified in the strain record (1-D array).
- **Minima-Extrema Indexes**: Indexes for the minima values that were identified (1-D array).
- **Minima Values**: The minima values that were identified in the strain record (1-D array).

For future use with the SHM system in monitoring mode, *Determine Extrema.vi*, was created to identify extrema in multiple strain records that are passed to the subVI. The 2-D array of strain data must be passed into the subVI with each row of the array corresponding to one strain record. Input to the subVI, *Determine Extrema.vi*, are as follows:

www.manaraa.com

- **Array of Sensor Data**: The strain records for multiple sensors (2-D array with each sensor strain record in one row of the array).
- **Maxima Threshold Array (+)**: The minimum value to be achieved for an event extrema to be considered an event maximum (1-D array with indexes of the thresholds matching those of the corresponding strain record in the sensor array).
- **Minima Threshold (-):** The maximum value to be achieved for an event extrema to be considered an event minimum (1-D array with indexes of the thresholds matching those of the corresponding strain record in the sensor array).

Output from the subVI, *Determine Extrema.vi*, are as follows:

- **Maxima Detected (T/F):** Reports true or false depending on whether or not a maxima was detected in the strain record (1-D array with indexes of the values matching those of the corresponding strain record in the sensor array).
- **Count of Maxima:** Number of maxima determined in each strain record (1-D array with indexes of the values matching those of the corresponding strain record in the sensor array).
- **Maxima Values:** The maxima values that were identified in each strain record (2-D array with the row indexes matching those of the sensor array).
- **Maxima-Extrema Start Indexes:** Extrema start indexes (ESIs) for each peak within each strain record (2-D array with the row indexes matching those of the sensor array).
- **Maxima-Extrema Indexes:** Indexes for the maxima values that were identified (2-D array with the row indexes matching those of the sensor array).
- **Maxima-Extrema End Indexes:** Extrema end indexes (EEIs) for each peak within each strain record (2-D array with the row indexes matching those of the sensor array).
- **Data Points between Maxima:** Number of data points between adjacent maxima in a strain record (2-D array with the row indexes matching those of the sensor array).
- **Minima Detected (T/F):** Reports true or false depending on whether or not a minima was detected in the strain record (1-D array with indexes of the values matching those of the corresponding strain record in the sensor array).
- **Count of Maxima:** Number of minima determined in each strain record (1-D array with indexes of the values matching those of the corresponding strain record in the sensor array).
- **Minima Values:** Minima values that were identified in each strain record (2-D array with the row indexes matching those of the sensor array).
- **Minima-Extrema Start Indexes:** Extrema start indexes (ESIs) for each valley within each strain record (2-D array with the row indexes matching those of the sensor array).
- **Minima-Extrema Indexes:** Indexes for the minima values that were identified (2-D array with the row indexes matching those of the sensor array).
- **Minima-Extrema End Indexes:** Extrema end indexes (EEIs) for each valley within each strain record (2-D array with the row indexes matching those of the sensor array).

www.manaraa.com

- **Data Points between Minima:** Number of data points between adjacent minima in a strain record (2-D array with the row indexes matching those of the sensor array).

The subVI, *Determine Extrema.vi*, has much more information that is exported than the subVI, *Determine Extrema – One Sensor.vi*. The subVIs were designed in this way because *Determine Extrema.vi* is only used in the in the VI, *2 - Configure FCB Filter.vi*, which only requires information pertaining to extrema values and locations for use in the strain record display. However, the subVI, *Determine Extrema.vi*, is used in the extrema matching process that is discussed Section 5.2.5 as well as the monitoring mode of the SHM system, which is discussed in Section 5.3; both of these applications require much more information about the strain record of each sensor.

After event extrema are identified for the filtered data by *Determine Extrema – One Sensor.vi*, all data are ready for the strain record display. Through use of the data selection control (#15) the user is able to simultaneously display one more of the following data sets for the active sensor: (1) raw data, (2) zeroed data, (3) the filtered strain record resulting from the Chebyshev filter, (4) extrema identified in the Chebyshev data, (5) the filtered strain record resulting from the Butterworth filter, and (6) extrema identified in the Butterworth data. Figure 5.43b illustrates the strain record display that was used during configuration the filter settings of B-SG-BF-H of the US30 SHM system. Presented in the display are the control configurations and resulting zeroed data, Chebyshev filtered data with event extrema, and Butterworth filtered data with event extrema. Review of the presented data reveals the followings:

- Comparison of zeroed and filtered data to illustrate the frequencies that were removed from the strain record.
- Comparison of filtered data to illustrate the significant differences that result from differing filtering types.
- The slight time delay of the filtered data records that develop during the filtering processes.

In both filtering procedures, the dynamic responses and noise in strain record have been removed to produce smooth vehicular events. Note, however, that the extrema values differ significantly between the Butterworth filtered data and the Chebyshev filtered data; the Butterworth identified extrema are much lower than that of the Chebyshev, and in addition, have a poor fit to the zeroed data. This reinforces the information presented in Section 2.5.2 of the literature review where

www.manaraa.com

the Butterworth filter was presented as being maximally flat with higher peak detection error than that produced by the Chebyshev filter. The error of the Butterworth filter could potentially be reduced by increasing the order of the filter, but since the Chebyshev filter accomplishes accurate filtering at the lower filter order (which requires less processor resources), it was selected for use in the US30 SHM system. The causes of the brief time delay of the filtered data are concisely addressed in literature [86, 87], but the slight delay is inherent to the process with IIR filters. The strain record displayed in Fig. 5.43b was used to generated Figs. 5.4 and 5.30, and the time delay of the filtered data in those figures, as well as Figs. 5.19 - 5.29, was removed for illustrative purposes.

The program, *2 - Configure FCB Filter.vi*, was written to allow the user to scan through multiple configurations of the filtering process as well as the thresholds for extrema identification. If changes are made to controls #6, 10, 12, or 14 - 19, the strain record display is immediately updated to reveal the impact of those changes on the demonstration data. The user is also able to use the zoom features (control #20) to change the view of the strain record for more detailed display of the zeroed and filtered data, which is especially useful when attempting to visually determine the frequencies that remain in the filtered strain record. When the final configuration for an active sensor is reached, the user must depress control #22 to temporarily store the filter configuration in LabVIEW memory; to save the temporarily stored configurations to the filter file save path specified in control #21, the user must depress control #23. The resulting filter file is a 2-D array of data that contains filtering configurations as well as extrema identification parameters. Each row represents the settings for one sensor (according to the sensor array indexes specified in control #5), and columns zero, one, two, three, and four are the cut-off frequency (Hz), filter order, passband ripple (dB), maxima threshold ($\mu\varepsilon$), and minima threshold ($\mu\varepsilon$), respectively, for each sensor. This process may be repeated as many times as desired until the user manually stops the program.

Table 5.1 presents the finalized filtering and extrema identification configurations that were established for each sensor in the US30 SHM system. During the configuration process and review of all PSD plots presented in Fig. 4.42, the following conclusions were determined:

www.manaraa.com

Table 5.1. Sensor array indexes and configurations for filtering and identification of event extrema.

Sensor	Aggregate Array Index	Sensor Array Index	Cut-off Frequency (Hz)	Order	Passband Ripple (dB)	Maxima Threshold (με)	Minima Threshold (με)
B-NG-BF-H	2	0	0.3500	2	0.0873	2.0	-2.0
B-NS-BF-H	3	1	0.2750	2	0.0873	2.0	-2.0
B-SS-BF-H	4	2	0.3500	2	0.0873	2.0	-2.0
B-SG-BF-H	5	3	0.3500	2	0.0873	2.0	-2.0
C-SG-BF-H	6	4	0.6250	2	0.0873	2.0	-2.0
C-FB(SS)-BF-H	7	5	0.3250	2	0.0873	2.0	-2.0
C-SS-WB-V	8	6	0.6500	2	0.0873	2.0	-2.0
C-SG-CB(5)-V	9	7	0.3750	2	0.0873	2.0	-2.0
C-SG-CB(4)-V	10	8	0.3750	2	0.0873	2.0	-2.0
C-SG-CB(3)-V	11	9	0.3750	2	0.0873	2.0	-2.0
C-SG-CB(2)-V	12	10	0.4000	2	0.0873	2.0	-2.0
C-SG-CB(1)-V	13	11	0.4000	2	0.0873	2.0	-2.0
A-NS-WB-V	14	12	0.5000	2	0.0873	2.0	-2.0
A-SS-WB-V	15	13	0.5000	2	0.0873	2.0	-2.0
D-SG-BF-H	16	14	0.4000	2	0.0873	2.0	-2.0
D-SS-BF-H	17	15	0.4000	2	0.0873	2.0	-2.0
D-NS-BF-H	18	16	0.4000	2	0.0873	2.0	-2.0
D-NG-BF-H	19	17	0.3500	2	0.0873	2.0	-2.0
C-NG-BF-H	20	18	0.5500	2	0.0873	2.0	-2.0
C-FB(NS)-BF-H	21	19	0.2750	2	0.0873	2.0	-2.0
C-NS-WB-V	22	20	0.4000	2	0.0873	2.0	-2.0
C-NG-CB(5)-V	23	21	0.3500	2	0.0873	2.0	-2.0
C-NG-CB(4)-V	24	22	0.3500	2	0.0873	2.0	-2.0
C-NG-CB(3)-V	25	23	0.3500	2	0.0873	2.0	-2.0
C-NG-CB(2)-V	26	24	0.3500	2	0.0873	2.0	-2.0
C-NG-CB(1)-V	27	25	0.3500	2	0.0873	2.0	-2.0
E-NG-BF-H	28	26	0.6500	2	0.0873	2.0	-2.0
E-NG-CB(5)-V	29	27	0.3250	2	0.0873	2.0	-2.0
E-NG-CB(1)-V	30	28	0.4000	2	0.0873	2.0	-2.0
E-NS-WB-V	31	29	0.5500	2	0.0873	2.0	-2.0
E-FB(NS)-BF-H	32	30	0.2750	2	0.0873	2.0	-2.0
E-FB(SS)-BF-H	33	31	0.3000	2	0.0873	2.0	-2.0
E-SS-WB-V	34	32	0.3250	2	0.0873	2.0	-2.0
E-SG-CB(5)-V	35	33	0.3250	2	0.0873	2.0	-2.0
E-SG-CB(1)-V	36	34	0.3250	2	0.0873	2.0	-2.0
E-SG-BF-H	37	35	0.5750	2	0.0873	2.0	-2.0
F-SG-BF-H	38	36	0.4000	2	0.0873	2.0	-2.0
F-SS-BF-H	39	37	0.4000	2	0.0873	2.0	-2.0
F-NS-BF-H	40	38	0.4000	2	0.0873	2.0	-2.0
F-NG-BF-H	41	39	0.4000	2	0.0873	2.0	-2.0

Note: [ ] denotes information written to the filter file, *FCB Filter - Chebyshev.txt*

www.manaraa.com

- For FOSs installed on the girders at midspan of all spans (i.e. B-SG-BF-H, D-NG-BF-H, F-SG-BF-H, etc.), the frequencies for quasi-static vehicular events were determined to be in the range of 0.35 - 4.0 Hz. For FOSs installed on the girders near support locations (i.e. C-NG-BF-H, E-SG-BF-H, etc.), the frequencies for the quasi-static events were determined to be approximately 0.55 - 0.65 Hz.

- The fundamental frequency of the bridge for the first mode of vibration for all spans was determined to be approximately 2.9 Hz. This frequency was identified in the PSD plots of nearly all FOSs installed on bottom flanges of girders, and it was also verified in the strain records by examining the free vibration response of the girders following events with large magnitudes. This value also agrees with the information from other literature findings that the fundamental frequencies of highway bridges are typically within 2 - 5 Hz [88].

- Strain records for FOSs installed on stringers or floor beams (i.e. B-NS-BF-H, C-SS-WB-V, C-FB(NS)-BF-H, D-SS-BF-H, etc.) were developed from a wide variety of frequencies. Strains were generated from the global response of the bridge (girder frequencies for the quasi-static response and fundamental frequencies) as well as localized frequencies for quasi-static responses that result from traffic events (approximately 2.0 - 2.5 Hz).

- Frequencies for quasi-static responses for FOSs in the cut-back regions agree with those of the girders (0.325 - 0.4 Hz), which reinforces the explanation that strains in cut-back regions develop from relative girder displacements. The 2.9 Hz fundamental frequency of the girders was not within the PSD for these sensors, but a higher frequency, 3.9 Hz, did appear that was barely detectable in the PSD plots of other sensors in the bridge.

Because the stringer frequencies for quasi-static vehicular events (2.0 - 2.5 Hz) were close to the fundamental frequency of the bridge spans (approximately 2.9 Hz), selection of cut-off frequencies for the stringers required more investigation than those of the girders. Figure 5.45a presents the identified extrema for an event in the strain record of D-SS-BF-H (previously displayed in Fig. 5.24b) when the filter cut-off frequency was set to 2.5 Hz and the extrema thresholds were set to ± 2 με. As illustrated, the resulting filtered data and identified extrema consisted of a local vehicular event as well as the free vibration response following the event. Since the objective of the filtering process is to remove all frequencies except that of the quasi-static response, this configuration was not suitable. As a result, two options were available: (1) adjust the thresholds such that the free vibration extrema were not detected, or (2) decrease the filter cut-off frequency to remove all frequencies except those resulting from the global response of the bridge (girder frequencies for the quasi-static response). Since adjusting the extrema thresholds would also affect the identification of extrema from smaller vehicles such as cars and small trucks, it was decided to lower the cut-off frequency for filtering the strain records of sensors installed on stringers and floor beams. Figure 5.45b illustrates the identified extrema in D-SS-BF-H for the lower cut-off frequency, 0.40 Hz, which

www.manaraa.com

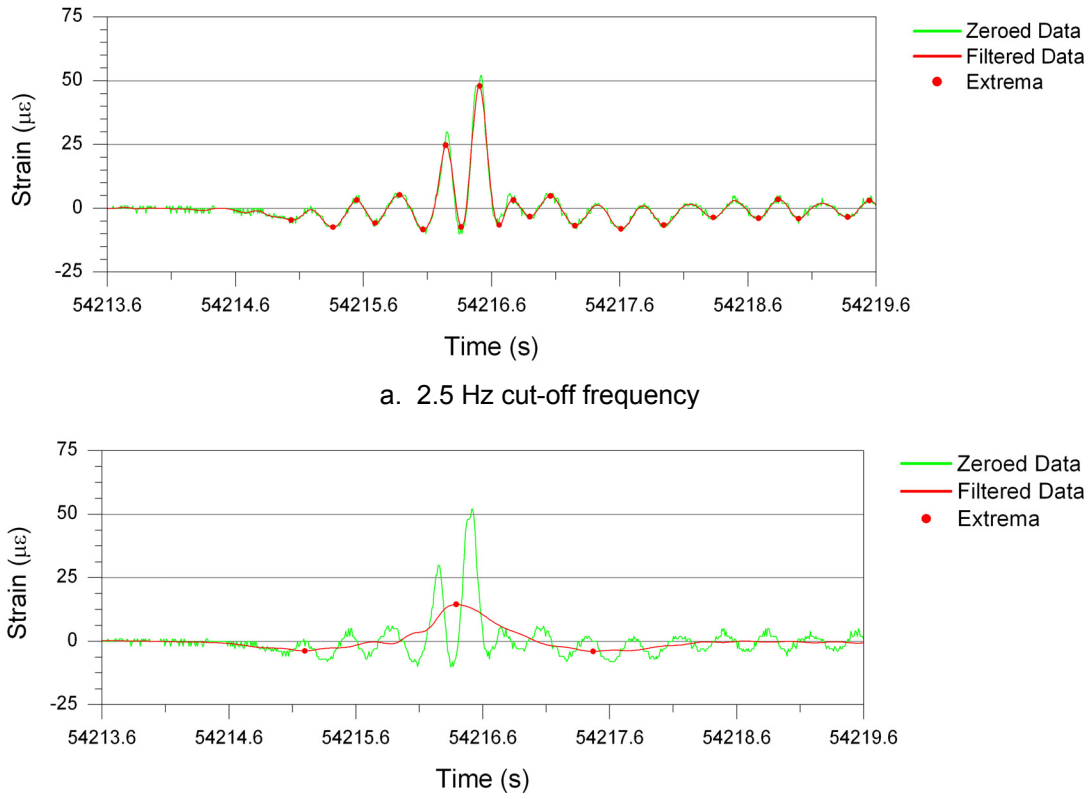

a. 2.5 Hz cut-off frequency

b. 0.40 Hz cut-off frequency

Figure 5.45. D-SS-BF-H: comparison of filtered data and identified extrema for different cut-off frequencies.

matched the cut-off frequency for D-SG-BF-H.

The cause of the 3.9 Hz frequency in the PSD plots of cut-back region sensors was not identified. Potential sources of this frequency include out-of-phase free vibration of the north and south girders or coupling of free vibration modes for differing degrees of freedom. Regardless of the source(s), the frequency is removed during the filtering process.

5.2.4 Defining Sensor Classifications and Longitudinal Locations

As illustrated in Fig. 5.37, after the filtering configurations have been established for all sensors in the SHM system, sensor information must be input into the system to classify each sensor as a TS or NTS. In addition, the longitudinal location of each sensor within the bridge must be specified, which is required for the extrema matching process. To accomplish these relatively simple

www.manaraa.com

tasks, two different programs were developed: *3 - Input Sensor Locations.vi* and *4 - Select Target Sensors.vi* (See Appendix E).

The front panel for the program, *3 - Input Sensor Locations.vi*, is presented in Fig. 5.46, and a brief description of the labeled controls and indicators are as follows:

1. **Sensor Locations File Save Path Control:** Path to the data file that is to be used for demonstration.
2. **Sensor Labels Control:** The labels to be used for each sensor, which are listed in the order of appearance in control #4.
3. **Sensor Indexes Control:** Sensor array indexes for the corresponding sensors listed in control #2.
4. **Sensor Locations Control:** Listbox for entering sensor longitudinal locations.
5. **Save Locations Control:** If depressed, the listed longitudinal locations are saved to the file specified in control #1.

When the VI is activated, the sensor labels in control #2 are automatically displayed in the left column of control #4. The user must simply enter the corresponding sensor longitudinal locations in the right column of control #4, as displayed in Fig. 5.46 for the US30 SHM system. Since the longitudinal locations of the sensors are used on a relative basis in the extrema matching process, the origin for determining the location of each sensor was arbitrarily chosen as the west end of the north girder in the US30 bridge. After control #5 is depressed, the 1-D array of sensor locations is written to the file specified in control #1 according to the array indexes specified in control #3.

The front panel for the program, *4 - Select Target Sensors.vi*, is presented in Fig. 5.47, and a brief description of the labeled controls and indicators are as follows:

1. **Sensor Classification File Save Path Control:** Path to the data file that is to be used for demonstration.
2. **Sensor Labels Control:** The labels to be used for each sensor, which are listed in the order of appearance in control #4.
3. **Sensor Indexes Control:** Sensor array indexes for the corresponding sensors listed in control #2.
4. **Select Target Sensors Control:** Listbox for selecting the TSs in the SHM system.
5. **Save Selection Control:** If depressed, the selected sensors are classified as TSs and all unselected sensors are saved as NTSs to the file specified in control #1.

www.manaraa.com

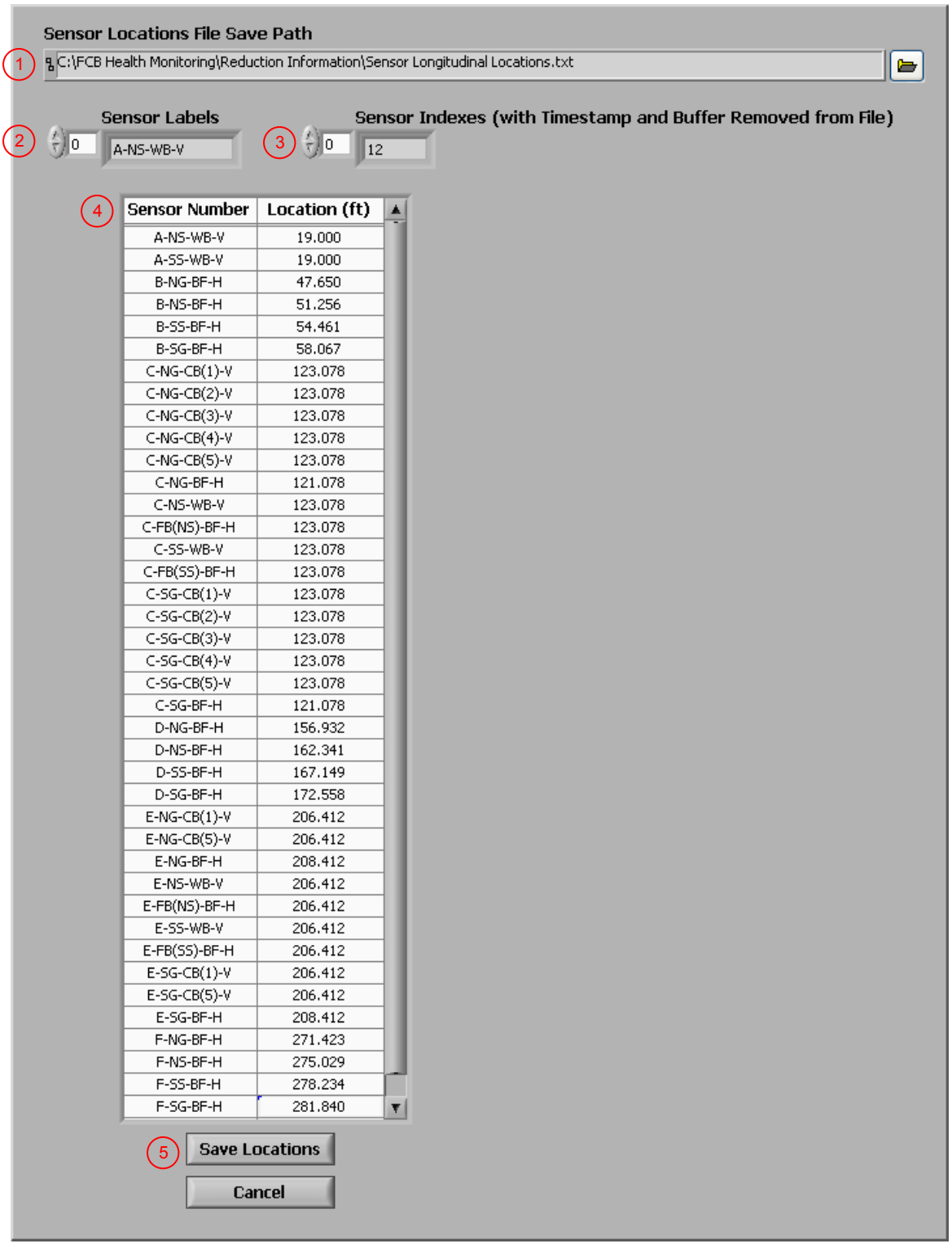

Figure 5.46. Front panel controls for inputting sensor longitudinal locations (*3 - Input Sensor Locations.vi*).

www.manaraa.com

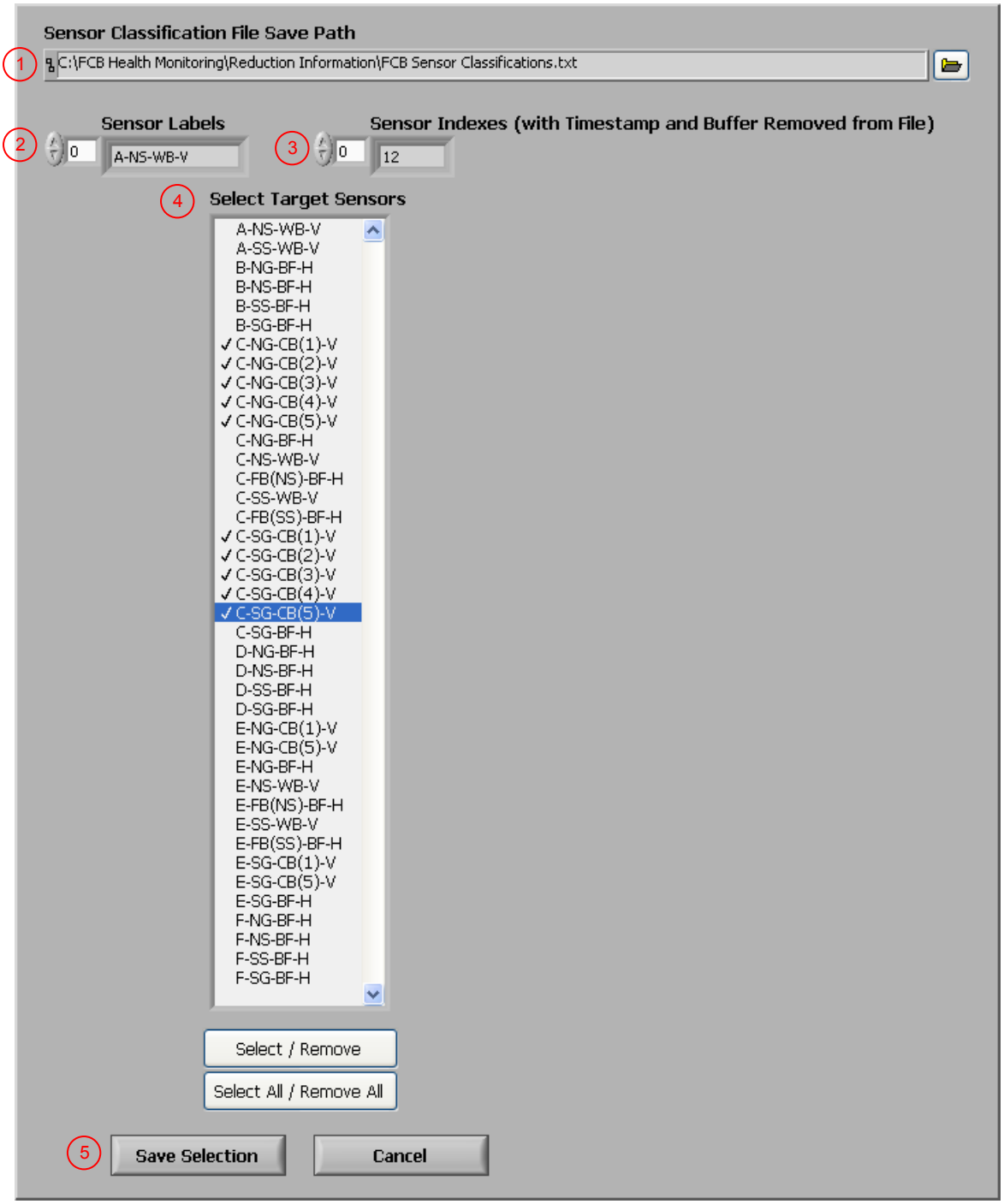

Figure 5.47. Front panel controls for defining sensor classifications (*4 - Select Target Sensors.vi*).

www.manaraa.com

When the program is activated, the sensor labels in control #2 are automatically displayed in control #4 and are available for selection. As displayed in Fig. 5.47, a check mark is placed by all sensors that have been selected for TS classification in the US30 SHM system, which were previously listed in Section 5.1.4. After control #5 is depressed, the 1-D array of classifications is written to the file specified in control #1 according to the array indexes specified in control #3. If a sensor was selected for TS classification, then a unit value was written to its index in the file; if a sensor was unselected, and thus assigned a NTS classification, a zero value was written to its index in the file. Table 5.2 lists the sensor longitudinal locations and classifications as specified in the US30 SHM system.

5.2.5 Generation of Training Information

As illustrated in Fig. 5.37, after the SHM system is configured to reduce strain records and extract event extrema, training data are generated to develop relationships among TSs and NTSs. To achieve this task, three programs were developed:

- *5 - Develop SHM Training Files.vi*
- *6 - Assemble SHM Training Files.vi*
- *7 - View Results - Assembled SHM Training Files.vi*

The first two programs are used to generated and organize the training data, while the third program is used to review the relationships that were developed from the system configurations. If necessary, the SHM system configuration may be changed and training data regenerated until relationships are determined to be satisfactory.

It was discussed in Section 5.1.4 that extrema corresponding to the same vehicular events between one TS and one NTS are matched to form (x,y) data points on a plot. As the extrema matching procedure is applied to continuous data for specified time, the matched event extrema form relationships on the x-y plot. Because extrema can be maxima or minima and because two sensors are considered at one time, up to four relationships can be established for each TS-NTS combination (See Fig. 5.37):

1. TS maxima matched with NTS maxima relationship (MAMAR)

www.manaraa.com

Table 5.2. Sensor array indexes, longitudinal locations, and classifications.

Sensor	Aggregate Array Index	Sensor Array Index	Longitudinal Location (ft)	Classification (0 = NTS, 1 = TS)
B-NG-BF-H	2	0	47.650	0
B-NS-BF-H	3	1	51.256	0
B-SS-BF-H	4	2	54.461	0
B-SG-BF-H	5	3	58.067	0
C-SG-BF-H	6	4	121.078	0
C-FB(SS)-BF-H	7	5	123.078	0
C-SS-WB-V	8	6	123.078	0
C-SG-CB(5)-V	9	7	123.078	1
C-SG-CB(4)-V	10	8	123.078	1
C-SG-CB(3)-V	11	9	123.078	1
C-SG-CB(2)-V	12	10	123.078	1
C-SG-CB(1)-V	13	11	123.078	1
A-NS-WB-V	14	12	19.000	0
A-SS-WB-V	15	13	19.000	0
D-SG-BF-H	16	14	172.558	0
D-SS-BF-H	17	15	167.149	0
D-NS-BF-H	18	16	162.341	0
D-NG-BF-H	19	17	156.932	0
C-NG-BF-H	20	18	121.078	0
C-FB(NS)-BF-H	21	19	123.078	0
C-NS-WB-V	22	20	123.078	0
C-NG-CB(5)-V	23	21	123.078	1
C-NG-CB(4)-V	24	22	123.078	1
C-NG-CB(3)-V	25	23	123.078	1
C-NG-CB(2)-V	26	24	123.078	1
C-NG-CB(1)-V	27	25	123.078	1
E-NG-BF-H	28	26	208.412	0
E-NG-CB(5)-V	29	27	206.412	0
E-NG-CB(1)-V	30	28	206.412	0
E-NS-WB-V	31	29	206.412	0
E-FB(NS)-BF-H	32	30	206.412	0
E-FB(SS)-BF-H	33	31	206.412	0
E-SS-WB-V	34	32	206.412	0
E-SG-CB(5)-V	35	33	206.412	0
E-SG-CB(1)-V	36	34	206.412	0
E-SG-BF-H	37	35	208.412	0
F-SG-BF-H	38	36	281.840	0
F-SS-BF-H	39	37	278.234	0
F-NS-BF-H	40	38	275.029	0
F-NG-BF-H	41	39	271.423	0

Note: denotes information written to the file, *Sensor Longitudinal Locations.txt*
denotes information written to the file, *FCB Sensor Classifications.txt*

www.manaraa.com

2. TS maxima matched with NTS minima relationship (MAMIR)
3. TS minima matched with NTS maxima relationship (MIMAR)
4. TS minima matched with NTS minima relationship (MIMIR)

The program, *5 - Develop SHM Training Files.vi*, was developed to perform the matching process for a collection of raw data files that have been selected for use in the training process. The front panel for this VI is presented in Fig. 5.48, and a brief description of the labeled controls and indicators are as follows:

1. **Data Files Directory Source Path Control:** Directory containing the raw data files to be used in the training process.
2. **Training Files Directory Save Path Control:** Top-level directory to which training folders/files are written.

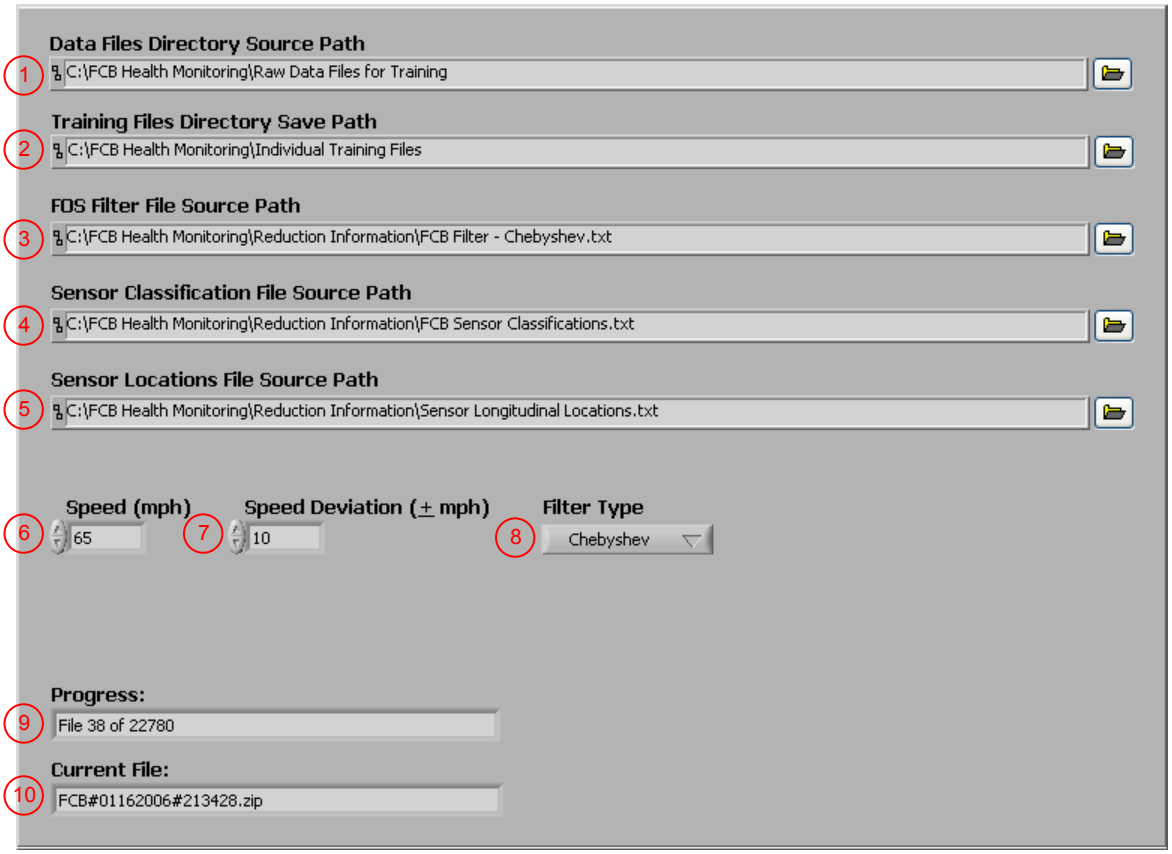

Figure 5.48. Front panel controls for developing training files from raw data files (*5 - Develop SHM Training Files.vi*).

www.manaraa.com

3. **FOS Filter File Source Path Control:** Path to the file containing filter configurations and extrema identification parameters for each sensor (file generated with the VI, *2 - Configure FCB Filter.vi*).

4. **Sensor Classification File Source Path Control:** Path to the file containing sensor classifications (file generated with the VI, *4 - Select Target Sensors.vi*).

5. **Sensor Locations File Source Path:** Path to the file containing sensor longitudinal locations within the bridge (file generated with the VI, *3 - Input Sensor Locations.vi*).

6. **Speed (mph) Control:** Expected average speed for a representative sample of traffic.

7. **Speed Deviation (± mph) Control:** Deviation (mph) to be used with the expected average speed to define the expected speed range for a representative sample of traffic.

8. **Filter Type Control:** Specifies the type of lowpass frequency filter, Chebyshev or Butterworth, to be applied to the data file.

9. **Progress Indicator:** Progress of the training file generation process.

10. **Current File Indicator:** Name of the current file in the process.

The primary objectives of the program are to reduce the data, extract the event extrema, and form all four relationships for every possible TS-NTS combination for every data file in the source directory (control #1). In this process, several previously discussed operations are performed on every data file to extract event extrema for matching:

- Data is extracted from the compressed file (*WindowsXP Unzip Data.vi* and *UnzipDataXP.dll*) and read into LabVIEW memory as a 2-D array.
- The timestamp and buffer columns are removed from the 2-D array. The DAR is determined from the timestamp, and file continuity is verified through use of the buffer (*Check File Continuity.vi*).
- Data are checked for flickers (*Remove Zero Flicker.vi*).
- Baselines are determined (*Determine Baselines.vi*) and the raw strain record is zeroed for each sensor.
- Filter configurations and extrema identification parameters are read into LabVIEW memory from the filter file specified in control #3. For each strain record in the file, the data are filtered according to control #8 (*Butterworth Filter.vi* or *Chebyshev Filter.vi*), and extrema information is extracted (Determine Extrema.vi).

After all extrema information has been determined (i.e. extrema values, ESIs, EIs, and EEIs) in all strain records, the extrema matching process is performed by the subVI, *Match Extrema.vi* (See Appendix E). In this subVI, a windowing procedure is used to match the maximum absolute strain values between corresponding events in TSs and NTSs records. This extreme value was selected

www.manaraa.com

because it theoretically always occurs when a vehicle is in the vicinity of a sensor. In addition, it is also theoretically the largest magnitude that is achieved during an event, and thus, it is reliable and repeatable. However, since the sensors have different longitudinal locations, the maximum absolute strain value does not occur at the same time within the strain records of all sensors in a data file. As a result, the extrema matching process must compensate for the time difference in order to accurately identify corresponding extrema between two strain records.

Since it was previously shown that vehicular events occur in many patterns and magnitudes within strain records, the general matching procedure was developed by using influence lines. Presented in Fig. 5.49 are three influence lines that have been conceptually converted to strain records to illustrate the windowing procedure that is used for extrema matching. The strain records represent those of B-SG-BF-H, D-SG-BF-H, and F-SG-BF-H that have been classified as NTS, TS, and NTS, respectively, for this example. As illustrated, the maximum absolute strains in each record (i.e. E_{1B}, E_{2D}, and E_{3F}) occur at different times, or array indexes. In the matching subVI, the extrema information for one TS and one NTS are simultaneously considered. Using the extrema information determined by the subVI, *Determine Extrema.vi*, the TS window is first identified for E_{2D} by using $ESI_{TS,D}$ and $EEI_{TS,D}$; $EI_{TS,D}$ is also located within the window. This window is resized and projected to the general location in the NTS records where the corresponding extrema is expected to be located; projected along with the window projection is the expected exact location of the extrema match. Note that the TS window was projected to lower array indexes for NTS,B and to higher array indexes for NTS,F.

For the procedures illustrated in Fig. 5.49 and performed by *Match Extrema.vi*, the projections were accomplished as follows:

$$WSI_{NTS} = ESI_{TS} + ESIP \tag{5.2}$$

$$WEI_{NTS} = EEI_{TS} + EEIP \tag{5.3}$$

$$EI_{NTS} = EI_{TS} + EIP \tag{5.4}$$

www.manaraa.com

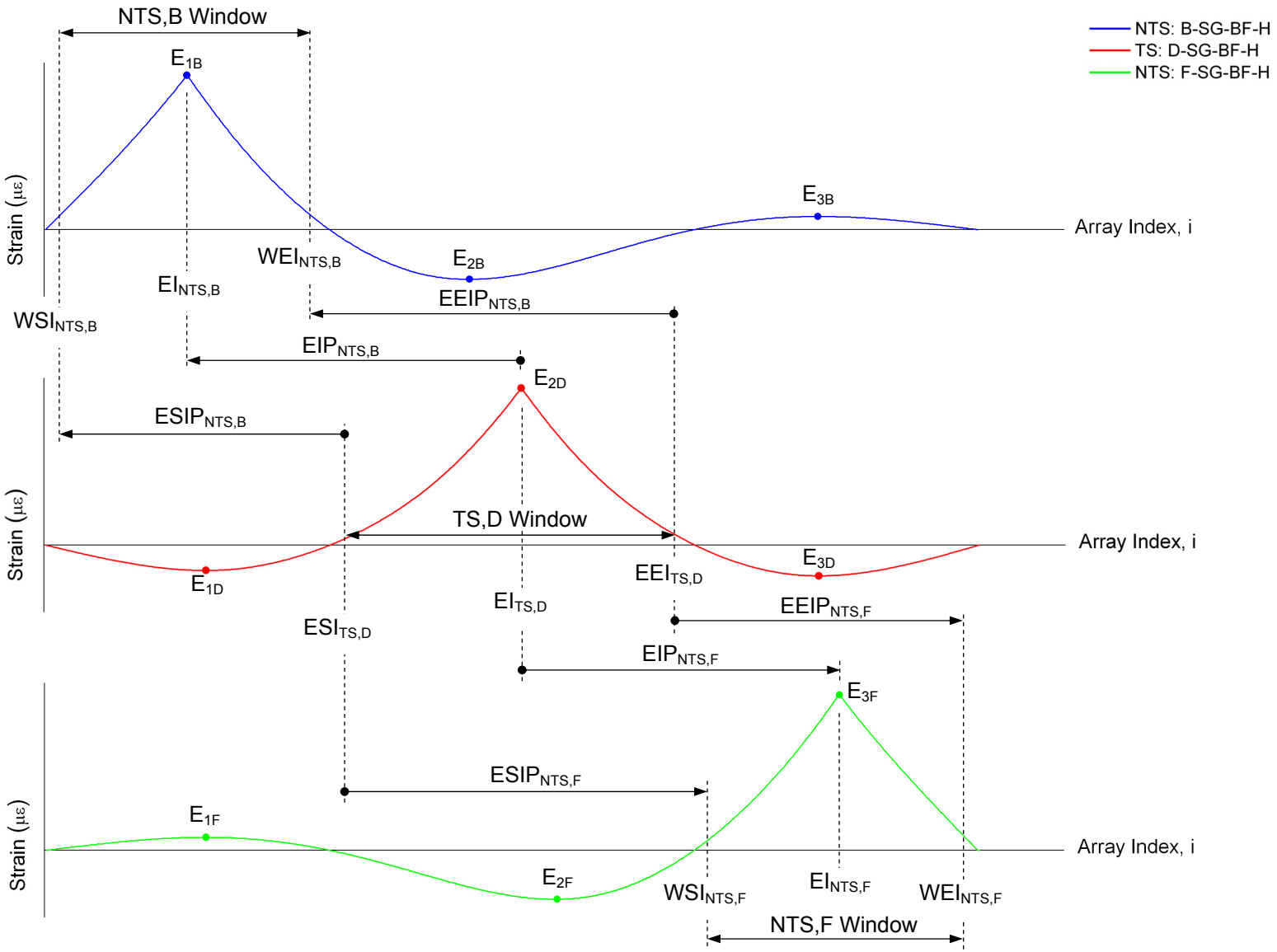

Figure 5.49. Fundamental approach to extrema matching process (*Match Extrema.vi*).

www.manaraa.com

where,

WSI_{NTS} = Projected start index of the NTS window
WEI_{NTS} = Projected end index of the NTS window
EI_{NTS} = Projected extreme value index within the NTS window
ESI_{TS} = Extreme value start index for the TS
EEI_{TS} = Extreme value end index for the TS
EI_{TS} = Extreme value index for the TS
ESIP = Extreme value start index projection shift (indexes)
EEIP = Extreme value end index projection shift (indexes)
EIP = Extreme value index projection shift (indexes)

The projection shifts are determined through use of the specified speed range, use of the relative distance between the TS and NTS, and utilization of the DAR. For determination of speed range values:

$$LS = S - SD \tag{5.5}$$

$$AS = S \tag{5.6}$$

$$HS = S + SD \tag{5.7}$$

where,

LS = Low speed for traffic traversing the bridge (ft/s)
AS = Average speed for traffic traversing the bridge (ft/s)
HS = High speed for traffic traversing the bridge (ft/s)
S = Converted speed specified in control #6 of Fig. 5.48 (ft/s)
SD = Converted speed deviation specified in control #7 of Fig. 5.48 (ft/s)

For determination of the relative locations of the TS and NTS:

$$D = L_{NTS} - L_{TS} \tag{5.8}$$

where,

D = Relative distance between the TS and NTS (ft)
L_{NTS} = Longitudinal location of the NTS (ft)
L_{TS} = Longitudinal location of the TS (ft)

Review of values in Table 5.2 illustrates that calculation of the relative distance between the TS and NTS, *D*, can be positive or negative, which ultimately controls the direction of the window projection. The window projection shifts are calculated as follows:

For all D:

$$EIP = \frac{D}{AS}[DAR] \tag{5.9}$$

www.manaraa.com

where,

DAR = Data acquisition rate (samples/s)

For D < 0 (projection to lower NTS array indexes),

$$ESIP = \frac{D}{LS}(DAR) \tag{5.10}$$

$$EEIP = \frac{D}{HS}(DAR) \tag{5.11}$$

For D $\geq$ 0 (projection to the same or higher NTS array indexes),

$$ESIP = \frac{D}{HS}(DAR) \tag{5.12}$$

$$EEIP = \frac{D}{LS}(DAR) \tag{5.13}$$

Note that the only difference among Eqns. 5.9 - 5.13 are the speeds that were used in the calculations. The calculation of EIP utilized AS to achieve an accurate estimate for the NTS extreme value index, while ESIP and EEIP were calculated to determine a conservative window width, and thus, switched LS and HS in the calculations.

If an extreme value is located within the projected NTS window, the TS and NTS extrema are matched to form a (x,y) pair for the corresponding relationship (i.e. MAMAR, MAMIR, MIMAR, or MIMIR). If multiple NTS extrema of the same type (i.e. maxima or minima) are within the NTS window, then the extrema value with the array index that is closest to EI_{NTS} is selected for the match. Note in Fig. 5.49 that the matching process was performed for only the TS extreme value that was determined to be the maximum absolute strain in the record. The subVIs performing the data operations, however, are only able to determine the extrema values and indexes in a strain record and do not have knowledge of vehicle position on the bridge. As illustrated in Fig. 5.50, the matching subVI performs the matching procedure for every identified TS extrema rather than for only the maximum absolute strain; if a NTS extreme value is windowed, it is automatically assumed to be a correct match. Because of this approach, three types of matches can be formed: direct matches, indirect matches, and mismatches (See Fig. 5.50). Direct matches are defined to be those that developed between TS and NTS maximum absolute strain values (as expected) and ultimately

www.manaraa.com

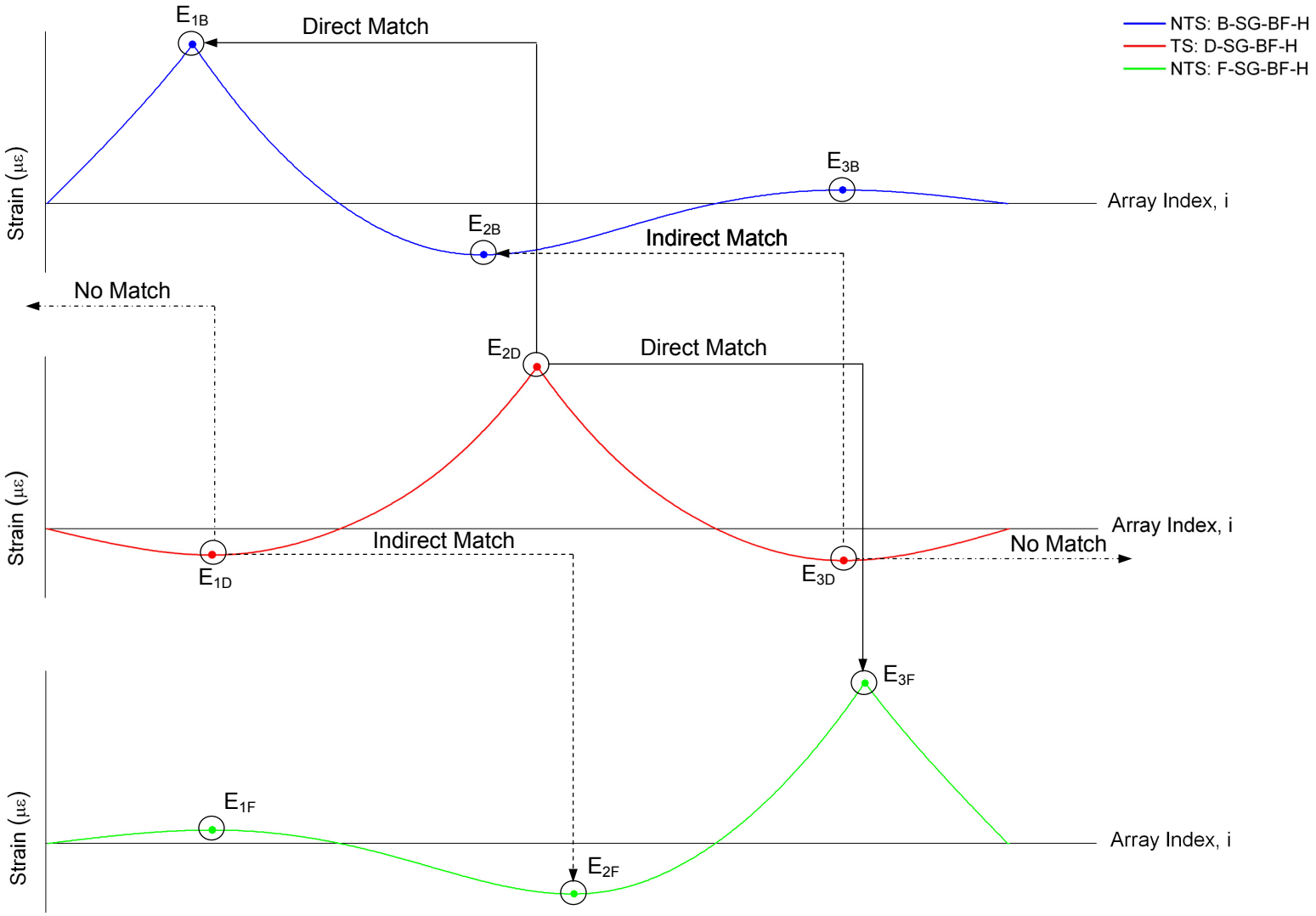

Figure 5.50. Illustration of direct matches and indirect extrema matches (mismatches not presented).

www.manaraa.com

formed a distinguishable relationship (i.e. E_{2D}-E_{1B} and E_{2D}-E_{3F}). Indirect matches are defined to be those that developed but not between TS and NTS maximum absolute strain values; because the indirect matches developed repeatedly and consistently, however, a distinguishable relationship is still formed (i.e. E_{3D}-E_{2B} and E_{1D}-E_{2F}). Because of the occurrence of indirect matches, it is possible for more than one useable relationship to form between a TS and NTS. Finally, mismatches are defined to be those that developed but not between TS and NTS maximum absolute strain values, and in addition, did not form a relationship.

It was demonstrated in Section 5.1 that the pattern and magnitudes of vehicular events are different due to variety in the geometries of the vehicles that traverse the bridge. However, use of the matching approach has been proven to be applicable to actual strain records obtained from the US30 bridge, which are significantly more complex than the strain records that were developed from influence lines in Fig. 5.49. The matching process for approximately 270 seconds of data for B-SG-BF-H and C-NG-CB(1)-V is illustrated in Fig. 5.51. Figure 5.51a presents the reduced, filtered data with extrema identified for the TS and NTS. To help illustrate the matching that occurred, four (of the 46 existing) matched extrema pairs have been identified. In Fig. 5.51b, a close up is displayed for one event from Fig. 5.51a, and the TS and NTS windows used in the matching process are included. For the TS minima that has been windowed, two extrema are encompassed within the corresponding NTS window and form Match B and Match C, which are direct and indirect matches, respectively. The matching results for all extrema in Fig. 5.51a are presented in Figs. 5.51c-f in the form of TS extrema versus NTS extrema. Successful matching for the MIMAR and MIMIR, but not the MAMAR or MAMIR, reinforces that the matching patterns that are illustrated in Fig. 5.51b are repeatable and consistent. Detailed example calculations for the matching process are provided in Appendix F for the event extrema that were considered in Fig. 5.51b.

Having discussed the operations performed by Match Extrema.vi, the following inputs that are required by the subVI are as follows:

- **Sensor Classifications:** Values (1 or 0) representing the classification of each sensor (1-D array developed by the VI, *4 - Select Target Sensors.vi*).
- **Speed (mph):** Expected average speed for a representative sample of traffic (scalar).

www.manaraa.com

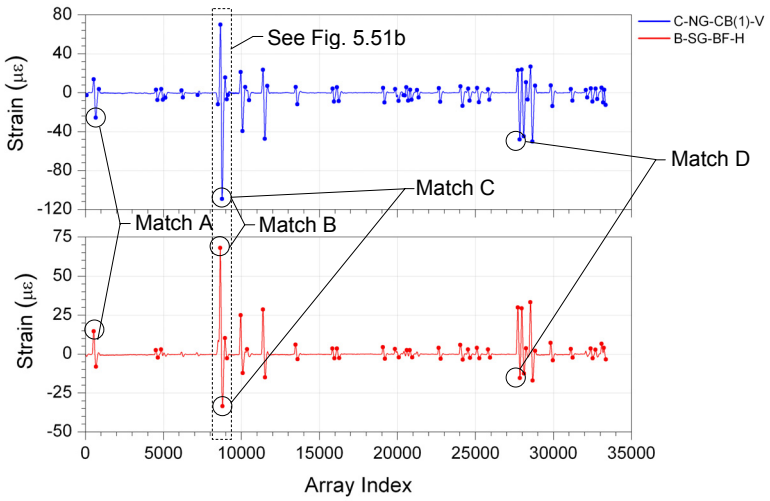

a. Filtered strain records and identified extrema for C-NG-CB(1)-V and B-SG-BF-H

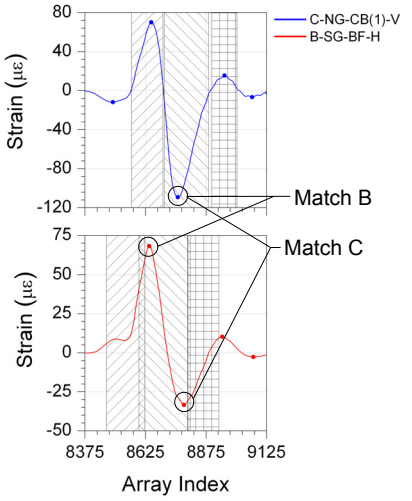

b. Close up view of Fig. 5.51a and the windows used in extrema matching

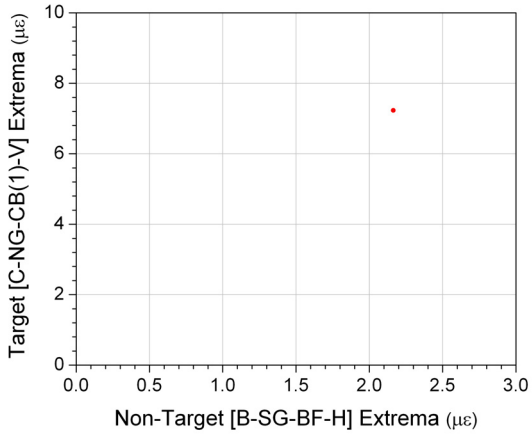

c. MAMAR matched extrema (mismatch)

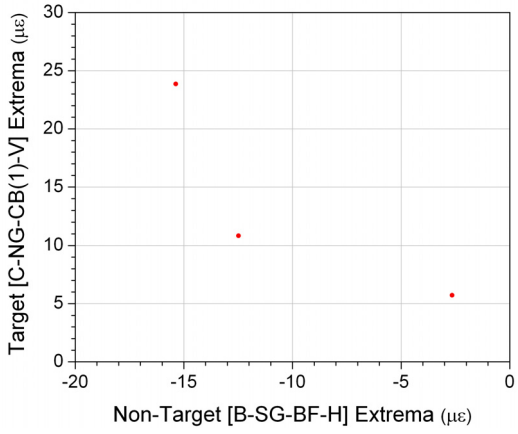

d. MAMIR matched extrema (mismatch)

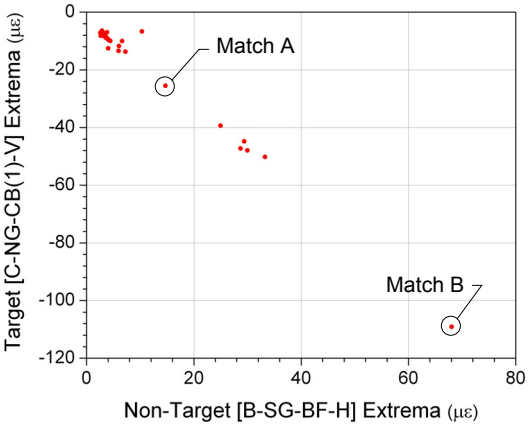

e. MIMAR matched extrema (direct match)

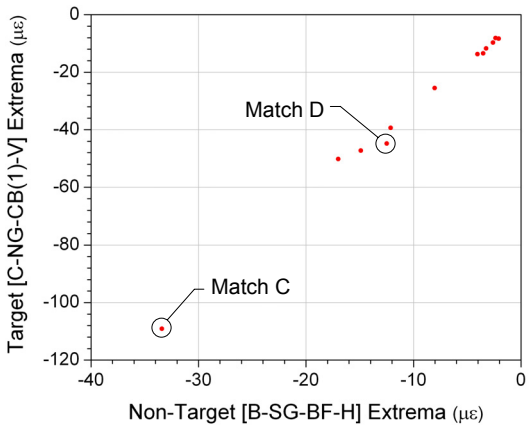

f. MIMIR matched extrema (indirect match)

Figure 5.51. Example of extrema matching for 270 seconds of data from the US30 SHM System.

www.manaraa.com

- **Speed Deviation (± mph):** Deviation (mph) to be used with the expected average speed to define the expected speed range for a representative sample of traffic (scalar).

- **Target-Extrema Values:** Either *Maxima Values* or *Minima Values*, which are direct outputs from the subVI, *Determine Extrema.vi* (2-D array). Selection is based on the desired relationship formed in the matching process.

- **Target-Extrema Start Indexes:** Either *Maxima-Extrema Start Indexes* or *Minima-Extrema Start Indexes*, which are direct outputs from the subVI, *Determine Extrema.vi* (2-D array). Selection is based on the desired relationship formed in the matching process.

- **Target-Extrema Indexes:** Either *Maxima-Extrema Indexes* or *Minima-Extrema Indexes*, which are direct outputs from the subVI, *Determine Extrema.vi* (2-D array). Selection is based on the desired relationship formed in the matching process.

- **Target-Extrema End Indexes:** Either *Maxima-Extrema End Indexes* or *Minima-Extrema End Indexes*, which are direct outputs from the subVI, *Determine Extrema.vi* (2-D array). Selection is based on the desired relationship formed in the matching process.

- **Non-Target-Extrema Values:** Either *Maxima Values* or *Minima Values*, which are direct outputs from the subVI, *Determine Extrema.vi* (2-D array). Selection is based on the desired relationship formed in the matching process.

- **Non-Target-Extrema Indexes:** Either *Maxima-Extrema Indexes* or *Minima-Extrema Indexes*, which are direct outputs from the subVI, *Determine Extrema.vi* (2-D array). Selection is based on the desired relationship formed in the matching process.

- **Data Acquisition Rate (Hz):** The DAR of the data collection (scalar).

- **Sensor Longitudinal Locations:** Longitudinal locations for all sensors (1-D array developed by the VI, *3 - Input Sensor Locations.vi*).

Outputs from the subVI, *Match Extrema.vi*, are as follows:

- **Matched Target Extrema:** The TS extrema values that have been matched (3-D array with one TS per page, one NTS per row, and on extreme value per column).

- **Matched Non-Target Extrema:** The NTS extrema values that have been matched (3-D array with one TS per page, one NTS per row, and on extreme value per column).

Note that the inputs control the relationship that is formed by the operations of the matching subVI. Therefore, *Match Extrema.vi*, is called four times by the VI, *5 - Develop SHM Training Files.vi*, to attempt for form all four relationships for every TS-NTS combination. After the matching subVI has exported the two 3-D arrays of matched extrema for each relationship, the two arrays are combined into one 4-D array, where the volume (fourth dimension) index applies to the classification of the extrema, either TS extrema (volume = 0) or NTS extrema (volume = 1). Each 4-D array is then flattened into a string and saved as a binary file in a folder that has been created for the data file

www.manaraa.com

being considered. As a result, for each data file contained in the source directory of control #1 of Fig. 5.48, a folder is generated in the save directory (control #2) with four binary files (one per relationship). The names of the new folder and files maintain the original file name along with additional information to identify each folder and its contents. Illustrated in Fig. 5.52a are the new folders that were created for the files in the source directory (See Fig. 5.39). Examples of the four binary files contained within one folder are presented in Fig. 5.52b.

As depicted in Fig. 5.37, after the training files have been created for every raw data file being used in the training process, the individual training files for each relationship type must be assembled into a common directory structure that organizes the training data by TS-NTS combinations and relationship types. This process is accomplished by the program, *6 - Assemble SHM Training Files.vi*. The front panel for this VI is presented in Fig. 5.53, and brief descriptions of the labeled controls and indicators are as follows:

1. **Training Files Source Directory Control:** Directory containing the folders with training files (directory to which results were written by the VI, *5 - Develop SHM Training Files.vi*).
2. **Assembled Training Files Save Directory Control:** Directory to which assembled training data is written.
3. **Non-Target Sensor Labels Control:** NTS labels that are listed in the order that they appear in the sensor array.
4. **Target Sensor Labels Control:** TS labels that are listed in the order that they appear in the sensor array.
5. **Creating Directory Indicator:** Indicates green when the assembled training data directory is being created in the source directory (control #1).
6. **Progress Indicator:** Progress of the training file generation process.

The resulting directories and assembled data files created by this VI are illustrated in Fig. 5.54. Within the primary saved directory (control #2 in Fig. 5.53), the assembled relationship files for each TS-NTS combination are achieved by opening the desired TS and NTS directories. Note that the file sizes in Fig. 5.54c are considerably different, which indicates that some relationships have many more matched extrema than others. As a result, the relationship file sizes may be useful indicators pertaining to the relative strength and reliability of the relationships.

www.manaraa.com

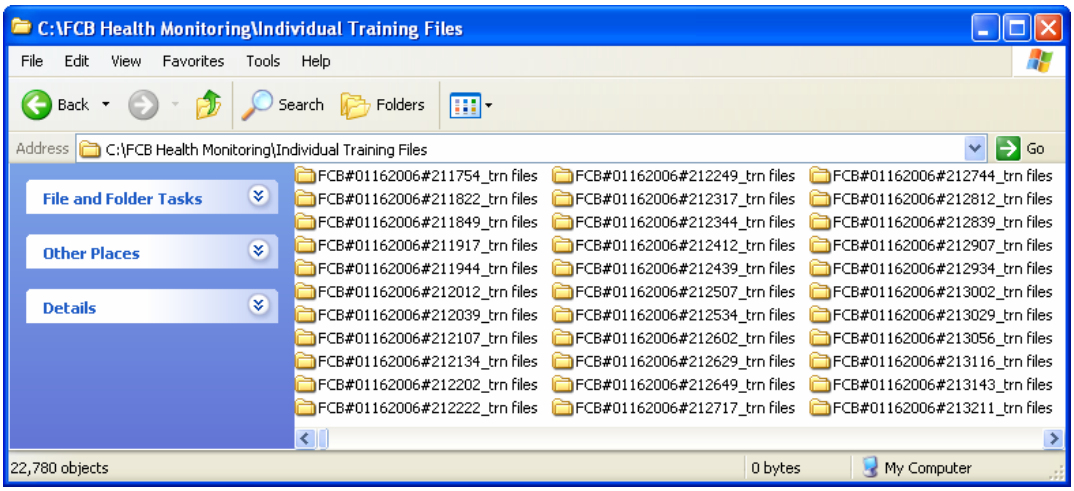

a. Directories containing training files (See source directory in Fig. 5.39)

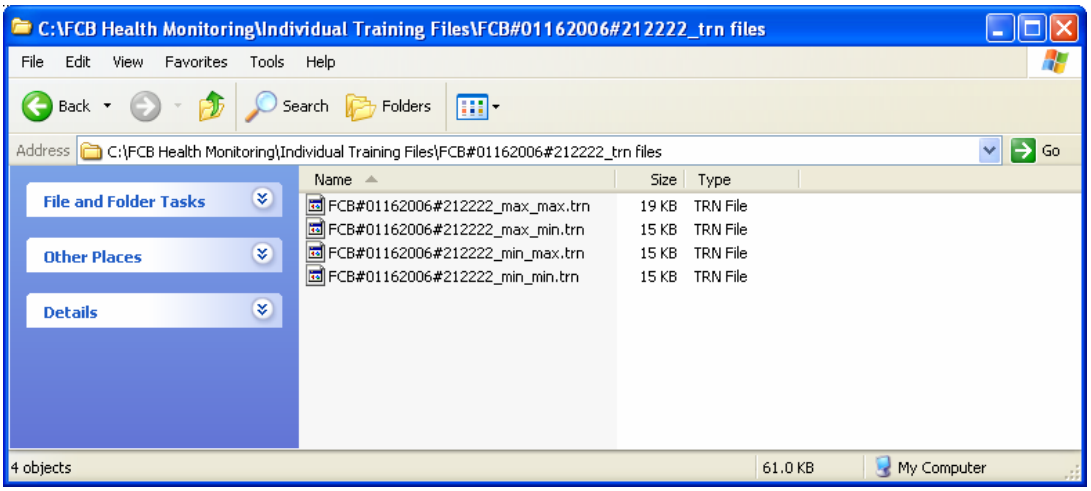

b. Four training files within a directory

Figure 5.52. Examples of directories and training files that were generated during training (*5 - Develop SHM Training Files.vi*).

After all training data has been created and assembled, the program, *7 - View Results - Assembled SHM Training Files.vi*, was developed to load the data and determine if the matching procedures were successful. In addition, the program can be used to compare multiple sets of training data in order to determine the amount that is sufficient for training the SHM system. The front panel for this VI is presented in Fig. 5.55, and brief descriptions of the labeled controls and indicators are as follows:

www.manaraa.com

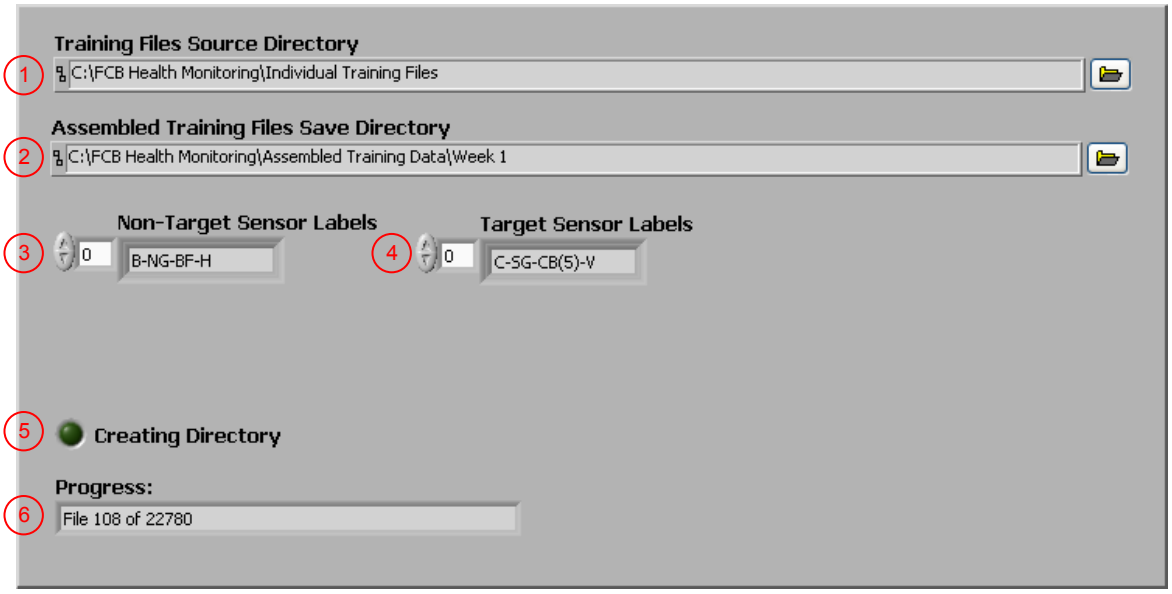

Figure 5.53. Front panel controls and indicators for assembling the training files (*6 - Assemble SHM Training Files.vi*).

1. **Assembled Training Files Source Directory(s) Path Control:** Top level directory containing the assembled training files (directory to which results were written by the VI, *6 - Assemble SHM Training Files.vi*). More than one directory may be specified for comparison of multiple sets of assembled training data.

2. **Non-Target Sensor Labels Control:** NTS labels that are listed in the order that they appear in the sensor array.

3. **Target Sensor Labels Control:** TS labels that are listed in the order that they appear in the sensor array.

4. **Target Sensor Selection Control:** Selected TS for the plotted relationship.

5. **Non-Target Sensor Selection Control:** Selected NTS for the plotted relationship.

6. **Assembled Training Files Available for Display Control:** Listbox of relationship files that are available for display for the selected sensors.

7. **Clear Graph Control:** If depressed, the graph is cleared prior to selection of a new file from control #6. Otherwise, a new file selection is overlaid on the existing plot.

8. **Matched Extrema Indicator:** Scatter plot of the training data (matched extrema) for the selected sensor combination and relationship(s).

When the program is activated, controls #1 - 5 are used to assemble the correct directory path which contains the four training files for the active TS-NTS combination. This action is performed for each source directory listed in control #1. All training files within these directories are

www.manaraa.com

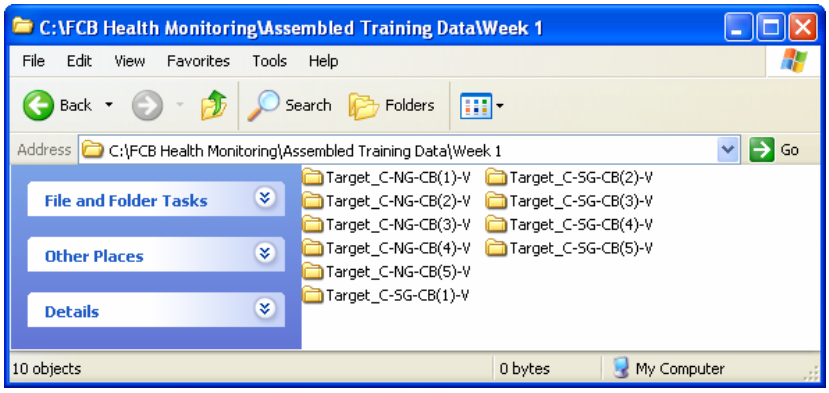

a. TS directories

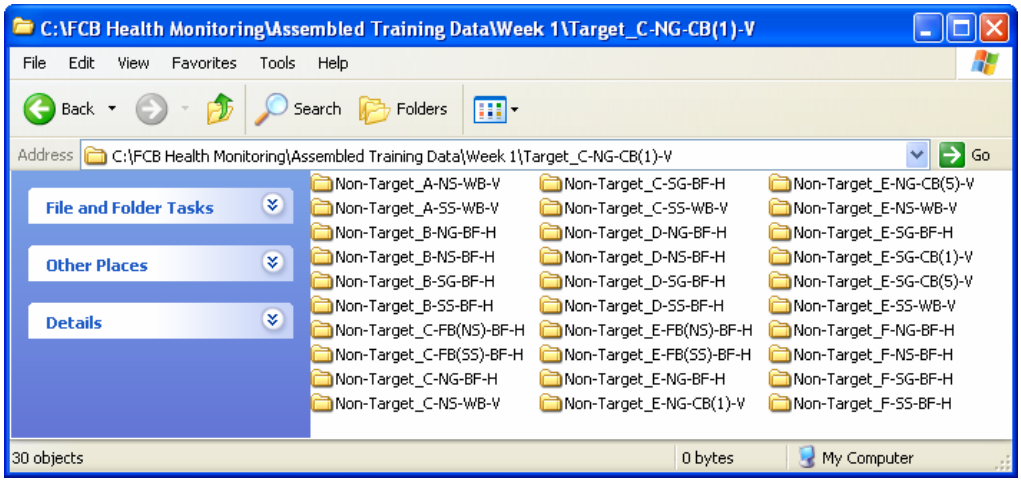

b. NTS directories within a TS directory

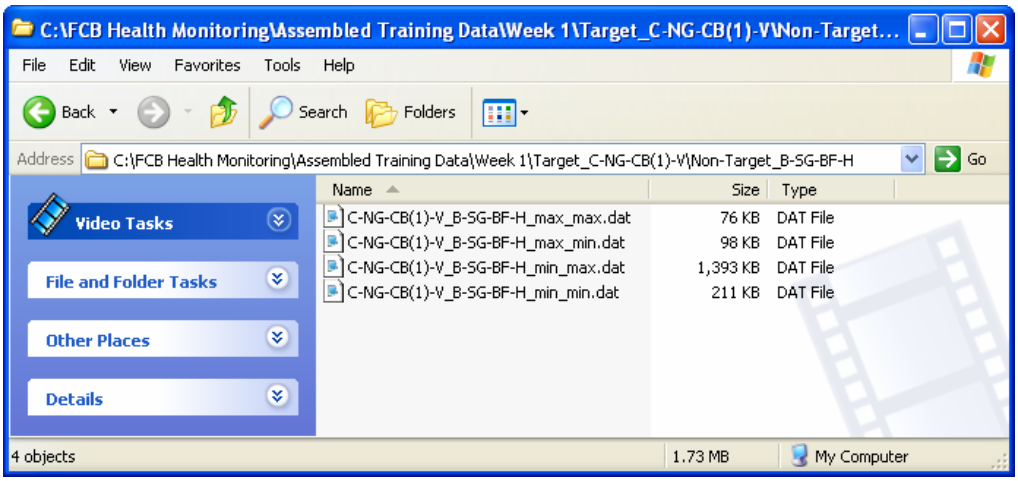

c. Four relationship files within a TS-NTS directory

Figure 5.54. Example displays of the assembled directory structure and resulting training data (*6 - Assemble SHM Training Files.vi*).

www.manaraa.com

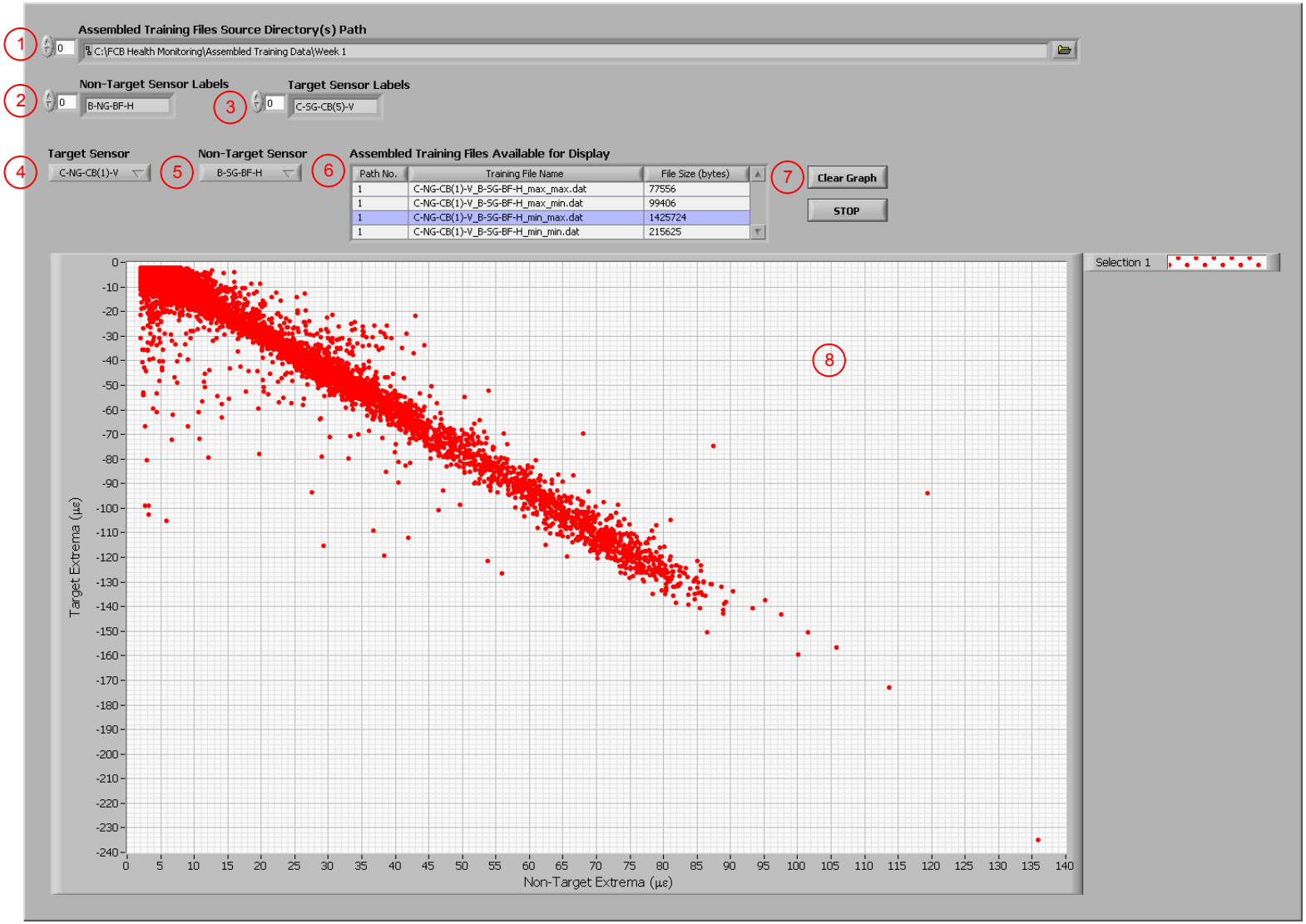

Figure 5.55. Front panel controls and indicators for reviewing assembled training data from one directory (*7 - View Results - Assembled SHM Training Files.vi*).

www.manaraa.com

collected and displayed for selection in control #6 along with the file size. As previously mentioned, the largest data file within the group of four for the selected TS-NTS combination is usually the most reliable relationship that formed during training data generation. When a file is selected, the matched extrema within are displayed on the graph (indicator #8) in the form of TS extrema versus NTS extrema. As more training files are selected, they are added to the displayed data set in a unique color. To clear the graph prior to file selection, control #7 must be depressed.

Figure 5.56 illustrates the use of the program to determine the amount of training data that was required to sufficiently train the SHM system. To perform this comparison, the individual training files corresponding to day one, day two, day three, and day four (from the original week of individual training files) were separately assembled into training data. Each top level directory of the assembled data sets was included in the source directory control (#1) of the program, and for the displayed sensor, the assembled training data for each time segment was displayed as illustrated in Fig. 5.56. By comparing the four individual days of training data with that of one week, it is evident that no new characteristics of the relationship were introduced by the weekly data. As a result, it is expected that four days of data would have been sufficient to train the SHM system. To be conservative, however, an entire week of training data was utilized to train the system.

Figures 5.57a-f present selected relationships that developed between TSs and NTSs during the training process of the US30 SHM system. Review of these figures reveals the following observations and conclusions:

- Each plot includes clusters of data points that shape the existing relationship, and in addition, outliers that do not closely agree with the cluster.
- In some figures, such as Figs. 5.57a and 5.57d-f, two clusters of data points are evident, whereas one cluster is evident in other figures. The number of clusters in a plot has been determined to depend on the sensitivity of the strains in the sensors to the transverse position of the vehicle traversing the bridge.
- The compactness of the clusters differs among the plots. Factors causing compactness variability have been primarily related to the sensitivity of the strains in the sensors to traffic variability such as the transverse positions of the vehicles as well as the patterns and combinations of the vehicles as they traverse the bridge.
- The presence and occurrence of outliers differs among the plots. Outliers have been proven to be either the result of uncommon traffic events or mismatches that occur during the extrema matching process.

www.manaraa.com

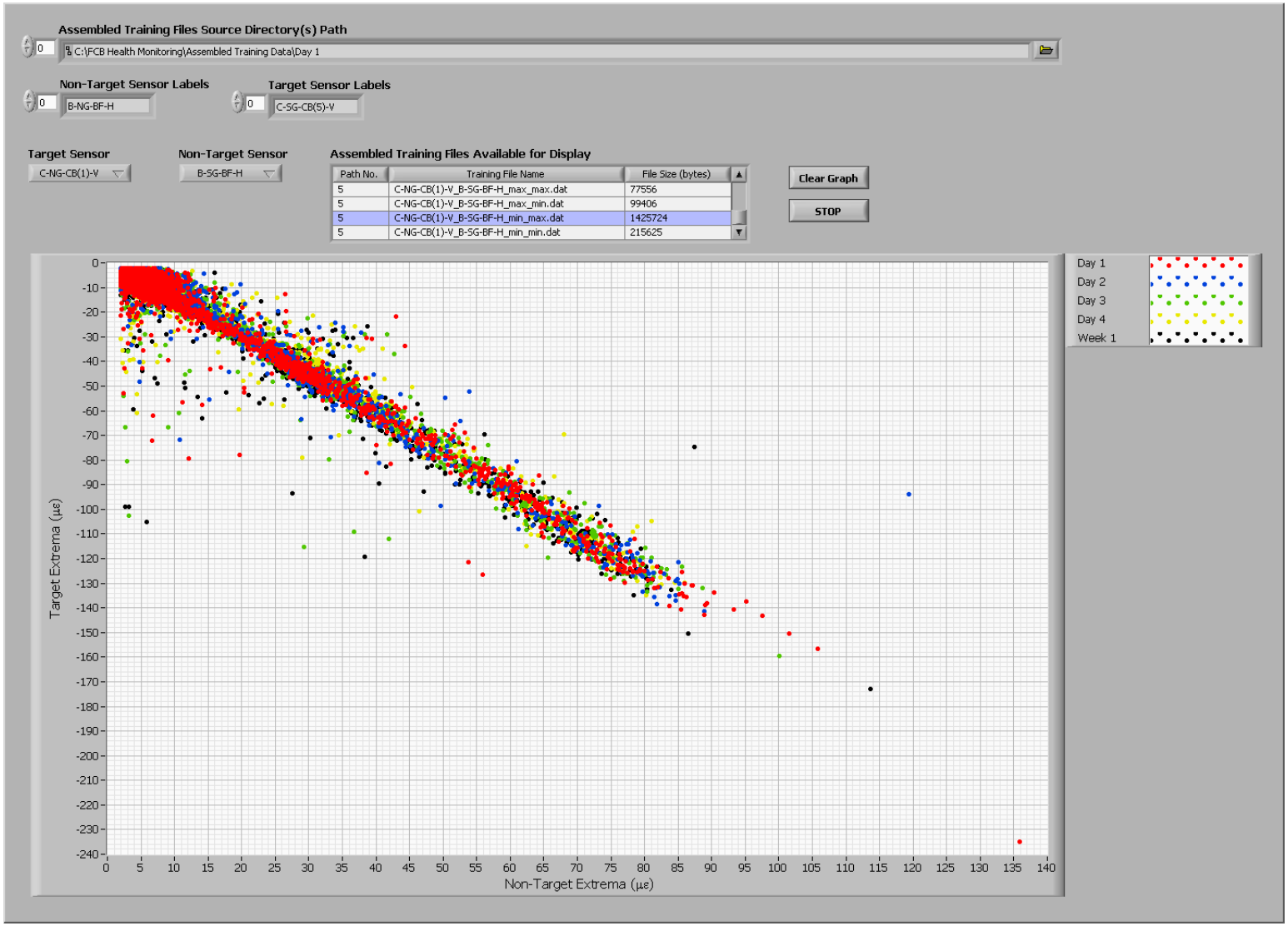

Figure 5.56. Comparison of training data for various time periods (*7 - View Results - Assembled SHM Training Files.vi*).

www.manaraa.com

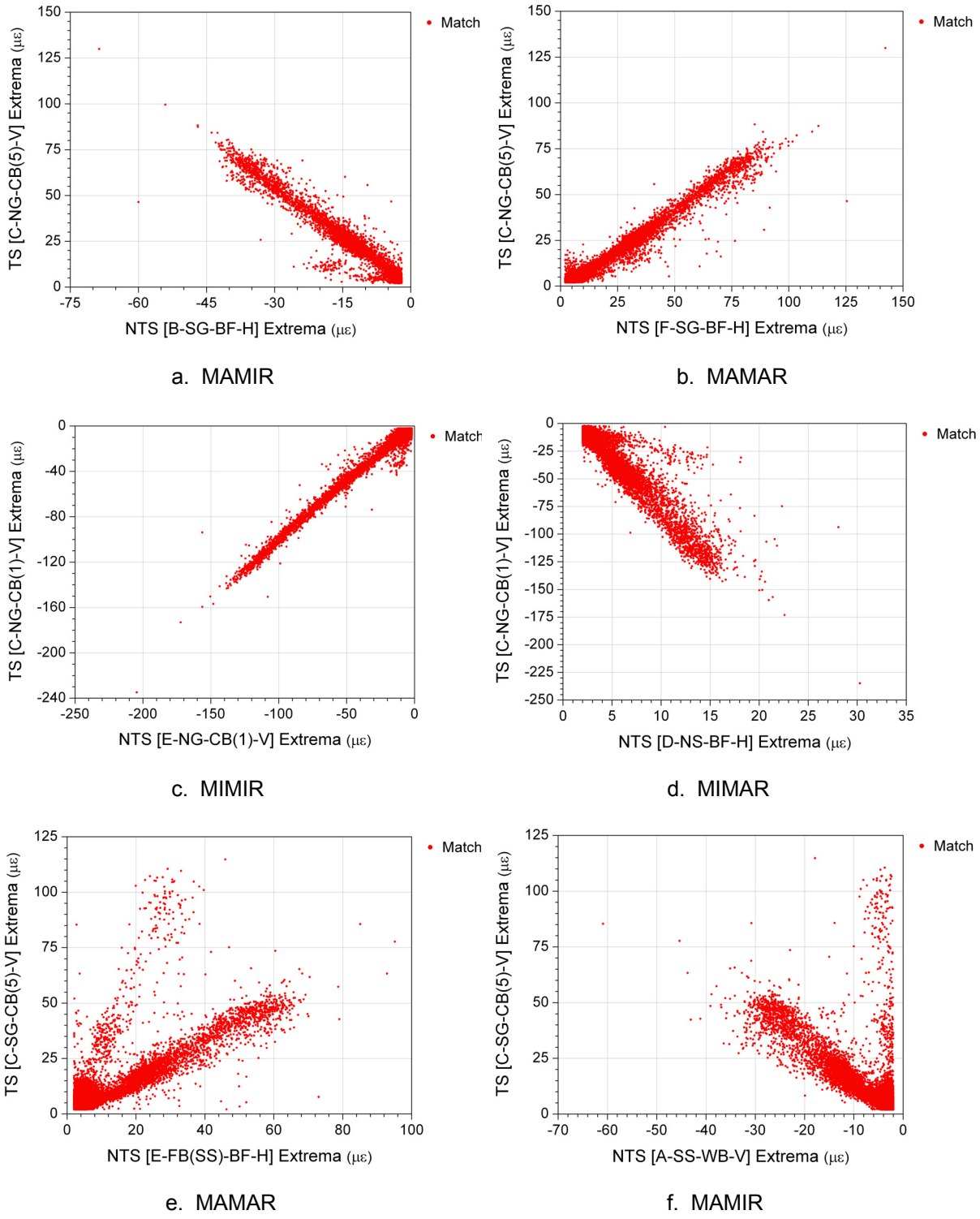

Figure 5.57. Selected relationships that formed during training from one week of US30 bridge data.

www.manaraa.com

The filter configurations for sensors in the SHM system were determined to be factors that significantly affect the development of relationships among the sensors in the SHM system. As discussed in Section 5.2.3 and demonstrated in Fig. 5.45, investigation was required in order to determine suitable cut-off frequencies for filtering the strain records from sensors installed on the stringers. As part of this investigation, the training process was completed for two different filter configurations: one configuration included cut-off frequencies for stringer and floor beam sensors in the range of 2.0 - 2.5 Hz, and the cut-off frequencies for sensors on stringers and floor beams in the other configuration were in the range of 0.275 - 0.65 Hz. The cut-off frequencies for girder sensors remained the same in both configurations.

In general, when comparing results from the high cut-off frequencies with those of the low cut-off frequencies within each relationship, the clusters were nearly always more disperse in the results from the high cut-off frequencies. Two drastic examples of this change are illustrated in Figs. 5.58a-b. With the high cut-off frequency settings, the free vibration response of the bridge was not removed from the strain record. As a result, many extrema were identified in the strain records that did not correspond to quasi-static vehicular events. Consequently, successful extrema matching significantly decreased, and the relationship plot was dominated by mismatched events. In some cases, relationships that formed with the low cut-off frequency configuration hardly developed or did not develop with the high frequency configuration, and an example of this case is presented in Fig. 5.58c. Three possible causes of this situation were identified: (1) The presence of high frequencies in the strain record decreased the success rate of identifying event extrema, (2) the change in event patterns with the high cut-off frequencies resulted in identified extrema that were not within the NTS window used in the matching procedure, and (3) higher occurrence of mismatched events as previously discussed. Because of the obviously problems associated with high cut-off frequencies for the stringer and floor beam sensors, it was determined to use the lower cut-off frequencies in the training and monitoring phases of the system.

5.2.6 Establishment of Limit Sets

As illustrated in Fig. 5.37, after training data has been generated and relationships have

www.manaraa.com

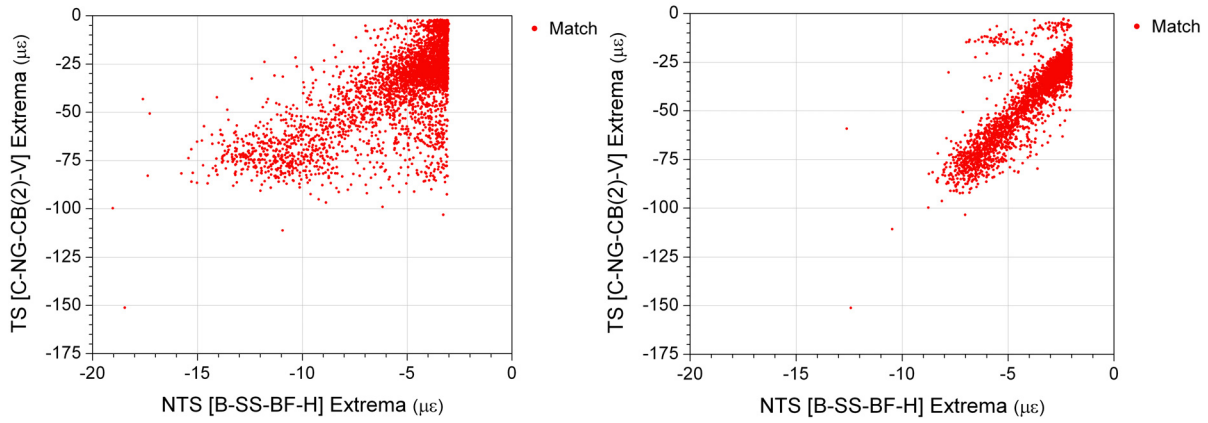

a. B-SS-BF-H: filter cut-off frequencies 2.5 Hz (left) and 0.35 Hz (right)

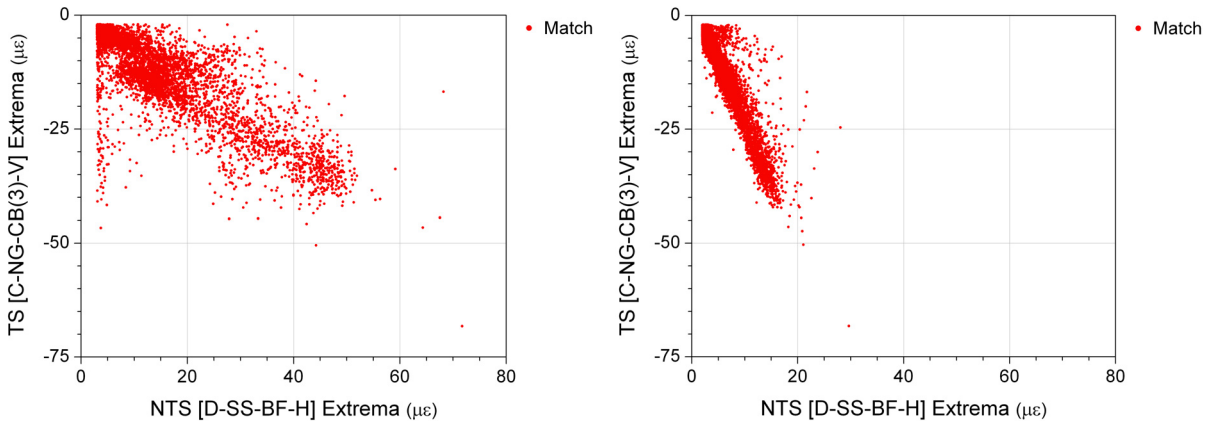

b. D-SS-BF-H: filter cut-off frequencies 2.5 Hz (left) and 0.40 Hz (right)

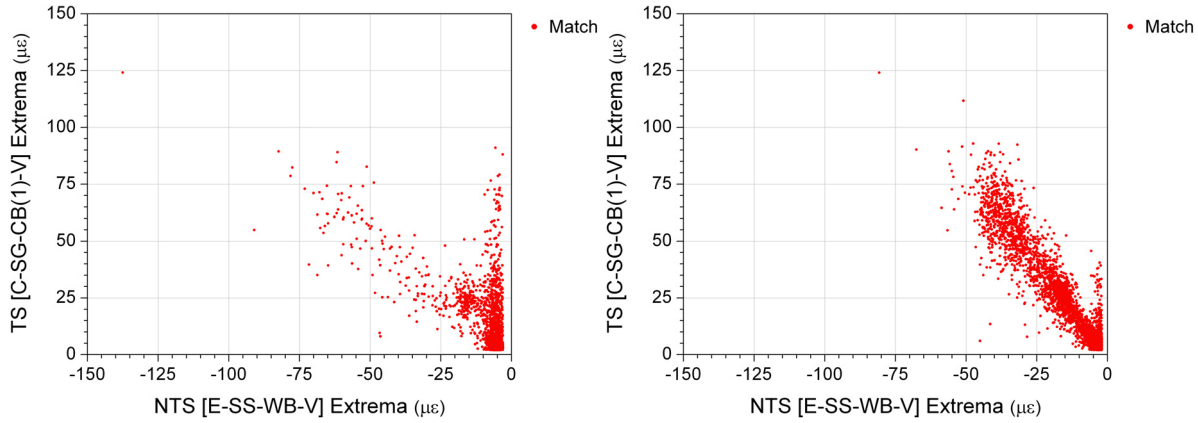

c. E-SS-WB-V: filter cut-off frequencies 2.0 Hz (left) and 0.325 Hz (right)

Figure 5.58. Comparison of changes in training relationships by altering the NTS cut-off frequency.

www.manaraa.com

visually been identified, each relationship must be defined by limit sets. Limit sets are similar to the elliptical control regions of the bivariate control charts discussed in Section 2.3.4 (See Fig. 2.3), and just as the control regions identify when a process is in control, the limits sets simply define typical bridge behavior based on the condition of the bridge when training data was collected. Two programs were developed to assist the user in the process of defining relationships:

- *8 - Define Limits.vi*
- *9 - View Results - Defined Limits.vi*

The first program is used to define the limits, and the second program is used to review the limit sets after they have been defined.

Through use of the VI, *8 - Define Limits.vi*, training data for a selected relationship is displayed and the user outlines the cluster(s) of data points with upper and lower limits that define typical behavior. A manual approach was used in this system for the following reasons:

- A manual approach involves the user much more than an autonomous mathematical approach. As a result, the user has more knowledge of how the system operates, and as a result, may develop a higher comfort level with the use of the system.
- As illustrated in Fig. 5.57, some relationships have two clusters, and thus, require two limit sets to define the relationship. Recognizing the need for and performing operations to establish two limits sets would be difficult to autonomously perform mathematically.
- Four sets of training data have been developed, but not all sets are useful for bridge analysis. Identification of useful and useless data sets would be hard to define mathematically.

The front panel display with labeled controls and indicators for this VI is presented in Fig. 5.59, and brief descriptions of the labeled controls and indicators are as follows:

1. **Assembled Training Files Source Directory Path Control:** Top level directory containing the assembled training files (directory to which results were written by the VI, *6 - Assemble SHM Training Files.vi*).
2. **Limit Files Save Directory Path Control:** Top level directory to which limit sets are written.
3. **Non-Target Sensor Labels Control:** NTS labels that are listed in the order that they appear in the sensor array.
4. **Target Sensor Labels Control:** TS labels that are listed in the order that they appear in the sensor array.
5. **Create New Directory? Control:** If true (depressed), a directory structure is created in the top level directory (control #2) for organizing the limit sets by TS-NTS combinations. If false, the program resumes with a previously created directory structure.

www.manaraa.com

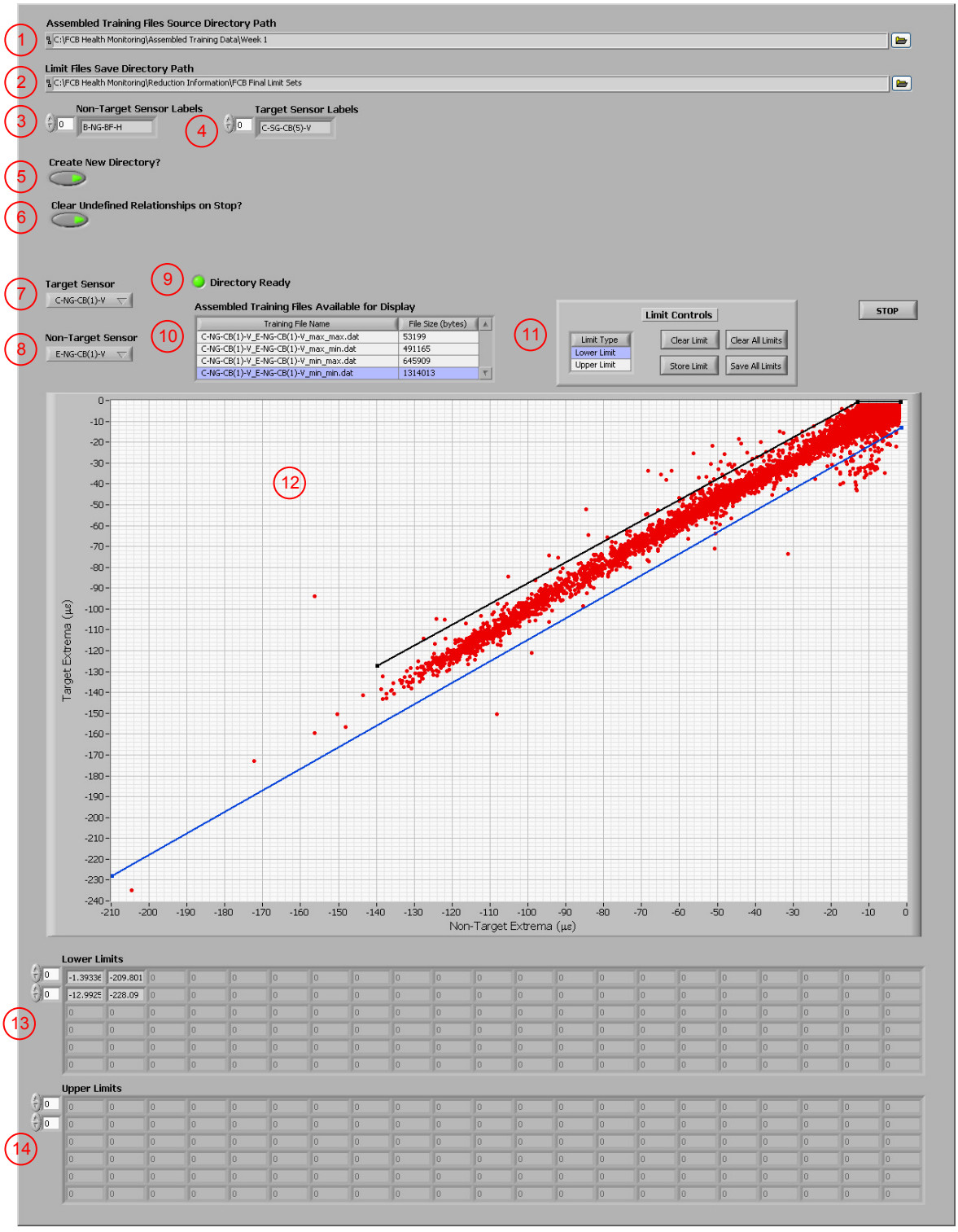

Figure 5.59. Front panel controls and indicators for establishing limit sets to define relationships (*8 - Define Limits.vi*).

www.manaraa.com

6. **Clear Undefined Relationships on Stop? Control:** If true (depressed), all undefined limit files are deleted when the program is stopped. If false, the limit files remain in order to be established in the future.

7. **Target Sensor Selection Control:** Active TS for the plotted training data and limits sets being defined.

8. **Non-Target Sensor Selection Control:** Active NTS for the plotted training data and limits sets being defined.

9. **Directory Ready Indicator:** When true (green), the directory structure is ready and the program is ready to begin defining limits.

10. **Assembled Training Files Available for Display Control:** Listbox of files available for display based on the active TS-NTS combination.

11. **Limit Set Controls:** Controls for creating and saving defined limits. **Limit Type** (upper or lower) registers the limit in the correct array, **Clear Limit** erases the limit currently being defined, **Store Limit** registers the limit in temporary memory, **Clear All Limits** erases all limits in the temporary memory, and **Save All Limits** writes all limit sets in the temporary memory to the proper file in the save directory (control #2).

12. **Training Data Indicator and Limit Sets Control:** Graph that displays training data while the user outlines the desired relationship with the mouse.

13. **Lower Limits Indicator:** Lists the data points that define a lower limit that has been stored in temporary memory.

14. **Upper Limits Indicator:** Lists the data points that define an upper limit that has been stored in temporary memory.

When the program is executed and control #5 is set to true, a new directory structure is created within the primary save directory specified in control #2 in order to organize the storage of defined limit sets by TS-NTS combinations. When indicator #9 displays true, creation of the directory structure is complete, and the program is ready for the user to select a desired TS and NTS. The assembled training data files for the selected sensor combination are displayed in the listbox control (#10), and when one is selected as displayed in Fig. 5.59, the training data are displayed on the graph (indicator #12).

Each limit within a set is defined by data points with linear interpolation between two adjacent points. One limit at a time, the user must use the mouse to click on the graph at the desire locations of data points, and a line is automatically drawn between the previous point and the current point. When all points for a limit have been established, the user must select the appropriate type of limit and store the limit in temporary memory. After all desired limits for one TS-NTS relationship have

www.manaraa.com

been defined and stored in temporary memory, the save button must be activated to write the limit sets to an automatically created file path within the directory structure that was previously discussed.

As illustrated in Fig. 5.59, relationships are displayed in black while they are being defined. When a limit is stored in the temporary memory, however, it is converted to blue color, and the data points defining the limit are added to indicators #13 or #14. If the user wishes to end the program before all relationships have been defined, control #6 must be set to false before the program is terminated. Upon re-entry, control #5 must be set to false to prevent the previously saved limits from being overwritten. After all relationships have been defined by limit sets and the user is ready to terminate the program, control #6 must be set to true; when the stop button is depressed, the VI clears all empty limit set files from the save directory. The resulting directories and limit set files that are created by this VI are illustrated in Fig. 5.60.

The program, *9 - View Results - Defined Limits.vi*, was developed to review limit sets after they have been saved. The front panel display with labeled controls and indicators for this VI is presented in Fig. 5.61, and brief descriptions of the labeled controls and indicators are as follows:

1. **Assembled Training Files Source Directory Path Control:** Top level directory containing the assembled training files (directory to which results were written by the VI, *6 - Assemble SHM Training Files.vi*).
2. **Limit Files Source Directory Path Control:** Top level directory containing defined limit sets (directory to which results were written by the VI, *8 - Define Limits.vi*).
3. **Non-Target Sensor Labels Control:** NTS labels that are listed in the order that they appear in the sensor array.
4. **Target Sensor Labels Control:** TS labels that are listed in the order that they appear in the sensor array.
5. **Target Sensor Selection Control:** Active TS for the plotted training data and limits sets.
6. **Non-Target Sensor Selection Control:** Active NTS for the plotted training data and limits sets.
7. **Limit Sets Available for Display Control:** Listbox of limit set files that are available for display based on the active TS-NTS combination.
8. **Training Data and Limit Sets Indicator:** Graph that displays training data and defined limit sets for the active TS-NTS combination and specified relationship from control #7.
9. **Lower Limits Indicator:** Lists the data points that define the displayed lower limit(s).

www.manaraa.com

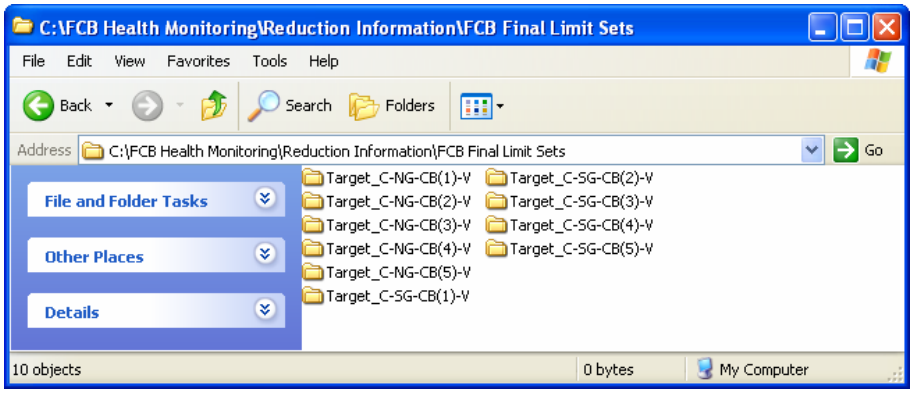

a. TS directories

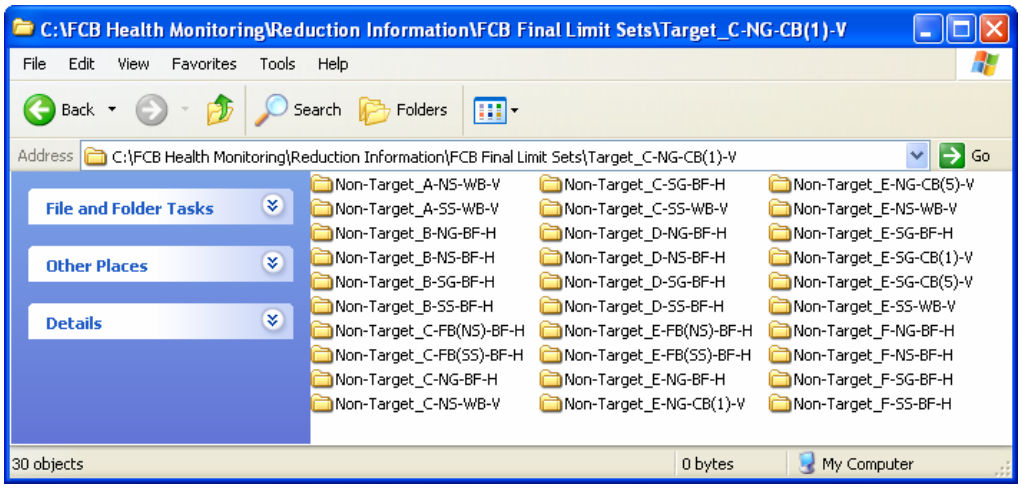

b. NTS directories within a TS directory

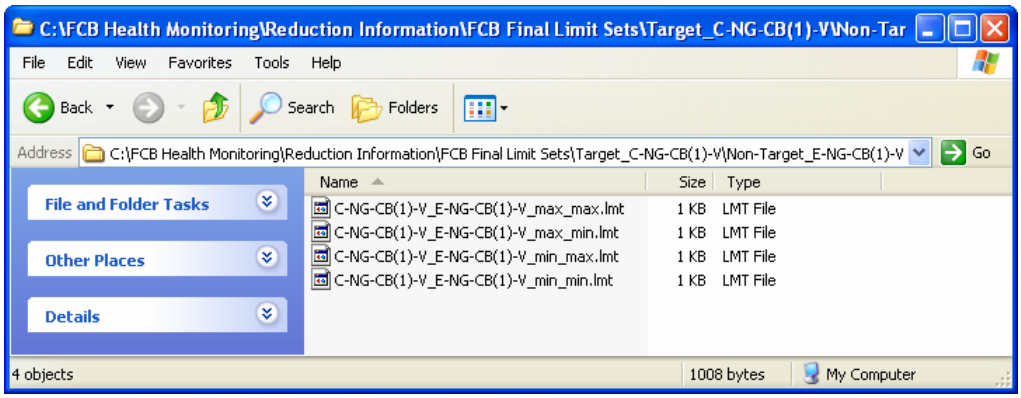

c. Four limit set files within a TS/NTS directory

Figure 5.60. Example displays of the limit set directory structure and defined limit set files (*8 – Define Limits.vi*).

www.manaraa.com

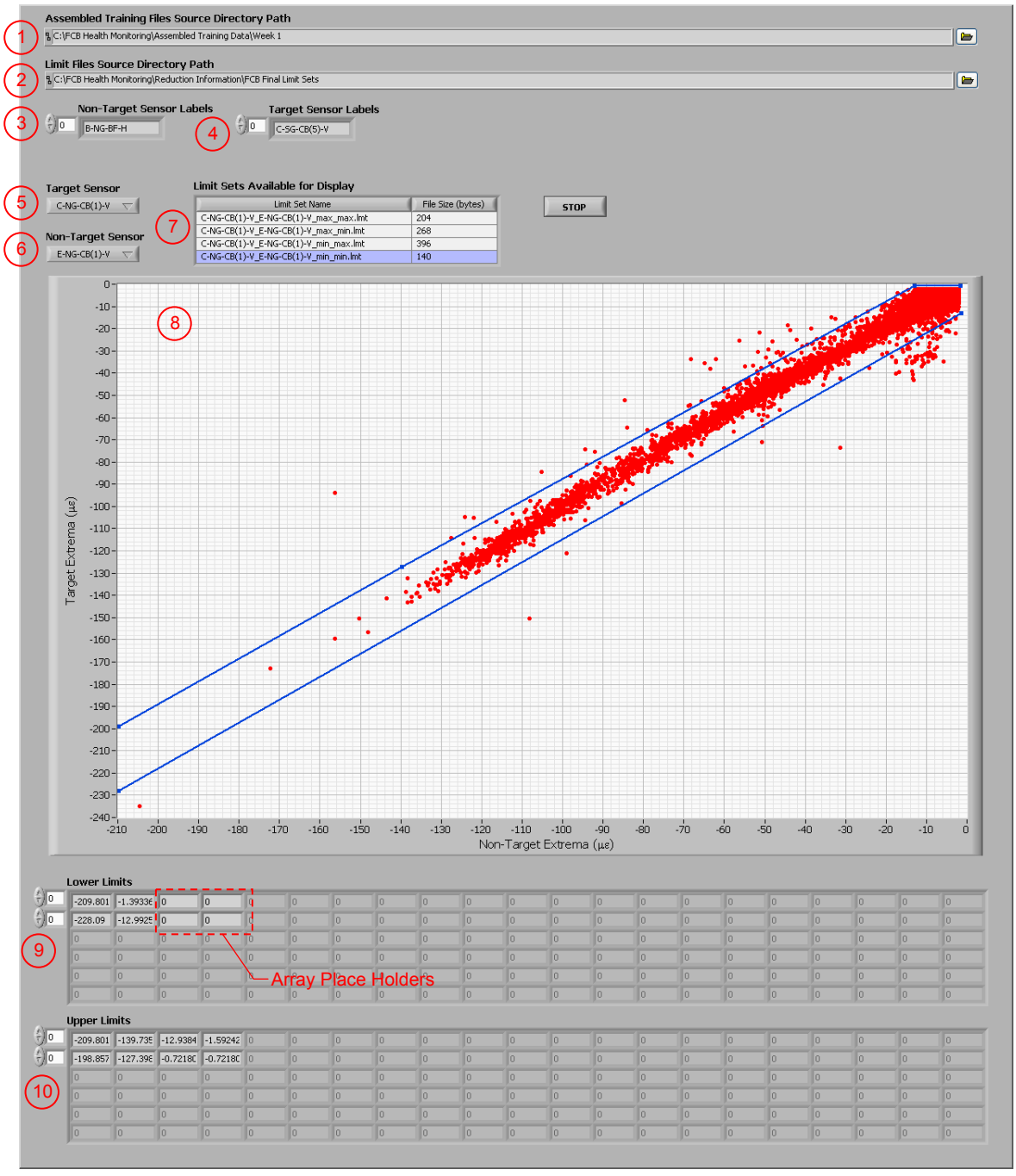

Figure 5.61. Front panel controls and indicators for establishing limit sets to define relationships (*9 - View Results - Defined Limits.vi*).

www.manaraa.com

10. **Upper Limits Indicator:** Lists the data points that define the displayed upper limit(s).

The front panel displayed in Fig. 5.61 is very similar to that in Fig. 5.59, except it does not have save controls to create or alter limit sets. However, for controls and indicators that are common to both VIs, the operations are exactly the same. If the limit sets are reviewed and revisions are required, the user must re-enter the VI, *8 - Define Limits.vi*, create new limits sets for those requiring revision, and resave the limit sets.

Figure 5.62 presents limit sets that were established to define the selected relationships presented in Figs. 5.57 - 5.58. Notice that the limit sets defining each relationship are unique. Some relationships required two limit sets to complete define the relationship, whereas others only required one set. In addition, the widths of the limits sets vary among the examples, making some relationships more sensitive to changes in bridge behavior than others that were developed. However, all relationships were developed by using US30 bridge measured performance data, and thus, define the structural behavior of the bridge at the time when the data was collected. This state of condition could be a damaged or undamaged state, but in either case, the data is useable in training as long as the measured behavior is consistent and repeatable.

While the training process attempts to form four relationships for every TS-NTS combination, Table 5.3 presents a summary of all relationships that were actually defined for use in the US30 SHM system. Review of Table 5.3 reveals the following observations:

- There were 415 relationships that were defined among all TS-NTS combinations, which amounted to an average of 41.5 defined relationships per TS and 1.4 relationships per TS-NTS combination.
- Each TS-NTS combination had at least one defined relationship.
- There was tremendous consistency in the relationships that were defined for corresponding TSs in the north and south cut-back regions.
- The TS-NTS combinations with the most defined relationships were those that were developed with a NTS in the cut-back region of Section E (i.e. E-NG-CB(1)-V, E-NG-CB(5)-V, E-SG-CB(1)-V, or E-NG-CB(5)-V).

The results in Table 5.3 illustrate that even though the training process attempts to develop four relationships for every TS-NTS combination, not all of the relationships are formed or are useable in the SHM system. In addition, the results also prove that more than one relationship can be formed

www.manaraa.com

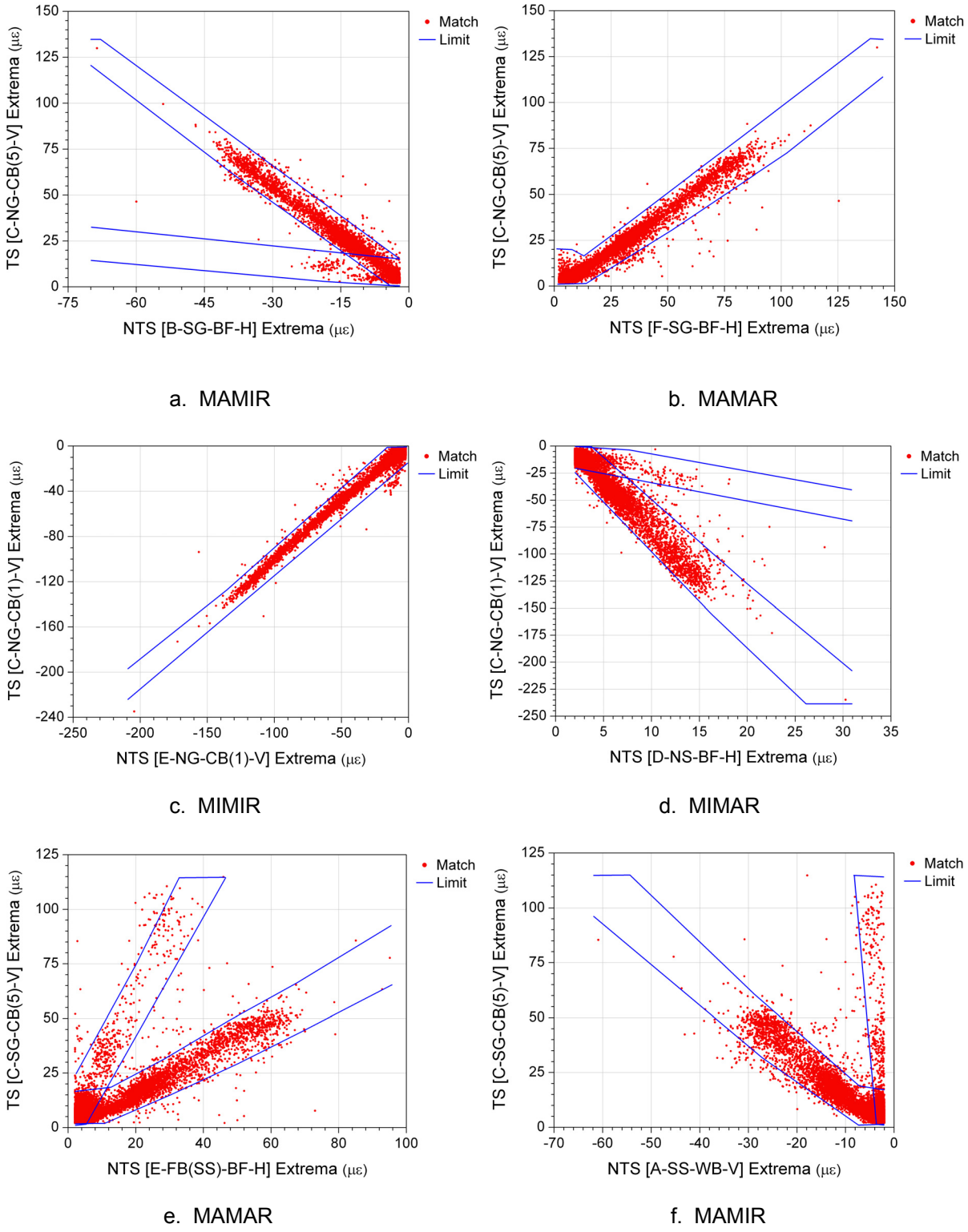

Figure 5.62. Selected limit sets that define relationships in the US30 SHM system.

www.manaraa.com

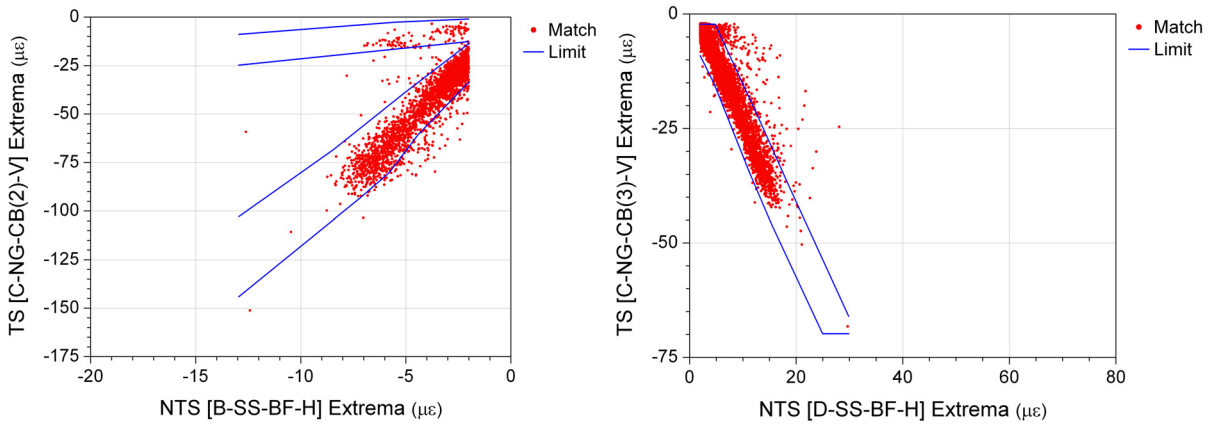

g. MIMIR

h. MIMAR

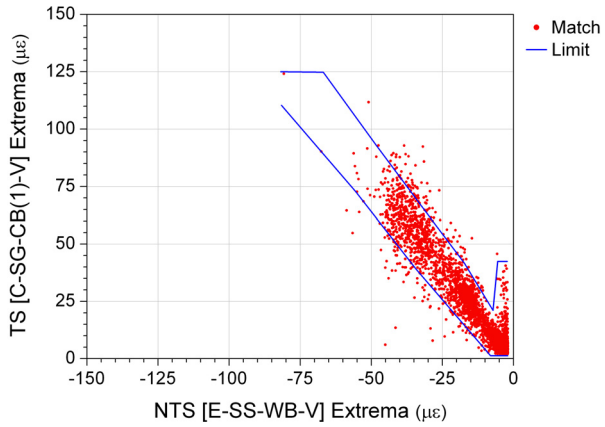

i. MAMIR

Figure 5.62. (continued).

between a TS and NTS due to indirect matching, which was initially suggested by the results of Fig.5.51. Moreover, fact that the highest number of relationships per TS-NTS combination were achieved when the NTS was a cut-back region sensor suggests that the success of the matching process increases as the similarity between event patterns in TS and NTS strain records increases. Recalling that the type of extrema (i.e. maxima or minima) that are generated in a TS strain record when vehicles are in close proximity of the sensor depends on the transverse position of the vehicle in the bridge, it is not possible to determine with absolute certainty which defined relationships in Table 5.3 are developed from direct or indirect matching. However, knowledge of the matching that produced a relationship is not important to the functionality of the SHM system. The matching

www.manaraa.com

Table 5.3. Summary of defined relationships for TS-NTS combinations in the US30 SHM system.

Non-Target Sensor	Target Sensor																							
	C-SG-CB(5)-V				C-SG-CB(4)-V				C-SG-CB(3)-V				C-SG-CB(2)-V				C-SG-CB(1)-V				C-NG-CB(5)-V				C-NG-CB(4)-V				C-NG-CB(3)-V				C-NG-CB(2)-V				C-NG-CB(1)-V			
B-NG-BF-H																																				
B-NS-BF-H																																				
B-SS-BF-H																																				
B-SG-BF-H																																				
C-SG-BF-H																																				
C-FB(SS)-BF-H																																				
C-SS-WB-V																																				
A-NS-WB-V																																				
A-SS-WB-V																																				
D-SG-BF-H																																				
D-SS-BF-H																																				
D-NS-BF-H																																				
D-NG-BF-H																																				
C-NG-BF-H																																				
C-FB(NS)-BF-H																																				
C-NS-WB-V																																				
E-NG-BF-H																																				
E-NG-CB(5)-V																																				
E-NG-CB(1)-V																																				
E-NS-WB-V																																				
E-FB(NS)-BF-H																																				
E-FB(SS)-BF-H																																				
E-SS-WB-V																																				
E-SG-CB(5)-V																																				
E-SG-CB(1)-V																																				
E-SG-BF-H																																				
F-SG-BF-H																																				
F-SS-BF-H																																				
F-NS-BF-H																																				
F-NG-BF-H																																				
Totals by Type	19	12	5	5	18	12	-	-	2	3	18	12	6	4	18	13	6	6	20	13	21	17	2	5	19	11	-	-	3	7	21	16	5	6	21	17	5	7	22	18
Overall Totals	41				30				35				41				45				45				30				47				49				52			

Note: MAMAR
MAMIR
MIMAR
MIMIR

www.manaraa.com

process producing the relationships must merely be consistent and repeatable, which describes both direct and indirect matching. As illustrated in Fig. 5.37, the training process for the SHM system is complete after all limit sets have been defined for the training data.

5.3 SHM System Monitoring Mode Procedures

After the training process is complete, the SHM system is ready to operate in monitoring mode. As will be presented in the proceeding sections, four pieces of information that were generated during the training process are necessary for the operations that are conducted when the system is in monitoring mode:

- the filter file that contains filter configurations and extrema identification parameters
- the file containing sensor classifications
- the file containing sensor longitudinal locations
- the directory that contains the limits sets for each defined relationship

A detailed schematic of the procedures involved in mode is provided in Fig. 5.63, and as illustrated, six phases are completed to collect and assess the bridge performance data:

1. Data collection and storage
2. Preliminary reduction
3. Primary reduction
4. Extrema matching
5. Extrema evaluation
6. Report generation

Unlike the training process, the monitoring mode is completely autonomous and requires no user intervention after it has been configured and started. The operations performed by the monitoring mode software algorithms are described in detail in the subsequent sections.

5.3.1 Phase One: Data Collection and Storage

The front panel for the FCB SHM system, *Master FCB SHM System.vi*, during monitoring mode is displayed in Fig. 5.64. Comparison of Fig. 5.64 and Fig. 5.38a reveals that only control #8 (See Fig. 5.38) was changed to switch the FCB SHM system into monitoring mode. Data collection

www.manaraa.com

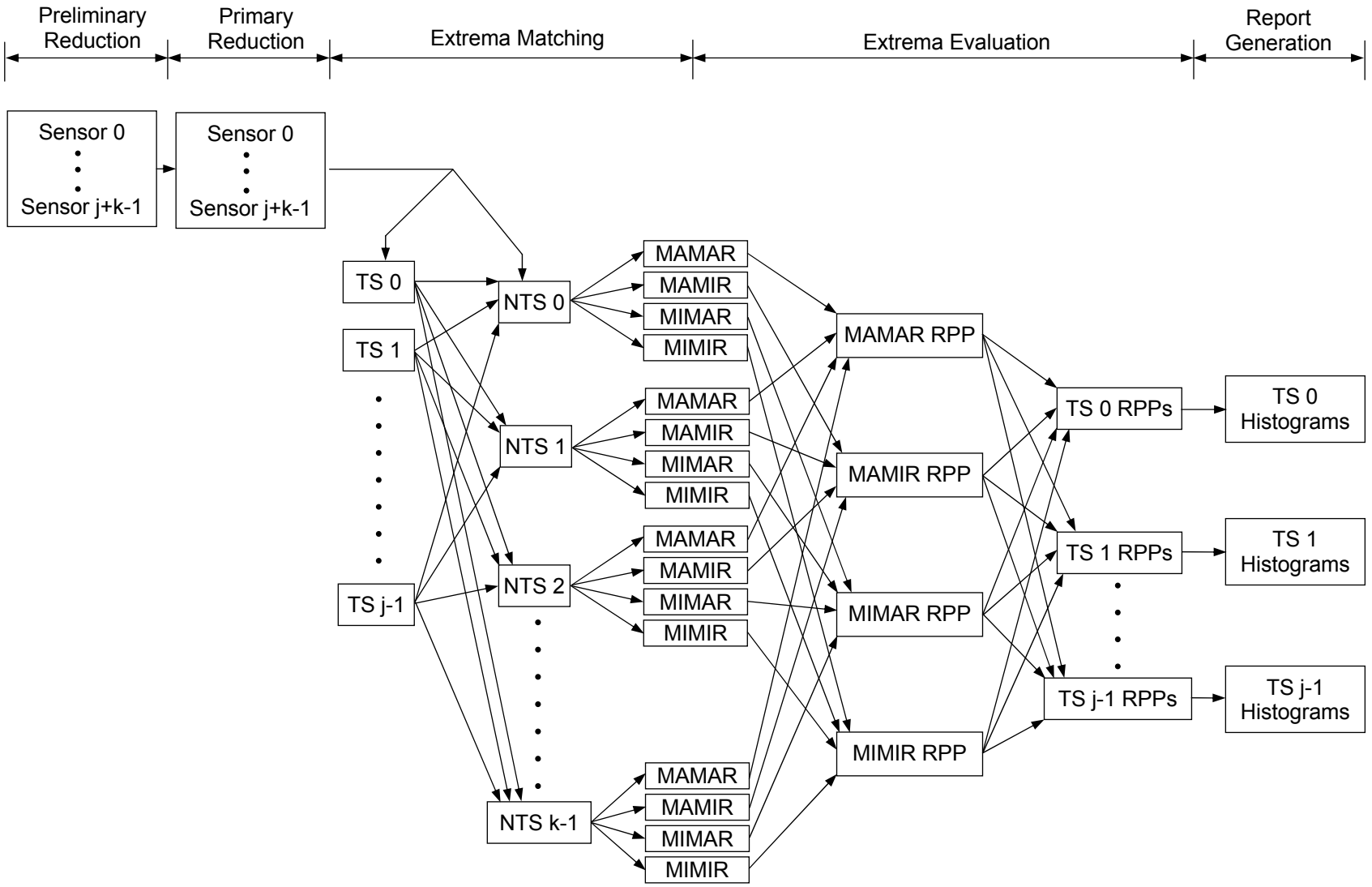

Figure 5.63. Overview of the phases in the FCB SHM monitoring process that are performed for each data file.

www.manaraa.com

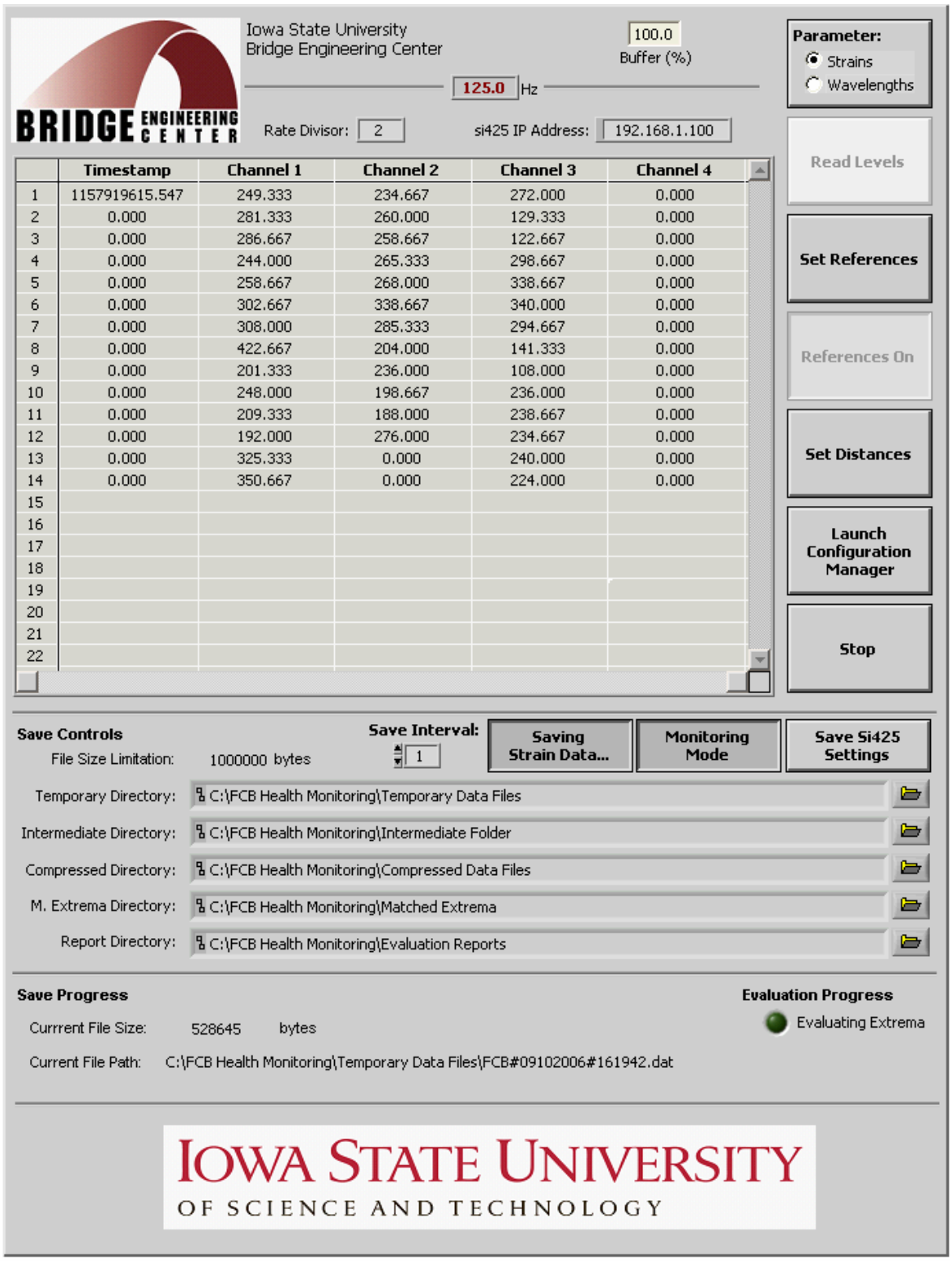

Figure 5.64. Front controls and indicators of FCB SHM system while operating in monitoring mode (*Master FCB SHM System.vi*).

www.manaraa.com

and storage with the system in monitoring mode is very similar to that which was performed with the system in training mode. Strain data are collected and written to a file in the temporary directory (control #11 in Fig. 5.38) with the same format that was discussed in Section 5.2.1. When the data file size exceeds the allowed limit (control #10), the data file is closed and moved to the intermediate folder (control #12). Rather than compressing the data as would be performed with the system in training mode, notification of a new file is sent to the subVI, *Synchronized Evaluation and Report Generation.vi*. Meanwhile, data collection continues and data are written to a new data file in the temporary directory. This repetitive process continues until the system is terminated.

The subVI, *Synchronized Evaluation and Report Generation.vi*, operates in parallel with the data collection and storage procedures. Essentially, this subVI remains dormant until it receives notification that a new data file has been created, closed, and moved into the intermediate folder. Upon notification, the subVI becomes active and autonomously performs all operations required to assess the bridge data and to generate a report that summarizes the evaluations. The required input, which is primarily composed of previously determined parameters, is as follows:

- **Filter Type Control:** The type of lowpass frequency filter, Chebyshev or Butterworth, to be applied to the data file (scalar).
- **Time Duration for Report Control:** Time limit in seconds for each evaluation report that is generated (scalar).
- **Speed (mph) Control:** Expected average speed for a representative sample of traffic (scalar).
- **Speed Deviation (± mph) Control:** Deviation (mph) to be used with the expected average speed to define the expected speed range for a representative sample of traffic (scalar).
- **Save Matched Extrema?/Save Original Strain Data Control:** For each set of data, if set to true, the data are saved after the evaluation process. Otherwise, the data are deleted after the evaluation process (cluster of two Boolean values).
- **Data File Source Directory Path Control:** Directory containing data files to be evaluated.
- **Compressed File Save Directory Path Control:** Directory in which data files are stored after they have been evaluated and compressed.
- **Matched Extrema Save Directory Path Control:** Directory in which the matched event extrema are stored after the data file contents have been evaluated.
- **Evaluation Report Save Directory Path Control:** Directory in which all evaluation reports are stored after they have been generated and compressed.

www.manaraa.com

- **Limit Sets Source Directory Path Control:** Directory to the folders that contain the limit sets for the defined TS-NTS relationships.
- **Filter File Source Path Control:** Path to the file that contains the settings for the selected lowpass frequency filter.
- **Sensor Classification File Path Control:** Path to the file that defines each sensor as a TS or NTS.
- **Sensor Locations File Path Control:** Path to the file that contains the longitudinal location of each sensor within the bridge.
- **New Evaluation Path? (IN) Control:** Specifies whether or not a new evaluation report is to be started prior to execution (Boolean).
- **Evaluation Path (IN) Control:** File path to which RPP values are being written for the current evaluation report.
- **Time Reference (IN) Control:** Timestamp reference corresponding to the time that the SHM system was switched to monitoring mode (scalar).
- **Iteration Number (IN) Control:** The number of times that the subVI has been called since the VI, *Master FCB SHM System.vi*, has been started (scalar).
- **Time Increment (IN) Control:** The numerical count of evaluation reports that have been created since the very first time that the SHM system was switched to monitoring mode (scalar).

A list of the output information from the subVI is as follows:

- Evaluation reports and accessory information written to the specified report directory
- **New Evaluation Path? (OUT) Indicator:** Specifies whether or not a new evaluation report is to be started prior to the next execution (Boolean).
- **Evaluation Path (OUT) Indicator:** File path to which RPP values are being written for the current evaluation report.
- **Time Reference (OUT) Control:** Timestamp reference corresponding to the time that the SHM system was switched to monitoring mode (scalar).
- **Time Increment (OUT):** The numerical count of evaluation reports that have been created since the very first time that the SHM system was switched to monitoring mode (scalar).

Nearly all input information is specified in the labeled controls in Fig. 5.38b, and the primary outputs are the evaluation reports that summarize results from the evaluation process. All other input and output information is developed and used internally by the system to determine when reports must be generated, and in addition, to recover from power outages at the US30 bridge. The subsequent

www.manaraa.com

paragraphs in Section 5.3 discuss the procedures performed by the subVI, *Synchronized Evaluation and Report Generation.vi*.

5.3.2 Phase Two: Preliminary Reduction

When the subVI, *Synchronized Evaluation and Report Generation.vi*, receives notification of a new data file in the intermediate directory, it automatically retrieves the file and reads it into LabVIEW memory. If control #34 in Fig. 38 is set to true, the subVI compresses the data file and moves it to the compressed file directory (control #13 in Fig. 5.38); if the control is set to false, the data file is closed and deleted.

With the data file in memory, the timestamp (column 0) and buffer (column 1) are removed, and thus, the remaining 2-D array of data is the sensor array. In preliminary reduction, the formatting and completeness of the data file is checked to make sure that it is useful and will not cause error in the operations within the proceeding phases. Thus, the following procedures are performed through use of the previously discussed subVIs:

- The number of sensors are verified to be correct, and zero value flickers that are created by the wavelength filter are removed. The number of sensors in the data file is technically assured to be correct during data collection (*Wavelength Filter – ISU BEC.vi*), but the count is confirmed as zero flicker values, if any, are removed (*Remove Flicker.vi*).
- The DAR is determined from the timestamp.
- Continuity of the file is confirmed (*Check File Continuity.vi*).
- The establishment of a baseline for each strain record is confirmed (*Determine Baselines.vi*).

If the data file fails to pass any of the previously listed confirmations, the data are erased from LabVIEW memory, and the evaluation process is terminated for that data. If all confirmations are passed, the data are passed on to the next phase.

5.3.3 Phase Three: Primary Reduction

In primary reduction, data are prepared for the extrema matching process. The procedures in this phase require the information that was written to the frequency filter file, which was developed and saved during the training process. Thus, this filter file is first read into LabVIEW memory as a 2-D array from the file path specified in control #29 in Fig. 5.38; the columns of the array are separated and dispersed accordingly to the subVIs that perform the following operations:

www.manaraa.com

- Each raw data strain record is zeroed with the baselines determined in preliminary reduction.
- Each strain record is filtered with the type of filter specified in control #24 in Fig. 5.38. For the US30 bridge, a Chebyshev (Type 1) IIR digital lowpass frequency filter (*Chebyshev Filter.vi*) is used according to the filter configurations that were established in the training process.
- All event extrema information is determined for every strain record (*Determine Extrema.vi*) according to the extrema identification parameters that were established in the training process.

Only the extracted extrema information is passed on to the next phase of reduction and evaluation, and all other information is discarded.

5.3.4 Phase Four: Extrema Matching

As illustrated in Fig. 5.63, the extrema information is separated according to TS and NTS classification and used in attempt to form the four types of relationship matches with the subVI, *Match Extrema.vi*. Thus, the procedures in this phase require information pertaining to sensor classifications and longitudinal locations in the bridge, which were determined and saved to files in the training process. Thus, these files are read into LabVIEW memory as 1-D arrays from the file paths specified in controls #30 and #31 in Fig. 5.38. The expected average speed and speed deviation are also required for the extrema matching process, which are specified in controls #25 and #26, respectively, in Fig. 5.38. With this information, the matching process is completed for all TS-NTS combinations (*Match Extrema.vi*) in the exact same way as it was accomplished during the training process. If control #27 of Fig. 5.38 is set to save matched extrema, which is the case for the US30 SHM system, the 4-D array of matched extrema is flattened into a binary string and saved to the directory specified in control #14 in Fig. 5.38.

5.3.5 Phase Five: Extrema Evaluation

After the matching process has been completed for all TS-NTS combinations, all TS extrema are assessed based on the relationships and limit sets that were established during the training process. Extrema are only evaluated, however, if their absolute values are greater than the thresholds specified in control #33 (Fig. 5.38b), and in addition, if the NTS value is within the range defined in each relationship. The evaluation process is completed through use of the subVI, *Evaluate Extrema.vi* (Appendix E). For one TS extrema (maximum or minimum value) at a time, all applicable

www.manaraa.com

matches and relationships are gathered. For each relationship, if the matched extrema pair is within one or more limit sets (between the upper and lower limits), a “pass” assessment is assigned; for outliers, a “fail” assessment is assigned (See Fig. 5.65). As illustrated in Fig. 5.63, when all assessments for one type of relationship have been completed, a relationship pass percentage (RPP) is computed from the output information from the subVI as follows:

$$\text{RPP}\ (\%) = \frac{\text{Number of "pass" assessments}}{\text{Total number of assessments}}(100) \tag{5.14}$$

For the TS extreme value being evaluated, one RPP is computed for every applicable relationship type (i.e. MAMAR and MAMIR RPPs for TS maxima and MIMAR and MIMIR RPPs for TS minima). Thus, it is possible to develop two RPPs for each TS extrema evaluation. For example, suppose a maximum value is being evaluated for C-NG-CB(5)-V, which has 45 defined extrema relationships. Assuming that all NTSs had matches to the TS maximum value, 21 MAMARs and 17 MAMIRs are applicable for the evaluation. If the number of “pass” assessments for each relationship type is 19 and 16, the corresponding MAMAR and MAMIR RPPs are 90.5% and 94.1%, respectively.

After this process has been completed for all extrema pertaining to one TS, the RPPs are grouped and written to one column of an autonomously created data file within the directory defined

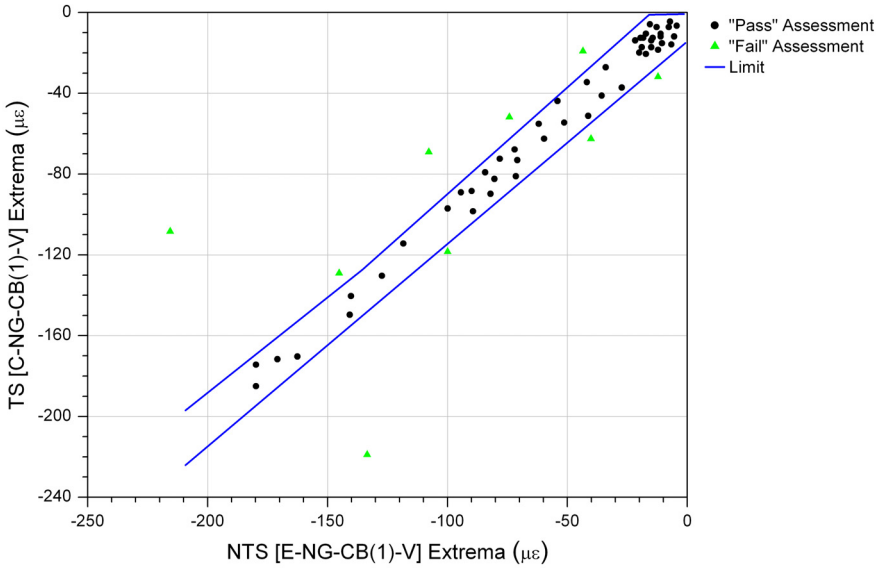

Figure 5.65. Identification of “pass” and “fail” relationship assessments for matched extrema.

www.manaraa.com

in control #15 in Fig. 5.38. This process is repeated for every TS in the bridge, and the product of this monitoring phase is a data file that contains one column of data for each TS in the SHM system; each column contains RPPs that are no longer identifiable by their relationship type. If control #34 (Fig. 5.38) is set to save data after evaluation, the raw data file is compressed and moved to the directory defined in control #13 of Fig. 5.38.

Having discussed the operations performed by *Evaluate Extrema.vi*, the following inputs that are required by the subVI are as follows:

- **Limit Files Source Directory Path:** Top level directory containing defined limit sets (directory to which results were written by the VI, *8 - Define Limits.vi*).
- **Relationship Type:** The type of relationship (MAMAR, MAMIR, MIMAR, or MIMIR) to be used in the assessment (scalar).
- **Matched Target Extrema:** The TS extrema values that have been matched (3-D array with one page per TS, one row per NTS, and one column per extreme value.
- **Matched Non-Target Extrema:** The NTS extrema values that have been matched (3-D array with one page per TS, one row per NTS, and one column per extreme value.
- **Target Threshold for Evaluation:** The value that must be exceeded by the TS extrema in order for it to be evaluated (scalar).
- **Non-Target Threshold for Evaluation:** The value that must be exceeded by the absolute value of the NTS extrema in order for it to be evaluated (scalar).
- **Target Sensor Labels:** TS labels that are listed in the order that they appear in the sensor array (1-D array).
- **Non-Target Sensor Labels:** NTS labels that are listed in the order that they appear in the sensor array (1-D array).

Output from the subVI is is as follows:

- **Number of Pass Assessments:** Number of pass assessments for evaluations (2-D array where each row is a TS and each column is an evaluation).
- **Number of Fail Assessments:** Number of fail assessments for evaluations (2-D array where each row is a TS and each column is an evaluation).
- **Total Number of Assessments:** Total number of assessments for evaluations (2-D array where each row is a TS and each column is an evaluation).

Since the number of extrema among the sensors may not be the same, the arrays containing extrema that are input into the subVI may contain zero value place holders. As a result, the subVI, *Remove*

www.manaraa.com

Training Zero Values.vi, was developed. This subVI is used to remove the place holders from 1-D arrays.

5.3.6 Phase Six: Report Generation

As soon as the data collection and extrema evaluation procedures have operated for a time duration that is longer that that which has been specified in control #32 in Fig. 5.38, which is one day (86,400 seconds) for the US30 SHM system, a report is autonomously created that summarizes the extrema evaluations that have been performed during that time period. This task is achieved by the subVI, *Generate FCB Report.vi* (Appendix E), which reads the RPPs from the file to which they were being saved. From these RPPs, two histograms are created for each TS. The first histogram that is created reports the numerical count of evaluations in each bin, where each bin is a five percent RPP range, and the second histogram reports the evaluations in each bin as a percentage of the total number of evaluations that have been performed during that particular time period. The results in the second histogram are standardized, and thus, allow for direct comparison of evaluation results for multiple time periods. After report generation is complete, the subVI compresses the report folder by utilizing the subVI, *WindowsXP Zip Files in Folder.vi*, which calls *ZipFilesXP.dll* to perform the compression. This procedure is repeated for every report that is generated by the SHM system. With the US30 SHM system, a file transfer protocol (FTP) utility automatically removes the compressed report file and delivers it to the bridge engineer for review at the end of each day.

Figure 5.66a presents examples of the folders and files that are contained within the evaluation report directory (control #15 in Fig. 5.38). The folder in Fig. 5.66a stores all information as it is being generated for the current report. Prior to execution of the subVI, *Generate FCB Report.vi*, this directory only contains the file to which RPPs are being written (See Fig. 5.66b). During report generation, the following information is added to the directory prior to compression: the evaluation report in hypertext markup language (HTML) format (example provided in Appendix G), accompanying figures for the report, and a data file containing infomation for each histogram. Such files are presented in Fig. 5.66c for the compressed report folder that is displayed in Fig. 5.66a and is waiting to be transferred to the bridge owner via the FTP utility. Finally, the text files contained in the

www.manaraa.com

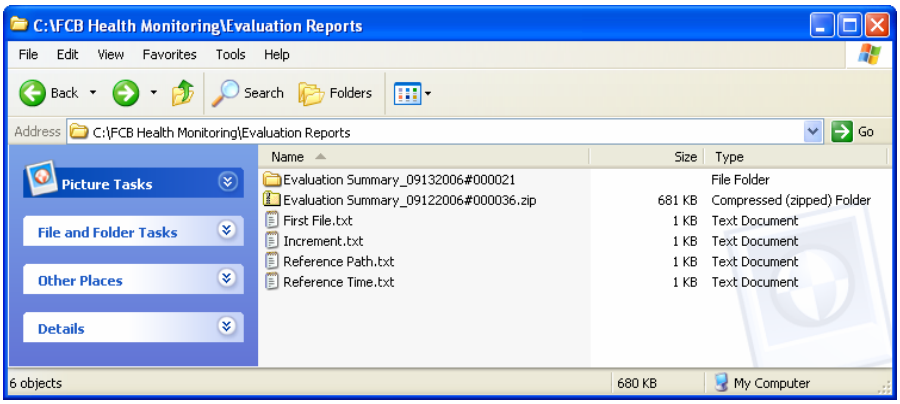

a. Evaluation report directory contents

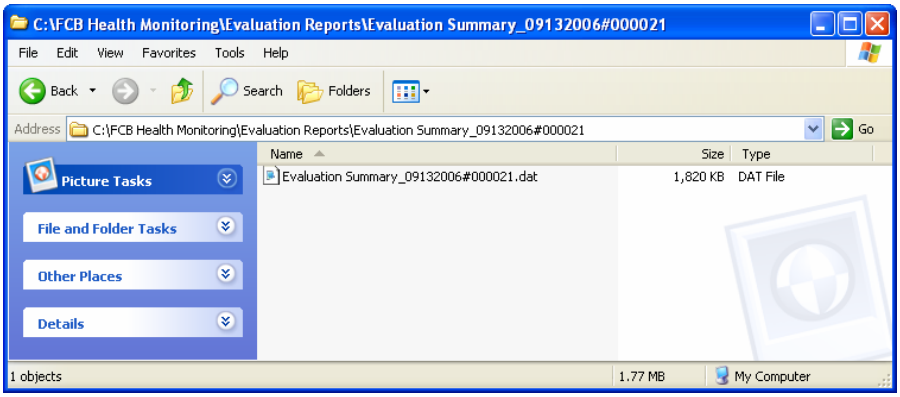

b. Current report folder contents

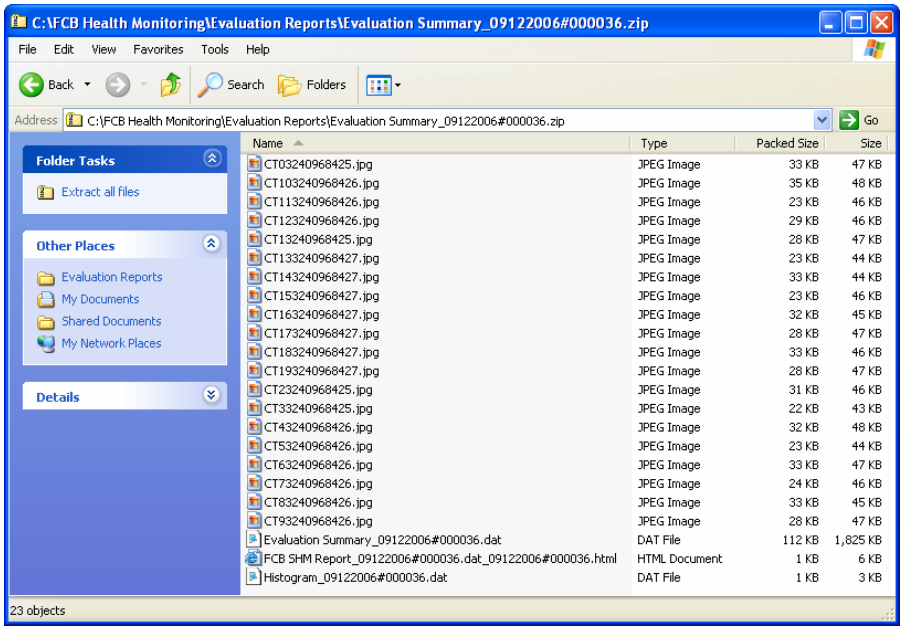

c. Completed (compressed) report folder contents

Figure 5.66. Report directory structure and files utilized in the generation of daily evaluation reports.

www.manaraa.com

window of Fig. 5.66a are autonomously created and updated by the SHM system and contain the following information:

- *First File.txt*: Contains the name of the first data file that was included in the current report.
- *Increment.txt*: Contains the numerical count of evaluation reports that have been created since the very first time that the SHM system was switched to monitoring mode.
- *Reference Path.txt*: Contains the file path to which RPP values are being written for the current report.
- *Reference Time.txt*: Timestamp value corresponding to the time that the SHM system was switched to monitoring mode.

The information within the files is updated, but names of the files never change. In addition, the files must never be moved from the directory in which they are autonomously created.

In Figs. 5.67a-g, the daily evaluation reports for all TSs for one week of monitoring have been displayed. The seven histograms were combined on each chart to aid day-to-day comparisons of TS behavior. Review of Figs. 5.67a-g reveals the following observations:

- The RPPs are not 100% for all extrema evaluations.
- Each histogram contains one dominant bin with high RPPs.
- Then number of evaluations for a given TS varies from day to day.
- Relatively comparing charts that report numerical counts of evaluations, fewer evaluations were performed for TSs located near the cut-back region inflection point than for those located farther away from the inflection point.
- Relatively comparing charts with standardized histograms, the variation among the dominant bins within one chart is larger for TSs that are located near the inflection point of the cut-back region than for those that are located father away from the inflection point. This variation appears to be similar for corresponding TSs between the two cut-back regions.
- Relatively comparing all types of charts, the distribution of the histogram to the inferior bins is much more noticeable for TSs that are located near the inflection point of each cut-back region than for those that are located father away from the inflection point.
- Comparing histograms that report numerical counts of evaluations within one chart, there is remarkable variation among the dominant bins. The pattern of the variation, however, is not consistent among all TSs.
- There are typically more evaluations performed for TSs in the north cut-back region than for those in the south cut-back region.

www.manaraa.com

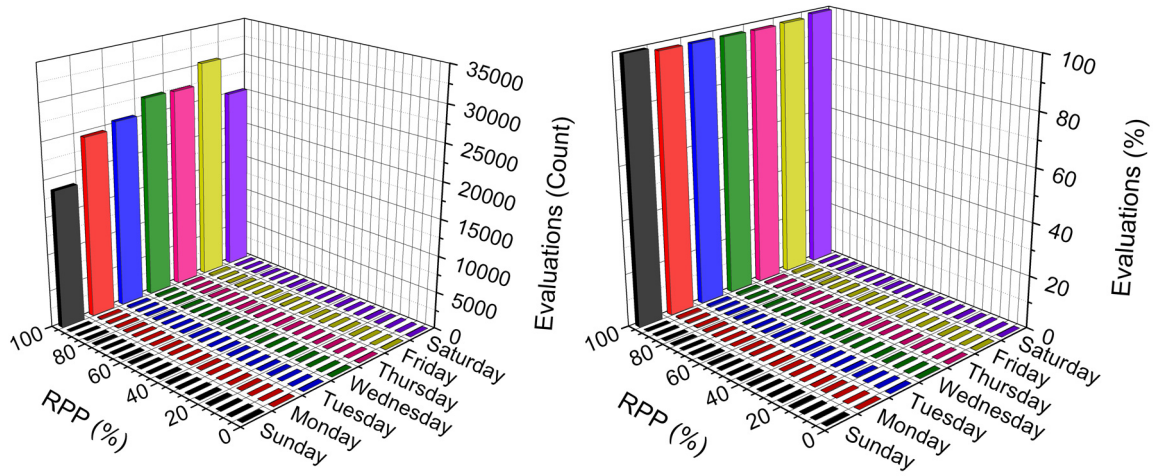

a. C-NG-CB(1)-V

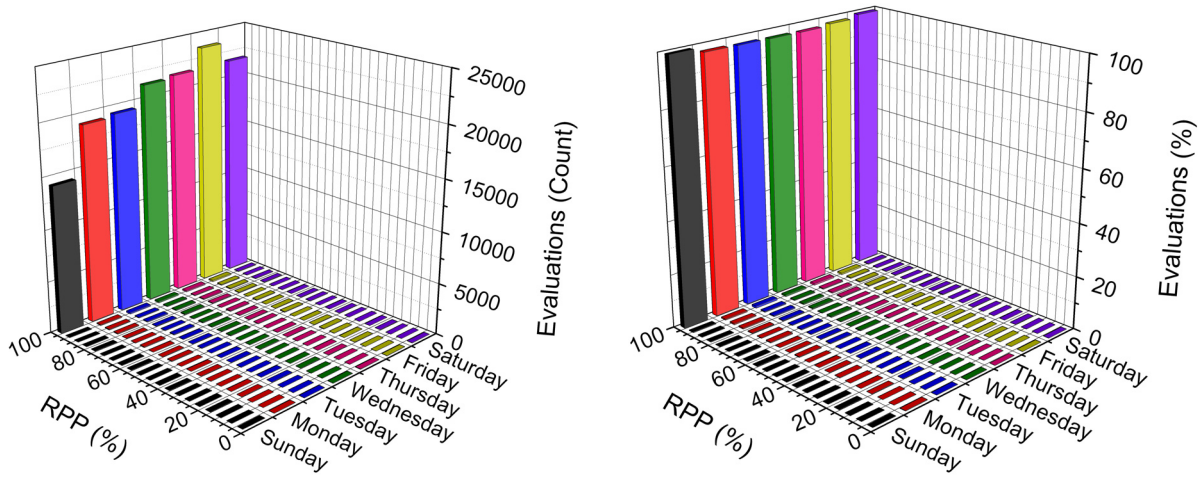

b. C-NG-CB(2)-V

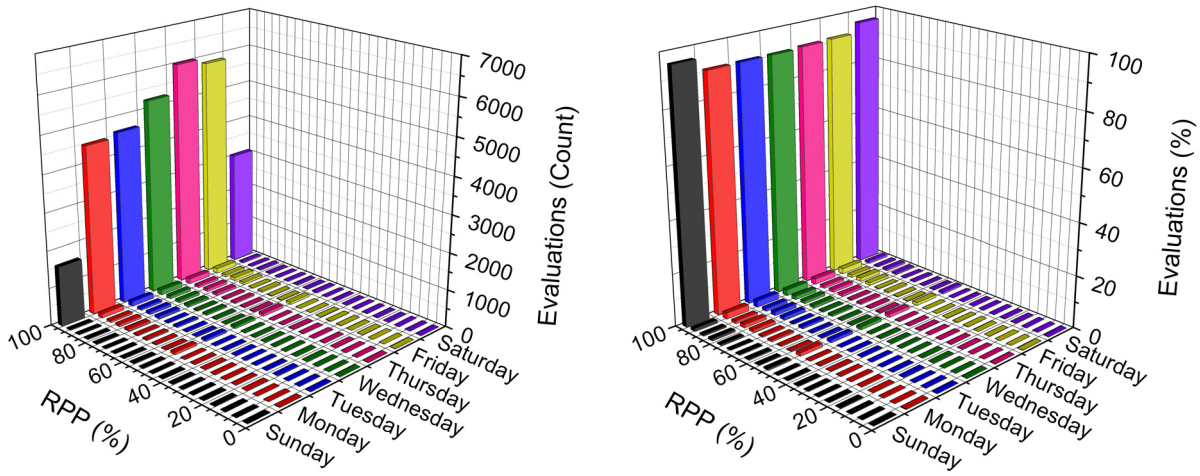

c. C-NG-CB(3)-V

Figure 5.67. Comparison of daily evaluation reports for TSs in the US30 SHM system.

www.manaraa.com

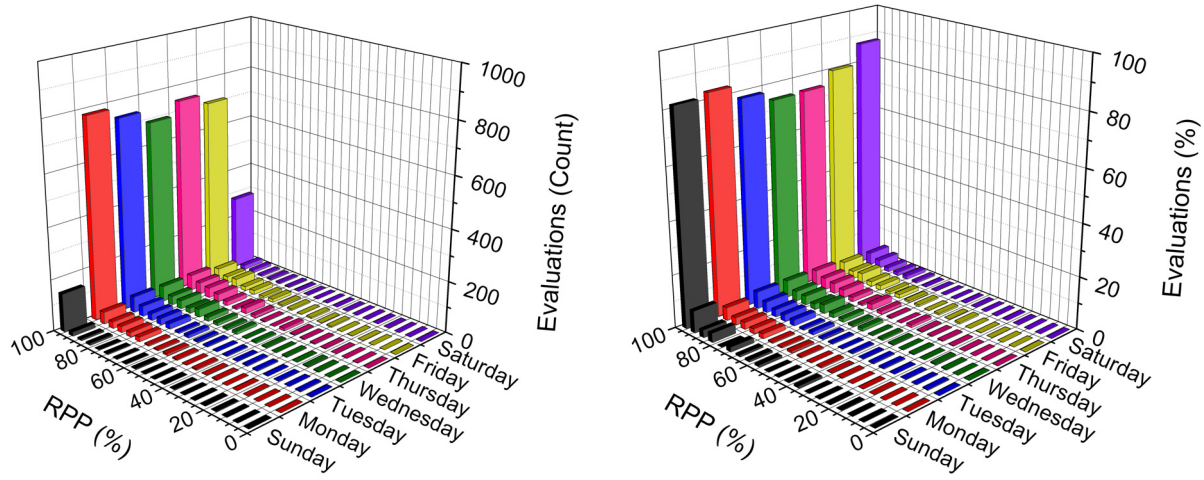

d. C-NG-CB(4)-V

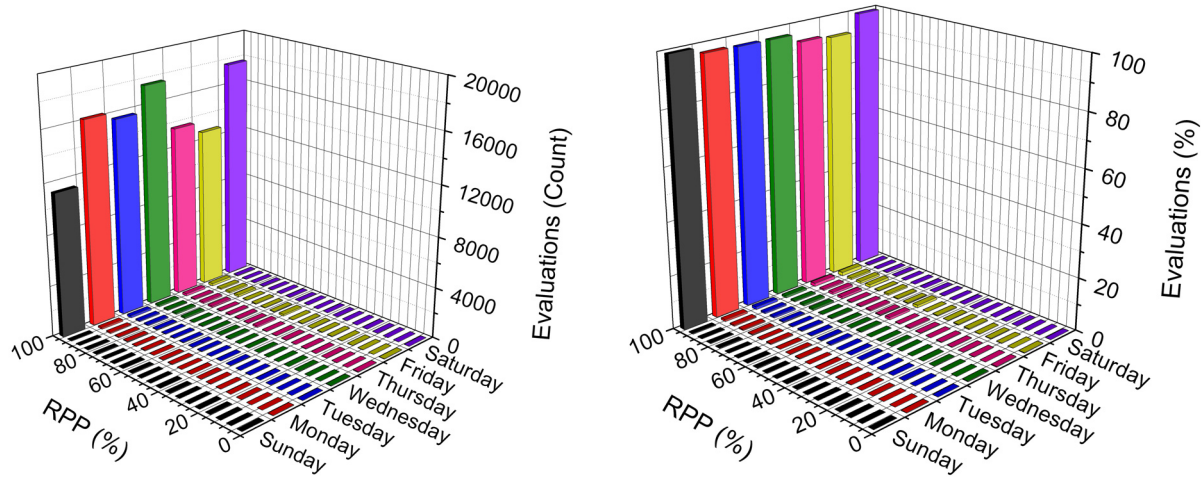

e. C-NG-CB(5)-V

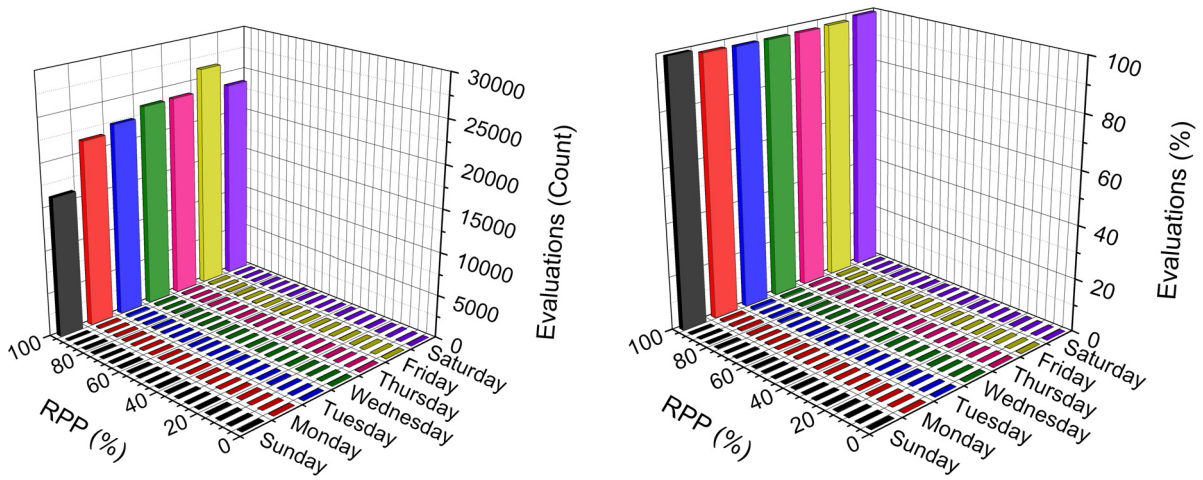

f. C-SG-CB(1)-V

Figure 5.67. (Continued).

www.manaraa.com

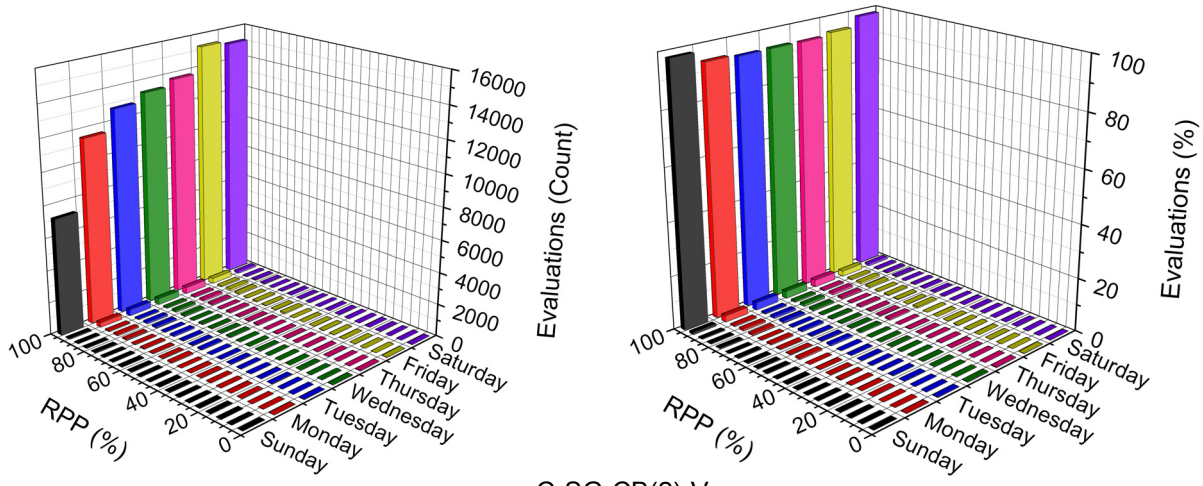

g. C-SG-CB(2)-V

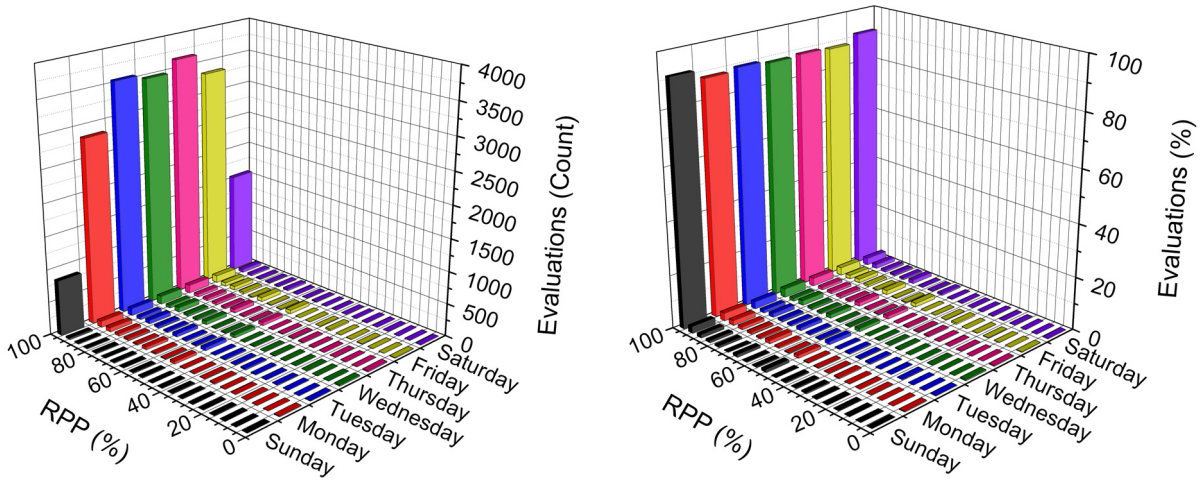

h. C-SG-CB(3)-V

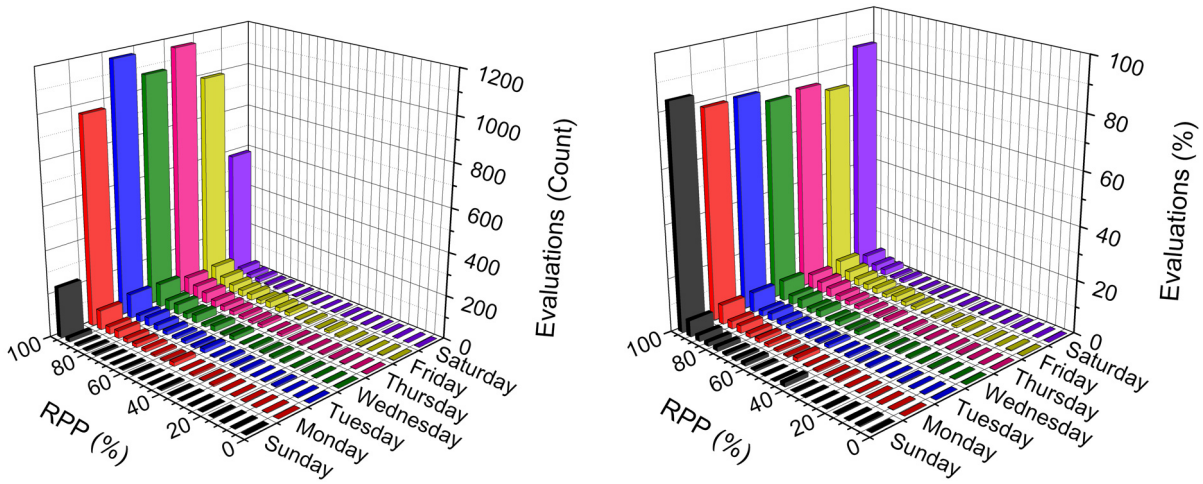

i. C-SG-CB(4)-V

Figure 5.67. (Continued).

www.manaraa.com

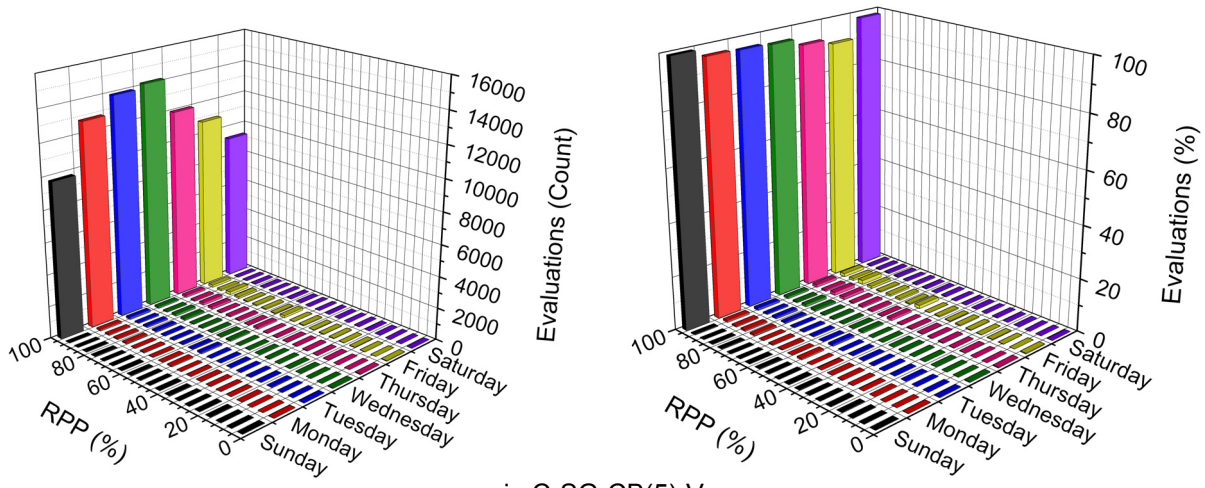

j. C-SG-CB(5)-V

Figure 5.67. (Continued).

- Within each chart for all TSs, there were no significant changes in histogram patterns among the seven days of evaluation results.

The fact that not all RPPs equal 100% is easily explained by reviewing Fig. 5.62 and noting that not all of the training data points are within the limits sets defining the relationships. In addition, the observed high variation in the number of daily evaluations within one chart is directly related to the volume of traffic traversing the bridge each day; in general, the weekday volumes of traffic are higher than those for the weekend days. Moreover, the observed differences among the charts are explained by reviewing the cut-back region structural responses illustrated in Fig. 5.32b and Fig. 5.33b. For sensors near the inflection points, strain values are smaller and less likely to exceed the required thresholds for extrema identification. As a result, fewer extrema are available for evaluation. In such a situation, the identified extrema may not constitute a representative sample, and histogram patterns may be skewed. Similarly, strains in the north cut-back region are larger than those in the south cut-back region when traffic travels in the south lane. Since the south lane is the driving lane, it is expected to be the popular lane for traffic traversing the bridge. Therefore, more extrema for evaluation are produced in the TS strain records of the north cut-back region. Finally, strain records containing small extrema are much flatter than those with high extrema. As a result, higher error is expected when locating the indexes of event extrema. As a result, the occurrence of mismatches will

www.manaraa.com

increase and cause lower RPPs to form, which explains the wider distribution of histogram patterns for TSs near the cut-back region inflection points.

In Figs. 5.68a-g, the weekly evaluation reports for all TSs for seven weeks of monitoring have been displayed. Each week of results was generated by combining RPP files from seven daily evaluation reports, and week one within each chart was formed by combining the results in Figs. 5.67a-g. In general, review of Figs. 5.68a-g reveals observations very similar to those previously listed for Figs. 5.67a-g. As a result, it can be concluded that the training process was performed for a suitable sample of traffic. However, one major difference exists between the daily and weekly evaluation results; the variation in numerical counts of weekly evaluations within one chart is much less than that which exists within one chart containing daily results. This was expected, however, since day-to-day traffic patterns fluctuate much more than week-to-week traffic patterns.

One unexpected result was the occurrence of the small inferior bin that developed during week four and is most obvious in the charts for C-SG-CB(3)-V, C-SG-CB(4)-V , and C-NG-CB(4)-V. The cause of this development is unknown. However, because it consistently developed in the results for corresponding sensors between the two cut-back regions, it is expected to be a related to a change in traffic, rather than a sensor or software malfunction. Fortunately, the bin disappeared and did not return. It is important reiterate, however, that there no major changes in the standardized histogram distributions for the 33 weeks of monitoring that has been performed. Thus, the ability of the SHM system to identify and evaluate repeatable bridge behavior has been proven.

It has been demonstrated that not all RPPs equal 100% during a time of constant bridge condition, and as a result, the FCB SHM system was not configured to identify damage based on an individual extreme value basis because of the highly likelihood of false alarms. Rather, damage is predicted to be identifiable based on changes in histogram patterns. If gradual damage begins to form in a cut-back region, the structural response similarly changes. Such a localized change will affect extrema that are recorded by TSs, which are close to the damage, but not by the NTSs that are farther away from the damage. As a result, fewer relationships will report “pass” for extrema evaluations, and the dominant bins displayed in Figs. 5.67 - 5.68 will become significantly distributed

www.manaraa.com

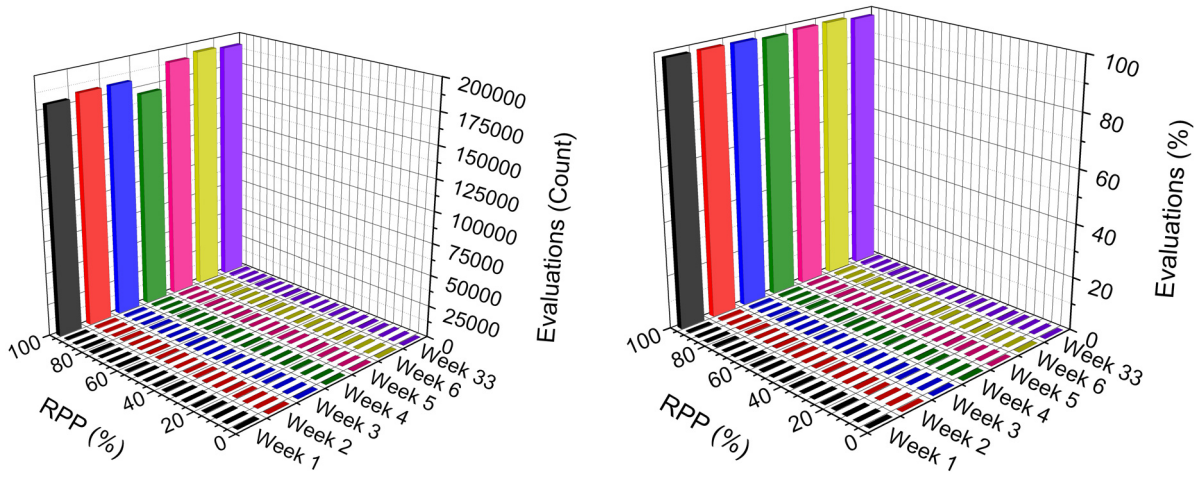

a. C-NG-CB(1)-V

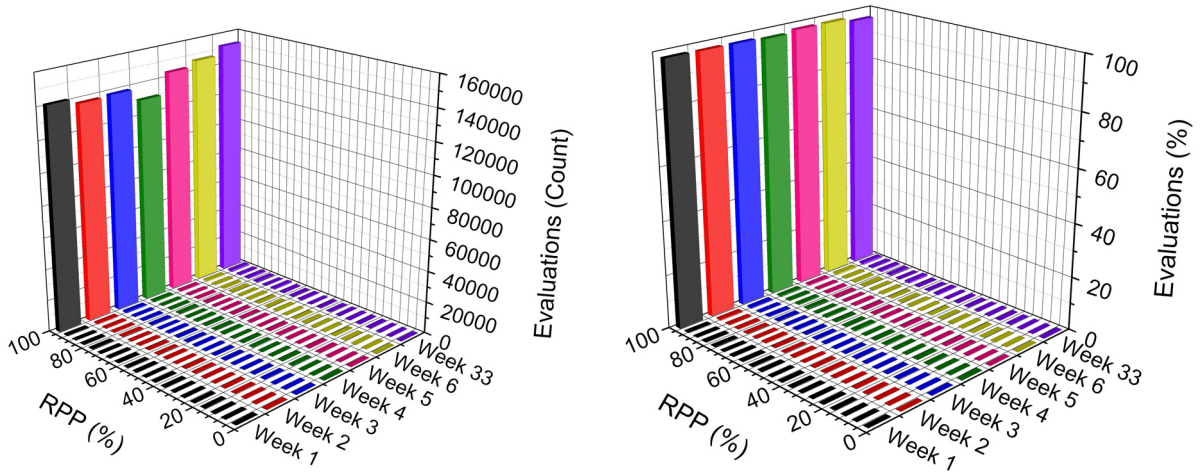

b. C-NG-CB(2)-V

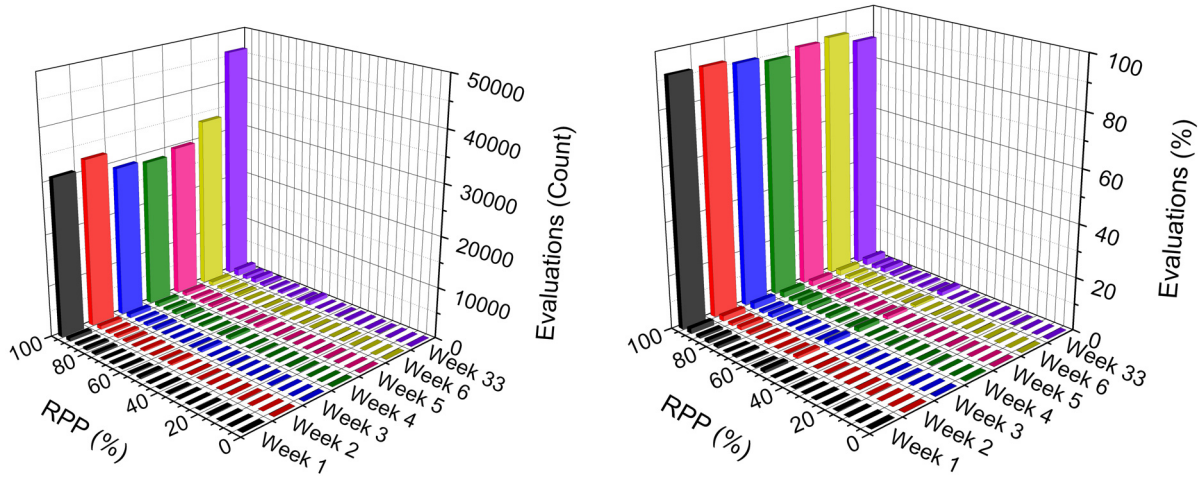

c. C-NG-CB(3)-V

Figure 5.68. Comparison of weekly evaluation reports for TSs in the US30 SHM system.

www.manaraa.com

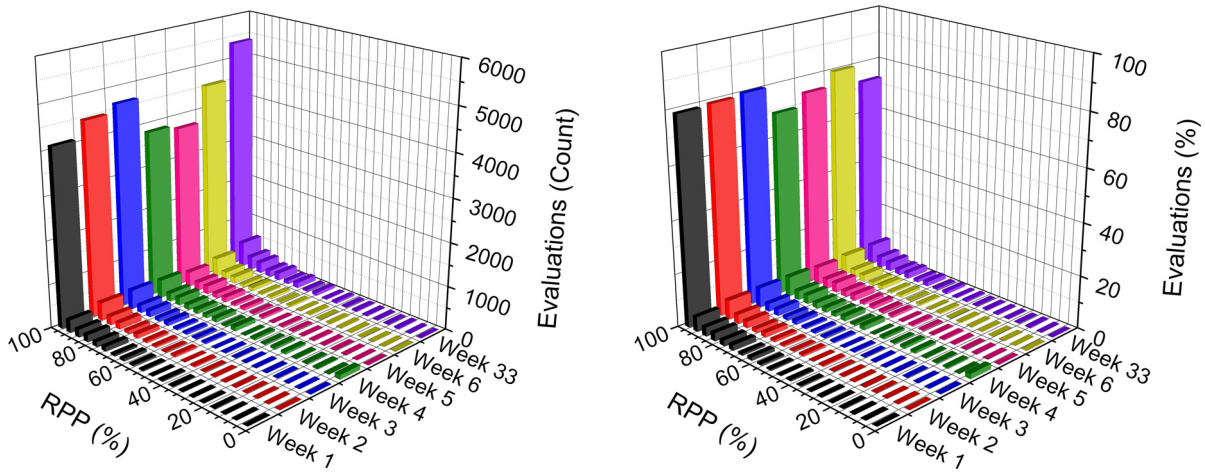

d. C-NG-CB(4)-V

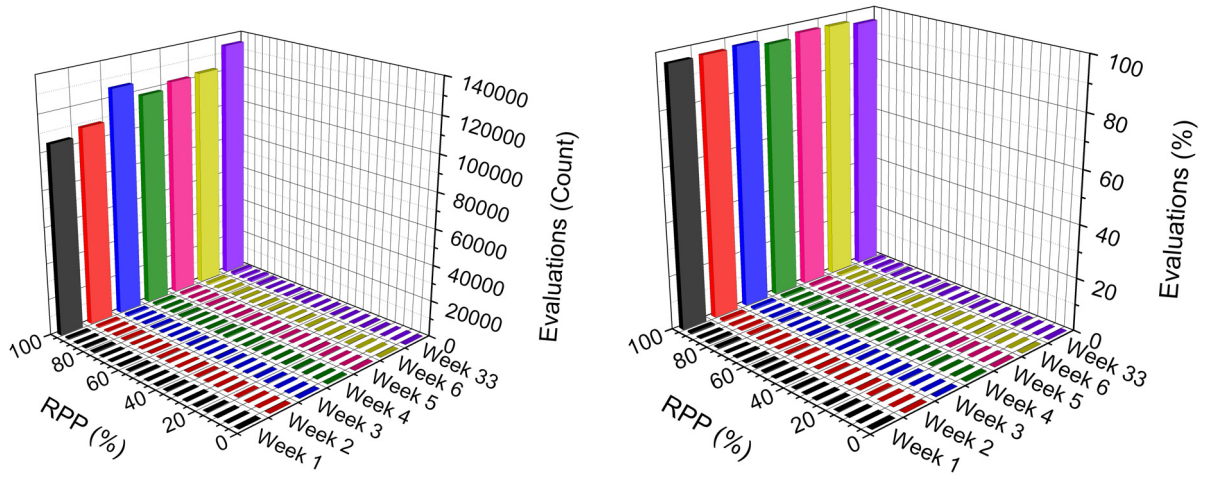

e. C-NG-CB(5)-V

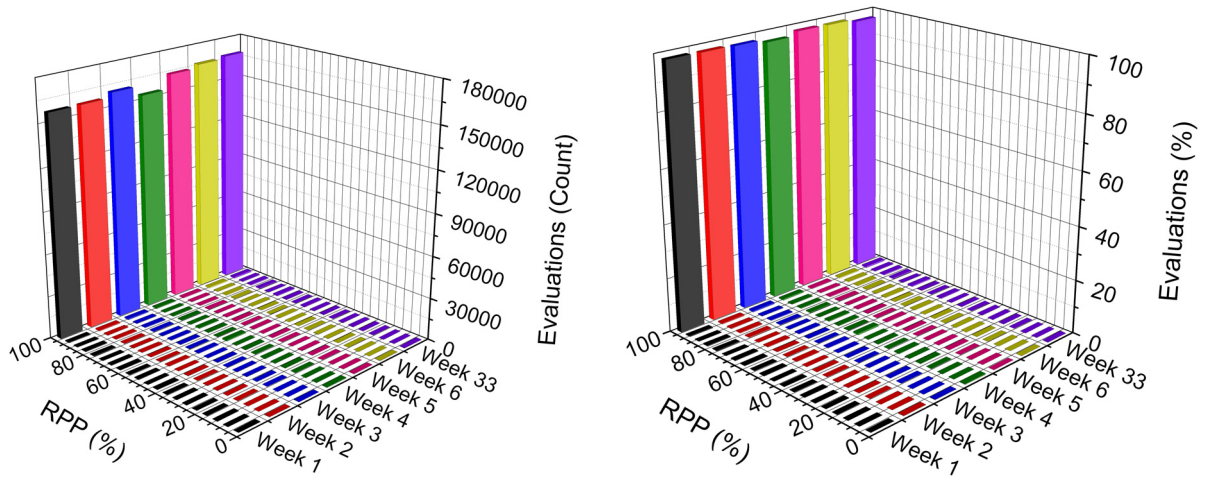

f. C-SG-CB(1)-V

Figure 5.68. (Continued).

www.manaraa.com

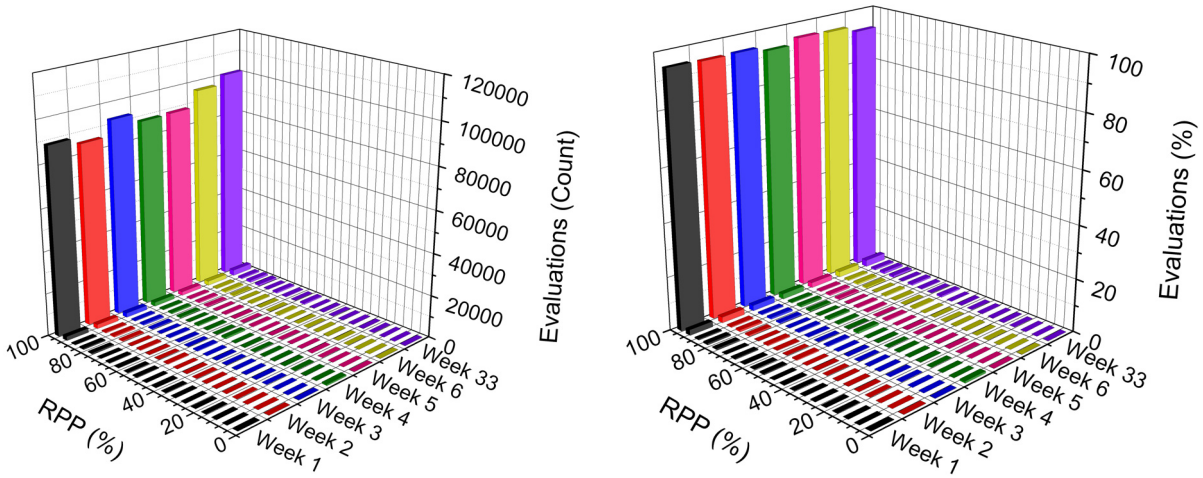

g. C-SG-CB(2)-V

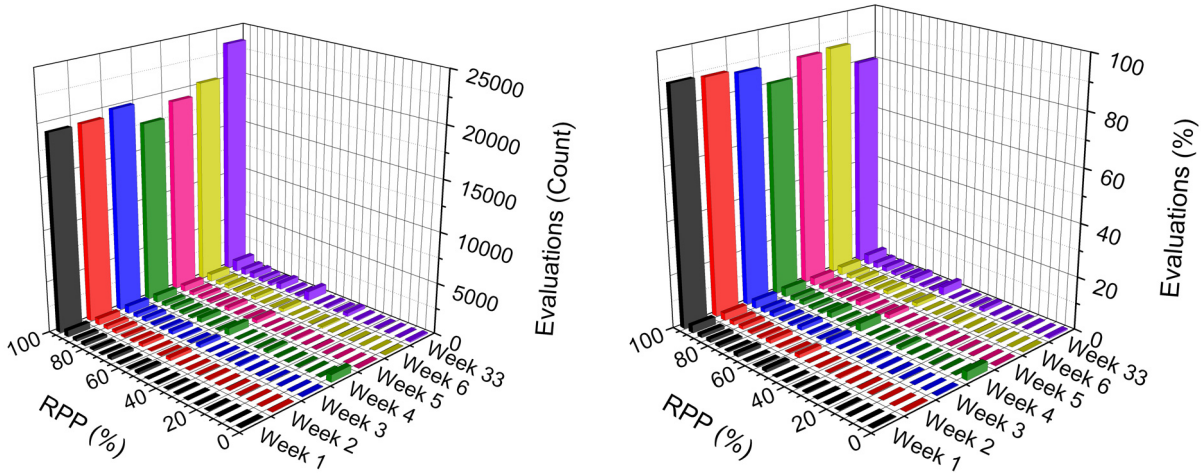

h. C-SG-CB(3)-V

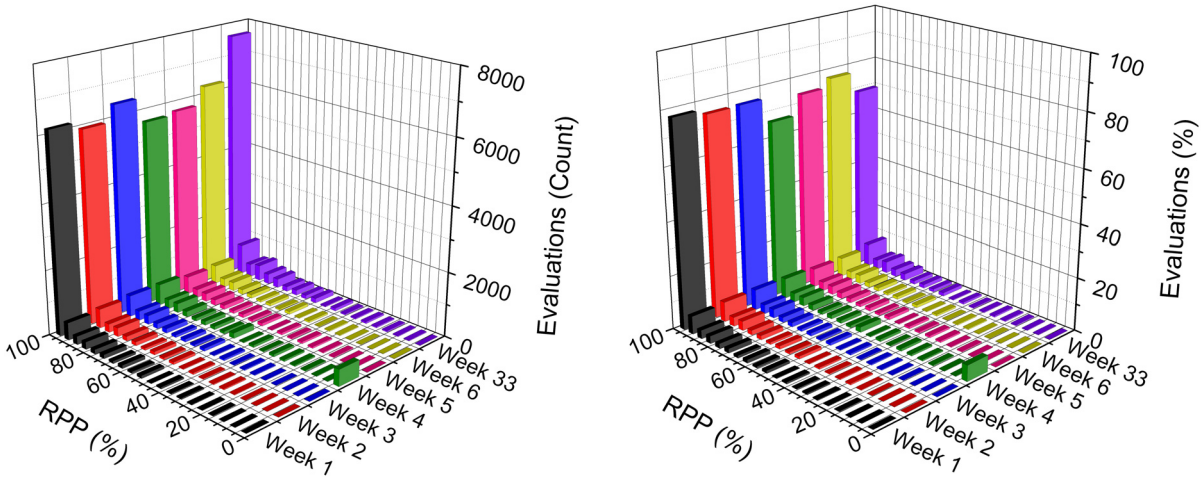

i. C-SG-CB(4)-V

Figure 5.68. (Continued).

www.manaraa.com

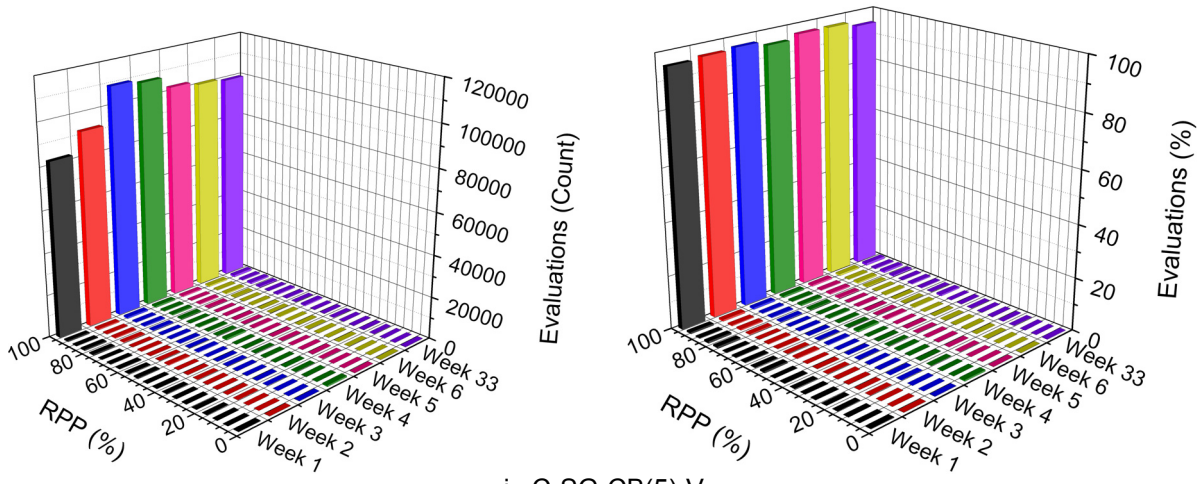

j. C-SG-CB(5)-V

Figure 5.68. (Continued).

across several bins. As the damage continues to grow, the dominant bin in each histogram is expected to return in the bin with RPP range of 0 - 5%. At this point, all relationships are reporting RPPs essentially equal to 0%, and the SHM system is longer able to illustrate damage growth. An example illustrating the expected histogram pattern changes for gradual damage formation and growth is presented for C-SG-CB(1)-V in Fig. 5.69a. If sudden and extreme damage occurs in a cut-back region, most relationships are expected to immediately report “fail” assessments, and thus, the dominant bin is expected to remain dominant, but will be shifted to a bin with significantly lower RPPs (i.e. 5-10% or 0-5%). Predicted histogram changes for sudden damage formation and growth are illustrated for C-SG-CB(1)-V in Fig. 5.69b.

Reviewing comparative histogram charts such as those presented in Figs. 5.67 - 5.69 for each TS allows one to estimate the location of the damage within a cut-back region. The TSs closest to the damage are expected to have the largest and most obvious changes in their histogram patterns, and those farther away from the damage will experience less change or perhaps no change at all. Thus, from the preceding discussion, it is predicted that three characteristics of damage are detectable through use of the evaluation reports:

- The presence of damage through identification of a change in the histogram patterns of one or more TSs.

www.manaraa.com

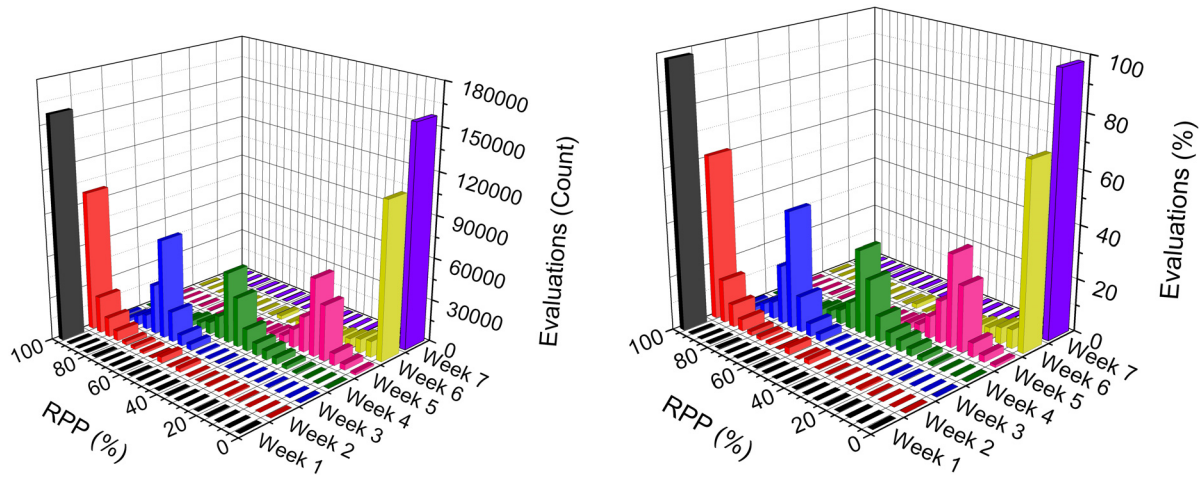

a. Gradual damage development and growth

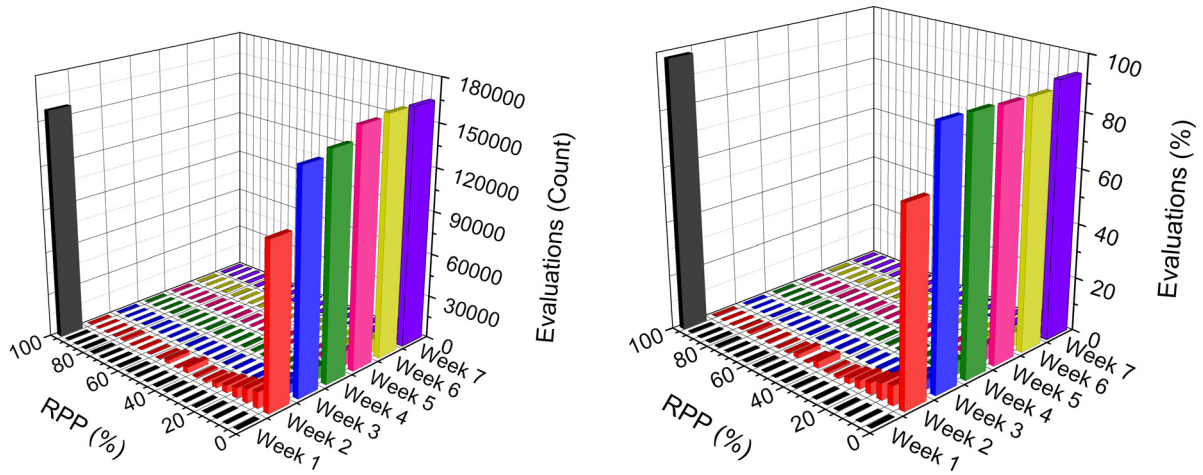

b. Sudden damage development and growth

Figure 5.69. C-SG-CB(1)-V: Predicted changes in histogram patterns damage formation and growth.

- The growth of damage through continued changes in histogram patterns among several sequential histograms for one or more TSs.
- The location of damage through identification of TSs that experienced histogram changes.

To determine the damage characteristics, however, the evaluation results must be reviewed and correctly interpreted by the bridge owner. As a result of presenting information in this way, the owner is able to decide when behavior has changed in the cut-back region and if there is the possibility of structural damage. Not only does this approach essentially eliminate the possibility of false alarms, but it also addresses criticisms of SHM that were presented Section 2.4. First, the

www.manaraa.com

visual format of the evaluation reports allows for easier interpretation of results by owners and managers for decision making on maintenance and management. Secondly, the presentation of the evaluation results is standardized, and the consistency of diagnostic methods depends on the owner that interprets the results.

Reviewing the four levels of damage detection presented in Section 2.3.1, proper use and interpretation of evaluation results from the FCB SHM system is predicted to allow for level two damage detection. This level of damage detection, and the success of the system as a whole, depends on the ability to identify and install TSs in damage-prone regions of the bridge and NTSs in locations of the bridge that are not prone to damage. While its ability to measure behavior change due to damage formation has not been proved, evaluation results presented in Figs. 5.68a-g have proven that the system has been stable and has recorded repeatable bridge behavior for more than 33 weeks of monitoring.

5.4 SHM System Performance and Distribution

The FCB SHM software, *Master FCB SHM System.vi*, is installed as a service on the local computer at the US30 bridge. By operating as a service, the program is able to restart if there is a power outage at the bridge site. Every time the program starts, it pauses for two minutes to allow the si425-500 to initialize, and then the monitoring process automatically begins. When the subVI, *Synchronized Evaluation and Report Generation.vi*, is called to evaluate a data file, it checks for the existence of the text files illustrated in Fig. 5.66a. If the files do not exist, the subVI assumes that the SHM system has just started the monitoring process, and thus, autonomously creates the files. If the files already exist, information is retrieved from the files to determine the point from which to resume in the evaluation and report generation process. With this configuration, the SHM system is able to resume from any intentional or unintentional system shut down.

Typical statistics for the FCB SHM system at the US30 bridge during 33 weeks of operation are as follows:

- Raw strain data are saved in approximately one MB file sizes, and approximately 3.4 gigabytes (GB) of raw strain data are collected in 24 hours.

www.manaraa.com

- The average time that is required to complete phases 2 - 6 of the reduction and evaluation process for each data file has been approximately 1.68 seconds. The time ranges from one to seven seconds, depending on the number of extrema that are extracted from within the data file.
- The average time that is required to generate a daily report from a RPP data file is has been approximately 8.7 seconds. The time required to generate a report has been observed to be essentially independent of the day of week for which it is being created.
- The extrema that are extracted from the data files and evaluated to assess the structural behavior of the bridge constitute, on average, 0.13% of the raw data that are collected. Percentages range from 0.01% to 0.38%, depending on the number of extrema that are extracted from within the data file.
- Matched extrema are saved following evaluation, but raw data files are deleted. The matched extrema files that are saved constitute approximately 5.5% of the uncompressed data size.

Based on the time requirements to perform each of the operations, the processing of one data file and potential report generation thereafter should always be finished before a new data file is created. The success of this rapid evaluation can be attributed to the fact that only the event extrema are being evaluated, rather than the entire data set. However, if there is unexpected overlap with processing and file creation, the software is designed to allow for file backup in the intermediate save directory until the normal one-to-one sequencing resumes.

As illustrated in Fig. 5.38b, controls are set in the US30 SHM system to save only the matched extrema and not the raw data. With this storage format, the available storage space on the local computer system is extended by approximately 94.5%. This option was included to address the data management and storage criticism of SHM, which was previously mentioned in Section 2.4.

The SHM system software, *Master FCB SHM System.vi*, performs as one system, but as previously presented, it is essentially composed of two components. The first component is the software that communicates with the data acquisition equipment to collect and store data, which is usually supplied by the equipment manufacturer. The second component is the subVI, *Synchronized Evaluation and Report Generation.vi*, which is called by the data collection component to reduce and evaluate a data file after it has been created. In addition, all programs that are used to train the SHM system were designed to be independent of the hardware that collects the data. With this software

www.manaraa.com

design, the VIs and subVIs that were developed in this research are usable with any data acquisition system and software as long as they are programmed to autonomously perform the following:

- Save continuous strain data in files with specified sizes
- Save data files in columns with tab delimited format, where the column zero is the timestamp, column one is the buffer, and all remaining columns compose the sensor array
- Use the subVI, *Create File Name.vi*, to name the saved data files, or develop code to name that data files in a format that is identical to that which is created by *Create File Name.vi*
- Be able to call the subVI, *Synchronized Evaluation and Report Generation.vi*, to perform the data reduction, evaluation, and report generation procedures after a data file has been saved.

Since the subVI, *Remove Zero Flicker.vi*, was specifically created to address filtering needs in the data collection utility of the si425-500 for this project, it is recommended that this subVI be removed from the SHM system software if it is used with other data acquisition systems.

www.manaraa.com

6. SUMMARY AND CONCLUSIONS

6.1 Summary

The FCB SHM system that was developed in this investigation enables bridge owners to remotely monitor bridges for gradual or sudden damage formation. The strain-based SHM system is trained with measured performance data to identify typical bridge responses when subjected to ambient traffic loads, and the knowledge that is learned during the training is used to evaluate newly collected data. At specified intervals, the SHM system autonomously generates evaluation reports that summarize the current behavior of the bridge. The evaluation reports are collected and distributed to the bridge owner for interpretation and decision making.

Hardware components that were selected for use in the FCB SHM were tested and scrutinized to validate their performance prior to installation in the US30 demonstration bridge. Fiber bragg grating FOSs with various sizes of CFRP packaging (See Table A1) and bonding adhesives (Appendix B) were researched and laboratory tested. In the testing, FOSs were bonded to steel coupons and subjected to cyclic tensile loads as well as sustained tensile loads. Results of the testing revealed that the 210x20mm SMS bonded with Loctite 392 adhesive proved to accurately measure cyclic mechanical strains. During high frequency and high magnitude cyclic testing, as well as during sustained loadings on the 15x20mm SMSs, it was revealed that the reduced CFRP packaging size created a condition that resulted in viscoelastic effects in the eight adhesives that were tested. When tested at the lower magnitudes and frequencies that were expected in the cut-back regions of the US30 bridge, however, the 15x20mm SMS bonded with Loctite H4500 was proven to be the only sensor/adhesive combination to be free of viscoelastic effects. Therefore, the following sensors and adhesives were determined to be adequate for use in the SHM system:

- 210x20mm SMSs bonded with Loctite 392 adhesive (Loctite 7387 activator)
- 15x20mm SMSs bonded with Loctite H4500 adhesive
- 220x20mm SMAs bonded with Loctite H4500 adhesive

As follow-up testing to further investigate the viscoelasticity that occurred in the adhesives, unpackaged FBGs were bonded to a steel coupon with the same adhesives that were previously

www.manaraa.com

used, and the testing was repeated. Results revealed that removal of the CFRP packaging eliminated viscoelasticity in nearly all adhesives.

Following installation of the 40 FOSs and accompanying hardware at the US30 bridge, the sensor/adhesive combinations were tested to validate their field performance when subjected to ambient traffic loadings in the presence of environmental conditions. In this testing, eight BDI sensors were installed next to FOSs, and comparisons were conducted between measurements that were obtained from each sensing technology. For all sets of sensors that were considered to capture the same structural response, there was excellent agreement between the FOSs and BDI sensors for both zeroed and filtered data sets. As a result, performances of the FOSs and hardware components of the system were validated and determined to be adequate for use in the FCB SHM system.

After all hardware components were installed and verified to be working correctly, the training process was initiated. In training mode, strain data are collected at the bridge and used to help the SHM system learn how to identify typical bridge performance. During this process for the US30 bridge, PSD plots were developed and used to configure a lowpass IIR Chebyshev filter for each FOS, which were utilized to remove dynamic responses from the strain data. Moreover, parameters for identification of quasi-static event extrema were determined. With these settings and parameters, one week of training data was filtered and event extrema were extracted and used to establish 415 relationships among TSs and NTSs in the bridge, which were comprised of MAMARs, MAMIRs, MIMARS, and MIMIRs. After limit sets were defined for each relationship, training was complete. For each step in the training process, a program with a GUI was developed and utilized. With the exception of defining limit sets, minimal user interaction was required to perform the training operations.

With the training process complete, the monitoring process was activated in the US30 SHM system. In this completely autonomous mode, the information obtained during the training is used to reduce future data and evaluate all TS extrema. In this process, strain records in data files are zeroed, filtered, and event extrema are extracted. After the matching process is completed for all extrema, the resulting matches are evaluated, and RPPs are collected. As this procedure is

www.manaraa.com

conducted, reports are autonomously generated that include two histograms for each collection of TS RPPs. The first histogram reports numerical counts of RPPs for each bin, and the second standardizes the contents of the first histogram, and thus, reports the contents of each bin as a percentage of the total evaluations that were performed. In the US30 SHM system, daily evaluation reports are generated, and an example is provided in Appendix G. After a report is generated, it is collected by a FTP utility and delivered to the bridge engineer for interpretation and decision making. By comparing consecutive reports for each sensor as illustrated in this research, it is expected that damage in the target region of the bridge will be detectable through one or both of the following:

- Gradual or sudden changes in histogram patterns that report lower RPPs for evaluations that were performed.
- Extreme changes in the numerical counts of evaluations that were performed during a report time period (relative to those that were typical) for each TS.

Since it is also predicted that the presence, growth, and general location of damage is detectable through correct interpretation of results, this SHM system is considered to be capable of achieving level two damage detection.

During the development of this SHM system, effort was given to reduce the obstacles that are considered to hinder practitioner acceptance of SHM. First, two options were included in the system that allow the user to specify the type of information that is to be saved, which addresses data management criticisms. One option is to compress and save all contents of the raw data files, and another option is to save only the matched extrema from the evaluation process. One or both options may be selected, but if only the second option is selected, the bridge owner has immediate access to reduced data instead of full data files. Such information is useful for viewing the trends of the resulting matched extrema as well as the extrema that are obtained from each vehicle that traversed the bridge. In addition, storing only the matched extrema makes much better use of the available hard drive space.

In addition to improving data storage procedures, significant effort was given to improve the methods that are used to present evaluation results to bridge owners. With the histogram approach developed and utilized in this research, identification of damage in the results merely requires visual

www.manaraa.com

review of graphs and does not require further calculations or understanding of one or more parameters that are calculated by the SHM system. By presenting the results in this familiar format, it is expected that bridge owners or managers will be more comfortable with interpretation of evaluation results. Finally, since the SHM system results require visual interpretation, bridge owners remain involved in the monitoring process, and the likelihood of false alarms has been essentially eliminated.

The training and evaluation programs have been developed to be independent of the hardware that is involved with the data collection process. As a result, the SHM system is versatile in that it can be used with any hardware as long as the data is stored in the same manner as that illustrated in this project, and as long as the accompanying system is able to call the evaluation programs. Thus, if the SHM system software is utilized with other data collection systems, additional programming will be required to the data collection software that accompanies those systems. If used with the si425-500 interrogator, however, the FCB SHM system is completely packaged for distribution and use by the Iowa DOT and/or other bridge owning agencies.

6.2 Conclusions

Considering all aspects of this investigation, the following conclusions can be made about the development, installation, and performance of the FCB SHM system:

- Through 33 weeks of operation in the US30 bridge, the FCB SHM system has been proven to be reliable and capable of autonomously collecting and evaluating continuous strain data for steel girder bridges that support one-way traffic.
- Review of bridge evaluation reports has proven the ability of the SHM system to continually identify and evaluate repeatable bridge behavior. The consistency of the standardized histograms among the 33 weeks of monitoring illustrates that the structural behavior in target regions of the bridge has not changed. Since damage has not occurred, however, the ability of the system to detect damage has not been proven or disproved.
- Success of the SHM system depends on the ability to identify and place TSs in the damage-prone regions of the bridge and NTSs in the regions of the bridge that are not prone to damage. Fortunately in the FCBs, the cut-back regions are the known problematic areas that are susceptible to fatigue crack formation.
- Due to consistency among the standardized histogram patterns for the 33 weeks of monitoring, the SHM system has been proven to be unaffected by environmental changes. Temperatures during this period varied from -7°F (-22°C) to 100°F (38°C), which is a range of 107°F (60°C) [89]. For the US30 bridge, training the system during one season has been proven to be adequate for all seasons thus far.

www.manaraa.com

- The SHM system has been proven to be robust and capable of autonomously resuming the monitoring process after power outages have occurred. In addition, the long-range wireless technology incorporated into the system has been proven to be useful for both distributing evaluation reports as well as receiving software updates, if required. Thus, the SHM system has been proven to be capable of operating as a remote, stand-alone system.

- Success of the system can primarily be attributed to the following:

    - The significant laboratory testing that was performed on the FOSs and various adhesives, which was used to aid sensor and adhesive selection to ensure quality measurements.
    - The pattern recognition training and monitoring approaches that utilized relationships among TSs and NTSs, which resembled those of bivariate control charts.

- The FCB SHM system is immediately deployable to FCBs or girder bridges that support one-way traffic. The training and evaluation software that was developed is able to be used with any type of data collection system as long as the data collection system meets the requirements listed in Section 5.4.

www.manaraa.com

7. RECOMMENDED RESEARCH

Additional research is recommended to further enhance the FCB SHM system and to acquire more information about its capabilities. A brief description of several items that should be investigated are listed below, with brief discussion of each bulleted item in the paragraphs that follow:

- To give bridge owners an estimate of the degree of damage that is detectable by the SHM system, finite element analyses should be conducted with progressive levels of damage in the cut-back regions. In addition, the analyses should provide sequential histogram pattern changes that correlate to crack propagation. These results will serve as guides to the bridge owners to help quantify the size of the crack or damage based on the observed histogram patterns.

- To decrease the time required to train the system, mathematical methods should be investigated for developing limit sets that define the TS-NTS relationships. Such methods should allow the owner to define parameters that control the mathematical approach. As a result, the process of defining relationships will be faster and require less manual effort from the user, but still allow the user to control how the limits are defined.

- To increase the valuable information that is reported to the Iowa DOT, development of an accessory subVI should be investigated to help the system to distinguish between cars, straight trucks, and semis. Such an add-on could compliment the system and provide details about the composition and density of traffic that utilizes the US30 bridge.

- To increase the versatility of the SHM system, further development should be considered to make it applicable for use with girder bridges that support two-way traffic.

- To increase the damage detection range of the SHM system, further development should be considered to allow for sensors to serve as both TSs and NTSs.

For the finite element analysis, it is recommended that two levels of modeling be used: (1) a coarse model that is developed from shell elements and subjected to various vehicular loads and combinations, and (2) fine submodels of the cut-back regions that utilize brick elements, as well as boundary conditions and shape functions that are determined from the coarse model. Submodeling is beneficial because it allows for more detailed modeling that is required to achieve accurate strains in localized regions, and in addition, provides for more control over the degree of damage and crack propagation that is modeled in the cut-back regions. After the analyses have been conducted with various levels of damage in cut-back regions, the magnitudes of change should be determined for matched extrema. With these results, histogram pattern changes should be investigated to determine the theoretical level of damage that is detectable by the system.

www.manaraa.com

It is perceived that mathematical development of limit sets can be accomplished by utilizing linear least squares fitting techniques. Upper and lower limits can be defined as three standard deviations above and below the linear fit to the matched extrema, respectively, and thus creating a 99.7% confidence interval similar to the methods of traditional control charts. Moreover, controls could be incorporated that allow the user to select the desired confidence interval that is to be achieved during development of the limit sets. To autonomously perform these mathematical operations, however, the software must be capable of first identifying the number of limit sets that are required to define a relationship, and then segregate the data accordingly as to the matched extrema that are to be used for each least squares fit.

The vehicular events within the strain records of sensors on stringers (both vertical and horizontal) theoretically change more than those on girders due to variations in the geometries of the vehicles that cross the bridge. Using this information, it is predicted that a subVI could be created to identify the types of vehicles within the traffic volumes that traverse the bridge. The subVI could potentially use the frequencies of the quasi-static events, the number and type of extrema produced in each event, or perhaps the magnitudes of the extrema in each event to identify vehicle types. In order to perform these operations, however, the filter cut-off frequencies for the sensors on the stringers must be adjusted to capture the localized responses in the strain records, rather than the current settings that identify the global bridge responses in the records.

To make the SHM system applicable for bridges with two-way traffic, the matching subVI must be adjusted. Instead of projecting the NTS window in one direction within a NTS strain record, it must project the window in two directions (forward and backward in the NTS record) to find the corrected extrema match. With this method of matching, however, it is likely that the number of indirect matches or mismatches will increase. One possible alternative is to use pattern recognition among TS and NTS strain records to identify the direction of traffic and to perform the matching process. With either method, however, the relationships that are formed will now be related to the direction of the traffic, and thus, the evaluation subVI must be correspondingly adjusted to identify the applicable relationships for each extrema evaluation.

www.manaraa.com

For sensors to serve as both TSs and NTSs, the elements within the matching and evaluation subVIs in the LabVIEW code must be removed that separate operations based on the classification of the sensors. In addition, the code must be adequately adjusted such that operations are conducted based on sensors serving as both TSs and NTSs. For a given number of sensors, this change will create more relationships that require limit sets. As a result, it is recommended that this research be conducted after the development of mathematical methods that establish limit sets.

www.manaraa.com

APPENDIX A: FOS SPECIFICATIONS

www.manaraa.com

Table A1. FOS specifications for laboratory validation testing.

FOS Name	Test Used	Packaging	Dimensions (LxWxD)		Grating Length (mm)	Fiber Type	Recoating	Bandwidth @ 3 dB (nm)	Minimum Reflectivity (%)	Proof Test (kpsi)	Grating Profile
			English (in.)	Metric (mm)							
Unpackaged FBG	CT1, CT2	NA	NA	NA	10	SMF28	Acrylate	< 0.3	90	> 100	Apodized with SLSR =12 db
210x20mm SMS	CT1, CT2	CFRP	8.26x0.8x0.04	210x20x1	10	SM Polyimide	Polyimide	< 0.3	90	> 100	Apodized with SLSR =12 db
15x10mm SMS	CT1, CT2	CFRP	0.59x0.4x0.04	15x10x1	5	SM Polyimide	Polyimide	< 0.5	90	> 100	Apodized with SLSR =12 db
15x20mm SMS	CT3, CT4, CT5, CT6	CFRP	0.59x0.8x0.04	15x20x1	5	SM Polyimide	Polyimide	< 0.5	85	> 100	Apodized with SLSR =12 db
44x12mm SWS	CT7, CT8	SS	1.73x0.47x0.08	44x12x1	10	SMF28	Acrylate	< 0.3	90	> 100	Apodized with SLSR =12 db
27x12mm SWS	CT7, CT8	SS	1.06x0.47x0.08	27x12x1	5	SM Polyimide	Polyimide	< 0.5	85	> 100	Apodized with SLSR =12 db

Note: SM = Singlemode
CT = Coupon Test
NA = Not Applicable
SS = Stainless Steel
SMF = Singlemode Fiber
FBG = Fiber Bragg Grating
SWS = Surface-Weldable Sensor
SMS = Surface-Mountable Sensor
SLSR = Side Lobe Suppression Ratio
CFRP = Carbon Fiber Reinforced Polymer

www.manaraa.com

Table A2. Specifications and accessory information for FOSs in the US30 FCB SHM system.

	FOS	Sensor Type	Grating Length (mm)	CW (nm)	Location in Fiber		Packaging Dimensions (LxWxD)		Bandwidth @ -3 dB (nm)
					(ft)	(mm)	(in.)	(mm)	
Channel 1 (Fiber 1)	A-NS-WB-V	210x20mm SMS	10	1577.5	52.86	16.110	8.26x0.8x0.04	210x20x1	< 0.3
	A-SS-WB-V	210x20mm SMS	10	1582.5	66.93	20.400	8.26x0.8x0.04	210x20x1	< 0.3
	B-NG-BF-H	210x20mm SMS	10	1517.5	121.41	37.005	8.26x0.8x0.04	210x20x1	< 0.3
	B-NS-BF-H	210x20mm SMS	10	1522.5	169.01	51.513	8.26x0.8x0.04	210x20x1	< 0.3
	B-SS-BF-H	210x20mm SMS	10	1527.5	197.34	60.147	8.26x0.8x0.04	210x20x1	< 0.3
	B-SG-BF-H	210x20mm SMS	10	1532.5	221.40	67.479	8.26x0.8x0.04	210x20x1	< 0.3
	C-SG-BF-H	210x20mm SMS	10	1537.5	291.71	88.910	8.26x0.8x0.04	210x20x1	< 0.3
	C-FB(SS)-BF-H	210x20mm SMS	10	1542.5	308.14	93.918	8.26x0.8x0.04	210x20x1	< 0.3
	C-SS-WB-V	210x20mm SMS	10	1547.5	322.64	98.335	8.26x0.8x0.04	210x20x1	< 0.3
	C-SG-CB(5)-V	220x20mm SMA*	5	1552.5	338.48	103.165	8.26x0.8x0.04	210x20x1	< 0.5
	C-SG-CB(4)-V	220x20mm SMA*	5	1557.5	338.65	103.215	8.26x0.8x0.04	210x20x1	< 0.5
	C-SG-CB(3)-V	220x20mm SMA*	5	1562.5	338.81	103.265	8.26x0.8x0.04	210x20x1	< 0.5
	C-SG-CB(2)-V	220x20mm SMA*	5	1567.5	338.98	103.315	8.26x0.8x0.04	210x20x1	< 0.5
	C-SG-CB(1)-V	220x20mm SMA*	5	1572.5	339.14	103.365	8.26x0.8x0.04	210x20x1	< 0.5
Channel 2 (Fiber 2)	D-SG-BF-H	210x20mm SMS	10	1517.5	239.25	72.921	8.26x0.8x0.04	210x20x1	< 0.3
	D-SS-BF-H	210x20mm SMS	10	1522.5	267.66	81.578	8.26x0.8x0.04	210x20x1	< 0.3
	D-NS-BF-H	210x20mm SMS	10	1527.5	284.25	86.636	8.26x0.8x0.04	210x20x1	< 0.3
	D-NG-BF-H	210x20mm SMS	10	1532.5	311.99	95.091	8.26x0.8x0.04	210x20x1	< 0.3
	C-NG-BF-H	210x20mm SMS	10	1537.5	355.32	108.297	8.26x0.8x0.04	210x20x1	< 0.3
	C-FB(NS)-BF-H	210x20mm SMS	10	1542.5	372.00	113.381	8.26x0.8x0.04	210x20x1	< 0.3
	C-NS-WB-V	210x20mm SMS	10	1547.5	386.08	117.672	8.26x0.8x0.04	210x20x1	< 0.3
	C-NG-CB(5)-V	220x20mm SMA*	5	1552.5	402.34	122.628	8.26x0.8x0.04	210x20x1	< 0.5
	C-NG-CB(4)-V	220x20mm SMA*	5	1557.5	402.51	122.678	8.26x0.8x0.04	210x20x1	< 0.5
	C-NG-CB(3)-V	220x20mm SMA*	5	1562.5	402.67	122.728	8.26x0.8x0.04	210x20x1	< 0.5
	C-NG-CB(2)-V	220x20mm SMA*	5	1567.5	402.83	122.778	8.26x0.8x0.04	210x20x1	< 0.5
	C-NG-CB(1)-V	220x20mm SMA*	5	1572.5	403.00	122.828	8.26x0.8x0.04	210x20x1	< 0.5
Channel 3 (Fiber 3)	E-NG-BF-H	210x20mm SMS	10	1517.5	228.18	69.547	8.26x0.8x0.04	210x20x1	< 0.3
	E-NG-CB(5)-V	15x20mm SMS	5	1522.5	239.25	72.921	8.26x0.8x0.04	210x20x1	< 0.5
	E-NG-CB(1)-V	15x20mm SMS	5	1527.5	245.95	74.963	8.26x0.8x0.04	210x20x1	< 0.5
	E-NS-WB-V	210x20mm SMS	10	1532.5	261.04	79.562	8.26x0.8x0.04	210x20x1	< 0.3
	E-FB(NS)-BF-H	210x20mm SMS	10	1537.5	275.45	83.954	8.26x0.8x0.04	210x20x1	< 0.3
	E-FB(SS)-BF-H	210x20mm SMS	10	1542.5	289.87	88.349	8.26x0.8x0.04	210x20x1	< 0.3
	E-SS-WB-V	210x20mm SMS	10	1547.5	303.95	92.640	8.26x0.8x0.04	210x20x1	< 0.3
	E-SG-CB(5)-V	15x20mm SMS	5	1552.5	319.87	97.493	8.26x0.8x0.04	210x20x1	< 0.5
	E-SG-CB(1)-V	15x20mm SMS	5	1557.5	327.41	99.791	8.26x0.8x0.04	210x20x1	< 0.5
	E-SG-BF-H	210x20mm SMS	10	1562.5	338.31	103.113	8.26x0.8x0.04	210x20x1	< 0.3
	F-SG-BF-H	210x20mm SMS	10	1567.5	417.93	127.380	8.26x0.8x0.04	210x20x1	< 0.3
	F-SS-BF-H	210x20mm SMS	10	1572.5	463.02	141.121	8.26x0.8x0.04	210x20x1	< 0.3
	F-NS-BF-H	210x20mm SMS	10	1577.5	496.37	151.287	8.26x0.8x0.04	210x20x1	< 0.3
	F-NG-BF-H	210x20mm SMS	10	1582.5	530.57	161.709	8.26x0.8x0.04	210x20x1	< 0.3

Note:

SM = Singlemode
CW = Center Wavelength
FBG = Fiber Bragg Grating
SMS = Surface-Mountable Sensor
SLSR = Side Lobe Suppression Ratio
CFRP = Carbon Fiber Reinforced Polymer

* All within the same packaging

For all FOSs:

Packaging Material: CFRP
Fiber Type: SM Polyimide
FBG Recoating: Polyimide
Minimum Reflectivity: 85%
Proof Test: 100 kpsi
Grating Profile: Apodized with SLSR = 12 db

www.manaraa.com

Sensor:

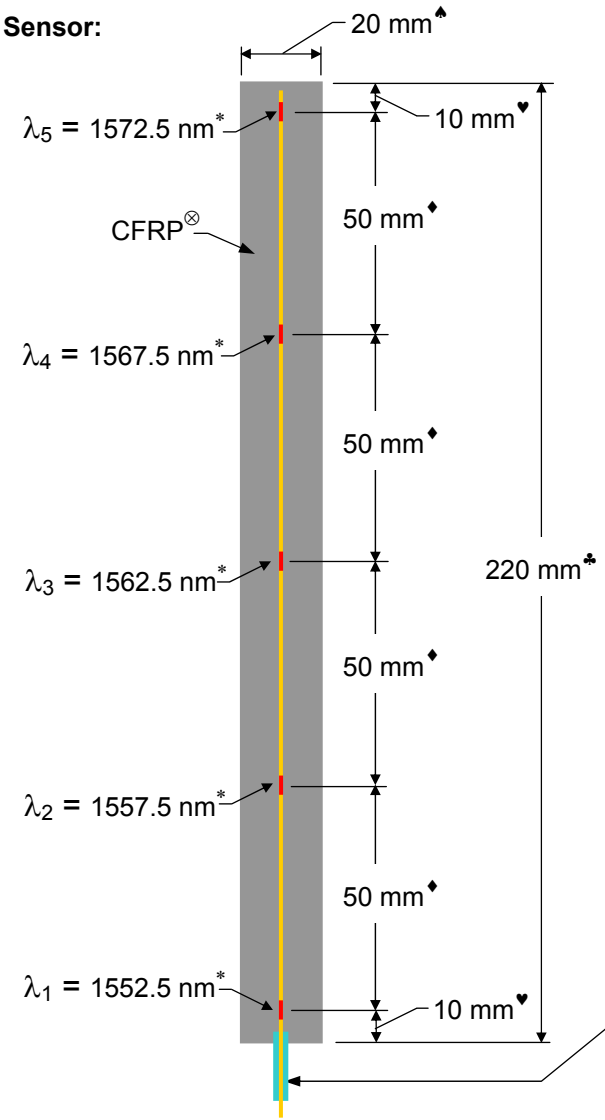

Lead Pigtail:
- 1.0m length
- No connector
- 900µm furcation tubing

Specifications:

FBGs:
- Designated center wavelengths, λ_i
- Grating Lengths = 5 mm
- Bandwidth < 0.5 nm

Fiber:
- SM Polyimide
- 900µm furcation tubing on lead pigtail
- Connector: None

Tolerances:

* ± 0.5 nm

⊗ FRP Thickness: 1 mm ± 0.5 mm

♠ ± 1 mm

♦ ± 5 mm

♥ No defined tolerance. Dimension is assumed to be the required length to adequately hold 0.9mm loose tube on pigtail. Distance can be adjusted, if needed, to ensure that the overall length of the sensor does not exceed 220 mm.

♣ No defined tolerance. Dimension is to be the overall length of the sensor while still meeting tolerance requirements for all other dimensions. Dimension (overall length of sensor) must not exceed 220 mm.

Figure A1. Specifications of the 220x20mm SMAs.

www.manaraa.com

APPENDIX B: ADHESIVE SPECIFICATIONS

www.manaraa.com

Technical Data Sheet

LOCTITE® 330

July 2004

PRODUCT DESCRIPTION

LOCTITE® 330 provides the following product characteristics:

Technology	Acrylic
Chemical Type	Urethane methacrylate ester
Appearance (uncured)	Slightly cloudy, colorless to pale yellow liquid[LMS]
Components	One component - requires no mixing
Viscosity	High
Cure	Anaerobic with activator
Application	Bonding

LOCTITE® 330 is a general purpose adhesive is used to bond metal, wood, ferrite, ceramic and plastic materials. Applications include tool handles, appliances, sporting goods and decorative trim.

TYPICAL PROPERTIES OF UNCURED MATERIAL

Specific Gravity @ 25 °C	1.05
Flash Point - See MSDS	
Viscosity, Brookfield - RVT, 25 °C, mPa·s (cP):	
Spindle 7, speed 20 rpm	45,000 to 90,000[LMS]
Viscosity, EN 12092 - SV, 25 °C, after 180 s, mPa·s (cP):	
Shear rate 20 s^{-1}	30,000 to 70,000

TYPICAL CURING PERFORMANCE

Cure Speed vs. Substrate

The rate of cure will depend on the substrate used. The graph below shows the shear strength developed with time on grit blasted steel lap shears and tested according to ISO 4587. (Activator 7387 applied to one surface)

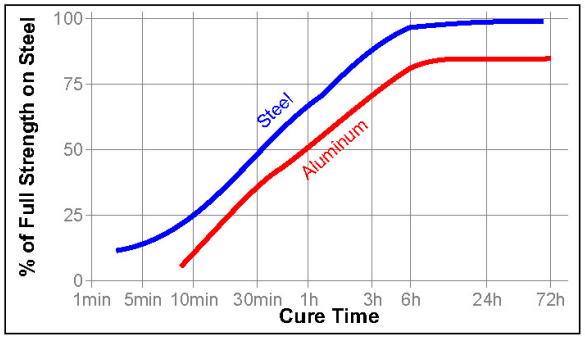

Cure Speed vs. Bond Gap

The rate of cure will depend on the bondline gap. The following graph shows shear strength developed with time on grit blasted steel lap shears at different controlled gaps and tested according to ISO 4587. (Activator 7387 applied to one surface.)

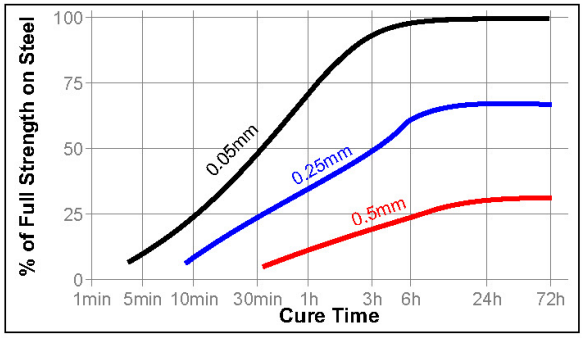

TYPICAL PROPERTIES OF CURED MATERIAL

Physical Properties:

Coefficient of Thermal Expansion, ASTM D 696, K^{-1}	8×10^{-6}
Coefficient of Thermal Conductivity, ASTM C 177, W/(m·K)	0.10
Specific Heat, kJ/(kg·K)	0.30

TYPICAL PERFORMANCE OF CURED MATERIAL

Adhesive Properties

After 24 hours @ 22 °C, Activator 7387 on 1 side

Lap Shear Strength, ISO 4587:

Mild steel (grit blasted)	N/mm²	15 to 30
	(psi)	(2,175 to 4,350)

Tensile Strength, ISO 6922:

Mild steel (grit blasted)	N/mm²	12 to 22
	(psi)	(1,740 to 3,190)

After 24 hours @ 22 °C, Activator 7387 or 7386 on 2 sides

Tensile Strength, ISO 6922:

Mild steel (grit blasted)	N/mm²	≥16.50[LMS]
	(psi)	(≥2,390)

TYPICAL ENVIRONMENTAL RESISTANCE

Cured for 1 week @ 22 °C, Activator 7387 on 1 side

Lap Shear Strength, ISO 4587:

Mild steel (grit blasted):

0.25 mm gap

Hot Strength

Tested at temperature

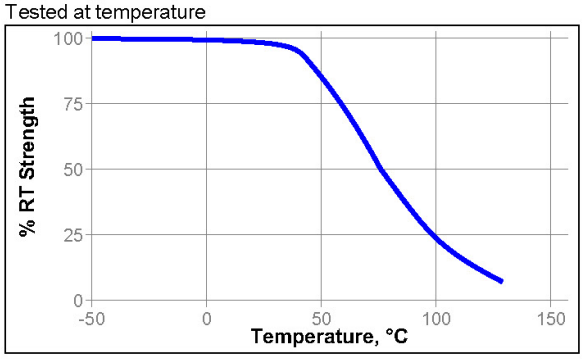

Henkel Technologies

www.manaraa.com

Heat Aging
Aged at temperature indicated and tested @ 22 °C

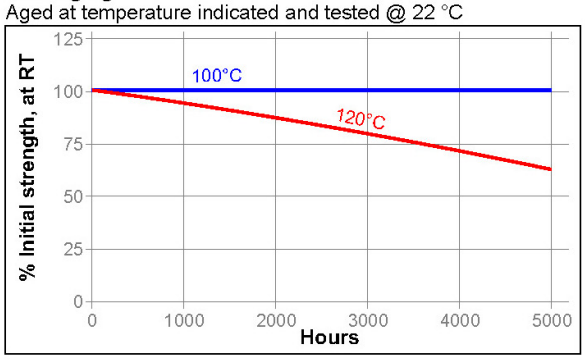

Chemical/Solvent Resistance
Aged under conditions indicated and tested @ 22 °C.

		% of initial strength	
Environment	**°C**	**350 hr**	**720 hr**
Acetone	22	10	10
Motor Oil	87	90	66
Unleaded Gasoline	22	20	20
Phosphate ester	87	93	75
Water Glycol 50/50	87	60	60

GENERAL INFORMATION

This product is not recommended for use in pure oxygen and/or oxygen rich systems and should not be selected as a sealant for chlorine or other strong oxidizing materials.

For safe handling information on this product, consult the Material Safety Data Sheet (MSDS).

Where aqueous washing systems are used to clean the surfaces before bonding, it is important to check for compatibility of the washing solution with the adhesive. In some cases these aqueous washes can affect the cure and performance of the adhesive.

Directions for use

1. For best performance bond surfaces should be clean and free from grease.
2. To ensure a fast and reliable cure, Activator 7387 or 7386 should be applied to one of the bond surfaces and the adhesive to the other surface. Parts should be assembled within 15 minutes.
3. The recommended bondline gap is 0.1mm. Where bond gaps are large (up to a maximum of 0.5 mm), or faster cure speed is required, Activator 7387 or 7386 should be applied to both surfaces. Parts should be assembled immediately (within 1 minute).
4. Excess adhesive can be wiped away with organic solvent.
5. Bond should be held clamped until adhesive has fixtured.
6. Product should be allowed to develop full strength before subjecting to any service loads (typically 24 to 72 hours after assembly, depending on bond gap, materials and ambient conditions).

Loctite Material Specification[LMS]
LMS dated March 11, 1996. Test reports for each batch are available for the indicated properties. LMS test reports include selected QC test parameters considered appropriate to specifications for customer use. Additionally, comprehensive controls are in place to assure product quality and consistency. Special customer specification requirements may be coordinated through Henkel Loctite Quality.

Storage
Store product in the unopened container in a dry location. Storage information may be indicated on the product container labeling.
Optimal Storage: 8 °C to 21 °C. Storage below 8 °C or greater than 28 °C can adversely affect product properties
Material removed from containers may be contaminated during use. Do not return product to the original container. Henkel Corporation cannot assume responsibility for product which has been contaminated or stored under conditions other than those previously indicated. If additional information is required, please contact your local Technical Service Center or Customer Service Representative.

Conversions
(°C x 1.8) + 32 = °F
kV/mm x 25.4 = V/mil
mm / 25.4 = inches
N x 0.225 = lb
N/mm x 5.71 = lb/in
N/mm^2 x 145 = psi
MPa x 145 = psi
N·m x 8.851 = lb·in
N·mm x 0.142 = oz·in
mPa·s = cP

Note
The data contained herein are furnished for information only and are believed to be reliable. We cannot assume responsibility for the results obtained by others over whose methods we have no control. It is the user's responsibility to determine suitability for the user's purpose of any production methods mentioned herein and to adopt such precautions as may be advisable for the protection of property and of persons against any hazards that may be involved in the handling and use thereof. In light of the foregoing, **Henkel Corporation specifically disclaims all warranties expressed or implied, including warranties of merchantability or fitness for a particular purpose, arising from sale or use of Henkel Corporation's products. Henkel Corporation specifically disclaims any liability for consequential or incidental damages of any kind, including lost profits.** The discussion herein of various processes or compositions is not to be interpreted as representation that they are free from domination of patents owned by others or as a license under any Henkel Corporation patents that may cover such processes or compositions. We recommend that each prospective user test his proposed application before repetitive use, using this data as a guide. This product may be covered by one or more United States or foreign patents or patent applications.

Trademark usage
LOCTITE is a trademark of Henkel Corporation

Reference 1

www.manaraa.com

Technical Data Sheet

LOCTITE® 392™

June 2005

PRODUCT DESCRIPTION

LOCTITE® 392™ provides the following product characteristics:

Technology	Acrylic
Chemical Type	Modified acrylic
Appearance (uncured)	Translucent beige to dark amber[LMS]
Components	One component - requires no mixing
Viscosity	Medium
Cure	Activator
Secondary Cure	Heat
Application	Bonding

LOCTITE® 392™ may be used for applications which require very fast assembly. This adhesive is particularly suited to DC motor assembly, magnet bonding and bonding of pre-coated sheet metal. Automated assembly lines with short cycle times will benefit from the rapid cure charecteristics of LOCTITE® 392™. The product has the capability to produce tough, durable bonds with outstanding impact and peel resistance.

TYPICAL PROPERTIES OF UNCURED MATERIAL

Specific Gravity @ 25 °C	1.16
Flash Point - See MSDS	
Viscosity, Brookfield - HBT, 25 °C, mPa·s (cP):	
Spindle TA, speed 2.5 rpm, Helipath	20,000 to 80,000[LMS]
Spindle TA, speed 20 rpm, Helipath	6,500 to 17,500[LMS]

TYPICAL CURING PERFORMANCE

LOCTITE® 392™ is designed to be used with Activator 7380™ or 7387™ and cured at room temperature. Cure charecteristics are measured by determining fixture time (handling time) and speed of cure.

Fixture Time

Fixture time is defined as the time to develop a shear strength of 0.1 N/mm² .

Fixture Time, ISO 4587, seconds:	
Steel, with Activator 7380™ on 1 side:	
0 gap	≤25
0.25 mm gap	≤330

Cure Speed vs. Activator

The graph below shows shear strength developed with time using Activator 7380™ on steel lap shears and tested according to ISO 4587.

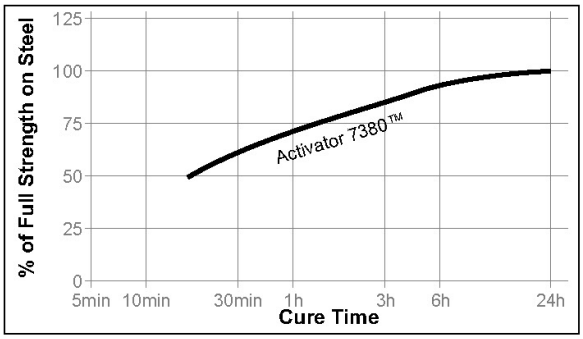

Cure Speed vs. Temperature

Heat can be used to effect or accelerate cure when surface priming operations are undesireable. Typical heat cure conditions consist of heating and maintaining bondline at a temperature shown in the graph below for the corresponding time specified. Optimum conditions for heat cure should be determined on the actual assemblies.

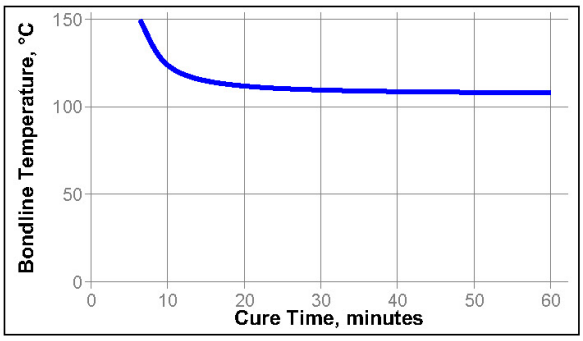

TYPICAL PROPERTIES OF CURED MATERIAL

Physical Properties:

Shore Hardness, ISO 868, Durometer D		65
Elongation, ISO 527, %		130
Tensile Strength, ISO 527	N/mm²	18.6
	(psi)	(2,700)
Tensile Modulus, ISO 527	N/mm²	144.8
	(psi)	(21,000)

TYPICAL PERFORMANCE OF CURED MATERIAL

Adhesive Properties

After 24 hours @ 22 °C, Activator 7380™ on 1 side

Lap Shear Strength, ISO 4587:		
Steel	N/mm²	≥11.7[LMS]
	(psi)	(≥1,696)

Henkel Technologies

www.manaraa.com

After 48 hours @ 22 °C, Activator 7380™ on 1 side

Lap Shear Strength, ISO 4587:

Steel :		
0 gap	N/mm²	17.2
	(psi)	(2,500)
0.25 mm gap	N/mm²	15.8
	(psi)	(2,300)
0.5 mm gap	N/mm²	14.5
	(psi)	(2,100)
Aluminum :		
0 gap	N/mm²	11
	(psi)	(1,600)
Zinc dichromate :		
0 gap	N/mm²	11
	(psi)	(1,600)

TYPICAL ENVIRONMENTAL RESISTANCE

After 48 hours @ 22 °C, Activator 7380™ on 1 side

Heat Aging

Heat aged for 2000 hours

Lap Shear Strength, ISO 4587:

Steel:		
@ 93°C	N/mm²	13.1
	(psi)	(1,900)
@ 121°C	N/mm²	9
	(psi)	(1,300)
@ 150°C	N/mm²	3.4
	(psi)	(500)

Humidity Resistance

Conditioned in 50°C condensing humidity

Lap Shear Strength, ISO 4587:

Steel:		
1 week	N/mm²	13
	(psi)	(1,900)
2 weeks	N/mm²	9.3
	(psi)	(1,350)
4 weeks	N/mm²	3.4
	(psi)	(500)

Chemical/Solvent Resistance

Aged under conditions indicated and tested @ 22 °C.

		% of initial strength
Environment	**°C**	**720 h**
Air reference	87	100
Water/glycol 50/50	87	30
Gasoline	87	10
Motor oil (MIL-L-46152)	87	100

GENERAL INFORMATION

This product is not recommended for use in pure oxygen and/or oxygen rich systems and should not be selected as a sealant for chlorine or other strong oxidizing materials.

For safe handling information on this product, consult the Material Safety Data Sheet (MSDS).

Directions for use

1. For best performance bond surfaces should be clean and free from grease.
2. To ensure a fast and reliable cure, Activator 7380™ or 7387™ should be applied to one of the bond surfaces and the adhesive to the other surface. Parts should be assembled within 15 minutes.
3. The recommended bondline gap is 0.1mm. Where bond gaps are large (up to a maximum of 0.5 mm), or faster cure speed is required, Activator 7380™ or 7387™ should be applied to both surfaces. Parts should be assembled immediately (within 1 minute).
4. Excess adhesive can be wiped away with organic solvent.
5. Bond should be held clamped until adhesive has fixtured.
6. Product should be allowed to develop full strength before subjecting to any service loads (typically 24 to 72 hours after assembly, depending on bond gap, materials and ambient conditions).

Loctite Material Specification[LMS]

LMS dated January 3, 2003. Test reports for each batch are available for the indicated properties. LMS test reports include selected QC test parameters considered appropriate to specifications for customer use. Additionally, comprehensive controls are in place to assure product quality and consistency. Special customer specification requirements may be coordinated through Henkel Quality.

Storage

Store product in the unopened container in a dry location. Storage information may be indicated on the product container labeling.

Optimal Storage: 8 °C to 21 °C. Storage below 8 °C or greater than 28 °C can adversely affect product properties. Material removed from containers may be contaminated during use. Do not return product to the original container. Henkel Corporation cannot assume responsibility for product which has been contaminated or stored under conditions other than those previously indicated. If additional information is required, please contact your local Technical Service Center or Customer Service Representative.

Conversions

(°C x 1.8) + 32 = °F
kV/mm x 25.4 = V/mil
mm / 25.4 = inches
µm / 25.4 = mil
N x 0.225 = lb
N/mm x 5.71 = lb/in
N/mm² x 145 = psi
MPa x 145 = psi
N·m x 8.851 = lb·in
N·m x 0.738 = lb·ft
N·mm x 0.142 = oz·in
mPa·s = cP

www.manaraa.com

Note

The data contained herein are furnished for information only and are believed to be reliable. We cannot assume responsibility for the results obtained by others over whose methods we have no control. It is the user's responsibility to determine suitability for the user's purpose of any production methods mentioned herein and to adopt such precautions as may be advisable for the protection of property and of persons against any hazards that may be involved in the handling and use thereof. In light of the foregoing, **Henkel Corporation specifically disclaims all warranties expressed or implied, including warranties of merchantability or fitness for a particular purpose, arising from sale or use of Henkel Corporation's products. Henkel Corporation specifically disclaims any liability for consequential or incidental damages of any kind, including lost profits.** The discussion herein of various processes or compositions is not to be interpreted as representation that they are free from domination of patents owned by others or as a license under any Henkel Corporation patents that may cover such processes or compositions. We recommend that each prospective user test his proposed application before repetitive use, using this data as a guide. This product may be covered by one or more United States or foreign patents or patent applications.

Trademark usage

Except as otherwise noted, all trademarks in this document are trademarks of Henkel Corporation in the U.S. and elsewhere. ® denotes a trademark registered in the U.S. Patent and Trademark Office.

Reference 0.4

www.manaraa.com

Technical Data Sheet

LOCTITE® 410

May 2004

PRODUCT DESCRIPTION

LOCTITE® 410 provides the following product characteristics:

Technology	Cyanoacrylate
Chemical Type	Ethyl cyanoacrylate
Appearance (uncured)	Black liquid[LMS]
Components	One part - requires no mixing
Viscosity	High
Cure	Humidity
Application	Bonding
Key Substrates	Metals, Plastics and Rubbers

LOCTITE® 410 is a rubber toughened adhesive with increased flexibility and peel strength along with enhanced resistance to shock.

TYPICAL PROPERTIES OF UNCURED MATERIAL

Specific Gravity @ 25 °C	1.10
Viscosity, Brookfield - RVT, 25 °C, mPa·s (cP):	
Spindle 3, speed 20 rpm	1,700 to 5,000[LMS]
Flash Point - See MSDS	

TYPICAL CURING PERFORMANCE

Under normal conditions, the atmospheric moisture initiates the curing process. Although full functional strength is developed in a relatively short time, curing continues for at least 24 hours before full chemical/solvent resistance is developed.

Cure Speed vs. Substrate

The rate of cure will depend on the substrate used. The table below shows the fixture time achieved on different materials at 22 °C / 50 % relative humidity. This is defined as the time to develop a shear strength of 0.1 N/mm² .

Fixture Time, ISO 4587, seconds:

Steel (degreased)	60 to 120
Aluminum	10 to 30
Neoprene	15 to 25
Rubber, Nitrile	15 to 25
ABS	20 to 50
PVC	50 to 100
Polycarbonate	30 to 90
Phenolic	20 to 60

Cure Speed vs. Bond Gap

The rate of cure will depend on the bondline gap. Thin bond lines result in high cure speeds, increasing the bond gap will decrease the rate of cure.

Cure Speed vs. Activator

Where cure speed is unacceptably long due to large gaps, applying activator to the surface will improve cure speed. However, this can reduce ultimate strength of the bond and therefore testing is recommended to confirm effect.

TYPICAL PROPERTIES OF CURED MATERIAL

After 24 hours @ 22 °C

Physical Properties:

Coefficient of Thermal Expansion, ASTM D 696, K^{-1}	80×10^{-6}
Coefficient of Thermal Conductivity, ASTM C 177, W/(m·K)	0.10
Glass Transition Temperature, ASTM E 228, °C	120

Electrical Properties:

Dielectric Constant / Dissipation Factor, ASTM D 150:

0.05 kHz	2.30 / <0.02
1 kHz	2.30 / <0.02
1,000 kHz	2.30 / <0.02
Volume Resistivity, ASTM D 257, Ω·cm	10×10^{15}
Dielectric Breakdown Strength, ASTM D 149, kV/mm	25

TYPICAL PERFORMANCE OF CURED MATERIAL

Adhesive Properties

After 24 hours @ 22 °C

Lap Shear Strength, ISO 4587:

Steel (grit blasted)	N/mm²	22
	(psi)	(3,190)
Aluminum (etched)	N/mm²	15
	(psi)	(2,175)
ABS	N/mm²	>6
	(psi)	(>870)
PVC	N/mm²	>6
	(psi)	(>870)
Polycarbonate	N/mm²	>5
	(psi)	(>725)
Phenolic	N/mm²	10
	(psi)	(1,450)
Neoprene	N/mm²	>10
	(psi)	(>1,450)
Nitrile	N/mm²	>10
	(psi)	(>1,450)

Tensile Strength, ISO 6922:

Steel (grit blasted)	N/mm²	18.50
	(psi)	(2,680)

After 48 hours @ 22 °C

Lap Shear Strength, ISO 4587:

Steel (grit blasted)	N/mm²	≥15.80[LMS]
	(psi)	(≥2,290)

Cured for 24 hours @ 22 °C, followed by 24 hours @ 121 °C, tested @ 22 °C

Lap Shear Strength, ISO 4587:

Steel (grit blasted)	N/mm²	≥19.30[LMS]
	(psi)	(≥2,800)

Henkel Technologies

www.manaraa.com

TYPICAL ENVIRONMENTAL RESISTANCE

After 1 week @ 22 °C

Lap Shear Strength, ISO 4587:

Mild steel (grit blasted)

Hot Strength

Tested at temperature

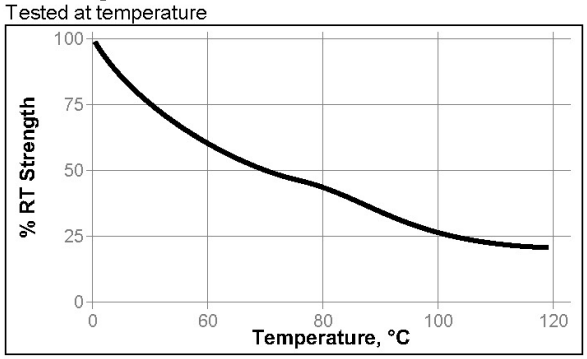

Heat Aging

Aged at temperature indicated and tested @ 22 °C

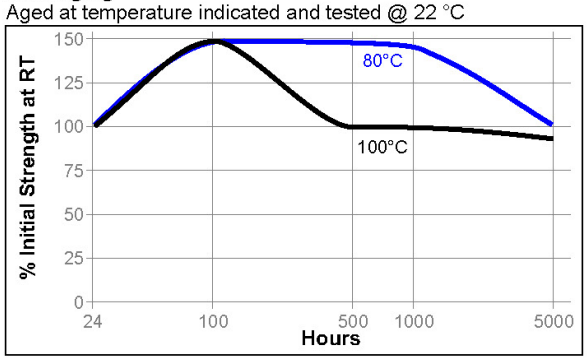

Chemical/Solvent Resistance

Aged under conditions indicated and tested @ 22 °C.

		% of initial strength		
Environment	**°C**	**100 hr**	**500 hr**	**1000 hr**
Motor Oil	40	85	85	85
Gasoline	22	90	70	70
Isopropanol	22	75	75	75
Industrial Methylated spirit	22	95	95	80
1,1,1 Trichloroethane	22	80	70	50
Freon TA	22	90	90	85
Heat/Humidity 95% RH	40	100	100	100

GENERAL INFORMATION

This product is not recommended for use in pure oxygen and/or oxygen rich systems and should not be selected as a sealant for chlorine or other strong oxidizing materials.

For safe handling information on this product, consult the Material Safety Data Sheet (MSDS).

Directions for use

1. For best performance bond surfaces should be clean and free from grease.
2. This product performs best in thin bond gaps (0.05 mm).
3. Excess adhesive can be dissolved with Loctite cleanup solvents, nitromethane or acetone.

Loctite Material Specification[LMS]

LMS dated June 13, 2001. Test reports for each batch are available for the indicated properties. LMS test reports include selected QC test parameters considered appropriate to specifications for customer use. Additionally, comprehensive controls are in place to assure product quality and consistency. Special customer specification requirements may be coordinated through Henkel Loctite Quality.

Storage

Store product in the unopened container in a dry location. Storage information may be indicated on the product container labeling.

Optimal Storage: 2 °C to 8 °C. Storage below 2 °C or greater than 8 °C can adversely affect product properties. Material removed from containers may be contaminated during use. Do not return product to the original container. Henkel Corporation cannot assume responsibility for product which has been contaminated or stored under conditions other than those previously indicated. If additional information is required, please contact your local Technical Service Center or Customer Service Representative.

Conversions

(°C x 1.8) + 32 = °F
kV/mm x 25.4 = V/mil
mm / 25.4 = inches
N x 0.225 = lb
N/mm x 5.71 = lb/in
N/mm² x 145 = psi
MPa x 145 = psi
N·m x 8.851 = lb.in
N·mm x 0.142 = oz.in
mPa·s = cP

Note

The data contained herein are furnished for information only and are believed to be reliable. We cannot assume responsibility for the results obtained by others over whose methods we have no control. It is the user's responsibility to determine suitability for the user's purpose of any production methods mentioned herein and to adopt such precautions as may be advisable for the protection of property and of persons against any hazards that may be involved in the handling and use thereof. In light of the foregoing, **Henkel Corporation specifically disclaims all warranties expressed or implied, including warranties of merchantability or fitness for a particular purpose, arising from sale or use of Henkel Corporation's products. Henkel Corporation specifically disclaims any liability for consequential or incidental damages of any kind, including lost profits.** The discussion herein of various processes or compositions is not to be interpreted as representation that they are free from domination of patents owned by others or as a license under any Henkel Corporation patents that may cover such processes or compositions. We recommend that each prospective user test his proposed application before repetitive use, using this data as a guide. This product may be covered by one or more United States or foreign patents or patent applications.

المنارة للاستشارات

www.manaraa.com

Trademark usage
LOCTITE is a trademark of Henkel Corporation

Reference 1

www.manaraa.com

LOCTITE
1001 Trout Brook Crossing
Rocky Hill, CT 06067-3910
Telephone: (860) 571-5100
FAX: (860) 571-5465

Product Description Sheet
Speedbonder® Product H3000
formerly Hysol® H3000

Industrial Products, May 2002

Description

Loctite® Speedbonder® H3000 is a general purpose, two component, room temperature curing, 1:1 mix ratio, methacrylate adhesive system. H3000 is formulated to yield high peel and shear strength. This adhesive forms resilient bonds and maintains its strength over a wide range of temperatures. H3000 is suitable for bonding a variety of substrates with a minimum of surface preparation. Primer 2000, a wipe-on metal adhesion promoter, is suggested when bonding metals for harsh environments.

Recommended Substrates: PVC, polycarbonate, acrylic, ABS, stainless steel and FRP

Features

Non-sagging gaps filled to .375 inch
Superior impact and peel strength
Little or no surface preparation
Offers excellent tolerance to off-ratio mixing
Rapid room temperature cure
100% reactive
Excellent environmental resistance

Typical Uncured Properties	Part A	Part B	Mixed
Open Time @ 70°F, mins	---	---	4 to 6
Fixture Time @ 70°F, mins	---	---	12 to 15
Color	Cream	Tan	Cream
Viscosity, cP	45,000 to 85,000	8,000 to 40,000	---
Specific Gravity	1.07	1.06	1.07
Weight per Gallon, Lbs	8.92	8.91	8.91
Mix Ratio			
By weight	1	1	---
By volume	1	1	---

Typical Cured Properties	Typical Value
Tensile Strength, psi, ASTM D 638	4,100 to 4,300
Elongation, %, ASTM D 638	20 to 30
Shear Strength @ 180°F, psi, Etched Aluminum ASTM D 1002	1,900 to 2,100

Shear Strength, psi, ASTM D1002	Typical Value
Etched Aluminum	4000
Aluminum	2940
Anodized Aluminum	1840
Steel	4150
Stainless Steel	3540
Zinc Dichromate	1980
Polycarbonate	960
Fiberglas	1740
Gelcoat	1490

T-peel, pli, ASTM D1876	Typical Value
Steel	45
Aluminum	20
Etched Alumunum	30

Side Impact Strength, kJ/m^2, GM9751P test	Typical value
Aluminum	25 to 30

Shear Strength after Environmental Exposure, psi, ASTM D 1002		
	2 Weeks	4 Weeks
120°F/100% RH	1250	2170

Peak Exotherm Curve –10 Gram Mass

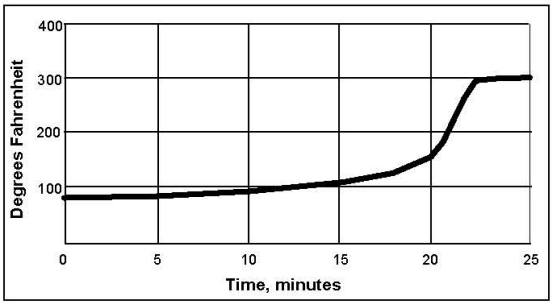

Development of Bond Strength

Strength Build on FRP

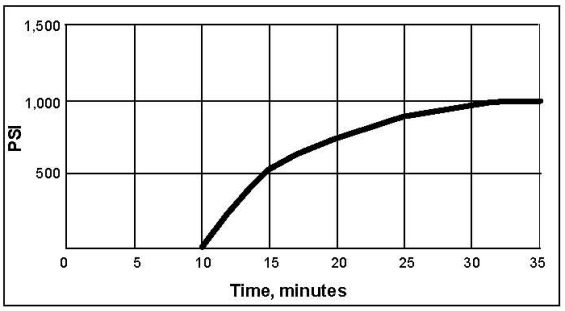

GENERAL INFORMATION

This product is not recommended for use in pure oxyger and/or oxygen rich systems and should not be selected as a sealant for chlorine or other strong oxidizing materials.

For safe handling information on this product, consult the Material Safety Data Sheet, (MSDS).

NOT FOR PRODUCT SPECIFICATIONS
THE TECHNICAL DATA CONTAINED HEREIN ARE INTENDED AS REFERENCE ONLY.
PLEASE CONTACT LOCTITE CORPORATION QUALITY DEPARTMENT FOR ASSISTANCE AND RECOMMENDATIONS ON SPECIFICATIONS FOR THIS PRODUCT.
ROCKY HILL, CT FAX: +1 (860)-571-5473 DUBLIN, IRELAND FAX: +353-(1)-451 - 9959

www.manaraa.com

Handling and Application

Mixing: It is highly recommended that either meter mix equipment or cartridges with static mix nozzles be used to properly ratio and dispense the adhesive. For hand mixing, combine Part A and Part B in the correct ratio and mix thoroughly. Once mixed, H3000 should achieve a uniform color. This is important! Heat buildup during and after mixing is normal. To reduce the likelihood of exothermic reaction or excessive heat buildup, mix less than 100 grams at a time. Mixing smaller amounts will minimize heat buildup.

Applying: Bonding surfaces should be clean, dry, and free of contamination. Extensive surface preparation is not required for H3000, and good bonds can be formed on most substrates after a solvent wipe. To assure maximum bond strength, surfaces must be mated within the adhesive's open time. Use enough material to completely fill the joint when parts are clamped.

Curing: Parts should remain undisturbed during the interval of time between the material's open time and fixture time. After the fixture time is achieved the material has reached handling strength. Temperature below 55°F will slow the cure; above 85°F will accelerate the cure rate.

Clean Up: It is important to clean up excess adhesive from the work area and application equipment before it cures. Denatured alcohol and many common industrial solvents are suitable for removing uncured adhesive. Speedbonder H3000 is flammable. Keep containers tightly closed after use. Keep away from heat, sparks, and open flames.

Storage

Speedbonder adhesives should be stored in unopened containers in a dry location at 40°F +/- 5 F. For further specific shelf life information, contact your local Technical Service Center.

Packaging

50ml EPS cartridges
400ml EPS cartridges
5 Gallon Pails
55 Gallon Drums

The data contained herein are furnished for information only and are believed to be reliable. We cannot assume responsibility for the results obtained by others over whose methods we have no control. It is the user's responsibility to determine suitability for the user's purpose of any production methods mentioned herein and to adopt such precautions as may be advisable for the protection of property and of persons against any hazards that may be involved in the handling and use thereof. In light of the foregoing, **Loctite Corporation specifically disclaims all warranties expressed or implied, including warranties of merchantability or fitness for a particular purpose, arising from sale or use of Loctite Corporation's products. Loctite Corporation specifically disclaims any liability for consequential or incidental damages of any kind, including lost profits.** The discussion herein of various processes or compositions is not to be interpreted as representation that they are free from domination of patents owned by others or as a license under any Loctite Corporation patents that may cover such processes or compositions. We recommend that each prospective user test his proposed application before repetitive use, using this data as a guide. This product may be covered by one or more United States or foreign patents or patent applications.

Note

Loctite, Hysol and Speedbonder are Registered Trademarks of Loctite Corporation U.S.A.

www.manaraa.com

LOCTITE
1001 Trout Brook Crossing
Rocky Hill, CT 06067-3910
Telephone: (860) 571-5100
FAX: (860) 571-5465

Product Description Sheet
Speedbonder® Product H3300
formerly Hysol® H3300

Industrial Products, October 2002

Description

Loctite® Speedbonder® H3300 is a highly thixotropic, two component, room temperature curing, 1:1 mix ratio, methacrylate adhesive system. H3300 is formulated to provide fixturing strength within 6 - 12 minutes. This adhesive forms resilient bonds and maintains its strength over a wide range of temperatures. H3300 is suitable for bonding a variety of substrates with a minimum of surface preparation.

Recommended Substrates: PVC, polycarbonate, acrylic, ABS, stainless steel and FRP

Features

Non-sagging gaps filled to .375 inch
Superior impact and peel strength
Little or no surface preparation
Offers excellent tolerance to off-ratio mixing
Rapid room temperature cure
100% reactive
Excellent environmental resistance

Typical Uncured Properties	Part A	Part B	Mixed
Open Time @ 70°F, mins	--	--	4 to 6
Fixture Time @ 70°F, mins	--	--	6 to 12
Color	Pale Milky White	Tan to Yellow	Light Yellow
Viscosity, cP	85,000 to 125,000	80,000 to 160,000	--
Specific Gravity	1.03	1.05	1.04
Weight per Gallon, Lbs	8.58	8.75	8.67
Mix Ratio			
By weight	1	1	--
By volume	1	1	--

Typical Cured Properties	Typical Value
Tensile Strength, psi, ASTM D 638	4100-4300
Elongation, %, ASTM D 638	20-40
Shear Strength @ 77°F, psi, Etched Aluminum ASTM D 1002	3,000 Minimum
Shear Strength @ 180°F, psi, Etched Aluminum ASTM D 1002	1900-2100
Hardness, Shore D	75-80

Shear Strength, psi, ASTM D1002	Typical Value
Aluminum	3250
Steel	3810
Stainless Steel	2900
Zinc Dichromate	1100
Polycarbonate	990
Fiberglas	>1650
Gelcoat	>1420

Side Impact Strength, kJ/m^2, GM9751P test	Typical value
Aluminum	25 to 30

Shear Strength after Environmental Exposure, psi, Steel, ASTM D 1002		
	2 Weeks	4 Weeks
120°F/100% RH	2630	1710

Block Shear, ASTM D4501, psi	Typical Value
PVC	2120
ABS	1880

T-peel, pli, ASTM D1876	Typical Value
Steel	45 to 55
Aluminum	15 to 20
Etched Alumunim	30

Peak Exotherm Curve –10 Gram Mass

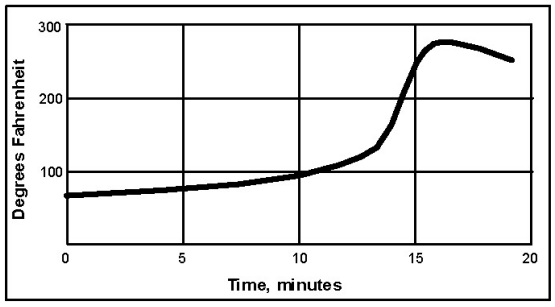

Development of Bond Strength

Strength Build on FRP

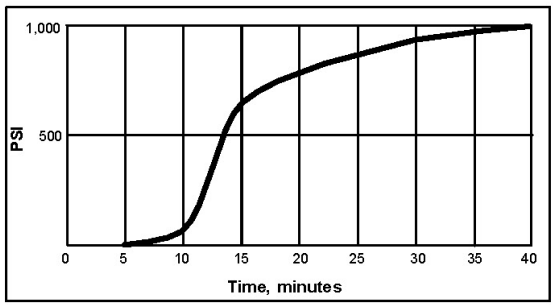

GENERAL INFORMATION

This product is not recommended for use in pure oxyger and/or oxygen rich systems and should not be selected as a sealant for chlorine or other strong oxidizing materials.

For safe handling information on this product, consult the Material Safety Data Sheet, (MSDS).

NOT FOR PRODUCT SPECIFICATIONS
THE TECHNICAL DATA CONTAINED HEREIN ARE INTENDED AS REFERENCE ONLY.
PLEASE CONTACT LOCTITE CORPORATION QUALITY DEPARTMENT FOR ASSISTANCE AND RECOMMENDATIONS ON SPECIFICATIONS FOR THIS PRODUCT.
ROCKY HILL, CT FAX: +1 (860)-571-5473 DUBLIN, IRELAND FAX: +353-(1)-451 - 9959

www.manaraa.com

Handling and Application

Mixing: It is highly recommended that either meter mix equipment or cartridges with static mix nozzles be used to properly ratio and dispense the adhesive. For hand mixing, combine Part A and Part B in the correct ratio and mix thoroughly. Once mixed, H3300 should achieve a uniform color. This is important! Heat buildup during and after mixing is normal. To reduce the likelihood of exothermic reaction or excessive heat buildup, mix less than 100 grams at a time. Mixing smaller amounts will minimize heat buildup.

Applying: Bonding surfaces should be clean, dry, and free of contamination. Extensive surface preparation is not required for H3300, and good bonds can be formed on most substrates after a solvent wipe. To assure maximum bond strength, surfaces must be mated within the adhesive's open time. Use enough material to completely fill the joint when parts are clamped.

Curing: Parts should remain undisturbed during the interval of time between the material's open time and fixture time. After the fixture time is achieved the material has reached handling strength. Temperature below 55°F will slow the cure; above 85°F will accelerate cure rate.

Clean Up: It is important to clean up excess adhesive from the work area and application equipment before it cures. Denatured alcohol and many common industrial solvents are suitable for removing uncured adhesive. Speedbonder H3300 is flammable. Keep containers tightly closed after use. Keep away from heat, sparks, and open flames.

Storage

Speedbonder adhesives should be stored in unopened containers in a dry location at 40°F +/- 5 F. For further specific shelf life information, contact your local Technical Service Center.

Packaging

50ml EPS cartridges
400ml EPS cartridges
5 Gallon Pails
55 Gallon Drums

Note

The data contained herein are furnished for information only and are believed to be reliable. We cannot assume responsibility for the results obtained by others over whose methods we have no control. It is the user's responsibility to determine suitability for the user's purpose of any production methods mentioned herein and to adopt such precautions as may be advisable for the protection of property and of persons against any hazards that may be involved in the handling and use thereof. In light of the foregoing, **Loctite Corporation specifically disclaims all warranties expressed or implied, including warranties of merchantability or fitness for a particular purpose, arising from sale or use of Loctite Corporation's products. Loctite Corporation specifically disclaims any liability for consequential or incidental damages of any kind, including lost profits.** The discussion herein of various processes or compositions is not to be interpreted as representation that they are free from domination of patents owned by others or as a license under any Loctite Corporation patents that may cover such processes or compositions. We recommend that each prospective user test his proposed application before repetitive use, using this data as a guide. This product may be covered by one or more United States or foreign patents or patent applications.

Loctite, Hysol and Speedbonder are Registered Trademarks of Loctite Corporation U.S.A.

www.manaraa.com

LOCTITE
1001 Trout Brook Crossing
Rocky Hill, CT 06067-3910
Telephone: (860) 571-5100
FAX: (860) 571-5465

Product Description Sheet
Speedbonder® Product H4500
formerly Hysol® H4500

Industrial Products, May 2002

Description
Loctite® Speedbonder® H4500 is a highly thixotropic, two component, room temperature curing, 10:1 mix ratio methacrylate adhesive system formulated specifically for bonding metals such as stainless steel, steel and aluminum. The unique formulation of H4500 allows bonding to metals without the use of a primer. This adhesive contains a corrosion inhibiting additive to insure long term bond durability even when exposed to moisture prone environments. Speedbonder H4500 forms resilient bonds and maintains its strength over a wide range of temperatures with minimum surface preparation.

Recommended Substrates: steel, aluminum, stainless steel, epoxy coated metal, SMC, and many plastics

Features
Internal metal primer
100% reactive
Superior impact and peel strength
Excellent environmental resistance
Little or no surface preparation
Offers excellent tolerance to off-ratio mixing
Rapid room temperature cure
Non-sagging gaps filled to ½"

Typical Cured Properties	Typical Value
Tensile Strength, psi, ASTM D 638	3400 to 3600
Elongation, %, ASTM D 638	20 to 30
Peel Strength, pli, ASTM D 3167	60
Hardness, Shore D	40 to 45

Typical Uncured Properties	Part A	Part B	Mixed
Open Time @ 70°F, mins	--	--	4 to 6
Fixture Time @ 70°F, mins	--	--	15 to 20
Color	Cream	Tan	Pale Yellow
Viscosity, cP	45,000 to 63,000	40,000 to 67,000	--
Specific Gravity	1.01	1.06	1.01
Weight per Gallon, Lbs	8.40	8.83	8.45
Mix Ratio			
By weight	9.5	1	--
By volume	10	1	--

Shear Strength, psi, ASTM D1002	Typical Value
Aluminum	4120
Steel	4310
Stainless Steel	4130
Zinc Dichromate	2810
Anodized Aluminum	3180
Polycarbonate	850
Fiberglas	>1760
Gelcoat	>1460

Side Impact Strength, kJ/m^2, GM9751P test	Typical value
Aluminum	35 to 40

Block Shear, ASTM D4501, psi	Typical Value
PVC	2200
ABS	1560

T-peel, pli, ASTM D1876	Typical Value
Steel	35 to 40
Aluminum	20

Peak Exotherm Curve –10 Gram Mass

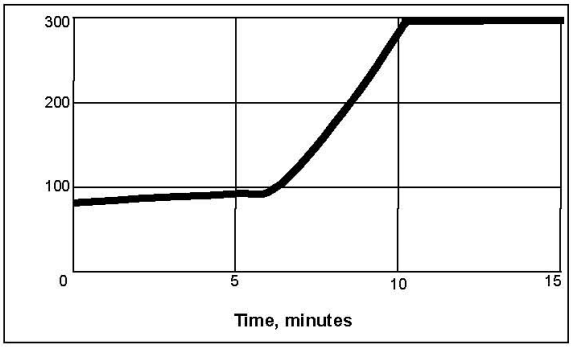

Development of Bond Strength
Strength Build on FRP

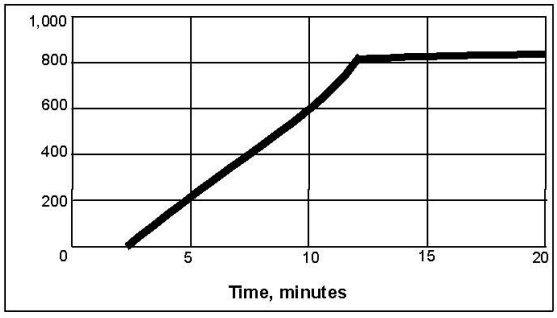

Performance of cured Material
Strength vs Temperature
Tensile Lap Shear Strength, ASTM D 1002, psi, 24 hour cure, Etched Aluminum

Test Temperature	Typical value
-40ºF	3500
-20ºF	4100
75ºF	4500
180ºF	2600
250ºF	780

NOT FOR PRODUCT SPECIFICATIONS
THE TECHNICAL DATA CONTAINED HEREIN ARE INTENDED AS REFERENCE ONLY.
PLEASE CONTACT LOCTITE CORPORATION QUALITY DEPARTMENT FOR ASSISTANCE AND RECOMMENDATIONS ON SPECIFICATIONS FOR THIS PRODUCT.
ROCKY HILL, CT FAX: +1 (860)-571-5473 DUBLIN, IRELAND FAX: +353-(1)-451 - 9959

www.manaraa.com

Tensile Lap Shear after Environmental Exposure
ASTM D 1002, psi
FRP/FRP coupons are 1"by 1", 30 mil bondline; Aluminum is etched with 5 mil bondline. All samples cured three days at 77ºF prior to exposure. Shear strength after 30 day exposure

	FRP	Etched Aluminum
Control	>800	4500
Water	>800	1000
Salt Water	>700	250
Unleaded Gasoline	>750	4000
Diesel Fuel	>750	4000
95ºF/100% RH	>800	600
Motor Oil	>800	4100
Antifreeze	>700	3300

GENERAL INFORMATION
This product is not recommended for use in pure oxygen and/or oxygen rich systems and should not be selected as a sealant for chlorine or other strong oxidizing materials.

For safe handling information on this product, consult the Material Safety Data Sheet, (MSDS).

Handling and Application
Mixing: It is highly recommended that either meter mix equipment or cartridges with static mix nozzles be used to properly ratio and dispense the adhesive. For hand mixing, combine Part A and Part B in the correct ratio and mix thoroughly. Once mixed, H4500 should achieve a uniform color. This is important! Heat buildup during and after mixing is normal. To reduce the likelihood of exothermic reaction or excessive heat buildup, mix less than 100 grams at a time. Mixing smaller amounts will minimize heat buildup.

Applying: Bonding surfaces should be clean, dry, and free of contamination. Extensive surface preparation is not required for H4500, and good bonds can be formed on most substrates after a solvent wipe. To assure maximum bond strength, surfaces must be mated within the adhesive's open time. Use enough material to completely fill the joint when parts are clamped.

Curing: Parts should remain undisturbed during the interval of time between the material's open time and fixture time. After the fixture time is achieved the material has reached handling strength. Temperature below 55°F will slow the cure; above 85°F will accelerate cure rate.

Clean Up: It is important to clean up excess adhesive from work area and application equipment before it hardens. Denatured alcohol and many common industrial solvents are suitable for removing uncured adhesive. Speedbonder H4500 is flammable. Keep containers tightly closed after use. Keep away from heat, sparks, and open flames.

Storage
Speedbonder adhesives should be stored in unopened containers in a dry location at 40°F +/- 5 F. For further specific shelf life information, contact your local Technical Service Center.

Packaging
490ml EPS cartridges
5 Gallon Pails
55 Gallon Drums

Note
The data contained herein are furnished for information only and are believed to be reliable. We cannot assume responsibility for the results obtained by others over whose methods we have no control. It is the user's responsibility to determine suitability for the user's purpose of any production methods mentioned herein and to adopt such precautions as may be advisable for the protection of property and of persons against any hazards that may be involved in the handling and use thereof. In light of the foregoing, **Loctite Corporation specifically disclaims all warranties expressed or implied, including warranties of merchantability or fitness for a particular purpose, arising from sale or use of Loctite Corporation's products. Loctite Corporation specifically disclaims any liability for consequential or incidental damages of any kind, including lost profits.** The discussion herein of various processes or compositions is not to be interpreted as representation that they are free from domination of patents owned by others or as a license under any Loctite Corporation patents that may cover such processes or compositions. We recommend that each prospective user test his proposed application before repetitive use, using this data as a guide. This product may be covered by one or more United States or foreign patents or patent applications.

Loctite, Hysol and Speedbonder are Registered Trademarks of Loctite Corporation U.S.A.

www.manaraa.com

MA820 Technical Data Sheet

Benefits

No Primer Required on Metal
High Toughness
100% Reactive
Non-Sagging
Available with Glass Beads - For fixed Bondline Gap

Characteristics

Room Temperature Cure
Working Time[2]
4 - 6 minutes
Fixture Time[3]
18 – 25 minutes
51°F Flash Point
Operating Temperature
-67°F to 250°F
Gap Filling to 0.5 inch
Mixed Density
8.33 lbs./gal (1.00 g/cc)

Chemical Resistance[4]

Excellent resistance to
- Hydrocarbons
- Acids and Bases (3-10 pH)
- Salt Solutions

Susceptible to:
- Polar Solvents
- Strong Acids and Bases

Recommended for:

ABS
Acrylics
Aluminum
FRP
Gelcoats[6]
PVC
Polyesters (including DCPD modified)
Steel, Carbon[7]
Steel, Stainless
Styrenics
Urethanes (General)
Vinyl Esters

Plexus® MA820 is a two-part methacrylate adhesive designed for structural bonding of metals without primers. In addition, MA820 does a superb job of bonding thermoplastic and composite assemblies with no surface preparation[1]. Combined at a 10:1 ratio, MA820 has a working time of 4 to 6 minutes and achieves 75% of ultimate strength in 15 to 18 minutes. This product provides a unique combination of high strength, excellent fatigue endurance, outstanding impact resistance, and superior toughness. Plexus MA820 is available in gray and is supplied in ready-to-use cartridges, 5 gallon pails or 50 gallon drums. The product can be dispensed as a non-sagging gel using standard meter-mix equipment. ITW Plexus recommends the ***MixPac MC08-32 nozzle*** for this product and a minimal bond gap of 0.03 inches. Versions are available with glass bead spacers to provide fixed bondline gaps of 0.03 inches.

Physical Properties (Uncured) –Room Temperature

	Adhesive	Activator
Viscosity, cP	90,000 – 120,000	50,000 – 80,000
Color	Off-White	Gray
Density, lbs./gal (g/cc)	8.26 (0.99)	8.95 (1.07)
Mix Ratio by Volume	10	1
Mix Ratio by Weight	9.2	1

Mechanical Properties (Cured) –Room Temperature

Tensile (ASTM D638)

Strength, psi	3300-3700
Modulus, psi	75,000 – 100,000
Strain to Failure (%)	75-100

Lap Shear (ASTM D1002)

Cohesive Strength, psi	2000 – 2400

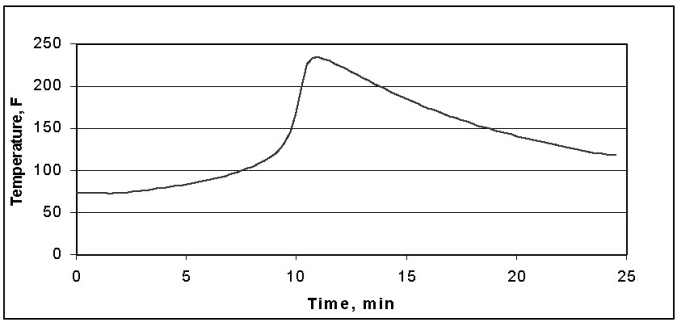

Typical Exotherm Curve for MA820 at 75°F (10 grams)[5]

www.manaraa.com

HANDLING AND APPLICATION

Plexus® MA820 adhesive (Part A) is flammable. Contents include Methacrylate Ester. Keep containers closed after use. Wear gloves and safety glasses to avoid skin and eye contact. Wash with soap and water after skin contact. In case of eye contact, flush with water for 15 minutes and get medical attention. Harmful if swallowed. Keep out of reach of children. Keep away from heat, sparks, and open flames. Reference the Material Safety Data Sheet for more complete safety information.

Note: Because of the rapid curing features of this product, large amounts of heat are generated when large masses of material are mixed at one time. The heat generated by the exotherm resulting from the mixing of large masses of adhesive can result in the release of entrapped air, steam, and volatile gases. To prevent this, use only enough material as needed for use within the working time for the product and confine gap thickness to no more than 0.5 inch. Questions relative to handling and applications should be directed to ITW Plexus at 800-851-6692.

DISPENSING ADHESIVE

MA820 may be applied manually or with automated equipment. Automated application may be accomplished with a variety of 10 to 1 meter mix equipment delivering both components to a static mixer. **ITW Plexus recommends the *MixPac MC08-32 nozzle* for proper mixing and a minimal bond gap of 0.03 inches**. For information concerning meter-mix equipment, contact ITW Plexus Sales Representatives. Pre-measured cartridges are also available, as well as the hand-held guns with which to dispense the adhesive. For more information, contact ITW Plexus at (800) 851-6692. To assure maximum bond strength, surfaces must be mated within the specified working time. Use sufficient material to ensure the joint is completely filled when parts are mated and clamped. All adhesive application, part positioning, and fixturing should occur *before* the working time of the mix has expired. After indicated working time, parts must remain undisturbed until the fixture time is reached. Automated equipment should be constructed of stainless steel or aluminum. Avoid contact with copper or copper containing alloys in all fittings, pumps, etc. Seals and gaskets should be made of Teflon, Teflon-coated PVC foam, ethylene/propylene or polyethylene. Avoid the use of Viton, BUNA-N, Neoprene or other elastomers for seals and gaskets. Clean up is easiest *before* the adhesive has cured. Citrus terpene or N-methyl pyrolidone (NMP) containing cleaners and degreasers can be used for best results. If the adhesive is already cured, careful scraping, followed by a solvent wipe may be the most effective method of clean up.

EFFECT OF TEMPERATURE

Application of adhesive at temperatures between 65°F and 80°F will ensure proper cure. Temperatures below 65°F will slow cure speed; above 80°F will increase cure speed. The viscosities of Parts A and B of this adhesive are affected by temperature. To ensure consistent dispensing in meter-mix equipment, adhesive and activator temperatures should be held reasonably constant throughout the year.

STORAGE AND SHELF LIFE

Shelf life of MA820 adhesive (Part A) is 1 year from day of shipment from ITW Plexus. Shelf life of activator (Part B), including cartridges that contain activators, is 9 months from day of shipment. Shelf life is based on continuous storage between 55°F and 75°F. Long term exposure above 75°F will reduce the shelf life of these materials. Prolonged exposure of activators, including cartridges that contain activators, above 100°F quickly diminishes the reactivity of the product and should be avoided. Shelf life can be extended by refrigeration (45°F - 55°F). These products should never be frozen.

Notes

1. ITW Plexus strongly recommends that all substrates be tested with the selected adhesive in the anticipated service conditions to determine suitability.
2. Working Time: The time elapsed between the moment Parts A and B of the adhesive system are combined and thoroughly mixed and the time when the adhesive is no longer useable. Times presented were tested at 75°F.
3. Fixture Time: The interval of time after which surface being joined will support a 2 lb. (1 kg) dead weight on a 1/2 inch (12.7 mm) overlap joint 1 inch (25.4 mm) wide without movement. Times presented were tested at 75°F.
4. Resistance to chemical exposure varies greatly based on several parameters including; temperature, concentration, bondline thickness, and duration of exposure. The chemical resistance guidelines listed assume long term exposures at ambient conditions.
5. In a typical bond line, exotherm temperatures will be lower than the temperatures shown.
6. Urethane-modified super-weathering gelcoats may require an alternate adhesive. As with all substrates, these gelcoats should be tested with the selected adhesive to determine suitability.
7. Exterior applications require the use of coatings that will inhibit oxidation of the steel.

All information on this data sheet is based on laboratory testing and is not intended for design purposes. ITW Plexus makes no representations or warranties of any kind concerning this data. Due to variance of storage, handling and application of these materials, ITW Plexus cannot accept liability for results obtained.

www.manaraa.com

ASHLAND
INFOTECH™

ASHLAND SPECIALTY CHEMICAL COMPANY
SPECIALTY POLYMERS & ADHESIVES
Corporate Office: P.O. Box 2219, Columbus, OH 43216
800/322-6580 • 614/790-3333 • Fax: 614/790-3206

Drew Ameroid Deutschland GmbH,
SP&A European Technical Center
Fraunhoferstr, 3 • 25524 Itzehoe, Germany
Tel: +49 (0) 4821 778 480 • Fax: +49 (0) 4821 778 489

PLIOGRIP® Adhesive Systems

7773/220
7773/660

GENERAL DESCRIPTION:

PLIOGRIP 7700 cartridge adhesive systems are high performance, two-component polyurethane adhesives packaged in 110ml by 110ml or 330ml by 330ml, side-by-side cartridges.

PLIOGRIP 7700 series adhesives are high-strength, structural adhesives which are resistant to exposure to elevated temperatures, moisture, fuel, most solvents and chemicals.

The adhesive systems are tested using stringent performance specifications of all major domestic automotive manufacturers and heavy truck producers. They have been designed for ease of dispense with a hand-held, pump action gun.

PLIOGRIP 7773/220 and PLIOGRIP 7770/660 cartridge adhesive systems are designed for small, quick, durable bonding and repair jobs. The use of these products yields fast turnaround due to early sanding and painting capability.

		Prepolymer	Curative
TYPICAL COMPONENT PROPERTIES, NOMINAL:	**Viscosity, cps**	15,000	15,000 - 27,000

TYPICAL CURE CHARACTERISTICS OF MIXED ADHESIVES:	**Working Time:**	3.5 minutes @ 23°C
	Sanding Time:	30 minutes

TYPICAL PHYSICAL PROPERTIES OF CURED ADHESIVE:	**Tensile, MPa @ 23°C**	25.5
	Elongation, %	70
	Young's Modulus, MPa	517
	Density, g/cc	1.28
	Water, Absorption, %	<1.5
	Shrinkage	Imperceptible

TYPICAL TEST CONDITIONS:	**Substrate**	Structural Plastics including Automotive and Marine; Coated Metal
	Surface Preparation	Plastics - sand and clean Metal - Coated
	Adhesive System	PLIOGRIP 7773/220, PLIOGRIP 7773/660
	Initial Cure	Room Temperature

(Over)

This information contained herein is correct to the best of our knowledge. The recommendations or suggestions contained in this bulletin are made without guarantee or representation as to results. We suggest that you evaluate these recommendations and suggestions in your own laboratory prior to use. Our responsibility for claims arising from breach of warranty, negligence or otherwise is limited to the purchase price of the material. Freedom to use any patent owned by Ashland or others is not to be inferred from any statement contained herein.

© Copyright 2001, Ashland Inc.
® Registered Trademark, Ashland Inc.
™ Trademark, Ashland Inc.
* Registered Service Mark, American Chemistry Council

SPECIALTY POLYMERS & ADHESIVES
ASHLAND
Ashland Specialty Chemical Company

www.manaraa.com

HANDLING:

PLIOGRIP 7773/220 and PLIOGRIP 7773/660 adhesives contain ingredients which could be harmful if improperly handled. Contact with skin and eyes should be avoided and necessary protective equipment and clothing should be worn.

Ashland Specialty Chemical Company maintains Material Safety Data Sheets on all of its products. Material Safety Data Sheets contain health and safety information for your development of appropriate product handling procedures to protect your employees and customers.

Our Material Safety Data Sheets should be read and understood by all of your supervisory personnel and employees before using Ashland Specialty Chemical Company's products in your facility.

STORAGE AND SHELF LIFE:

Unopened cartridge stored indoors at 60° - 90°F (15° - 32°C)
2 Years

PACKAGING:

PLIOGRIP 7773/220 adhesive is packaged in 110ml by 110ml side-by-side cartridges for use with a hand-held dispensing gun.

PLIOGRIP 7773/660 adhesive is packaged in 330ml by 330ml side-by-side cartridges for use with a hand-held pneumatic gun.

ASCC PRODUCT CODE:

PLIOGRIP 7773/220 Cartridge Adhesive System: 583564
PLIOGRIP 7773/660 Cartridge Adhesive System: 583330

DOT LABEL REQUIREMENTS:

PLIOGRIP 7773/220 Cartridge Adhesive System - None Required
PLIOGRIP 7773/660 Cartridge Adhesive System - None Required

www.manaraa.com

APPENDIX C: STC INFORMATION FOR FOIL SENSORS

www.manaraa.com

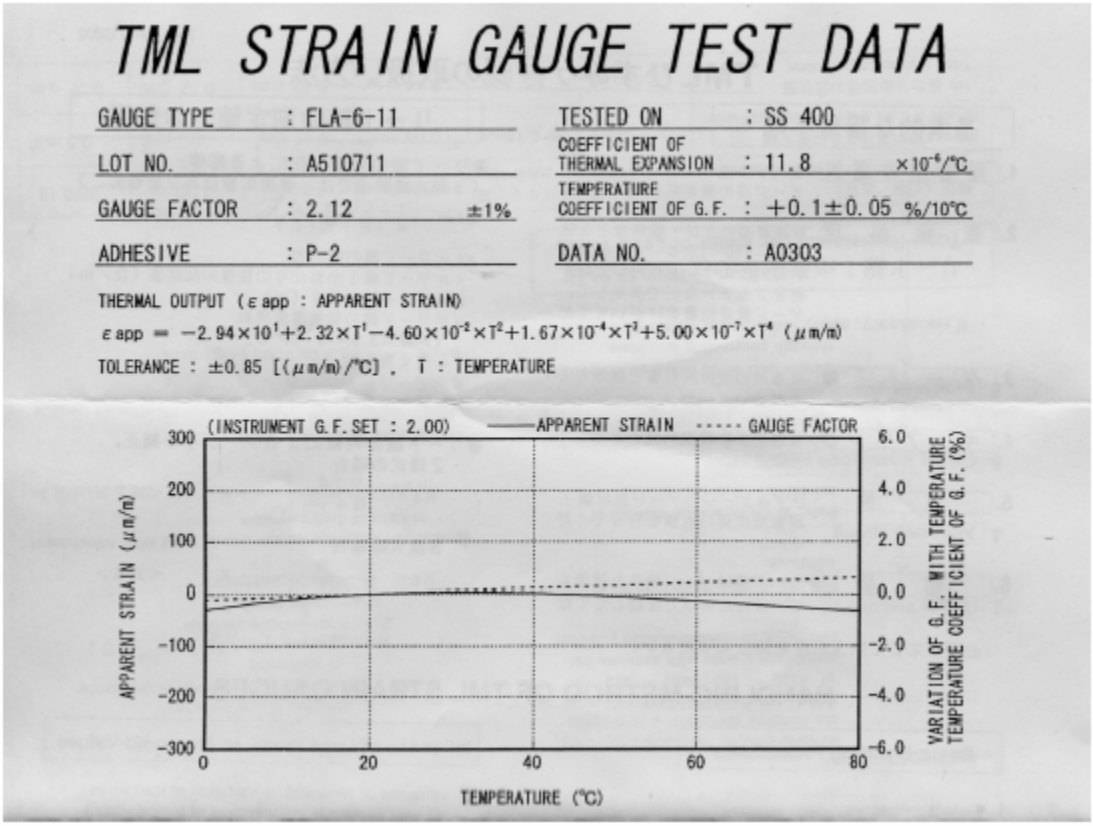

Figure C1. STC information for TML FLA-6-11 foil sensors.

www.manaraa.com

APPENDIX D: SI425-500 INTERROGATOR SPECIFICATIONS

www.manaraa.com

s

optical sensing

Optical Sensing Interrogator | si425

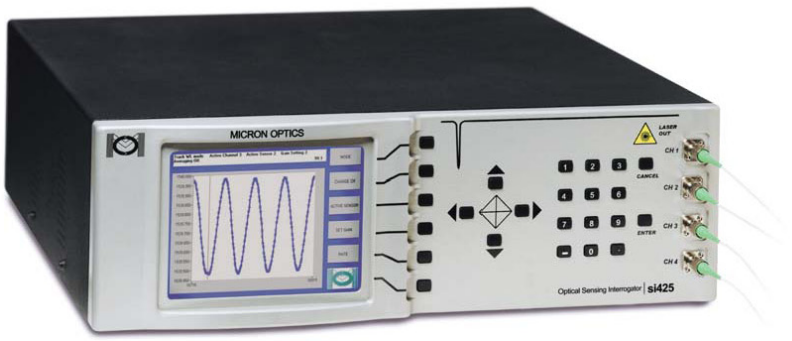

Applications

- Measurements using FBG strain gages, temperature probes, and pressure sensors
- Dynamic, simultaneous measurements of hundreds of sensors on multiple fibers
- Continuous structural health monitoring of ships, aircraft and other complex structures
- Permanent installations for tracking the condition and performance in smart structures like bridges, dams, and tunnels

Description

The **si425 Optical Sensing Interrogator** is installed today monitoring hundreds of active structures. Users rely on the **si425's** ability to make fast, simultaneous, measurements of hundreds of fiber-optic strain and temperature sensors that indicate the health of their bridges, dams, tunnels and buildings.

The rugged **si425** combines an industrial PC with **Micron Optics'** robust, high-power, low-noise swept laser source. The **Micron Optics si425** is a complete standalone multi-FBG-sensor system that provides high optical power, and rapid measurement of up to 512 sensors on four fibers. It is expandable to 8 or 16 channels, and its modular design allows customization volume applications.

Micron Optics instruments are installed in hundreds of challenging applications all over the world, from large-span bridges in China to earthquake monitors in California to aircraft tests in Europe.

Where are Micron Optics Instruments Deployed?

- **Civil Structures/Civionics (bridges, dams, tunnels, buildings, etc.)**
- **Energy (wind turbines, pipelines, nuclear reactors, etc.)**
- **Aerospace Vehicles (composite structures, wind tunnels, dynamic tests, etc.)**
- **Oil & Gas (well reservoir management, platform structural health monitoring, etc.)**
- **Marine Vessels (hull, mast, rudder, submarine pressure tests, etc.)**
- **Transportation (railways, roadways, etc.)**
- **Homeland Security (perimeter intrusion, shipping container integrity, etc.)**
- **Research (medical devices, military armor, chemical sensing, etc.)**

MICRON OPTICS

Micron Optics, Inc.
1852 Century Pl, NE
Atlanta, GA 30345
ph: 404/325-0005
fax: 404/325-4082
www.micronoptics.com

www.manaraa.com

si425 | Optical Sensing Interrogator

PRELIMINARY

Specifications		si425-500	si425-200
Optical			
Number of Optical Channels		4 (up to 16)	1 (up to 16)
Wavelength Range	a	1520-1570 nm (1510-1590 nm available)	
Wavelength Stability	b	2 pm typ, 5 pm max	
Wavelength Repeatability	c	0.5 pm at full speed, 0.05 pm with 250 averages	
Dynamic Range	d	25 dB	15 dB
Scan Frequency	e	250 Hz	50 Hz
Max Sensors per Channel		128	32
Optical Connectors		FC/APC (E2000 available)	
Mechanical			
Dimensions		134 mm x 432 mm x 451 mm	
Weight		15.5 kg (34 lbs)	
Color LCD Display		162 mm (diagonal)	No
Environmental			
Operating Temperature		10° to 40°C	
Operating Humidity		0 to 80%, non-condensing	
Storage Temperature		-20° to 70°C	
Storage Humidity		0 to 95%, non-condensing	
Electrical			
Input Voltage		100 VAC to 240 VAC, 50/60 Hz input (24 VDC available)	
Power Consumption		80 W typ, 150 W Max	
Interfaces		Ethernet	
Protocols		Custom MOI protocol via Ethernet	
Data Management			
On-Board Firmware		Instrument control, GUI management	
Remote Software		Peak detection, data logger, peak tracking, and instrument control	
LabVIEW™ Source Code		Allows for customization of remote software	
Options			
8-16 Channel Expansion		Please see our 8 or 16 channel sm040 multiplexers	
Local Data Storage	f	80GB Internal hard drive	

060919v

Notes:

a 65,536 data points distributed over either 50nm or 80nm. Effect on performance is minimal.
b Captures effects of long-term use over full operating temperature range of the instrument.
c Per NIST Technical Note 1297, 1994 Edition, Section D.1.1.2, definition of "repeatability [of results of measurements]"
d Defined as laser launch power minus detection noise floor. 25dB over 3 gain stages. 15dB over 2 gain stages.
e Scan frequency is 125Hz for si425-500 for 100 or more sensors.
f Hard drive operating conditions may differ from si425 specifications.

si425 / 060919 / acs2sv1 / SPECIFICATIONS ARE SUBJECT TO CHANGE WITHOUT NOTICE

s
optical sensing

MICRON OPTICS
Micron Optics, Inc.
1852 Century Pl, NE
Atlanta, GA 30345
ph: 404/325-0005
fax: 404/325-4082
www.micronoptics.com

www.manaraa.com

Optical Sensing Interrogator | si425

Connections

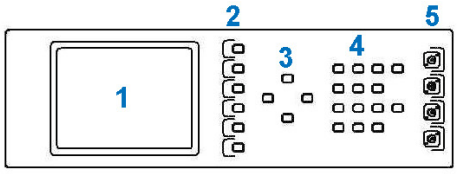

Front Panel View

1) LCD Display, used for viewing data
2) Menu Keys, used for navigation through options menus
3) Arrow Keys, used for incrementing integer data inputs
4) Number Keys, used to entering numeric data
5) FC/APC Connectors, used for connecting optical sensors

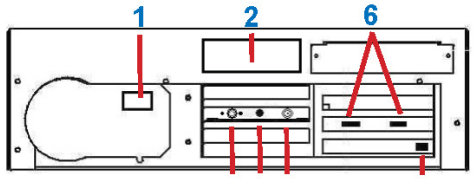

Rear Panel View

1) Connector for AC line cord
2) Label, including instrument serial number and calibration date
3) Accessories port
4) On/Off power switch
5) BNC connector for sync output, used for si425/system synchronization
6) USB connectors for keyboard attachment (intended for diagnostics),
7) RJ45 connector for Ethernet cable.

Data Analysis Using On-Board Controls and LabVIEW™ Remote Utility

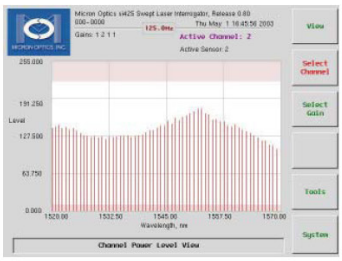

Channel Power View

Used for system setup. Relative power of each sensor is displayed. See instant response to gain settings.

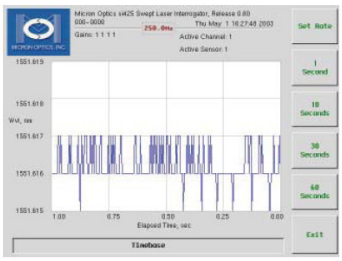

Sensor Wavelength View

Shows sensor values as a function of time.

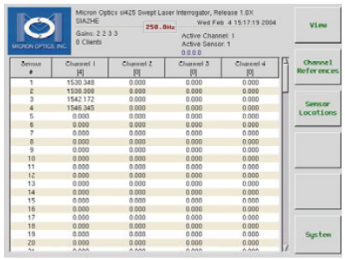

Table View

Shows dozens of sensor readings simultaneously.

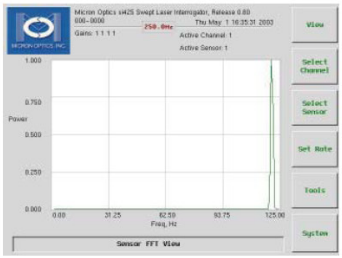

FFT View

Fast Fourier Transform (FFT) View shows frequency content for individual sensors.

MICRON OPTICS
Micron Optics, Inc.
1852 Century Pl, NE
Atlanta, GA 30345
ph: 404/325-0005
fax: 404/325-4082
www.micronoptics.com

www.manaraa.com

si425 | Optical Sensing Interrogator

Benefits

- **No Calibration -** The si425 never needs calibration. Wavelength is calibrated automatically on every scan.
- **Robust Operation -** The si425 survives harsh environments. Tests at professional facilities, meticulous customer evaluations, and tests at Micron Optics headquarters prove how well Micron Optics products are designed and built.
- **Huge FBG Sensor Capacity -** The si425 can monitor a huge number of multiplexed fiber Bragg grating sensors. With 80nm of wavelength range per channel and up to 16 optical channels, users of the system have great flexibility in designing their sensing system to maximize the number of sensors per interrogator, and to minimize total solution cost.
- **Fast Peak Detection -** The si425's on-board peak detection circuitry is fast and efficiency. That's why so many simultaneous measurments can be made at 250Hz.
- **Rack Mountable -** The si425 is designed for use in a convention instrument rack, in a protective enclosure at the measurment site, or on a lab bench. It is shown to withstand shock, vibration, and wide temperature extremes while performing to spec.
- **Verifiable Performance -** The performance we quote is the performance you'll get. Some manufacturers boast fantastic numbers for accuracy, resolution, and repeatability, but how will they perform in your application? Our specs apply over the entire operating range of temperature, humidity and vibration.
- **Modular Design -** The si425 is offered in three standard models. Custom configurations allow optimization of unit costs and feature sets for volume customers. Some si425 instruments have a built-in display and front panel controls. All use Ethernet to network to external PCs for additional data analysis.

Channel Expansion Modules

- **sm040-416 (16-channel Switch Extension):** 1U box converting four optical channel I/O from si425-500 to 16 optical channel I/O for sensor arrays. Product pricing includes all necessary jumpers, standard 100V/220V operation, control software and Ethernet command set providing access through LabVIEWTM.
- **sm040-408 (8-channel Switch Extension):** 1U box converting four optical channel I/O from si425-500 to 8 optical channel I/O for sensor arrays. Product pricing includes all necessary jumpers, standard 100V/220V operation, control software and Ethernet command set providing access through LabVIEWTM.
- **sm040-016 (16-channel Coupler Extension):** This 1U chassis contains four 1x4 couplers to accommodate connection of up to four fibers per channel. All fibers are scanned simultaneously. This provides no net gain of wavelength range or sensor capacity; it is solely intended to provide more fiber connection options.
- **sm040-008 (8-channel Coupler Extension):** This 1U chassis contains four 1x2 couplers to accommodate connection of up to two fibers per channel. All fibers are scanned simultaneously. This provides no net gain of wavelength range or sensor capacity; it is solely intended to provide more fiber connection options.

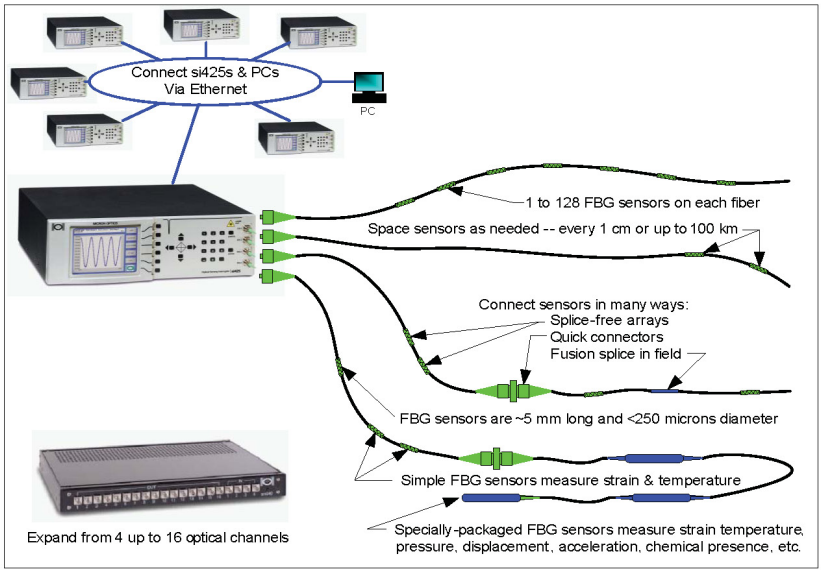

si425 / 060919 / acs2sv1 / SPECIFICATIONS ARE SUBJECT TO CHANGE WITHOUT NOTICE

MICRON OPTICS
Micron Optics, Inc.
1852 Century Pl. NE
Atlanta, GA 30345
ph: 404/325-0005
fax: 404/325-4082
www.micronoptics.com

www.manaraa.com

APPENDIX E: VIs, SUBVIs, VB DLLs

(Electronic Attachments)

www.manaraa.com

APPENDIX F: SAMPLE CALCULATIONS FOR FIGURE 5.51

www.manaraa.com

Calculations for the windowing procedure that is illustrated in Fig. 5.51 are provided for the following TS extrema:

TS Extrema #1:	TS Extrema #2:	TS Extrema #3:
Value = 69.9 με	Value = -109.1 με	Value = 15.6 με
ESI = 8567	ESI = 8699	ESI = 8898
EI = 8649	EI = 8759	EI = 8952
EEI = 8698	EEI = 8887	EEI = 9002

Parameters for use in *Match Extrema.vi* are as follows:

Speed = 65 mph
Speed Deviation = 10 mph

Therefore,

LS = 65 - 10 mph = 55 mph = 80.667 ft/s (5.5)
AS = 65 mph = 95.333 ft/s (5.6)
HS = 65 + 10 mph = 75 mph = 110.000 ft/s (5.7)

Sensor longitudinal locations from Table 5.2 are as follows:

$L_{B\text{-}SG\text{-}BF\text{-}H}$ = 58.067 ft

$L_{C\text{-}NG\text{-}CB(1)\text{-}V}$ = 123.078 ft

Thus,

D = 58.067 – 123.078 = -65.011 (5.8)

-65.011 < 0 ∴ Use equations 5.9 – 5.11

$$ESIP = \frac{-65.011}{80.667}(125) = -100.740 \quad (5.10)$$

$$EEIP = \frac{-65.011}{110.000}(125) = -73.876 \quad (5.11)$$

$$EIP = \frac{-65.011}{95.333}(125) = -85.242 \quad (5.9)$$

For TS Extrema #1:

WSI_{NTS} = 8567 – 100.740 = 8466.3 (5.2)
WEI_{NTS} = 8698 – 73.876 = 8624.1 (5.3)

No NTS extrema within window
Thus, no matches were formed.

EI_{NTS} = 8649 – 85.242 = 8563.8 (5.4)

www.manaraa.com

For TS Extrema #2:

WSI_{NTS} = 8699 – 100.740 = 8598.3 (5.2)

WEI_{NTS} = 8887 – 73.876 = 8813.1 (5.3)

Two NTS extrema within window
Thus, Match B and Match C were formed.

EI_{NTS} = 8759 – 85.242 = 8673.7 (5.4)

For TS Extrema #3:

WSI_{NTS} = 8898 – 100.740 = 8797.3 (5.2)

WEI_{NTS} = 9002 – 73.876 = 8928.1 (5.3)

No NTS extrema within window
Thus, no matches were formed.

EI_{NTS} = 8952 – 85.242 = 8866.8 (5.4)

www.manaraa.com

APPENDIX G: EXAMPLE EVALUATION REPORT FOR THE US30 BRIDGE

www.manaraa.com

US30 Bridge Evaluation Summary for the Files:

FCB#09132006#000021 - FCB#09142006#000002

Target Sensor C-SG-CB(5)-V

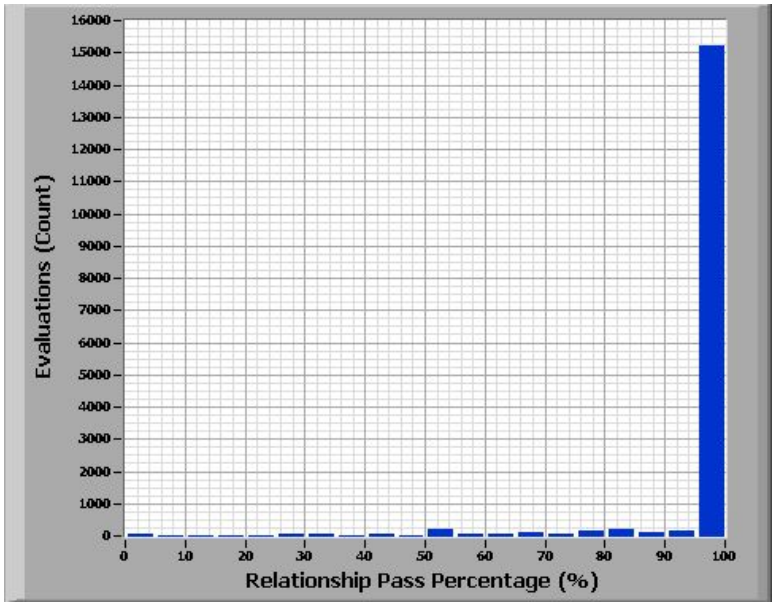

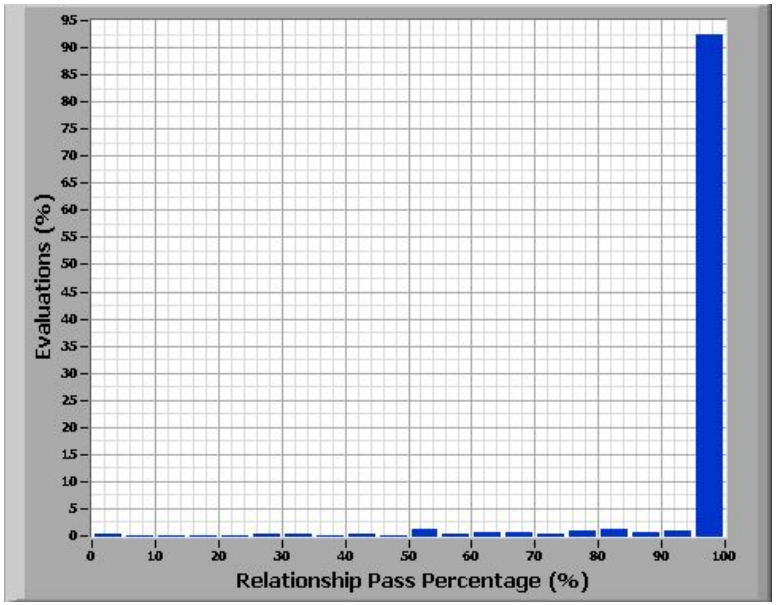

www.manaraa.com

US30 Bridge Evaluation Summary for the Files:

FCB#09132006#000021 - FCB#09142006#000002

Target Sensor C-SG-CB(4)-V

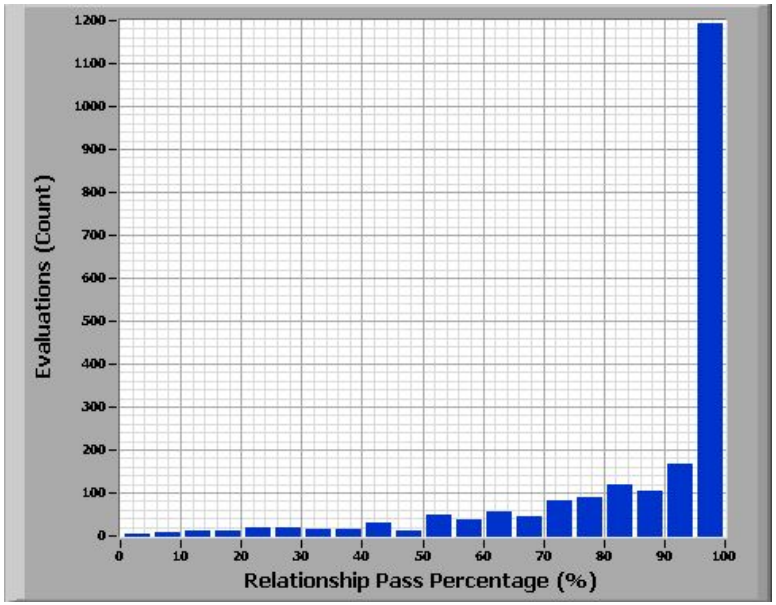

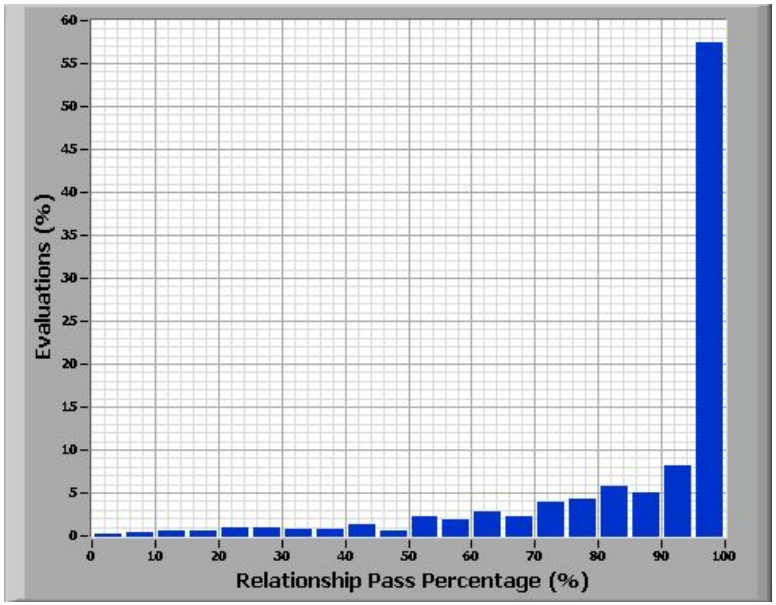

www.manaraa.com

US30 Bridge Evaluation Summary for the Files:

FCB#09132006#000021 - FCB#09142006#000002

Target Sensor C-SG-CB(3)-V

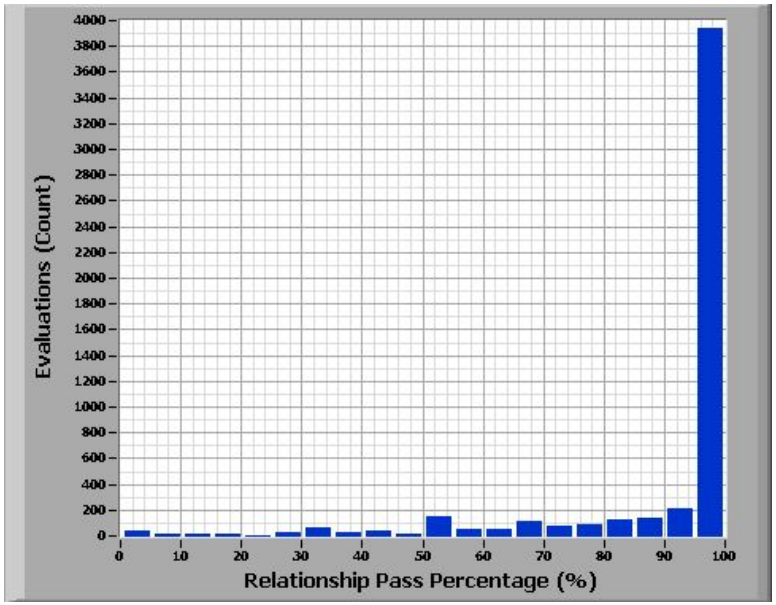

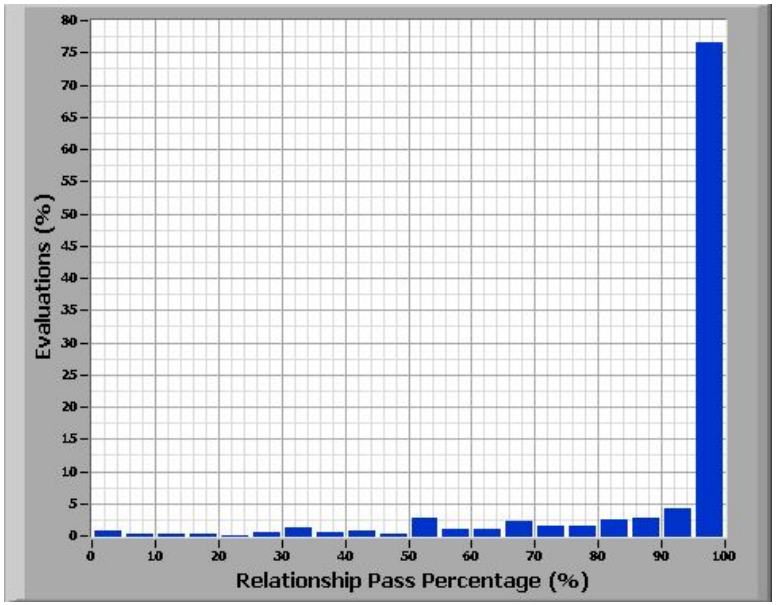

www.manaraa.com

US30 Bridge Evaluation Summary for the Files:

FCB#09132006#000021 - FCB#09142006#000002

Target Sensor C-SG-CB(2)-V

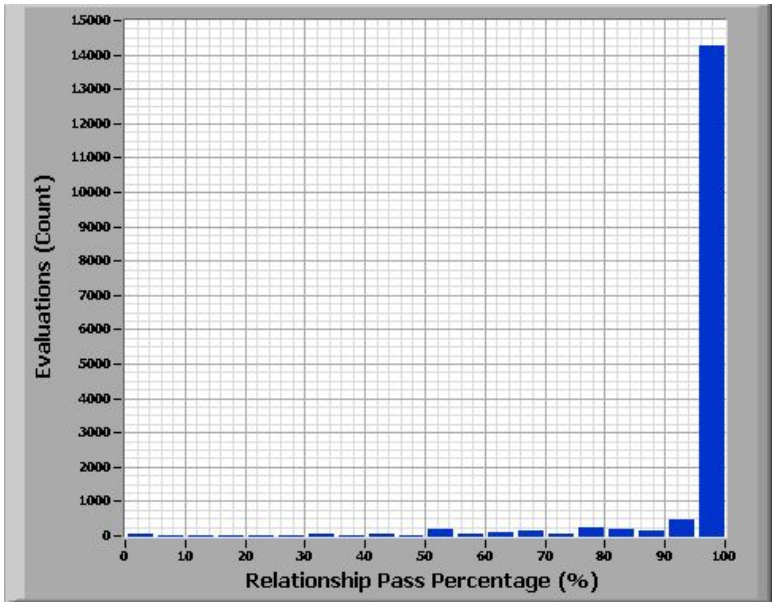

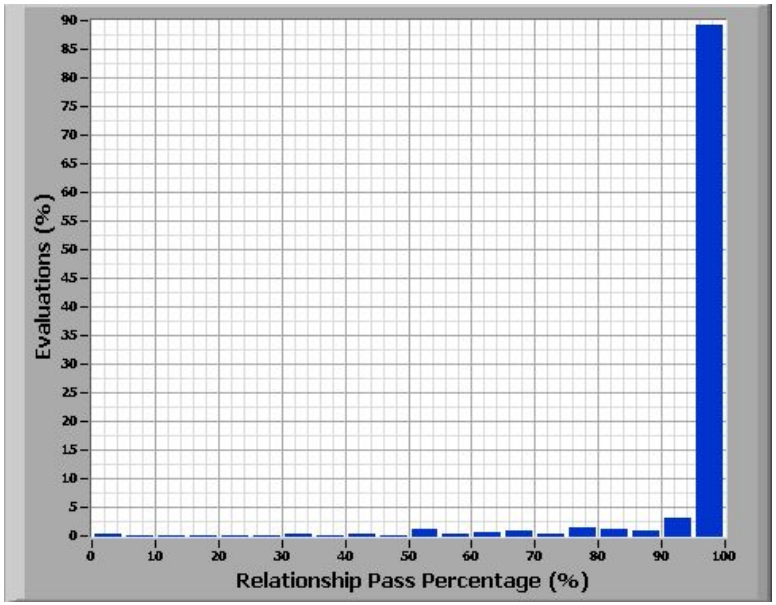

www.manaraa.com

US30 Bridge Evaluation Summary for the Files:

FCB#09132006#000021 - FCB#09142006#000002

Target Sensor C-SG-CB(1)-V

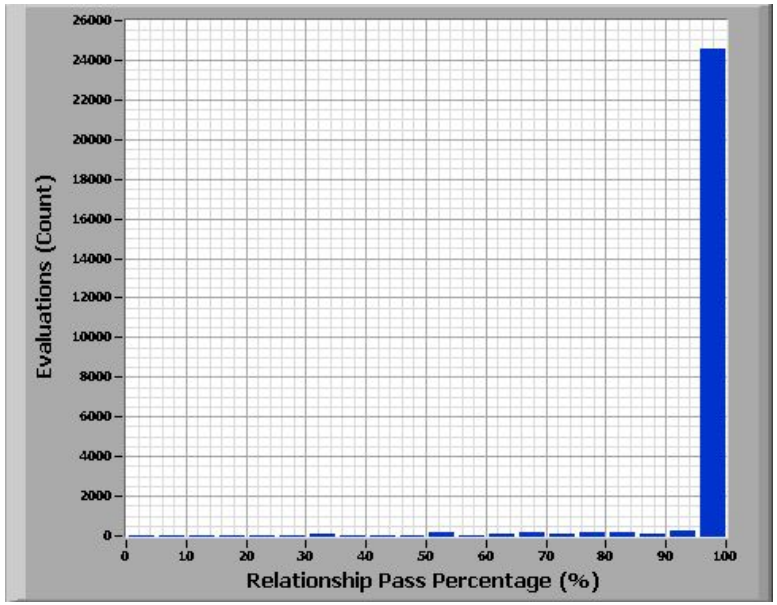

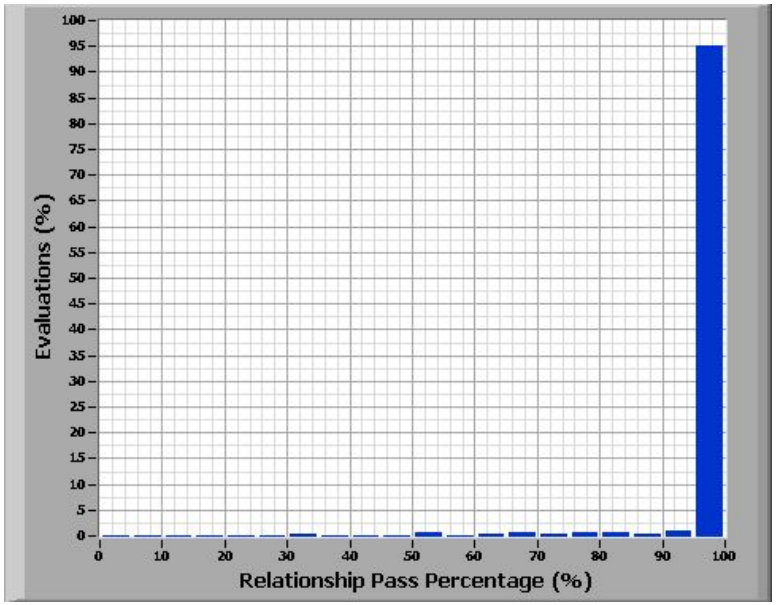

www.manaraa.com

US30 Bridge Evaluation Summary for the Files:

FCB#09132006#000021 - FCB#09142006#000002

Target Sensor C-NG-CB(5)-V

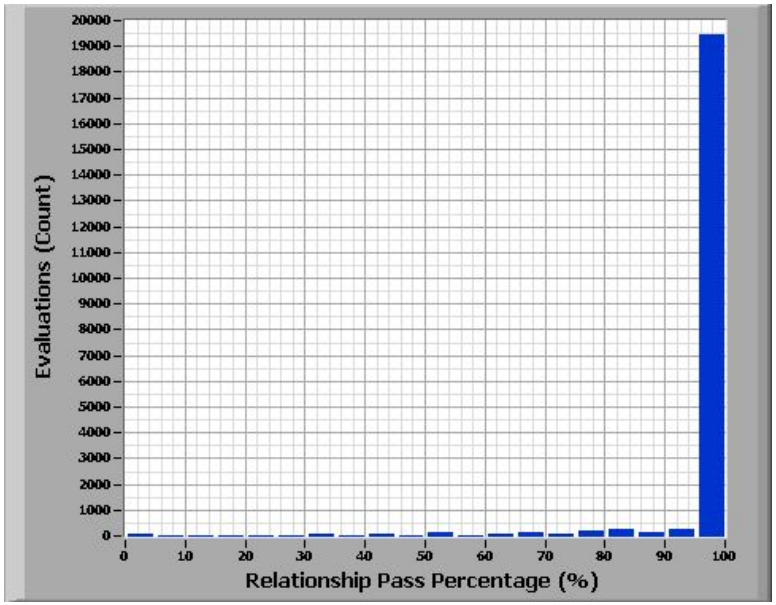

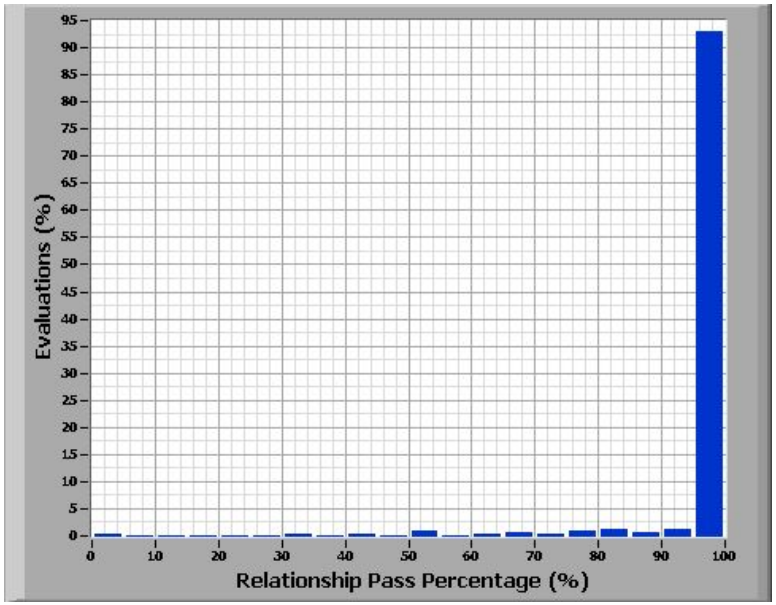

www.manaraa.com

US30 Bridge Evaluation Summary for the Files:

FCB#09132006#000021 - FCB#09142006#000002

Target Sensor C-NG-CB(4)-V

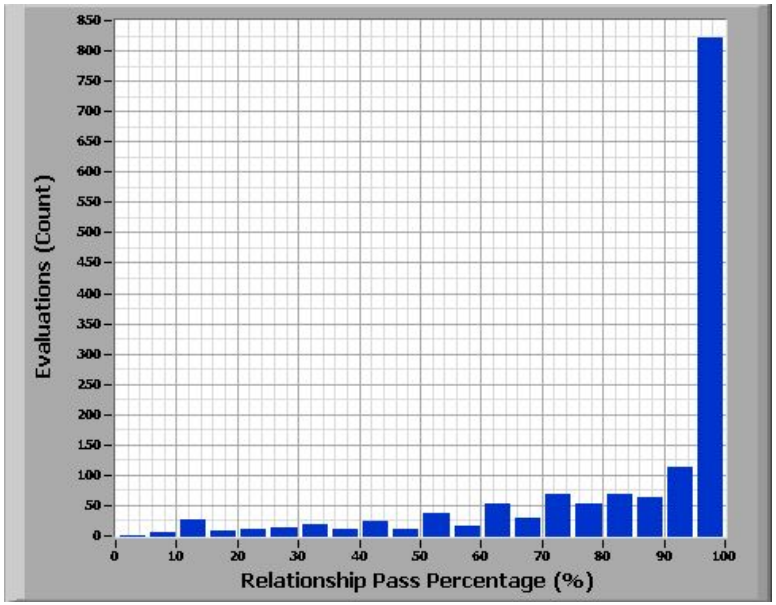

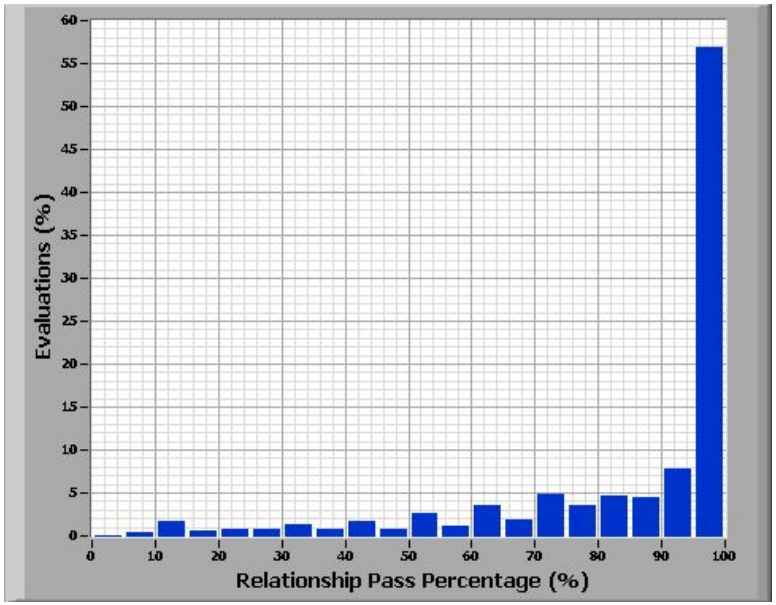

www.manaraa.com

US30 Bridge Evaluation Summary for the Files:

FCB#09132006#000021 - FCB#09142006#000002

Target Sensor C-NG-CB(3)-V

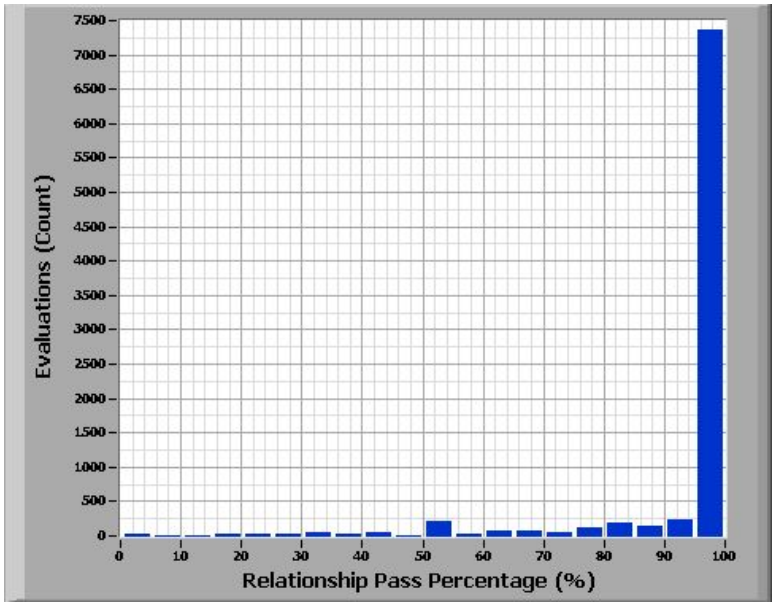

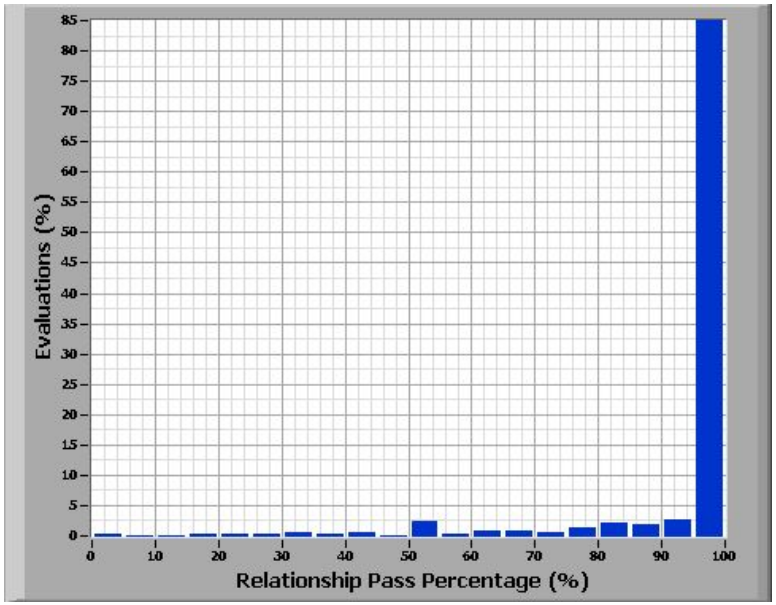

www.manaraa.com

US30 Bridge Evaluation Summary for the Files:

FCB#09132006#000021 - FCB#09142006#000002

Target Sensor C-NG-CB(2)-V

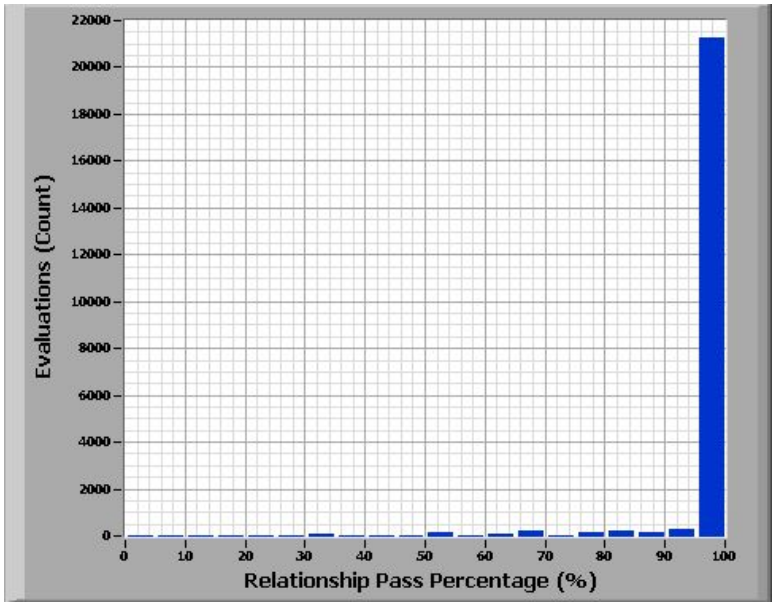

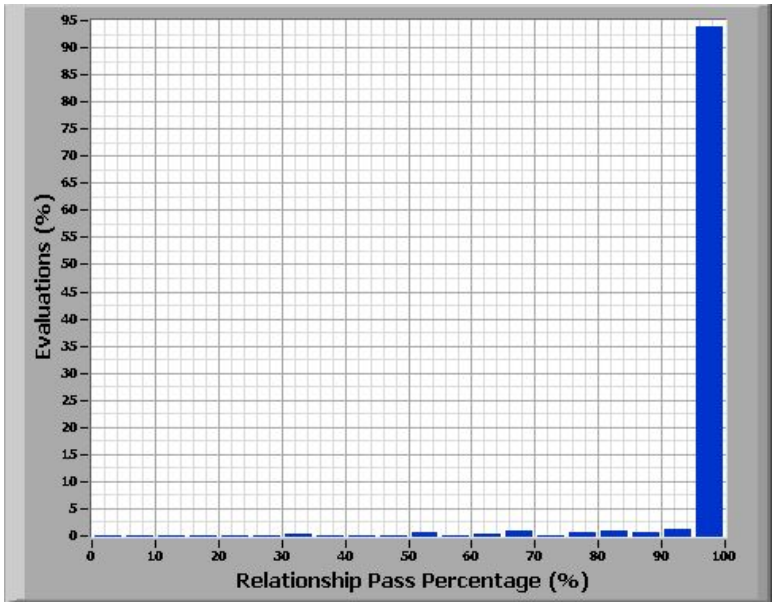

www.manaraa.com

US30 Bridge Evaluation Summary for the Files:

FCB#09132006#000021 - FCB#09142006#000002

Target Sensor C-NG-CB(1)-V

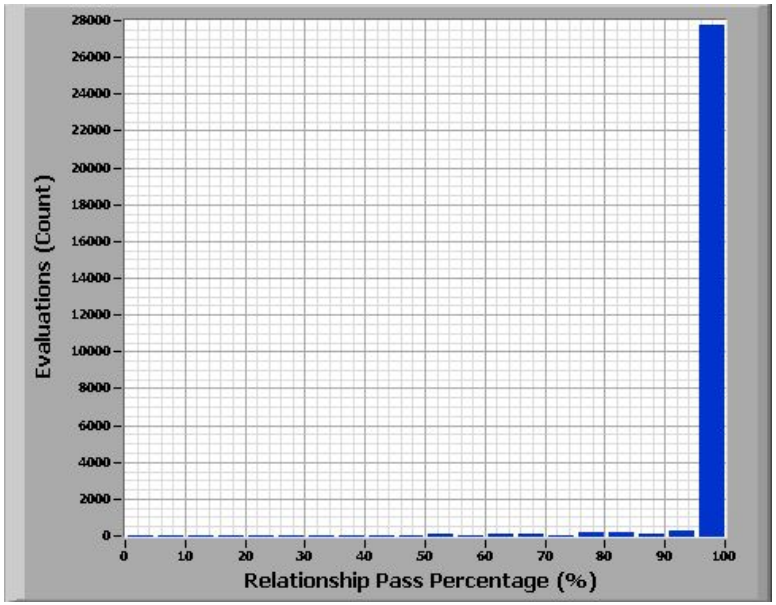

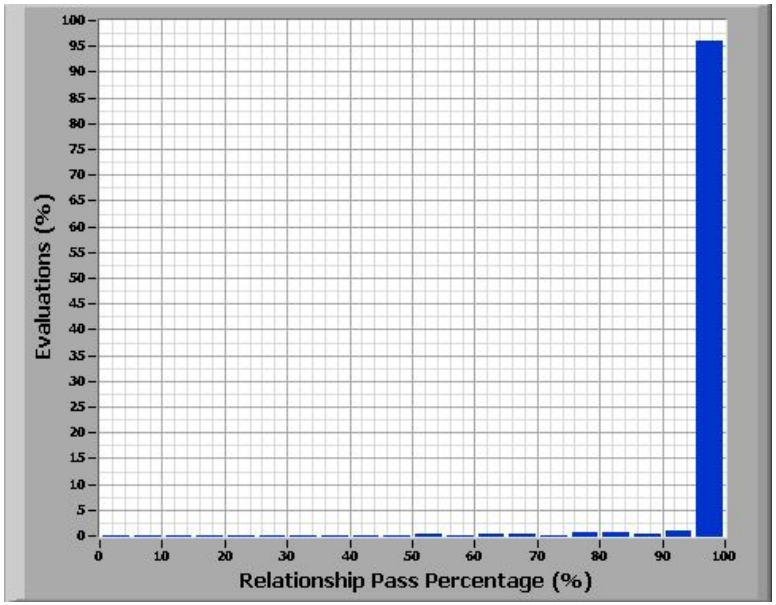

www.manaraa.com

REFERENCES

1. American Association of State Highway and Transportation Officials (AASHTO). (2004). *Manual for Maintenance Inspection of Bridges*, Washington, D.C.

2. Fisher, John W. (1984). *Fatigue and Fracture in Steel Bridges,* John Wiley & Sons, Inc.

3. Wipf, T. J., Phares, B. M., Greimann, L. F., Doornink, J. D., Hemphill, D. J., and Lu, P. (2005). "The remote continuous structural health monitoring of the East 12th Street Bridge", Final Report, Iowa Department of Transportation, 136 pp.

4. Small, E. P., Philbin, T., Fraher, M., and Romack, G. P. (2000). "Current status of bridge management system implementation in the United States." Eighth International Bridge Management Conference, *Transportation Research Circulator 498*, TRB, NRC, Vol. 1, A1-A16.

5. Chong, K. P., Carino, N. J., and Washer, G. (2003). "Health monitoring of civil infrastructures." *Smart Materials and Structures*, Vol. 12, 483-493.

6. Connor, R. J., Dexter, R., and Mahmoud, H. (2005). *Inspection and management of bridges with fracture-critical details, a synthesis of highway practice*. NCHRP Synthesis 354, Transportation Research Board, Washington, D.C.

7. Moore, M., Phares, B. M., Graybeal, B., Rolander, D. (2001). *Reliability of Visual Inspection for Highway Bridges, Volume I: Final Report*. Federal Highway Administration, Report No. FHWA-RD-01-020, 486 pp.

8. Ghorbanpoor, A., and Benish, N. (2003). *Non-Destructive Testing of Wisconsin Highway Bridges*. Final Report, Wisconsin Highway Research Program, Project No. 0092-00-15, 102 pp.

9. American Society for Testing and Materials (ASTM) International. (2006). ASTM E 165-02, "Standard test method for liquid penetrant examination." *Annual Book of ASTM Standards*, Vol. 03.03, 62-71.

10. American Society for Testing and Materials (ASTM) International. (2006). ASTM E 709-01, "Standard guide for magnet particle examination." *Annual Book of ASTM Standards*, Vol. 03.03, 297-322.

11. American Society for Testing and Materials (ASTM) International. (2006). ASTM A 577/ A 577M-90, "Standard specifications for ultrasonic angle-beam examination of steel plates." *Annual Book of ASTM Standards*, Vol. 01.04, 315-317.

12. American Society for Testing and Materials (ASTM) International. (2006). ASTM A 435/A 435M-90, "Standard specifications for straight-beam ultrasonic examination of steel plates." *Annual Book of ASTM Standards*, Vol. 01.04, 256-257.

13. American Society for Testing and Materials (ASTM) International. (2006). ASTM E 587-00, "Standard practice for ultrasonic angle-beam examination by the contact method." *Annual Book of ASTM Standards*, Vol. 03.03, 266-273.

14. American Society for Testing and Materials (ASTM) International. (2006). ASTM A 898/898M-91, "Standard specifications for straight beam ultrasonic examination of rolled steel structural shapes." *Annual Book of ASTM Standards*, Vol. 01.04, 517-519.

www.manaraa.com

15. American Society for Testing and Materials (ASTM) International. (2006). ASTM E 1106-86, "Standard method for primary calibration of acoustic emission sensors." *Annual Book of ASTM Standards*, Vol. 03.03, 543-551.

16. American Society for Testing and Materials (ASTM) International. (2006). ASTM E 650-97, "Standard guide for mounting piezoelectric acoustic emission sensors." *Annual Book of ASTM Standards*, Vol. 03.03, 280-285.

17. American Society for Testing and Materials (ASTM) International. (2006). ASTM E 569-02, "Standard practice for acoustic emission monitoring of structures during controlled stimulation." *Annual Book of ASTM Standards*, Vol. 03.03, 250-253.

18. American Society for Testing and Materials (ASTM) International. (2006). ASTM E 94-04, "Standard guide for radiographic examination." *Annual Book of ASTM Standards*, Vol. 03.03, 1-11.

19. American Society for Testing and Materials (ASTM) International. (2006). ASTM E 1955-04, "Standard radiographic examination for soundness of welds in steel by comparison to graded ASTM E 390 reference radiographs." *Annual Book of ASTM Standards*, Vol. 03.03, 1056-1057.

20. Ko, J. M., and Ni, Y. Q. (2005). "Technology developments in structural health monitoring of large-scale bridges." *Engineering Structures*, 27(12), 1715-1725.

21. Yoo, S. H., and Kim, B. S. (2000). "Characterization of a crack in a plate using strain mode shapes." *Proc. of the International Modal Analysis Conference (IMAC-XVIII)*, San Antonio, TX, 1790-1795.

22. Patil, D. P., and Maiti, S. K. (2003). "Detection of multiple cracks using frequency measurements." *Engineering Fracture Mechanics*, Vol. 70, 1553-1572.

23. Wang, G. and Barkey, M. E. (2004). "Fatigue cracking and its influence on dynamic response characteristics of spot welded specimens." *Experimental Mechanics*, 44(5), 512-521.

24. Verreman, Y. (1994). "Monitoring short fatigue cracks with miniature strain gages." *Experimental Mechanics*, 34(3), 208-216.

25. Fujimoto, Y., and Yue, J. (2005). "Depth estimation of surface cracks based on the measurement of crack opening deformation and numerical-experimental iteration." *Journal of Marine Science and Technology*, 10(4), 203-210.

26. Younis, N. T., and Mize, J. (1996). "Discrete averaging effects of a strain gage at a crack tip." *Engineering Fracture Mechanics*, 55(01), 147-153).

27. Ihn, J. B., and Chang, F. K. (2004). "Detection and monitoring of hidden fatigue crack growth using a built-in piezoelectric sensor/actuator network: I. Diagnostics." *Smart Materials and Structures*, Vol. 13, 609-620.

28. Ihn, J. B., and Chang, F. K. (2004). "Detection and monitoring of hidden fatigue crack growth using a built-in piezoelectric sensor/actuator network: II. Validation using riveted joints and repair patches." *Smart Materials and Structures*, Vol. 13, 621-630.

www.manaraa.com

29. Casas, J. R., and Paulo, J. S. (2003). "Fiber optic sensors for bridge monitoring." *Journal of Bridge Engineering*, 8(6), 362-373.

30. Udd, E. (1991). *Fiber Optic Sensors: An Introduction for Engineers and Scientists*. Wiley & Sons, Inc.

31. Zhou, G., and Sim, L. M. (2002). "Damage detection and assessment in fibre-reinforced composite structures with embedded fibre optic sensors – review." *Smart Materials and Structures*, Vol. 11, 925-939.

32. Hale, K. F (1992). "An optical-fibre fatigue crack-detection and monitoring system." *Smart Materials and Structures*, Vol. 1, 156-161.

33. Leung, C. K. Y., Elvin, N., Olson, N., Morse, T. F., and He, Y. (2000). "A novel distributed optical crack sensor for concrete structures." *Engineering Fracture Mechanics*, 65(2), 133-148.

34. Leung, C. K. Y. (2001). "Fiber optic sensors for concrete structures: the future." *Non-Destructive Testing and Evaluation International*, 34(2), 85-94.

35. Olson, N., Leung, C. K. Y., and Meng, A. (2005). "Crack sensing with a multimode fiber: experimental and theoretical studies." *Sensors and Actuators, A: Physical*, 118(2), 268-277.

36. Yang, Z. L., Liu, G. R., and Lam, K. Y. (2002). "An inverse procedure for crack detection using integral strain measured by optical fibers." *Smart Materials and Structures*, Vol. 11, 72-78.

37. Peters, K., Studer, M., Botsis, J., Iocco, A., Limberger, H., and Salthe, R. (2000). "Embedded optical fiber bragg grating sensor in a nonuniform strain field; measurements and simulations." *Experimental Mechanics*, 41(1), 19-28.

38. Studer, M. and Peters, K. (2004). "Multi-scale sensing for damage identification." *Smart Materials and Structures*, Vol. 13, 283-294.

39. Hill, P. C., Eggleton, B. J. (1994). "Strain gradient chirp of fibre bragg gratings." *Electronics Letters*, 30(14), 1172-1174.

40. Degen, B. (2006). "Shear design and behavior of ultra-high performance concrete." M.S. Thesis, Department of Civil, Construction, and Environmental Engineering, Iowa State University, 146 pp.

41. Doebling, S. W., Farrar, C. R., and Prime, M. B. (1998). "A summary review of vibration-based damage identification methods." *The Shock and Vibration Digest*, 30(2), 91-105.

42. Rytter, A. (1993). "Vibration based inspection of civil engineering structures." Ph.D. Dissertation, Department of Building Technology and Structural Engineering, Aalborg University, Denmark.

43. Sohn, H., Farrar, C., Hemez, F., Shunk, D., Stinemates, D., and Nadler, B. (2003). "A review of structural health monitoring literature: 1996 – 2001." Los Alamos National Laboratory Report, LA-13976-MS.

www.manaraa.com

44. Farrar, F. R, and Jauregui, D. A. (1997). "Comparative study of damage identification algorithms applied to a bridge: I. Experiment." *Smart Materials and Structures*, Vol. 7, 704-719.

45. Farrar, F. R, and Jauregui, D. A. (1997). "Comparative study of damage identification algorithms applied to a bridge: II. Numerical Study." *Smart Materials and Structures*, Vol. 7, 720-731.

46. Woodward, C., White, K. R., and Minor, J. (1994). "Global NDT of a fracture critical bridge." *NDE: An Answer for an Aging World*, March 21-25, New Orleans, LA, 200-202.

47. Idriss, R. L., White, K. R., Woodward, C. B., and Jaurequi, D. V. (1995). "After-fracture redundancy of two-girder bridge: testing of the I-40 bridges over Rio Grande." *Proc. of the Fourth International Bridge Engineering Conference*, August 28-30, San Francisco, CA, 316-326.

48. Iwasaki, A., Todoroki, A., Sugiya, T., Izumi, S., and Sakai, S. (2005). "Unsupervised statistical damage diagnosis for structural health monitoring of existing structures." *Smart Materials and Structures*, Vol. 14, S154-S161.

49. Kesavan, A., Deivasigamani, M., John, S., and Herszberg, I. (2005). "Damage critically assessment in complex geometric structures using strain response-based signal processing techniques." *Smart Structures and Materials 2005: Smart Structures and Integrated Systems, Proc. of SPIE*, Vol. 5764, 542-552.

50. Wong, K. Y., Chan, W. Y. K., Man, K. L., Mak, W. P. N., and Lau, C. K. (2000). "Structural health monitoring results on Tsing Ma, Kap Shui Mun, and Ting Kau Bridges." *Nondestructive Evaluation of Highways, Utilities, and Pipelines IV, Proc. of SPIE*, Vol. 3995, 288-299.

51. Li, Z.X., Chan, T. H. T., and Ko, J. M. (2001). "Fatigue damage model for bridge under traffic loading: application made to Tsing Ma Bridge." *Theoretical and Applied Fracture Mechanics*, 35(1), 81-91.

52. Ni, Y. Q, Zhou, X. T., Ko, J. M., and Wang, B. S. (2000). "Vibration-based damage localization in the Ting Kau bridge using probabilistic neural networks." *Advances in Structural Dynamics*, Vol. 2, 1069-1076.

53. Caicedo, J. M., and Dyke, S. J. (2005). "Experimental validation of structural health monitoring for flexible bridge structures." *Structural Control and Health Monitoring*, 12(304), 425-443.

54. Maeck, J., Peeters, B., and De Roeck, G. (2001). "Damage identification on the Z24 bridge using vibration monitoring." *Smart Materials and Structures*, Vol. 10, 512-517.

55. Zhao, J., and DeWolf, J. T. (2002). "Dynamic monitoring of steel girder highway bridges." *Journal of Bridge Engineering*, 7(6), 350-356.

56. Khalil, A., Greimann, L., Wipf, T. J., Wood, D. (1998). "Modal testing for nondestructive evaluation of bridges: issues." *Proceedings of Crossroads 2000*, Aug. 19-20, Ames, IA, 109-112.

www.manaraa.com

57. Khalil, A. (1999). "Aspects in nondestructive evaluation of steel plate girder bridges." Ph.D. Dissertation, Department of Civil and Construction Engineering, Iowa State University, 228 pp.

58. Farrar, C. R., and Doebling, S. W. (1998). "An overview of modal-based damage identification methods." Proc. of EUROMECH 365 International Workshop: DAMAS 97, Structural Damage Assessment Using Advanced Signal Processing Procedures, Sheffield, U.K.

59. Tennyson, R. C., Mufti, A. A., Rizkalla, S., Tadros, G., and Benmokrane, B. (2001). "Structural health monitoring of innovative bridges in Canada with fiber optic sensors." *Smart Materials and Structures*, Vol. 10, 560-573.

60. Mohammed, M. Karasaridis, A., Pantazzopoulou, S., and Hatzinakos, D. (2002). "Structural health monitoring of smart structures." *Smart Materials and Structures*, Vol. 11, 581-589.

61. Doornink, J. D., Phares, B. M., Zhou, Z., Ou, J., Graver, T. W., and Xu, Z. (2004). "Fiber bragg grating sensing for structural health monitoring of civil structures." *Proceedings of the International Symposium on Advances and Trends in Fiber Optics (ATFO)*, October 11-15, Chongqing, China.

62. Graver, T., Inaudi, D., and Doornink, J. D. (2004). "Growing market acceptance for fiber-optic solutions in civil structures." *Fiber Optic Sensor Technology and Applications III, Proceedings of SPIE*, Vol. 5589, p 44-55.

63. Phares, B. M. and LaViolette, M. D. Personal communication, June 28, 2006.

64. Seim, J., Udd, E., Schulz, W., and Laylor, H. (1999). "Health monitoring of an Oregon historical bridge with fiber bragg grating sensors." *Smart Structures and Materials 1999: Smart Systems for Bridges, Structures, and Highways, Proceedings of SPIE*, Vol. 3671, 128-134.

65. Doornink, J. D., Lee, Y. S., Wipf, T. J., and Phares, B. M. (2005). "Current state-of-the-practice and state-of-the-art in structural health monitoring of bridges and components." Unpublished manuscript.

66. Huang, S., Zhao, T., and Chen, W. (1997). "The evaluation of the bridge pavement samples using an optical fiber sensor system." *Smart Materials, Structures, and Integrated Systems, Proceedings of SPIE*, Vol. 3241, 347-352.

67. Wang, J. N., and Tang, J. L. (2005). "Using fiber bragg grating sensors to monitor pavement structures." *Transportation Research Record 1913*, 165-176.

68. Idriss, R. L., Kodindouma, M. B., Kersey, A. D., and Davis, M. A. (1998). "Multiplexed bragg grating optical sensors for damage evaluation in highway bridges." *Smart Materials and Structures*, Vol. 7, 209-216.

69. Davis, M., Bellemore, D., Berkoff, T., Kersey, A., Putnam, M., Idriss, R., and Kodinduma, M. (1996). "Fiber-optic sensors system for bridge monitoring with both static load and dynamic modal sensing capabilities." *Nondestructive Evaluation of Bridges and Highways, Proceedings of SPIE*, Vol. 2946, 219-232.

www.manaraa.com

70. Yong, Z., Fu, Y., Chen, W., Huang, S., and Bennet, K. D. (2003). "Health monitoring system for Dafosi cable-stayed bridge." *Smart Structures and Materials 2003: Smart Systems and Nondestructive Evaluation for Civil Infrastructures, Proceedings of SPIE*, Vol. 5057, 289-297.

71. Liu, P. L. and Sun, S. C. (1997). "The application of artificial neural networks on the health monitoring of bridges." *Structural Health Monitoring, Current Status and Perspectives*, Stanford University, Palo Alto, CA, 103-110.

72. Montgomery, D. C. (2004). *Introduction to Statistical Quality Control*, v. 5e, John Wiley & Sons, Inc.

73. Mitra, A. (1998). *Fundamentals of Quality Control and Improvement*, v. 2, Prentice Hall, Inc., Upper Saddle River, NJ.

74. Mandel, B. J. (1969). "The regression control chart." *Journal of Quality Control*, 1(1), 1-9.

75. Hoon, S., Czarnecki, J. A., and Farrar, C. (2000). "Structural health monitoring using statistical process control." *Journal of Structural Engineering*, 126(11), 1356-1363.

76. Kullaa, J. (2003). "Damage detection of the Z24 Bridge using control charts." *Mechanical Systems and Signal Processing*, 17(1), 163-170.

77. Brownjohn, J. M. W., Moyo, P., Omenzetter, P., and Chakraborty, S. (2005). "Lessons from monitoring the performance of highway bridges." *Structural Control and Health Monitoring*, 12(3-4), 227-244.

78. Packham, D. E. (2005). *Handbook of Adhesion*, 2nd Edition, John Wiley & Sons, West Sussex, England.

79. Petrie, E. M. (2000). *Handbook of Adhesives and Sealants*, McGraw-Hill, New York, NY.

80. Comyn, J. (1997). *Adhesion Science*, The Royal Society of Chemistry, Cambridge, UK.

81. Callister, Jr., W. D. (2000). *Materials Science and Engineering: An Introduction*, 5th Edition, John Wiley & Sons, Inc.

82. Takiguchi, M., Izumi, S., and Yoshida, F. (2004). "Rate-dependent shear deformation of ductile acrylic adhesive and its constitutive modeling." *Proc. of the Institution of Mechanical Engineers, Part C: Journal of Mechanical Engineering Science*, 218(6), 623-629.

83. Gunawan, M., Davila, L. T., Wong, E. H., Mhaisalkar, S. G. Tsai, T. K., and Osiymemi, S. (2004). "Static and cyclic studies in nonconductive adhesives." *Thin Solid Films, Proc. of the International Conference on Materials for Advanced Technologies (ICMAT 2003)*, Vol. 462-463, 419-426.

84. Chernenkoff, R. A. (1992). "Cyclic creep effects in single-overlap bonded joints under constant-amplitude testing." *Proc. of the Symposium on Cyclic Deformation, Fracture, and Nondestructive Evaluation of Advanced Materials*, ASTM Special Publication n. 1157, 190-204.

85. Proakis, J. G., and Manolakis, D. G. (1996). *Digital Signal Processing: Principles, Algorithms, and Applications*, 3rd Edition, Prentice Hall, Inc., Upper Saddle River, NJ.

www.manaraa.com

86. National Instruments. (2004). *LabVIEW Analysis Concepts*, National Instruments Corporation, Austin, TX, 231 pp.

87. Smith, S. W. (1997). *The Scientist and Engineer's Guide to Digital Signal Processing*, California Technical Publishing, 640 pp. Also available online at http://www.dspguide.com.

88. Cantieni, R. (1983). "Dynamic load tests on highway bridges in Switzerland: 60 years experience of EMPA." *Tech. Rep. 211*, Swiss Federal Laboratory for Materials Testing and Research, Dubendorf, Switzerland.

89. National Weather Service (2006). Climate data obtained from http://www.weather.gov/climate/index.php?wfo=dmx (September 30, 2006).

www.manaraa.com

ACKNOWLEDGEMENTS

The investigation presented in this report was conducted by the Bridge Engineering Center at Iowa State University. The research was sponsored by the Iowa Department of Transportation, Highway Division, and the Iowa Highway Research Board. The author wishes to thank Doug Wood, ISU Research Laboratory Manager, for his significant contributions to the laboratory and field testing that was performed in this research.

www.manaraa.com